Edited by
Mahdi Sharifzadeh

Design and Operation of Solid Oxide Fuel Cells

The Systems Engineering Vision for Industrial Application

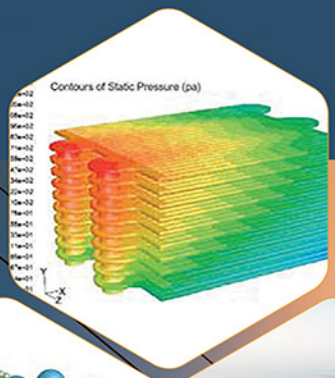

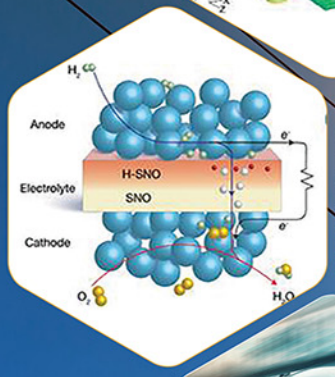

Design and Operation of Solid Oxide Fuel Cells

The Systems Engineering Vision for Industrial Application

This page intentionally left blank

Design and Operation of Solid Oxide Fuel Cells

The Systems Engineering Vision for Industrial Application

Edited by

Mahdi Sharifzadeh

Sharif Energy Research Institute (SERI), Sharif University of Technology, Tehran, Iran

ACADEMIC PRESS

An imprint of Elsevier

Academic Press is an imprint of Elsevier
125 London Wall, London EC2Y 5AS, United Kingdom
525 B Street, Suite 1650, San Diego, CA 92101, United States
50 Hampshire Street, 5th Floor, Cambridge, MA 02139, United States
The Boulevard, Langford Lane, Kidlington, Oxford OX5 1GB, United Kingdom

Notices
Knowledge and best practice in this field are constantly changing. As new research and experience broaden our understanding, changes in research methods, professional practices, or medical treatment may become necessary.

Practitioners and researchers must always rely on their own experience and knowledge in evaluating and using any information, methods, compounds, or experiments described herein. In using such information or methods they should be mindful of their own safety and the safety of others, including parties for whom they have a professional responsibility.

To the fullest extent of the law, neither the Publisher nor the authors, contributors, or editors, assume any liability for any injury and/or damage to persons or property as a matter of products liability, negligence or otherwise, or from any use or operation of any methods, products, instructions, or ideas contained in the material herein.

British Library Cataloguing-in-Publication Data
A catalogue record for this book is available from the British Library

Library of Congress Cataloging-in-Publication Data
A catalog record for this book is available from the Library of Congress

ISBN: 978-0-12-815253-9

Publisher: Katie Hammon
Acquisition Editor: Maria Convey
Editorial Project Manager: Lindsay Lawrence
Production Project Manager: Mohana Natarajan
Cover Designer: Christian Bilbow

Typeset by MPS Limited, Chennai, India

Contents

List of contributors

Tohid N. Borhani
School of Water, Energy and Environment, Cranfield University, Bedford, Bedfordshire, United Kingdom

Wenqian Chen
Department of Chemical Engineering, Imperial College London, London, United Kingdom

Mohsen Foroughi Doust
Chemical & Petroleum Engineering Department, Sharif University of Technology, Tehran, Iran; Sharif Energy Research Institute (SERI), Sharif University of Technology, Tehran, Iran

Mohsen Foroughidoust
Chemical & Petroleum Engineering Department, Sharif University of Technology, Tehran, Iran; Sharif Energy Research Institute (SERI), Sharif University of Technology, Tehran, Iran

Maryam Ghadrdan
Research & Technology, Equinor ASA, Fornebu, Norway

Aliakbar Ghaffari
School of Chemistry, College of Science, University of Tehran, Tehran, Iran

Ehsan Haghi
University of Waterloo, Canada

Mirko Hu
IMT School for Advanced Studies, Lucca, Italy

Rui Jing
College of Energy, Xiamen University, Xiamen, P.R. China

Venkatesan Krishnan
School of Science, Engineering and Design, Teesside University, Middlesbrough, United Kingdom

Venkatesan Venkata Krishnan
School of Science, Engineering and Design, Teesside University, Middlesbrough, United Kingdom

Mojtaba Meghdari
Chemical & Petroleum Engineering Department, Sharif University of Technology, Tehran, Iran

Alireza Mohammadzadeh
Department of Mechanical Engineering, Sharif University of Technology, Tehran, Iran; Sharif Energy Research Institute (SERI), Sharif University of Technology, Tehran, Iran

Seyedeh Kiana Naghib Zadeh
Sharif Energy Research Institute (SERI), Sharif University of Technology, Tehran, Iran; Department of Mechanical Engineering, Sharif University of Technology, Tehran, Iran

Meysam Qadrdan
Cardiff University, United Kingdom

Davood Rashtchian
Department of Chemical & Petroleum Engineering, Sharif University of Technology, Tehran, Iran

Majid Saidi
School of Chemistry, College of Science, University of Tehran, Tehran, Iran

Mohammad Hassan Saidi
Sharif Energy Research Institute (SERI), Sharif University of Technology, Tehran, Iran; Department of Mechanical Engineering, Sharif University of Technology, Tehran, Iran

Nilay Shah
Department of Chemical Engineering, Centre for Process Systems Engineering (CPSE), Imperial College London, London, United Kingdom

Mahdi Sharifzadeh
Department of Chemical Engineering, Centre for Process Systems Engineering (CPSE), Imperial College London, London, United Kingdom

Giorgio Triulzi
School of Management, Universidad de los Andes, Bogotá, Colombia; Sociotechnical Systems Research Center, Massachusetts Institute of Technology, MA, United States

Christopher Williams
Cardiff University, United Kingdom

Xiandong Xu
Cardiff University, United Kingdom

Zhihui Zhang
College of Energy, Xiamen University, Xiamen, P.R. China

Yingru Zhao
College of Energy, Xiamen University, Xiamen, P.R. China

Preface

Fossil fuels are projected to remain the dominant source of energy in the foreseeable future. Nevertheless, their dwindling reserves and associated pollutions have motivated intensive research for finding alternative resources as well as more efficient utilization of these carbon-intensive fuels. Solid oxide fuel cells (SOFCs) are one of the most promising electrochemical technologies offering several pathways for decarbonization. First, they are not constrained to the Carnot limits, offering very high energy conversion efficiencies. Second, they are flexible to utilize a wide range of fuels, including those extracted from renewable resources. They are also highly modular, but adaptable to be integrated with a variety of applications and services including vehicles and mobile applications, remote or distributed power generation, as well as large-scale industrial power generation. Most of all, the unmixed nature of the involved electrochemical reactions offers one of the most promising technologies for carbon capture integration.

Nonetheless, such unique characteristics come at the price of more convoluted processes. Considering the enormous options for process integration and intensification, the number of alternative solutions grows sharply with the size of the problem, thereby requiring efficient methodologies with tailor-made solution algorithms for decision-support. Such methodologies should be able to systematically generate alternative candidate solutions and then, quantitatively based, screen on rigorous performance indicators. Nevertheless, the design indicators for SOFC systems are to large extent competing and conflicting, including economic performance, environmental footprints, operation safety, flexibility, and process controllability. Most of all, many of the involved decisions span over a broad spectrum of spatial and temporal scales, extending from the molecular design of SOFC materials, microstructures, and grains to the involved electrochemical reactions and transport phenomena, phase behavior, and fluid dynamics, and further to process equipment, plant-wide operation, and energy supply chains. The key observation is that the design and operation of SOFC systems is a multiscale and multifaceted research area, requiring the involvement of experts from several science and engineering disciplines.

Design and Operation of Solid Oxide Fuel Cells aims to address this need by providing a multidisciplinary perspective on the systems engineering of SOFC systems. The book has two parts. The first offers in-depth insights into the theoretical foundation of the underlying phenomena, design considerations, and operational strategies. The features of interest include the technological growth of SOFCs among other fuel cell technologies, thermodynamic considerations, mechanical properties, engineering the materials for SOFCs, multiscale modeling and optimization of SOFC systems, process synthesis, integration, and intensification, process control, fault analyses, operational safety, and loss prevention. The second part of the book is application-oriented and explores topics such as the fuel flexibility in SOFC systems with emphasis on the application of renewable

energies and reversible solid oxide cells (ReSOCs) for energy storage, as mobile applications in cars, trucks, locomotives, undersea vehicles, and aircrafts, as well as stationary and distributed applications for power generation and the utilization of SOFCs for waste minimization.

We hope that this contribution will impact the research field, especially through promoting a multidisciplinary vision for systems engineering of solid oxide fuel cells, and welcome all constructive feedback from readers.

Dr. Mahdi Sharifzadeh, on behalf of all coauthors
October 2019

PART

Theory and Concept

1

This page intentionally left blank

CHAPTER

Technological change in fuel cell technologies

1

Mirko Hu[1], Giorgio Triulzi[2,3] and Mahdi Sharifzadeh[4]

[1]*IMT School for Advanced Studies, Lucca, Italy*

[2]*School of Management, Universidad de los Andes, Bogotá, Colombia*

[3]*Sociotechnical Systems Research Center, Massachusetts Institute of Technology, MA, United States*

[4]*Sharif Energy Research Institute, Sharif University of Technology, Tehran, Iran*

1.1 Introduction to technological change

The ability to quantify technical change in technology is an important input for business and research strategic decisions [1]. Betting on the winning technology and correctly identifying or even predicting the technology's life cycle are important determinants of business success and long-term survival in the market place [2]. When we talk about objective quantification of technological change we can consider either the diffusion of technology in the market from a mainly economic perspective or the improvement of functional performance [3].

The diffusion of technology adoption in the market, typically follows an S-shaped curve [1,4] as pictured in Fig. 1.1. In the S-shaped model it is clear how in the different technological life cycle phases, there are different factors contributing to the spread of the technology [5,6]. Initially most of the resources are invested in the research and development (R&D) field. In this phase the main component that pushes the adoption is the learning-by-searching factor, which generates different designs that are adopted by different niches of early adopters. The scaling-up of production following the emergence of a dominant design represents the turning point. When the technology is introduced in the market the learning-by-doing factor reinforces the existing learning-by-searching factor and drives the penetration of the technology into the market. Furthermore, a specific group of technologies such as mass-produced technologies (e.g., solar PV) benefits from the economies of scale effect [7,8], which is the unit cost reduction derived by the production in series of a large quantity of a specific product. During the market maturity stage the technology reaches the peak of the diffusion rate, which then starts to wear off as both learning-by-

Design and Operation of Solid Oxide Fuel Cells. DOI: https://doi.org/10.1016/B978-0-12-815253-9.00001-X

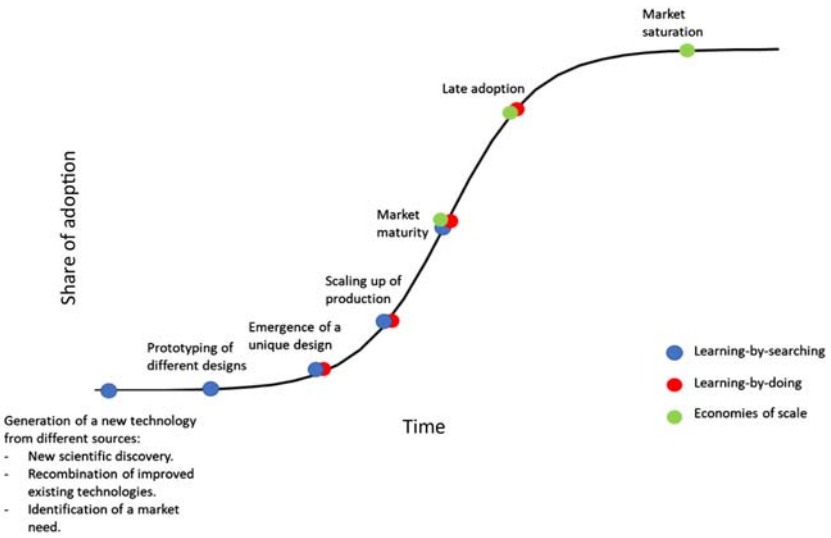

FIGURE 1.1

Technology life cycle with the main contributors to the growth rate.

searching and learning-by-doing disappear. The technology diffusion arrives at a saturation point that is usually explained either by having served all available users or by an upper limit given by technical constraints that limit further improvement in performance or cost [1]. It is at this stage that efforts to design newer technologies ramp up.

The curves used to represent the S-shaped technological life cycle of a technology are the logistic curves. The equations are inspired by the behavior of biological systems and they are characterized by the presence of an upper limit. Eqs. (1.1)–(1.3) are the most commonly used equations in the field of technological change.

$$\text{Pearl} - \text{Reed} \quad Y = \frac{L}{1 + a\widehat{e}(-bt)} \quad Y_l = \ln\left[\frac{Y}{L-Y}\right] = -\ln a + bt \tag{1.1}$$

$$\text{Fisher} - \text{Pry} \quad \frac{Y}{L-Y} = e^{2a(t-t_0)} \quad Y_l = \ln\left[\frac{Y}{L-Y}\right] = 2a(t-b) \tag{1.2}$$

$$\text{Gompertz} \quad Y = Le^{be^{-kt}} \quad Y_l = \ln\left[\frac{Y}{L-Y}\right] = \ln b - kt \tag{1.3}$$

On the other hand if the focus of attention is not market diffusion of a given technology, but rather its performance improvement rate, Moore's law (1.4) and

Wright's law (1.5) are to the functional forms that best serve the task [9–11]. In [12] we found the different applications of S-shaped curves and Moore's law.

$$\text{Moore} \quad Y = Y_0 e^{bt} \quad \ln Y = \ln Y_0 + bt + e_t \tag{1.4}$$

$$\text{Wright} \quad Y = aX^{(\ln b/\ln 2)} \quad \ln Y = \ln a + \left(\frac{\ln b}{\ln 2}\right)\ln X \tag{1.5}$$

Eqs. (1.4) and (1.5) describe the improvement of the performance or cost of a technology, Moore's law in time, and Wright's law as a function of cumulative production. Sahal [13] demonstrated that the two laws are fundamentally equivalent when cumulative production increases exponentially over time. In this case a generalized version of Moore's law is sufficient to describe performance (or cost) improvement of a technological domain [10].

Summing up, technology adoption on the one hand and performance and cost improvements on the other hand are two faces of the same coin. Learning effects, as well as the physical characteristics of the technology, determine its improvement rate, which, in turn, is related to its adoption rate. Furthermore, as a technology diffuses its cumulative production and learning effects helps further decreasing its cost and improving its performance. The curves depicting technological diffusion have a typical S-shaped curve where the different technological phases are visible. The curves for performance growth are usually exponential, therefore, they are linear on a semilogarithmic scale, the slopes of the curves are used to compare the growth rates of different technologies. The purpose of the diffusion curve is to identify the stage of the technology. The purpose of the performance growth curve is to quantify the speed of improvement of a specific technology to compare it with alternative technologies and inform investment decisions (Table 1.1).

When we analyze a technology we need to address two other important issues, namely (1) defining a performance measure for the technology and (2) characterizing the nature of the technology itself. First, depending on the properties we are considering, it is possible to create several performance measures [14]. Nevertheless, in the literature, technologies with specific operations are linked to

Table 1.1 Main differences between technological diffusion curves and performance growth curves.

	Technological diffusion	Performance improvement curve
Content	Market diffusion, learning effects	Performance improvement, cost reductions
Plot	S-shaped	Exponential or power law
Purpose	Identifying technological stage and actions to take	Identifying fast-growing technologies

Table 1.2 Technological operations and related performance measurements [15].

Operation	Relative performance measurement	Unit
Storage	Stored specific energy	Wh/L
	Energy storage density	Wh/kg
	Stored energy per unit cost	Wh/USD(year)
Transformation	Specific power	W/L
	Power density	W/kg
	Power per unit cost	W/USD(year)
Transportation	Powered distance	W × km
	Powered distance per unit cost	W × km/USD(year)

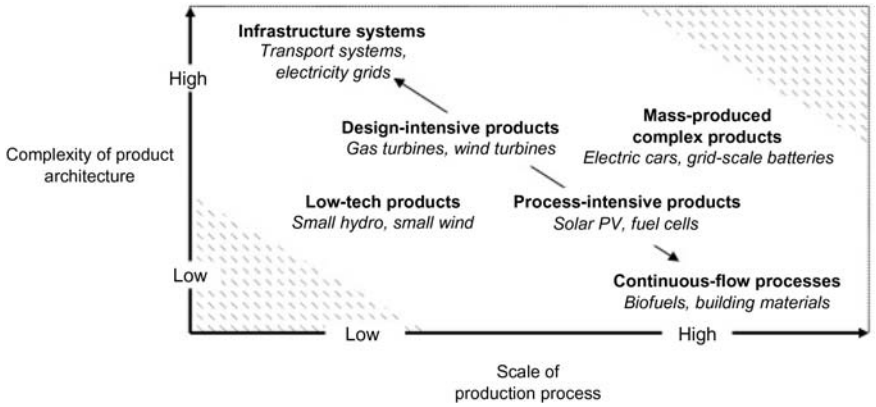

FIGURE 1.2

Classification of various energy technologies [16].

fixed performance measurements. In the case of fuel cells, it could be convenient to use the stored energy per unit cost or the power per unit cost [15] thanks to the double operation mode of the technology that can either store energy or generate power. Moreover, these measurements include the technical and the economic aspects of the technology (Table 1.2).

Second, it is important to classify technologies into categories because different technologies follow different patterns of innovation. Huenteler et al. [16] recognized that process-intensive products such as solar PV or fuel cells have few technological components and are produced in large scales, so the technological domains advance initially by focusing on product innovation and then by focusing on process innovation (Fig. 1.2).

In the case of recent technologies there could be a lack of the data that we need to build performance growth curves. Therefore patent data, which is highly available, is used instead.

1.2 A survey of the patents related to various fuel cell technologies

1.2.1 Fuel cell technologies

The rapid consumption of fossil fuels and the need for new sustainable sources of energy led to the discovery of various hydrogen production methods and the invention of fuel cell technologies [17]. Hydrogen technologies, which comprise fuel cell technologies, have several advantages compared to other green power technologies. First, the energy generated is less pollutant if the hydrogen is produced through clean methods. Second, the fuel used is considered safe. Third, the energy generated has high quality characteristics. Last, hydrogen technologies could overcome the problem of the intermittent nature of the other green power technologies such as solar and wind systems [18]. Additional important advantages of fuel cells are the light weight of the devices in the case of mobile applications, the maximum achievable theoretical efficiency that is not limited by the Carnot efficiency and is up to 80% combined to high temperature thermal machines, the high efficiency in low power applications (in the range of 40%–60% [19,20]), and the electrical adaptability of the fuel cells to the load. Moreover, other interesting properties are the mechanical simplicity of the devices, for example, few moving parts or none, and quiet or completely silent functioning [21] (Fig. 1.3).

Due to the variety of fuel cell technologies the range of possible applications is very broad. Historically NASA sustained the initial research in the technological domain of fuel cells for manned space missions. The industry applied the same technologies to transportation and stationary power generation. Only recently, with the reduction of the fuel cell dimensions, has the fuel cell technology spread to portable applications or even wearable and implantable uses [23].

Solid oxide fuel cells (SOFCs) have very high efficiency and can produce clean electricity out of several types of fuel [24]. Moreover, as SOFCs operate at high temperature conditions, they present several side effects such as high reaction rates, tolerance to impurities, and the possibility to use them as steam generators to extract further energy. Another use of SOFCs is as electrolyzers. SOFCs can produce hydrogen by using excess electricity. In industry, high temperature electrolysis can capture low-grade heat to improve the kinetics of electrochemical reactions that are endothermic. However, one of the most interesting combinations for the future of sustainable energy is the use of both intermittent green power technologies and solid oxide electrochemical technology [25].

In Fig. 1.4 there is a representation of the structure of the fuel cell classifications in the cooperative patent classification (CPC) system. In Table 1.3 we compare fuel cell technology categories in the same patent classification system. It is possible to recognize that the division of fuel cells is made according to the corresponding electrolyte typology. Namely, Nafion used by proton exchange membrane fuel cell (PEMFC) and the derived fuel cells [direct alcohol fuel cell

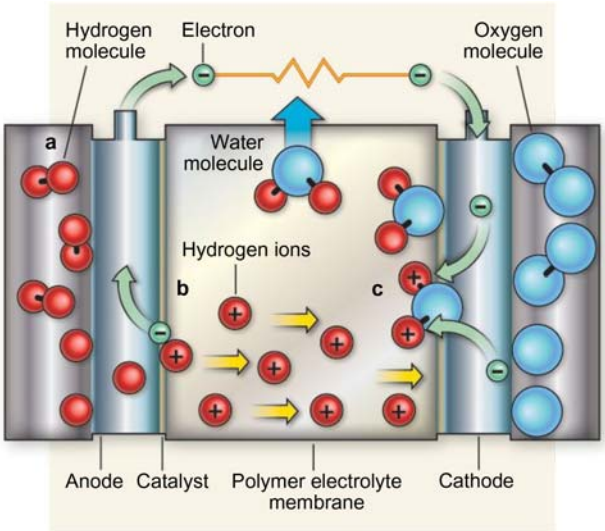

FIGURE 1.3

A hydrogen fuel cell. (A) Channeling of H_2 to the anode, H_2 is split into H atoms. (B) Catalyst splits hydrogen ions (H +) and electrons. H + passes through polymer electrolyte membrane (PEM) and electrons become current. (C) Channeling O_2 to the cathode and the formation of water with electrons and H + [22].

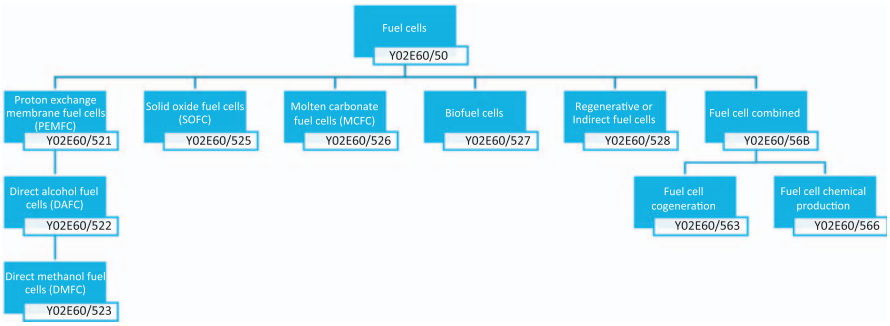

FIGURE 1.4

Hierarchical representation of fuel cell classifications.

(DAFC), direct methanol fuel cell (DMFC)], yttria stabilized zirconia by SOFC, molten carbonates by molten carbonate fuel cell (MCFC), and mixed organic and inorganic electrolytes by biofuel cells. Regenerative fuel cells are based on the same types of fuel cells with the additional ability to reverse the electrochemical process.

Table 1.3 Comparative table of fuel cell technology subgroups in the patent database.

CPC Code	Technology	Electrolyte	Operating temperature (°C)	Typical power	Electrical efficiency	Applications	Advantages	Disadvantages	References
Y02E60/521	Proton exchange membrane fuel cells (PEMFC)	Nafion	50–100	<1–250 kW	53%–58%	Backup power; portable power; transportation	Reduced corrosion; manageable electrolyte; quick start-up	Expensive catalysts; expensive electrolyte; high sensitivity to fuel impurities	[26–28]
Y02E60/522	Direct alcohol fuel cells (DAFC)	Nafion	120–140	300 W–5 kW	<70%	Military; space programs; backup power; transportation	More choices of materials; low activation voltage	Intolerant of CO and CO_2	[28,29–32]
Y02E60/523	Direct methanol fuel cells (DMFC)	Nafion	60–130	<5 kW	63%	Transportation; portable applications	Easy fuel storage; simple structure without thermal management	Low power density, fuel crossover, high cost	[33–35]
Y02E60/525	Solid oxide fuel cells (SOFC)	Yttria stabilized zirconia	500–1000	1 kW–30 MW	<70%	Portable applications; residential power; transportation; power plants	Flexible fuel choice; high overall efficiency; impurities and CO tolerance; absence of liquid in cell; low costs	Long heat up and cool down time	[24,36–38]
Y02E60/526	Molten carbonate fuel cells (MCFC)	Molten lithium, sodium, potassium carbonates	600–700	100 kW–10 MW	45%–50%	Stationary power generators; distributed power and heat generation	No use of noble catalyst; use of CO as fuel	Component degradation; material and production costs	[39–42]
Y02E60/527	Biofuel cells	Thionin diffusing mediator; organic substrate; solutions	3–80	<10 μW–50 mW	25%–81%	Powering microelectronic systems; environmental remediation; sanitation systems	Low operation temperatures; use of mild reactions; cost of biocatalysts	Degradation of enzymes; low power output; unclear stability and durability conditions	[43,44]
Y02E60/528	Regenerative or indirect fuel cells, for example, redox flow type batteries	Nafion; yttria stabilized zirconia	50–900	1 kW–30 MW	<58%	Space vehicles, satellites, submarines, aircraft, energy supply system	Round-trip energy conversion, high specific energy density, H_2O as fuel carrier, light-weight, durable	Expensive electrocatalysts; fragility of the Nafion binder; degradation and cost of the polymer membrane, bipolar plates, gas diffusion packing	[45–49]

One challenge of studying technological development through patent analysis is to keep pace with the rapidly growing number of patents in the domain. There are several papers in the literature that carried out patent analyses on fuel cell technologies [32]. Barrett [50] studied the opportunities, key companies, and emerging trends through patent analysis. Huang and Yang [51] focused more on companies, countries, and authors associated with published papers and patents related to fuel cells. Reports such as Refs. [52,53] are very comprehensive case studies that guide possible stakeholders in their decisions on investing, or not, in the technology. These studies are focused primarily on publication growth, geography, and key companies of the patent activity. However, they rarely compare the different fuel cell technologies. In our study we try to close this gap.

As Fig. 1.5 shows, if we do not consider the general classification code for fuel cells, SOFCs have the largest number of patents, with 1139 in total. This corresponds to 18% of the patents related to fuel cell technologies. DMFC patents are the second-most numerous with 978 (15%) patents. Surprisingly the PEMFC class has fewer patents than its subtechnology class. Both PEMFC and RFC have 11% of the patents (696 and 709, respectively).

From 1976 to 2015 the number of USPTO patents granted to fuel cell technologies has increased from 8 in 1976 to 1356 in 2016, as shown in Fig. 1.6. In 2016 there was a peak of published patents and in 2017 the number of published patents was more than halved (579). The data for 2018 was incomplete at the time of writing this book. As discussed in [53] the decreasing worldwide trend started in 2007 and the authors pointed out that the global economic crisis was the main cause of the smaller number of published patents in the fuel cell sector.

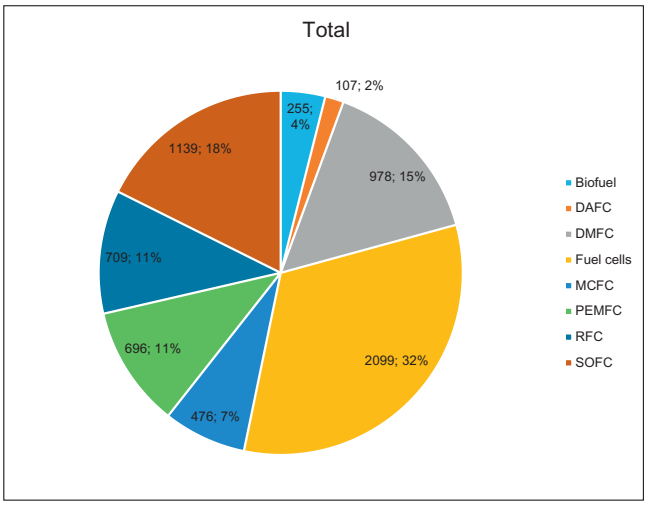

FIGURE 1.5

Total number of patents published for each category.

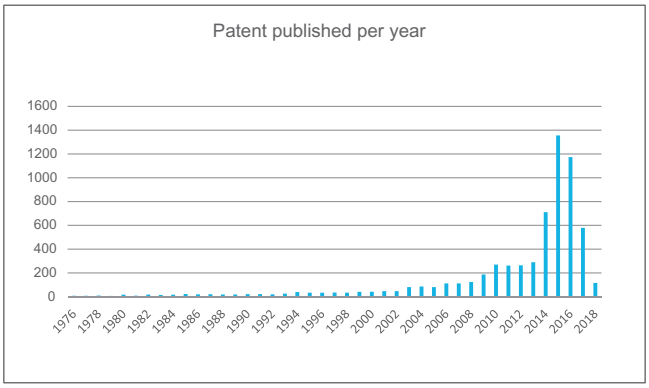

FIGURE 1.6

Total patents granted per year.

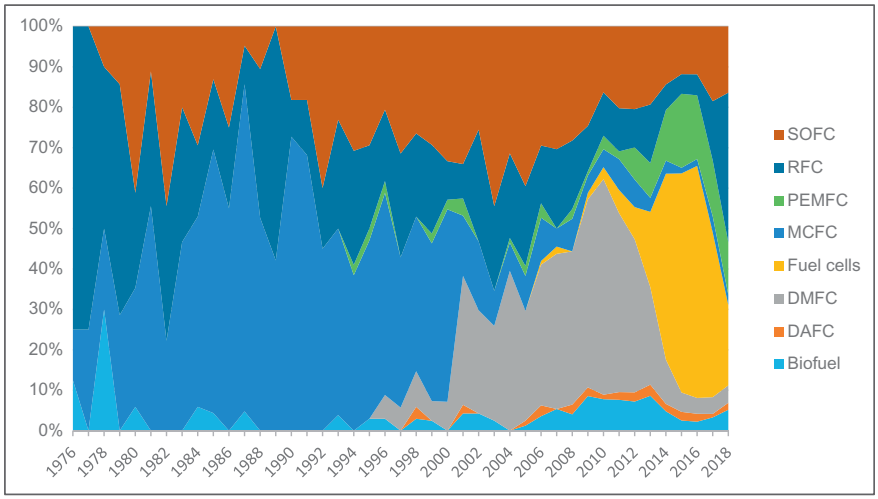

FIGURE 1.7

Ratio of patenting activity among different fuel cell technological domains per year. The data is derived from the patent grant year.

In Fig. 1.7 we can observe the initial predominance of regenerative and indirect fuel cell patents. The technology dominance in the patenting activity is quickly substituted by the introduction of SOFC technology and the steady presence of a small percentage of MCFC-related patents. MCFC and SOFC technologies gain more and more space in the patenting landscape at

regenerative and indirect fuel cell technology expenses. In 1995 DMFC patents started to appear, whereas the share of MCFC patents began to decrease. In 2007 we observe the first patents classified generically as fuel cells, a class that quickly became predominant in the following years. In the last two years (2016–2018), we observe that the share of regenerative or indirect fuel cell patents started to increase again. DAFC and biofuel cell technologies have been niche technologies since their appereance in the patenting landscape (1975 and 1998, respectively).

In Fig. 1.8 we can obtain two main pieces of information. Namely (1) the four most active applicant countries and (2) their patenting portfolio in the fuel cell technological domain. Most of the patent applications are from US companies and institutions with almost 2500 patents. The other main countries are Japan, Korea, and Germany. Surprisingly, the number of general fuel cell patents having a Japanese assignee is as large as for US ones, despite the lower number of total Japanese patents. Moreover it seems that US applicants have been quite active in the regenerative or indirect fuel cell and MCFC technologies. On the other hand, none of the other applicant countries published many patents in those classes of fuel cell technologies. In Japan and Korea the DMFC technology is quite popular. United States and Japan applicants also hold many SOFC patents. We discuss the motivations behind these figures in Section 1.3 in which we analyze the patenting activity of the main companies doing research on fuel cells.

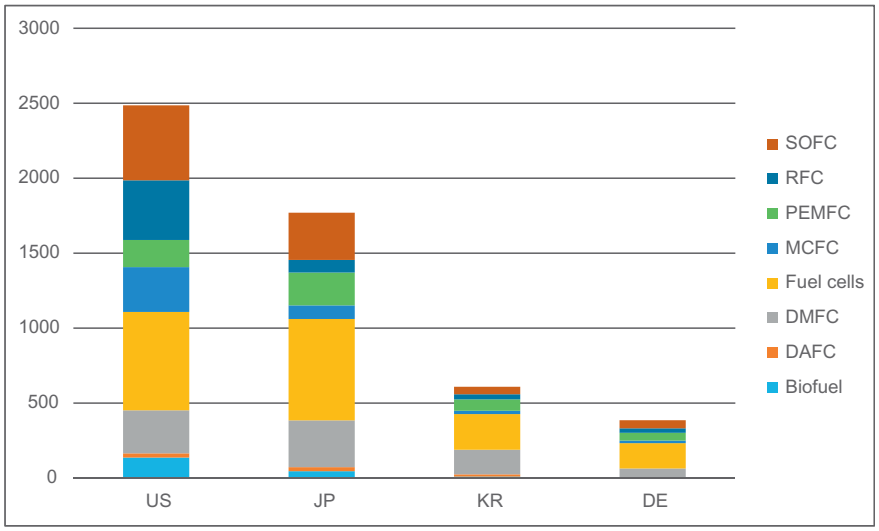

FIGURE 1.8

Total number of patents published per applicant country.

1.3 A survey of industrial research (company review)

Research in the fuel cell technology domain has been shifting from educational and academic purposes to industrial applications since 2007 when this technology entered the commercialization stage [52]. In Fig. 1.9 it is observed that the top companies and institutions that were leading the patenting activity in fuel cell technology started to decrease their relative contribution from 2005, while new companies emerged in the patenting landscape. The top applicants before 2005 were mainly nonprofit research institutions focusing on the energy research (The United States Department of Energy, Institute of Gas Technology, Energy Research Corporation).

The current situation shows a totally different landscape. In Table 1.4, if we ignore the applicants labelled as 'N/A', the principal applicants are companies in the automotive, power generation, or electric and electronic device sectors. Bloom Energy Corporation and Honda Motor Co., Ltd. have been the most active for the SOFC technology with 66 and 52 patents, respectively, whereas the other applicants do not have more than 11 patents in this field. Samsung Sdi Co., Ltd. and Kabushiki Kaisha Toshiba have been leading the patenting activity for DMFC with 122 and 74 patents, respectively. PEMFC patents are well distributed among all the top applicants, whereas, unsurprisingly, DAFC and biofuel fuel cell patents are scarce through all the companies considered for they are not

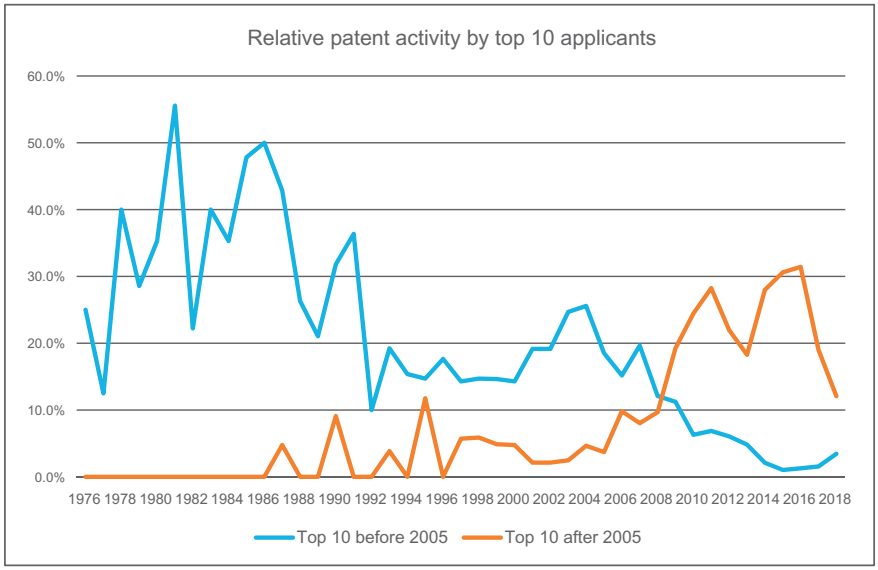

FIGURE 1.9

Relative patent activity by top 10 applicants before 2005 versus top 10 applicants after 2005.

Table 1.4 Top 10 applicants and their patent portfolio.

Applicant	SOFC	RFC	PEMFC	MCFC	Fuel cells	DMFC	DAFC	Biofuel	Grand total
N/A	71	45	40	20	33	24	4	14	251
Honda Motor Co., Ltd.	52	4	37	1	148	1			243
Gm Global Technology Operations, Inc.		1	29		163	2	8	2	205
Toyota Jidosha Kabushiki Kaisha	8	1	21	2	166		3	2	203
Bloom Energy Corporation	66	20	21	18	71	4	1		201
Samsung Sdi Co., Ltd.	9	1	13		37	122	8		190
Kabushiki Kaisha Toshiba	3	2	4	15	2	74			100
Nissan Motor Co., Ltd.	11	3	19	2	58	6			99
Panasonic Intellectual Property Management Co., Ltd.	7		10		56	1		1	75
Hyundai Motor Company	1		9		56	2	1		69
Grand total	228	77	203	58	790	236	25	19	1636

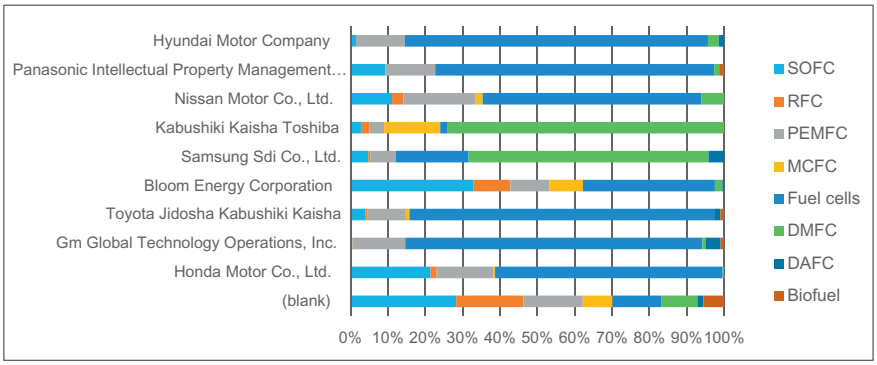

FIGURE 1.10

Comparison of the patent portfolios of the top 10 applicants.

suitable for the sectors taken into consideration here (mainly automotive and power generation). Although MCFC and RFC had a glorious past it seems that currently companies prefer focusing on other fuel cell technologies.

In Fig. 1.10 it is even clearer how Bloom Energy Corporation, Samsung Sdi Co., Ltd., and Kabushiki Kaisha Toshiba R&D departments decided to focus on specific fuel cell technologies (DMFC and SOFC) rather than applying for more general fuel cell patents. Bloom Energy Corporation, Nissan Motor Co., Ltd., and Honda Motor Co., Ltd. are the applicants with the most diversified portfolio. Car manufacturing companies seem to have a similar portfolio with a comparable ratio of SOFC, PEMFC, and general fuel cell patents.

1.4 Quantification of the technological changes in solid oxide fuel cells

From the patent analysis it is possible to observe the predominance of SOFC technology in the patenting landscape since its introduction. The flexibility of the SOFC applications is also evident by observing the presence of the related patents in the portfolios of most of the top applicants. SOFC technology has already entered the mature phase and that could possibly translate into profits for companies that invested in the development of the technology [54]. Moreover, during the mature stage fast cost reductions are expected. The velocity of the maturation is reflected by the learning rate, which is a measure in learning curve methodology. In this method the cost reduction is measured with respect to the doubling of the production capacity in accordance with Wright's law [55]. Depending on the stage of the SOFC technology, the authors calculated a learning rate variable from 14% to 17% for the R&D stage, and 27% ± 15% for the following stages (Table 1.5). Wei et al. [56] compared the learning rates of several fuel cell

Table 1.5 Learning and cost reduction phenomena in different stages for solid oxide fuel cells [55].

Learning rates (%)	Pure learning phenomena	Learning + EoS for only materials	Learning + EoS for only equipment	Learning + automation ($\beta = 0.7$)	All reduction cost phenomena
Research and development (R&D) stage	16	16	16	16	16
Pilot stage	27	44	28	36	44
Early commercial stage	1	5	12	10	12
All stages included	20	27	22	28	35

technologies in the United States and Japanese markets. The author observed that data related to SOFCs production in California showed very low or near-zero cost reduction and consequently a nearly absent effective technological advance. The techno-economic studies on SOFC technology focused on economic factors such as the economies of scales and manufacturing systems. The increasing importance of the manufacturing technologies for the construction of the SOFCs demonstrates that the technological changes in SOFCs are shifting from being related to the product performance to the exploration of more cost-efficient production processes [55].

1.5 Methodology

We performed the technological forecasting on fuel cells by adapting the procedure developed by Benson and Magee [57] to Patentsview.org API and using the CPC system introduced in 2013 [58]. The procedure starts from a patent database that collects patent data such as patent number, publication year, citation references, and number of times a patent is cited. With a script we connected to the patent database to retrieve the patents relevant to the technological domain considered and we saved the data in a comma-separated values (csv) file. With another script we selected the important data from the csv file and we cleaned it up, thereby transforming the patent data into structured data. In the next step we performed some simple statistical analyses on the structured data such as the calculation of the average publication year and the count of cited patents within three years from the publication year of each patent in the relevant set (Fig. 1.11).

The first problem was to identify the best patent database. There are several options, some of which are free while others need a license. ESPACENET and Patentsview are two examples of free patent databases. In our initial work we used Patentsview because it affords the possibility of downloading bulk patent

data. The original method developed by Benson and Magee was based on keyword searches and the classification overlap method (COM). The COM method was used to identify the most representative international patent classification (IPC) code and the United States patent classification (USPC) code for the technological domain from a set of patents initially retrieved using only a list of keywords. Then the patents labeled with the most representative IPC and UPC codes were intersected to find a set of patents highly relevant to the technological domain. The methodology used in this chapter to retrieve the relevant set of patents is different as we used CPC codes only. CPC codes were developed jointly by the European patent office and the US patent and trademark office in an effort to create a single system that could potentially replace the IPC system and the USPC system. The CPC system can be considered as a more detailed version of the IPC system. In the case of fuel cell technologies we found that it provides specific subclasses that allow distinguishing different types of fuel cells neatly.

In Table 1.6 the main CPC codes related to fuel cell technologies are listed.

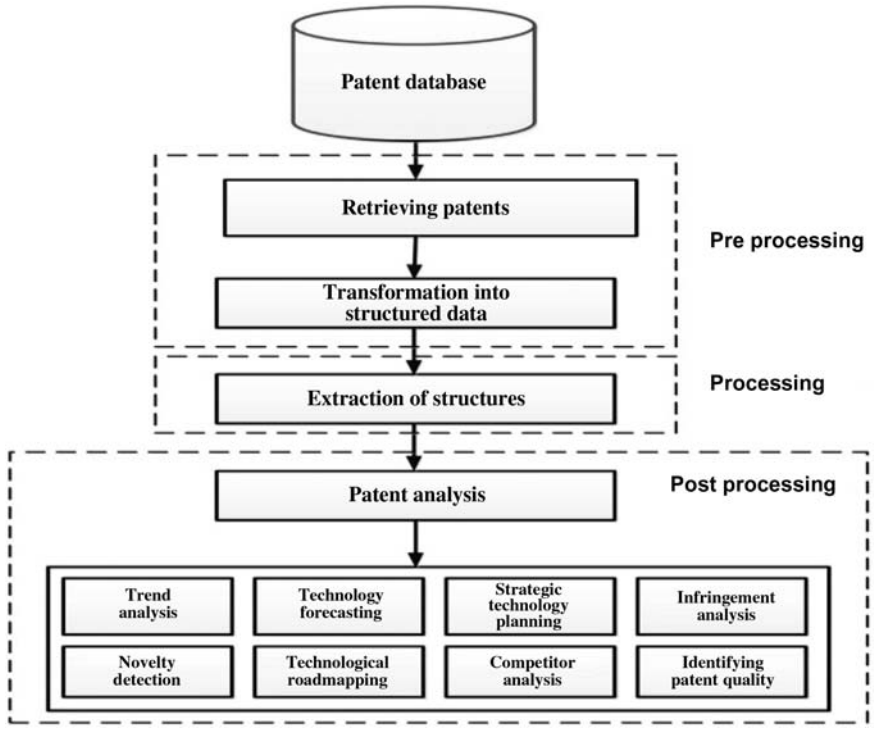

FIGURE 1.11

Patent analysis process [59].

Table 1.6 CPC codes and corresponding fuel cell technologies.

Y02E60/50	Fuel cells
Y02E60/521	Proton exchange membrane fuel cells (PEMFC)
Y02E60/522	Direct alcohol fuel cells (DAFC)
Y02E60/523	Direct methanol fuel cells (DMFC)
Y02E60/525	Solid oxide fuel cells (SOFC)
Y02E60/526	Molten carbonate fuel cells (MCFC)
Y02E60/527	Biofuel cells
Y02E60/528	Regenerative or indirect fuel cells, for example, redox flow type batteries
Y02E60/56B	Fuel cell combined
Y02E60/563	Fuel cell cogeneration
Y02E60/566	Fuel cell chemical production

We fed the CPC codes to the script one by one and saved the obtained patent data related to the years from 1976 to 2015. We estimated the performance improvement rate of each fuel cell subtechnology following the methodology developed by Triulzi et al. [60]. These authors proposed several potential patent-based predictors of the technological improvement rate based on theoretical conjectures. These predictors reflected four properties of a technological domain, namely (1) the immediacy, (2) pace of obsolescence, (3) centrality, and (4) the concentration of new assignees in the patenting landscape.

Triulzi et al. selected 30 technological domains for which they already had the historical performance time series data that they used to estimate the observed yearly performance improvement rates for each domain. The heterogeneity in the 30 improvement rates allowed them to have enough variance to test different patent-based predictors. Then the authors [50] collected the patent data using the COM method described briefly in the previous section and computed several patent-based measures for each domain. After testing different measures as predictors of the technological improvement rate, Triulzi et al. found that the most accurate and reliable estimation was given by Eq. (1.6) with an $R^2 = 0.63$.

$$\text{Predicted yearly performance improvement rate for a technology domain } i = e^{(6.15987 \times \text{average normalized patent centrality} i - 5.01885)} \times e^{\frac{\sigma_i^2}{2}} \tag{1.6}$$

The authors used a measure of centrality called search path node pair (SPNP) normalized through a citation network randomization procedure to correct for differences in time of appearance and citation practices across technologies. The raw SPNP measure was initially developed by Hummon and Dereian in 1989 [61]. This method measured the centrality of a node within a citation network by counting the number of paths entering and exiting through that node. The centrality used in the estimation of the improvement rate is the average normalized overall

centrality of a domain's patents computed with respect to the whole patent citation network including all patents granted by the USPTO between 1976 and 2015. This is the same measure that we use in this book.

1.6 Results

In this section we present the results of the research. We organized the results in three subsections. In the first subsection we analyze overlaps and interconnections between the different patent sets. The second subsection deals with a centrality analysis of the most important patent sets with the least overlaps. In the last subsection we report the estimation of the performance improvement rate for each fuel cell technology and a rationalization of the technology development of the two fastest-improving technologies.

1.6.1 Evaluation of patent sets: overlaps and interconnections

In Fig. 1.4 the CPC code "Y02E60/50" is a general code to classify patents related to the general technological domain "fuel cells." The codes starting with "Y02E60/52" are the classifications used for the patents according to the design or the type of the fuel cells contained in the patents. "Y02E60/522" is a subtype of "Y02E60/521" and "Y02E60/523" is a subtype of "Y02E60/522". It can be noticed from the number of patents that a subtype code does not necessarily have fewer patents. As an example, Y02E60/521 has 416 patents, whereas its subgroup Y02E60/523 has 903 patents. This means that researchers put more patenting efforts into the more specific technology of DMFC rather than the more general technology of PEMFC.

Y02E60/56B is a code that includes both fuel cells with cogeneration technologies and fuel cells with the production of chemicals. The former technology relies on the fact that fuel cells produce water vapor at a high temperature and a gas turbine can use the water vapor to produce electricity. On the other hand, fuel cell reactors can produce useful chemicals along with electricity generation with a process called electrochemical cogeneration [62].

Fig. 1.12 shows the overlaps between the main patent sets. The values on the diagonal represent the share of patents that are uniquely found in the subdomain under observation (row-wise). On the other hand, we calculated the values off-diagonal as the number of patents shared between the two patent sets divided by the total number of patents in the patent set located on the row. We can observe that most of the subdomains have a high percentage of patents uniquely belonging to that patent set. This percentage is relatively low only for PEMFC, DAFC, and SOFC (61%, 33%, and 57%, respectively). PEMFC shares its patents with the SOFC set (3%). DAFC has a large overlap with DMFC (33%). We expected such overlap as DMFCs are a DAFC subtechnology. The SOFC set shares patents with the general fuel cells patent set (22%) and PEMFC patent set (18%).

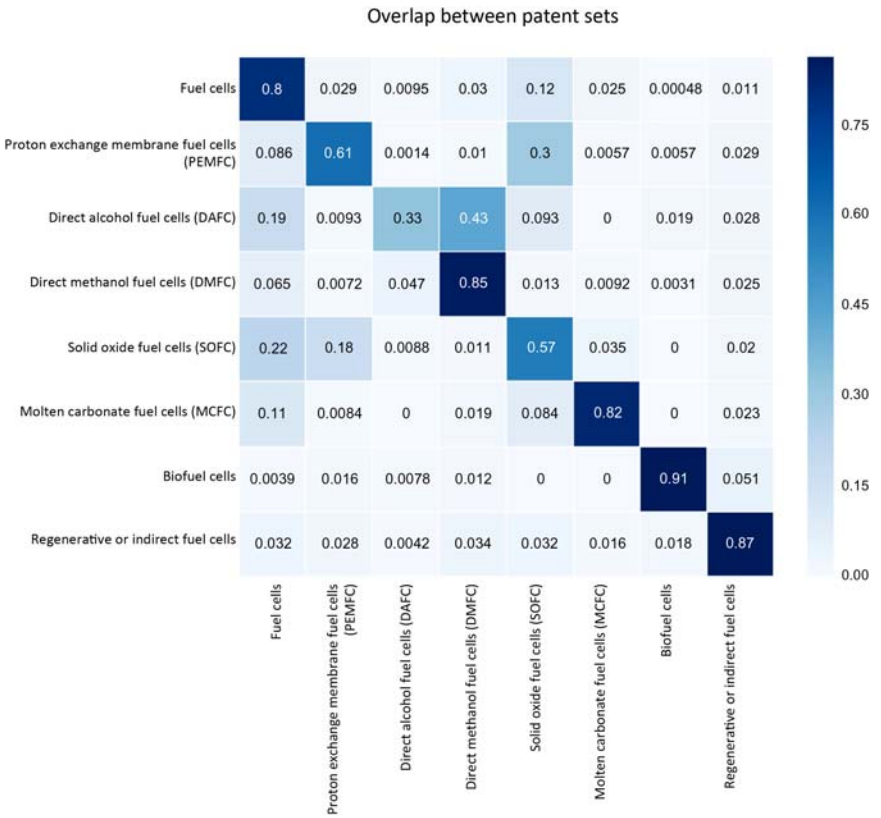

FIGURE 1.12

The overlap between the major fuel cell technologies.

Fig. 1.13 shows an analysis of the cross-technologies citations. The analysis is useful to understand whether, and how much, two technologies are related. We followed the work and the methodology developed by Alstott et al. [63]. The authors used citations as a measure to assess the knowledge relatedness between technological domains. More precisely, they calculated the z-scores of the number of citations between any pair of subdomains. These are calculated as the difference between the number of citations from one domain to another and its expected number of citations were randomly made,[1] divided by the standard

[1] The expectation is formulated by randomly rewiring citations between patents preserving each time the filing year of the citing and the cited patent, the number of citations made and received by each patent and the share of citations that go to other patents of the same class. The expected number of citations given these constraints is an hypergeometrically distributed random variable. As such, we can compute its expected value and standard deviation analytically. Alstott et al. [62] show how to do that.

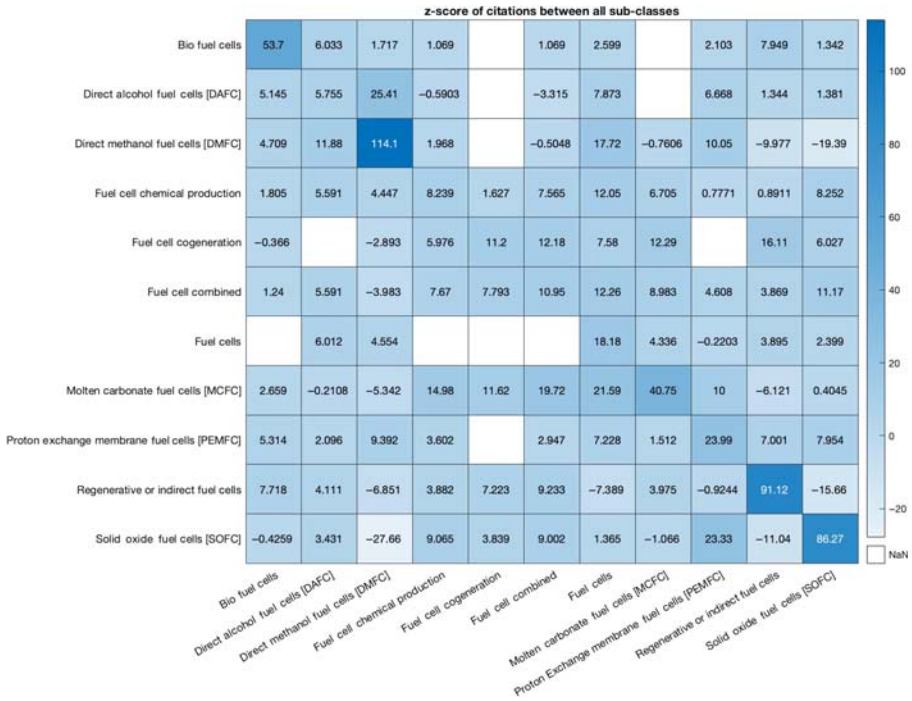

FIGURE 1.13

The *z*-scores of citations between the major fuel cell technology patent sets.

deviation. The higher the *z*-scores, the more related the two technological subdomains are. Darker colors correspond to stronger relatedness and blank cells correspond to the impossibility to calculate the *z*-scores due to the absence of observed citations. We can observe in Fig. 1.13 that there are several large *z*-scores on the diagonal. In particular the large values on the diagonal for biofuel cells, DMFC, RFC, and SOFC shows that these are relatively independent clusters of patents. DMFC is the domain that has the least knowledge relatedness with other domains. We can explain this fact by observing Fig. 1.4. DMFC is a very specific subclass of PEMFC, therefore the knowledge relatedness is very low.

1.6.2 Patent centrality analysis

We used patent centrality values to obtain the mean centrality of the technological domains and subdomains. These were filled in Eq. (1.6) to estimate the yearly performance improvement rates for each fuel cell technology. We also performed an analysis of the most central patents in each set to rank them by their

importance in the overall patent citation network. We used as filters a normalized measure of the patent citations within 3 years from filing and the centrality measure described briefly in the methodology section. The two measures allow us to get the most important patents and to avoid those patents that received few citations. By analyzing 30 of the most central and highly cited patents in each subdomain, it was possible to reconstruct the main technological trajectories for the development of the technology.

In Table 1.7 most of the MCFC central patents are related to the general structure of the fuel cells. The composition of the devices is described carefully by the patents. Patents 4169917, 4192906, 4554225, 4943496, and 5811202 belong to this typology. Among the remaining central patents there are patents that describe the structure of a fully internally manifolded fuel cell stack (4753857, 4769298, 5045413, 5077148, 5227256), patents that contain the improvement to the electrolyte design (4818639, 4761348, 5399443), and patents focused on the design of the plate separator (5698337, 4977041, 6040076, 6410178). Patent 6458477 proposed a fuel cell for a high-efficiency power system with an operating range from 20°C to 2000°C.

Regarding SOFC in Table 1.8 the most central patents from 1978 to 1992 (4226692, 4344904, 4330633, 4609562, 4614628, 4920014, 4950562, 5171645,

Table 1.7 Top 30 most central patents for molten carbonate fuel cell (MCFC) subdomain.

Patent number	Filing year	Organization	Title
4169917	1978	Energy Research Corporation	Electrochemical cell and separator plate thereof
4192906	1978	Energy Research Corporation	Electrochemical cell operation and system
4250230	1979	In Situ Technology, Inc.	Generating electricity from coal in situ
4308299	1980	General Electric Company	Lithiated nickel oxide
4511636	1983	Individual(s)	
4514475	1984	Individual(s)	
4554225	1984	Tokyo Shibaura Denki Kabushiki Kaisha	Molten carbonate fuel cell
4753857	1986	Ishikawajima-Harima Jukogyo Kabushiki Kaisha	Laminated fuel cell
4659635	1986	The United States Government as represented by the Department of Energy	Electrolyte matrix in a molten carbonate fuel cell stack
4818639	1987	Gas Research Institute	Molten carbonate electrolyte creepage barrier

(*Continued*)

Table 1.7 Top 30 most central patents for molten carbonate fuel cell (MCFC) subdomain. *Continued*

Patent number	Filing year	Organization	Title
4769298	1987	Ishikawajima-Harima Jukogyo Kabushiki Kaisha	Laminated fuel cell
4761348	1987	The United States of America as represented by the Secretary of the Air	Electrolytic cell stack with molten electrolyte migration control
4977041	1988	Ishikawajima-Harima Heavy Industries Co., Ltd.	Fuel cell and method of ameliorating temperature distribution thereof
4943496	1989	Hitachi, Ltd.	Fuel cell, electrode for the cell and method of preparation thereof
5045413	1990	Institute of Gas Technology	Fully internal manifolded fuel cell stack
5077148	1990	Institute of Gas Technology	Fully internal manifolded and internal reformed fuel cell stack
5227256	1991	Institute of Gas Technology	Fully internal manifolded fuel cell stack
5185220	1991	MSW Power Corporation	Fuel cell clamping force equalizer
5409784	1993	Massachusetts Institute of Technology	Plasmatron-fuel cell system for generating electricity
5348814	1993	Matsushita Electric Industrial Co., Ltd.	Internal reforming type molten carbonate fuel cell
5399443	1994	Electric Power Research Institute, Inc.	Fuel cells
5698337	1996	Energy Research Corporation	Process for preparing a separator plate for a melt carbonate fuel cell and separator plate prepared according to this process
5811202	1997	MSW Power Corporation	Hybrid molten carbonate fuel cell with unique sealing
6045933	1998	Honda Giken Koygo Kabushiki Kaisha	Method of supplying fuel gas to a fuel cell
6040076	1998	MSW Power Corporation	One piece fuel cell separator plate
6410178	1999	Aisin Takaoka Co., Ltd.	Separator of fuel cell and method for producing same
6458477	2000	ZTE Corporation	Fuel cell stacks for ultra-high efficiency power systems
7491431	2004	NanoGram Corporation	Dense coating formation by reactive deposition
7279655	2004	Pliant Corporation	Inductively coupled plasma/partial oxidation reformation of carbonaceous compounds to produce fuel for energy production
7781695	2007	Pliant Corporation	Inductively coupled plasma/partial oxidation reformation of carbonaceous compounds to produce fuel for energy production

Table 1.8 Top 30 most central patents for the solid oxide fuel cell (SOFC) subdomain.

Patent number	Filing year	Organization	Title
4226692	1978	Individual(s)	Solid state combustion sensor
4344904	1980	Sumitomo Aluminium Smelting Company, Limited	Sintering method of zirconia
4330633	1981	Teijin Limited	Solid electrolyte
4609562	1984	Westinghouse Electric Company LLC	Apparatus and method for depositing coating onto porous substrate
4614628	1984	Massachusetts Institute of Technology	Solid electrolyte structure and method for forming
4920014	1988	Sumitomo Metal Mining Co., Ltd.	Zirconia film and process for preparing it
4950562	1989	Toa Nenryo Kogyo Kabushiki Kaisha	Solid electrolyte type fuel cells
5171645	1991	Gas Research Institute	Zirconia-bismuth oxide graded electrolyte
5342703	1992	NGK Insulators, Ltd.	Solid electrolyte type fuel cell and method for producing the same
5160618	1992	Air Products and Chemicals, Inc.	Method for manufacturing ultrathin inorganic membranes
5409371	1994	IGR Enterprises	Oxygen welding and incorporating a novel gas separation system
5993989	1997	Siemens Westinghouse Power Corporation	Interfacial material for SOFC
6004688	1997	Board of Regents, The University of Texas System	SOFC and doped perovskite lanthanum gallate electrolyte therefor
6372375	1999	CeramPhysics	Ceramic fuel cell
6287432	1999	Standard Oil Company	Solid multi-component membranes, electrochemical reactor components, electrochemical reactors and use of membranes, reactor components, and reactor for oxidation reactions
6609582	1999	Delphi Technologies, Inc.	Power generation system and method
6207311	1999	Siemens Westinghouse Power Corporation	SOFC operable over wide temperature range
6165431	1999	Eltron Research, Inc.	Methods for separating oxygen from oxygen-containing gases
6607821	2001	NanoProducts Corporation	Applications and devices based on nanostructured nonstoichiometric substances

(*Continued*)

Table 1.8 Top 30 most central patents for the solid oxide fuel cell (SOFC) subdomain. *Continued*

Patent number	Filing year	Organization	Title
6548424	2001	ASM Microchemistry Oy	Process for producing oxide thin films
6602595	2002	NanoProducts Corporation	Nanotechnology for inks and dopants
6787264	2002	General Electric Company	Method for manufacturing fuel cells, and articles made therewith
6777353	2003	ASM Microchemistry Oy	Process for producing oxide thin films
7648785	2004	Eaton Corporation	Clean power system
7213397	2005	Eaton Corporation	Mechanism and method of combined fuel reformer and dosing system for exhaust aftertreatment and anti-idle SOFC APU
7326611	2005	Micron Technology, Inc.	DRAM arrays, vertical transistor structures and methods of forming transistor structures and DRAM arrays
7413687	2005	U.T. Battelle, LLC	Low temperature proton conducting oxide devices
7569876	2007	Micron Technology, Inc.	DRAM arrays, vertical transistor structures, and methods of forming transistor structures and DRAM arrays
8463529	2009	Eaton Corporation	System and method of operating internal combustion engines at fuel rich low-temperature-combustion mode as an on-board reformer for SOFC-powered vehicles
8304818	2010	Micron Technology, Inc.	Dram arrays, vertical transistor structures, and methods of forming transistor structures and dram arrays

5342703, 5160618) are related to the electrolyte, either to an innovative structure or composition or to the method of producing it. After 1992 patents started to focus on improving the operation of the SOFC technologies. Engineers started to investigate new applications of SOFCs (5409371) and to extend the technology operating range by using novel materials (5993989, 6004688, 6372375, 6287432). Since 2000 there have been three main technological trajectories; namely, power generation (6609582, 7648785, 7213397), low temperature operation (7413687, 8463529), and improvements in the manufacturing process (7326611, 7569876, 8304818).

The fuel cell combined subdomain is a relatively recent subdomain. Table 1.9 includes central patents with filing years succeeding 1999 and has a

Table 1.9 Top 30 most central patents for the fuel cell combined subdomain.

Patent number	Filing year	Organization	Title
6214485	1999	Northeastern University	Direct hydrocarbon fuel cells
6793711	2000	Eltron Research, Inc.	Mixed conducting membrane for carbon dioxide separation and partial oxidation reactions
6479178	2001	Northeastern University	Direct hydrocarbon fuel cells
6902838	2001	General Motors Corporation	Cogeneration system for a fuel cell
6815102	2002	General Electric Company	Energy management system for a rotary machine and method therefor
6834831	2002	The Boeing Company	Hybrid SOFC aircraft auxiliary power unit
7067208	2002	Ion America Corporation	Load matched power generation system including a SOFC and a heat pump and an optional turbine
7118818	2002	Rolls-Royce, plc	SOFC system
7410713	2002	General Electric Company	Integrated fuel cell hybrid power plant with recirculated air and fuel flow
6871491	2003	Robert Bosch GmbH	Combustion system having an emission control device
6896988	2003	FuelCell Energy, Inc.	Enhanced high efficiency fuel cell/turbine power plant
7045231	2003	Protonetics International, Inc.	Direct hydrocarbon reforming in protonic ceramic fuel cells by electrolyte steam permeation
7147072	2004	Delphi Technologies, Inc.	Method and apparatus for providing hybrid power in vehicle
7216246	2004	Kabushiki Kaisha Toshiba	Electronic apparatus and supply power setting method for the apparatus
7465512	2004	Rolls-Royce, plc	SOFC stack
7520350	2004	individual(s)	System and method for extracting propulsion energy from motor vehicle exhaust
7575822	2004	Bloom Energy Corporation	Method of optimizing operating efficiency of fuel cells
7213397	2005	Eaton Corporation	Mechanism and method of combined fuel reformer and dosing system for exhaust aftertreatment and anti-idle SOFC APU
7250690	2005	Samsung Techwin Co., Ltd.	Distributed power generation system using a fuel cell and a method of controlling the same
7370666	2005	Sprint Communications Company L.P.	Power system with computer-controlled fuel system

(*Continued*)

Table 1.9 Top 30 most central patents for the fuel cell combined subdomain. *Continued*

Patent number	Filing year	Organization	Title
7358622	2007	Samsung Techwin Co., Ltd.	Distributed power generation system using a fuel cell and a method of controlling the same
7615875	2007	Sprint Communications Company L.P.	Power system for a telecommunications facility
7635926	2007	Sprint Communications Company L.P.	Redundant mobile power supply system
7878280	2007	Bloom Energy Corporation	Low pressure hydrogen fueled vehicle and method of operating same
8182658	2008	Kabushiki Kaisha Toyota Jidoshokki	Electrochemical device and exhaust gas purification apparatus
8071246	2009	Bloom Energy Corporation	Method of optimizing operating efficiency of fuel cells
8221911	2009	Sumitomo Electric Industries, Ltd.	Method for operating redox flow battery and redox flow battery cell stack
8403258	2009	Airbus Operations GmbH	Power regulating device for an aircraft
8463529	2009	Eaton Corporation	System and method of operating internal combustion engines at fuel rich low-temperature-combustion mode as an on-board reformer for SOFC-powered vehicles
8349504	2010	Individual(s)	Electricity, heat and fuel generation system using fuel cell, bioreactor and twin-fluid bed steam gasifier

miscellaneous collection of central patents which combine the different fuel cell technologies with cogeneration production technologies such as electricity production without emission of undesired gases (6214485, 6479178, 7213397, 8349504, 6871491, 7520350), synthesis gas production (6793711), and mechanical (and electrical) power generation (6902838, 6815102, 6896988, 6834831, 7250690, 7358622).

Concerning PEMFC in Table 1.10 it is possible to observe that the most central patents are very recent. More than two-thirds of the central patents were filed after 2000 and almost one-third of the patents were filed in the biennium 2011 and 2012. Therefore we can divide the central patent set into three main groups, namely (1) the period from 1993 to 1999, (2) the period from 2002 to 2009, and (3) the period from 2011 to 2012. In the first period engineers focused mainly on improving the transportation of H^+ through the electrolyte (5336570, 5458989, 5509942, 6312846). Central patents were also about the insulator (5912088) and general PEMFC structure (6103412). In the second period the central patents are

Table 1.10 Top 30 most central patents for the proton exchange membrane fuel cell (PEMFC) subdomain.

Patent number	Filing year	Organization	Title
5336570	1993	Individual(s)	Hydrogen powered electricity generating planar member
5458989	1994	Individual(s)	Tubular fuel cells with structural current collectors
5509942	1994	Individual(s)	Manufacture of tubular fuel cells with structural current collectors
5912088	1997	Plug Power Inc.	Gradient isolator for flow field of fuel cell assembly
6103412	1998	Mazda Motor Corporation	Polymer electrolyte fuel cell
6287717	1998	Gore Enterprise Holdings, Inc.	Fuel cell membrane electrode assemblies with improved power outputs
6312846	1999	Integrated Fuel Cell Technologies, Inc.	Fuel cell and power chip technology
7056614	2002	Honda Giken Koygo Kabushiki Kaisha	Membrane electrode assembly and fuel cell unit
6867159	2003	Ballard Power Systems Inc.	Application of an ionomer layer to a substrate and products related thereto
7338692	2003	3M Innovative Properties Company	Microporous PVDF films
6991866	2004	Integrated Fuel Cell Technologies, Inc.	Fuel cell and power chip technology
7029779	2004	Integrated Fuel Cell Technologies, Inc.	Fuel cell and power chip technology
7465512	2004	Rolls-Royce, plc	SOFC stack
7691514	2004	The Regents of the University of California	Polymer–zeolite nanocomposite membranes for proton-exchange-membrane fuel cells
7799485	2005	Nissan Motor Co., Ltd.	Fuel cell system and composition for electrode
8518594	2007	Encite, LLC	Power cell and power chip architecture
8834700	2007	Encite, LLC	Method and apparatus for electrochemical reaction
8389175	2008	UTC Power Corporation	Fuel cell having a stabilized cathode catalyst
8663868	2008	3M Innovative Properties Company	Microporous Polyvinylidenefluoride (PVDF) films
8343684	2009	Individual(s)	Fuel cell device and system
8153318	2011	Individual(s)	Method of making a fuel cell device
8257884	2011	Individual(s)	Method of making a fuel cell device
8293429	2011	Individual(s)	Method of making a fuel cell device

(*Continued*)

Table 1.10 Top 30 most central patents for the proton exchange membrane fuel cell (PEMFC) subdomain. *Continued*

Patent number	Filing year	Organization	Title
8309266	2011	Individual(s)	Fuel cell device and system
8409764	2011	Individual(s)	Fuel cell device and system
8449702	2011	Bloom Energy Corporation	Method for SOFC fabrication
8968957	2011	Honda Motor Co., Ltd.	Fuel cell
8293417	2012	Individual(s)	Solid oxide fuel cell device
8911916	2012	Honda Motor Co., Ltd.	Fuel cell
8936887	2012	Samsung Electronics Co., Ltd.	Composite electrolyte membrane for fuel cell, method of manufacturing the membrane, and fuel cell including the membrane

mostly related to the improvement of the previous design by increasing durability and performance and reducing costs (7056614, 6867159, 6991866, 7029779, 7691514, 7799485, 8518594, 8834700, 8389175, 8343684). Finally, in the third period most central patents are related to methods to make PEMFCs (8153318, 8257884, 8293429, 8309266) and new designs (8409764, 8968957, 8911916, 8936887).

Regarding biofuel cells in Table 1.11 the first central patents can be traced back to 1975, at the beginning of the patenting activity. The patent (3941135) is related to a biofuel cell compatible with a heart pacemaker and, hence, for biomedical purposes. The second-oldest central patent is 4117202, which is the application of biofuel cells to the conversion of solar power to electricity via biological processes. The remaining patents until 2001 focused on enzymatic fuel cells (4224125, 4490464, 6294281, 6500571, 6531239, 6495023). In 2003, organizations started to study how to reduce the dimensions of the biofuel cells for biomedical implants (7160637, 7368190, 7687186, 7816025). The latest central patents are related to power generation through microbial fuel cells (8663852, 8012616, 7927749, 8518566).

Finally, the central patents of RFC technology are evenly spread through the years from 1974 to 2007 (Table 1.12). We can recognize three main periods. In the first period researchers focused on different ways to build a battery that can charge and discharge through reduction−oxidation cells (3981745, 3994745, 3996064, 4133941, 4159366, 4192910). There are also patent numbers 4021323 and 4215182 which deal with solar conversion. In the 1980s and 1990s, engineers were interested in lowering the operating temperature of regenerative fuel cells (4410606, 4738904), improving efficiency through new materials such as the all-

Table 1.11 Top 30 most central patents for the biofuel cell subdomain.

Patent number	Filing year	Organization	Title
3941135	1975	Siemens Aktiengesellschaft	Pacemaker with biofuel cell
4117202	1977	Individual(s)	Solar powered biological fuel cell
4224125	1978	Matsushita Electric Industrial Co., Ltd.	Enzyme electrode
4490464	1982	Individual(s)	Electrode for the electrochemical regeneration of coenzyme, a method of making said electrode, and the use thereof
4541908	1984	Ajinomoto Company, Inc.	Heme protein immobilized electrode and its use
6294281	1998	TheraSense, Inc.	Biological fuel cell and method
6500571	1999	Powerzyme, Inc.	Enzymatic fuel cell
6531239	2001	TheraSense, Inc.	Biological fuel cell and methods
6495023	2001	Michigan State University	Electrochemical methods for generation of a biological proton motive force and pyridine nucleotide cofactor regeneration
7258938	2002	Sharp Kabushiki Kaisha	Polymer electrolyte fuel cell
7005273	2002	TheraSense, Inc.	Method for the determination of glycated hemoglobin
7482072	2003	GRIntellectual Reserve, LLC	Optimizing reactions in fuel cells and electrochemical reactions
7160637	2003	The Regents of the University of California	Implantable, miniaturized microbial fuel cell
7368190	2003	Abbott Diabetes Care Inc.	Miniature biological fuel cell that is operational under physiological conditions, and associated devices and methods
7018735	2003	Abbott Diabetes Care Inc.	Biological fuel cell and methods
7709133	2005	UT-Battelle, LLC	Electrically conductive cellulose composite
7635530	2005	The Board of Trustees of the University of Illinois	Membraneless electrochemical cell and microfluidic device without pH constraint
7687186	2006	Canon Kabushiki Kaisha	Enzyme electrode, and sensor and biofuel cell using the same
7816025	2007	Canon Kabushiki Kaisha	Enzyme electrode, enzyme electrode producing method, sensor and fuel cell each using enzyme electrode
7871739	2007	Sony Corporation	Fuel cell and electronic device

(*Continued*)

Table 1.11 Top 30 most central patents for the biofuel cell subdomain. *Continued*

Patent number	Filing year	Organization	Title
7695850	2007	Panasonic Corporation	Electrode for use in oxygen reduction
7858243	2008	University of Wyoming Research Corporation	Influential fuel cell systems including effective cathodes and use with remediation efforts
7888433	2008	GM Global Technology Operations LLC	Sulfonated-polyperfluoro-cyclobutane-polyphenylene polymers for PEM fuel cell applications
8114544	2009	HRL Laboratories, LLC	Methods and apparatus for increasing biofilm formation and power output in microbial fuel cells
7709113	2009	The Penn State Research Foundation	Bio-electrochemically assisted microbial reactor that generates hydrogen gas and methods of generating hydrogen gas
8785059	2009	Smith & Nephew, Inc.	Power generation
8663852	2010	University of Massachusetts	Aerobic microbial fuel cell
8012616	2010	The Government of the United States of America, as represented by the Secretary of the Navy	Advanced apparatus for generating electrical power from aquatic sediment/water interfaces
7927749	2010	Xerox Corporation	Microbial fuel cell and method
8518566	2010	Oakbio, Inc.	Multielectrode microbial fuel cells and fuel cell systems and bioreactors with dynamically configurable fluidics

vanadium redox battery (4786567, 6468688), and transforming "traditional" technologies such as SOFC into two-mode, energy storage and energy recovery, technologies (5492777, 7150927). In the third period the central patents focused on the invention on hydrogen storage and generation devices (6875536, 7282294, 7879205).

1.6.3 Technology performance improvement analysis and discussion of possible drivers of faster performance improvements

Fig. 1.14 compares the observed yearly functional performance improvement rates of 30 technological domains studied in previous works [14,60] with the estimated

Table 1.12 Top 30 most central patents for the regenerative fuel cell subdomain.

Patent number	Filing year	Organization	Title
3981745	1974	United Technologies Corporation	Regenerative fuel cell
3996064	1975	The United States of America as represented by the Secretary of the Air	Electrically rechargeable REDOX flow cell
4021323	1975	Texas Instruments Incorporated	Solar energy conversion
3994745	1976	Ford Motor Company	Secondary battery with separate charge and discharge zones
4133941	1977	The United States of America as represented by the Secretary of the Air	Formulated plastic separators for soluble electrode cells
4159366	1978	The United States of America as represented by the Secretary of the Air	Electrochemical cell for rebalancing redox flow system
4192910	1978	Individual(s)	Catalyst surfaces for the chromos/chromic redox couple
4215182	1979	Institute of Gas Technology	Conversion of solar energy to chemical and electrical energy
4310396	1980	Societe d'Etudes et de Recherches en Sources d'Energie Nouvelles (SERSEN)	Method for desalination of water, in particular sea water
4410606	1982	Individual(s)	Low temperature thermally regenerative electrochemical system
4738904	1986	Hughes Aircraft Company	Low temperature thermoelectrochemical system and method
4814241	1987	Director-General of Agency of Industrial Science and Technology	Electrolytes for redox flow batteries
4786567	1988	Unisearch Limited, A.C.N.	All-vanadium redox battery
4874483	1989	Chiyoda Corporation	Process for the preparation of redox battery electrolyte and recovery of lead chloride
5346778	1992	Energy Partners, Inc.	Electrochemical load management system for transportation applications
5376470	1993	Rockwell International Corporation	Regenerative fuel cell system
5492777	1995		

(*Continued*)

Table 1.12 Top 30 most central patents for the regenerative fuel cell subdomain. *Continued*

Patent number	Filing year	Organization	Title
		Westinghouse Electric Corporation	Electrochemical energy conversion and storage system
5631099	1995	Individual(s)	Surface replica fuel cell
6468688	1998	Pinnacle ARB Limited	High energy density vanadium electrolyte solutions, methods of preparation thereof and all-vanadium redox cells and batteries containing high energy vanadium electrolyte solutions
6507169	2001	Farnow Technologies PTY Limited	Energy storage system
6516905	2001	Ballard Power Systems Inc.	Vehicle with a fuel cell system and method for operating the same
6579638	2001	Individual(s)	Regenerative fuel cell system
6620539	2001	Energy Conversion Devices, Inc.	Fuel cell cathodes and their fuel cells
6692862	2001	Squirrel Holdings Ltd.	Redox flow battery and method of operating it
6641945	2002	Individual(s)	Fuel cell
6875536	2002	Texaco Ovonic Fuel Cell LLC	Catalytic hydrogen storage composite material and fuel cell employing same
7226675	2002	Ovonic Battery Company, Inc.	Very low emission hybrid electric vehicle incorporating an integrated propulsion system including a fuel cell and a high power nickel metal hydride battery pack
7150927	2003	Bloom Energy Corporation	SORFC system with non-noble metal electrode compositions
7282294	2004	General Electric Company	Hydrogen storage-based rechargeable fuel cell system and method
7879205	2007	Samsung Electronics Co., Ltd.	Hydrogen generating apparatus, fuel cell power generation system, method of controlling hydrogen generating quantity and recorded medium recorded program performing the same

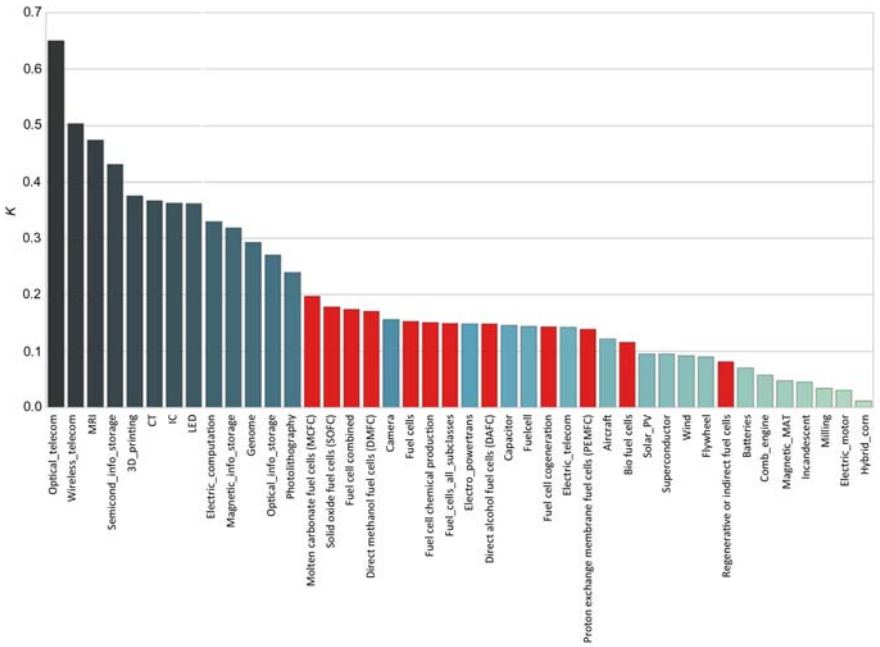

FIGURE 1.14

The performance improvement rate of the major fuel cell technologies (shown in *red*) and 30 other technological domains.

growth rates of 12 major fuel cell subdomains. We can observe that the fuel cell subdomains are estimated to improve at a rate between 8% and 20% per year. This puts them in a mid-range of improvement speed, bounded by "photolithography" on the upper end and "batteries" on the lower end. MCFC and SOFC are the fastest-growing fuel cell technologies, whereas the RFC subdomain is the slowest.

Fig. 1.15 shows a probabilistic comparison of the estimated growth rates of the main fuel cell subdomains. The left panel shows the probability density function (PDF) of the estimated rate. As we can see it is very unlikely that the actual improvement rate for any fuel cell technology would be faster than 50%−60% a year. The right panel shows the cumulative distribution obtained from the results reported in the left panel. We can interpret this cumulative function by observing that, for instance, there is a 50% chance that all actual improvement rates are below 20% a year. Based on the PDFs, we can estimate the likelihood that one observed subdomain is improving faster than another domain. This likelihood is reported in Fig. 1.16 for any pair of domains. This figure confirms that the fuel cell subdomains that are likely to be the fastest improving are SOFC and MCFC, whereas biofuel cell and RFC are likely to be the slowest.

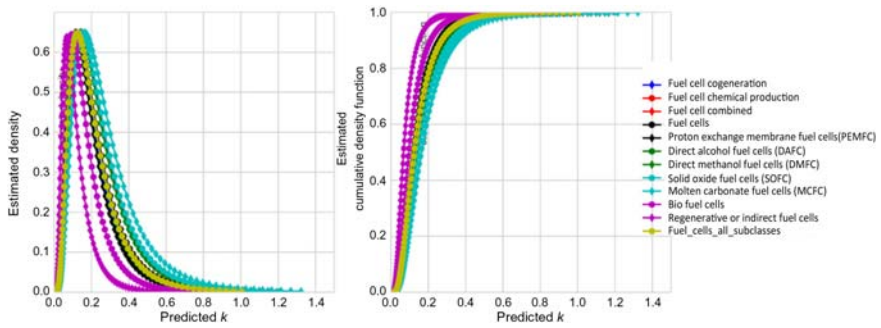

FIGURE 1.15

Probability density functions of the estimated performance improvement rates of the main fuel cell technologies.

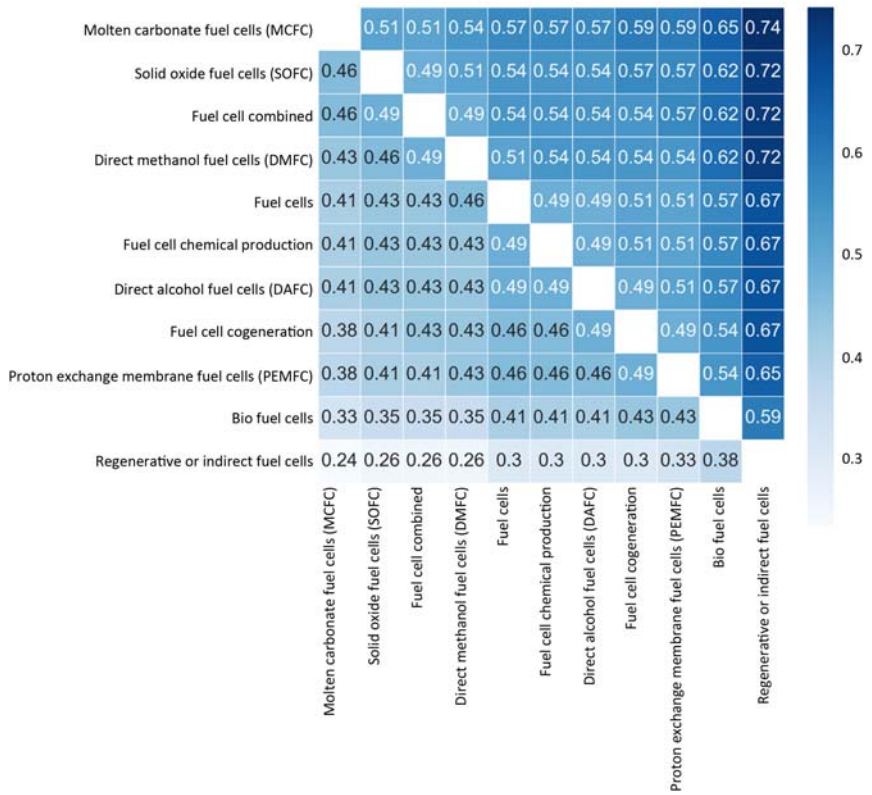

FIGURE 1.16

Heatmap representing the likelihood that an observed technological subdomain is growing faster than another subdomain.

In the following paragraphs we compare the history, barriers, and key drivers of the two faster-growing technologies, namely SOFC and MCFC.

The invention of SOFCs has its roots in the mid-19th century with the first discoveries related to a fuel cell capable of producing energy through the combination of hydrogen and oxygen [38]. Scientists had been improving the technology and from a patent citation network analysis and it emerges that one of the fundamental patents in the development of the technology (4510212) was granted in 1985 by the USPTO to an invention by the US department of energy [32]. The patent described an innovative configuration of the SOFC that improves the thermomechanical properties of the technology [64]. The first applications of solid conductors were lamps [65]. Currently the main applications are in the field of clean power generation, but there are some technical barriers that are limiting the potential advancement of this technology [66]. Milewski recognized the main technical limitations for the SOFCs that span from thermal to design and efficiency issues. On the other hand the major driver for the technological improvement of SOFC technology has always been the higher efficiency achievable compared to the thermal machines under the same operating conditions [38]. Furthermore the key drivers that led to the development of the SOFCs rather than the other fuel cell technologies are the possibility of directly using natural gas [67]. Current barriers and key drivers of SOFC technology are summarized in Table 1.13. Because of the maturity stage of the SOFC technology, technical and nontechnical factors are important for its technological development.

MCFCs along with SOFCs are both considered high-temperature fuel cells. Nevertheless MCFC technology is unpopular [70] compared to its main technological competitor. Even though the two technologies share the starting decade of development (the 1960s) and MCFC technology was apparently more advantageous, during the 1980s SOFCs quickly advanced technologically thanks to the R&D efforts of Westinghouse Power Corporation. In the same years the problems related to the building materials of MCFCs started to emerge. Currently the technology has entered the commercialization phase and the next step is the realization of a pilot plant to convince the market that the technology is convenient. The success of the MCFCs is strictly linked to energy prices. The lower they are, the

Table 1.13 Current barriers and key drivers of solid oxide fuel cell (SOFC).

Barriers	Key drivers	References
• Low thermal resistance • Complexity of reforming of hydrocarbon fuels • Insufficient overall energy efficiency • Insufficient utilization of the fuel in the anode	• Higher efficiency achievable compared to thermal machines • Fuel flexibility • Energy demand (since the Oil Crisis in 1974) • Environmental concerns	[38,66–69]

Table 1.14 Current barriers and key drivers of molten carbonate fuel cell (MCFC).

Barriers	Key drivers	Reference
• Low energy costs • Liberalization of energy market • Competition with fast advancing technologies	• Environmental protocols and legislation • Bonuses for clean power generation systems • Rise of the energy demand (e.g., coal gasification) • Unique advantage of MCFC	[71]

least convenient is the adoption of the technology. Moreover, other nonfuel cell technologies are being developed rapidly such as Stirling engines and small gas turbines. The key drivers for the technological development of MCFCs are the changes in the energy market (higher energy prices predicted) and the legislations (stringent environmental laws). Furthermore MCFC technology has to be developed in those applications where the fuel cell is the most advantageous such as with biogas, for the tolerance of the technology to the gas composition [71]. In Table 1.14 we sum up the nontechnical barriers and the key drivers that apply to MCFC performance improvement.

1.7 Conclusion and future research direction

Fuel cell technologies are exiting the hype phase and are approaching maturity stage with a very fast improvement rate. Fuel cells have many applications and they can function in a wide range of operating conditions. Moreover the materials used for the different fuel cell technologies are very diverse. United States, Japan, Korea, and Germany are leading the patenting activity due to the geographical presence of firms strongly interested in the development of the fuel cell technologies applied to the products that they make. Interestingly, historically the development of the technological domain was first sustained by mostly nonprofit institutions and currently by the industry (automotive, power generation, appliances). The shift demonstrates that fuel cells have scientific and economic interests. Among the various fuel cell technologies, MCFC and SOFC are quite promising, and they have reached a mature stage in which fast technological growth, fueled by several learning factors, is expected. In accordance, we identified MCFC as the fastest-improving technology among the fuel cell technologies. SOFC comes second. By observing the patent analysis results of SOFC it is possible to notice the initial popularity of the technology that was gradually substituted by the newest fuel cell technologies. Currently MCFC has reached the commercialization stage and it is ready to be demonstrated.

Technological forecasting is a fast-changing field; therefore, it is necessary to revise the results of the current research frequently using the latest advances in scientometrics. Some suggested research directions are:

1. Improving the accuracy of the growth prediction with actual historical performance data for commercialized fuel cell technologies.
2. Using the central patents analysis to define barriers.
3. Performing a predictive cost analysis using the forecasting tools.
4. Identifying the life-cycle stage in a quantitative way.

References

[1] J. Martino, Technological Forecasting for Decision Making, vol. XXXIII, 1993. doi:10.1007/s13398-014-0173-7.2.

[2] G. Triulzi, Looking for the right path: technology dynamics, inventive strategies and catching-up in the semiconductor industry, Datawyse / Universitaire Pers Maastricht, Netherlands, 2015.

[3] T.U. Daim, G. Rueda, H. Martin, P. Gerdsri, Forecasting emerging technologies: use of bibliometrics and patent analysis, Technol. Forecast. Soc. Change 73 (2006) 981–1012.

[4] R. Brown, Managing the "S" curves of innovation, J. Mark. Manag. 7 (1991) 189–202. Available from: https://doi.org/10.1108/EUM0000000002597.

[5] P. Balachandra, H.S.K. Nathan, B.S. Reddy, Commercialization of sustainable energy technologies, Renew. Energy 35 (2010) 1842–1851.

[6] A. Grübler, N. Nakićenović, D.G. Victor, Dynamics of energy technologies and global change, Energ. Policy 27 (1999) 247–280.

[7] A.D. Sagar, B. Van Der Zwaan, Technological innovation in the energy sector: R&D, deployment, and learning-by-doing, Energ. Policy 34 (2006) 2601–2608. Available from: https://doi.org/10.1016/j.enpol.2005.04.012.

[8] S. Kahouli-Brahmi, Technological learning in energy–environment–economy modelling: a survey, Energ. Policy 36 (2008) 138–162. Available from: https://doi.org/10.1016/j.enpol.2007.09.001.

[9] S.R. Walk, Quantitative technology forecasting techniques, Technological Change, InTech, 2012.

[10] C.L. Magee, S. Basnet, J.L. Funk, C.L. Benson, Quantitative empirical trends in technical performance, Technol. Forecast. Soc. Change 104 (2016). Available from: https://doi.org/10.1016/j.techfore.2015.12.011.

[11] B. Nagy, J.D. Farmer, Q.M. Bui, J.E. Trancik, Statistical basis for predicting technological progress, PLoS One 8 (2013) e52669.

[12] C.L. Benson, C.L. Magee, Data-Driven Investment Decision-Making: Applying Moore's Law and S-Curves to Business Strategies, ArXiv Prepr ArXiv180506339, 2018.

[13] Sahal, D., 1979. A theory of progress functions. AIIE Trans. 11 (1), 23–29.

[14] C.L. Benson, C.L. Magee, Quantitative determination of technological improvement from patent data, PLoS One 10 (2015) e0121635. Available from: https://doi.org/10.1371/journal.pone.0121635.

[15] H. Koh, C.L. Magee, A functional approach for studying technological progress: extension to energy technology, Technol. Forecast. Soc. Change 75 (2008). Available from: https://doi.org/10.1016/j.techfore.2007.05.007.
[16] J. Huenteler, T.S. Schmidt, J. Ossenbrink, V.H. Hoffmann, Technology life-cycles in the energy sector—technological characteristics and the role of deployment for innovation, Technol. Forecast. Soc. Change 104 (2016) 102−121. Available from: https://doi.org/10.1016/j.techfore.2015.09.022.
[17] R. Kothari, D. Buddhi, R.L. Sawhney, Comparison of environmental and economic aspects of various hydrogen production methods, Renew. Sustain Energy Rev. 12 (2008) 553−563.
[18] M. Beccali, S. Brunone, M. Cellura, V. Franzitta, Energy, economic and environmental analysis on RET−hydrogen systems in residential buildings, Renew. Energy 33 (2008) 366−382.
[19] U.S. Department of Energy, Comparison of Fuel Cell Technologies [Internet]. Energy Efficiency and Renewable Energy. 2016 <https://www.energy.gov/eere/fuelcells/comparison-fuel-cell-technologies> (accessed 03.09.18).
[20] L. Honorio, J. Bartaire, R. Bauerschmidt, T. Ohman, Z. Tihanyi, H. Zeinhofer, et al., Efficiency in Electricity Generation, 2003, Union of the Electricity Industry − EURELECTRIC, technical report, access (18/08/2019) from http://payesh.saba.org.ir/saba_content/media/image/2016/07/8412_orig.pdf.
[21] Á. Varga, Introduction to fuel cell technology, Fuel Cell Electronics Packaging, Springer, 2007, pp. 1−32.
[22] L. Schlapbach, Technology: hydrogen-fuelled vehicles, Nature 460 (2009) 809.
[23] C. Spiegel, Designing and Building Fuel Cells, vol. 87, Citeseer, 2007.
[24] N.Q. Minh, Solid oxide fuel cell technology—features and applications, Solid State Ionics 174 (2004) 271−277.
[25] M. Andersson, B. Sundèn, Technology Review—Solid Oxide Fuel Cell, ENERGIFORSK, 2017.
[26] K. Scott, A.K. Shukla, Polymer electrolyte membrane fuel cells: principles and advances, Rev. Environ. Sci. Biotechnol. 3 (2004) 273−280. Available from: https://doi.org/10.1007/s11157-004-6884-z.
[27] S. Mekhilef, R. Saidur, A. Safari, Comparative study of different fuel cell technologies, Renew. Sustain Energy Rev. 16 (2012) 981−989. Available from: https://doi.org/10.1016/J.RSER.2011.09.020.
[28] M. Winter, R.J. Brodd, What are batteries, fuel cells, and supercapacitors? 2004. https://doi.org/10.1021/CR020730K.
[29] A. Di Blasi, V. Baglio, A. Stassi, C. D'Urso, V. Antonucci, A.S. Arico, Composite polymer electrolyte for direct ethanol fuel cell application, ECS Trans. 3 (2006) 1317−1323. Available from: https://doi.org/10.1149/1.2356251.
[30] C. Lamy, E.M. Belgsir, J.-M. Léger, Electrocatalytic oxidation of aliphatic alcohols: application to the direct alcohol fuel cell (DAFC), J. Appl. Electrochem. 31 (2001) 799−809. Available from: https://doi.org/10.1023/A:1017587310150.
[31] S. Maddipati, R. Nandigam, S. Kim, V. Venkatasubramanian, Learning patterns in combinatorial protein libraries by Support Vector Machines, Comput. Chem. Eng. (2011). Available from: https://doi.org/10.1016/j.compchemeng.2011.01.017.
[32] B. Verspagen, Mapping technological trajectories as patent citation networks: a study on the history of fuel cell research, Adv. Complex Syst. 10 (2007) 93−115.

[33] Fuel Cell Today Limited, FCT - Fuel Cell Technologies - DMFC [Internet]. 2011. <http://fuelcelltoday.com/technologies/dmfc> (accessed 03.09.18).
[34] A.S. Aricò, V. Baglio, V. Antonucci, Direct methanol fuel cells: history, status and perspectives, Electrocatal Direct Methanol Fuel Cells, Wiley, 2009, pp. 1–78.
[35] F. Samimi, M.R. Rahimpour, Direct methanol fuel cell, Methanol, Elsevier, 2017, pp. 381–397.
[36] R.M. Ormerod, Solid oxide fuel cells, Chem. Soc. Rev. 32 (2003) 17–28.
[37] A.B. Stambouli, E. Traversa, Solid oxide fuel cells (SOFCs): a review of an environmentally clean and efficient source of energy, Renew. Sustain Energy Rev. 6 (2002) 433–455.
[38] K. Huang, J.B. Goodenough, Solid Oxide Fuel Cell Technology: Principles, Performance and Operations, Elsevier, 2009.
[39] Espacenet. Cooperative patent classification (CPC) [Internet]. 2017. <https://worldwide.espacenet.com/help?locale = en_EP&method = handleHelpTopic&topic = cpc> (accessed 07.09.18).
[40] C. Rayment, S. Sherwin, Introduction to Fuel Cell Technology, Dep Aerosp Mech Eng Univ Notre Dame, Notre Dame, 2003, pp. 11–12.
[41] E. Antolini, The stability of molten carbonate fuel cell electrodes: a review of recent improvements, Appl. Energy 88 (2011) 4274–4293.
[42] P. Tomczyk, MCFC versus other fuel cells—characteristics, technologies and prospects, J. Power Sources 160 (2006) 858–862. Available from: https://doi.org/10.1016/J.JPOWSOUR.2006.04.071.
[43] S. Cosnier, A.J. Gross, F. Giroud, M. Holzinger, Beyond the hype surrounding biofuel cells: what's the future of enzymatic fuel cells? Curr. Opin. Electrochem. (2018). Available from: https://doi.org/10.1016/J.COELEC.2018.06.006.
[44] R.A. Bullen, T.C. Arnot, J.B. Lakeman, F.C. Walsh, Biofuel cells and their development, Biosens. Bioelectron. 21 (2006) 2015–2045. Available from: https://doi.org/10.1016/J.BIOS.2006.01.030.
[45] Y. Wang, D.Y.C. Leung, J. Xuan, H. Wang, A review on unitized regenerative fuel cell technologies, part-A: unitized regenerative proton exchange membrane fuel cells, Renew. Sustain Energy Rev. 65 (2016) 961–977. Available from: https://doi.org/10.1016/J.RSER.2016.07.046.
[46] J. Andrews, A. Doddathimmaiah, Regenerative fuel cells, Fuel Cell Mater. (2008) 344–385.
[47] U. Ugurlu, R. Wichman, Enabling low-resolution ADC with high-order modulations for millimeter-wave systems, in: 2016 IEEE Int. Conf. Commun., IEEE, 2016, pp. 1–6. <https://doi.org/10.1109/ICC.2016.7510846>.
[48] S.-Y. Huang, P. Ganesan, H.-Y. Jung, B.N. Popov, Development of supported bifunctional oxygen electrocatalysts and corrosion-resistant gas diffusion layer for unitized regenerative fuel cell applications, J. Power Sources 198 (2012) 23–29.
[49] G.L. Soloveichik, Regenerative fuel cells for energy storage, Proc. IEEE 102 (2014) 964–975.
[50] S. Barrett, Patent analysis identifies trends in fuel cell R&D, Fuel Cells Bull. 2005 (2005) 12–13.
[51] M.-H. Huang, H.-W. Yang, A scientometric study of fuel cell based on paper and patent analysis, Journal of Library and Information Studies 11 (2013) 1–24.
[52] Fuel Cell Today, Fuel Cell Patent Review, 2012.

[53] Blue Vine Consultants, HGF, Fuel Cell Industry & Patent Overview, 2015.
[54] Y.-H. Chen, C.-Y. Chen, S.-C. Lee, Technology forecasting and patent strategy of hydrogen energy and fuel cell technologies, Int. J. Hydrogen Energy 36 (2011) 6957–6969.
[55] R. Rivera-Tinoco, K. Schoots, B. Van Der Zwaan, Learning curves for solid oxide fuel cells, Energy Convers. Manag. 57 (2012) 86–96.
[56] M. Wei, S.J. Smith, M.D. Sohn, Analysis of fuel cell markets in Japan and the US: experience curve development and cost reduction disaggregation, 2016.
[57] C.L. Benson, C.L. Magee, A hybrid keyword and patent class methodology for selecting relevant sets of patents for a technological field, Scientometrics 96 (2013) 69–82. Available from: https://doi.org/10.1007/s11192-012-0930-3.
[58] Espacenet, Cooperative Patent Classification (CPC), n.d. <https://worldwide.espacenet.com/help?locale = en_EP&method = handleHelpTopic&topic = cpc> (accessed 07.09.18).
[59] A. Abbas, L. Zhang, S.U. Khan, A literature review on the state-of-the-art in patent analysis, World Pat. Inf. 37 (2014) 3–13. Available from: https://doi.org/10.1016/j.wpi.2013.12.006.
[60] G. Triulzi, J. Alstott, C.L. Magee, Estimating Technology Performance Improvement Rates by Mining Patent Data, 2018.
[61] N.P. Hummon, P. Dereian, Connectivity in a citation network: the development of DNA theory, Soc. Networks 11 (1989) 39–63.
[62] W. Wiyaratn, Reviews on fuel cell technology for valuable chemicals and energy co-generation, Eng. J. 14 (2010) 1–14.
[63] J. Alstott, G. Triulzi, B. Yan, J. Luo, Mapping technology space by normalizing patent networks, Scientometrics 110 (2017) 443–479.
[64] A.V. Fraioli, Solid Oxide Fuel Cell Having Compound Cross Flow Gas Patterns, 1985.
[65] H.-H. Möbius, On the history of solid electrolyte fuel cells, J. Solid State Electrochem. 1 (1997) 2–16.
[66] J. Milewski, W. Budzianowski, Recent key technical barriers in solid oxide fuel cell technology, Arch. Thermodyn. 35 (2014) 17–41.
[67] A. Hawkes, M. Leach, Solid oxide fuel cell systems for residential micro-combined heat and power in the UK: key economic drivers, J. Power Sources 149 (2005) 72–83.
[68] H. Yokokawa, History of high temperature fuel cell development, Handbook of Fuel Cells-Fundamentals, Technology, Applications, vol. 1, 2003, pp. 219–266.
[69] M. Lo Faro, V. Antonucci, P.L. Antonucci, A.S. Aricò, Fuel flexibility: a key challenge for SOFC technology, Fuel 102 (2012) 554–559.
[70] J.R. Selman, Molten-salt fuel cells—technical and economic challenges, J. Power Sources 160 (2006) 852–857.
[71] A. Dicks, A. Siddle, Assessment of commercial prospects of molten carbonate fuel cells, J. Power Sources 86 (2000) 316–323.

This page intentionally left blank

CHAPTER

Thermodynamics and energy engineering

2

Venkatesan Venkata Krishnan

School of Science, Engineering and Design, Teesside University, Middlesbrough, United Kingdom

2.1 Introduction to thermodynamics of energy conversions

Thermodynamics dictate limits to which energetic transformations can occur, that is, all energy is conserved in a process (First Law) and heat cannot be transferred from low to high temperature without the application of work, and heat cannot be completely converted to work (Second Law). The subject itself with its concepts and laws evolved from observing the operation of devices that convert heat to work (electricity is work, and is therefore included as well).

One of the key technology developments in the electrical age was the invention of the electrical motor operating on electrical power, produced by the generator (another key advance of this era), which, in turn, is operated by flow or pressure driven processes. Other than hydroelectric and wind power, the majority of electrical power arises from pressure driven flows derived from heat released by chemical reactions, namely burning of fuel. Hence, modern technology relies on the conversion of heat energy to work, that is, electricity.

This led to work or electricity production from heat via thermomechanical engines that operate in a cyclic mode, namely processes that operated in multiple stages with a working fluid which returns to the starting point, only to repeat itself, for example, the Brayton cycle, Rankine cycle, and the theoretical Carnot cycle.

Examples of thermomechanical engines include the steam turbine and, later, the gas turbine, which have been prime movers for the generation of electricity over the past century and earlier. Such devices are also known as heat engines and are usually characterized by a few attributes [1], such as:

1. They require a high-temperature heat source to provide high-quality heat.
2. The next stage is to convert this heat to work, that is, only possible if a flow is generated, via a device like a rotating shaft or impeller.
3. Not all the heat is converted to the work (as per the Second Law of thermodynamics) and a part of the heat is rejected to a low-temperature reservoir, that is, water bodies or atmosphere.

Design and Operation of Solid Oxide Fuel Cells. DOI: https://doi.org/10.1016/B978-0-12-815253-9.00002-1

4. It is a cyclic process, thus the stages are repeated.

This is reflected in the performance of commonly engineered products such as thermal power plants and in refrigerators (in the latter case, heat flows in the opposite direction with the addition of power) [1,2].

However, there are examples of cyclic processes that are not truly cyclic in the thermodynamic sense, namely internal combustion (IC) engines, although they do undergo a mechanical cycle. This concept can be demonstrated in an IC engine where fuel and air are brought in from outside and the exhaust gases upon combustion are released, that is, the working fluid is not conserved within the process. Nevertheless these are also included within the broad purview of heat engines.

Naturally, these cyclic processes are governed by efficiency, which is expressed as work produced or heat energy input. Engineers have for many generations worked on maximizing energy output by maximizing the efficiency of these processes, but they are limited by practical temperature constraints. The basic definition of efficiency arising from the First Law of thermodynamics [1–4], that is, $\eta = W_{(\text{net})}/Q_{\text{in}}$, where $W_{(\text{net})} = Q_{\text{in}} - Q_{\text{out}}$, can be applied to the theoretical Carnot engine efficiency, which is then transformed to $\eta_{\text{Carnot}} = 1 - T_c/T_H$. Therefore the higher the temperature of the hot heat source, or the lower the temperature of the cold heat sink, the higher the efficiency. However, this is the maximum possible efficiency achievable for a "reversible" process and is the efficiency limit for any "cyclic" process.

Thermodynamics has traditionally created and defined entities or variables that describe heat flows as enthalpy, reversible work as Gibbs free energy, and the concept of entropy, which describes the irreversibility of a process and is defined by the well-known formula $\mathrm{d}S = \mathrm{d}Q/T$, first identified by Clausius. Entropy is shown to be a state function as the cyclic integral (i.e., $\oint \mathrm{d}Q/T$) for a reversible Carnot cycle is zero. It is also an undeniable reality that all processes in nature are irreversible and, therefore, the concept of entropy generation assumes great significance. Hence the Clausius definition becomes an inequality (i.e., $\oint \mathrm{d}Q/T \leq 0$) which can then be rewritten as $\Delta S =$ change in entropy between one state and another $= \int_1^2 \mathrm{d}Q/T \geq 0$ [1].

2.2 Thermodynamics of electrochemical cells

Electrochemical cells that convert chemical energy directly into electricity are termed *galvanic cells* (as opposed to electrolytic cells where the process is the reverse) and include batteries and fuel cells. These are clear alternatives to thermomechanical engines and are not capped by Carnot efficiency limits.

Bearing in mind that the fuel cell is *not* a cyclic process with a working fluid and is actually a steady-state flow process [2], the statement of the First Law of thermodynamics is therefore expressed simply as $\Delta H = Q + W$ (where W is

$W_{electrical}$) due to the flow of electrons or ions in an electrochemical cell. The heat term (Q) can be replaced with $T\Delta S$, bringing in the concept of entropy (applied to a reversible and isothermal process) and leading to the expression $\Delta H = T\Delta S + W_{electrical}$.

As an electrical energy producer the focus of the technologist is maximizing $W_{electrical}$; the maximum value attainable is when the process is reversible, which may be expressed as $W_{electrical,max} = \Delta H - T\Delta S$. This is also equal to the change in the Gibbs free energy (ΔG) (as postulated by the Gibbs equation). Therefore the maximum efficiency of a fuel cell as represented by the First Law principles, which is $\eta_{cell,max} = W_{electrical,max}/\Delta H$, where ΔH will be the heat of the fuel cell reactions, namely electrochemical oxidation of hydrogen, or oxidation of syngas or methanol, depending on the type fuel utilized. Since hydrocarbon combustion reactions release condensable water, one can represent ΔH as either a higher heating value (HHV) or a lower one (LHV) [1–5]. The maximum work is also expressed in voltage terms, as nFE, where n is the number of electrons transferred per unit mole of limiting reactant, which is usually the fuel, while F is the Faraday's constant (96,487 Coulombs per mole of electrons transferred) and E is the Nernst voltage of the electrochemical cell. This can then be written more specifically as E^{o}, leading to the maximum value, which is known as thermodynamic efficiency [5] as shown in Eq. (2.1).

$$\eta_{cell,max} = \frac{W_{electrical,max}}{\Delta H} = \frac{\Delta G^{\circ}}{\text{HHV or LHV}} = \frac{nFE^{\circ}}{\text{HHV or LHV}} \tag{2.1}$$

If one were to use LHV instead of HHV [the former is used regularly for solid oxide fuel cells (SOFCs) since the product is vapor] the $\eta_{cell,max}$ will be higher. Therefore one school of thought insists that comparisons of thermodynamic efficiencies for different types of fuel cells should be done using the same basis (i.e., HHV) so it can be applicable to other types of fuel cells such as proton exchange membrane fuel cells, direct-methanol fuel cells, alkaline fuel cells, as well.

However, as will be discussed later in this chapter, many engineers and technologists have departed from this level of thinking and are urging the use of *exergy* as a way of defining the efficiency of a process, that is, defining efficiency in terms of the power produced relative to the maximum possible power achievable (exergy).

Coming back to the conventional First Law definition of efficiency, if one were to summarily compare the efficiency of cyclic or thermomechanical engines with electrochemical engines (fuel cells), the latter are not bound by operational temperature limits (as in a cyclic engine). They are, instead, limited by $T\Delta S$ and if the entropy generation approaches zero, thermodynamic efficiency can approach 100% (direct carbon-fueled SOFCs [6]), something that is highly improbable for cyclic engines operating under most industrial conditions.

For the case where solid phase carbon itself is a fuel, where the overall cell reaction is $C + O_2 \rightarrow CO_2$, the standard enthalpy changes in high temperature (600°C) is about -395.4 kJ/mol. For the same reaction the ΔS is only 1.6 J/K/

mol at the same temperature. Applying the Gibbs equation ($\Delta G = -394$ kJ/mol) implies that the fuel cell efficiency (thermodynamic) is almost 100% [6].

There are many instances where thermodynamic (reversible) efficiency exceeds theoretical Carnot engine efficiencies [5], although as the temperature increases beyond 800°C and if one assumes the cold reservoir temperature to be about 50°C, efficiencies of heat engines begin to surpass that of fuel cells (hydrogen can be taken as an example, although CO and syngas show similar trends). This need not be a dampener against high-temperature fuel cells (i.e., MCFCs and SOFCs) because all these devices operate irreversibly since no electrochemical process operates at infinitesimal current, just as no cyclic process operates under reversible conditions, and polarization losses at high temperatures are very low. As systems get more complex, heat management within the fuel cell system ensures high overall system efficiencies and, as such, high-temperature operation is the preferred choice, particularly for stationary applications. A more nuanced method for quantifying SOFC efficiency uses the concept of *exergy*, as discussed in Section 2.3.

2.3 Exergy concepts in heat to power conversions

The development of exergy as a concept is relevant to assessing the performance efficiency of an engine in relation to its maximum potential. Exergy is a more modern interpretation of the concept of Gibbs free energy that has been used significantly to describe thermodynamic efficiencies and is synonymous with maximum reversible work extractable in a fuel cell [5]. Exergy may also be described as a chemical equivalent of *potential energy* used in mechanical systems.

Exergy is initially postulated as the extent of departure of a system in its existing state from a reference state, which is quite simply the Earth's atmosphere (i.e., if a system has a temperature, pressure, or composition different from the environment then the system has exergy). A classic argument made to distinguish exergy from energy is that the atmosphere around us has considerable energy but no exergy, which means that any system in equilibrium with the atmosphere (or the reference state) in terms of temperature, pressure, and composition is incapable of doing work.

Therefore exergy refers to a system having a certain potential for doing work and once this work is done the system will reach a final state of equilibrium with its surroundings [3–5]. The route taken to achieve this transformation is also important in terms of whether the process is irreversible or reversible. The familiar term *irreversibility* can thus be equated to a new term, *exergy destruction*. Therefore in a system where one can reduce the irreversibility, then it can be said that the extent of exergy destruction is also reduced. In the case of fuel cells, reducing irreversibilities or lowering exergy destruction is achieved

by operating at regions of low polarization, that is, high voltage (low current density).

A basic postulation of exergy [1,4] for any state relative to a reference state (also termed as the dead state) is:

$$\text{Exergy } Ex = (U - U_o) + P_o(V - V_o) - T_o(S - S_o) + \text{KE} + \text{PE} \tag{2.2}$$

In many instances, and particularly in heat cycles, we ignore the kinetic energy (KE) and potential energy (PE) terms as they are zero at reference state. The above formulation is referred to in the literature as physical exergy and is applicable to systems where there are mass and enthalpy flows. If these flow processes contain heat evolution or heat supply term, Q, then the exergy value arising from that heat content can be postulated using the Carnot efficiency as shown in Eq. (2.3) [1,4].

$$\text{Exergy transfer from heat}, Ex_{\text{heat}} = Q\left(1 - \frac{T_o}{T}\right) \tag{2.3}$$

The concept of exergy has been extended to "chemical exergy" [4,5] as well. In the case of cyclic heat engines a thermomechanical term describes exergy [Eq. (2.2)], while in the case of a fuel cell a chemical component is also introduced, as discussed next.

The differential expression for Gibbs Energy, in terms of deviation from a thermodynamic equilibrium is written as follows [5]:

$$\partial G = V\partial P - S\partial T + \sum \mu_i \partial n_i \tag{2.4}$$

From here, integrating between the limits of the existing temperature and pressure (T, P) and the reference state (i.e., state of the environment) as mentioned earlier (T_o and P_o), exergy can be formulated as [1,3–5]:

$$\text{Physical and chemical exergy} = T_o(S - S_o) - (H - H_o) - \sum n_i(\mu_i - \mu_{i,o}) + X_{\text{heat}} \tag{2.5}$$

The term for chemical exergy for a system ($\overline{X^{\text{Chem}}}$) that comprises an ideal mixture ($i = 1$ to j) at a set of temperature and pressure conditions can be further formulated as:

$$\overline{X^{\text{Chem}}} = \sum n_i\left(\mu_i - \mu_{i,o}\right) = RT_o \sum_{i=1}^{j}\left(y_i \ln \frac{y_i}{y_i^e}\right) \tag{2.6}$$

Using exergy as a basis for calculating the effectiveness of an SOFC, standalone units or hybrid SOFC plants are useful since they directly attempt to identify irreversibilities at every stage in a plant. One can potentially identify a large irreversibility and adjust process variables to bring it down to an acceptable level. However, the overall exergetic efficiency can only be optimized through formulating the interactions between all process components. Further details on exergy formulations are discussed using specific examples in later sections.

2.4 Overview of basic modeling and conventional approaches to the energetics of solid oxide fuel cells

Modeling of SOFCs at various levels (viz., cell, stack, balance of plant) and the overall systems level have continued to progress over the past 25–30 years. Modeling approaches can be described as *0-dimensional*, *1-dimensional*, or by using a more advanced *computational fluid dynamic* (*CFD*) model [7]. 0D models are useful for overall systems or plant simulation and do not offer details related to the design and dimensions of individual components and/or their performance. In the 0D category, the modeling effort focusses on overall SOFC plant energetics and efficiency. These types of models are strongly rooted in thermodynamic concepts described in the introduction to this chapter. The classic treatment of energetics revolves around the First Law definition of efficiency starting from the very basic thermodynamic efficiency to the more modern understanding considering the irreversibility expressed as exergy destruction during cell operations.

1D models comprise electrochemical models with ionic or electronic transport formulations, Fick's law-type expressions (e.g., equimolar counter diffusion, combining gas phase binary diffusion, and Knudsen diffusion) for concentration polarization [8,9]. The main aim of these approaches is to model current–voltage curves and electrochemical impedance spectroscopy data via estimations of the different types of polarization/polarization resistances. In thermodynamic terms the focus has been on estimating the irreversibility in single or button cell performances.

Modeling approaches can also be classified based on length scales, that is, over cell component thicknesses ranging from small single cell or button cells (one-dimensional model) to large cell areas (2 or 3 dimensional models where fuel and air utilizations are key factors, and temperature or flow gradients that exist in 3 dimensions), which necessitate multiphysics (CFD) approaches (considering thermal effects, that is, heat transfer, flow coupled with chemical or electrochemical reactions, and accounting for material stresses and deformations) [10,11]. These are of great value toward stack and hotbox designs where heat effects, namely hot spots, and other degradation phenomena are of importance.

In this chapter the major thermodynamic analysis for SOFC standalone and hybrid systems fall under the category of 0D models as they relate to overall energetics calculations. However, the work done by Calise et al. [12] and Sciacovelli and Verda [13] combine the thermodynamic principles of exergetic analysis and entropy generation, with finite element modeling for a tubular SOFC itself using 1D models.

2.4.1 Modeling of solid oxide fuel cell–hybrid cycles

There are different types of processes designed around the SOFC stack, including standalone SOFC stack-systems [14–19], hybrid SOFC–steam turbines (SOFC–ST) [19,20], hybrid SOFC–gas turbines (SOFC–GT) [18,21–27] and

their combination (SOFC−GT−ST) [18,22,27] in a bid to boost the overall efficiency of electricity production. These hybrid energy configurations include a *bottoming cycle* where waste heat from the stack exhaust is extracted in different ways and is utilized in a thermodynamic cycle or heat engine to derive additional power prior to being irreversibly transferred to the environment.

To highlight the importance of the bottoming cycle one can go back to the concept of thermodynamic efficiency in Eq. (2.1) (i.e., $\eta_{\text{th}} = \Delta G/\Delta H = (\Delta H - T\Delta S)/\Delta H$) at the temperature of operation of the fuel cell, as explained in the following paragraph. From a thermodynamic perspective, the efficiency of a fuel cell is highest at the lowest temperatures (i.e., ambient temperatures). This is true for most cases, particularly for hydrogen and carbon monoxide, which are the most likely fuel components that participate in electrochemistry. Since the $T\Delta S$ term dominates with the increase in temperature, the maximum reversible work (ΔG) from a fuel cell decreases with a reduction in temperature. However, the lower the temperature the slower are the reaction kinetics and, consequently, the higher the polarization resistance (irreversibility), which will lower the operating efficiency drastically. Therefore to go to high temperatures as is done in SOFCs is a practical necessity despite the lower thermodynamic efficiency. The idea of the bottoming cycle is to use the fuel cell exhaust at high temperatures in a cyclic heat engine, thereby generating additional power or efficiency; the fuel cell operating at high temperature lowers the irreversibility's under those conditions, whereas the bottoming heat engine operates under a practical Rankine or Brayton cycle with steam or gas, respectively [5]. These cycles can utilize useful exergy to generate maximum work. Introducing bottoming cycles leads to lower exergy destruction, that is, if the bottoming cycles are not incorporated the corresponding exergy would doubtlessly be destroyed.

Larminie and Dicks [5] have discussed how to achieve efficiency limits for a fuel cell operating on hydrogen and for a Carnot cycle with a 100°C exhaust (T_2). Under the assumption that zero work is done (100% irreversibility), that is, $\Delta G = 0$, maximum temperature can be reached, $T_F = \Delta H/\Delta S$. This maximum temperature for the proposed Carnot engine (T_1) is used as the limit for a bottoming cycle. By fixing a suitable value as the low-temperature exhaust (sink), e.g., 100°C one can plot the Carnot efficiency limit as a function of temperature up to the maximum value, T_F.

$$\eta_{\text{Carnot}} = 1 - \frac{T_2}{T_1} \quad \text{for all} \quad T_1 \leq T_F \tag{2.7}$$

Meanwhile, the thermodynamic efficiency for hydrogen as fuel in the fuel cell is calculated as a function of temperature as well, as shown in Eq. (2.8).

$$\eta_{Th} = \frac{\Delta G}{\Delta H} \quad \text{from thermodynamic properties of the fuel cell reaction} \tag{2.8}$$

Calculations for the hydrogen-powered fuel cell−heat engine combined cycle show that the (thermodynamic) efficiency is a constant value throughout the

temperature range, assuming a purely reversible process [5]. Therefore operating as close to a reversible condition becomes the primary criteria of the process designer, that is, the design engineer can thus freely choose a reasonably high temperature for this purpose up till the maximum temperature limit, T_F, computed earlier.

Early SOFCs operating at 1000°C were particularly suited for hybrid process configurations. There are two very basic forms of bottoming cycles; one uses waste heat to generate steam and operate a steam turbine, and a second entails pressurized operation of a stack. This is followed by combustion, releasing the high-pressure exhaust gas to power a gas turbine. There have also been attempts to have a combined gas turbine, steam turbine bottoming cycle, and *steam injected in gas turbine (STIG)* in the bid to maximize efficiency.

2.4.2 Modeling of stack-system configurations

Furthermore, within the SOFC system itself configurations vary, such as total or partial internal reformation of fuel versus complete prereformation (external reformation). This can be combined with partial recirculation of flue gas exhaust into the anode system, which lowers the fresh feed steam requirements for natural gas reformation (Fig. 2.1) once the requisite steam-to-carbon ratio is maintained [15], and configuring the process by adjusting fuel utilization to either maximize electrical output or to strike a balance between electricity and heat production (combined heat and power). The very basic configuration must include an after-burner following the stack to combust unconverted fuel from the stack and in the process preheating the feedstock as seen in many process flow diagrams reviewed in this work.

Fig. 2.2 shows a very simple configuration by Peters et al. [16] that demonstrates the efficacy of anode recycling applicable to a hydrogen-fueled cell. Most of the other configurations include anode off-gas recycling as well. While there is no reformation and there is no requirement of moisture in the stack for this case, the authors condensed out the water formed in the stack, thereby recycling the hydrogen with the recycle ratio being almost 100% in one of their case studies. This configuration uses up parasitic power in the form of the anode recycle blower, but the fuel is nearly 100% hydrogen as it enters the stack (in case of 100% recirculation), thereby leading to high cell/stack performance. Enhancement of First Law efficiencies have been reported by recycling and removal of product water from the anode off-gas in this work.

For natural gas and hydrocarbons, partial external reformation or prereformation (methanation) of feedstock is the most widely used configuration in most SOFC stacks (almost all the configurations reviewed in this chapter) since the exothermic nature of the electrochemical oxidation is somewhat regulated by the endothermic reformation. This type of balancing is needed since airflow on the cathode side has to be increased for the removal of excess heat. This would

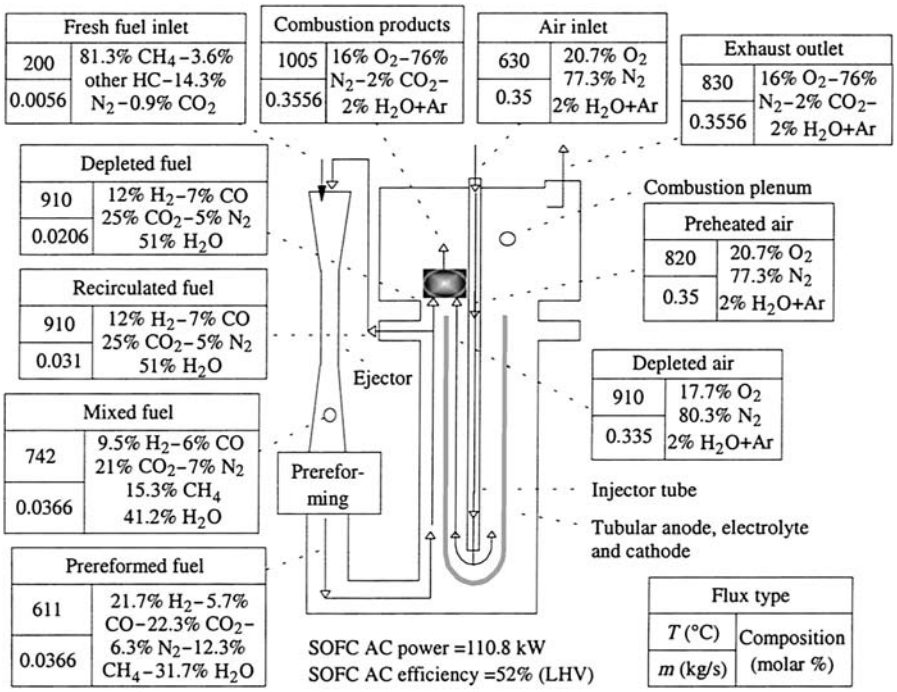

FIGURE 2.1

Tubular solid oxide fuel cell (SOFC) stack configuration with calculated values [15].

lead to higher power consumption for the air blower and add to the parasitic power consumption in an SOFC system.

Chan et al. [17] demonstrated a configuration wherein all reformation occurs externally (discussed further in Section 2.8, on exergy calculations). Published in 2002 this type of configuration was reflective of the earlier state-of-the-art. A totally different configuration involving complete internal reformation within the stack was discussed by Calise et al. [24,25]. In practical terms this adds to the complexity of the anode material and energy balance, but will be very optimal in terms of thermal gradients in the cell. In cases of partial or total internal reformation, Gibbs free energy minimization algorithms for multireaction equilibria [1–4] are used to predict exit anode compositions, discussed further on in this chapter.

Other schemes that will be discussed further onward in this chapter include biomass gasification integrated SOFC plant for CHP (Rokni et al. [21,28] and Panopolous et al. [29]). In some of these case studies efficiencies are calculated using the First Law of thermodynamics basis, whereas in many others the concept of exergy is used where the performance efficacy of the system is correlated with the irreversibility in the operation.

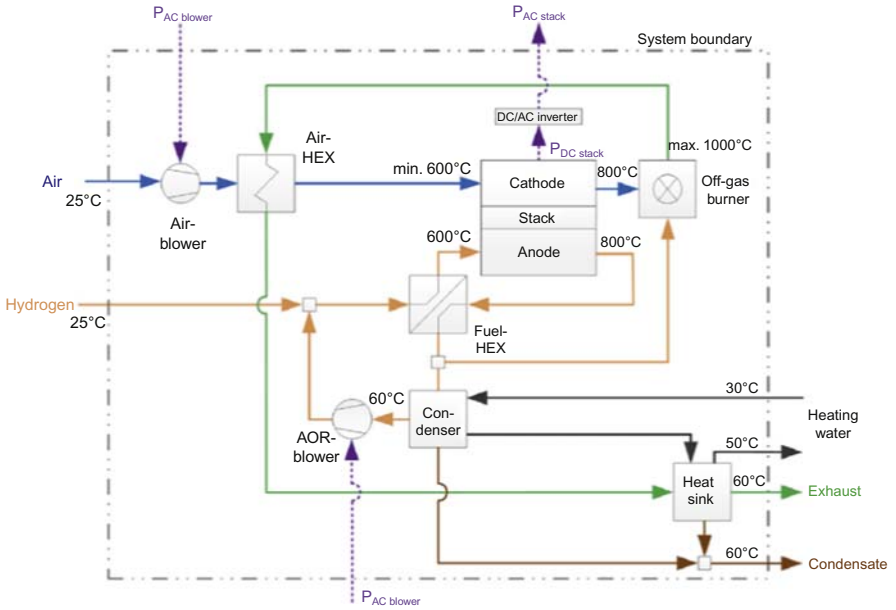

FIGURE 2.2

Systems layout for hydrogen-powered solid oxide fuel cell stack with anode recycling, off-gas recirculation, and condensation [16].

2.5 Fuel utilization in the anode of an solid oxide fuel cell stack

Fuels such as natural gases are always cofed with moisture (about 2.5 to 1 steam-to-carbon ratio, to prevent coking on Ni-catalysts) available from a steam boiler and undergo either partial or total internal reformation to syngas in the anode of the SOFC stack. Complicating this is the added variable of partial recycling of the anode off-gas, which has the advantage of recycling part of the steam. This lowers the latent heat demand arising from fresh water and helps in enhancing efficiency [15,16], notwithstanding the detrimental effect of feed dilution. The recycle ratio is also adjusted to maintain the safe steam-to-carbon ratio in the anode of a stack.

As an example, for the configuration outlined in Fig. 2.1, Campaneri [15] formulated a First Law-based electrical efficiency term(LHV basis) to include fuel utilization, U_f (or fuel utilization factor) as:

$$\eta_{el} = \frac{W_{el}}{\text{LHV}} = \frac{nFE}{\text{LHV}} = \frac{nFV_{cell}U_f\Gamma_{H2}}{\text{LHV}} \tag{2.9}$$

In this example, Campaneri [15] has used Γ_{H2} as the fuel equivalent hydrogen content, which can then be written as $\Gamma_{H2} = X_{H2} + X_{CH4} + X_{CO}$, where X_{CH4} and

X_{CO} are the fractions of methane and CO that contribute to hydrogen formation as per the reformation and water gas shift (WGS), respectively.

The reactions are the following:

$$CH_4 + H_2O \rightarrow CO + 3H_2$$

$$CO + H_2O \leftrightarrow CO_2 + H_2O$$

Therefore the fuel utilization factor, U_f, may be expressed as:

$$U_f = \frac{N_{H2,consumed}}{(N_{H2,in} + N_{CO,in} + 4N_{CH4,in})} \tag{2.10}$$

The factor of 4 in the denominator is due to the fact that the consumption of one mole of methane generates 4 moles of hydrogen, overall.

U_f is a global number for fuel utilization where a single pass conversion measure across the cell or stack can also be evaluated based on the recycle ratio of the anode off-gas (e.g., U_f of 85% compares to 69% conversion per pass, for the example used) [15].

In the cases of partial or total internal reformation and anode recycling estimating fuel utilization requires a complex calculation. Typically within the SOFC stack the hydrocarbon is not expected to undergo direct electrochemical oxidation as a dominant pathway given that the Ni-catalyst facilitates reformation in the presence of steam, followed by a WGS equilibrium. The WGS reaction is primarily an equilibrium step under most SOFC operating conditions. The likely components that undergo electrochemical oxidation are CO and H_2 or in some cases only H_2. In the case of the latter, the CO is either converted completely via the shift reaction or unreacted. Therefore there are instances where authors have used fuel utilization (U_f) calculated based on hydrogen alone. Campanari [15] used U_f based on hydrogen undergoing the electrochemical reaction only, that is, the assumption being that CO (in equilibrium with CO_2) passes through the fuel cell stack as unutilized fuel and is finally combusted in the after-burner. However, this assumption may not be entirely true under modern-day configurations where the anodes are complex and multifunctional, for example, Ni (or Ni-bimetallic) with ceria (Gd-doped ceria or Sm-doped ceria).

The fuel cell configuration described by Campanari [15], as do many other configurations [15–28,30], incorporates an after-burner that combusts all unconverted fuel from the SOFC stack in a plenum chamber, generating high-grade heat (high temperature) which is integrated within the process.

The heat generated from the combustor can be enhanced by lowering the fuel utilization in the stack (using less electrical power), thus releasing surplus heat for commercial applications. On the other hand, increasing fuel utilization (using more electricity) will produce less heat in the after-burner, thus leaving much less for commercial heating applications. This is usually dictated by the market requirements for heat and power, that is, SOFC systems that are tailored for combined heat and power applications may have the flexibility to adjust U_f levels to

meet customer demands for heat versus electricity. High-grade heat from the combustor after heat integration can also be directed to appropriate bottoming cycles for generating additional power, as seen in later sections of the chapter.

Alternatively as shown in configurations by Haseli et al. [24] in Fig. 2.3, a small portion of methane (natural gas) fuel is split and used in the after-burner to raise the temperature of the exhaust appropriately for facilitating bottoming cycles, namely gas or steam turbines with enhanced heat recovery.

In the analysis provided by Calise et al. [25], internal reformation and WGS reaction achieve equilibrium within the stack itself for a totally internally reformed fuel cell and is only hydrogen generated from these reactions that participates in the electrochemical reaction. This is the same as Campanari's assertion [15] reported earlier. In this example, there are no anode recycle streams and, therefore, fuel utilization is directly related to the amount of hydrogen reacted in the cell. Fuel utilization has a critical influence on individual efficiencies, namely SOFC versus steam turbine cycle, and is discussed further as exergy destruction.

Calise et al. [26] discuss the strategy for part-load versus full-load operations for a hybrid SOFC−GT where options range from varying fuel and airflow rates, combustor bypass, gas turbine bypass to gas turbine rotor speed. Fuel utilization in the SOFC stack can be one of the tunable parameters to address variable loads. The former can be achieved by variation in fuel mass flow rate or even air mass flow rate, combustor bypass, and stack bypass of the fuel (as shown in a few models in [24]) on the SOFC stack side in addition to variations in gas turbine operations.

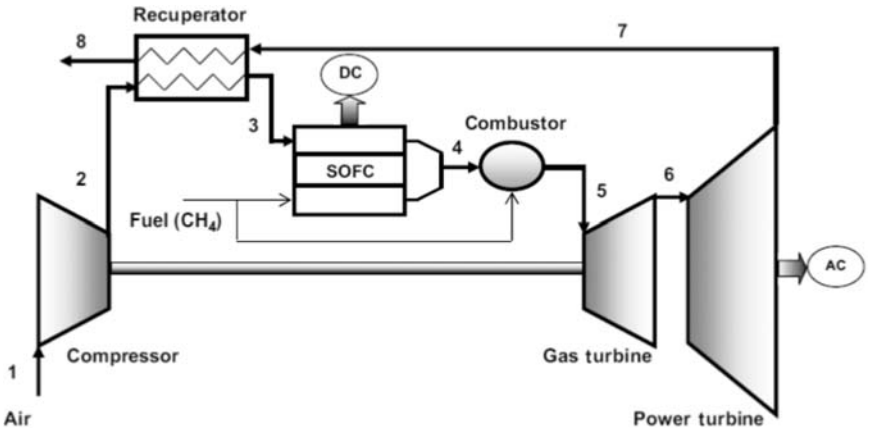

FIGURE 2.3

Solid oxide fuel cell (SOFC) stack−gas turbine and power turbine hybrid flow diagram [24].

For a very simple case of a hydrogen-powered SOFC stack [16] with the configuration shown in Fig. 2.2, the very basic concepts of fuel utilization and the effect of recycling are presented in Eqs. (2.11) and (2.12):

$$U_f = \frac{\dot{N}_{\text{H2,reacted}}}{\dot{N}_{\text{H2,in}}}.100 \tag{2.11}$$

$$\text{RR} = \frac{\dot{N}_{\text{Recirculated}}}{\dot{N}_{\text{Anode Out}}}.100 \tag{2.12}$$

U_f being the stack utilization based on molar component flows and RR being the recycle ratio based on total flows. Fuel utilization of the system is therefore expressed as:

$$U_{f,\text{system}} = \frac{U_f}{1 - \text{RR} \cdot (1 - U_f)} \tag{2.13}$$

van Biert et al. [19] also distinguished the basis for fuel utilization, namely the single pass fuel utilization ($U_{f,\text{single pass}}$) versus the global fuel utilization ($U_{f,g}$) as a function of the recirculation ratio.

$$U_{f,\text{single pass}} = \frac{1 - \text{RR}}{(1 - \text{RR}) \cdot U_{f,g}} \cdot U_{f,g} \tag{2.14}$$

which is the same as Eq. (2.13) after reorganization.

To summarize, it is important to note that fuel utilization is one of the key parameters that determine efficiency of electrical power generated by SOFC or SOFC−hybrid plants. In the following sections, we will review some of the results that demonstrate how fuel utilization can affect the exergy utilized in the SOFC stack and thereby influence the overall system efficiency, and that there is usually an optimal solution for this factor.

2.6 Efficiency calculations in solid oxide fuel cell stacks

Rokni [20], in their SOFC−steam turbine (Rankine cycle) hybrid and in their SOFC−Stirling engine hybrids have defined efficiency by combining thermodynamic efficiency, voltage efficiency, and fuel utilization. Having postulated the thermodynamic efficiency, η_{rev} (as shown earlier), and the voltage efficiency, η_V, as:

$$\eta_{\text{rev}} = \frac{\Delta G_{\text{Fuel}}}{\text{LHV}_{\text{Fuel}}} \tag{2.15}$$

$$\eta_V = \frac{V}{E_{\text{Nernst}}} \tag{2.16}$$

an expression for overall electrical efficiency is formulated accounting for operating voltage (voltage efficiency) and fuel utilization (U_F), as:

$$\text{Overall efficiency} = \eta_{\text{Rev}}\eta_V U_F = \frac{P_{\text{SOFC}}}{\left(\text{LHV}_{\text{H2}}\dot{n}_{\text{H2,in}} + \text{LHV}_{\text{CO}}\dot{n}_{\text{CO,in}} + \text{LHV}_{\text{CH4}}\dot{n}_{\text{CH4,in}}\right)} \quad (2.17)$$

This value is only for the SOFC stack and is an efficiency term based on the First Law.

The calculation for hydrogen, CO, and methane inlet flows can be set via a material balance, although the extent of reaction can be determined by considering multireaction equilibrium—these results are inserted in the denominator in Eq. (2.14). This is a standard calculation using the criterion of Gibbs free energy minimization considering all the species (viz., H_2, CO, CO_2, H_2O, CH_4, and N_2) which is explained in various thermodynamics textbooks [1–4]. In systems software packages such as Aspen Plus, the Gibbs reactor option is used for these calculations. Rokni [20] used the traditional method of Lagrange multipliers [1–4] and arrived at final compositions of the stack exhaust with the above equilibrium assumptions. In the case of a prereformer, yet again, the Gibbs free energy minimization algorithm is used to get the exit concentrations.

Peters et al. [16] used a very simple hydrogen-fueled SOFC standalone system and investigated the effect of anode off-gas recycling for the efficiency of the system. The simulation of the system with anode off-gas recycling is compared to that of a nonrecycling system. Parameters such as recycle ratio and electrical demands on the recycle blower will influence the overall efficiency of the process and there appears to be an optimal solution to the usage of anode gas recycling.

The overall power calculations [16] are based very simply on overall power output, starting from the stack (i.e., DC power). This is then converted to AC power using a suitable value for inverter efficiency. Additionally in any SOFC power plant, "parasitic power" losses occur, predominantly composed of blower power consumption.

The overall electrical efficiency is:

$$\eta_{\text{Elec}} = \frac{(U_{\text{cell}} \cdot N_{\text{cell}} \cdot A_{\text{cell}} \cdot i_{\text{cell}})\eta_{\text{Inv}} - \text{Blower power, AC}}{\dot{m}_{\text{H2in}}\text{LHV}_{\text{H2}}} \quad (2.18)$$

where, U_{cell}—cell voltage; N_{cell}—number of cells in stack; A_{cell}—area of each cell; i_{cell}—operating current density of the cell, η_I—inverter efficiency. The terms in the denominator are self-explanatory and reflect the total heat input to the system. In this work [16] this is a First Law-based efficiency term and does not treat the efficiency based on exergy analysis.

Peters et al. [16] defined the term thermal efficiency (not to be confused with the thermodynamic efficiency discussed earlier) as - heat output divided by the total heat input, provided by the entering fuel, namely hydrogen, in this case.

$$\eta_{\text{Thermal}} = \frac{\sum \dot{Q}_{\text{Heat sink}}}{\dot{m}_{\text{H2in}}.\text{LHV}_{\text{H2}}} \quad (2.19)$$

Isentropic efficiencies of the blower are modified by using factors to adjust the irreversibility and mechanical blower efficiency.

However, a Second Law treatment toward the calculation of efficiency is particularly relevant for SOFCs since the focus of the process engineer is to avoid as much irreversibility as possible. This means utilizing as much of the exergy available for power and heat, and the efficiency calculated in this way is considered a more pragmatic measure of the efficacy of a process. This is discussed further along in later sections.

2.7 Estimating efficiencies and irreversibility's in solid oxide fuel cell–hybrid processes

As discussed in Section 2.4.1 bottoming cycles are very attractive in generating additional power, and some more heat, for low-grade heat applications like domestic hot water. Some of the bottoming cycles include steam turbines (Rankine cycle), reciprocating pumps (Stirling cycle [20,28] or Seiliger cycle [19]), gas turbine (Brayton cycle), and steam and gas turbines in series. SOFCs can also be connected to a biomass gasifier, which is primarily a "topping" cycle, generating fuel to the SOFC stack [21,28,30]. However, the allothermic biomass gasifier [29] receives the exhaust heat from the SOFC stack and, in that sense, becomes a bottoming cycle.

SOFC–heat engine hybrids can be extended to their fullest potential wherein the heat from the exhaust of the gas turbine (located downstream of the afterburner that follows the SOFC stack) is used to generate steam from the fresh water supply. The idea is to utilize fully the flue gas heat to make steam in the heat recovery steam generator (HRSG) section.

HRSGs can be used to generate steam for heating purposes or to drive a steam turbine to generate more electricity. If used for cogeneration with either a gas turbine or a gas turbine–SOFC hybrid, HRSGs can maximize plant efficiencies. In such a situation the overall capital costs will be higher due to the very high inventory of equipment (viz., SOFC stack, gas turbine, HRSG balance of plant equipment such as evaporators and steam drums, and steam turbines) [31].

Typical plant data involving HRSG application [31] demonstrate that for a burner or fuel cell exhaust flue gas flow (mostly CO_2 and water vapor) the rate of 702 kg/s at an inlet temperature of 596°C HRSG can recover about 371 MW of heat (as steam) resulting in an outlet venting temperature of 119°C. Exhaust gases at temperatures of 430°C–650°C are typically used for steam production. HRSGs extract heat from the hot flue gases by convection or radiation, or both, and the water is pumped to sufficiently high pressure to produce high-pressure steam.

Bang-Møller et al. [22] examined the combination of the SOFC stack with a microgas turbine to produce combined power and heat. The fuel feedstock was obtained from gasifying the biomass and the energy balance depicted in a Sankey diagram (Fig. 2.4).

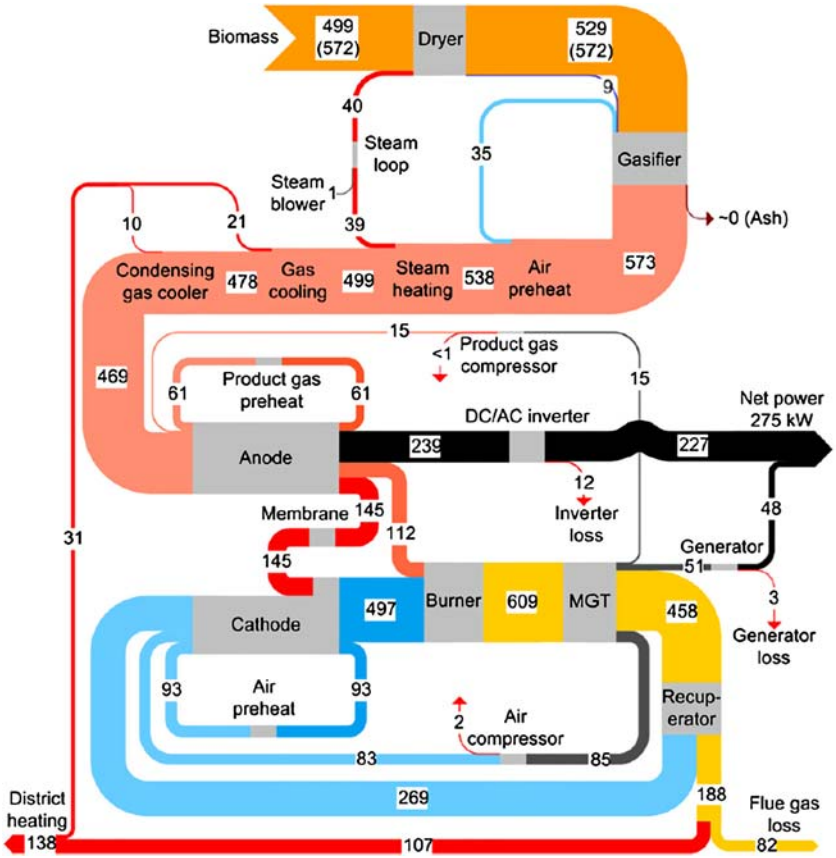

FIGURE 2.4

Sankey diagram of the energy flows (values in kW) in the reference case. The wet and dry biomass flows are evaluated using lower heating values in the illustration (values on a higher heating value basis written in parentheses) [22].

The energy flows over the entire process flow diagram shown in the Sankey diagram are very clearly marked at each stage of the process. The input biomass has an LHV of 499 kW, while the electrical power generated by the SOFC stack is 275 kW (about 55% efficiency, based on the First Law). From the First Law type of calculation it follows that 45% of the enthalpy is given off as heat out of which about 138 kW is used for heating. That leaves 82 kW of heat lost via flue gas and another 4 kW lost elsewhere within the process. The loss of 82 kW in flue gas is only an apparent inefficiency as any further usage of this low-grade heat appears to be the only way to improve the process efficiency. Therefore Bang-Møller et al., effectively pointed out the value of using exergy as a more

meaningful Second Law basis calculation. The exergy data is discussed later on in the chapter.

Arsalis [23] showed process calculations for SOFC−GT−ST (HRSG). The gas and steam turbines with HRSG (an example of a bottoming cycle) can maximize overall plant efficiency. The first part of the plant is the SOFC with the fuel compressor, followed by a gas turbine. The temperature of operation of the SOFC is about 1000°C, which allows for successive bottoming cycles. Steam-to-carbon ratios, pressure, fuel utilization, and SOFC operating temperatures were key parameters for SOFC stacks. The second part of the plant [23] is the HRSG, which is implemented in up to 3 pressure stages as seen in many commercial plants, described earlier [31]. The number of pressure stages is also a design parameter, for example, 1 or 2 or 3 stages, or another 3-stage configuration with reheating between stages. Arsalis [23] estimated efficiencies and costing results for all these configurations.

The final performance efficiencies were calculated (using MATLAB simulations) assuming seasonal variations in load demand, which are compartmentalized within times and then averaged out over the full year, as described by Eq. (2.17). Considering seasonal variations, time-averaged efficiency is evaluated as:

$$\eta_{\text{tot}} = \sum_i \frac{\dot{W}_i \Delta t_i}{\dot{Q}_H \Delta t_i} \tag{2.20}$$

where, $\dot{W}_i$ is the power output for that period of time (Δt_i) and corresponds to either 25%, 50%, 75%, or 100% loads and $\dot{Q}_H$ is the heat supplied in terms of total LHV and flow rate of the fresh fuel.

Arsalis [23] summed up the ratio of the work done to the heat input, over the ith interval where each interval has a certain load factor (i.e., 25%, 50%, or 75% of 100% load). Given Δt_i, the time duration of the i^{th} interval, this equation provides a yearly average of overall efficiency, which is about 60% with small variations. This type of efficiency analysis is still based upon the First Law definition. However, an efficiency of about 68% has been simulated for the case of a 10 MWe SOFC−GT−ST hybrid cycle with a triple pressure with reheat HRSG. For such SOFC hybrid plants, fuel utilization plays a key role as well—a maximum efficiency is reached with a fuel utilization of 85%. This indicates that the more the fuel utilization in the stack the more the power is generated with higher efficiency, although very high fuel utilization causes severe fuel dilution and lowering of performance, thereby leading to efficiency loss (Fig. 2.5).

Haseli et al. [24] discussed a SOFC−hybrid operating at 1000°C with a conventional gas turbine configuration. In addition to a First Law assessment (material and energy balance) they have also carried out a Second Law analysis of the cycle (entropy generation). The latter method attempts to proportion the total irreversibility among the individual components of the entire process. Entropy generation calculations are carried out for each component and added up for the process as a whole. Parametric studies investigating the effect of the compression

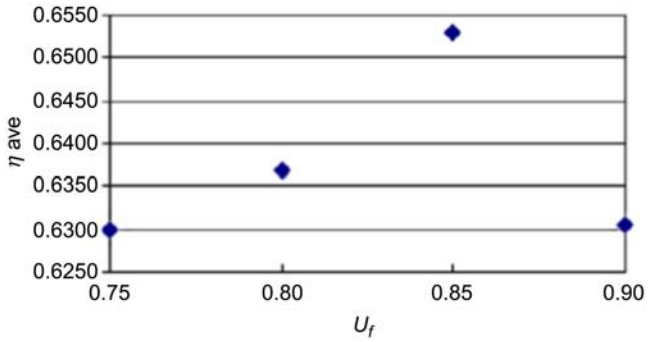

FIGURE 2.5

Variation of First Law efficiency with stack fuel utilization [23].

ratio in the gas turbine and the effect of turbine inlet temperature (TIT) on the irreversibility are also discussed.

The fuel supplied is methane and it is assumed to undergo internal reformation to syngas (the flow of steam is, however, not shown in the flow diagram, but it can be assumed that the fuel supply could well be a fuel−steam mixture) that undergoes electrochemical oxidation. Electrochemical oxidation of methane is also considered as a possible route toward the conversion of the latter and is included in the simulation software. There is no anode recycling in this process. Moreover a small part of the methane supply bypasses the SOFC stack and is fed to the combustor (also known as the after-burner or in some cases the tail gas oxidizer) to ensure that significant heat is available for the gas and power turbines at sufficiently high pressure.

The $T-S$ diagram of the GT−SOFC cycle (Fig. 2.6) is a good representation of the irreversibility occurring in the SOFC−GT assembly. The stages identified in the $T-S$ diagram are correlated with the nodes in the process flow diagram shown in Fig. 2.3. Although air as a working fluid undergoes compositional differences and is not conserved the paths from 1 through to 8 are good representations of entropy changes vis-à-vis temperature, and for a full estimate of entropy generated for all the equipment used in the process. Effective work was done only in sections 3−4, and 5−7 of Figs. 2.3 and 2.6, although part of the expansion work in 5−7 is consumed to counter the work done by the compressor in nodes 1−2. The process flow diagram in Fig. 2.3 is elementary in the sense that it does not show steam generation for the fuel internal reformation nor does it show the preheat of the fuel. Nevertheless the approach is useful since there is a direct illustration of thermodynamic cycles in a $T-S$ diagram.

Haseli et al. [24] did a component-by-component energy and entropy balance (i.e., compressor, turbines, SOFC, recuperator, and combustor) (Fig. 2.7).

All entropy terms can be added now (i.e., summing up the entropy) for each equipment or process occurring in the SOFC plant and simplifying the mass flow

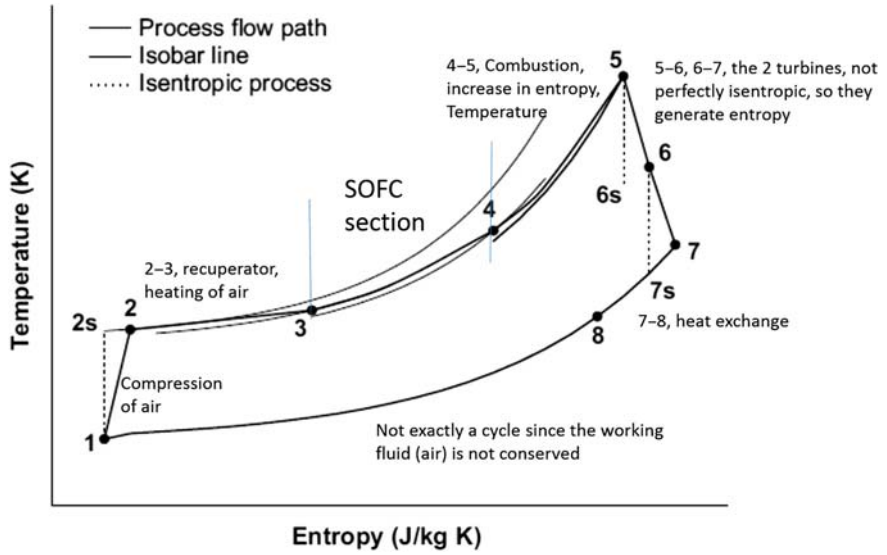

FIGURE 2.6

T–S diagram of a solid oxide fuel cell (SOFC) stack–gas turbine cycle used in Fig. 2.3 [24].

terms (viz., $\dot{m}_1 = \dot{m}_2 = \dot{m}_3$) and with the other set of terms (i.e., $\dot{m}_5 = \dot{m}_6 = \dot{m}_7 = \dot{m}_8$; and $\dot{m}_{\text{fuel}} = \dot{m}_{\text{fuel,FC}} + \dot{m}_{\text{FC,comb}}$) in place a final expression for entropy generation across the entire plant can be formulated as shown in Eq. (2.21).

$$S_{\text{Gen}}^{\text{Cycle}} = \dot{m}_8 s_8 - \dot{m}_1 s_1 - (\dot{m}s)_{\text{fuel}} - \frac{\dot{Q}_{\text{comb}}}{T_{\text{comb}}} + \frac{\dot{Q}_{\text{Loss}}}{T_{\text{Sink}}} \tag{2.21}$$

This expression is a consequence of lumping together all individual components together as a system boundary, as is usually done to formulate entropy generation in a system vis-à-vis the surroundings (Fig. 2.8).

The process simulation software that calculates the individual compositions of the streams and their overall enthalpies and entropies can thus make estimates of the entropy generations as a function of certain parameters such as the compression ratio of the compressor (r_p) and TIT (Fig. 2.9A and B). The latter is also connected with the fuel utilization in the stack and is, therefore, an important parameter.

The TIT is a function of the adiabatic flame temperature of the combustor or after-burner downstream of the SOFC stack. The lower the TIT the higher the overall plant efficiency, which suggests that if the fuel utilization is lower the TIT will be higher, but efficiency will also be lower, namely higher irreversibility, despite leading to higher power output.

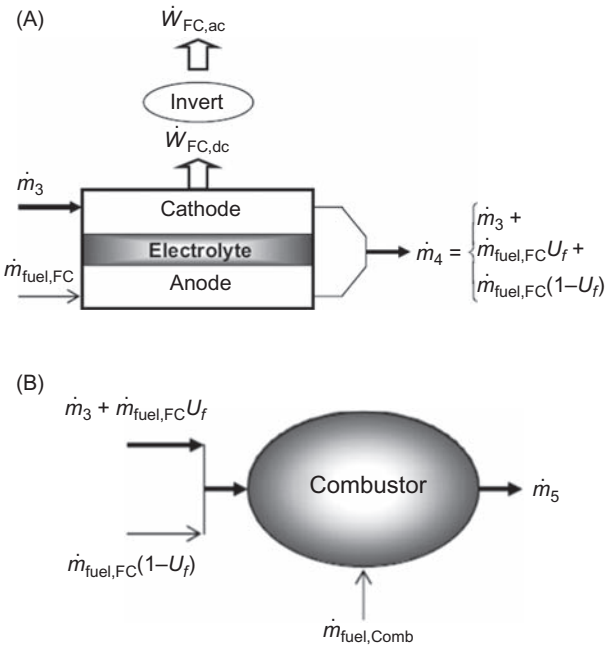

FIGURE 2.7

(A) Schematic of solid oxide fuel cell section with inlet and outlet flows [24]. (B) Schematic of post-solid oxide fuel cell combustor section with inlet and outlet flows [24].

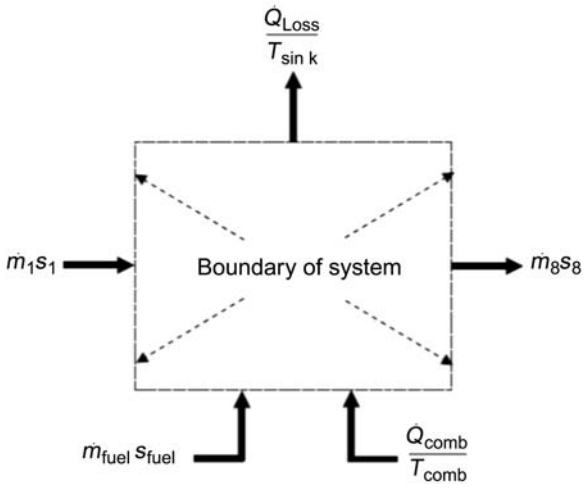

FIGURE 2.8

Entropy balance schematic of overall control volume for the gas turbine–solid oxide fuel cell cycle [24].

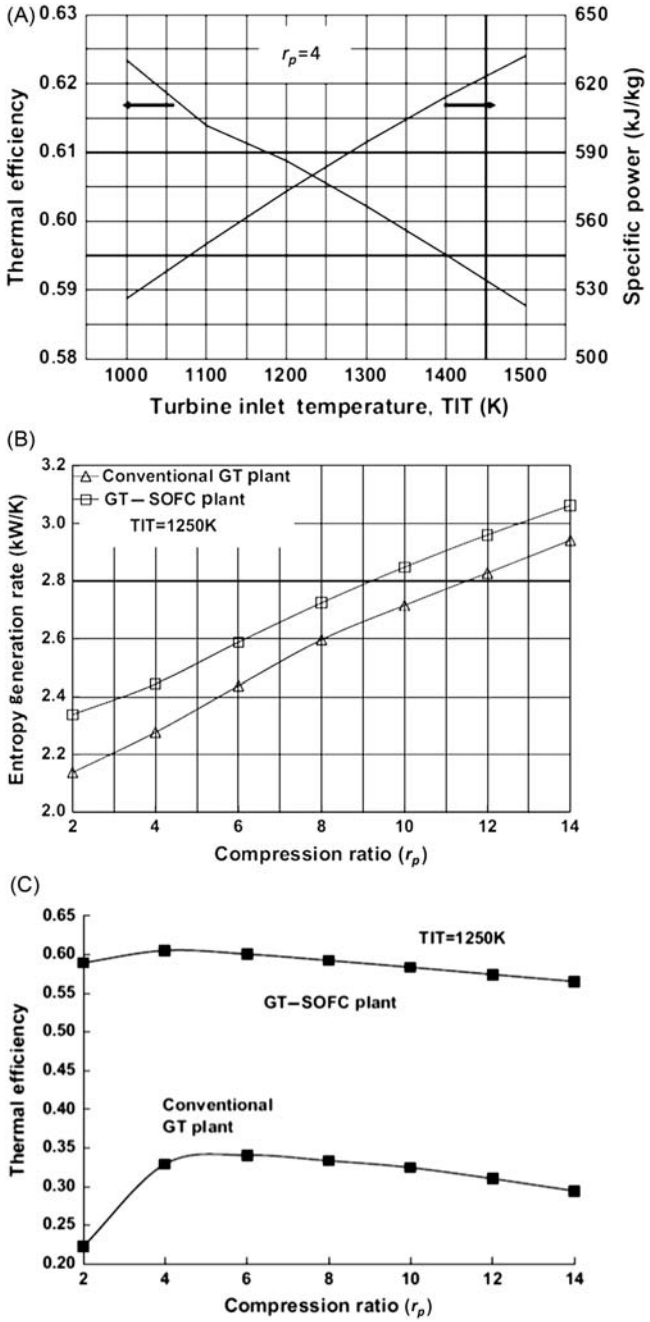

FIGURE 2.9

(A) Effects of turbine inlet temperature (TIT) on the thermal efficiency and specific power input of a gas turbine–solid oxide fuel cell (GT–SOFC) plant of Fig. 2.3 using a compression ratio of 4 [24]. (B) Comparison of the entropy generation rate versus the compression ratio for a gas turbine plant with and without the SOFC [24]. (C) Comparison of the thermal (electrical) efficiency at various compression ratios between a GT plant with and without a SOFC stack [24].

Additionally entropy generation is enhanced with compression ratio and is higher for a GT−SOFC hybrid plant than for a GT plant on its own. However, Fig. 2.9C reveals superior performance of the GT−SOFC hybrid in the form of thermal efficiency, which is higher for most compression ratios than the corresponding GT alone plant. Therefore given the seemingly misleading results of higher entropy production and yet resulting in higher efficiencies the exergy destruction analysis may be more revealing as a way to compare cycles under various parametric variations.

In another configuration by Rokni the SOFC stack is integrated with a Rankine cycle [20] using a HRSG (Fig. 2.10A and B), discussed earlier, and in another set with a Stirling cycle [21,30]. The Rankine cycle−SOFC stack operates using natural gas as feedstock [20], while the Stirling cycle−SOFC stack has been investigated for many fuels (viz., natural gas, methanol, ethanol, dimethyl ether (DME) [21]) and with the biomass gasified effluent syngas.

Rokni [20] simulated an SOFC−Rankine hybrid cycle wherein two different methods for fuel processing were used, one with adiabatic steam reformation (ASR) (Fig. 2.10B) and one with a catalytic partial oxidizer (CPO) (Fig. 2.10A) in order to evaluate the thermodynamics of each process configuration. From a practical standpoint, in case of high-pressure operations generally used in SOFC−GT combines there are material degradation and safety issues; therefore, the SOFC stack with Rankine cycle (HRSG) offers a safer and lasting solution, providing good combined cycle efficiencies.

The simulations in Rokni's work were carried out using an inhouse software tool called dynamic network analysis (DNA), which computes thermodynamic calculations. The key aspects of this software include equations of state models for fluids, numerical solvers for differential and algebraic equations, and a detailed library for component calculations (e.g., heat exchangers, dryers, burners, etc.). Rokni [20,21,30] used the DNA software extensively for all the system calculations reviewed. The methodology is essentially to solve the mass and energy balance for all components across all equipment, including heat losses from components.

The HRSG configuration entails preheating of the incoming air to the SOFC stack by the off-gases from the HRSG. Rokni [20] focused on this and examined its effect on plant efficiencies. The simulation of the SOFC−Rankine cycle hybrid was discussed earlier with reference to the anode outlet composition calculations using the Gibbs free energy minimization method. The same method is also used for prereformer calculations, assuming outlet equilibrium. Rokni used the same Gibbs free energy approach for his calculations for all the systems investigated.

The after-burner exhaust following the SOFC stack provides high-quality heat and is now passed through an HRSG and achieved in three stages, namely (1) the economizer, which heats the pressurized water to the steam temperature, followed by (2) the evaporator that converts the liquid to vapor, and then (3) the super

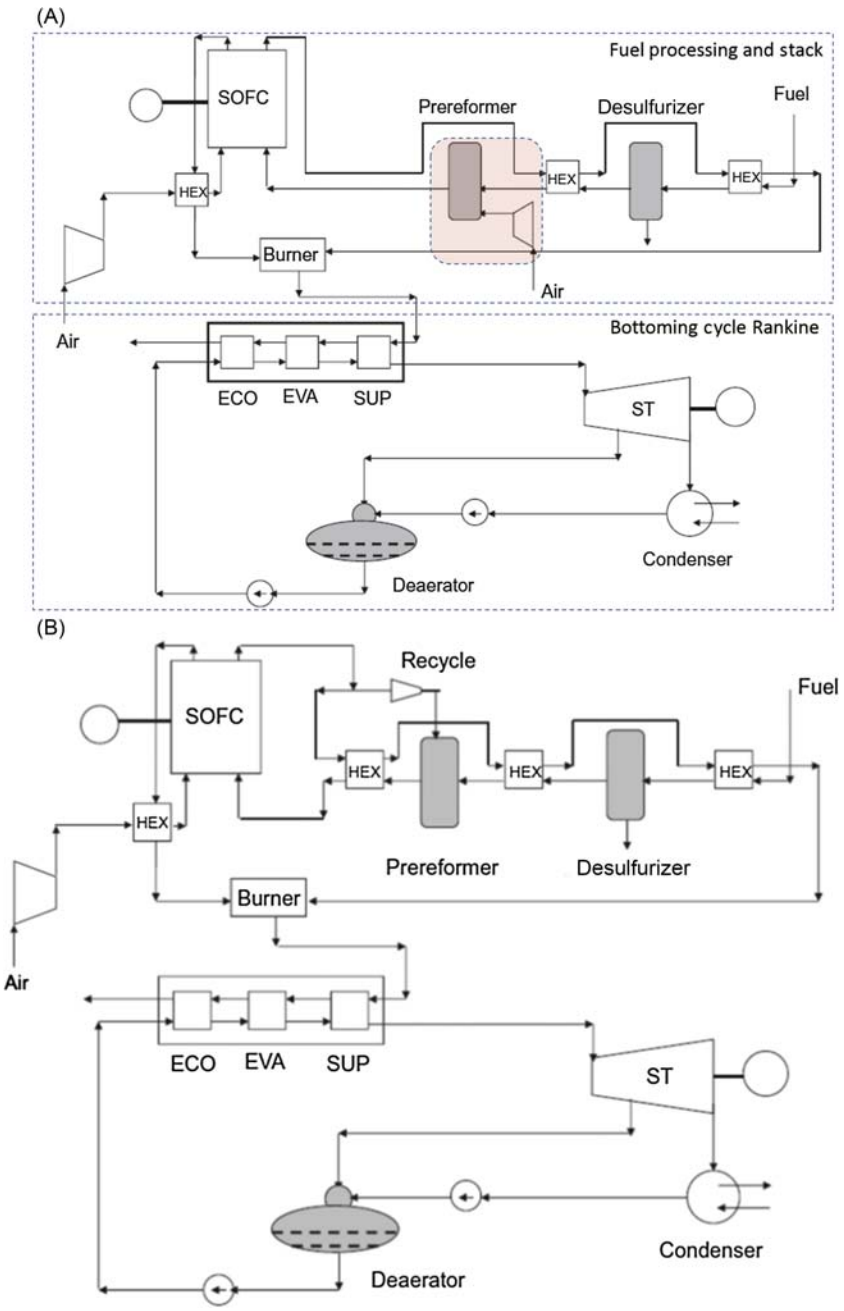

FIGURE 2.10

(A) Combined solid oxide fuel cell–steam turbine (SOFC–ST) cycle plants with catalytic partial oxidation reformer; bottoming cycle and Rankine cycle with a single pressure level [20]. (B) Combined SOFC–ST cycle plants with adiabatic steam reformer; bottoming cycle and Rankine cycle with a single pressure level [20] . ECO, Economiser; EVA, Evaporator; SUP, Superheater; HEX, Heat Exchanger.

heater (SUP). These three stages were described earlier [31] and by van Biert [19] as key elements of a modern HRSG unit.

The power generated is calculated as follows. As discussed earlier the thermodynamic efficiency as well as the voltage efficiency and fuel utilization are all lumped together and represented as the overall efficiency term.

$$\text{Electrical power production, } P_{SOFC} = \eta_{Rev}\eta_V U_f[\text{LHV}_{H2}.\dot{n}_{H2,in} + \text{LHV}_{CO}.\dot{n}_{CO,in} + \text{LHV}_{CH4}.\dot{n}_{CH4}]$$

which is in effect Eq. (2.14) rewritten. Since this process configuration uses external partial reformation the fuel entering the stack has an equilibrium mixture of H_2, CO, and CH_4.

Evaluation of the overall efficiency of an integrated system can be done by combining individual stages (i.e., the SOFC stack and the HRSG steam turbine). An effectiveness term for the HRSG unit is also used in this calculation, defined as:

$$\varepsilon_{HRSG} = \frac{T_{HRSG,in} - T_{HRSG,out}}{T_{HRSG,in} - T_{Air}} \tag{2.22}$$

where ε_{HRSG} is the effectiveness factor for the HRSG.

The overall efficiency (η_{Th}) is therefore:

$$\eta_{Th} = \eta_{SOFC} + \eta_{ST}\left(1 - \eta_{SOFC}\right)\varepsilon_{HRSG} \tag{2.23}$$

where the steam cycle efficiency is formulated as:

$$\eta_{ST} = \frac{\text{Power from steam cycle}}{\text{Heat available through HRSG}} \tag{2.24}$$

In a comparative assessment of the ASR versus the CPO the simulation shows slightly higher efficiencies of the overall plant (Table 2.1) with CPO prereformation. Refer to Fig. 2.10A and B for the corresponding process configuration. One of the characteristics for the CPO is that the off-gases are at a higher temperature, which means that the feeding temperature for the Rankine cycle (steam turbine) is higher. This is to be expected because the CPO is an exothermic process while the ASR is endothermic. This will result in higher power from the steam cycle and slightly higher energy efficiency as shown in Table 2.1.

The key changes in configuration reveal a very small increase in overall thermal efficiency (term used by the author; it is important to clarify that this means electrical efficiency since it relates to the total power produced) for the CPO system vis-à-vis the ASR system. The fuel dilution incurred due to CPO prereformation is somewhat offset by the anode recycle in the ASR configuration, which provides similar dilution of the fuel feed. Consequently the efficiency of the SOFC stack alone is a mere 1% higher for the ASR. The average stack temperatures are in the region of 750°C and if one were to increase them to about 800°C the efficiencies for all stages will be enhanced further. From a practical point of view higher temperatures do pose greater harm to the stack components in terms of materials degradation (e.g., seals, Cr-poisoning), most so for planar SOFCs.

Table 2.1 Comparison of catalytic partial oxidizer (CPO) prereformation versus adiabatic steam reformation (ASR) [20].

Stream, variable	CPO prereformer configuration	ASR prereformer configuration
Heat recovery steam generation (HRSG) gas side inlet temperature (from after-burner) (°C)	526.3	455.6
HRSG gas side outlet temperature (from after-burner) (°C)	218.2	232
Steam turbine inlet temperature (°C)	496.3	425.6
Steam turbine pressure (bar)	69.97	59.97
Steam turbine inlet mass flow (kg/s)	6.33	5.47
Overall plant power output (MW)	38.03	36.72
Power output from solid oxide fuel cell (SOFC) cycle only (MW)	31.04	31.23
Power output from steam turbine cycle only (MW)	6.99	5.49
Efficiency of the SOFC stack alone (%)	51.4	52.4
Overall thermal efficiency (electrical), lower heating value basis (%)	63	61.7

In the same work Rokni [20] added a level of complexity to the process by introducing cathode air preheating. The author emphasized that the HRSG gas outlet temperature is still high (i.e., 218°C−232°C) and wanted to use this further for preheating the inlet cathode air. The end result is that the HRSG gas outlet temperatures may be brought down to as low as 90°C with very little consequence to the SOFC power generated and the SOFC efficiency compared to the earlier configurations. However, the steam turbine power output is enhanced, thereby raising the overall power output and efficiency to about 68%. Table 2.2 shows the changes in the values for this configuration.

The plant efficiency, steam turbine process efficiency, and the SOFC stack efficiencies for CPO and ASR cases may be evaluated as a function of fuel utilization in the stack in the range from 72% to 82%. The general conclusion is that the overall hybrid plant efficiencies decreased with increased SOFC stack utilization, probably indicating that the Rankine cycle is more sensitive to the stack fuel utilization and that the loss of fuel for the HRSG influences the power generated in the latter.

Rokni [21] used another bottoming cycle attached to an SOFC stack (i.e., the Stirling cycle) while keeping the overall plant power production at 10 kW with a variety of fuels. The hybrid process comprises the after-burner, which combusts the unconverted fuel from the anode. The after-burner is now a part of the Stirling engine (1−5 kW), which is a combination of 2 isochoric and 2 isothermal steps as discussed in various thermodynamics textbooks [1−4]. The Stirling engine combustor is cooled by circulating water, for example, in a domestic household.

Table 2.2 Catalytic partial oxidation (CPO) prereformation versus adiabatic steam reformation (ASR) [20].

Stream, variable	CPO prereformer configuration	ASR prereforming configuration
Heat recovery steam generation (HRSG) gas side inlet temperature (from after-burner) (°C)	526.3	455.6
HRSG gas side outlet temperature (from after-burner) (°C)	218.2	232
Steam turbine inlet temperature (°C)	496.3	425.6
Steam turbine pressure (bar)	69.97	59.97
Steam turbine inlet mass flow (kg/s)	6.33	5.47
Overall plant power output (MW)	41.06	40.34
Power output from solid oxide fuel cell (SOFC) cycle only (MW)	30.92	31.03
Power output from steam turbine cycle only (MW)	10.14	9.21
Efficiency of the SOFC stack alone (%)	51.2	52.3
Overall thermal efficiency (electrical), lower heating value basis (%)	68	67.7

In this work SOFC stacks are powered using not only natural gas but also ammonia, DME, methanol, and ethanol [21]. For DME, methanol, and ethanol a "methanation reaction" integrated with steam reformation wherein conversion of syngas (from reformation) to methane occurs and is included as well in the fuel utilization. Ammonia does not require any fuel processing. Keeping the feed mass flow rate constant during the variation of fuel utilization from 75% to 80%, the power from the bottoming cycle increases with a decrease in fuel utilization in the SOFC stack since more fuel is now burnt in the combustor. Net efficiency from the plant increased with the decrease in stack fuel utilization (except in the case of ammonia) just as observed in the earlier simulation [20].

On the other hand, increase in stack operating temperature increases overall efficiency due to the complex interplay of various phenomena; lowering stack temperature is linked with lower fuel utilization due to lower electrochemical kinetics. Lowering stack temperature also entails adjustment in the temperature of the prereformer, which, in turn, may affect the extent of prereformed or methanated feed fuel. If the overall fuel utilization in the stack is lowered because of these factors the quantity of unconverted fuel available for the combustor is higher and the power produced via the Stirling cycle may be more, which could lead to increased plant efficiency.

Using the energy and mass balances calculated by a process Table 2.3 shows the variations in the process using the Stirling cycle and the appropriate modifications in fuel processing for the various types of fuels used.

Table 2.3 A hybrid plant operating at 10 kW total electrical power output with fuel utilization = 80% [21].

Parameter	NG fuel, catalytic partial oxidizer (CPO) (fuel processing)	Dimethyl ether fuel	Ethanol fuel	Methanol fuel	Ammonia
		(Adiabatic steam reformation/ methanation) and partial recycling			Only preheated
Fuel flow (kg/h)	1.33	2.13	2.15	3.06	3.34
Airflow (kg/h)	58.44	60.82	52.09	71	58.71
CPO/meth, inlet temp (°C)	525	300	300	300	N/A
CPO/meth, outlet temp (°C)	650	595	528	566	N/A
Burner outlet temp (°C)	1256	1304.8	1346.9	1200.1	1152.2
Stirling outlet temp (°C)	632.8	635.2	637.4	630.0	627.6
Stirling power (kW)	1.105	1.177	1.121	1.121	1.062
Parasitic power consumption (kW, air blower)	0.131	0.135	0.116	0.158	0.135
Net solid oxide fuel gas (SOFC) power output (kW)	8.895	8.823	8.879	8.879	8.938
Thermal efficiency, lower heating value (%)	59.03	58.58	62.62	59.04	57.89
SOFC plant efficiency (%, Stirling is constant at about 26.1%)	52.5	51.7	55.6	51.9	51.8

The efficiency of an SOFC plant operating on ethanol is shown to be the highest owing to the lowest airflow in the cathode, which results in the lowest consumption of parasitic power (via the air blower). Much of the data is dependent upon SOFC polarization models; however, it shows the strong dependency of overall performance on fuel utilization and the various interrelated parameters, as discussed above.

Going one step further [30] a biomass gasification plant is integrated with the SOFC stack and the Stirling cycle as shown in Fig. 2.11.

The anode exit gas composition and the methanator exit compositions were established using Gibbs free energy minimization as done in an earlier work by

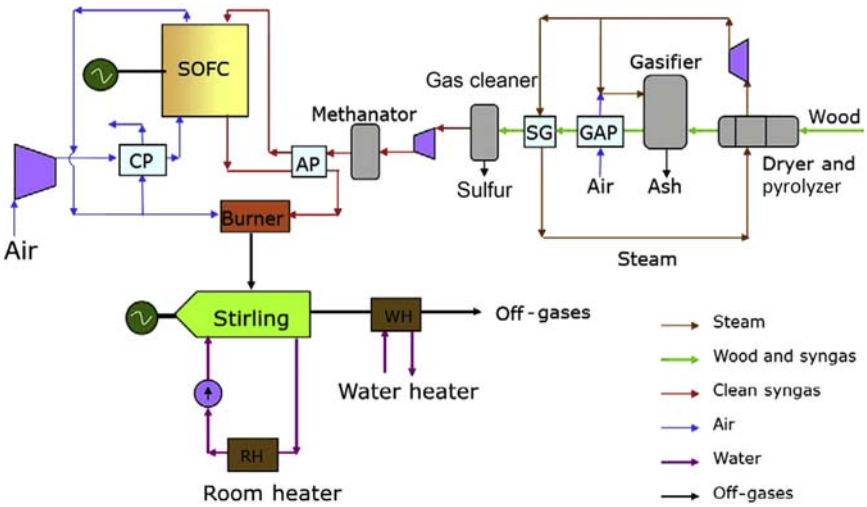

FIGURE 2.11

System layout for integrated biomass gasification, solid oxide fuel cell (SOFC) stack and Stirling cycle as the bottoming cycle with combined heat and power output [30]. CP, Cathode Preheater; AP, Anode Preheater; GAP, Gasifier Air Preheater; SG, Steam Generator.

the same author. In this work [30] Rokni also carried out an economic analysis in addition to the energy balance and efficiency calculations for the plant; however, this is beyond the scope of this chapter. For a plant of 120 kW electrical power output the calculations for an SOFC fueled by wood chip biomass yield a First Law efficiency of only 41% for the full plant partly because of the quality of the fuel syngas, which comprises a large proportion of diluents.

In summary, in several of the above examples in combined cycles, notwithstanding the fundamental representation of the electrochemistry via the Butler–Volmer equation, the emphasis has been on calculations of plant efficiency based on the considerations of the First Law. There have been some examples wherein entropy changes were calculated step-by-step in each node of a combined cycle process and added up to give a measure of the overall entropy generation in the power plant. In Section 2.8 case studies that show the usage of exergy and the Second Law of thermodynamics for determining the efficiency of SOFC or SOFC–hybrid systems are presented.

2.8 The exergy approach (Second Law) for estimating irreversibility in processes

Throughout this chapter so far various configurations were analyzed and showed how SOFC operating parameters like fuel utilization (U_f), stack operating

temperature, extent and type of prereformation, anode recycling, along with other parameters such as gas turbine compression ratio (r_p) and TIT together affect the electrical efficiency based on the First Law of thermodynamics. In this section the emphasis is on the cumulative exergy utilization for the whole process obtained by making exergy balances for each element of the process. The notion of exergy was introduced and in the case of the SOFC stack, prereformer, and combustor both *physical* and *chemical exergies* need to be considered since there are compositional changes. However, for heaters, turbines, and compressors physical exergy numbers are enough. To recap, exergy is the extent of departure of a system in its existing state from a reference state and it represents the "potential" for performing work by the system. Every time work is done (i.e., electricity is generated) part of the exergy is utilized and part of it is destroyed. By controlling the irreversibility (exergy destruction) in devices like SOFC stacks, it is possible to evaluate an optimal target for utilization of available exergy.

In this section a few examples are discussed where energy and entropy balances and notably exergy terms are formulated. The main objective is to study methods by which irreversibility under operating conditions is accounted for so that it may be minimized.

The physical exergy may be written as [16,30]:

$$E_{\text{Phy},n} = (H_n - H^o) - T_o(S_n - S^o) \tag{2.25}$$

where the subscript "n" refers to the stream number or node number in the nomenclature [17]. This term is inclusive of each of the components in the stream (e.g., CO, H_2, CO_2, etc.).

Chemical exergy is formulated by [29]:

$$e_{\text{Chem},n} = \sum\nolimits_i x_i E_{o,i} + RT_o \sum\nolimits_i x_i \ln[x_i] \tag{2.26}$$

where x_i is the mole fraction of component "i"; $E_{o,i}$, is the specific exergy of the component "i" at standard conditions—standard (reference) environmental conditions are usually 298.15K (T_o), and 1.013 bar (P_o). All individual exergies need to be summed up in the proportion of their molar fractions to obtain a specific exergy value, e_{Chem} (J or kJ/mol), which is then multiplied by the total molar flow rate for the stream (N_n) of interest $E_{\text{Chem},n} = N_n\ e_{\text{Chem},n}$, and added to the physical exergy.

In Chan et al. [17] exergy computations for the SOFC standalone plant operating on methane for each stream were done using the above formulae. Two different types of efficiencies were computed (First Law-based efficiency calculated to be 62%, and Second Law-based efficiency at about 60%). The key difference between the First Law and Second Law was attributed by Chan et al. [17] to the fact that the chemical exergy of the fuel is higher than its corresponding LHV.

For a hybrid allothermic biomass gasification process integrated with a SOFC stack, exergetic calculations were carried out by Panopolous et al. [29]. Since the heat available in each stream has enough exergy to perform work, another way of

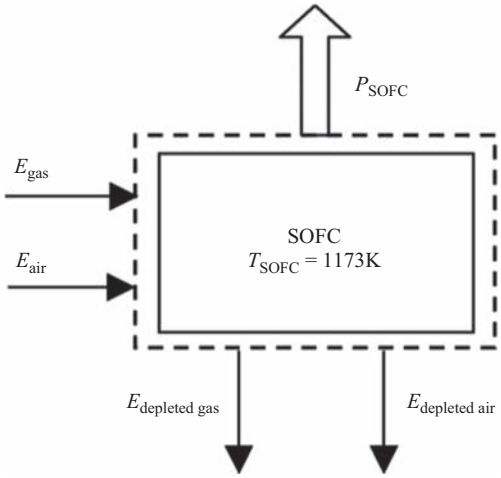

FIGURE 2.12

Control volume for solid oxide fuel cell (SOFC) stack of the flowsheet in Fig. 2.12 [29].

estimating the latter is to use the Carnot efficiency. Exergy of each heat stream in the flowsheet can be calculated based on a Carnot factor relative to a sink temperature, T_o, since heat, Q, is available for work and Carnot efficiency represents the maximum potential for work (which is, in effect, the exergy) and thus exergy for any process in that stream is computed.

For material streams the exergy values will include the chemical exergies and will apply to units like SOFC stack, prereformers, and combustors. The equation can be thus rewritten for exergy changes in the heat streams (physical exergy) and the exergy for changes in the material streams (chemical exergy). A full balance of the chemical and physical exergies executed in this manner gives an estimate of the overall exergy utilization [29]. For the SOFC stack alone Panopolous et al., conducted an exergy balance by making the former the control volume (Fig. 2.12) and using the Aspen Plus software tool for processing the heat and mass balance. FORTRAN codes are used to solve the electrochemical models and equations (e.g., Butler−Volmer equation). The operating temperature of the SOFC was 900°C with the off-gas from the stack going into a secondary fixed-bed combustor (Fig. 2.13). Being an allothermic biomass gasification reactor the heat from the fixed-bed combustor is used for the gasification of biomass.

The overall exergy balances for heat streams and material streams are expressed as [29]:

$$\left[\sum_{\text{IN}} E_j + \sum_{\text{IN}} E^{Q}{}_{T_{\text{IN}}}\right] - \left[\sum_{\text{OUT}} E_k + \sum_{\text{OUT}} E^{Q}{}_{T_{\text{OUT}}}\right] - I = \sum_{\text{OUT}} E^{\text{Work}} \tag{2.27}$$

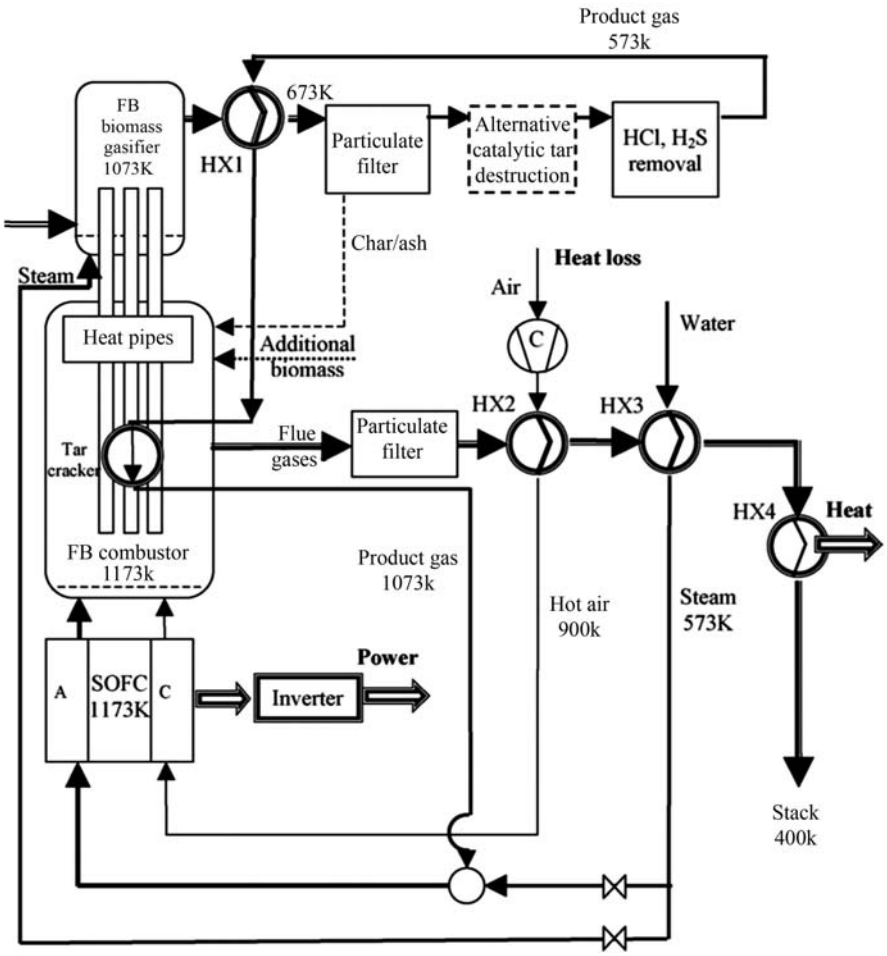

FIGURE 2.13

Flowchart of the combined solid oxide fuel cell (SOFC) or allothermal biomass gasification power plant where biomass gasification acts like the bottoming cycle [29].

This expression consists of the exergy flows in and out (material and energy flows [denoted by a superscript Q]). The term I, refers to the exergy "losses" due to energy dissipation and/or material losses. The right-hand side output power produced by the process is the control volume.

The electrical efficiencies for the SOFC based on the Second Law of thermodynamics (i.e., based on the exergy of the material streams) is:

$$\eta_{\text{exer,Elec}} = \frac{P_{\text{SOFC}}}{\text{Exergy}_{\text{Fuel}} + \text{Exergy}_{\text{Air}}} \tag{2.28}$$

Calise et al. (SOFC−GT hybrid) [25] assumed the equilibrium for the steam reformation and WGS reactions with hydrogen being the only fuel undergoing electrochemical oxidation. The exergy formulations for the SOFC stack are:

$$\{\left[\dot{n}_{\mathrm{In}}e\tilde{x}_{\mathrm{Chem,in}}+\dot{m}_{\mathrm{In}}ex_{\mathrm{Phys,in}}\right]-\left[\dot{n}_{\mathrm{Out}}e\tilde{x}_{\mathrm{Chem,out}}+\dot{m}_{\mathrm{Out}}ex_{\mathrm{Phys,out}}\right]\}_{\mathrm{Anode}}$$
$$+\{\left[\dot{n}_{\mathrm{In}}e\tilde{x}_{\mathrm{Chem,in}}+\dot{m}_{\mathrm{In}}ex_{\mathrm{Phys,in}}\right]-\left[\dot{n}_{\mathrm{Out}}e\tilde{x}_{\mathrm{Chem,out}}+\dot{m}_{\mathrm{Out}}ex_{\mathrm{Phys,out}}\right]\}_{\mathrm{Cathode}}=\dot{E}x_D+V_{\mathrm{cell}}.I \tag{2.29}$$

where, $e\tilde{x}_{\mathrm{Chem,in}}$, molar specific chemical exergy, kJ/mol; $ex_{\mathrm{Phys,in}}$, mass specific physical exergy, kJ/kg; $\dot{E}x_D$, exergy destruction rate, kW.

For a SOFC stack, $\dot{E}x_D$, is the exergy destruction rate to which is added the $V_{Cell}{\cdot}I$, which is the useful work done. This formulation is very much on the lines of Panopolous et al. [29] and given in Eq. (2.27).

Calise et al. [25] demonstrated the difference between the First Law expressions of efficiency [Eq. (2.30)] and the Second Law (exergetic) value [Eq. (2.31)].

$$\eta_{\mathrm{1st\ law}}=\frac{V_{\mathrm{Cell}}\cdot I}{z\cdot\Delta h_{\mathrm{H_2}}} \tag{2.30}$$

where z is the rate of reaction (i.e., hydrogen consumption in the stack).

In Eq. (2.41) the left-hand side of the equation may be written simply as the changes in inlet and outlet exergies for the cathode and anode as $\Delta Ex_{\mathrm{Chem,Anode}}$, $\Delta Ex_{\mathrm{Chem,Cathode}}$, $\Delta Ex_{\mathrm{Phys,Anode}}$, $\Delta Ex_{\mathrm{Phys,Cathode}}$. By adding all the left-hand side terms they can be arranged as $\Delta\mathrm{Exergy}_{\mathrm{SOFC,total}}$ and incorporated into an efficiency term as:

$$\eta_{\mathrm{Exergy}}=\frac{V_{\mathrm{Cell}}\cdot I}{(-\Delta\mathrm{Exergy}_{\mathrm{SOFC,total}})} \tag{2.31}$$

The formulation of exergies is done in the same way as before, that is, by including the chemical and physical exergy of all the components. The full-scale exergy balance of the SOFC stack is done by considering the fuel and the air together and considering the exergy destroyed. As in all cases $V_{\mathrm{Cell}}{\cdot}I$ correlations are obtained using activation polarization Butler−Volmer models, ohmic resistance estimates, and concentration polarization models by considering the effects of fuel dilution along the cell geometry within the stack. After completing material and energy balances, by using a simulation software tool the same type of exergy formulations can be done for all the other unit operations in the hybrid plant.

Without going into the details of the values obtained by the simulation a brief summary of parametric studies on the plant performance is presented here. To begin with, under operating conditions of any equipment maximum exergy destruction occurs in the SOFC stack (compared to heat exchangers, compressors, turbines, combustors, etc.). Calise et al. also obtained trends that show that the higher the fuel utilization in the stack the higher the plant efficiency (including

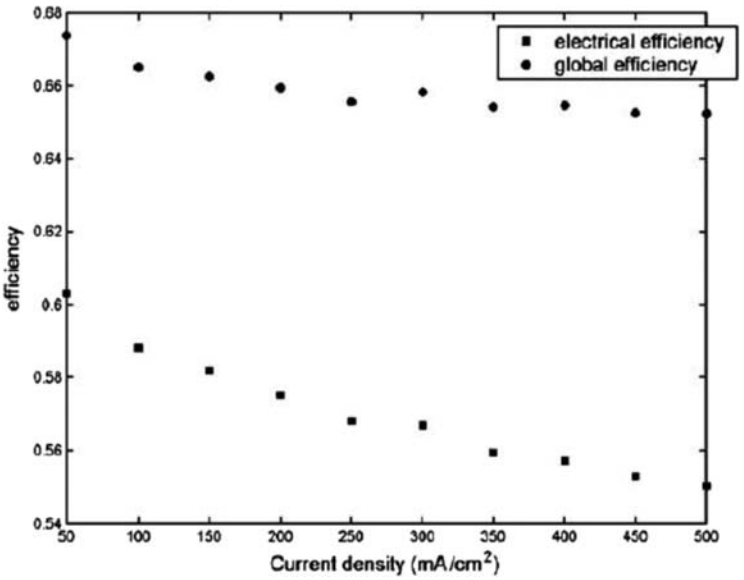

FIGURE 2.14

Plant efficiencies versus current density [25].

efficiency of the SOFC system). This is because, obviously, more fuel is converted via the electrochemical step and, consequently, a smaller amount of fuel is sent to the combustor, allowing less power in the bottoming cycle (gas turbine). This appears to be different from the trends shown by Rokni [19,28], part of which could be explained by different plant configurations. Another important point demonstrated by Calise [25] in Fig. 2.14, is that by operating at lower current densities (higher cell voltage), exergy destruction is reduced, due to lower overpotentials. Therefore in order to ensure maximum fuel utilization, lower current densities and, consequently, higher cell area (and higher capital cost) is the preferred route. The exergetic calculations shown in Fig. 2.15 show the effect of the current density on electrical efficiency and the destroyed exergy.

A similar approach toward the calculation of component-by-component irreversibilities by Bavarsad [27] showed very similar trends (using FORTRAN code and calculating the detailed material and energy balance for a SOFC−GT hybrid with HRSG bottoming cycle). The author also carried out a stage-by-stage exergy balance and identified the irreversibility at each stage (i.e., the exergy destroyed). Given the fact that the maximum power is derived from the SOFC stack it is also logical to expect the maximum exergy destruction from it as well.

A valuable insight from their data is that SOFCs operating toward higher currents invariably lead to more irreversibility. Higher currents would also result in higher power delivered by the stack, but will release more heat (more exergy destruction) in the stack, which will then have to be counter-balanced by higher

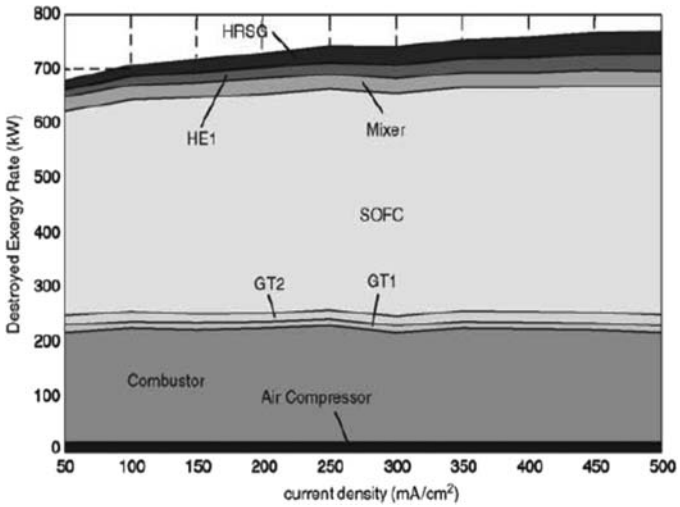

FIGURE 2.15

Local exergy destruction rates versus current density [25]. *HRSG*, Heat recovery steam generation; *GT*, gas turbine; *SOFC*, solid oxide fuel cell.

air flows and, consequently, more parasitic power consumption. Therefore there has to be a balance between system power density and system efficiency.

Motaher et al. [28] analyzed a SOFC−GT hybrid whose performance was enhanced by steam injection (STIG). The SOFC stack encompasses the internal reformation of the fuel and here again hydrogen was considered the fuel for electrochemical oxidation. Here the method used is to estimate the irreversibility at each stage and the SOFC stack performance is simulated in much the same way as discussed earlier (i.e., usage of Butler−Volmer kinetics to estimate polarization).

Motaher et al. [28], defined an exergetic efficiency term, ψ, in the following manner for any unit in the process (i.e., SOFC stack or fresh feed−recycled gas mix or gas turbine):

$$\psi_{\text{unit}} = 1 - \frac{\dot{I}_{\text{unit}}}{\sum \text{Exergy In}_{\text{unit}}} \tag{2.32}$$

where $\dot{I}_{\text{unit}}$ represents the irreversibility (in W or kW) from that unit. In a multicomponent system this term will include a summation of the irreversibilities for each component, which is the resultant exergy defect (input exergies−output exergies from the respective units).

To distinguish between the total system efficiency (First Law basis) and the system exergetic efficiency (Second Law basis), Motaher et al., used Eqs. (2.33) and (2.34). The total work done by the hybrid system is represented as $\dot{W}_{\text{Sys}}$ and in case of the exergetic efficiency the term $(\dot{m}_{\text{fuel}}\varepsilon_f)_{\text{Sys}}$ is used, where $\dot{m}_{fuel}$ is the

rate of fuel consumption and the specific exergy utilized in the process, given by ε_f.

$$\eta_{\text{sys}} = \frac{\dot{W}_{\text{sys}}}{(\dot{m}_{\text{fuel}}\text{LHV})_{\text{sys}}}, \quad \text{which is the 1st law definition of efficiency} \tag{2.33}$$

$$\psi_{\text{sys}} = \frac{\dot{W}_{\text{sys}}}{(\dot{m}_{\text{fuel}}\varepsilon_f)_{\text{sys}}}, \quad \text{which is the 2nd law definition of efficiency} \tag{2.34}$$

As shown in Fig. 2.16 a comparative assessment of the irreversibilities is shown, wherein the authors have demonstrated that STIG configuration with the gas turbine in the GT−SOFC hybrid drastically improves overall exergetic efficiency of the plant to 65.34% (by reducing irreversibilities in the exhaust stream) from 58%, which was achievable with a gas turbine−SOFC hybrid. While the nuances of the STIG are not very relevant to this review there is another clear demonstration that irreversibilities are very high in the SOFC stack and this should serve as a reminder that considerable enhancements in the SOFC stack are necessary to boost the overall systems efficiency (or exergetic efficiency) in hybrid systems.

Among the latest work in this area Van Biert et al. [19] in analyzing the efficiency of several hybrid cycles formulated exergy similarly as:

$$\dot{E}x_{\text{loss}}, \text{exergy loss} = \left[P_{\text{AC,out}} - P_{\text{AC,in}}\right] + \sum(\dot{E}x_{\text{in}} - \dot{E}x_{\text{out}}) \tag{2.35}$$

$\dot{E}x$ is a combination of physical and chemical exergy.

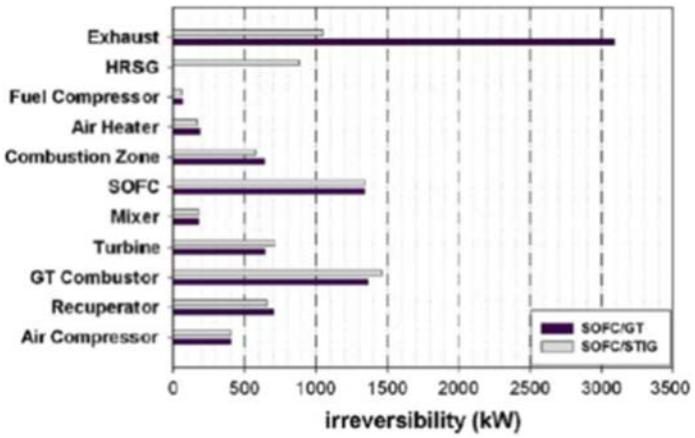

FIGURE 2.16

Comparison of the irreversibility in system components of the solid oxide fuel cell stack−gas turbine (SOFC−GT) base case versus SOFC−GT (steam injected in gas turbine, STIG) system [28].

$$\dot{E}x_{\text{Phys}} = \dot{n} \cdot \{(h - h_o) - T_o \cdot (s - s_o)\} \tag{2.36}$$

$$\dot{E}x_{\text{Chem}} = n \cdot \left\{ \sum\nolimits_j y_i \cdot ex_j + RT_o \sum\nolimits_j y_j \cdot \ln y_j \right\} \tag{2.37}$$

where s is the specific entropy, ex_j, is the specific exergy of component j, and R being the universal gas constant; the subscript "o" indicates the reference environmental conditions and y_i the mole fractions of each component in the stream.

Another term, relative exergy loss, is introduced here, which is based on the exergy of the fuel input to the stack and is not the exergetic efficiency as described earlier.

$$\delta_k = \frac{\dot{E}x_{\text{loss},k}}{\dot{E}x_{\text{fuel,in}}} \cdot 100\% \tag{2.38}$$

Without going into the details of the various hybrid cycles it is instructive to examine the broad conclusions of the SOFC standalone system in light of the exergetic values. First, the system efficiency increases with higher global fuel utilization (700°C stack operation), an observation that is similar to that by Calise et al. [26], for exactly the same reasons discussed earlier (i.e., higher cell voltage, lower overpotentials). The efficiency reported here was 62.7% for a global fuel utilization of 90%. Of course in most SOFC stacks such high fuel utilization may not be practical given the constraints of concentration polarization, particularly in anode-supported cell geometries.

Similarly, relative exergy losses [defined in Eq. (2.35)] obtained at cell operation of 700°C and at a cell voltage of 0.7 V are high for lower fuel utilization (viz., 65%) since the exhaust from the stack still has high exergy. At high fuel utilizations, $\sim$90%, the air that goes to the burner is relatively in excess vis-à-vis the unconverted fuel; hence, more exergy is destroyed in the air preheater due to the high heat duty.

The abovementioned examples show how engineers address the processes considering the exergy footprint and evolve strategies to mitigate exergy destruction. For example, the fuel utilization in the stack may be lowered to an acceptable value and the expected exergy loss mitigated by adding a bottoming cycle.

Exergetic analysis for heavy hydrocarbons with advanced fuel processing

As discussed by Nehter et al. [32], the usage of heavy fuels requires external reformation to the extent that the all higher hydrocarbons be converted to a mixture of methane and syngas. Auxiliary power units (APUs) operating on SOFCs in diesel vehicles (viz., trucks) tend to lower diesel emissions during idling since idling times of trucks operating over long distances is significant. Fuel processing prior to the APU stacks is required and can be done by any of the methods such as steam reformation (SR), catalytic partial oxidation (CPOx, or POx) or autothermal reformation (ATR).

Kang et al. [33] used a surrogate fuel hexadecane ($C_{16}H_{34}$), which is very similar to the average molecular weight of commercial diesel and is a straight chain molecule as most of the diesel fraction is. However, as the authors report, the fuel-processing data for the surrogate molecule is not a good comparison with commercial diesel since the latter has a small proportion of aromatics, which are more refractory toward SR.

The three mechanisms of fuel processing are reviewed as:

SR:

$$C_{16}H_{34} + 32H_2O \rightarrow 49H_2 + 16CO_2; \quad \Delta H = 2336 \text{ kJ/mol}$$

POx:

$$C_{16}H_{34} + 16O_2 \rightarrow 17H_2 + 16CO_2; \quad \Delta H = -5694 \text{ kJ/mol}$$

ATR:

$$C_{16}H_{34} + 16H_2O + 8O_2 \rightarrow 33H_2 + 16CO_2; \quad \Delta H = -1739 \text{ kJ/mol}$$

As the authors mention, ATR can be controlled to be net exothermic or net endothermic by adjustment of the O_2-to-moisture ratio. It offers lower hydrogen yield compared to SR, but higher than POx. Other advantages are the lowered propensity for carbon deposition, which is a vital characteristic for complex fuels. It is interesting to note that by adjusting the ratio of O_2 to fuel and correspondingly the moisture levels, one can obtain the standard ΔH to be 0 kJ/mol (at 298K). A value of $O_2/C_{16}H_{34}$ of 5.78 provides this figure. However, this is obtained using a stoichiometric amount of moisture in the feed. Higher quantities of moisture are needed to suppress coking.

In Fig. 2.17 the authors plot an "efficiency" value of a fuel processing for an ATR system as given by the equation:

$$\text{Efficiency}(\%) = \frac{(\text{Flow rate of Hydrogen produced}) \cdot (\text{LHV of Hydrogen})}{(\text{LHV of fuel}) \cdot (\text{Feed fuel flow rate})} \tag{2.39}$$

Fig. 2.17 shows how at the O_2/C_{16} value of 5.78 a maximum value of efficiency is obtained, which is approximately 91%. This relates to the production rate of hydrogen, which is essential for the input to the SOFC stack in terms of stack performance.

Additionally Kang et al., report from their experimental results [33] that there are nonuniformities within the catalytic bed when ATR is in progress, for example, initially there is stronger tendency towards POx whereas toward the latter part of the bed SR dominates. Therefore there are temperature gradients across the catalyst bed that are not ideal and are not in-keeping with the exact thermoneutral reaction that is expected. This type of nonideality is more in keeping with the kinetics of the competing reactions rather than thermodynamics.

Nehter et al. [32] reported an exergetic analysis of two basic fuel-processing operations and compared them in terms of exergetic efficiency. As mentioned earlier in the chapter, the exergy of a fuel containing stream is equal to the Gibbs free energy calculated with respect to the environmental conditions used as reference, namely ambient temperature of 25°C, 1 bar atmospheric pressure, and a

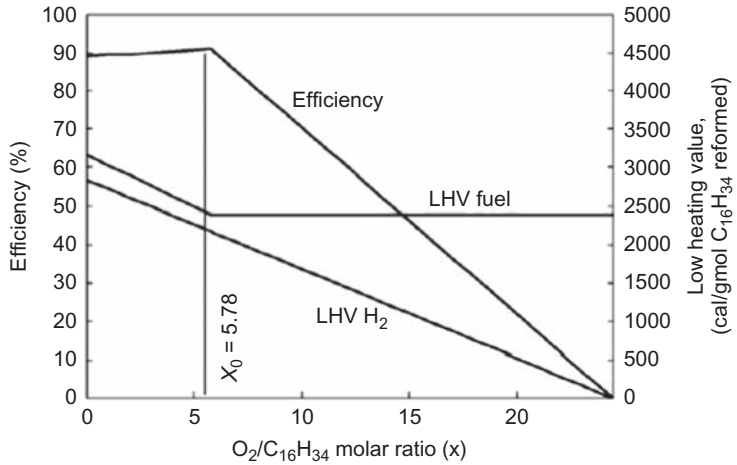

FIGURE 2.17

Thermal efficiency as a function of oxygen to diesel surrogate–fuel ratio [33]. *LHV,* Lower heating value.

standard air composition (N_2, O_2, and rare gases, with CO_2 and moisture at approximately 0.00031 and 0.03171, respectively). Expressions for exergy calculations were discussed earlier in this chapter. With respect to an input stream (e.g., fuel feedstock) whose physical exergy can be calculated as mentioned earlier (E_{in}) an exiting stream is shown to lose part of the exergy based on either work or chemical reactions and, thus, leaves the process with a physical exergy of E_{out}. The exergetic efficiency can be postulated as shown in Eq. (2.40).

$$\eta_{ex} = \frac{E_{out}}{E_{in}} \tag{2.40}$$

However, as per Nehter's nomenclature, the above term (Eq. 2.40) is only the physical exergy efficiency wherein E_{out} and E_{in} are the physical exergy numbers for the fuel entering and leaving the fuel processor, respectively. The chemical exergy term ($\eta_{ex,Chem,FP}$) was considered separately, as (E_{fuel} being the LHV of the diesel surrogate fuel, in this case):

$$\eta_{ex,Chem,FP} = \frac{W_{Rev,SOFC}}{E_{fuel}} \tag{2.41}$$

The reversible work in a SOFC $W_{Rev,SOFC}$ has been calculated as a function of the integral of the Gibbs free energy change as a function of the fuel utilization [FU] (measure of dilution) at the respective temperature of cell operation:

$$W_{Rev,SOFC} = \int_{FU1}^{FU2} \Delta G(T)\mathrm{d(FU)} \tag{2.42}$$

In other words, the chemical exergy, which is equivalent to the reversible work, is now averaged over a range of feedstock dilution.

In this manner the authors have computed the effect of fuel processing on the overall exergetic efficiency for two types of fuel processing approaches; namely SR (500°C and 750°C) and CPO. While the SR consumed heat with a small component of exothermicity induced by methanation, as in the case of 500°C, the CPO released heat due its strong exothermicity. However, chemical exergy is lowered immensely in the case of CPO since about 32% of the diesel is precombusted prior to the SOFC stack. This translates into an overall exergetic efficiency of the SOFC and fuel processing together of about 58%, remaining approximately invariant at both fuel-processing temperatures. Interestingly, the SR−SOFC system showed an overall exergetic efficiency of 86%−87% at both temperatures of fuel processing, which is considerably higher than that for the CPO fuel processor. The analysis shows that despite the high heat available in the case of the CPO and the heat consumption in case of the SR, chemical exergy of the reformate is the deciding factor in the overall exergetic efficiency of the process. These are, of course, thermodynamic efficiencies and do not take into account the overpotentials in the SOFC, but provide a useful upper limit as a function of the choice of fuel processing. A similar analysis is applicable to other fuels as well.

2.9 Summary and conclusion

In this chapter key concepts of thermodynamics as applied to SOFC stacks and systems and SOFC-bottoming cycle hybrid systems are presented. The emphasis here is to understand, after review of several process simulations, how efficiencies of SOFC or SOFC-combined cycles are calculated, initially with the principles of the First Law of thermodynamics, and second, using exergetic concepts and exergy analysis. The general concepts of free energy, reversibility (and, consequently, irreversibility), and entropy as applied to SOFC stacks and associated systems are reviewed via a few select case studies. Since many of the solutions derived from the case studies use advanced software there is not much discussion on each of the material and energy balance solutions calculated. Instead variations in key energetic parameters like electrical efficiency and exergy destruction as functions of fuel utilization, current densities, and process configuration are presented to showcase the current state of the art of thermodynamics and its evolution.

Exergetic formulations and exergetic efficiencies offer a realistic assessment of the performance and effectiveness of all types of engines and equipment for SOFCs, gas turbines, heat exchangers, and combustors. Exergy excludes completely that part of enthalpy that can never be used for work; hence exergetic efficiency only provides a relative value of work accomplished in relation to the maximum work permissible. Therefore exergetic efficiency is based on the

Second Law of thermodynamics and not on the traditional work−enthalpy definition (First Law).

Many of the processes reviewed are simulated using zero-dimensional models. Although a few researchers have combined exergy analysis with finite element modeling there are good possibilities toward integrating exergy and thermodynamics with CFD-type heat transfer (fluid mechanics) electrochemistry in the future, that is, exergy formulation at a differential level.

The hybridization of SOFCs with gas turbines, steam turbines, HRSG, and others serve to enhance both First Law and Second Law (exergetic) efficiencies, but, as shown in many simulations, SOFC stack irreversibilities still play a major. There are many instances reviewed in this chapter that show how SOFC stack performances are limited by high irreversibilities (exergy destruction). Exergy calculations and exergy trends, therefore, indicate a few areas for technological breakthroughs, namely better-performing SOFC cells. These are:

1. Advanced cathodes to lower cathodic overpotentials, for example, higher ionic conductivities, higher electronic conductivities, etc.
2. Multifunctional anodes, which can absorb a higher degree of internal fuel reformation. To facilitate this, catalytic functionalities that are more effective toward CO oxidation in addition to hydrogen oxidation are required.
3. Advanced microstructures for cathodes and anodes that enhance three phase boundaries, thereby leading to lower polarization.
4. Thinner and dimensionally stable electrolytes in addition to combinations with higher ionic conduction leading to lower ohmic polarization. To achieve this there needs to be advanced manufacturing processes that offer precision in dimension in addition to materials compatibility and dimensional stability.

Other major challenges relating to SOFCs, namely degradation of electrodes, chromium poisoning, and cost reduction are independent of thermodynamics or systems analysis, and are the subject of material physicochemical investigations.

References

[1] Y.A. Cengel, M.A. Boles, Thermodynamics - An Engineering Approach, fifth ed., McGraw Hill, New York, 2005.
[2] J.M. Smith, H.C. Van Ness, M.M. Abbott, Chapter 10: Introduction to Chemical Engineering Thermodynamics 7th Ed., 2005, McGraw Hill, Boston, MA.
[3] G. Hoogers, (Ed.), Chapter 3: Fuel Cell Technology Handbook, 2003, CRC Press, Boca Raton, FL.
[4] M.J. Moran, H.N. Shapiro, D.D. Boettner, M.B. Bailey, Chapter 7: Principles of engineering thermodynamics 8th Ed., 2015, Wiley, Singapore.
[5] J.J. Larminie, A. Dicks, Fuel Cell Systems Explained, second ed., Wiley, 2003.
[6] D. Cao, Y. Sun, G. Wang, Direct carbon fuel cell: fundamentals and recent developments, J. Power Sources 167 (2007) 250−257.

[7] F. Calise, M. Dentice d'Accadia, G. Restuccia, Simulation of a tubular solid oxide fuel cell through finite volume analysis: effects of the radiative heat transfer and exergy analysis, Int. J. Hydrogen Energy 32 (2007) 4575–4590.
[8] H. Zhu, R.J. Kee, A general mathematical model for analyzing the performance of fuel-cell membrane-electrode assemblies, J. Power Sources 117 (2003) 61–74.
[9] S.A. Hajimolana, M.A. Hussain, W.M.A.W. Daud, M. Soroush, A. Shamiri, Mathematical modeling of solid oxide fuel cells: a review, Renew. Sustain. Energy Rev. 15 (2011) 1893–1917.
[10] F. Arpino, N. Massarotti, Numerical simulation of mass and energy transport phenomena in solid oxide fuel cells, Energy 34 (2009) 2033–2041.
[11] M. Peksen, A coupled 3D thermofluid-thermomechanical analysis of a planar type production scale SOFC stack, Int. J. Hydrogen Energy 36 (2011) 11914–11928.
[12] F. Calise, G. Ferruzzi, L. Vanoli, Parametric exergy analysis of a tubular solid oxide fuel cell (SOFC) stack through finite-volume model, Appl. Energy 86 (2009) 2401–2410.
[13] A. Sciacovelli, V. Verda, Entropy generation analysis in a monolithic-type solid oxide fuel cell (SOFC), Energy 34 (2009) 850–865.
[14] G. De Lorenzo, et al., Thermoelectric characterization of an intermediate temperature solid oxide fuel cell system directly fed by dry biogas, Energy Convers. Manag. 127 (2016) 90–102.
[15] S. Campanari, Simulation and thermodynamic analysis of a tubular SOFC module, J. Power Sources 92 (2000).
[16] R. Peters, et al., Efficiency analysis of a hydrogen-fueled solid oxide fuel cell system with anode off-gas recirculation, J. Power Sources 328 (2016) 105–113.
[17] S.H. Chan, C.F. Low, O.L. Ding, Energy and exergy analysis of simple SOFC power systems, J. Power Sources 103 (2002) 188–200.
[18] L. Barelli, G. Bidini, F. Gallorini, A. Ottaviano, An energetic-exergetic comparison between PEMFC and SOFC-based micro-CHP systems, Int. J. Hydrogen Energy 36 (2011) 3206–3214.
[19] L. van Biert, T. Woudstra, M. Godjevac, K. Visser, P.V. Aravind, A thermodynamic comparison of solid oxide fuel cell-combined cycles, J. Power Sources 397 (2018) 382–396.
[20] M. Rokni, Thermodynamic analysis of an integrated solid oxide fuel cell cycle with a rankine cycle, Energy Convers. Manag. 51 (2010) 2724–2732.
[21] M. Rokni, Thermodynamic analysis of SOFC (solid oxide fuel cell)-Stirling hybrid plants using alternative fuels, Energy 61 (2013) 87–97.
[22] C. Bang-Møller, M. Rokni, B. Elmegaard, Exergy analysis and optimization of a biomass gasification, solid oxide fuel cell and micro gas turbine hybrid system, Energy 36 (2011) 4740–4752.
[23] A. Arsalis, Thermoeconomic modeling and parametric study of hybrid SOFC-gas turbine-steam turbine power plants ranging from 1.5 to 10 MWe, J. Power Sources 181 (2008) 313–326.
[24] Y. Haseli, I. Dincer, G.F. Naterer, Thermodynamic modeling of a gas turbine cycle combined with a solid oxide fuel cell, Int. J. Hydrogen Energy 33 (2008) 5811–5822.
[25] F. Calise, M. Dentice d'Accadia, A. Palombo, L. Vanoli, Simulation and exergy analysis of a hybrid solid oxide fuel cell (SOFC)–gas turbine system, Energy 31 (2006) 3278–3299.

[26] F. Calise, A. Palombo, L. Vanoli, Design and partial load exergy analysis of hybrid SOFC-GT power plant, J. Power Sources 158 (2006) 225–244.
[27] P.G. Bavarsad, Energy and exergy analysis of internal reforming solid oxide fuel cell-gas turbine hybrid system, Int. J. Hydrogen Energy 32 (2007) 4591–4599.
[28] S. Motahar, A.A. Alemrajabi, Exergy based performance analysis of a solid oxide fuel cell and steam injected gas turbine hybrid power system, Int. J. Hydrogen Energy 34 (2009) 2396–2407.
[29] K.D. Panopoulos, L. Fryda, J. Karl, S. Poulou, E. Kakaras, High temperature solid oxide fuel cell integrated with novel allothermal biomass gasification. Part II: Exergy analysis, J. Power Sources 159 (2006) 586–594.
[30] M. Rokni, Thermodynamic and thermoeconomic analysis of a system with biomass gasification, solid oxide fuel cell (SOFC) and Stirling engine, Energy 76 (2014) 19–31.
[31] J. Hunt, <https://www.powerengineeringint.com/articles/decentralized-energy/print/volume-9/issue-3/features/heat-recovery-steam-generators-design-options-and-benefits.html>, 2008.
[32] P. Nehter, J.B. Hansen, P.K. Larsen, A techno-economic comparison of fuel processors utilizing diesel for solid oxide fuel cell auxiliary power units, J. Power Sources 196 (2011) 7347–7354.
[33] I. Kang, J. Bae, Autothermal reforming study of diesel for fuel cell application, J. Power Sources 159 (2006) 1283–1290.

CHAPTER

3 Mechanical engineering of solid oxide fuel cell systems: geometric design, mechanical configuration, and thermal analysis

Alireza Mohammadzadeh[1,2,*], Seyedeh Kiana Naghib Zadeh[1,2,*], Mohammad Hassan Saidi[1] and Mahdi Sharifzadeh[1]

[1]*Sharif Energy Research Institute (SERI), Sharif University of Technology, Tehran, Iran*

[2]*School of Mechanical Engineering, Sharif University of Technology, Tehran, Iran*

3.1 Introduction

Solid oxide fuel cells (SOFCs) are highly efficient, electrifying generators which directly convert chemical energy into electrical power. Fuel cells convert the chemical energy stored in fuels into electrical energy without burning the fuel and making gaseous pollutants. As they operate in high temperatures a wide range of fuels can be fed to them and both hydrogen and hydrocarbons can be used as the fuel. The operating temperature of a cell can be as high as 1000°C or for a low-temperature SOFC as low as 400°C [1] depending on the ionic conductivity, electric conductivity, and other properties of the electrolytes and layers of the cell [2]. SOFC's high-operating temperature requires them to be subtly designed, fabricated, and analyzed. From a mechanical perspective the geometry of a device is an important parameter in the distribution of stresses, temperatures, and the concentration of species and, consequently, its electrochemical performance. Analogous to heat or mass exchangers, the arrangement of cells and flow configuration is another important parameter for determining the performance of an SOFC stack. Hence the first part of this chapter is allocated to the geometry and configuration of SOFC cells and stacks. In addition, there are limited numbers of materials that can be used in the structure of high-temperature devices such as SOFCs. This limited choice of materials is not only expensive, but also requires special technics. Therefore the second section of this chapter is devoted to the fabrication methods used for manufacturing SOFCs. The commercialization of this technology highly depends on the reliability of SOFC modules and requires

* Both authors contributed equally to this chapter.

Design and Operation of Solid Oxide Fuel Cells. DOI: https://doi.org/10.1016/B978-0-12-815253-9.00003-3

the identification of various failure modes, which are discussed later on. Furthermore the thermal analysis of SOFCs is considered and discussed in Section 3.4. The chapter ends with a conclusion and summary section where the most potent research areas for further investigation are proposed.

3.2 Configuration and geometry

All SOFCs contain four main elements, namely a porous anode, dense electrolyte, porous cathode [which together are called the membrane electrode assembly (MEA)], and an interconnector. If there is only one MEA in an SOFC it is called a single cell or short stack. However, SOFCs with more than one MEA with a series or parallel layout for producing more power and voltage are called SOFC stacks. On both sides of each MEA there is a ceramic or metallic membrane for collecting electrical produced current, called the interconnector. The electrochemical reactions occur where the electrolyte and electrodes meet each other. This important place is called the triple phase boundary (TPB) and determines the active area of an SOFC. A set of one or more MEAs with some interconnectors form the SOFC cell or stack. There are three main categories of SOFCs based on their temperature, cell support, and geometry.

High-temperature, intermediate-temperature, and low-temperature SOFCs operate at approximately 1000°C, 800°C, and 600°C (or lower), respectively. The electrolyte and electrode materials, cell geometry, and the involved reactions are the major parameters that determine the operating temperature of a certain SOFC type. High-temperature SOFCs are the most electrically efficient among SOFCs [3].

The main reason for the high cost of SOFCs is their high-operating temperature, which requires expensive materials to ensure stability and durability under elevated temperatures. The materials that can be used as electrolytes in SOFCs are required to have high-ionic and low-electrical conductivity. In addition they must be stable when exposed to reducing and oxidizing environments. Yttria-stabilized zirconia (YSZ) is the most common material used as electrolytes in SOFCs. However, operating SOFCs at relatively low temperatures allows the use of a wide range of inexpensive materials for other parts of the cell, resulting in reducing the cost of their fabrication [1]. One of the main materials that satisfies these properties is gadolinia-doped ceria, or GDC ($Gd_{0.1}Ce_{0.9}O_{1.95}$), which can be applied at relatively low temperatures (below 600°C).

In each cell there must be a section that provides mechanical strength as well as structural support, and is generally thicker than other layers. There are five types of SOFCs based on the kind of part used for structural support: *cathode supported* and *anode* which are categorized under electrode-supported SOFCs; *electrolyte supported*, *porous substrate-supported*, and *interconnector or metallic* supported SOFCs. When the main parts are used as the supporting section (i.e.,

first three types) the cell is called self-supporting and when the other parts are used as the supporting section (i.e., last two types) the cell is called and external supporting SOFC. Electrolyte-supported SOFCs have some advantages over electrode-supported ones, including less susceptibility to redox and other failures. However, the thicker the electrolyte layer is the higher the operating temperature and ohmic resistance will be. Thus higher temperature and ionic resistance make electrolyte-supported SOFCs undesirable [4] making the electrode-supported (especially anode-supported) SOFCs the most common type of SOFC.

3.2.1 Cell geometric configurations

SOFCs are divided into two main geometry types, namely tubular and planar configurations. Planar configurations have advantages in power density, production cost, and thermal-cycle stability over tubular geometries. The higher power density of planar SOFCs in comparison to tubular ones is due to their lower electrical path and resistance. Their lower production cost is because of the applicability of mass-production methods for manufacturing planar SOFCs [5]. In contrast, tubular SOFCs are better in high-temperature sealing, stability of thermal cycling, and mechanical strength due to their symmetric shapes. They also have faster start-up and shut-down operations in comparison to planar SOFCs. For mobile applications high voltage and fast start-up are needed simultaneously. Planar SOFCs due to their low structural stability and tubular SOFCs due to their low power density cannot provide high voltage and fast start-up and, hence, are not appropriate for mobile applications. In Sections 3.2.1.1–3.2.1.5 other geometrical configurations introduced by researchers to overcome these disadvantages are discussed.

3.2.1.1 Integrated planar (segmented in series) solid oxide fuel cells

An integrated planar SOFC (IP-SOFC) or an SOFC segmented in series (SIS-SOFC) is a configuration between planar and tubular that was designed and promoted by Rolls–Royce. Fig. 3.1 presents a schematic view of an IP-SOFC.

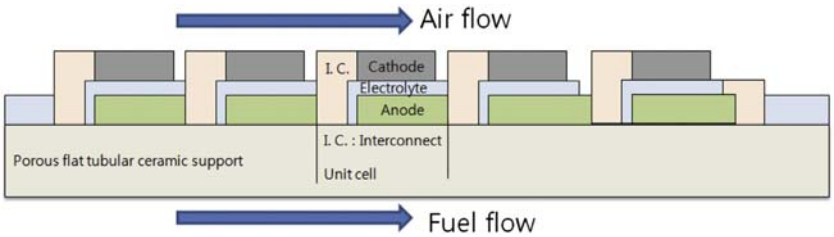

FIGURE 3.1

A schematic view of an integrated planar (IP) or segmented in series (SIS) solid oxide fuel cell (SOFC) [5].

This geometry has some advantages over regular planar and tubular designs. The smaller number of interconnectors used in the design helps lower the weight and cost of the IP-SOFC over other designs [6]. In addition the shorter and simpler external mechanical and electrical connection (current path) improves the cell performance and the power density of the SIS-SOFC over regular geometries [5]. However, the main limitations of this geometry are its relatively weak sealing and integrity of the interconnectors, which can be minimized by microstructural optimization and suitable material selection [6].

Bujalski et al. [7] compared the transient performance of an IP-SOFC with planar and tubular ones in thermal cycling experiments. They found that during temperature ramping or its fall, start-up and shut-down procedures of the cell were smaller than critical size and no damage will occur. Thus they suggested that cell size should be reduced to a millimeter-scale.

3.2.1.2 Cone-shaped solid oxide fuel cells

The concept of cone-shaped SOFCs comes from the SIS design. In this design, as shown in Fig. 3.2, several conically shaped tubular SOFCs are gathered in series. As the single SOFCs are fitted to each other, this design is self-supporting. The fuel flows from the core of the cells and passes one by one, while the oxidant flows over outside the stack [8]. This configuration is similar to tubular SOFCs in fuel and air passage and since its shape is like a cone they are called cone-shaped tubular SOFCs. This geometry was introduced by Sui and Liu [8].

3.2.1.3 Flat tubular solid oxide fuel cells

Another common geometric configuration for SOFCs is flat tubular SOFCs (FT-SOFC). In this design planar and tubular configuration are combined to produce an SOFC with higher cell power density by reducing electrical losses as well as better thermal stability and sealing. However, the thermal resistance of this configuration is relatively high. Fig. 3.3 presents a schematic view of a flat tubular SOFC. There is an anode porous substrate with extruded channels for fuel

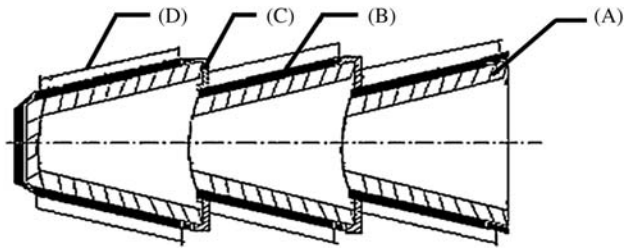

FIGURE 3.2

Schematic view of a cone-shaped SOFC: (A) anode, (B) electrolyte, (C) interconnect materials, (D) cathode [9].

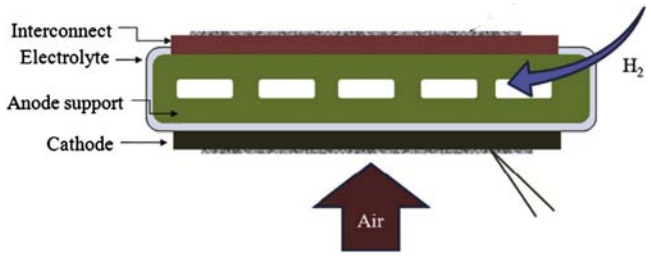

FIGURE 3.3

A schematic view of a flat tubular SOFC [10].

passage, an electrolyte layer, as well as an interconnector layer around the anode. Fuel flows through the channels and oxidant flows over the cathode. The cross-section of channels can be any arbitrary shape. This configuration was suggested and designed by Siemens–Westinghouse.

Interconnectors have two essential duties in this configuration; they connect cells electronically and they are barriers between the fuel and oxidant of neighboring cells. Thus they should be relatively impermeable to gas, have high chemical stability in both fuel and oxidizer, and have high-electronic conductivity. In this regard the main challenge that researchers faced was the design and material selection for the interconnectors in FT-SOFCs. There are two main types of interconnectors, namely metallic and ceramic. Ceramic interconnectors have lower electrical conductivity and are expensive in comparison to metallic counterparts. However, ceramic interconnectors have negligible permeability to gas. Hence in a flat tubular configuration in which the fuel and oxidizer are in contact with the interconnector, using ceramic materials is mandatory [11].

3.2.1.4 Honeycomb solid oxide fuel cells

This design consists of a series of cells. The early configuration of this design is electrolyte-supported, as shown in Fig. 3.4A. Here the electrolyte layer forms a honeycomb structure supporting the cell. Due to the thickness of the electrolyte layer in this configuration it has a higher ohmic resistance and, consequently, lower electrochemical performance. In addition, some channels are for the passage of air while others are for the passage of fuel. To solve this problem another type of cell has been suggested where the electrode provides the structural support of the honeycomb and the design is electrode-supported. Fig. 3.4B illustrates an electrode-supported honeycomb SOFC. In an electrode-supported SOFC the structural support is provided by one of the electrodes, while the other electrode is inside each channel. Therefore each channel can act as an independent SOFC [12]. The durability of this type of cell is high enough for increasing the start-up rate up to 100°C/min [13]. This design was first proposed by ABB.

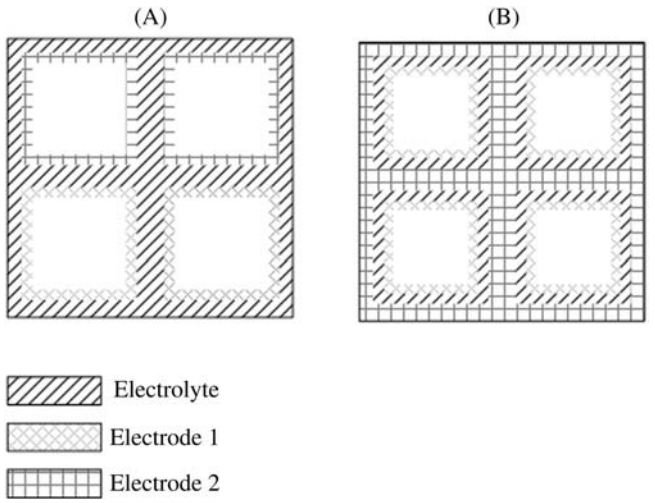

FIGURE 3.4

Schematic view of a honeycomb SOFC: (A) electrolyte-supported, and (B) electrode-supported.

3.2.1.5 Microtubular solid oxide fuel cells

As it is evident from the name of this geometry that it is a tubular SOFC with a diameter in the scale of 5 mm or smaller. Because of the small size of all their parts, especially the wall thickness, they are highly resistant to thermal shocks. Therefore they reach their operating temperature in a relatively short time, in the order of a minute, in comparison to large-scale SOFCs with a start-up that takes one hour or more. In addition, with decreasing the diameter of the tubes the ratio of the surface-to-volume increases, thus the power density of these types of cells improves drastically. Despite these advantages, small diameter of the cell reduces the cell capability to collect electrical current. Manufacturing microtubular SOFCs (MT-SOFCs) is challenging [6]. Phase inversion is the common method for MT manufacturing which is introduced in Section 3.3.6.

There are several other designs aimed at exploiting the advantages of planar and tubular SOFC geometries while reducing their disadvantages. Delta 8 or triangular design is one example of such a configuration and was proposed by Nagel et al. [14]. This new design entails a tubular geometry with a triangular cross-section as shown in Fig. 3.5. The authors found that this geometry had sealing properties similar to tubular SOFCs while, at the same time, the current path is short in comparison to planar SOFCs.

The electrochemical performance of different SOFC geometric and stack configurations are presented in Table 3.1.

The focus of the above discussions was the cell geometries. For designing stack SOFCs it is important to note that a free expansion length must be

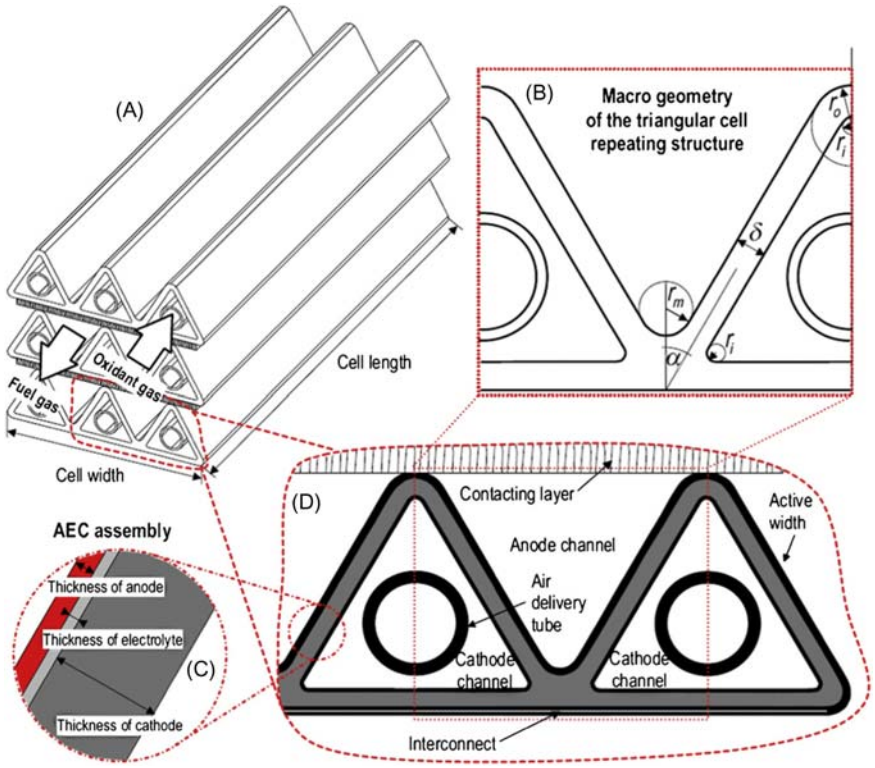

FIGURE 3.5

Schematic view of a delta 8 or triangular SOFC [14].

considered for the expansion and shrinkage of adjacent cells due to high-temperature gradients frequently occurring during start-up and shut-down operations [14]. The stack configurations are discussed in Section 3.2.2.

3.2.2 Stack configurations

Cells are compactly assembled to create an SOFC stack in order to produce more voltage and power. In stacks the distribution of the fuel and oxidant flows and their orientation relative to each other are important parameters for ensuring flow uniformity, temperature distribution, and chemical potential throughout the stack. The uniformity of the flow is a key parameter in determining stack performance. Its significance is due to the fact that the uniformity of the oxidant flow over the cathode results in a better cooling effect. In addition, uniform fuel distribution results in homogenous species transport in the anode. The orientation of the fuel and the oxidant flow relative to each other can be co-, counter-, or cross-flow in analogy to other heat or mass exchange equipment. The other important design

Table 3.1 Electrochemical performance of different cells studied by various researchers.

Geometry type	Fabrication method	Number of cells in a stack	Anode/electrolyte/cathode	Fuel	Temperature (°C)	Output
Flat tubular SIS-SOFC [5]	Extrusion, screen printing and dip coating	Five cells	Ni–ScSZ/ScSZ–GDC/ LSCF–GDC, LSCF	3% humidified H_2 and air	800	0.62 W/ cm^2
Cone-shaped SOFC [8]	Slip casting	Three cells	NiO–GDC/YSZ/LSCF–GDC	Humidified H_2 and air	800	0.9 W and 2.9 V OCV
Cone-shaped SOFC [9]	Dip coating	–	NiO–YSZ/YSZ/LSM–YSZ	Humidified H_2 and air	850	1 W/cm^2
Cone-shaped SOFC [15]	Gel casting and dip coating	Four cells	NiO–YSZ/YSZ/LSM–YSZ	3% humidified H_2 and air	800	3.4 W
Cone-shaped SOFC [1,16]	Slip casting and dip coating	Two cells	NiO–GDC/GDC (15 μm)/ BSCF–GDC	Moist H_2 and air	400	1.86 V OCV
Flat tube [10]	Screen printing and extrusion	–	Lanthanum–manganese-doped $CaTiO_3$ perovskite interconnector	3% humidified H_2 and air	800	0.207 W/ cm^2
Honeycomb SOFC [12]	Extrusion, dip coating, and slurry injection	–	NiO–GDC/10ScSZ/LSM Cathode supported	Humidified H_2 and air	650	2 W/cm^3
Microtubular SOFC [17]	Phase inversion and dip coating	Single cell	NiO–YSZ (240 μm)/YSZ (10 μm)/LSM–SDC (20 μm)	H_2 and air	600/800	0.277/ 0.752 W/ cm^2
Micro-tubular SOFC [18]	Phase inversion, dip coating, and high-temperature cosintering	Single cell	NiO–YSZ/YSZ/LSM–YSZ with electrode catalyst	15% humidified H_2 and air	750	0.78 W/ cm^2
Single-chamber SOFC [19]	Dry pressing and screen printing	Single cell	NiO–CGO/CGO (150 μm)/ LSCF–CGO (70–30 wt.%) (30 μm)	$CH_4/O_2 = 2$	600	0.26 W/ cm^2

BSCF: $Ba_{1-y}Sr_yCo_{1-x}Fe_xO_3$; CGO: gadolinia-doped ceria; GDC: gadolinium-doped ceria; LSCF: $La_{0.5}Sr_{0.5}Fe_{0.5}Co_{0.5}O_3$; LSM: $La_{1-x}Sr_xMnO_3$; LSM–YSZ: La_2ZrO_7 and $SrZrO_3$; ScSZ: scandia-stabilized zirconia; SDC: Sm-doped ceria; YSZ: yttria-stabilized zirconia.

considerations are header and distributors of each flow. The common design for manifolds are the stacks with single-inlet/single-outlet and double-inlet/single-outlet configurations. The single-inlet/single-outlet configuration contains spinal, serpentine, radial, and Z-flows.

Most studies on the effect of the flow configuration on cell performance are approached numerically. Some studies compared different flow configuration including co, cross, and counter configurations with respect to the flow uniformity and temperature distribution. Choudhary and Sanjay [20] investigated different cell parameters in a planar stack with co and counter-flow configurations numerically. They observed that the co-flow configuration results in thermal stress as its temperature distribution as well as current density distribution are more uniform. Kupecki et al. [21] investigated cross-, co-, and counter-flow configurations for a 1 kW planar stack numerically. They reported that cross-current configuration was superior because of its even temperature distribution.

Almost all numerical studies consider uniform flow in their simulation. However, Huang et al. [22] experimentally and numerically studied the validity of the flow uniformity assumption in different planar stacks with a single and double inlet. They compared their results with the results of a similar simulation where the uniform flow was assumed. The authors concluded that uniform flow is a valid assumption and does not affect the results significantly. They also observed that adding some small guides near the inlet and the outlet areas of the double-inlet/single-outlet stack increased the power density of the cell by about 11%.

3.3 Fabrication methods of solid oxide fuel cell elements

A thicker functional layer results in higher operating temperature and ohmic resistance [4]. For instance, Kim et al. [23] reported that decreasing electrolyte thickness from 10.5 to 6.5 μm, increases maximum power density from 0.74 to 1.12 W/cm^2. Thus the main challenge in fabricating SOFCs is to manufacture electrodes or electrolytes that have thinner layers. The main cost-effective SOFC fabrication methods are tape casting, screen printing, different coating, and deposition methods. All of the components in an SOFC can be fabricated using one or more methods of fabrication, for example, an anode can be fabricated using tape casting while the cathode can be fabricated using the screen-printing method. The choice of method of production for each component is mainly based on the resulting electrochemical and mechanical performance as well as the durability of the final cell. In Sections 3.3.1–3.3.6 various fabrication methods of different parts of an SOFC will be discussed.

3.3.1 Tape casting

As it is obvious from the name of this method, a slurry is cast to prepare flexible tapes for electrode and electrolyte support and functional layers with a thickness

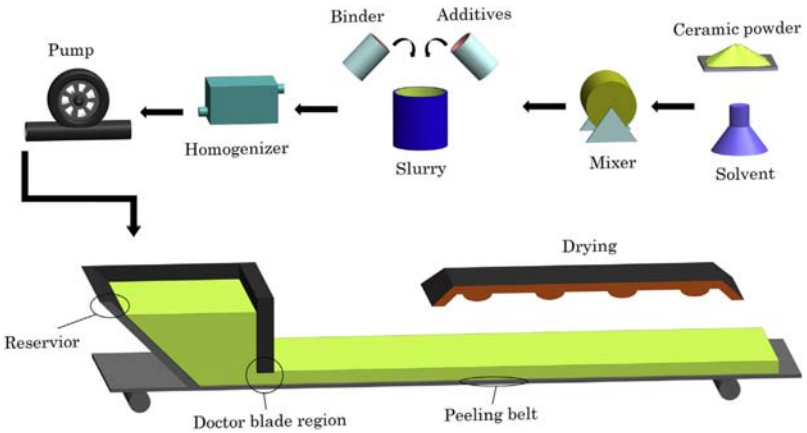

FIGURE 3.6

A schematic view of the tape-casting method [30].

of 10−1000 μm. Fig. 3.6 presents a schematic view of the tape-casting method. Almost all slurries in this method contain ceramic and polymer powders, solvents, binders, and plasticizers. However, the exact amount of each substance in the slurry is not fixed and has profound impact on the SOFC's characteristics. A high concentration of solid particles (solid loading) and binder in the slurry mixture increases the solid particle network strength and viscosity of the mixture. The former is desirable and improves the electrochemical and mechanical performances of the SOFC [24−26]. However, the latter is undesirable and makes removing air bubbles from the slurry more difficult. Air bubbles in the structure of fabricated tape make it nonuniform. Furthermore decreasing the tape density decreases the electrochemical performance of the SOFC [27,28]. This fabrication process is cost effective for mass production in comparison to other methods of fabrication [29]. The limitation of the tape-casting method is its slow processing procedures which limits its scale-up.

Faes et al. [31] and Kluczowski et al. [32] suggested the use of ceramic or powder injection molding (CIM or PIM) with a higher rate of production. Both studies investigated anode-supported planar SOFCs and concluded that the electrochemical performance of the final SOFC is comparable to equivalent SOFCs produced from the tape-casting method.

3.3.2 Screen printing

In the screen-printing method, screen mesh and ink (or paste) are the main parts of the manufacturing process. Ink or paste is produced from ceramic and polymers powders, binders, and solvents. The screen mesh is a stencil in which the empty sections produce the final shape of the fabricated layer. The screen mesh is

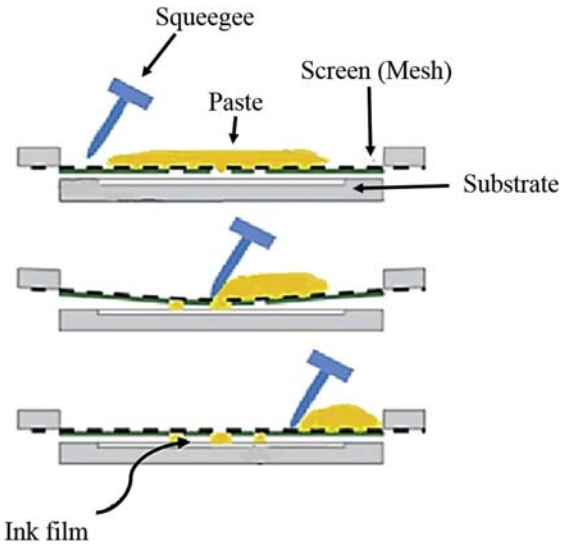

FIGURE 3.7

Schematic view of screen-printing method [33].

placed slightly above the bottom layer on the screen frame, and a thin film of ink or paste lies on the screen mesh. Using a squeegee, the ink or paste is forced to adhere to the bottom layer in the form of the screen mesh. After sintering a layer in the form of the screen mesh with a thickness of 10−200 μm will be printed on the sublayer. A schematic of each step in the screen-printing method is illustrated in Fig. 3.7. As the screen is used for producing a pattern on a layer, this method is very useful for fabricating porous layers. It is worthy to note that this method does not allow acceptable performance for fabricating support layers and usually is used for fabricating other layers such as functional ones [4]. Thus another method is needed for producing the supporting layer.

Several researchers reported that the quality of the final layer is affected by the process parameters and materials used. One of the main parameters that affect electrochemical and mechanical parameters is the ink's composition and viscosity. The lower or higher viscosity of the ink causes pores in the final layer or ink spreading in sublayers [34].

3.3.3 Dip coating

Dip coating is also known as slurry or vacuum slurry dip coating. This method is usually used for fabricating functional layers. Similarly to the screen-printing method, this method uses slurry in the fabrication process. The slurry is a combination of ceramic powder, solvent, binder, and dispersant. In the dip-coating method the supporting layer is soaked in the slurry. Then the slurry jar comes

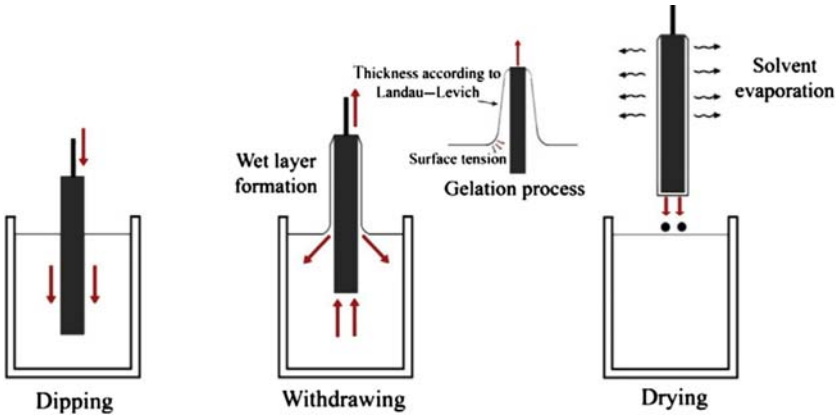

FIGURE 3.8

A schematic view of the dip-coating method [38].

down (or the supported layer comes up) and a film of slurry attaches to the supporting layer. After the coated slurry is dried in ambient temperature the supported layer with its new dip-coated layer are sintered [35]. The smoothness and thickness of the layer can be controlled by modifying the solid loads in the slurry and the draw-up speed of the supporting layer from the slurry jar. Layers with the thickness of a few microns to hundreds of microns can be produced using this method [36]. The usual duration for soaking the supporting layer in the jar initially is about 30 seconds [23,35]. Yamaguchi et al. [37] reported that the density of the electrolyte layer coated on the anode-supported layer in a tubular SOFC is highly affected by the shrinkage of the sublayer during the cosintering process. Fig. 3.8 illustrates the dip-coating method.

3.3.4 Slurry spin coating

The slurry spin-coating method uses centrifugal forces for a spin motion in order to produce a uniform layer. Fig. 3.9 presents a schematic view of this method of manufacturing. The slurry which is used in this method is similar to other fabrication methods. As shown in Fig. 3.9, a certain amount of the slurry is placed on the center of the spin axis above the supporting layer, and will be spread over the plate by its rotation. Constant speed rotation of the axis and centrifugal force allows the slurry to form a uniform layer. The angular velocity of the spin is an important parameter in determining the thickness of the layer, and has an inverse relation to each other. In addition the speed of the rotation can be adjusted in order to fabricate coating layers of desirable thickness [39]. Like the other methods containing slurry, the composition and the viscosity of the slurry determines the thickness of the resulting layer and also the length of the TPB. Lower viscosity causes lower adherence of the slurry to the sublayer and thus a lower TPB volume [40].

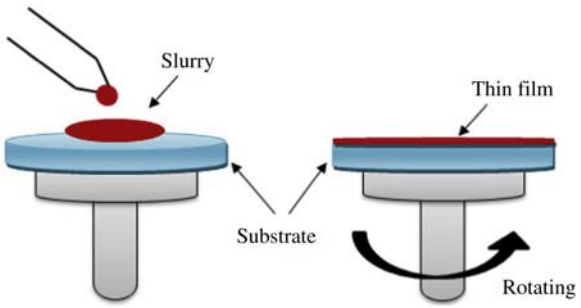

FIGURE 3.9

A schematic view of the spin-coating method [4].

3.3.5 Spray coating

The thermal spray-coating method has a lower production cost in comparison to other common methods especially the first two methods discussed. The main disadvantage of this method is that it needs additional surface modification because spraying ceramics like YSZ under room temperature induces a surface with some pores and cracks, which are undesirable for coatings. Some of the modification methods are high-temperature sintering, chemical densification, and spark-plasma sintering. The first and essential step for producing a dense layer using this method is melting the powder. The melting point of ceramic materials like YSZ is as high as 2700°C, while for methods involving high-temperature plasma spraying with gas the temperature required can be as high as 10,000K. Vacuum plasma spraying (VPS) and atmospheric plasma spraying (APS) are two subdivisions of the plasma spraying method based on their operating pressure. The former method operates at about 50 mbar and the latter operates at the atmospheric pressure. Substrate density in the VPS method is higher than the APS method because of the higher particle velocity in the VPS process. Through analyzing the causes for the development of pores and cracks in coating process Vaßen and coworkers [3] introduced a new spraying condition for diminishing the number and the size of the cracks in coatings without needing any additional treatment. They applied YSZ as a coating material and reported that this method produces thin electrolyte and anode layers with acceptable electrochemical performance. A cathode produced via the screen-printing method, however, is better than a cathode produced via this spray-coating method. In addition the authors reported that applying a further layer as a diffusion barrier between the substrate and anode can decrease the rate of degradation of the cell.

3.3.6 Phase inversion

This method of fabrication is commonly used for manufacturing MT-SOFCs, especially hollow-fiber types. The phase-inversion method is relatively

inexpensive, simple, and fast in comparison to the other methods of fabrication. In this method a viscous slurry is smoothly injected into a cool water bath using a spinneret. The injected slurry is called the microtubular precursor (MTP). After about 30 minutes the molecules in the water and MTP will be exchanged and a porous fiber as an electrode is fabricated.

The other methods of fabrication which are not as common as the abovementioned are: decalcomania, electrophoretic deposition (EPD), direct deposition, pulsed-laser deposition, (PLD), aerosol-assisted chemical vapor deposition, spray pyrolysis, atomic-layer deposition, and electron-beam evaporation. These methods can be categorized as chemical vapor deposition (CVD), electrochemical vapor deposition (EVD), physical vapor deposition (PVD), and spraying methods.

One of the main features which can increase the performance of an SOFC is the length of the TPB. The impregnation of electrodes with a suitable catalyst can increase the TPB length. By impregnating a porous electrode in a dense electrolyte layer the pores of the electrode behave as an O^{2-} transport bridge. Thus the ionic conductivity in the electrode (cathode) and the electrolyte, as well as the total performance of the cell, will increase [41]. Nanowires with the high-surface area can serve as a straight path as suggested by Zhao et al. [42]. This concept was applied to the MT-SOFCs by Yang et al. [18].

These methods of fabrication do not have any control over the produced pores. In conventional methods, since a molten resin is mixed with the main material, there is no control of the shape, size, and distribution of pores. Yoon et al. [43] developed a new method for controlling the pores and paths appearing in the porous layer. First, a cell produced using powder pressing and sintering method. After production of the cell, pores and pathways in different shapes with different distribution form in the cell using the laser-ablation technique. The resulting cells are called microarchitectured SOFCs. The authors reported 9%−17% improvement in current density and 7%−19% enhancement in power density in microarchitectured SOFCs.

3.4 Reliability and mechanical performance

The large power density of a single cell or stack and the number of its cycles increases the possibility of its failure. Almost all mechanical failures are due to thermochemical stresses being higher than the resistance stresses of a part in a cell. For analyzing the reliability of a cell, different stresses must first be recognized and then their effect on different parts of the cell must be studied. The main reason for stress is that there are several layers with different physical and chemical properties attached to each other. Their different behavior subject to dramatic variations of temperature from ambient temperature to about 1000°C makes a lot of thermomechanical stresses and chemically induced stresses due to the nonstoichiometric condition in the system and causes mechanical failure. The cell or

stack in high-manufacturing temperature is stress-free as different components adjust relative to each other. Hence the highest residual stress occurs under room temperature. A wide range of parameters including fabrication methods, thermomechanical properties of the materials, and the geometry of the cell affect the reliability and durability of an SOFC, and are the focus of this section.

Nakajo et al. [44] studied the mechanical properties of different materials used in intermediate-temperature, anode-supported SOFCs. The materials and layers considered in this study include Ni−YSZ anodes, YSZ electrolytes, and YDC, GDC, LSM, or LSCF cathodes. One of the main conclusions in this study was that the thermal expansion coefficient (CTE) of YSZ was the lowest compared to the other materials. This causes only tensile stress in the anode. However, the CTE of the materials in the other layers overlaps with materials in the anode over a wide range of temperatures, that is, spanning from ambient to operating temperatures. Thus the nature of the stress in these layers may switch from tensile to compressive, and vice versa. It is predicted that LSCF ($La_{0.5}Sr_{0.5}Fe_{0.5}Co_{0.5}O_3$) cathodes almost always are under tensile stress. Predicting the type of stress can be useful in the mechanical design of the cell.

The New Energy and Industrial Technology Development Organization (NEDO) divided the mechanism of mechanical failure into three main categories of deformation of a cell due to *asymmetry*, *propagation of a mechanical defect*, and *effect of irregular operations*. Cell asymmetry can be either mechanical or chemical. Different electrodes on each side of the electrolyte make the cell mechanically asymmetric. In addition the nonstoichiometric injection of oxide forms some gaps in the cell, especially cells with lanthanum chromite, which is more serious than mechanical asymmetry. A crack, especially in the electrolyte or the interconnector, can grow and cause severe failure. Cracks bigger than a critical size cause gas leakage, so temperature increases gradually at some points. This higher temperature causes more failure as well as exposure of the electrode to the oxidizing gases [45]. Furthermore the oxidization of Ni particles, which is called redox, adjacent to an electrolyte crack causes high stress occurring on the crack. It should be noted that the deficit of fuel increases the possibility of Ni particle reduction−oxidation reactions, while the deficit of air may cause oxygen nonstoichiometric expansion (chemical expansion) of the electrode. This is problematic when the electrode provides the structural support to the cell.

As with redox, some of the degradation and thermomechanical problems are, to some extent, reversible and some are not. Reduction−oxidation is a reversible process and by reintroduction of H_2 to the anode, NiO can be converted to Ni again; however, it may cause serious and irreversible failures. A cell with sulfur poisoning and early stage carbon deposition can regenerate itself [46]. However, cracking and delamination are not reversible issues. Identifying the type of failure is important for choosing the method of repair, such as requiring in situ repair or total replacement of the damaged part. The mechanism and the reason for each failure is different, but all of them decrease the cell electrical potential under constant-current load. Thus the DC potential of the cell in constant current is not

a diagnostic indicator and other diagnostic technics are needed [47]. In Sections 3.4.1–3.4.3 various failures and their diagnostic methods are discussed.

3.4.1 Redox

In the case of a shortage of fuel near the anode the Ni particles in the anode structure start to oxidize and degrade, called anode reduction–oxidation malfunction or redox. Redox is one of the main modes of failure in anode-supported SOFCs. Redox and oxidation are destructive processes. If they happen beyond a critical value the cell will be irreversibly damaged. Sarantaridis et al. [48] studied the critical value of oxidation whether directly by air or electrochemically induced. Electrochemical oxidation damage and crack formation in the substrate are irreversible only after 5% Ni is oxidized. In contrast, until 50% oxidation directly by air, no irreversible failure appears. Redox commonly appears by electrolyte cracking.

The partial pressure of oxygen and fuel are indicators of the ratio of the oxidizer and the fuel in the cell. The higher partial pressure of oxygen than oxygen partial pressure at equilibrium state can be a sign of anode reduction–oxidation or redox. The simulation of anode redox, based on the concept of discrepancy in oxygen partial pressure, and introducing this method for diagnosing redox was done by Larrain et al. [49] and Faes et al. [50]. In addition, anode reduction–oxidation causes expansion of the anode. Therefore evaluating the local stresses in the anode and adjacent layers at operating or room temperatures can be applied for diagnosing redox faults [51].

The other important observation in redox is that the amount of residual stress decreases via reduction. Sun et al. [52] reported that the residual stress of Ni(O)/YSZ SOFC is −600 MPa before reduction and −450 MPa after reduction. From the strength of material knowledge, we know that when low stress is applied to a material its deformation is in the elastic region and reversible; however, when applied stress is higher than a critical value the deformation is in the plastic region and irreversible. Based on this concept and observations they concluded that residual stress decreases because of large plastic deformation during the reduction process. Frandsen et al. [53] reported this decrement of residual stress as reduction creep during redox at a high rate of about 10^4. Creep is the slow change of material shape and properties with the passage of time. It relieves the residual stress in a solid and its rate is usually small. Hence reduction creep rate is much larger than usual operating creep.

3.4.2 Delamination

Delamination is the detachment of the electrolyte and the electrode layers. The gap between the electrolyte and the electrode decreases all types of conductivity drastically, which results in decrement of cell performance. Delamination reduces the effective area of the cell and causes distinguishable changes in the impedance spectrum of the cell in comparison to the other malfunctions. Thus drawing the

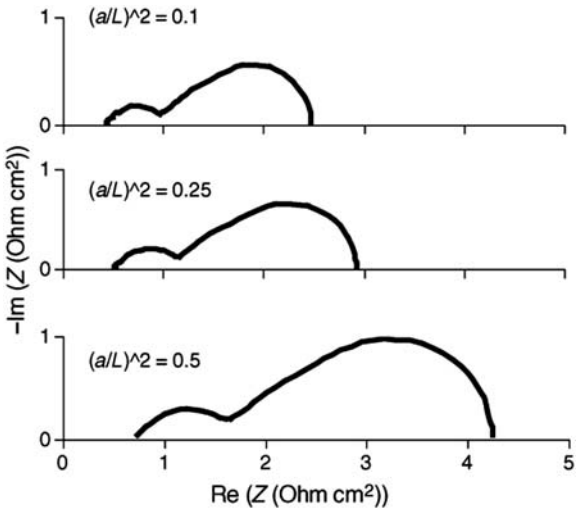

FIGURE 3.10

Effect of the delamination length on the impedance spectrum of an SOFC [54].

impedance spectrum of an intact cell and a delaminated cell can be helpful in detection of delamination [54,55]. This diagnosis method is called electrochemical impedance spectroscopy (EIS). Fig. 3.10 shows the effect of delamination length on the impedance spectrum developed via a computational model.

The other suggested method for diagnosing delamination is based on the oxygen pressure in the cell. If the oxygen pressure in the interface of the cathode and electrolyte exceeds a critical value (about 1200 atm), delamination will occur. Therefore the chemical potential that is directly related to the oxygen pressure in the electrode can be monitored for delamination diagnosis [56].

3.4.3 Degradation

The microstructure and porous structure of the electrodes is very important for transportation of ions, gas, and electrons, and consequently the electrochemical performance of the cell. In addition the electrochemically active areas of the cell are TBP sites that depend on the microstructure and morphology of the electrodes. The initial microstructure of the electrodes is determined by the fabrication method and its related parameters such as sintering temperature, powder composition, and so on. The operating conditions and malfunctions of the cell such as the impurities of the fuel, redox, thermal cycling, and aging modify the microstructure of the electrode reversibly or irreversibly.

Brus et al. [57] compared the morphology of a 100 W SOFC stack over 3700 hours operation using a combination of focused ion beam (FIB) and scanning electron microscope (SEM) (FIB−SEM). They observed a nonhomogenous

change in the microstructure in different regions of the cell and the most decrement of TPB length was reported near the inlet of the cell stack.

An important issue that has not yet been considered in this chapter is the effect of fuel impurities on cell degradation and mechanical failure. Sulfur impurities in hydrocarbons fuels form H_2S and contaminate the cell materials. If sulfur poisoning is in an early stage, using sulfur-free fuels repair this poisoning. However, excessive sulfur poisoning induces irreversible failures.

Spectroscopy after and before cell operation can provide much useful information about cracks and deformations of cells. In addition, in situ spectroscopy can give a lot of information about the dynamic interaction of different parts of a cell. Bozzini et al. [58] applied in situ photoelectron microscopy in order to investigate the microstructure of a single-chamber SOFC with an Ni-based anode, YSZ (100) single crystal electrolyte, and Au−MnO_2 cathode operated at 600°C, with CH_4 and O_2 1:1 fuel and oxidant mixture during operation. They continuously monitored the chemical state and distribution of the cell when electrodes are fully oxidized and after the reduction of the anode. Although they reported that the long-time operation of the cell does not change the chemical state and morphology of the electrodes, they illustrated that the degradation of the cell causes high morphological changes.

Kumada et al. [59] investigated the mechanical status of an anode-supported single cell using Acoustic Emission (AE) and SEM monitoring during start-up and shut-down operations. They observed vertical cracks in the cell and some cracks in the reproducible part of the glass seal during the shut-down operation. This study revealed that the AE method can be used for detecting sealing and cell cracks, separately.

Another important factor which causes failure is the external load on the cell. The contact area of the SOFC layers plays an important role in the contact resistance between layers, thus different parts of an SOFC should be pressed by external force to each other for better and more contact. As the behavior of the sealant materials changes under high-operating temperatures, their behavior under different temperatures must be analyzed precisely. Dey et al. [60] reported that with an external load the stress will be concentrated near the edge of the electrode and channel contact. In addition, their simulation showed that pressure in the range of 0.05−0.1 MPa is safe for the external load of the considered SOFC during operation.

3.5 Thermal analysis

The high-operating temperature of SOFCs offers advantages and disadvantages. Due to ionic conductivity of the electrolyte, SOFCs produce higher power output with higher efficiency at higher temperatures. Thus the SOFCs operate at high temperatures in the range of 600°C−1000°C. On the other hand, failures due to thermal fatigue and induced thermal stresses in cell components are the two main disadvantages of high-operating temperatures. Thus temperature must be kept below a limit.

In this regard thermal analysis of the SOFC is crucial to ensure system reliability. However, thermal analysis of an SOFC system through experimental

investigations is quite expensive and time consuming. Alternatively, thermal modeling offers a low-cost method to optimize, increase efficiency, examine the feasibility of new designs, and evaluate their performance.

Thermal modeling is also used to investigate different SOFC configurations in order to quantify electrochemical performance, mitigate temperature gradients, and, consequently, reduce principal stresses.

Another area of interest for SOFC thermal investigation is the examination of start-ups and shut-downs of system operation or the fluctuations in the operating temperature. The thermal transient modeling and thermal management of the SOFC system are discussed in Sections 3.5.1 and 3.5.2, respectively.

3.5.1 Thermal modeling

Chyou et al. [61] developed an integrated model to simulate heat transfer in an interconnect which was enveloped by insulation to reduce the heat loss to the environment. The simulation model consists of a computer code capable of analyzing the steady-state, discrete, electrochemical model (ECM) and a finite element model (FEM) to simulate heat transfer within the interconnect. The simulation framework was such that the temperature distribution was calculated by the ECM in the reaction zone of the interconnect under adiabatic conditions. The results were used as a thermal boundary in the 2D FEM heat-transfer analysis to estimate overall thermal parameters. Among the parameters the heat loss was fed back to the ECM to produce a more realistic model. Then through iterative evaluation of both ECM and FEM a unified temperature distribution was found. Combining ECM with FEM made their proposed model more cost-effective and less time-consuming compared to CFD models. Thus an efficient computational methodology was proposed for the integration of electrochemical and heat-transfer analyses that could be used as a fast design tool for SOFCs.

Mounir et al. [62] developed an ECM capable of determining the temperature variation induced by electrochemical reactions, air, and fuel flow. The model was applied in order to predict performance analysis of a multicell IP-SOFC. The results revealed that ohmic and activation losses dominate cell performance, while reducing the electrolyte cell thickness could improve cell performance and increasing the operating temperature results in ohmic loss reduction.

A tubular SOFC was investigated through a mathematical and an experimental study by Tonekabonimoghadam et al. [63]. An isothermal macrotubular SOFC model was developed by dividing a macrotubular SOFC into six MT-SOFC subsystems connected in series. The model was capable of simulating the performance of an SOFC by considering mass, momentum, diffusion through porous media, electrochemical reactions, and heat generation in the subsystems. The model could successfully simulate the dependence of the current density on cell potential, thermal energy generation from electrochemical reactions, as well as voltage irreversibility losses. The results showed that efficiencies of electrical and thermal power generation increased by around 50% when the operating

temperature increased from 923K to 1023K. It was also shown that the maximum electrical power increased by increasing the fuel-flow rate.

Detailed SOFC thermal modeling should incorporate all the physics and processes involved, such as fluid flow and electrochemical equations. Moreover in order to the study structural behavior of the system, the temperature distribution calculated from heat transfer, fluid flow, and electrochemical coupling should be applied to structural analysis of the system to enable estimating the thermal stresses. Generally the principal stress in the SOFC is induced by thermal stresses that are caused by the mismatch of the coefficient of thermal expansion (CTE) between different SOFC components.

In a numerical study Chiang et al. [64] simulated the thermal-fluid behavior as well as thermal stress analysis of a planar anode-supported SOFC. Utilizing the commercial Star-CD software and the MARC finite element analysis (FEA) they built a 3D integrated numerical model and investigated the effects of anode porosity on the temperature gradient, thermal stress, and performance of positive electrode−electrolyte−negative electrode (PEN). The 3D CAD model of the PEN was developed using Solidworks and CATIA that was then imported to the PATRAN and Gridgen for meshing the geometry. Afterward, using the Star-CD and es-SOFC module, the electrochemical, fluid flow, and heat-transfer analysis of the PEN were performed to obtain its current−voltage ($I-V$) characteristic curves as a function of the anode porosity and temperature field within the fuel cell. The simulated $I-V$ characteristics of the SOFC were then validated with experimental observations (Fig. 3.11). Finally the temperature distribution obtained from Star-CD was used as an input for the structural analysis in MARC FEA. By utilizing this integrated simulation procedure the maximum principal

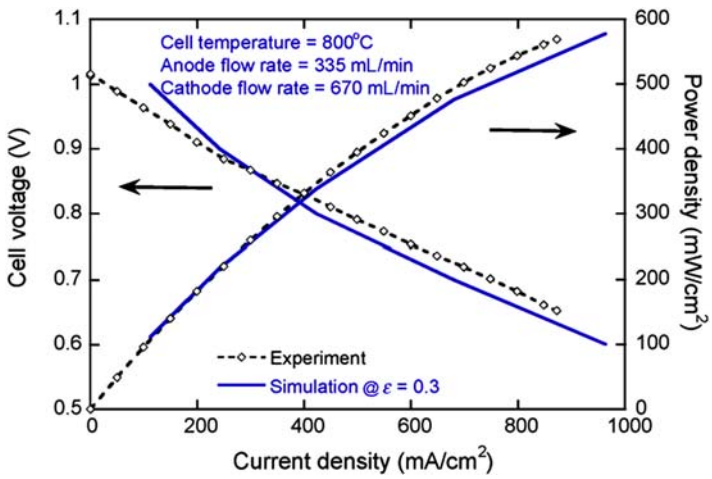

FIGURE 3.11

Comparison of experimental and numerical results for variation of cell voltage and power density versus current density [60].

stress induced within the PEN was investigated as a function of porosity, operating voltage, and temperature gradient.

Results demonstrate that the maximum principal stress within the PEN rises at a higher current and higher temperature gradient (Fig. 3.12).

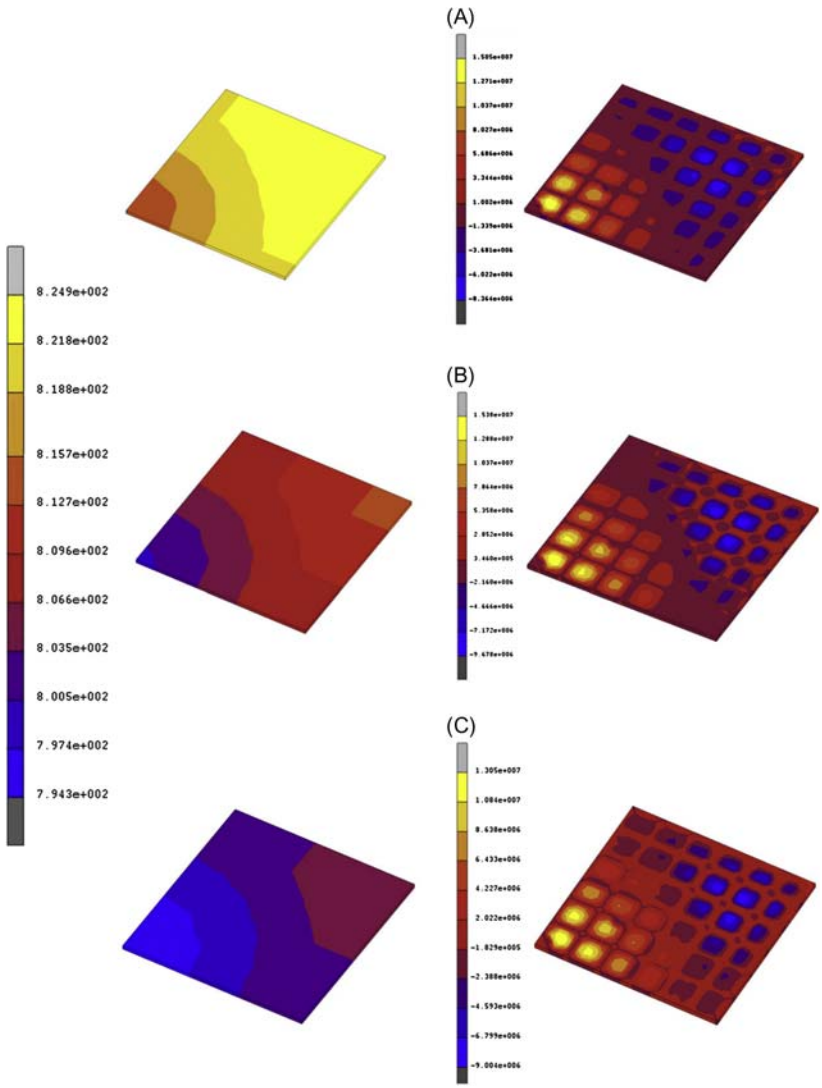

FIGURE 3.12

Temperature gradient distributions (left) and thermal stress distributions (right) in positive electrode–electrolyte–negative electrode (with porosity of 0.5 in all cases) at cell voltages of: (A) 0.7 V; (B) 0.8 V; and (C) 0.9 V [64].

It is also shown that the power density and cell voltage increase with increasing porosity in the range of $0.2 < \varepsilon < 0.5$ (Fig. 3.13).

The effect of adding an uniform load to the upper interconnect were also studied. It was shown that the maximum principal stresses do not change dramatically with increasing the load magnitude (Table 3.2). Therefore it was concluded that the temperature gradient and the CTE mismatches between fuel-cell components were the principle causes of stress distribution within the PEN.

The results showed that the thermal stress within the PEN is lower at lower temperature gradients, which is recommended to be limited to less than 10.6°C/mm to retain the structural integrity of the SOFC.

Ni [65] developed a 2D thermofluid model of a planar SOFC through incorporating a CFD model with an ECM. Hydrogen was used as the fuel in this SOFC with a porous anode and cathode in a co-flow configuration. Results showed that increasing the H_2 molar fraction or higher inlet velocity can increase the Nernst

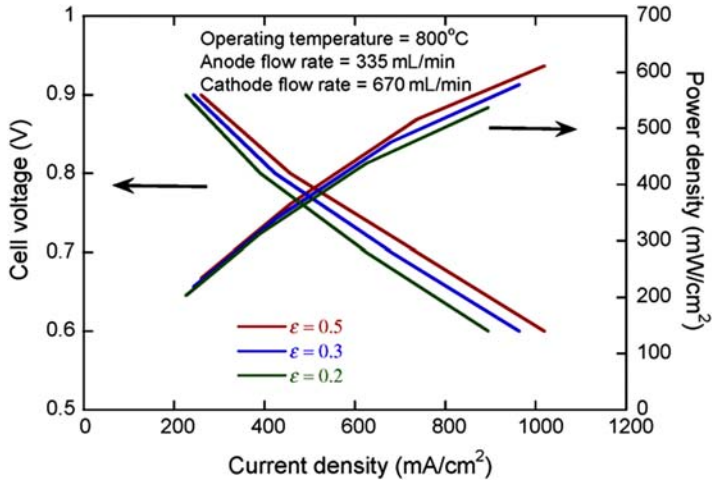

FIGURE 3.13

Variation of cell voltage and power density with current density as functions of anode porosity [64].

Table 3.2 Maximum principal stresses in the positive electrode–electrolyte–negative electrode (PEN) and interconnect at various loads (in the case of $V = 0.7$ and porosity = 0.3) [64].

Load (kg/cm)	PEN (MPa)	Interconnect (MPa)
0.5	18.7 (−10.5)	42.9 (−4.7)
1	18.7 (−11.1)	42.9 (−5.0)
5	18.1 (−15.2)	42.3 (−7.5)

potential and, consequently, leads to an increase in the SOFC's electric output. Furthermore, increasing electrode porosity increased the SOFC's power output. However, changing electrode permeability did not affect the SOFC's performance remarkably. The simulation data showed good agreement with experimental data of the Nusselt number and friction factor.

Mounir et al. [66] extended their previous studies [58,61] by conducting structural analysis with the goal of evaluating the probability of survival of IP-SOFCs. A thermoelectrochemical model was applied to estimate the temperature profiles which were then used to find the thermal stress distribution in the multiple-cell module. In this study the effects of the CTE difference as well as the Young's modulus difference between materials used in IP-SOFCs were taken into account. The results showed that generated thermal stresses at the inlet fuel-flow section were moderate, while the IP-SOFC cell undergoes high stresses at the outlet section. It was also found that the probability of survival of the electrolyte is lower than other components. The results showed that in the IP-SOFC stack, constituting of five bundles, the first bundle produced the maximum power of 200 W while the second bundle's production increased by 10% and increased around 20% for in the fourth bundle. However, the probability of survival decreases by 12% for the fifth bundle (Fig. 3.14).

Wang et al. [67] developed a 3D numerical model based on FEM to calculate thermal stresses in a planar SOFC. A stack consisting of five components, including cell, metallic interconnect, seal, and anode/cathode current collectors were considered as the simulation domain (Fig. 3.15). The results showed that the maximum stress concentration area appeared at the corners of the components. The effect of the stack components on the maximum stress concentration was also investigated. The mismatch of the CTE between the interconnect and the seal is a crucial parameter to determine the thermal stress distribution in the stack. This study also revealed that various compressive loads do not affect the stress distribution. Different seal designs were also investigated and it was found that the elastic modulus had a prominent role in the induced stresses by interconnects and seals.

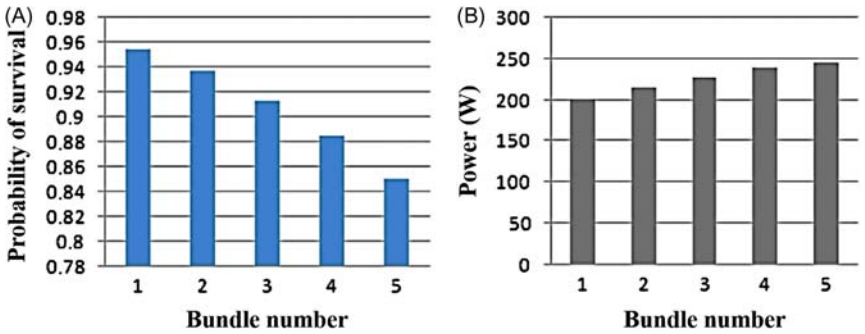

FIGURE 3.14

Bundle-to-bundle evolution for (A) probability of survival and (B) output power [66].

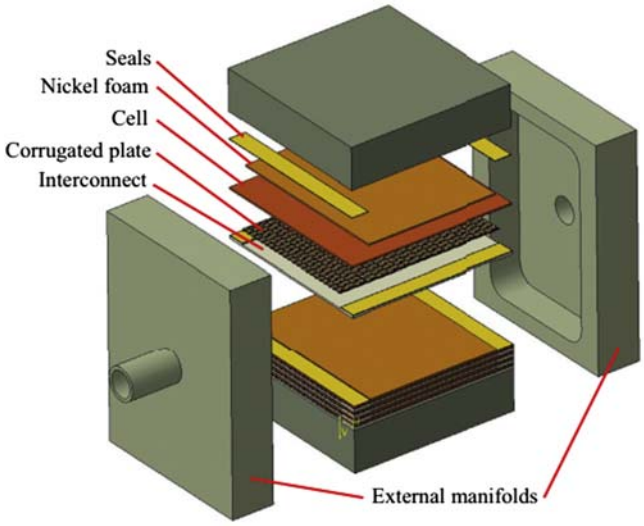

FIGURE 3.15

Geometry of planar SOFC stack 5-cell units [67].

The most prominent challenge in SOFC simulation is to develop and solve fully coupled multiphysics simulation in which all the governing equations corresponding to the involved phenomena of the system are considered. These include continuity, momentum, species transport, heat transfer, charge transport, and electrochemical reactions. In this regard most studies have incorporated several pieces of software or codes with or without simplifying assumptions in a fully coupled or segregated manner.

Serincan et al. [68] developed a 2D axisymmetric computational fluid dynamic model incorporating mass, momentum, energy, and charge balances to simulate the multiphysical nature of the steady-state behavior of a MT-SOFC. An anode-supported SOFC containing a ceria-based electrolyte was studied. Such configuration enabled them to take into account the performance losses caused by internal leakage currents since the ceria-based electrolyte lets the electrons leak through the electrolyte. The results of the modeled polarization curves were in good agreement with the experimental data for a set of various working temperatures (Fig. 3.16).

Considering a fuel cell-test furnace that was modeled separately allowed Serincan et al. [68] to assess the oxygen concentration distribution as well as the temperature distribution inside the furnace, and to obtain a more realistic simulation. Then the results of the separately solved furnace models were utilized as a boundary condition for the fuel-cell simulation.

Based on their previous thermal-fluid model [68] Serincan et al. [69] developed a multiphysics model to investigate the thermal stresses in MT-SOFCs. The

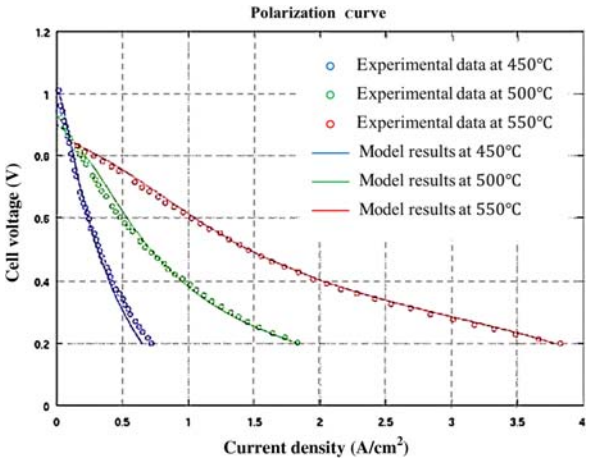

FIGURE 3.16

Comparison between experimental (*circle markers*) and model results (*solid lines*) for polarization curves [68].

composite structure approximation was utilized to theoretically evaluate the mechanical properties of the anode and cathode. Knowing the mechanical properties is one of the prerequisites for structural analysis. Furthermore they considered the mismatch between thermal expansion coefficients, as well as the interactions between the cell, sealant, and alumina tube in order to have a more realistic model of the problem. The results showed that spatial temperature distribution did not have a significant effect, while the interactions between the cell and the support structure as well as the residual stress had a substantial impact on the overall stress distribution.

Wei et al. [70] developed a multiphysics 3D model incorporating two commercial packages, namely ANSYS-FLUENT and ANSYS. The model was capable of simulating the thermal-fluid-electrical field as well as thermal-stress distribution. The numerical calculation procedure incorporated the continuity, momentum, energy, and species transport equations as well as current continuity equations and electrochemical reactions. These equations were solved in the ANSYS Fluent and SOFC modules in a coupled manner. Then the resulting temperature distribution was used as the input for the ANSYS software to find the stress distribution in the computational domain (Fig. 3.17).

Moreover a new design of counter-flow channels was proposed and a feasibility study was done using the developed model. The results showed that the proposed design could produce a more uniform flow and current density distribution as well as lower-stress distribution.

The previous SOFC simulation models were developed based on simplified geometries or using relatively easy-to-couple equations. Li et al. [71] developed the first fully coupled multiphysics numerical model that also utilized high-

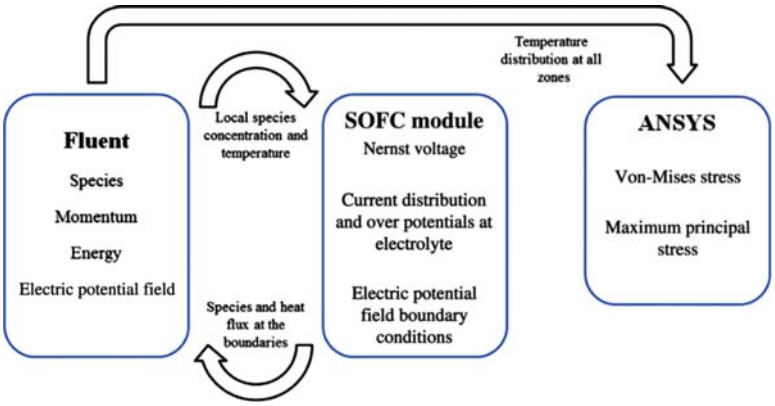

FIGURE 3.17

Coupling of flow solver, SOFC module, and stress-analysis solver [70].

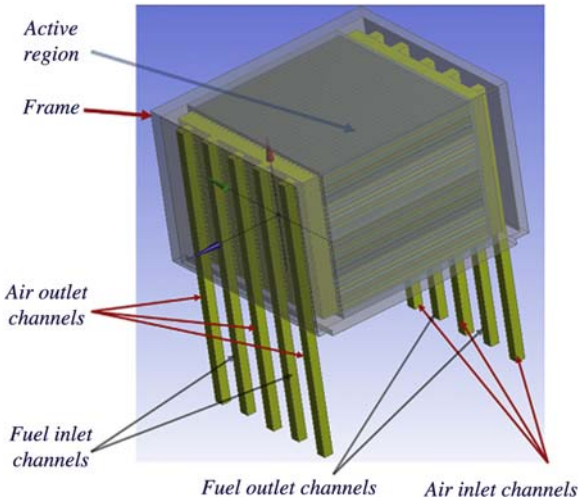

FIGURE 3.18

High-resolution geometry of a 30-cell pSOFC stack with extended gas flow channels for numerical simulations [71].

resolution geometry. All the stack components such as flow channels, manifolds, cathode−electrolyte−anode assemblies, interconnects, seals, and frames were considered in the numerical model (Fig. 3.18).

The multiphysics fully coupled governing equations of momentum, mass, species, heat transfer, charge transports, electrochemical reaction, and methane-steam reforming as well as the gas-shift reactions were incorporated in the developed model.

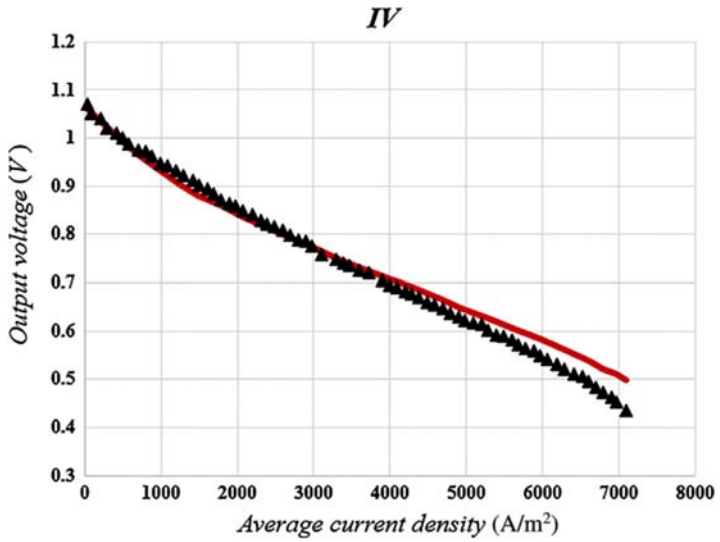

FIGURE 3.19

Comparison of the theoretical (*red solid line*) and experimental (*black triangles*) *I–V* curves for a one-cell stack operated at 750°C [71].

The numerical model was developed by combining in-house created multiphysics modules using the commercial software FLUENT. The *I–V* characteristic curve calculated from the simulation model was validated with experimental data (Fig. 3.19). Thus the proposed fully coupled multiphysics model could be used as a reliable tool for SOFC design and development.

3.5.2 Thermal transient modeling

SOFCs require high-operating temperatures to reach high-ion conductivity in the electrolyte. Therefore the SOFC module should be heated up before the fuel is supplied to the stack. This heating-up, transient operation should entail changing the temperature from ambient to around 700°C quickly, while keeping the temperature gradient and net-fuel consumption as low as possible.

A computational model was developed by Ki and Kim [72] to find temperature distributions in solid structures and gas channels of an SOFC stack during the start-up operation. The start-up operation was modeled using two different heat-up methods, namely using hot air through the cathode channel or with an electrical furnace. Results of simulation for 1 kW planar SOFC showed that the required net-heating energy to reach a uniform temperature profile was similar for both heating methods. It was also demonstrated that in the air-heating case, having a constant mass flow rate of air through the stack would result in a larger amount of heat loss compared to a constant speed for the air flow.

Selimovic et al. [73] developed an in-house simulation code that was capable of anticipating steady-state and transient temperature distribution (heat-up, start-up, and shut-down operations). They determined the thermal stress induced by the difference in thermal expansion coefficients of the SOFC's components under high-temperature gradient. The in-house simulation was then used to assess the electrochemical and thermal performances of a planar SOFC. The output of the simulation determined the temperature distribution of the SOFC, which was then used in another model to estimate the thermal-stress components. The thermal loading's maximum principal stress was calculated and compared with the yield strength data reported in the literature. The knowledge of the maximum stress and its difference with yield stress could be used to improve the structural reliability of planar SOFCs. The ultimate design objective was to enhance the reliability of the SOFC during start-up, shut-down, and transient operations. The investigated cases were ceramic or metallic interconnects, hydrogen-/methane-fueled cells with cross-/co-/counter-flow configurations. The results showed that the largest stress occurred in a methane-fueled ceramic cell at the interface between the electrolyte and anode. It was observed that in the heat-up operation both interconnect types required about the same amount of time to reach the operating temperature. Concerning the start-up transition, the cell with the ceramic interconnect needed about 30 minutes when fed by hydrogen and an hour when fed by methane to reach the operational temperature. Furthermore the principal stress occurring in the cell domain is higher when the cell is fueled by methane than that with hydrogen. Concerning the shut-down operation, all investigated configurations would take a similar amount of time, about 4 hours, to cool down to about 100K.

Serincan et al. [74] developed a 2D axisymmetric transient CFD model by integrating mass, species, momentum, energy, and ionic and electronic charge conversion to study the dynamic response of a MT-SOFC based on an extension of their previous models [68,69] discussed in the previous Section 3.5.1. They also considered the internal current leakage since the ceria-based electrolyte was considered in the SOFC. The step change in voltage was taken into account and the current density response was studied. The cell exhibited an overshoot in the current density response immediately after the input step due to fast electrochemical reactions occurring in the electrodes (Fig. 3.20). It was shown that the dynamic response of the cell was controlled by heat transfer. Consequently it was also predicted that the time scale of the SOFC was in the order of 20 seconds.

The response of the cell to abrupt failure in the fuel-supply system was also studied. The results showed that cell reaction continues for about 4 seconds until all the hydrogen is consumed (Fig. 3.21). However, due to internal current leakage the electrochemical reaction could not be utilized and the cell stops producing external current. As the result, the cell response to the fuel-supply intruption which was observed by the output current occurred in less than 1 second.

A 2D axisymmetric model was developed by Amiri et al. [75] to investigate thermal transients of a MT-SOFC. The simulation results showed good agreement

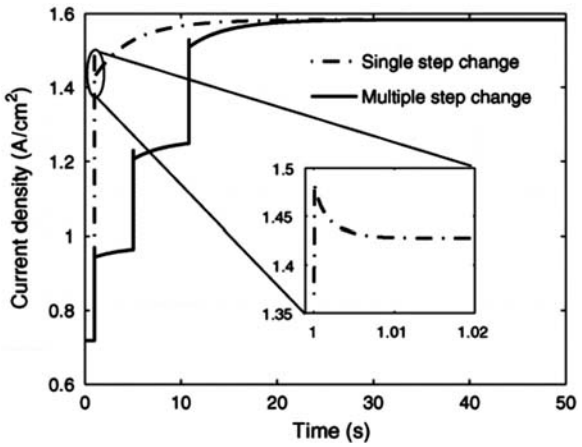

FIGURE 3.20

Current density response of the SOFC to two cases: (1) single-step change in voltage from 0.7 to 0.4 V at $t = 1$ s (*dashed line*), (2) multiple-step change in voltage from 0.7 to 0.6 V at $t = 1$ s then 0.6–0.5 V at $t = 6$ s and 0.5–0.4 V at $t = 11$ s (*solid line*) [71].

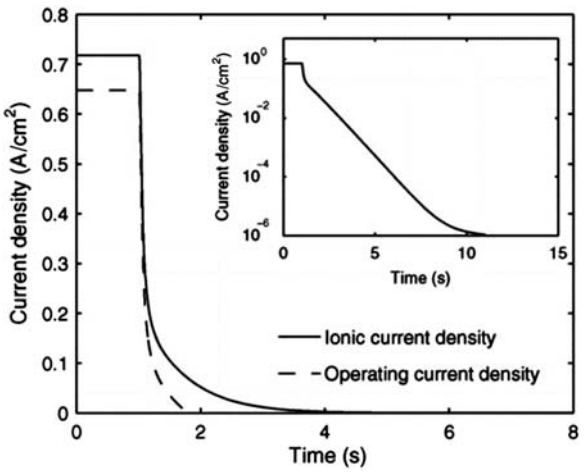

FIGURE 3.21

Ionic (*solid line*) and electronic (*dashed line*) current density response of the SOFC to failure in fuel supply at $t = 1$ s [71].

with experimental results. The model was used to simulate the transient behavior of the cell to a step-change in cell current and air flow. The results revealed that two transients determined the thermal response of the system. The faster transient was related to the heat transfer in the cell and the slower transient was associated with the heat transfer though the furnace walls. The fast thermal transients' time

constant was of the order of 2 seconds, which was expected for the MT-SOFC. The mass transfer and electrochemical reactions—introduced transients were very fast with time constants of a fraction of a second. Thus the transients of the system were controlled by thermal transients. Consequently, a fast electric response is the result of the small thermal mass of the system. When a step current was drawn from the cell the voltage showed a sharp drop that was followed by gradual recovery due to the increase in the temperature of the cell.

3.5.3 Configuration

Recknagle et al. [76] developed a 3D thermofluid electrochemical model to simulate a planar SOFC stack. The model integrated Star-CD a commercial CFD software with an experimentally validated ECM. Three flow configurations were investigated which were the co-flow, counter-flow, and cross-flow stack designs. Then the effects of flow configuration on temperature distribution, current density, and fuel species was studied. The results showed that for identical average cell temperature and fuel, the co-flow configuration had the most uniform temperature distribution and, thus, the smallest temperature gradients.

Tan et al. [77] investigated the effects of the flow configuration in SOFCs using a quasi-3D model. Various flow configurations including co, counter, and cross-flow as well as alternated air flow in parallel or perpendicular to the fuel flows were investigated (Fig. 3.22).

These flow configurations were analyzed for four fuel utilization (FU) amounts, namely 0.193, 0.386, 0.579, and 0.772. Fuel utilization is a nondimensional parameter equal to the ratio of the fuel consumed by the cell to generate the electric current to the total supply of fuel [77]. The results showed that the

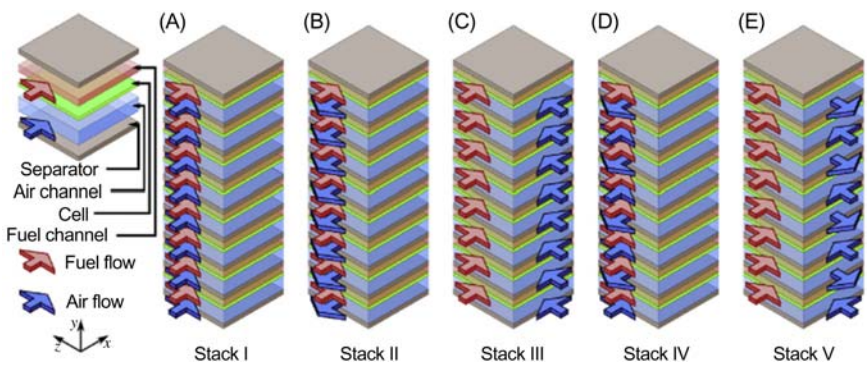

FIGURE 3.22

Flow configurations: (A) co-flow, (B) counter-flow, (C) cross-flow, (D) alternate air flow in parallel direction to the fuel flow, and (E) alternate air flow in perpendicular direction to the fuel flow [75].

counter-flow configuration had a higher voltage efficiency than co-flow and cross-flow configurations with the same FU. However, variability analysis (using an interquartile range) showed that the counter-flow configuration possessed the highest dispersion of current density. It was revealed that increasing the average current density worsened the nonuniformity. It was also reported that alternating the air-flow direction in the stack would allow better heat circulation in the air, which resulted in a more symmetrical temperature distribution as well as shifting the high-temperature region to the cell center. Supplying alternating air-flow from two different directions into the stack caused high-voltage efficiency due to high-cell temperature distribution with low dispersion, which increased the ion conductivity.

A 3D model was developed by Pianko-Oprych et al. [78] based on the similar numerical procedure utilized in Wei et al. [70] in order to investigate the effect of the flow channel and fuel cell arrangement on the thermal stresses and electrochemical performance of a MT-SOFC. The computation model was created by coupling a CFD and computational structural mechanics using ANSYS software. Three cell arrangements of a 48 anode supported MT-SOFC and their flow channels were considered (as depicted in Fig. 3.23). The first configuration (Fig. 3.23A) is denoted by case C-I (circular-internal air inlet) in which 12 fuel cells were distributed in 4 rows circularly. The second (Fig. 3.23B) and third (Fig. 3.23C) configurations represent two hexagonally distributed fuel cells in MT-SOFC with external and internal air cooling respectively. In H-E and H-I terminology denote hexagonally distributed fuel cells in the MT-SOFC with external air flow direction as well as internal air flow direction respectively. It should be noted that the cooling air entering the air distributor (i.e., located in the middle of the stack) is radially distributed between fuel cells toward the stack housing in the C-I and H-I cases (the internal cases). By comparison, in case H-E, the cooling air was supplied longitudinally from inlet channels located in the housing toward the outlet channel located in the middle of the stack.

The results showed that the uniform temperature distribution of the case H−E caused the smallest axial and total stresses as well as the smallest total displacement of the assembly. It should be noted that the constant flow velocity boundary condition was assumed for all cases rather than the constant mass flow rate. Thus the case with bigger air-inlet surface would have better cooling. Here the H−E case had the largest air-inlet surface and the C−I case had the lowest air-inlet surface.

Fardadi et al. [79] developed a dynamic SOFC model to investigate the effect of flow arrangement on temperature distribution and gradient under the transient and steady-state operations of the cell. Then an efficient feedback controller was proposed to minimize the temperature gradient in the SOFC during power variation. A modified cross-flow configuration (Fig. 3.24C) was also introduced to lessen the temperature gradients. The results showed that the suggested multiinput−multioutput feedback controller was capable of minimizing the temperature gradients in steady-state and transient operations.

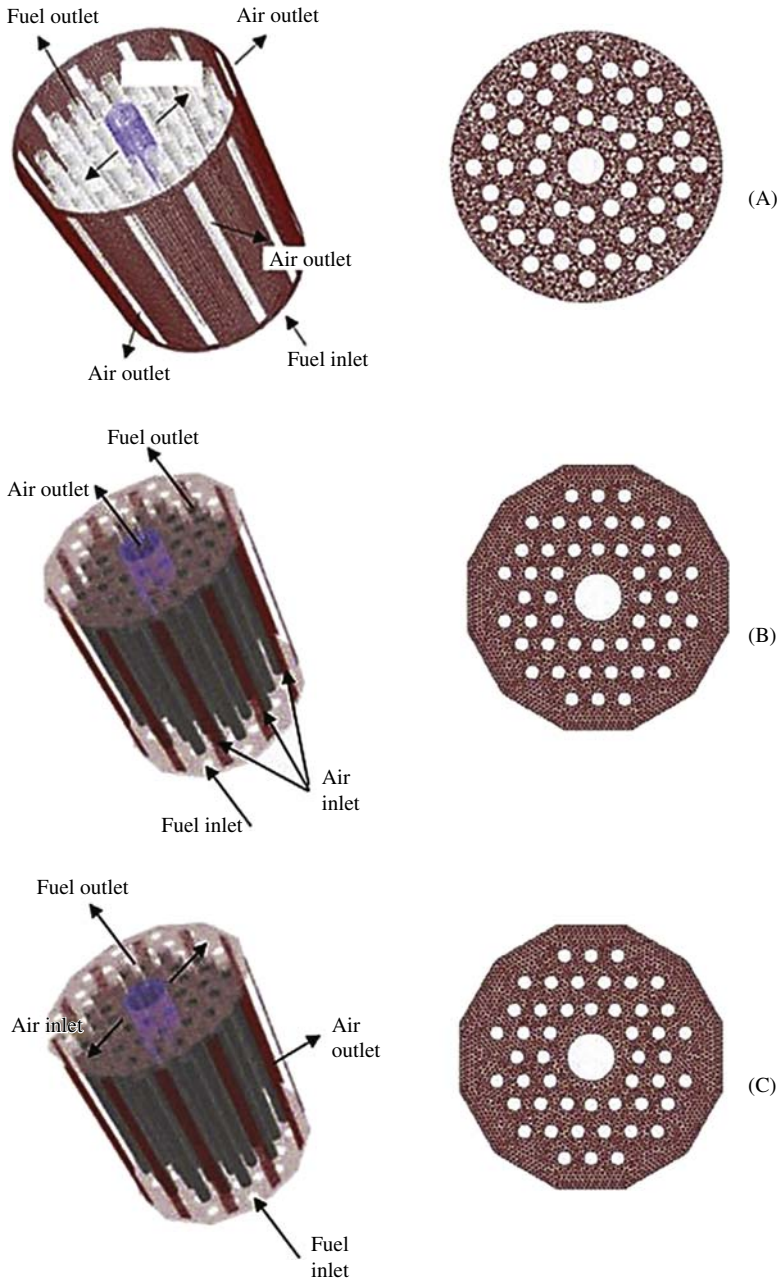

FIGURE 3.23

Anode-supported microtubular SOFC stack cases in which fuel cells are distributed: (A) **circularly** with an **internal** air flow direction (case **C**–**I**); (B) **hexagonally** with an **external** cooling air flow direction (case **H**–**E**); and (C) **hexagonally** with an **internal** cooling air flow direction (case **H**–**I**) [78].

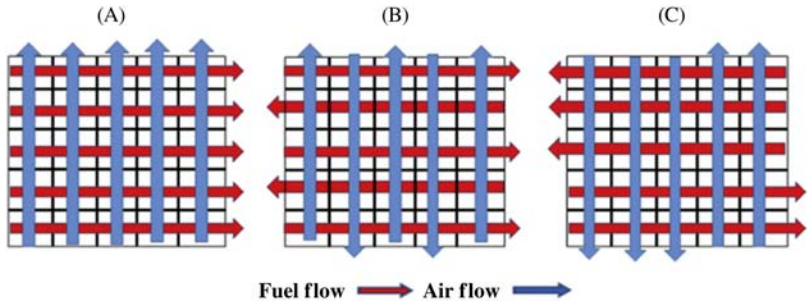

FIGURE 3.24

Flow arrangements: (A) traditional cross-flow design (basic arrangement), (B) reversed cross-flow, and (C) modified cross-flow [79].

The results suggested that this flow modification will result in lower temperature gradients (33K−39K) and a lower maximum-temperature difference across the cell (76K vs 124K), which implies more uniform temperature profiles (standard deviation of 22.5 against 26.5) and a higher efficiency (+1.4%) in comparison to the conventional cross-flow arrangement with a modest modification.

In case of open-loop operation, nonuniform distribution of the air-flow rate resulted in lower temperature gradients and smoother distribution for regular and modified cross-flow, but at the expense of a 3% lower efficiency in comparison to the uniform flow rate. However, using the nonuniform air flow rate and the modified flow simultaneously resulted in the best temperature distribution as well as a modest efficiency loss of 1.6%.

The results revealed that for a power variation of $\pm$ 15% a controller capable of regulating airflow and inlet temperature could achieve lower temperature gradients during transient response (14K against 27K for regular cross-flow).

3.5.4 Thermal management

Since SOFCs consist of ceramic components the challenges of thermal expansion coefficient (CTE) mismatch and large thermal gradients need to be addressed and avoided. The former challenge could be overcome by selecting suitable materials with relatively close CTEs, while the latter could be resolved by designing appropriate control strategies.

Since the minimum operating temperatures of SOFCs are high, the cooling down of the system should be avoided if it is required to be operated instantly. This could be done using passive and active strategies for temperature control by incorporating suitable thermal insulation or maintaining system temperature, respectively. One of the critical aspects of the thermal management of an SOFC system is the number of start-up cycles regardless of the system design. This would not be a problem for stationary operations with just a couple of shut-downs

per year. However, in the case of mobile applications, SOFC possibly undergoes multiple daily start-ups and shut-downs. For this case the operating temperature of the system could be maintained by system insulation for short, daily start-ups and shut-down times. However, the passive strategy may not be adequate for longer times. Thus keeping the system temperature around operating temperature through active heating may be required.

Apfel et al. [80] developed an FEM simulation to study a whole SOFC system during steady and transient operations. Three strategies for temperature control investigated in this study are depicted in Fig. 3.25A–C. The first (Fig. 3.25A) strategy is to allow cooling down of the system as slowly as possible, which could be achieved by utilizing adequate insulation (passive controlling).

It is evident from Fig. 3.25A that the stack should be heated before restarting the system, which will take some time due to limited input thermal power as well as avoiding thermal stresses.

In order to avoid these limitations the second strategy (Fig. 3.25B) could be used. In this case the stack is held at the desired operating temperature through continuous heating of the stack. However, keeping the system at an operating temperature in the range of 800°C–1000°C may cause problems regarding safety aspects and customer acceptance. Therefore the third strategy (Fig. 3.25C) was considered as a possible control strategy while retaining the advantages of the first and second strategies. In this case, the system is completely shut down for say 24 h and then reheated periodically. Using active and passive methods (i.e., an appropriately chosen isolation thickness and periodic reheating) the SOFC stack is kept above the minimum operating temperature. Thus the whole system can always be started abruptly.

The additional fuel consumption for the three strategies are listed in Table 3.3. The results show that the amount of additional fuel needed to keep the system at, or near, the desired operation temperature was not high for strategies (B) and (C) in comparison to strategy (A). Moreover, for strategy (A) the thermal loss was minimum (i.e., highest efficiency) in contrast to the two other strategies since the mean temperature between stack and ambience was the lowest. In addition, the decrease of efficiency due to thermal losses for strategies (B) and (C) were identical since the temperature difference between the stack and ambience was roughly equal.

Effective thermal management is crucial for the successful design of small-scale SOFC systems (<1 kW). While controlling separate processes that occur in each component of the system is important, managing the heat transfer from or to the components is another crucial aspect of system-level design.

Kattke and Braun [81] presented a modeling approach capable of capturing the thermal interactions among the components, which was then applied to the process-system design. The developed system-level thermal model considered the thermal interactions between system components including a reformer, burner, recuperator, and SOFC stack with the enclosure inner wall and the circulating cavity gas using thermal-resistance analysis. Three cases were considered for 1.1 kW SOFC system: in the first case (case A) the recuperator exhaust gases

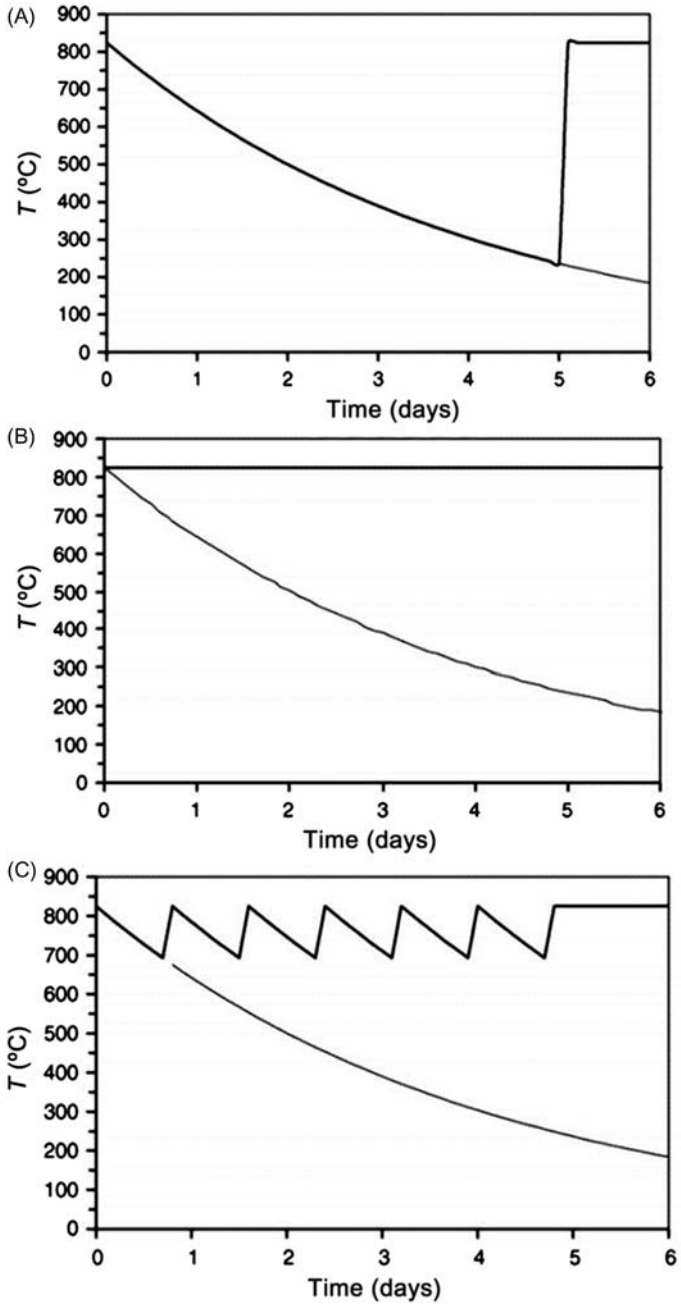

FIGURE 3.25

Different system strategies for prolonged periods of standstill: (A) only passive insulation, (B) active heating to maintain temperature, and (C) short reheating cycles so less energy is needed [79].

Table 3.3 Comparison of fuel consumption due to thermal losses and electricity production for the three strategies of thermal management.

Strategy	Fuel to compensate thermal loss during 6 days (MJ)	Fuel for operation over a given period (MJ)		
		1 h	5 h	24 h
(A)	11.4	45	225	1080
(B)	17.9			
(C)	19.4			

Stack data: nominal power: 5 kW, SOFC efficiency: 50%, burner efficiency: 80% [79].

were circulated within the enclosure resulting in forced convection within the enclosure (i.e., an integrated system model with forced convection). For the second case (case B) the recuperator exhaust gases were directly plumbed out of the enclosure resulting in natural convection within the enclosure (i.e., integrated system model with natural convection). In the third case (case C) a quasi-adiabatic system model was considered, which implies zero-heat transfer from recuperator, CPOx reformer, and burner, thereby avoiding the stack from cooling.

The results showed that when the conventional adiabatic thermodynamic model (case C) was used in the system design, the required stack oxidant flow rate was overpredicted by 84%, requiring a 90% larger recuperator heat duty compared with the thermally integrated system model (case B). In addition, in comparison to case A (circulating recuperator exhaust gas in the hot-box enclosure), case C overpredicted oxidant flow rate by 204% and recuperator heat duty by 221%. In case A, the oxidant usage was reduced by 39% compared to case B. The results also showed the importance of enclosure gas circulation for sizing the system components. Another important observation was that the external thermal boundary conditions had little effect on the overall system's operating performance due to the large enclosure surface area compared to system component areas. Although the thermal-resistance analysis with the system-level approach in this study was not validated experimentally it provided an understanding of the coupled heat transport phenomena among the SOFC components without requiring complicated and time-consuming 3D thermal-fluid simulations.

Detailed and accurate modeling of SOFCs' thermal management and their transient modeling of start-up and shut-down operations require considering the thermal contact resistance as a necessary input parameter.

Dillig et al. [82] measured the thermal contact resistance between different components of an SOFC stack repeating unit in the temperature range of 150°C−800°C. Thermal contact resistances between the interconnector and Ni-mesh (R_{c1}), Ni-mesh and anode (R_{c2}), and cathode and interconnector (R_{c3}) (Fig. 3.26) were calculated based on the measured data (Table 3.4).

Cao et al. [83] developed thermal management of a kW-scale SOFC system (including a planar SOFC stack, burner, and two heat exchangers (Fig. 3.27) using

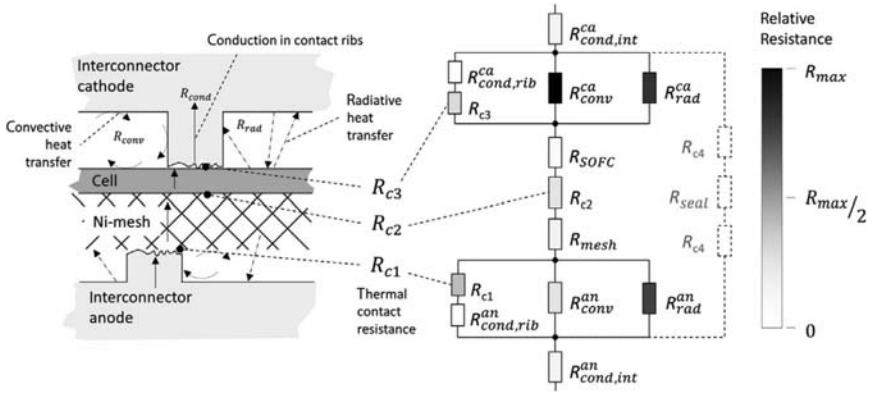

FIGURE 3.26

Schematic of heat-transfer mechanisms perpendicular to cell plane in SOFC stacks (left). Representation with thermal resistances [81] (right).

Table 3.4 Resulting heat transfer resistances for an solid oxide fuel cell stack repeating unit at different temperature levels (measured contact resistances are in bold typeface) [83].

	Relevant cross-section	**350°C**	**650°C**	**800°C**
	10^{-4} m²	**10^{-4}K m²/W**	**10^{-4}K m²/W**	**10^{-4}K m²/W**
$R^{ca}_{cond,int}$	7.07	0.22	0.20	0.19
$R^{ca}_{cond,rib}$	2.36	0.31	0.28	0.27
R_{c3}	**2.36**	**4.65**	**3.85**	**3.38**
R^{ca}_{conv}	4.71	97.69	72.96	65.27
R^{ca}_{rad}	4.71	224.00	68.88	43.84
R^{ca}_{SOFC}	7.07	1.03	0.99	1.09
R_{c2}	**7.07**	**14.34**	**9.54**	**8.18**
R_{mesh}	7.07	4.06	3.50	3.26
R^{an}_{rad}	4.71	201.60	61.99	39.46
R^{an}_{conv}	4.71	8.37	6.11	5.40
R_{c1}	**2.36**	**8.68**	**6.06**	**4.29**
$R^{an}_{cond,rib}$	2.36	0.22	0.20	0.19
$R^{an}_{cond,int}$	7.07	0.22	0.20	0.19
R_{ru}	7.07	41.17	30.24	26.13

a MATLAB/Simulink platform. The main objetive was to maximize system efficiency (while ensuring system safety) through temperature management which was conducted by utilizing an air bypass around the heat exchangers.

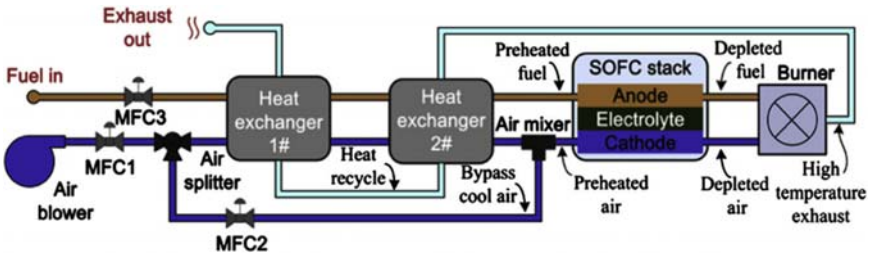

FIGURE 3.27

Schematic of a kW-scale SOFC system [83].

Moreover the effects of operating parameters including FU, air excess (AE) ratio, bypass ratio, and stack voltage (SV) on the system performances (e.g., system efficiency, stack inlet, stack outlet, and burner temperatures) were investigated. Notably an optimal relationship between the system efficiency and operating parameters were proposed. Then by utilizing the optimal relationship a transverse optimization was performed to calculate the maximum system efficiency as well as the safe operating parameters at any efficient SV operation point. As the operating voltage range varied from 104 to 84.5 V, the maximum system efficiency decreased from 54.1% to 24.2% in which the stack inlet and outlet temperatures were kept constant at 978K and 1063K, respectively. This control strategy enabled the SOFC system to work at optimum operating conditions. The results also revealed two important system characteristics. First, the control design of the SOFC system was nonlinear and requires a switching control structure. Second, if the temperature of the upstream stack is controlled, the burner will operate within the safe temperature zone.

Dilling and Karl [84] developed a 2D thermoelectrochemical model for a solid oxide cell system. A high-temperature, solid oxide cell could be operated in an electrolyzer cell or fuel-cell mode. The results revealed that integrating heat pipes into the stack structure as the proposed electrolyzer cell results in the reduction of temperature gradients. At the operating voltage of 1.29 V no thermal gradients were produced and no temperature control was required.

In an experimental study, Zeng et al. [85] designed a new tubular heat pipe−solid oxide fuel cell (HP−SOFC) that was capable of minimizing the temperature gradient within the SOFC. Thus the proposed HP−SOFC had better electrochemical performance and lowered thermal stresses. They integrated a heat pipe with liquid sodium metal with a tubular SOFC that consisted of five layers, namely heat-functional, current-collecting, anode, electrolyte, and cathode layers (Fig. 3.28).

In addition, a porous media (Fig. 3.28B) was also utilized to measure the HP−SOFC's electrochemical performance under the extreme operating condition of the methane flame. The results showed that the temperature gradient along the axis of the SOFC was reduced from 31K/cm in the conventional SOFC to 13K/cm in the proposed HP−SOFC. In the extreme methane condition the

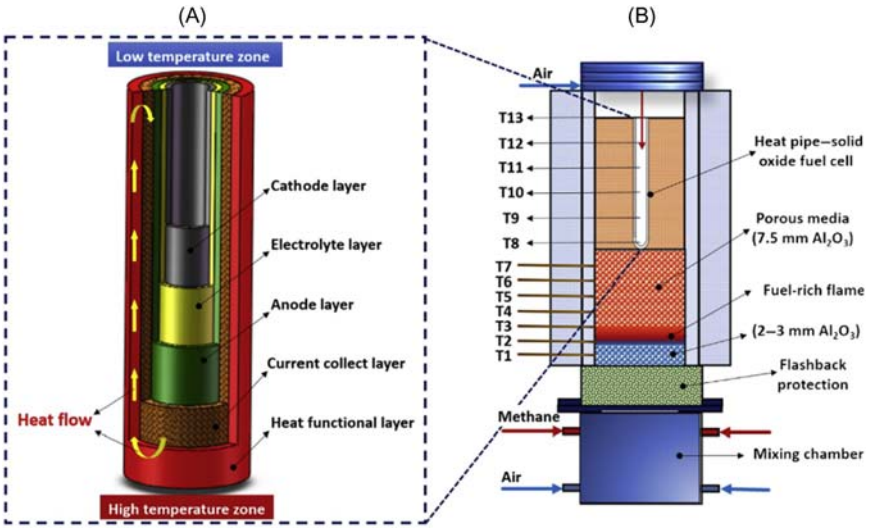

FIGURE 3.28

Heat pipe–solid oxide fuel cell structure and experimental setup [84]. (A) HP–SOFC structure and (B) experimental setup.

HP–SOFC had better performance compared to conventional SOFCs. It was reported that at an equal inlet air-flow rate and equivalence ratio (i.e., the ratio of methane-to-air flow rate fraction to methane-to-air flow rate fraction at stoichiometric condition) a maximum power density of 120 mW/cm^2 was reached for the HP–SOFC, while the maximum achievable power density for a conventional SOFC is around 73 mW/cm^2. Thus it can be inferred that utilizing the heat pipe with liquid sodium metal as the heat-transfer medium improved the SOFC's performance.

3.6 Conclusion

The primary purpose of this chapter was to analyze SOFCs with respect to their mechanical features. From the mechanical engineering viewpoint, studying the stresses and the factors that induce them are necessary in order to quantify their impact on the SOFC key performance indicators. Therefore the first part of the chapter was dedicated to discussing different geometries and configurations of SOFCs alone and within those stacks. As extensively discussed, planar and tubular are the main geometric configurations of SOFCs. However, these configurations do not completely satisfy the requirements for mobile applications. Hence other geometries such as IP-SOFCs, cone-shaped SOFCs, and MT-SOFCs that

essentially combine the two primary designs were proposed by the researchers. MT-SOFCs with high resistance to thermal shocks and fast start-up seems to be one of the best available choices. Gathering cells for producing higher power introduced the concept of SOFC stacks. Their key features of interest include determining the temperature and stress distribution, which were discussed in this chapter. Fabrication methods are another major research area that profoundly affects the residual stresses in the cells. Here, different fabrication methods were introduced. Common large-scale fabrication methods of SOFCs are dip coating and screen printing for fabrication of functional layers, and tape casting for the supported and functional layers. Phase inversion is a relatively quick method used for manufacturing SOFCs in microscale (i.e., MT-SOFCs).

The chapter also discussed the mechanical performance and reliability of SOFCs. As SOFCs are high-temperature dependent devices, their extreme operating conditions also influence the induced stresses in the cells. In this respect, various malfunctions related to the operational and manufacturing conditions were discussed. Typical problems related to SOFCs are degradation (change in the microstructure of porous electrodes), delamination (gap between electrode and electrolyte layers), and redox (a common problem in Ni-based anodes and the reduction−oxidation of anode particles due to the shortage of fuel). They are studied deeply on that part.

The thermal analysis of different cells was presented. Since the experimental thermal analysis of SOFCs is expensive and time-consuming, thermal modeling would be more practical and is often examined first. Several SOFC modeling studies were discussed. The main purpose of thermal modeling is to find the temperature distribution that is required as the input for the structural analysis of SOFCs. SOFCs' transient operation is important because temperature must be raised from room temperature to operating temperature (about 700°C). Finally, some of the thermal management studies and methods for SOFCs are mentioned. The results show that thermal management could reduce temperature gradients, which keeps the SOFC structures safe with respect to thermal stresses. However, the main purpose of thermal management is to maintain SOFCs' temperature in a limited range for instant start-ups.

3.7 Future perspectives

Based on the critical review of the research in the field the following potent areas for future research are proposed:

- Thermal simulation of SOFC systems play an important role in the design of the system since temperature distribution is essential to calculate stress distribution in SOFCs' components. One of the main challenges in this regard is coupling the heat transfer, electrochemical, fluid flow, and structural equations. Therefore it is expected that in future simulation software tools that

are capable of integrating multiple physics will be the frontier in the theoretical research in the field rather than developed in-house codes.
- Parametric optimization of SOFC design, configuration, and geometry have profound impacts on the mechanical characteristics of SOFCs and, therefore, remain a major research area. New geometric configurations need to be developed.
- Mobile application requirements.
- Fabrication of SOFCs using common methods is a time-consuming process that poses a key barrier for commercialization. Development of cost-efficient fabrication methods that ensure proper microstructure and high length of TPB as well as inducing less residual stress are crucial for the mass production of SOFCs, and offers a potent research area.
- The operating temperature of an SOFC is highly related to its electrolyte properties. High-ionic conductivity, low-electrical conductivity, and stability of the material are the main required properties. Research on materials with desirable properties under lower temperatures could greatly improve the performance of SOFCs and reduce their cost.
- Thermal transient modeling is another important aspect of SOFC system design and reliability. Modeling more realistic thermal transients based on more detailed multiphysics simulation models could open up new avenues for the thermal management of SOFCs.

References

[1] J. Ding, J. Liu, G. Yin, Fabrication and characterization of low-temperature SOFC stack based on GDC electrolyte membrane, J. Memb. Sci. 371 (1–2) (2011) 219–225.
[2] T. Ishihara, N.M. Sammes, O. Yamamoto, Chapter 4 - Electrolytes, in: S.C. Singhal, K. Kendall (Eds.), High Temperature and Solid Oxide Fuel Cells, Elsevier Science, Amsterdam, 2003, pp. 83–117.
[3] D. Marcano, G. Mauer, R. Vaßen, A. Weber, Manufacturing of high performance solid oxide fuel cells (SOFCs) with atmospheric plasma spraying (APS) and plasma spray-physical vapor deposition (PS-PVD), Surf. Coatings Technol. 318 (2017) 170–177.
[4] L.S. Mahmud, A. Muchtar, M.R. Somalu, Challenges in fabricating planar solid oxide fuel cells: a review, Renew. Sustain. Energy Rev. 72 (2017) 105–116.
[5] D.-W. Kim, et al., Fabrication and operating characteristics of a flat tubular segmented-in-series solid oxide fuel cell unit bundle, Energy 72 (2014) 215–221.
[6] B. Timurkutluk, C. Timurkutluk, M.D. Mat, Y. Kaplan, A review on cell/stack designs for high performance solid oxide fuel cells, Renew. Sustain. Energy Rev. 56 (2016) 1101–1121.
[7] W. Bujalski, C.M. Dikwal, K. Kendall, Cycling of three solid oxide fuel cell types, J. Power Sources 171 (1) (2007) 96–100.
[8] J. Sui, J. Liu, An electrolyte-supported SOFC stack fabricated by slip casting technique, ECS Trans. 7 (1) (2007) 633–637.

[9] Y. Bai, J. Liu, H. Gao, C. Jin, Dip coating technique in fabrication of cone-shaped anode-supported solid oxide fuel cells, J. Alloys Compd. 480 (2) (2009) 554–557.
[10] N. Raeis Hosseini, N.M. Sammes, J.S. Chung, Manganese-doped lanthanum calcium titanate as an interconnect for flat-tubular solid oxide fuel cells, J. Power Sources 245 (2014) 599–608.
[11] B.K. Park, et al., La-doped $SrTiO_3$ interconnect materials for anode-supported flat-tubular solid oxide fuel cells, Int. J. Hydrogen Energy 37 (5) (2012) 4319–4327.
[12] T. Yamaguchi, S. Shimizu, T. Suzuki, Y. Fujishiro, M. Awano, Development and evaluation of a cathode-supported SOFC having a honeycomb structure, Electrochem. Solid-State Lett. 11 (7) (2008) B117–B121.
[13] T. Yamaguchi, S. Shimizu, T. Suzuki, Y. Fujishiro, M. Awano, Evaluation of extruded cathode honeycomb monolith-supported SOFC under rapid start-up operation, Electrochim. Acta 54 (5) (2009) 1478–1482.
[14] F.P. Nagel, T.J. Schildhauer, S.M.A. Biollaz, A. Wokaun, Performance comparison of planar, tubular and Delta8 solid oxide fuel cells using a generalized finite volume model, J. Power Sources 184 (1) (2008) 143–164.
[15] Y. Liu, Y. Tang, J. Ding, J. Liu, Electrochemical performance of cone-shaped anode-supported segmented-in-series SOFCs fabricated by gel-casting technique, Int. J. Hydrogen Energy 37 (1) (2012) 921–925.
[16] J. Ding, J. Liu, A novel design and performance of cone-shaped tubular anode-supported segmented-in-series solid oxide fuel cell stack, J. Power Sources 193 (2) (2009) 769–773.
[17] C. Chen, M. Liu, L. Yang, M. Liu, Anode-supported micro-tubular SOFCs fabricated by a phase-inversion and dip-coating process, Int. J. Hydrogen Energy 36 (9) (2011) 5604–5610.
[18] C. Yang, C. Jin, F. Chen, Micro-tubular solid oxide fuel cells fabricated by phase-inversion method, Electrochem. commun. 12 (5) (2010) 657–660.
[19] L.P. Sun, M. Rieu, J.P. Viricelle, C. Pijolat, H. Zhao, Fabrication and characterization of anode-supported single chamber solid oxide fuel cell based on $La_{0.6}Sr_{0.4}Co_{0.2}Fe_{0.8}O_3 - \delta - Ce_{0.9}Gd_{0.1}O_{1.95}$ composite cathode, Int. J. Hydrogen Energy 39 (2) (2014) 1014–1022.
[20] T. Choudhary, Sanjay, Computational analysis of IR-SOFC: thermodynamic, electrochemical process and flow configuration dependency, Int. J. Hydrogen Energy 41 (2) (2016) 1259–1271.
[21] J. Kupecki, J. Milewski, A. Szczesniak, R. Bernat, K. Motylinski, Dynamic numerical analysis of cross-, co-, and counter-current flow configuration of a 1 kW-class solid oxide fuel cell stack, Int. J. Hydrogen Energy 40 (45) (2015) 15834–15844.
[22] C.M. Huang, S.S. Shy, C.H. Lee, On flow uniformity in various interconnects and its influence to cell performance of planar SOFC, J. Power Sources 183 (1) (2008) 205–213.
[23] S.-D. Kim, et al., Effects of anode and electrolyte microstructures on performance of solid oxide fuel cells, J. Power Sources 169 (2) (2007) 265–270.
[24] L.F.G. Setz, I. Santacruz, M.T. Colomer, S.R.H. Mello-Castanho, Tape casting of strontium and cobalt doped lanthanum chromite suspensions, J. Eur. Ceram. Soc. 30 (14) (2010) 2897–2903.
[25] M.R. Somalu, V. Yufit, I.P. Shapiro, P. Xiao, N.P. Brandon, The impact of ink rheology on the properties of screen-printed solid oxide fuel cell anodes, Int. J. Hydrogen Energy 38 (16) (2013) 6789–6801.

[26] M.R. Somalu, V. Yufit, N.P. Brandon, The effect of solids loading on the screen-printing and properties of nickel/scandia-stabilized-zirconia anodes for solid oxide fuel cells, Int. J. Hydrogen Energy 38 (22) (2013) 9500–9510.
[27] W. Schafbauer, N.H. Menzler, H.P. Buchkremer, Tape casting of anode supports for solid oxide fuel cells at Forschungszentrum Jülich, Int. J. Appl. Ceram. Technol. 11 (1) (2014) 125–135.
[28] M. Michálek, G. Blugan, T. Graule, J. Kuebler, Comparison of aqueous and non-aqueous tape casting of fully stabilized ZrO_2 suspensions, Powder Technol. 274 (2015) 276–283.
[29] S. Lee, K. Lee, Y. Jang, J. Bae, Fabrication of solid oxide fuel cells (SOFCs) by solvent-controlled co-tape casting technique, Int. J. Hydrogen Energy 42 (3) (2017) 1648–1660.
[30] M. Jabbari, R. Bulatova, A.I.Y. Tok, C.R.H. Bahl, E. Mitsoulis, J.H. Hattel, Ceramic tape casting: a review of current methods and trends with emphasis on rheological behaviour and flow analysis, Mater. Sci. Eng. B 212 (2016) 39–61.
[31] A. Faes, H. Girard, A. Zryd, Z. Wuillemin, J. Van herle, Fabrication of structured anode-supported solid oxide fuel cell by powder injection molding, J. Power Sources 227 (2013) 35–40.
[32] R. Kluczowski, M. Krauz, M. Kawalec, J.P. Ouweltjes, Near net shape manufacturing of planar anode supported solid oxide fuel cells by using ceramic injection molding and screen printing, J. Power Sources 268 (2014) 752–757.
[33] H.M. Mohamed, Screen-printed disposable electrodes: pharmaceutical applications and recent developments, TrAC Trends Anal. Chem. 82 (2016) 1–11.
[34] D. Burnat, P. Ried, P. Holtappels, A. Heel, T. Graule, D. Kata, The rheology of stabilised lanthanum strontium cobaltite ferrite nanopowders in organic medium applicable as screen printed SOFC cathode layers, Fuel Cells 10 (1) (2010) 156–165.
[35] H. Tikkanen, C. Suciu, I. Wærnhus, A.C. Hoffmann, Dip-coating of 8YSZ nanopowder for SOFC applications, Ceram. Int. 37 (7) (2011) 2869–2877.
[36] A. Torabi, T.H. Etsell, P. Sarkar, Dip coating fabrication process for micro-tubular SOFCs, Solid State Ionics 192 (1) (2011) 372–375.
[37] T. Yamaguchi, T. Suzuki, S. Shimizu, Y. Fujishiro, M. Awano, Examination of wet coating and co-sintering technologies for micro-SOFCs fabrication, J. Memb. Sci. 300 (1–2) (2007) 45–50.
[38] M.F. Mohd Yusoff, M.R. Abdul Kadir, N. Iqbal, M.A. Hassan, R. Hussain, Dipcoating of poly(ε-caprolactone)/hydroxyapatite composite coating on Ti6Al4V for enhanced corrosion protection, Surf. Coatings Technol. 245 (2014) 102–107.
[39] X. Xu, C. Xia, S. Huang, D. Peng, YSZ thin films deposited by spin-coating for IT-SOFCs, Ceram. Int. 31 (8) (2005) 1061–1064.
[40] H. Sun, W. Ma, J. Yu, X. Chen, H. Lin, Preparation and characterization of $La_{0.8}Sr_{0.04}Ca_{0.16}Co_{0.6}Fe_{0.4}O_3 - \delta - La_{0.9}Sr_{0.1}Ga_{0.8}Mg_{0.2}O_3$ composite cathode thin film for SOFC by slurry spin coating, J. Rare Earths 28 (6) (2010) 917–921.
[41] D. Ding, W. Zhu, J. Gao, C. Xia, High performance electrolyte-coated anodes for low-temperature solid oxide fuel cells: model and experiments, J. Power Sources 179 (1) (2008) 177–185.
[42] F. Zhao, Z. Wang, M. Liu, L. Zhang, C. Xia, F. Chen, Novel nano-network cathodes for solid oxide fuel cells, J. Power Sources 185 (1) (2008) 13–18.

[43] C. Yoon, M. Liu, D. Yuan, R. Guo, M. Liu, S. Das, Microarchitectured solid oxide fuel cells with improved energy efficiency (part II): fabrication and characterization, J. Power Sources 293 (2015) 883–891.
[44] A. Nakajo, et al., Compilation of mechanical properties for the structural analysis of solid oxide fuel cell stacks. Constitutive materials of anode-supported cells, Ceram. Int. 38 (5) (2012) 3907–3927.
[45] Z. Wuillemin, N. Autissier, A. Nakajo, M. Luong, J. Van herle, D. Favrat, Modeling and study of the influence of sealing on a solid oxide fuel cell, J. Fuel Cell Sci. Technol. 5 (1) (2008) 11016–11019.
[46] J.I. Gazzarri, O. Kesler, Short stack modeling of degradation in solid oxide fuel cells: part II. Sensitivity and interaction analysis, J. Power Sources 176 (1) (2008) 155–166.
[47] L. Barelli, E. Barluzzi, G. Bidini, Diagnosis methodology and technique for solid oxide fuel cells: a review, Int. J. Hydrogen Energy 38 (12) (2013) 5060–5074.
[48] D. Sarantaridis, R.A. Rudkin, A. Atkinson, Oxidation failure modes of anode-supported solid oxide fuel cells, J. Power Sources 180 (2) (2008) 704–710.
[49] D. Larrain, J. Van herle, D. Favrat, Simulation of SOFC stack and repeat elements including interconnect degradation and anode reoxidation risk, J. Power Sources 161 (1) (2006) 392–403.
[50] A. Faes, A. Hessler-Wyser, A. Zryd, J. Van herle, A review of RedOx cycling of solid oxide fuel cells anode, Membranes 2 (3) (2012).
[51] J. Laurencin, G. Delette, F. Lefebvre-Joud, M. Dupeux, A numerical tool to estimate SOFC mechanical degradation: case of the planar cell configuration, J. Eur. Ceram. Soc. 28 (9) (2008) 1857–1869.
[52] B. Sun, R.A. Rudkin, A. Atkinson, Effect of thermal cycling on residual stress and curvature of anode-supported SOFCs, Fuel Cells 9 (6) (2009) 805–813.
[53] H.L. Frandsen, et al., Accelerated creep in solid oxide fuel cell anode supports during reduction, J. Power Sources 323 (2016) 78–89.
[54] J.I. Gazzarri, O. Kesler, Non-destructive delamination detection in solid oxide fuel cells, J. Power Sources 167 (2) (2007) 430–441.
[55] J.I. Gazzarri, O. Kesler, Electrochemical AC impedance model of a solid oxide fuel cell and its application to diagnosis of multiple degradation modes, J. Power Sources 167 (1) (2007) 100–110.
[56] A.V. Virkar, A model for solid oxide fuel cell (SOFC) stack degradation, J. Power Sources 172 (2) (2007) 713–724.
[57] G. Brus, H. Iwai, A. Sciazko, M. Saito, H. Yoshida, J.S. Szmyd, Local evolution of anode microstructure morphology in a solid oxide fuel cell after long-term stack operation, J. Power Sources 288 (2015) 199–205.
[58] B. Bozzini, et al., In-situ photoelectron microspectroscopy during the operation of a single-chamber SOFC, Electrochem. Commun. 24 (2012) 104–107.
[59] K. Kumada, K. Sato, T. Hashida, Evaluation of mechanical damages in SOFCs during start/stop operation by using acoustic emission technique, ECS Trans. 78 (1) (2017) 2355–2363.
[60] T. Dey, D. Singdeo, J. Deshpande, P.C. Ghosh, Structural analysis of solid oxide fuel cell under externally applied compressive pressure, Energy Procedia 54 (2014) 789–795.
[61] Y.-P. Chyou, T.-D. Chung, J.-S. Chen, R.-F. Shie, Integrated thermal engineering analyses with heat transfer at periphery of planar solid oxide fuel cell, J. Power Sources 139 (1–2) (2005) 126–140.

[62] H. Mounir, A. El Gharad, M. Belaiche, M. Boukalouch, Non-isothermal and electrochemical modelling of the multi-cell module performance in the integrated-planar solid oxide fuel cell, Proc. Inst. Mech. Eng. A: J. Power Energy 224 (1) (2010) 23–33.
[63] S. Tonekabonimoghadam, et al., Mathematical modelling and experimental validation of an anode-supported tubular solid oxide fuel cell for heat and power generation, Energy 90 (2015) 1759–1768.
[64] L.-K. Chiang, H.-C. Liu, Y.-H. Shiu, C.-H. Lee, R.-Y. Lee, Thermal stress and thermo-electrochemical analysis of a planar anode-supported solid oxide fuel cell: effects of anode porosity, J. Power Sources 195 (7) (2010) 1895–1904.
[65] M. Ni, 2D thermal-fluid modeling and parametric analysis of a planar solid oxide fuel cell, Energy Convers. Manag. 51 (2010) 714–721.
[66] H. Mounir, M. Belaiche, A. El Marjani, A. El Gharad, Thermal stress and probability of survival investigation in a multi-bundle integrated-planar solid oxide fuel cells IP-SOFC (integrated-planar solid oxide fuel cell), Energy 66 (2014) 378–386.
[67] C. Wang, et al., Numerical simulation and analysis of thermal stress distributions for a planar solid oxide fuel cell stack with external manifold structure, Int. J. Hydrogen Energy 43 (45) (2018) 20900–20910.
[68] M.F. Serincan, U. Pasaogullari, N.M. Sammes, Computational thermal-fluid analysis of a microtubular solid oxide fuel cell, J. Electrochem. Soc. 155 (11) (2008) B1117.
[69] M.F. Serincan, U. Pasaogullari, N.M. Sammes, Thermal stresses in an operating micro-tubular solid oxide fuel cell, J. Power Sources 195 (15) (2010) 4905–4914.
[70] S.-S. Wei, T.-H. Wang, J.-S. Wu, Numerical modeling of interconnect flow channel design and thermal stress analysis of a planar anode-supported solid oxide fuel cell stack, Energy 69 (2014) 553–561.
[71] A. Li, C. Song, Z. Lin, A multiphysics fully coupled modeling tool for the design and operation analysis of planar solid oxide fuel cell stacks, Appl. Energy 190 (2017) 1234–1244.
[72] J. Ki, D. Kim, Computational model to predict thermal dynamics of planar solid oxide fuel cell stack during start-up process, J. Power Sources 195 (10) (2010) 3186–3200.
[73] A. Selimovic, M. Kemm, T. Torisson, M. Assadi, Steady state and transient thermal stress analysis in planar solid oxide fuel cells, J. Power Sources 145 (2) (2005) 463–469.
[74] M.F. Serincan, U. Pasaogullari, N.M. Sammes, A transient analysis of a micro-tubular solid oxide fuel cell (SOFC), J. Power Sources 194 (2) (2009) 864–872.
[75] S. Amiri, R. Hayes, P. Sarkar, Transient simulation of a tubular micro-solid oxide fuel cell, J. Power Sources 407 (2018) 63–69.
[76] K. Recknagle, R. Williford, L. Chick, D. Rector, M. Khaleel, Three-dimensional thermo-fluid electrochemical modeling of planar SOFC stacks, J. Power Sources 113 (1) (2003) 109–114.
[77] W.C. Tan, H. Iwai, M. Kishimoto, H. Yoshida, Quasi-three-dimensional numerical simulation of a solid oxide fuel cell short stack: effects of flow configurations including air-flow alternation, J. Power Sources 400 (2018) 135–146.
[78] P. Pianko-Oprych, T. Zinko, Z. Jaworski, Simulation of thermal stresses for new designs of microtubular solid oxide fuel cell stack, Int. J. Hydrogen Energy 40 (42) (2015) 14584–14595.

[79] M. Fardadi, D.F. McLarty, F. Jabbari, Investigation of thermal control for different SOFC flow geometries, Appl. Energy 178 (2016) 43–55.
[80] H. Apfel, M. Rzepka, H. Tu, U. Stimming, Thermal start-up behaviour and thermal management of SOFC's, J. Power Sources 154 (2) (2006) 370–378.
[81] K.J. Kattke, R.J. Braun, Implementing thermal management modeling into SOFC system level design, J. Fuel Cell Sci. Technol. 8 (2) (2011) 021009.
[82] M. Dillig, T. Biedermann, J. Karl, Thermal contact resistance in solid oxide fuel cell stacks, J. Power Sources 300 (2015) 69–76.
[83] H. Cao, X. Li, Z. Deng, J. Li, Y. Qin, Thermal management oriented steady state analysis and optimization of a kW scale solid oxide fuel cell stand-alone system for maximum system efficiency, Int. J. Hydrogen Energy 38 (28) (2013) 12404–12417.
[84] M. Dillig, J. Karl, Thermal management of high temperature solid oxide electrolyser cell/fuel cell systems, Energy Procedia 28 (2012) 37–47.
[85] H. Zeng, Y. Wang, Y. Shi, N. Cai, D. Yuan, Highly thermal integrated heat pipe–solid oxide fuel cell, Appl. Energy 216 (2018) 613–619.

CHAPTER

Engineering solid oxide fuel cell materials

4

Wenqian Chen

Department of Chemical Engineering, Imperial College London, London, United Kingdom

4.1 Introduction

A solid oxide fuel cell (SOFC) is an electrochemical device that generates electricity through the oxidation of a fuel such as hydrogen and hydrocarbons. Although SOFCs are advantageous in terms of energy conversion efficiency, power density and fuel flexibility in comparison to other types of fuel cells, [1] a significant cost reduction is needed for SOFCs to be a competitive energy-generation technology [2,3]. This can be achieved by improving the performance of cell components, while controlling the cost of materials and fabrication process.

The main components of an SOFC include two porous electrodes and a dense solid electrolyte (Fig. 4.1). The electrolyte should have high conductivity for oxide ions that are generated at the cathode and low conductivity for electrons that are generated at the anode [4]. It is usually a solid oxide that allows the passage of oxide ions via the oxygen vacancy hopping mechanism at an elevated temperature (typically 800°C−1000°C) [5,6]. On the other hand, the cathode is typically a porous oxide that allows the penetration of oxygen and catalyzes its reduction to oxide ions, whereas the anode is typically a porous ceramic−metallic composite that catalyzes the oxidation of fuels such as hydrogen and hydrocarbons [7,8].

In addition to the numerous reviews on the material perspectives of SOFCs [9−13], this chapter highlights both the selection and processing of materials for the various components of an SOFC cell as the material composition and microstructural characteristics have fundamental influences on the performance of each cell component. This chapter only discusses oxide-conducting SOFCs (Fig. 4.2A), which are the mainstream developments. Readers interested in proton-conducting SOFCs (Fig. 4.2B) should refer to other literature available [14]. The materials most commonly used in commercial SOFCs that operate at high temperatures (i.e., 800°C−1000°C) are first discussed as the state-of-the-art, followed by recent developments that enable the operation of SOFCs at intermediate (i.e., 650°C−800°C) and low temperatures (i.e., <650°C) (note: intermediate and low temperature are also referred to as reduced temperature in this chapter). The

Design and Operation of Solid Oxide Fuel Cells. DOI: https://doi.org/10.1016/B978-0-12-815253-9.00004-5

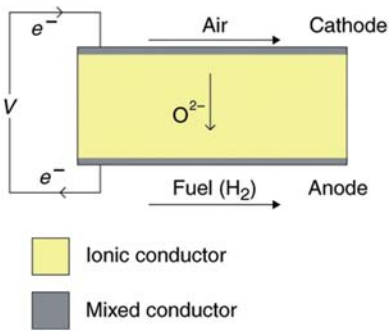

FIGURE 4.1

Typical structure of an solid oxide fuel cell (SOFC) [6].

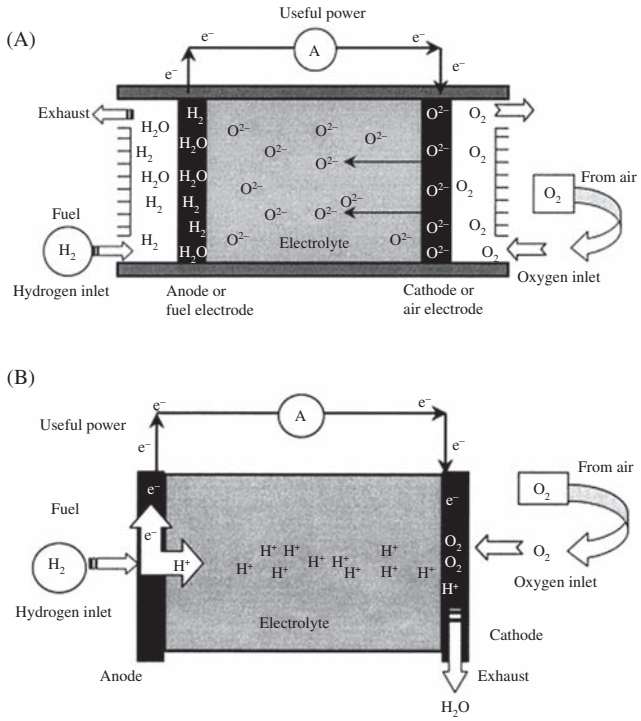

FIGURE 4.2

Schematics of (A) oxide-conducting and (B) proton-conducting solid oxide fuel cells (SOFCs) [1].

reduction of operation temperature can significantly lower the cost of SOFCs as more economical materials can be used and the rate of material degradation over time is reduced.

4.2 Electrolyte

The electrolyte in an SOFC conducts ions (i.e., oxide or protons) selectively against electrons and plays the most important role in determining the energy performance of the SOFC. Ideally, its ionic transference number should be higher than 0.99 and its electronic transference number should be less than 0.01 [4]. Furthermore, it should have chemical and thermal stability between room temperature (i.e., 20°C−25°C) and 1000°C under a wide range of oxygen-partial pressure. Its thermal expansion coefficient (TEC) should be compatible with those of the cathode and anode to prevent cracking during cell fabrication and operation. It should not react with the cathode and anode to produce side-products that hinder the conduction of ions.

4.2.1 Material selection for electrolyte

In order to efficiently conduct oxide ions, the electrolyte should have a host crystal structure with a large interionic open space that leads to considerable point defect disorder and low-migration enthalpy [15]. Doping a solid oxide with lower-valent cations can make the host lattice deficient in oxygen and hence create oxygen vacancies as charge-compensating defects [16]. Common examples include zirconia (ZrO_2) doped with yttria (Y^{3+}) or scandia (Sc^{3+}).

The oxide conductivity of electrolyte is strongly dependent on the operating conditions such as temperature (e.g., oxide conductivity increases with temperature in general; Fig. 4.3A) [17] as well as its physical properties such as composition (Fig. 4.3B) and microstructure. In terms of composition, the choice of oxide determines the overall crystal structure of the electrolyte and the choice of dopant cations determines the binding enthalpy between oxygen vacancies and the dopant cations in the defect associates. For instance, doped zirconias share the same cubic fluorite structure and scandia-stabilized zirconia (ScSZ) has higher oxide-ion conductivity than yttria-stabilized zirconia (YSZ) due to the lower-binding enthalpy within its defect associate as a result of smaller size mismatch between Sc^{3+} and Zr^{4+} relative to that between Y^{3+} and Zr^{4+} [18,19].

YSZ (Fig. 4.4A) is the most commonly used electrolyte for commercial high-temperature SOFCs [20]. The doping of ZrO_2 with Y_2O_3 helps to stabilize the cubic fluorite structure of ZrO_2 (Fig. 4.4B) at room temperature and enhance its oxide-ion conductivity. For instance, 8 mol.% Y_2O_3−ZrO_2 (8YSZ) has a stable cubic phase from room temperature to 2500°C and the highest ionic conductivity at 1000°C among various Y_2O_3 compositions (Fig. 4.3B) [21−23]. ZrO_2 can also be doped with other rare-earth oxides to enhance its oxide-ion conductivity. At 1000°C, the oxide-ion conductivity enhancement effect of the dopant cation follows the descending order of $Sc^{3+} > Yb^{3+} > Er^{3+} > Dy^{3+} > Gd^{3+} > Sm^{3+} > Nd^{3+}$ [24]. Although ScSZ has higher oxide-ion conductivity than YSZ,

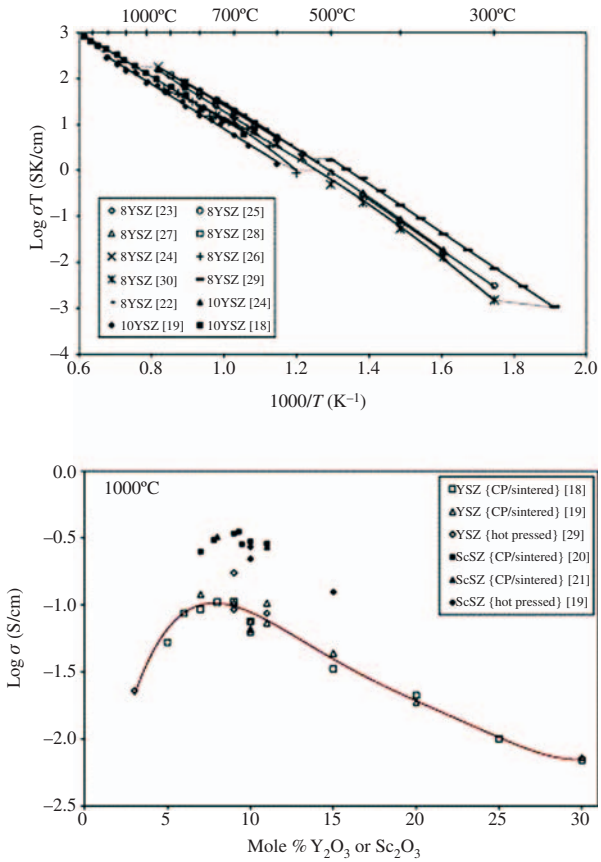

FIGURE 4.3

Oxide conductivity of yttria-stabilized zirconia (YSZ) (A) over a wide range of temperatures and (B) over a range of dopant compositions [19].

it has not been widely used in commercial SOFCs due to its high cost, aging behavior at high temperature, and complex phase assembly [25].

To develop electrolytes that are suitable for reduced-temperature operation, extensive research has been conducted on new compositions and microstructures. Besides ZrO_2, other fluorite structure oxides such as ceria (CeO_2) and bismuth oxide (Bi_2O_3) have been studied [28,29]. Ceria-based electrolytes have significantly higher conductivity than YSZ and ScSZ at the intermediate temperature (approximately 650°C−800°C) [30]. Doping CeO_2 with alkaline-earth oxides such as calcium oxide (CaO) and strontium oxide (SrO) as well as rare-earth oxides such as samarium oxide (Sm_2O_3) and gadolinium oxide (Gd_2O_3) can enhance the oxide-ion conductivity of CeO_2 [31−34]. Furthermore, ceria-based electrolytes have significantly higher stability with cathode materials than zirconia-based

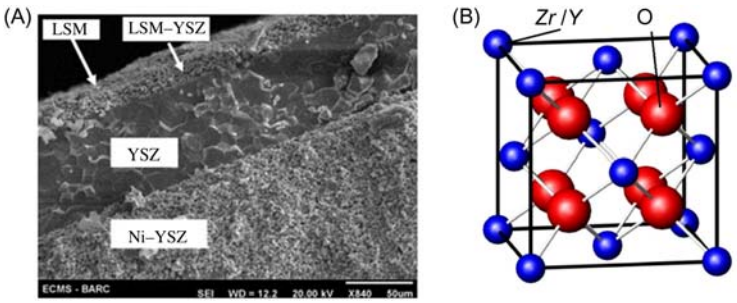

FIGURE 4.4

(A) Scanning electron microscope (SEM) image of yttria-stabilized zirconia (YSZ) electrolyte supported on Ni−YSZ anode and (B) fluorite structure of YSZ [26,27].

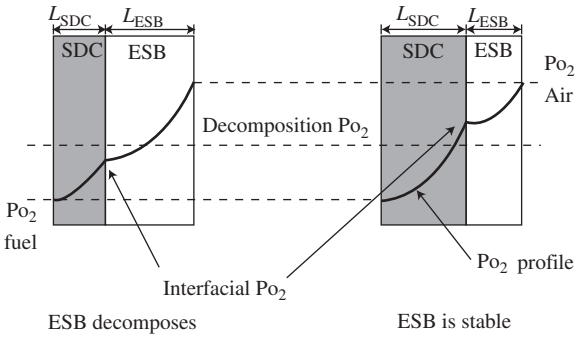

FIGURE 4.5

A bilayer composite consisting of samaria-doped ceria (SDC) and erbia-stabilized bismuth oxide (ESB) [38].

electrolytes [35]. Despite these desirable properties, challenges such as electronic conductivity and instability at low oxygen-partial pressures have to be overcome for the application of ceria-based electrolyte in intermediate-temperature SOFCs [18,29,36]. On the other hand, although Bi_2O_3 has even higher oxide-ion conductivity than CeO_2 and ZrO_2, it has stability issues at low oxygen-partial pressure and intermediate temperature (650°C−800°C) [19,37]. One way to overcome the disadvantages of ceria-based and bismuth oxide-based electrolytes is to develop a bilayer composite where the ceria-based electrolyte is at the anode and the bismuth oxide-based electrolyte is at the cathode (Fig. 4.5) [38].

Other major types of oxide that have been studied extensively for the application in reduced-temperature SOFCs include pyrochlore, perovskite, apatite, and LAMOX [12,19]. The pyrochlore has a structure similar to the cubic fluorite structure of ZrO_2 with one oxygen atom absent per unit cell [39]. Among the various pyrochlores, $Gd_2Zr_2O_7$ and its variants have the highest oxide-ion

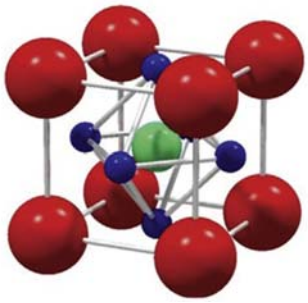

FIGURE 4.6

ABO_3 perovskite structure [47].

conductivity in the intermediate-temperature range [18,40,41]. The major problem for pyrochlores is their electronic conductivity, which has to be overcome for their application as the electrolyte in intermediate-temperature SOFCs [40].

Perovskites have ABO_3 stoichiometry, where a large cation (typically a rare-earth metal) occupies the A-site and a smaller cation (typically a transition metal) occupies the B-site (Fig. 4.6) [6]. Among the various types of perovskites, lanthanum gallate ($LaGaO_3$) and its variants have the best oxide-ion conductivity in the intermediate-temperature range [42,43]. However, the stability issue of gallium oxide (Ga_2O_3) and the formation of stable secondary phases during processing need to be overcome [44–46].

Apatite and LAMOX are relatively recent developments for oxide-ionic conductors. The apatites are typically lanthanum-based and share the general formula of $La_{10-x}M_6O_{26+y}$ (M = Si or Ga) [6]. Among the various apatites doped with strontium (Sr), $La_9SrGa_6O_{26.5}$ has consistently higher oxide-ion conductivity than YSZ over the intermediate and high-temperature ranges [48]. On the other hand, LAMOX refers to oxides based on $La_2Mo_2O_9$, whose development was based on the concept of lone–pair substitution [49–53]. These oxides were shown to have oxide-ion conductivity similar to the typical stabilized zirconias at 800°C, but there were contradictory results reported by other researchers [49,54]. Due to the novelty of apatites and LAMOX, more research is required to understand their chemical and physical properties to fully exploit their advantages over the conventional stabilized zirconia for their application in reduced-temperature SOFCs.

4.2.2 Processing methods for electrolyte

As the thickness of an electrolyte is proportional to its ohmic resistance, the key to the operation of SOFCs at reduced temperature is the development of a thin-film electrolyte that is supported by either the anode or cathode (Fig. 4.7). The common range of thin-film thickness is between 5 and 15 μm, which can be achieved industrially by screen printing [10].

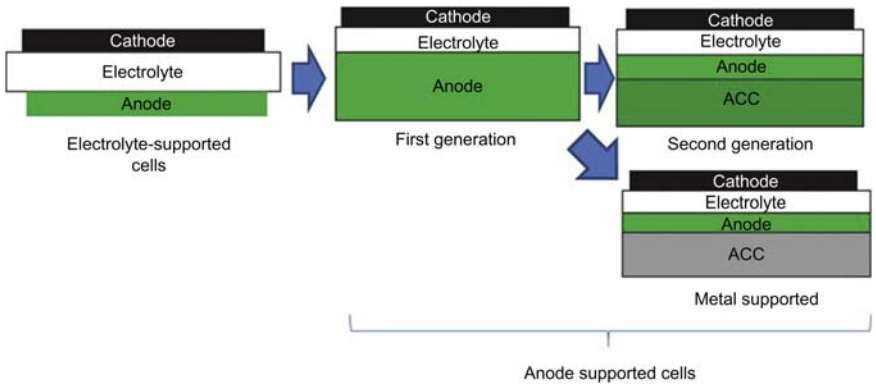

FIGURE 4.7

Structures of electrolyte-supported and anode-supported solid oxide fuel cells (SOFCs) [10].

For the fabrication of a thin-film electrolyte SOFC, ceramic particles of the electrolyte material are first dispersed in nonpolar organic solvents or water to form a suspension, which is then printed onto the supporting electrode (typically the anode). The resulting bilayer cell is sintered to densify the electrolyte before deposition of the remaining electrode material and the firing of the trilayer cell. These co-firing steps are important for achieving good interfacial bonding between the electrolyte and electrodes, but also limits the selection of materials for the electrolyte and electrodes to those with matching TECs.

The properties of the sintered electrolyte depend heavily on the properties of the starting ceramic particles, which can be synthesized via solid-state reaction or wet-chemical routes [55]. One important property of the starting particles is the size distribution, which affects the sintering kinetics at a specific temperature and the final particle-size distribution. For instance, previous results showed that the use of ScSZ particles with an average size of 3 nm could lower the sintering temperature by 150°C relative to the case of μm-sized particles and lead to the final grain size of 80 nm [56]. For grain size within the μm range, the grain interior has higher contribution to the overall oxide-ion conductivity than the grain boundary and smaller grain size leads to lower oxide-ion conductivity [57]. In the case of 8YSZ, (Fig. 4.8) the oxide-ion conductivity of the grain interior is two to three orders of magnitude higher than that of the grain boundary [58]. On the other hand, the phase purity of the starting particles is also important. For example, the presence of SiO_2 in the grain boundary of Gd-doped ceria ($Ce_{0.8}Gd_{0.2}O_{2-\delta}$) (CGO) could decrease the oxide-ion conductivity of CGO significantly [59]. Therefore, the processing procedure for the starting ceramic particles of electrolyte must be optimized to achieve a desirable size distribution and phase purity.

The wet-chemical routes for preparing the starting ceramic particles include solution combustion, co-precipitation, hydrothermal, sol−gel, and polymeric-

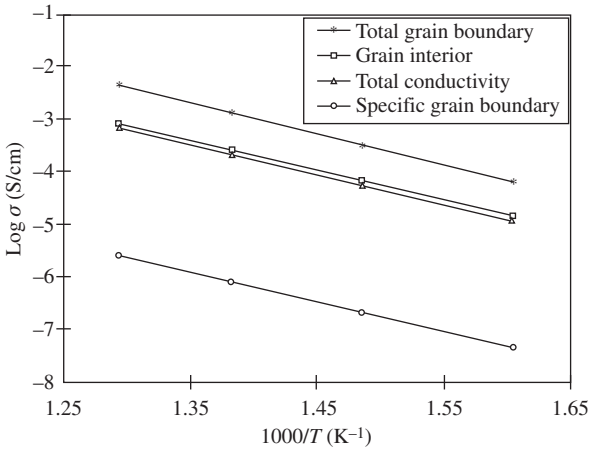

FIGURE 4.8

Ionic conductivity of 8 mol.% Y_2O_3–ZrO_2 (8YSZ) over a range of temperatures [58].

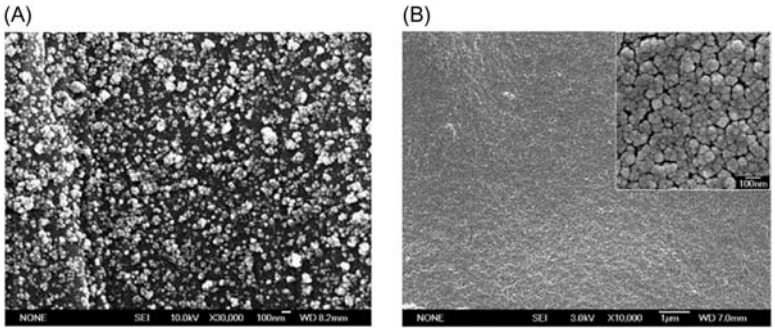

FIGURE 4.9

Field-emission scanning electron microscopy (FESEM) images of (A) 8 mol.% Y_2O_3–ZrO_2 (8YSZ) powder prepared by the hydrothermal process and (B) 8YSZ green film prepared from the powder in (A) [60].

complexing methods. [55] These methods offer higher phase purity, narrower particle-size distribution, and higher surface area than the conventional solid-state reaction method. For example, the hydrothermal method could prepare highly monodisperse 8YSZ nanoparticles with diameters of approximately 9 nm (Fig. 4.9A) [60]. The resulting nanoparticles also had a high coverage of hydroxyl groups on their surfaces, which allowed the green density of the corresponding 8YSZ film (Fig. 4.9B) on the anode to reach up to 51% before sintering. The monodispersity of particle size and high-green density of the film contributed to the sufficient densification of 8YSZ at a reduced sintering temperature of 1000°C and lower fabrication cost.

The wet-chemical methods are also suitable for new electrolyte materials such as CeO_2 and $LaGaO_3$. The co-precipitation method was employed to produce monodispersed Sm-doped CeO_2 nanoparticles that could be densified at lower temperatures (i.e., 1100−1200°C) to achieve excellent conductivity in comparison with particles produced by other methods [61]. On the other hand, the hydrothermal, sol−gel, and polymeric-complexing methods were able to produce doped $LaGaO_3$ with high-phase purity [62−64].

4.3 Cathode

At the cathode of an SOFC, gaseous oxygen combines with electrons to form oxide ions that diffuse through the electrolyte toward the anode. Unlike the electrolyte, the cathode should have high conductivity for electrons and oxide ions. In addition, it should be porous to allow the fast diffusion of oxygen to the cathode−electrolyte interface where the reduction of oxygen occurs. In terms of stability, its TEC should be compatible with the electrolyte and interconnect, and it should be chemically inert toward the electrolyte and interconnect at elevated temperatures.

4.3.1 Material selection for cathode

With the fabrication of thin-film electrolyte and the operation of an SOFC at reduced temperature, the overpotential loss at the cathode becomes an important area for improving the overall energy conversion efficiency [2,65]. The overpotential loss at the cathode is attributed to the high-activation energy for the oxygen−reduction reaction (ORR) where oxygen from the fuel is reduced to oxide ion. Due to their complexity, the exact mechanisms of ORR in different combinations of cathode/electrolyte are still under intensive research (Fig. 4.10). The general mechanism is believed to involve the sorption of oxygen onto/into the cathode, the conversion of the oxygen into certain electroactive intermediates. and the transfer of the electroactive intermediates to the electrolyte where the intermediates are incorporated as oxide ions [7].

As these steps contribute collectively to the overall activation energy of ORR, a suitable cathodic material should have high porosity to allow the fast diffusion

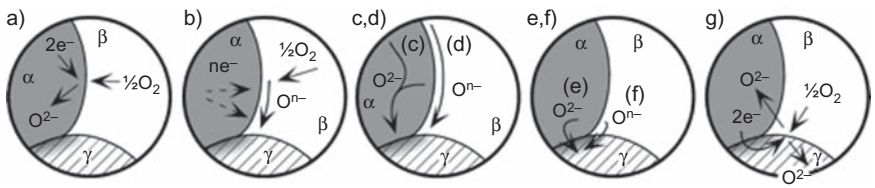

FIGURE 4.10

Proposed mechanisms of oxygen−reduction reaction (ORR) (phases α, β, and γ are the electronic, gas, and ionic phases, respectively) [7].

of oxygen, high conductivity for electrons and oxide ions, as well as high catalytic activity for ORR. A mixed ionic−electronic conductor (MIEC) has these desirable properties as its electrical and ionic conductivities allow the ORR to proceed throughout the cathode. One example of MIEC is $La_{1-x}Sr_{x-}MnO_{3\pm\delta}$ ($x \leq 0.5$) (LSM), which is the most widely used cathodic material for commercial high-temperature SOFCs [20].

LSM is a transition metal oxide with the perovskite structure (Fig. 4.6). It is the result of doping $LaMnO_3$ with SrO, where La^{3+} and Sr^{2+} have small ionic-size mismatch [66]. The substitution of La^{3+} with Sr^{2+} causes the oxidation of some manganese ions and increases the electron−hole concentration, resulting in a higher conductivity of electrons [67]. The electronic conductivity of LSM can be tuned with the concentration of Sr^{2+} as they are linearly proportional up to 50 mol.% Sr^{2+} [68]. When LSM is coupled with YSZ in commercial SOFCs, the presence of Sr^{2+} reduces the undesirable formation of $La_2Zr_2O_7$ at the interface between the cathode and electrolyte at high temperatures, but a concentration of Sr^{2+} higher than 30 mol.% will lead to the undesirable formation of $SrZrO_3$. Thus 30 mol.% Sr^{2+} is often considered as the optimal value for minimizing the formation of $La_2Zr_2O_7$ and $SrZrO_3$, which have high electrical resistance [69−74]. In addition, LSM is more stable than other transition metal oxides that contain iron (Fe) or cobalt (Co) and has little chemical expansivity [75−77].

Due to the absence of oxygen vacancies, LSM has low conductivity for oxide ions below 800°C, making it unsuitable for the operation at reduced temperature. One way to overcome this problem is the doping of LSM with a cation on the A-site and/or B-site to form oxygen vacancies. For instance, lanthanum (La) on the A-site can be substituted with other rare-earth cations including ytterbium (Yb), gadolinium (Gd), samarium (Sm), neodymium (Nd) praseodymium (Pr), and yttrium (Y), while keeping Sr on the A-site [78,79]. It was found that $Ln_{0.7}Sr_{0.3}MnO_3$ (Ln = Nd, Sm, and Pr) has consistently higher electrical conductivity than $La_{0.7}Sr_{0.3}MnO_3$ between 1200°C and 500°C (Fig. 4.11) [79]. Another study on $Pr_{1-x}Sr_xMnO_{3\pm\delta}$ showed that $Pr_{0.5}Sr_{0.5}MnO_3$ is the most promising cathodic material for low-temperature SOFCs due to its high conductivity (226 S/cm) at 500°C and its TEC (12×10^{-6}/K) that is compatible with ceria-based electrolyte [80]. The Ce-doped $SrMnO_3$ ($Sr_{1-x}Ce_xMnO_{3-\delta}$) is also a promising cathodic material for intermediate-temperature operation. For example, $Sr_{0.7}Ce_{0.3}MnO_{3-\delta}$ has a relatively stable high conductivity of 300 S/cm between 600°C and 800°C [81]. On the other hand, examples of B-site doping include LSM doped with Sc, aluminum (Al), and gallium (Ga) as well as $Sr_{1-x}Ce_xMnO_{3-\delta}$ doped with Sc (i.e., $Sr_{1-x}Ce_xMn_{1-y}Sc_yO_{3-\delta}$) have improved conductivities over the base materials at intermediate temperatures [81−83].

In addition to manganites, ferro-cobaltites and nikelates are also promising cathodic materials for reduced-temperature SOFCs. Among the ferro-cobaltites, $La_{1-x}Sr_xCo_{1-y}Fe_yO_{3-\delta}$ (LSCF) and $Ba_{1-x}Sr_xCo_{1-y}Fe_yO_{3-\delta}$ (BSCF) are the most promising candidates due to their high-electrical and ionic conductivities as well as high activities for ORR [84,85]. For example, LSCF has significantly lower

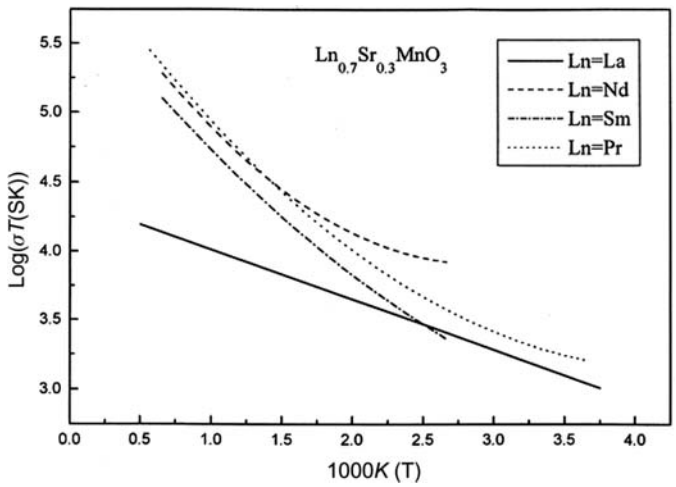

FIGURE 4.11

Electrical conductivity of $Ln_{0.7}Sr_{0.3}MnO_3$ (Ln = La, Nd, Sm, and Pr) [79].

electrode−polarization resistance than LSM between 600°C and 900°C as well as TEC that is compatible with the commonly used electrolytes at intermediate temperatures [86,87]. The formation of phases with high-electrical resistance due to the reaction between LSCF and YSZ can be avoided by the introduction of a CGO diffusion-barrier layer between the cathode and electrolyte or using CGO as the electrolyte [88,89]. On the other hand, although BSCF has significantly lower area-specific resistance (ASR) than other cathodic materials at reduced temperature, its high TEC and susceptibility to the poisoning of carbon dioxide (CO_2) still needs to be addressed [90−92]. For nikelates, $LaNi_{1-x}Fe_xO_{3-\delta}$ has high-electrical conductivity, moderate TEC, and stability in the air at reduced temperatures [93−95]. The formation of undesirable $La_2Zr_2O_7$ due to the reaction between $LaNi_{1-x}Fe_xO_{3-\delta}$ and zirconia-based electrolytes at sintering temperature can be overcome by placing a doped ceria layer between them [96]. The properties of various perovskite-type oxides are summarized in Table 4.1.

4.3.2 Processing methods for cathode

Synthetic methods of electrolyte are also applicable to cathodic and anodic materials. Among the wet-chemical methods, co-precipitation is the preferred choice for making monodispersed particles with high-phase purity. For the co-precipitation of LSM, $MnNO_3$, $SrNO_3$ and La_2O_3 were first dissolved in nitric acid and then ammonia solution was added into this mixture to adjust the pH value to 6−7. An aqueous solution of sodium carbonate was finally added into this mixture to yield LSM in the form of light-brown solids [97]. The final

Table 4.1 Properties of various perovskite-type oxides (σ_e and σ_i are electronic and ionic conductivities) [67].

Composition	Thermal expansion coefficient ($\times 10^{-6}$/K)	T (°C)	σ_e (S/cm)	σ_i (S/cm)
$La_{0.8}Sr_{0.2}MnO_3$	11.8	900	300	5.93×10^{-7}
$La_{0.7}Sr_{0.3}MnO_3$	11.7	800	240	–
$La_{0.6}Sr_{0.4}MnO_3$	13.0	800	130	–
$La_{0.8}Sr_{0.2}CoO_3$	19.1	800	1220	–
$La_{0.6}Sr_{0.4}CoO_3$	20.5	800	1600	0.22
$La_{0.8}Sr_{0.2}FeO_3$	12.2	750	155	–
$La_{0.6}Sr_{0.4}FeO_3$	16.3	800	129	0.0056
$Pr_{0.6}Sr_{0.4}MnO_3$	12.0	950	220	–
$Pr_{0.8}Sr_{0.2}FeO_3$	12.1	800	78	–
$Pr_{0.5}Sr_{0.5}FeO_3$	13.2	550	300	–
$La_{0.7}Sr_{0.3}Fe_{0.8}Ni_{0.2}O_3$	13.7	750	290	–
$La_{0.8}Sr_{0.2}Co_{0.8}Fe_{0.2}O_3$	20.1	600	1050	–
$La_{0.8}Sr_{0.2}Co_{0.2}Fe_{0.8}O_3$	15.4	600	125	–
$La_{0.6}Sr_{0.4}Co_{0.8}Fe_{0.2}O_3$	21.4	800	269	0.058
$La_{0.6}Sr_{0.4}Co_{0.2}Fe_{0.8}O_3$	15.3	600	330	0.008
$La_{0.4}Sr_{0.6}Co_{0.2}Fe_{0.8}O_3$	16.8	600	–	–
$Pr_{0.8}Sr_{0.2}Co_{0.2}Fe_{0.8}O_3$	12.8	800	76	0.0015
$Pr_{0.7}Sr_{0.3}Co_{0.2}Mn_{0.8}O_3$	11.1	800	200	4.4×10^{-5}

particles were shown to have the most suitable surface structure for catalyzing the oxidation of carbon monoxide to carbon dioxide in comparison with particles synthesized with drip pyrolysis, sol–gel and citrate methods.

The co-precipitation method is also suitable for making cathodic materials for reduced-temperature operations [98,99]. For instance, the particles of $(La_{1-x}A_x)_yMO_{3-\delta}$ (A = Sr or Ca; M = Fe or Mn) made with the carbonate co-precipitation method had more homogeneous composition and led to better cell performance than particles made with citrate and spray pyrolysis methods [98]. Similarly, the co-precipitation method produced $LaNi_{0.6}Fe_{0.4}O_3$ particles with high-phase purity (Fig. 4.12), which could be sintered at a lower temperature compared to particles synthesized with other methods [99].

4.4 Anode

The oxidation of fuel takes place at the anode of an SOFC where the oxide ion combines with a fuel compound such as hydrogen to produce electrons, which are transferred to the cathode via an external circuit. A suitable anodic material

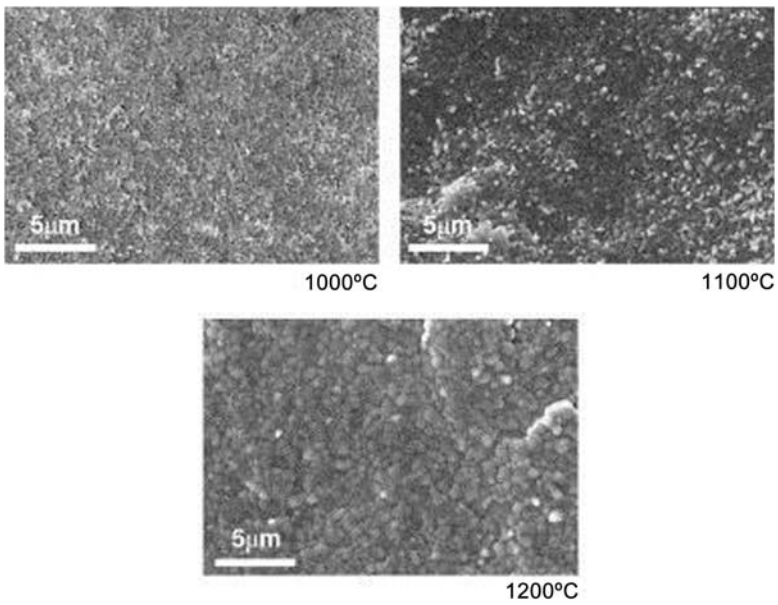

FIGURE 4.12

Scanning electron microscopy (SEM) images of $LaNi_{0.6}Fe_{0.4}O_3$ particles prepared by the coprecipitation method after calcination at different temperatures [99].

should have high activity for the oxidation reaction, high stability, high electrical and ionic conductivities, and TEC that is compatible with the electrolyte and interconnect.

4.4.1 Material selection for anode

Although Ni has high stability and high activity for the oxidation reaction its TEC has considerable mismatch with commonly used electrolytes such as YSZ. This challenge can be overcome by the incorporation of Ni particles into the framework of YSZ to form the ceramic−metallic composite Ni−YSZ (Fig. 4.13) whose TEC can be tuned with the ratio of Ni to YSZ [100]. Experimental results showed that lower-Ni content led to lower TEC in the presence of hydrogen [101]. In addition, the YSZ framework broadens the three-phase boundaries for the oxidation reaction due to its high conductivity for oxide ions and inhibits the agglomeration of Ni particles during operation [8]. The recommended composition for Ni−YSZ is 40 vol.% Ni and 60 vol.% YSZ, which has the lowest polarization resistance [102]. Due to these advantages, Ni−YSZ is the most commonly used anodic material for commercial SOFCs [20].

Ni−YSZ has several challenges to overcome. The material can degrade after a prolonged operation at high temperature due to Ni sintering, which reduces the

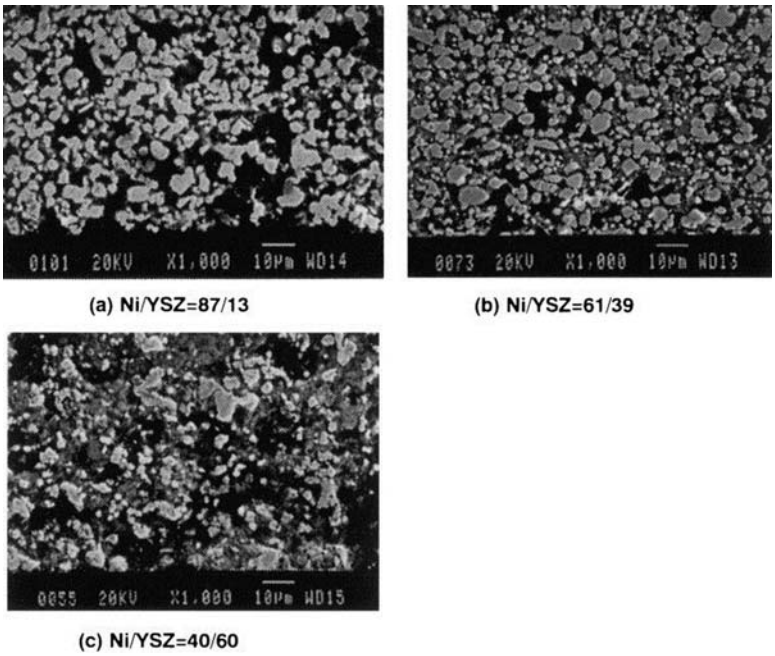

FIGURE 4.13

Scanning electron microscopy (SEM) images of Ni−YSZ cermet anodes with different volume ratios of Ni and YSZ [102].

specific-surface area of Ni particles as well as the contact area at the interface between the anode and electrolyte [103]. When hydrocarbons are used as fuels, Ni can be re-oxidized to NiO, causing the undesirable expansion of anode [104]. The use of hydrocarbon also makes it susceptible to carbon deposition (Fig. 4.14C, D, and F) and sulfur poisoning [105−107]. The problem of carbon deposition can be overcome with the addition of a transition metal oxide such as BaO, La_2O_3, Al_2O_3 and SnO_2 into Ni−YSZ [108−110], whereas sulfur poisoning can be overcome by the surface modification of Ni−YSZ with Nb_2O_5 and $BaZr_{0.1}Ce_{0.7}Y_{0.1}Yb_{0.1}O_{3-\delta}$ (BZCYYb) [111,112].

In order to improve the fuel flexibility of SOFCs several types of new materials have been investigated for better resistance to carbon deposition and sulfur poisoning, including noble metal-based materials, ceria-based materials, perovskites, and pyrochlores (Table 4.2) [11,12]. Noble metals such as copper (Cu) and gold (Au) have been incorporated into ceramic−metallic composites to counter the problem of carbon deposition [114−116]. Experimental results showed that Cu impregnated in a samaria-doped ceria (SDC) matrix remained stable due to its low activity for the oxidation of *n*-butane at 650°C and the Cu mainly served as the electronic conductor in the anode [114]. The performance of Cu−SDC in the

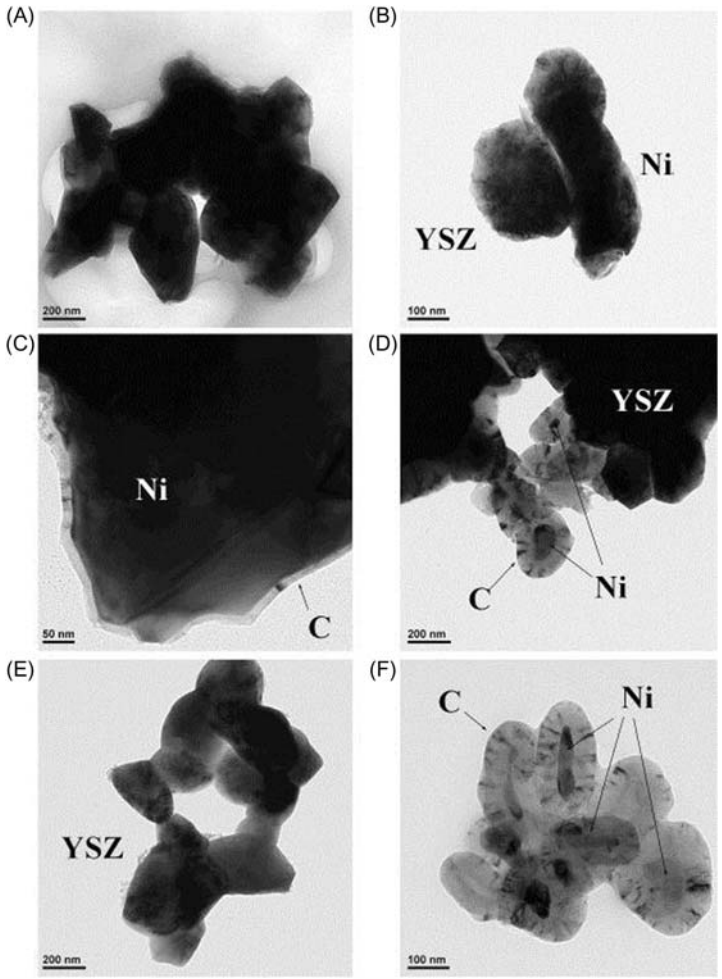

FIGURE 4.14

Transmission electron microscopy (TEM) images of Ni–YSZ operated (A and B) in hydrogen and (C–F) in syngas [113].

presence of hydrocarbons can be improved by the addition of Co to Cu to form bimetallic, ceramic–metallic composites [116,117].

In addition to its high conductivities for electrons and oxide ions, ceria has high catalytic activity for the oxidation of hydrocarbons such as methane. When combined with Zr, ceria has better stability and catalytic activity for the oxidation of hydrocarbons. For instance, the $Ce_xZr_{1-x}O_2$ series was shown to have higher catalytic activity than pure CeO and $Ce_{0.75}Zr_{0.25}O_2$ has the highest catalytic activity within this series [119]. Furthermore, ceria-based materials such as Cu–CeO_2 and

Table 4.2 Conductivities of various solid oxide fuel cell (SOFC) anodic materials at 800°C [118].

Material	DC conductivity (S/cm)	Advantage/disadvantage
$Sc_{0.3}Y_{0.1}Zr_{0.6}Ti_{0.2}O_{1.9}$	0.14	Operate at high temperature
$La_{0.8}Sr_{0.2}Fe_{0.8}Cr_{0.2}O_3$	0.5	Low conductivity
$La_{0.8}Sr_{0.2}Cr_{0.95}Ru_{0.05}O_3$	0.6	Expensive
$(La_{0.7}Sr_{0.3})_{1-x}Ce_xCr_{1-x}Ni_xO_3$	5.03	Carbon deposition
$Sr_{0.88}Y_{0.08}TiO_3$	64	High operating temperature
$CrTi_2O_5$	177	Expensive
Ni–YSZ	250	High operating temperature
$Ti_{0.34}Nb_{0.66}O_2$	340	Very expensive
$LaSrTiO_2$	360	No compatibility
Ni–SDC	573	Coke formation
Ni–GDC	1070	Coke formation
Cu–CeO_2	5200	Improved electronic conductivity
Cu–GDC	8500	Good thermal expansion and good electronic performance

DC, *Direct current;* GDC, *gadolinia-doped ceria;* SDC, *samaria-doped ceria;* YSZ, *yttria-stabilized zirconia.*

CGO can be incorporated into materials such as YSZ, $La_{0.75}Sr_{0.25}Mn_{0.5}Cr_{0.5}O_3$ and Nb-doped $SrTiO_3$ to enhance anodic performance [120–122].

Since Ni is prone to sulfur poisoning, numerous nickel-free perovskites such as $La_xSr_{1-x}BO_3$ (B = Ti, Cr, Mn, V) and their variants have been explored as alternative anodic materials [123–128]. For example, a series of Mn and Ti replaced complex perovskites, $Ln_{0.5}Sr_{0.5}Ti_{0.5}Mn_{0.5}O_{3\pm d}$ (Ln: Sm, Nd and La), was found to be chemically stable with CGO and YSZ at high temperatures (up to 1500°C) and $Nd_{0.5}Sr_{0.5}Ti_{0.5}Mn_{0.5}O_{3\pm d}$ had the highest electrical conductivity among these three perovskites [129,130]. Double perovskites such as $Pr_{0.5}Ba_{0.5}MnO_{3-\delta}$ (Mo-PBMO) and $Sr_2FeNb_{0.2}Mo_{0.8}O_{6-\delta}$ (SFNM20) also have been developed as potential anodic materials with resistance against carbon deposition and sulfur poisoning [131–133]. For example, SFNM20 was shown to remain stable against carbon deposition during the direction oxidation of methane at reduced temperatures (600°C–800°C) [133].

4.4.2 Processing methods for anode

Wet-chemical methods such as spray pyrolysis and co-precipitation are suitable for making high-performance anodic materials. For example, the spherical particles of Ni–YSZ with mean diameters of approximately 1 μm were

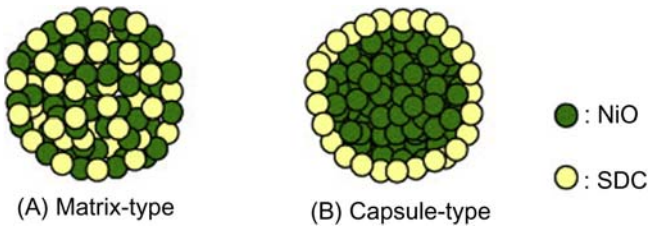

FIGURE 4.15

NiO–SDC composite particles with (A) matrix-type and (B) capsule-type structures [135].

prepared by spray pyrolysis where the NiO particles had a high coverage of fine YSZ particles on their surfaces [134]. This microstructure was found to be effective for suppressing the sintering of Ni at 1000°C and, hence, led to the long-term stability of the anode. Spray pyrolysis was also used to prepare matrix-type composite particles of SDC and NiO [135]. The resulting spherical particles were less prone to aggregation in comparison with their capsule-type counterparts (Fig. 4.15). Furthermore, the well-dispersed SDC particles did not obstruct the Ni-network structure among the matrix-type composite particles, leading to lower ohmic loss in comparison with capsule-type particles.

Co-precipitation can also produce monodispersed nanoparticles with high-phase purity for anodic materials. In the case of SDC, samarium nitrate hexahydrate ($Sm(NO_3)_3 \cdot 6H_2O$) and cerium nitrate hexahydrate ($Ce(NO_3)_3 \cdot 6H_2O$) were first dissolved in water and then the pH of the mixture was tuned to 9.5 with the addition of ammonia to initiate the co-precipitation [136]. The resulting monodispersed nanoparticles were approximately 11–14 nm in diameter and had significantly higher oxide conductivity than YSZ. Ni–SDC could also be prepared by co-precipitation using $Ce(NO_3)_3$, $Sm(NO_3)_3$, and $Ni(NO_3)_2$ as the precursors and $(NH_4)_2CO_3$ as the mineralizer [137]. The resulting particles had significantly higher conductivity and catalytic activity than particles prepared by mechanical mixing at 500°C and 800°C, showing that the co-precipitation method was suitable for preparing anodic materials for the operation of SOFCs at reduced temperatures.

4.5 Interconnect and sealant

In multiple-cell SOFCs, the interconnect allows the electrons to flow from the anode of one cell to the cathode of the adjacent cell, while being a physical barrier between the fuel and oxygen streams that enter the anode and cathode chambers (Fig. 4.16). Therefore, the interconnects should be non-porous to avoid the mixing of fuel and oxygen, while having high electrical conductivity and low

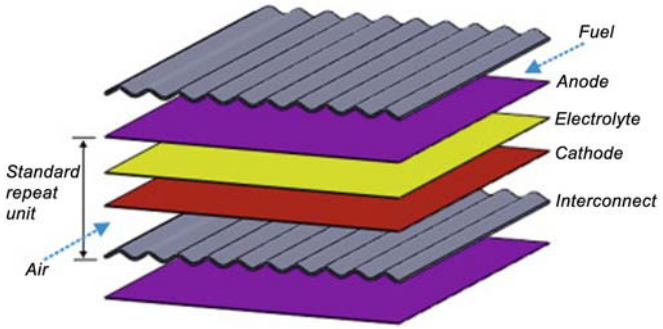

FIGURE 4.16

A standard planar solid oxide fuel cell (SOFC) [138].

oxide-ion conductivity. Furthermore, the ideal materials for interconnects should have stability, resistance to carbon deposition, sulfur poisoning, and oxidation as well as TEC that is compatible with the commonly used anodic and cathodic materials.

High-temperature SOFCs use ceramic interconnects that are normally based on lanthanum chromite ($LaCrO_3$) [139]. With a melting point higher than 2300°C, $LaCrO_3$ is one of the most stable perovskite oxides [140]. It has high-electrical conductivity above 800°C, TEC that is compatible with YSZ, and chemical stability under low-oxygen partial pressure [68,141,142]. Its conductivity can be improved by substituting La^{3+} with large cations such as Sr^{2+} and Ca^{2+} and replacing Cr^{3+} with small cations such as Cu^{2+} and Ni^{2+} [143,144]. Poor sinterability in air is the major challenge for $LaCrO_3$-based materials due to the volatilization of Cr species [145]. This can be overcome by sintering under reducing atmosphere or lowering the vapor pressure of Cr species [146–148].

For intermediate and low-temperature SOFCs, metallic alloys are the preferred materials for interconnects due to their high-electrical conductivity, ease of fabrication and handling, and relatively low cost. [149] The most popular choices are Cr, Fe, and Ni-based alloys due to their oxidation resistance [150]. Cr-based alloys such as $Cr_5FeY_2O_3$ and Fe–Cr-based alloys have high-oxidation resistance and TEC that are compatible with the cathodic and anodic materials. However, the excessive scale formation of Cr_2O_3 or Al_2O_3 on these alloys can substantially increase the ASR of interconnects [150–152]. On the other hand, Ni–Cr-based alloys have oxide scales that have high-electrical conductivity, but their TECs usually have significant mismatch with the other SOFC components [153].

Sealants play a critical role in ensuring the proper function of SOFCs by preventing gas leakage from the anode and cathode chambers. Compressive sealants are placed between sealing surfaces, which are then compressed constantly to achieve airtightness. Therefore, compressive sealants must be ductile and not form oxide in the presence of air. Noble metals such as gold and silver meet such

requirements [154,155]. Silver is the preferred choice due to its lower cost, but it can degrade due to cracking along the grain boundaries as well as the reaction of dissolved oxygen and hydrogen to form water [156,157]. To overcome this problem, silver or metal oxides such as Ag−CuO and Ag−V_2O_5 can be used instead [158]. Another possibility for metallic compressive sealants is heat-resistant Fe and Cr-based alloys such as FeCrAlY [12,150]. While mica alone cannot provide proper sealing, combining it with other materials such as glass and silver can make it a suitable compressive sealant [159,160]. Phlogopite ($KMg_3(AlSi_3O_{10})(OH)_2$) and muscovite ($KAl_2(AlSi_3O_{10})(F,OH)_2$) are the most commonly used mica-based sealants as they are stable up to 800°C [161−163].

Unlike their compressive counterparts, rigid sealants bind strongly with the sealing surfaces and, hence, should have TEC that is compatible with the binding SOFC components. Commonly used materials include glass, glass−ceramic, and metallic braze [164−170]. Examples of suitable glass and glass−ceramic are boroaluminosilicate, borosilicate, aluminosilicate, silicate, and borate, among which Ba-containing glass−ceramics are the most promising materials due to their relatively large TEC [166−169]. For example, the variants of $BaO−Al_2O_3−La_2O_3−B_2O_3−SiO_2$ with suitable ratios of B_2O_3 and SiO_2 were shown to have suitable binding and wetting characteristics, compatibility with YSZ in terms of TEC, as well as chemical stability with YSZ at 800°C−850°C over 100 hours [166]. However, Ba-containing glass−ceramics can form barium chromate when in contact with Cr-containing components, leading to an interface with high TEC and subsequent delamination [171].

On the other hand, a metallic braze is usually made of alloys that are stable in the presence of oxygen (e.g., Ag and Au-based alloys) [172,173]. To improve the wetting characteristics of the metallic braze, reactive metals such as Zr and Ti can be added into the alloy to reduce the formation of oxides [174]. An oxide and metal mixture that has an eutectic reaction can also be used [175]. For example, Ag−CuO can be used to braze perovskites and alumina [176,177].

4.6 Conclusion

State-of-the-art high-temperature SOFCs use YSZ as the electrolyte, Ni−YSZ as the anode and LSM as the cathode. The move from high-temperature to reduced-temperature operation for SOFCs demands the development of more conductive materials and better control of their physical properties such as particle size and film thickness to achieve high energy-conversion efficiency. In terms of cell design the electrode-supported, thin-film configuration minimizes the ohmic resistance of the electrolyte and, hence, is suitable for reduced-temperature SOFCs. The precise control of film thickness for the electrolyte can be achieved with screen printing, which needs optimization to prevent the appearance of defects. In terms of material development, the requirements for each cell component is different and new

materials generally need further improvement for industrial application. New materials should have chemical and thermodynamic stability at reduced temperatures as well as TECs that are compatible with the materials of adjacent cell components. The electrolyte material should have high conductivity for oxide ions and low conductivity for electrons at reduced temperature. Promising materials include doped zirconias and cerias such as ScSZ and CGO. For cathode, the material should have high activity for ORR and high porosity to enable the fast diffusion of oxygen. Examples of promising materials include manganites and ferro-cobaltites such as $Pr_{0.6}Sr_{0.4}MnO_3$ and LSCF. For anode, the materials should have activity for the oxidation of fuel as well as resistance to carbon deposition and sulfur poisoning. Potentially suitable materials include Ni−YSZ impregnated with transition metal oxides and SDC impregnated with noble metals. In terms of material processing, it is important to produce starting particles with high-phase purity and size monodispersity. The wet-chemical routes such as co-precipitation, hydrothermal, sol−gel, and polymeric-complexing methods are more advantageous than the conventional solid-state reaction to achieve these goals, but they need to be optimized for scaling-up to the industrial production level.

Abbreviations

8YSZ	8 mol.% Y_2O_3−ZrO_2
ASR	area-specific resistance
BSCF	$Ba_{1-x}Sr_xCo_{1-y}Fe_yO_{3-\delta}$
CGO	Gd-doped ceria
FESEM	field-emission scanning electron microscopy
LSCF	$La_{1-x}Sr_xCo_{1-y}Fe_yO_{3-\delta}$
LSM	$La_{1-x}Sr_{x-}MnO_{3\pm\delta}$
ORR	oxygen−reduction reaction
ScSZ	scandia-stabilized zirconia
SDC	samaria-doped ceria
SEM	scanning electron microscopy
SOFC	solid oxide fuel cell
TEC	thermal expansion coefficient
TEM	transmission electron microscopy
YSZ	yttria-stabilized zirconia

References

[1] A.B. Stambouli, E. Traversa, Solid oxide fuel cells (SOFCs): a review of an environmentally clean and efficient source of energy, Renew. Sustain. Energy Rev. 6 (5) (2002) 433−455.

[2] L.C. de Jonghe, C.P. Jacobson, S.J. Visco, Supported electrolyte thin film synthesis of solid oxide fuel cells, Annu. Rev. Mater. Sci. 33 (2003) 169−182.

[3] S. Badwal, Stability of solid oxide fuel cell components, Solid State Ionics 143 (1) (2001) 39–46.
[4] T. Liu, X. Zhang, X. Wang, J. Yu, L. Li, A review of zirconia-based solid electrolytes, Ionics (2016) 2249–2262.
[5] S.J. Skinner, Recent advances in perovskite-type materials for solid oxide fuel cell cathodes, Int. J. Inorg. Mater. 3 (2) (2001) 113–121.
[6] S.J. Skinner, J.A. Kilner, Oxygen ion conductors, Mater. Today 6 (3) (2003) 30–37.
[7] S.B. Adler, Factors governing oxygen reduction in solid oxide fuel cell cathodes, Chem. Rev. 104 (10) (2004) 4791–4843.
[8] W. Zhu, S.C. Deevi, A review on the status of anode materials for solid oxide fuel cells, Mater. Sci. Eng. A 362 (1–2) (2003) 228–239.
[9] A.M. Abdalla, S. Hossain, A.T. Azad, P.M.I. Petra, F. Begum, S.G. Eriksson, et al., Nanomaterials for solid oxide fuel cells: a review, Renew. Sustain. Energy Rev. 82 (2018) 353–368.
[10] M. Cassidy, Trends in the processing and manufacture of solid oxide fuel cells, Wiley Interdiscip. Rev.: Energy Environ. 6 (5) (2017) e248.
[11] F.S. Silva, T.M. Souza, Novel materials for solid oxide fuel cell technologies: a literature review, Int. J. Hydrogen Energy 42 (41) (2017) 26020–26036.
[12] N. Mahato, A. Banerjee, A. Gupta, S. Omar, K. Balani, Progress in material selection for solid oxide fuel cell technology: a review, Prog. Mater. Sci. 72 (2015) 141–337.
[13] E.D. Wachsman, K.T. Lee, Lowering the temperature of solid oxide fuel cells, Science (80-) 334 (6058) (2011) 935–939.
[14] S. Hossain, A.M. Abdalla, S.N.B. Jamain, J.H. Zaini, A.K. Azad, A review on proton conducting electrolytes for clean energy and intermediate temperature-solid oxide fuel cells, Renew. Sustain. Energy Rev. (2017) 750–764.
[15] J. Fergus, R. Hui, X. Li, D.P. Wilkinson, J. Zhang, Solid Oxide Fuel Cells: Materials Properties and Performance, CRC Press, 2016.
[16] J.A. Kilner, B.C.H. Steele, Mass Transport in Anion-Deficient Fluorite Oxides, Academic Press, New York, 1981.
[17] J.A. Kilner, C.D. Waters, The effects of dopant cation-oxygen vacancy complexes on the anion transport properties of non-stoichiometric fluorite oxides, Solid State Ionics 6 (3) (1982) 253–259.
[18] V.V. Kharton, F.M.B. Marques, A. Atkinson, Transport properties of solid oxide electrolyte ceramics: a brief review, Solid State Ionics 174 (1–4) (2004) 135–149.
[19] J.W. Fergus, Electrolytes for solid oxide fuel cells, J. Power Sources 162 (1) (2006) 30–40.
[20] F. Tietz, H.-P. Buchkremer, D. Stover, Components manufacturing for solid oxide fuel cells, Solid State Ionics 152–153 (2002) 373–381.
[21] J.M. Dixon, L.D. LaGrange, U. Merten, C.F. Miller, J.T. Porter II, Electrical resistivity of stabilized zirconia at elevated temperatures, J. Electrochem. Soc. 110 (4) (1963) 276–280.
[22] D.W. Strickler, W.G. Carlson, Ionic conductivity of cubic solid solutions in the system $CaO–Y_2O_3–ZrO_2$, J. Am. Ceram. Soc. 47 (3) (1964) 122–127.
[23] R.E.W. Casselton, Low field DC conduction in yttria-stabilized zirconia, Phys. Status Solidi 2 (3) (1970) 571–585.

[24] J. Molenda, K. Świerczek, W. Zajac, Functional materials for the IT-SOFC, J. Power Sources 173 (2) (2007) 657–670 (special issue).
[25] S. Omar, W. Bin Najib, N. Bonanos, Conductivity ageing studies on 1M10ScSZ (M^{4+} = Ce, Hf), Solid State Ionics 189 (1) (2011) 100–106.
[26] T. Mahata, S.R. Nair, R.K. Lenka, P.K. Sinha, Fabrication of Ni–YSZ anode supported tubular SOFC through iso-pressing and co-firing route, Int. J. Hydrogen Energy (2012).
[27] V. Vonk, N. Khorshidi, A. Stierle, H. Dosch, Atomic structure and composition of the yttria-stabilized zirconia (111) surface, Surf. Sci. (2013).
[28] H. Inaba, Ceria-based solid electrolytes, Solid State Ionics 83 (1–2) (1996) 1–16.
[29] B. Dalslet, P. Blennow, P.V. Hendriksen, N. Bonanos, D. Lybye, M. Mogensen, Assessment of doped ceria as electrolyte, J. Solid State Electrochem. 10 (8) (2006) 547–561.
[30] B.C.H. Steele, Oxygen ion conductors, High Conductivity Solid Ionic Conductors: Recent Trends and Applications, World Scientific, 1989, pp. 402–446.
[31] H. Yahiro, T. ohuchi, K. Eguchi, H. Arai, Electrical properties and microstructure in the system ceria–alkaline earth oxide, J. Mater. Sci. 23 (3) (1988) 1036–1041.
[32] H. Arai, T. Kunisaki, Y. Shimizu, T. Seiyama, Electrical properties of calcia-doped ceria with oxygen ion conduction, Solid State Ionics 20 (4) (1986) 241–248.
[33] H. Yahiro, K. Eguchi, H. Arai, Electrical properties and reducibilities of ceria–rare earth oxide systems and their application to solid oxide fuel cell, Solid State Ionics 36 (1–2) (1989) 71–75.
[34] K. Eguchi, T. Setoguchi, T. Inoue, H. Arai, Electrical properties of ceria-based oxides and their application to solid oxide fuel cells, Solid State Ionics 52 (1–3) (1992) 165–172.
[35] J.M. Ralph, C. Rossignol, R. Kumar, Cathode materials for reduced-temperature SOFCs, J. Electrochem. Soc. 150 (11) (2003) A1518.
[36] M.B. Mogensen, D. Lybye, K. Kammer Hansen, N. Bonanos, K. Kammer, N. Bonanos, Ceria revisited: electrolyte or electrode material? in: Proceedings Materials, vol. 2, 2005–07, 2005, pp. 1068–1074.
[37] N. Jiang, E.D. Wachsman, Structural stability and conductivity of phase-stabilized cubic bismuth oxides, J. Am. Ceram. Soc. 82 (11) (2004) 3057–3064.
[38] J.Y. Park, H. Yoon, E.D. Wachsman, Fabrication and characterization of high-conductivity bilayer electrolytes for intermediate-temperature solid oxide fuel cells, J. Am. Ceram. Soc. 88 (9) (2005) 2402–2408.
[39] J. Lian, L. Wang, J. Chen, K. Sun, R.C. Ewing, J.M. Farmer, et al., The order-disorder transition in ion-irradiated pyrochlore, Acta Mater. 51 (5) (2003) 1493–1502.
[40] S. Kramer, M. Spears, H.L. Tuller, Conduction in titanate pyrochlores: role of dopants, Solid State Ionics 72 (Pt 2) (1994) 59–66.
[41] S.A. Kramer, H.L. Tuller, A novel titanate-based oxygen ion conductor: $Gd_2Ti_2O_7$, Solid State Ionics 82 (1–2) (1995) 15–23.
[42] T. Ishihara, H. Matsuda, Y. Takita, Doped $LaGaO_3$ perovskite type oxide as a new oxide ionic conductor, J. Am. Chem. Soc. 116 (9) (1994) 3801–3803.
[43] M. Feng, J.B. Goodenough, A superior oxide-ion electrolyte, Eur. J. Solid State Inorg. Chem. 31 (8–9) (1994) 663–672.
[44] J. Stevenson, Effect of a-site cation nonstoichiometry on the properties of doped lanthanum gallate, Solid State Ionics 113–115 (1–2) (1998) 571–583.

[45] E. Djurado, M. Labeau, Second phases in doped lanthanum gallate perovskites, J. Eur. Ceram. Soc. 18 (10) (1998) 1397–1404.
[46] K. Yamaji, T. Horita, M. Ishikawa, N. Sakai, H. Yokokawa, Chemical stability of the $La_{0.9}Sr_{0.1}Ga_{0.8}Mg_{0.2}O_{2.85}$ electrolyte in a reducing atmosphere, Solid State Ionics 121 (1) (1999) 217–224.
[47] H.U. Habermeier, Thin films of perovskite-type complex oxides, Mater. Today (2007).
[48] H. Arikawa, H. Nishiguchi, T. Ishihara, Y. Takita, Oxide ion conductivity in Sr-doped $La_{10}Ge_6O_{27}$ apatite oxide, Solid State Ionics 136–137 (2000) 31–37.
[49] P. Lacorre, F. Goutenoire, O. Bohnke, R. Retoux, Y. Lallgant, Designing fast oxide-ion conductors based on $La_2Mo_2O_9$, Nature 404 (6780) (2000) 856–858.
[50] P. Lacorre, The LPS concept, a new way to look at anionic conductors, Solid State Sci. 2 (8) (2000) 755–758.
[51] F. Goutenoire, O. Isnard, R. Retoux, P. Lacorre, Crystal structure of $La_2Mo_2O_9$, a new fast oxide-ion conductor, Chem. Mater. 12 (9) (2000) 2575–2580.
[52] F. Goutenoire, O. Isnard, E. Suard, O. Bohnke, Y. Laligant, R. Retoux, et al., Structural and transport characteristics of the LAMOX family of fast oxide-ion conductors, based on lanthanum molybdenum oxide $La_2Mo_2O_9$, J. Mater. Chem. 11 (1) (2001) 119–124.
[53] S. Georges, F. Goutenoire, F. Altorfer, D. Sheptyakov, F. Fauth, E. Suard, et al., Thermal, structural and transport properties of the fast oxide-ion conductors $La_{2-x}R_xMo_2O_9$ (R = Nd, Gd, Y), Solid State Ionics 161 (3–4) (2003) 231–241.
[54] R. Subasri, H. Näfe, F. Aldinger, On the electronic and ionic transport properties of $La_2Mo_2O_9$, Mater. Res. Bull. 38 (15) (2003) 1965–1977.
[55] Z. Shao, W. Zhou, Z. Zhu, Advanced synthesis of materials for intermediate-temperature solid oxide fuel cells, Prog. Mater. Sci. (2012) 804–874.
[56] Z. Lei, Q. Zhu, Low temperature processing of dense nanocrystalline scandia-doped zirconia (ScSZ) ceramics, Solid State Ionics 176 (37–38) (2005) 2791–2797.
[57] B. Zhu, Solid oxide fuel cell (SOFC) technical challenges and solutions from nano-aspects, Int. J. Energy Res 33 (13) (2009) 1126–1137.
[58] M.C. Martin, M.L. Mecartney, Grain boundary ionic conductivity of yttrium stabilized zirconia as a function of silica content and grain size, Solid State Ionics 161 (1–2) (2003) 67–79.
[59] B. Steele, Appraisal of $Ce_{1-y}Gd_yO_{2-y/2}$ electrolytes for IT-SOFC operation at 500°C, Solid State Ionics 129 (1–4) (2000) 95–110.
[60] Q. Zhu, B. Fan, Low temperature sintering of 8YSZ electrolyte film for intermediate temperature solid oxide fuel cells, Solid State Ionics 176 (9–10) (2005) 889–894.
[61] H. Li, C. Xia, M. Zhu, Z. Zhou, G. Meng, Reactive $Ce_{0.8}Sm_{0.2}O_{1.9}$ powder synthesized by carbonate coprecipitation: sintering and electrical characteristics, Acta Mater. 54 (3) (2006) 721–727.
[62] T.-Y. Chen, K.-Z. Fung, Synthesis of and densification of oxygen-conducting $La_{0.8}Sr_{0.2}Ga_{0.8}Mg_{0.2}O_{2.8}$ nanopowder prepared from a low temperature hydrothermal urea precipitation process, J. Eur. Ceram. Soc. 28 (4) (2008) 803–810.
[63] K. Huang, M. Feng, J.B. Goodenough, Sol–gel synthesis of a new oxide-ion conductor Sr- and Mg-doped $LaGaO_3$ perovskite, J. Am. Ceram. Soc. 79 (4) (1996) 1100–1104.
[64] M. Shi, Y. Xu, A. Liu, N. Liu, C. Wang, P. Majewski, et al., Synthesis and characterization of Sr- and Mg-doped lanthanum gallate electrolyte materials prepared via the pechini method, Mater. Chem. Phys. 114 (1) (2009) 43–46.

[65] E. Ivers-Tiffée, A. Weber, D. Herbstritt, Materials and technologies for SOFC-components, J. Eur. Ceram. Soc. 21 (10–11) (2001) 1805–1811.
[66] R.D. Shannon, Revised effective ionic radii and systematic studies of interatomic distances in halides and chalcogenides, Acta Crystallogr. Sect. A 32 (5) (1976) 751–767.
[67] C.W. Sun, R. Hui, J. Roller, Cathode materials for solid oxide fuel cells: a review, J. Solid State Electrochem. 14 (7) (2010) 1125–1144.
[68] N.Q. Minh, T. Takahshi, Science and technology of ceramic fuel cells, Comp. Educ. 49 (March) (2013) 374–387.
[69] O. Yamamoto, Y. Takeda, R. Kanno, M. Noda, Perovskite-type oxides as oxygen electrodes for high temperature oxide fuel cells, Solid State Ionics 22 (2–3) (1987) 241–246.
[70] T. Kenjo, M. Nishiya, $LaMnO_3$ air cathodes containing ZrO_2 electrolyte for high temperature solid oxide fuel cells, Solid State Ionics 57 (3–4) (1992) 295–302.
[71] C. Clausen, C. Bagger, J.B. Bilde-Sørensen, A. Horsewell, Microstructural and microchemical characterization of the interface between $La_{0.85}Sr_{0.15}MnO_3$ and Y_2O_3-stabilized ZrO_2, Solid State Ionics 70–71 (Pt 1) (1994) 59–64.
[72] G. Stochniol, E. Syskakis, A. Naoumidis, Chemical compatibility between strontium-doped lanthanum manganite and yttria-stabilized zirconia, J. Am. Ceram. Soc. 78 (4) (1995) 929–932.
[73] T. Setoguchi, T. Inoue, H. Takebe, K. Eguchi, K. Morinaga, H. Arai, Fabrication and evaluation of flat thick film type solid oxide fuel cell, Solid State Ionics 37 (2–3) (1990) 217–221.
[74] H. Yokokawa, N. Sakai, T. Kawada, M. Dokiya, Thermodynamic analysis on interface between perovskite electrode and YSZ electrolyte, Solid State Ionics 40–41 (Pt 1) (1990) 398–401.
[75] J. Mizusaki, H. Tagawa, K. Naraya, T. Sasamoto, Nonstoichiometry and thermochemical stability of the perovskite-type $La_{1-x}Sr_xMnO_{3-\delta}$, Solid State Ionics 49 (C) (1991) 111–118.
[76] A. Atkinson, T.M.G.M. Ramos, Chemically-induced stresses in ceramic oxygen ion-conducting membranes, Solid State Ionics 129 (1) (2000) 259–269.
[77] S.B. Adler, Chemical expansivity of electrochemical ceramics, J. Am. Ceram. Soc. 84 (9) (2004) 2117–2119.
[78] T. Ishiham, T. Kudo, H. Matsuda, Y. Takita, Doped perovskite oxide, $PrMnO_3$, as a new cathode for solid-oxide fuel cells that decreases the operating temperature, J. Am. Ceram. Soc. 77 (6) (1994) 1682–1684.
[79] T.L. Wen, H. Tu, Z. Xu, O. Yamamoto, A study of $(Pr, Nd, Sm)_{(1-x)}Sr_xMnO_3$ cathode materials for solid oxide fuel cell, Solid State Ionics 121 (1–4) (1999) 25–30.
[80] G.C. Kostogloudis, N. Vasilakos, C. Ftikos, Preparation and characterization of $Pr_{1-x}Sr_xMnO_{3\pm\delta}$ ($x = 0$, 0.15, 0.3, 0.4, 0.5) as a potential SOFC cathode material operating at intermediate temperatures (500–700°C), J. Eur. Ceram. Soc. 17 (12) (1997) 1513–1521.
[81] S. Hashimoto, H. Iwahara, Structural, thermal and electrical properties of Ce-doped $SrMnO_3$, J. Electroceram. 4 (1) (2000) 225–231.
[82] J.M. Ralph, A.C. Schoeler, M. Krumpelt, Materials for lower temperature solid oxide fuel cells, J. Mater. Sci. 36 (5) (2001) 1161–1172.

[83] X. Yue, A. Yan, M. Zhang, L. Liu, Y. Dong, M. Cheng, Investigation on scandium-doped manganate $La_{0.8}Sr_{0.2}Mn_{1-x}Sc_xO_{3-\Delta}$ cathode for intermediate temperaturesolid oxide fuel cells, J. Power Sources 185 (2) (2008) 691–697.
[84] R. Pelosato, G. Cordaro, D. Stucchi, C. Cristiani, G. Dotelli, Cobalt based layered perovskites as cathode material for intermediate temperature solid oxide fuel cells: a brief review, J. Power Sources 298 (2015) 46–67.
[85] S.P. Jiang, Development of lanthanum strontium manganite perovskite cathode materials of solid oxide fuel cells: a review, J. Mater. Sci. 43 (21) (2008) 6799–6833.
[86] S.P. Jiang, W. Wang, Fabrication and performance of GDC-impregnated (La,Sr) MnO_3 cathodes for intermediate temperature solid oxide fuel cells, J. Electrochem. Soc. 152 (7) (2005) A1398–A1408.
[87] G.C. Kostogloudis, C. Ftikos, Properties of a-site-deficient $La_{0.6}Sr_{0.4}Co_{0.2}Fe_{0.8}O_{3-\delta}$-based perovskite oxides, Solid State Ionics 126 (1) (1999) 143–151.
[88] V.A.C. Haanappel, J. Mertens, A. Mai, Performance improvement of (La,Sr)MnO_3 and $(La,Sr)_x(Co, Fe)O_3$-type anode-supported SOFCs, J. Fuel Cell Sci. Technol. 3 (3) (2006) 263–270.
[89] B. Steele, Properties of $La_{0.6}Sr_{0.4}Co_{0.2}Fe_{0.8}O_{3-x}$ (LSCF) double layer cathodes on gadolinium-doped cerium oxide (CGO) electrolytes II. Role of oxygen exchange and diffusion, Solid State Ionics 106 (3–4) (1998) 255–261.
[90] Z. Shao, S.M. Halle, A high-performance cathode for the next generation of solid-oxide fuel cells, Nature 431 (7005) (2004) 170–173.
[91] B. Wei, Z. Lü, X. Huang, J. Miao, X. Sha, X. Xin, et al., Crystal structure, thermal expansion and electrical conductivity of perovskite oxides $Ba_xSr_{1-x}Co_{0.8}Fe_{0.2}O_{3-\delta}$ ($0.3 \leq x \leq 0.7$), J. Eur. Ceram. Soc. 26 (13) (2006) 2827–2832.
[92] A. Yan, M. Cheng, Y. Dong, W. Yang, V. Maragou, S. Song, et al., Investigation of a $Ba_{0.5}Sr_{0.5}Co_{0.8}Fe_{0.2}O_3$-delta based cathode IT-SOFC. I. The effect of CO_2 on the cell performance, Appl. Catal. B Environ. 66 (1–2) (2006) 64–71.
[93] R. Chiba, F. Yoshimura, Y. Sakurai, An investigation of $LaNi_{1-x}Fe_xO_3$ as a cathode material for solid oxide fuel cells, Solid State Ionics 124 (3) (1999) 281–288.
[94] R. Chiba, F. Yoshimura, Y. Sakurai, Properties of $La_{1-y}Sr_yNi_{1-x}Fe_xO_3$ as a cathode material for a low-temperature operating SOFC, Solid State Ionics 152–153 (2002) 575–582.
[95] H. Orui, K. Watanabe, R. Chiba, M. Arakawa, Application of $LaNi(Fe)O_3$ as SOFC cathode, J. Electrochem. Soc. 151 (9) (2004) A1412–A1417.
[96] R. Chiba, H. Orui, T. Komatsu, Y. Tabata, K. Nozawa, M. Arakawa, et al., $LaNi_{0.6}Fe_{0.4}O_3$–ceria composite cathode for SOFCs operating at intermediate temperatures, J. Electrochem. Soc. 155 (6) (2008) B575.
[97] R.J. Bell, G.J. Millar, J. Drennan, Influence of synthesis route on the catalytic properties of $La_{1-x}Sr_xMnO_3$, Solid State Ionics 131 (3) (2000) 211–220.
[98] J. Sfeir, S. Vaucher, P. Holtappels, U. Vogt, H.J. Schindler, J. Van herle, et al., Characterization of perovskite powders for cathode and oxygen membranes made by different synthesis routes, J. Eur. Ceram. Soc. 25 (12) (2005) 1991–1995 (special issue).
[99] M. Bevilacqua, T. Montini, C. Tavagnacco, G. Vicario, P. Fornasiero, M. Graziani, Influence of synthesis route on morphology and electrical properties of $LaNi_{0.6}Fe_{0.4}O_3$, Solid State Ionics 177 (33–34) (2006) 2957–2965.
[100] H.S. Spacil, Electrical Device Including Nickel-Containing Stabilized Zirconia Electrode, Google Patents, 1970.

[101] M. Mori, T. Yamamoto, H. Itoh, H. Inaba, H. Tagawa, Thermal expansion of nickel-zirconia anodes in solid oxide fuel cells during fabrication and operation, J. Electrochem. Soc. 145 (4) (1998) 1374–1381.
[102] H. Koide, Y. Someya, T. Yoshida, T. Maruyama, Properties of Ni/YSZ cermet as anode for SOFC, Solid State Ionics 132 (3–4) (2000) 253–260.
[103] X.Q. Yang, H.S. Lee, L.K. Hanson, J. McBreen, Z.S. Xu, T.A. Skotheini, et al., Characterization of Ni–YSZ anode degradation for substrate-type solid oxide fuel cells, J. Electroanal. Chem. Acta 143 (139) (1996) 225–625.
[104] M. Cassidy, G. Lindsay, K. Kendall, The reduction of nickel-zirconia cermet anodes and the effects on supported thin electrolytes, J. Power Sources 61 (1–2) (1996) 189–192.
[105] K. Nikooyeh, R. Clemmer, V. Alzate-Restrepo, J.M. Hill, Effect of hydrogen on carbon formation on Ni/YSZ composites exposed to methane, Appl. Catal. A Gen. 347 (1) (2008) 106–111.
[106] J.F.B. Rasmussen, A. Hagen, The effect of H_2S on the performance of Ni-YSZ anodes in solid oxide fuel cells, J. Power Sources 191 (2) (2009) 534–541.
[107] W. Wang, C. Su, Y. Wu, R. Ran, Z. Shao, Progress in solid oxide fuel cells with nickel-based anodes operating on methane and related fuels, Chem. Rev. (2013) 8104–8151.
[108] L. Yang, Y. Choi, W. Qin, H. Chen, K. Blinn, M. Liu, et al., Promotion of water-mediated carbon removal by nanostructured barium oxide/nickel interfaces in solid oxide fuel cells, Nat. Commun. 2 (1) (2011).
[109] A. Yan, M. Phongaksorn, D. Nativel, E. Croiset, Lanthanum promoted NiO-SDC anode for low temperature solid oxide fuel cells fueled with methane, J. Power Sources 210 (2012) 374–380.
[110] F. Wang, W. Wang, R. Ran, M.O. Tade, Z. Shao, Aluminum oxide as a dual-functional modifier of Ni-based anodes of solid oxide fuel cells for operation on simulated biogas, J. Power Sources 268 (2014) 787–793.
[111] S.H. Choi, J.H. Wang, Z. Cheng, M. Liu, Surface modification of Ni-YSZ using niobium oxide for sulfur-tolerant anodes in solid oxide fuel cells, J. Electrochem. Soc. 155 (5) (2008) B449–B454.
[112] S. Sengodan, M. Liu, T.-H. Lim, J. Shin, M. Liu, G. Kim, Enhancing sulfur tolerance of a Ni-YSZ anode through $BaZr_{0.1}Ce_{0.7}Y_{0.1}Yb_{0.1}O_3$-infiltration, J. Electrochem. Soc. 161 (5) (2014) F668–F673.
[113] T. Chen, W.G. Wang, H. Miao, T. Li, C. Xu, Evaluation of carbon deposition behavior on the nickel/yttrium-stabilized zirconia anode-supported fuel cell fueled with simulated syngas, J. Power Sources 196 (5) (2011).
[114] C. Lu, W.L. Worrell, J.M. Vohs, R.J. Gorte, A comparison of Cu-Ceria-SDC and Au-Ceria-SDC composites for SOFC anodes, J. Electrochem. Soc. 150 (10) (2003) A1357.
[115] S. Park, J.M. Vohs, R.J. Gorte, Direct oxidation of hydrocarbons in a solid-oxide fuel cell, Nature 404 (6775) (2000) 265–267.
[116] O. Costa-Nunes, R.J. Gorte, J.M. Vohs, Comparison of the performance of Cu-CeO_2-YSZ and Ni-YSZ composite SOFC anodes with H_2, CO, and syngas, J. Power Sources 141 (2) (2005) 241–249.
[117] S.-I. Lee, J.M. Vohs, R.J. Gorte, A study of SOFC anodes based on Cu-Ni and Cu-Co bimetallics in CeO_2–YSZ, J. Electrochem. Soc. 151 (9) (2004) A1319.
[118] S.P.S. Shaikh, A. Muchtar, M.R. Somalu, A review on the selection of anode materials for solid-oxide fuel cells, Renew. Sustain. Energy Rev. (2015).

[119] J. Kearney, J.C. Hernández-Reta, R.T. Baker, Redox and catalytic properties of Ce−Zr mixed oxide nanopowders for fuel cell applications, Catal. Today 180 (1) (2012) 139−147.
[120] X.J. Chen, Q.L. Liu, S.H. Chan, N.P. Brandon, K.A. Khor, High-performance cathode-supported SOFC with perovskite anode operating in weakly humidified hydrogen and methane, Fuel Cells Bull. 2007 (6) (2007) 12−16.
[121] S.P. Jiang, X.J. Chen, S.H. Chan, J.T. Kwok, GDC-impregnated $(La_{0.75}Sr_{0.25})(Cr_{0.5}Mn_{0.5})O_3$ anodes for direct utilization of methane in solid oxide fuel cells, J. Electrochem. Soc. 153 (5) (2006) A850−A856.
[122] P. Blennow, K.K. Hansen, L.R. Wallenberg, M. Mogensen, Electrochemical characterization and redox behavior of Nb-doped $SrTiO_3$, Solid State Ionics 180 (1) (2009) 63−70.
[123] O.A. Marina, N.L. Canfield, J.W. Stevenson, Thermal, electrical, and electrocatalytical properties of lanthanum-doped strontium titanate, Solid State Ionics 149 (1−2) (2002) 21−28.
[124] R. Mukundan, E.L. Brosha, F.H. Garzon, Sulfur tolerant anodes for SOFCs, Electrochem. Solid-State Lett. 7 (1) (2004) A5.
[125] P.R. Slater, D.P. Fagg, J.T.S. Irvine, Synthesis and electrical characterisation of doped perovskite titanates as potential anode materials for solid oxide fuel cells, J. Mater. Chem. 7 (12) (1997) 2495−2498.
[126] J. Canales-Vazquez, S.W. Tao, J.T.S. Irvine, Electrical properties in $La_2Sr_4Ti_6O_{19delta}$: a potential anode for high temperature fuel cells, Solid State Ionics 159 (1−2) (2003) 159−165.
[127] H. Kurokawa, L. Yang, C.P. Jacobson, L.C. De Jonghe, S.J. Visco, Y-doped $SrTiO_3$ based sulfur tolerant anode for solid oxide fuel cells, J. Power Sources 164 (2) (2007) 510−518.
[128] L. Aguilar, S. Zha, Z. Cheng, J. Winnick, M. Liu, A solid oxide fuel cell operating on hydrogen sulfide (H_2S) and sulfur-containing fuels, J. Power Sources 135 (1−2) (2004) 17−24.
[129] J. Jeong, A.K. Azad, H. Schlegl, B. Kim, S.W. Baek, K. Kim, et al., Structural, thermal and electrical conductivity characteristics of $Ln_{0.5}Sr_{0.5}Ti_{0.5}Mn_{0.5}O_{3\pm d}$ (Ln: La, Nd and Sm) complex perovskites as anode materials for solid oxide fuel cell, J. Solid State Chem. 226 (2015) 154−163.
[130] K. Kim, J. Jeong, A.K. Azad, S.B. Jin, J.H. Kim, X-ray photoelectron spectroscopic study of direct reforming catalysts $Ln_{0.5}Sr_{0.5}Ti_{0.5}Mn_{0.5}O_{3\pm\delta}$ (Ln = La, Nd, and Sm) for high temperature-operating solid oxide fuel cell, Appl. Surf. Sci. 365 (2016) 38−46.
[131] S. Sengodan, S. Choi, A. Jun, T.H. Shin, Y.W. Ju, H.Y. Jeong, et al., Layered oxygen-deficient double perovskite as an efficient and stable anode for direct hydrocarbon solid oxide fuel cells, Nat. Mater. 14 (2) (2015) 205−209.
[132] Y.F. Sun, Y.Q. Zhang, B. Hua, Y. Behnamian, J. Li, S.H. Cui, et al., Molybdenum doped $Pr_{0.5}Ba_{0.5}MnO_{3-\delta}$ (Mo-PBMO) double perovskite as a potential solid oxide fuel cell anode material, J. Power Sources 301 (2016) 237−241.
[133] H. Ding, Z. Tao, S. Liu, Y. Yang, A redox-stable direct-methane solid oxide fuel cell (SOFC) with $Sr_2FeNb_{0.2}Mo_{0.8}O_{6-\delta}$ double perovskite as anode material, J. Power Sources 327 (2016) 573−579.
[134] T. Fukui, S. Ohara, K. Mukai, Long-term stability of Ni-YSZ anode with a new microstructure prepared from composite powder, Electrochem. Solid State Lett. 1 (3) (1998) 120−122.

[135] M. Kawano, H. Yoshida, K. Hashino, H. Ijichi, S. Suda, K. Kawahara, et al., Synthesis of matrix-type NiO-SDC composite particles by spray pyrolysis with acid addition for development of SOFC cermet anode, J. Power Sources 173 (1) (2007) 45–52.
[136] Y.-P. Fu, S.-B. Wen, C.-H. Lu, Preparation and characterization of samaria-doped ceria electrolyte materials for solid oxide fuel cells, J. Am. Ceram. Soc. 91 (1) (2008) 127–131.
[137] X. Fang, G. Zhu, C. Xia, X. Liu, G. Meng, Synthesis and properties of Ni-SDC cermets for IT-SOFC anode by co-precipitation, Solid State Ionics 168 (1–2) (2004) 31–36.
[138] T.T. Molla, K. Kwok, H.L. Frandsen, Efficient modeling of metallic interconnects for thermo-mechanical simulation of SOFC stacks: homogenized behaviors and effect of contact, Int. J. Hydrogen Energy (2016).
[139] N. Sakai, H. Yokokawa, T. Horita, K. Yamaji, Lanthanum chromite-based interconnects as key materials for SOFC stack development, Int. J. Appl. Ceram. Technol. 1 (1) (2005) 23–30.
[140] W. Vielstich, H.A. Gasteiger, H. Yokokawa, Handbook of Fuel Cells: Fundamentals Technology and Applications: Advances in Electrocatalysis, Materials, Diagnostics and Durability, vol. 5, John Wiley & Sons, 2009.
[141] F. Tietz, Thermal expansion of SOFC materials, Ionics (Kiel) 5 (1–2) (1999) 129–139.
[142] T. Nakamura, G. Petzow, L.J. Gauckler, Stability of the perovskite phase $LaBO_3$ (B = V, Cr, Mn, Fe, Co, Ni) in reducing atmosphere I. Experimental results, Mater. Res. Bull. 14 (5) (1979) 649–659.
[143] J.W. Fergus, Lanthanum chromite-based materials for solid oxide fuel cell interconnects, Solid State Ionics 171 (1–2) (2004) 1–15.
[144] W.Z. Zhu, S.C. Deevi, Development of interconnect materials for solid oxide fuel cells, Mater. Sci. Eng. A 348 (1–2) (2003) 227–243.
[145] H.U. Anderson, Fabrication and property control of $LaCrO_3$ based oxides, Processing of Crystalline Ceramics, Springer, 1978, pp. 469–477.
[146] L. Groupp, H.U. Anderson, Densification of $La_{1-x}Si_xCrO_3$, J. Am. Ceram. Soc. 59 (9–10) (1976) 449–450.
[147] N. Sakai, T. Kawada, H. Yokokawa, M. Dokiya, T. Iwata, Sinterability and electrical conductivity of calcium-doped lanthanum chromites, J. Mater. Sci. 25 (10) (1990) 4531–4534.
[148] L.-W. Tai, P.A. Lessing, Tape casting and sintering of strontium-doped lanthanum chromite for a planar solid oxide fuel cell bipolar plate, J. Am. Ceram. Soc. 74 (1) (1991) 155–160.
[149] J.C.W. Mah, A. Muchtar, M.R. Somalu, M.J. Ghazali, Metallic interconnects for solid oxide fuel cell: a review on protective coating and deposition techniques, Int. J. Hydrogen Energy 42 (14) (2017) 9219–9229.
[150] Z. Yang, K.S. Weil, D.M. Paxton, J.W. Stevenson, Selection and evaluation of heat-resistant alloys for SOFC interconnect applications, J. Electrochem. Soc. 150 (9) (2003) A1188.
[151] W.Z. Zhu, S.C. Deevi, Opportunity of metallic interconnects for solid oxide fuel cells: a status on contact resistance, Mater. Res. Bull. 38 (6) (2003) 957–972.
[152] J. Wu, X. Liu, Recent development of SOFC metallic interconnect, J. Mater. Sci. Technol. (2010) 293–305.

[153] J.W. Fergus, Metallic interconnects for solid oxide fuel cells, Mater. Sci. Eng. A 397 (1–2) (2005) 271–283.
[154] A. Weber, A. Muller, D. Herbstritt, E. Ivers-Tiffee, Characterization of SOFC single cells, in: Proc. 7th Int. Symp. Solid Oxide Fuel Cells, No. 16, 2001, pp. 952–962.
[155] J. Duquette, A. Petric, Silver wire seal design for planar solid oxide fuel cell stack, J. Power Sources 137 (1) (2004) 71–75.
[156] Y.S. Chou, J.W. Stevenson, Novel silver/mica multilayer compressive seals for solid-oxide fuel cells: the effect of thermal cycling and material degradation on leak behavior, J. Mater. Res. 18 (9) (2003) 2243–2250.
[157] P. Singh, Z. Yang, V. Viswanathan, J.W. Stevenson, Observations on the structural degradation of silver during simultaneous exposure to oxidizing and reducing environments, J. Mater. Eng. Perform. 13 (2004) 287–294.
[158] K.S. Weil, C.A. Coyle, J.S. Hardy, J.Y. Kim, G.-G. Xia, Alternative planar SOFC sealing concepts, Fuel Cells Bull. 2004 (5) (2004) 11–16.
[159] S.P. Simner, J.W. Stevenson, Compressive mica seals for SOFC applications, J. Power Sources 102 (1–2) (2001) 310–316.
[160] Y.S. Chou, J.W. Stevenson, L.A. Chick, Ultra-low leak rate of hybrid compressive mica seals for solid oxide fuel cells, J. Power Sources 112 (1) (2002) 130–136.
[161] Y.S. Chou, J.W. Stevenson, Phlogopite mica-based compressive seals for solid oxide fuel cells: effect of mica thickness, J. Power Sources 124 (2) (2003) 473–478.
[162] Yshyung Chou, J.W. Stevenson, Thermal cycling and degradation mechanisms of compressive mica-based seals for solid oxide fuel cells, J. Power Sources 112 (2) (2002) 376–383.
[163] Y.S. Chou, J.W. Stevenson, Mid-term stability of novel mica-based compressive seals for solid oxide fuel cells, J. Power Sources 115 (2) (2003) 274–278.
[164] K.L. Ley, M. Krumpelt, R. Kumar, J.H. Meiser, I. Bloom, Glass–ceramic sealants for solid oxide fuel cells: part I: physical properties, J. Mater. Res. 11 (6) (1996) 1489–1493.
[165] N. Lahl, K. Singh, L. Singheiser, K. Hilpert, D. Bahadur, Crystallisation kinetics in AO-Al_2O_3-SiO_2-B_2O_3 glasses (A = Ba, Ca, Mg), J. Mater. Sci. 35 (12) (2000) 3089–3096.
[166] S.-B. Sohn, S.-Y. Choi, G.-H. Kim, H.-S. Song, G.-D. Kim, Stable sealing glass for planar solid oxide fuel cell, J. Non. Cryst. Solids 297 (2–3) (2002) 103–112.
[167] S.B. Sohn, S.Y. Choi, G.H. Kim, H.S. Song, G.D. Kim, Suitable glass-ceramic sealant for planar solid-oxide fuel cells, J. Am. Ceram. Soc. 87 (2) (2004) 254–260.
[168] C. Lara, M.J. Pascual, M.O. Prado, A. Durán, Sintering of glasses in the system RO-Al_2O_3-BaO-SiO_2 (R = Ca, Mg, Zn) studied by hot-stage microscopy, Solid State Ionics 170 (3–4) (2004) 201–208.
[169] C. Lara, M.J. Pascual, A. Durán, Glass-forming ability, sinterability and thermal properties in the systems RO-BaO-SiO_2 (R = Mg, Zn), J. Non. Cryst. Solids 348 (2004) 149–155.
[170] T.I. Khan, A. Al-Badri, Reactive brazing of ceria to an ODS ferritic stainless steel, J. Mater. Sci. 38 (11) (2003) 2483–2488.
[171] P. Batfalsky, V.A.C. Haanappel, J. Malzbender, N.H. Menzler, V. Shemet, I.C. Vinke, et al., Chemical interaction between glass-ceramic sealants and interconnect steels in SOFC stacks, J. Power Sources 155 (2) (2006) 128–137.

[172] M.C. Tucker, C.P. Jacobson, L.C. De Jonghe, S.J. Visco, A braze system for sealing metal-supported solid oxide fuel cells, J. Power Sources 160 (2) (2006) 1049–1057 (special issue).
[173] K.S. Weil, J.P. Rice, Substrate effects on the high-temperature oxidation behavior of a gold-based braze filler metal, Scr. Mater 52 (11) (2005) 1081–1085.
[174] J. Mei, P. Xiao, Joining metals to zirconia for high temperature applications, Scr. Mater. 40 (5) (1999) 587–594.
[175] K.S. Weil, C.A. Coyle, J.T. Darsell, G.G. Xia, J.S. Hardy, Effects of thermal cycling and thermal aging on the hermeticity and strength of silver-copper oxide air-brazed seals, J. Power Sources 152 (1–2) (2005) 97–104.
[176] C.C. Schüler, A. Stuck, N. Beck, H. Keser, U. Täck, Direct silver bonding - an alternative for substrates in power semiconductor packaging, J. Mater. Sci. Mater. Electron. 11 (5) (2000) 389–396.
[177] K.M. Erskine, A.M. Meier, S.M. Pilgrim, Brazing perovskite ceramics with silver/copper oxide braze alloys, J. Mater. Sci. 37 (8) (2002) 1705–1709.

CHAPTER

Multiscale modeling and optimization programing of solid oxide fuel cell systems

5

Mahdi Sharifzadeh

Sharif Energy Research Institute, Sharif University of Technology, Tehran, Iran

5.1 Introduction

The convoluted interactions between the transport phenomena and electrochemical reactions in solid oxide fuel cells (SOFCs) pose a significant challenge toward understanding and predicting their behavior. As shown in Fig. 5.1, such interactions span from the design of electrodes and electrolyte materials at molecular scales to fluid dynamics and phase interactions within process equipment, and further expands to the mass and energy flows across the process and through energy distribution and storage networks. Modeling and optimization programing are key enablers to understand this multiscale interactive behavior and optimize the key process indicators. This chapter presents a brief review of the research in the field with emphasis on the key decision variables and the diversity of involved applications. At the molecular scale, these decisions involve the reactant interactions with the electrode surface and their diffusion through the cell's material, expanding further to the composition, grain size, and microstructure of materials. At a higher level, the geometrical dimensions and the cells' configuration within the stack are modeled and optimized at the equipment scale. Beyond this, quantification and optimization of key process indicators through optimal process synthesis and integration with synergistic applications will be studied. The applications of SOFC-based systems expand further through the local and national energy networks.

5.2 Optimization of the electrochemical performance of cathodes

Haanappel et al. [4] studied the optimization of a $La_{0.65}Sr_{0.3}MnO_3$ (LSM)-based cathode in an anode-supported single cell. Four parameters used for the cathode functional layer (CFL) were investigated, namely: (1) the mass ratio of LSM/YSZ of the CFL; (2) the grain size of the LSM powder of the cathode current collector

Design and Operation of Solid Oxide Fuel Cells. DOI: https://doi.org/10.1016/B978-0-12-815253-9.00005-7

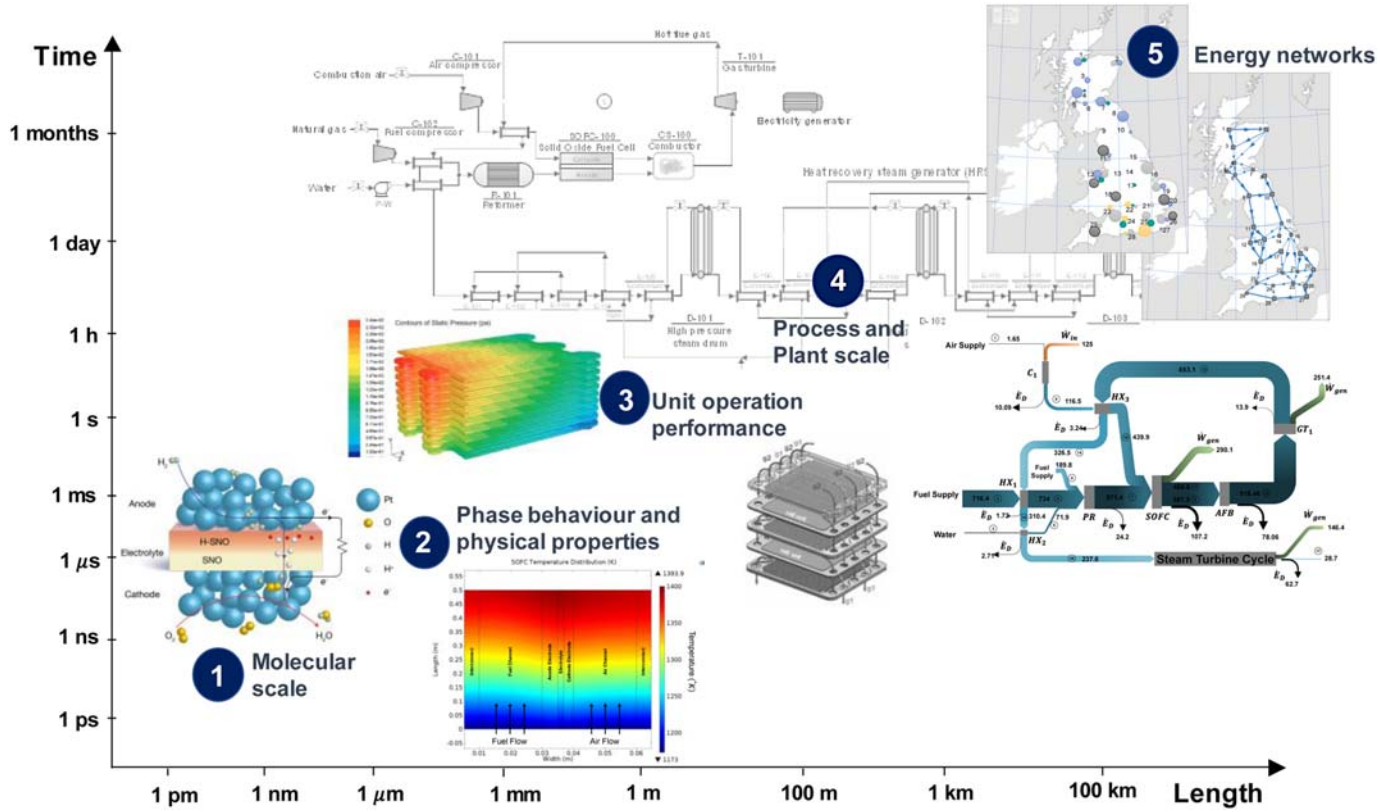

FIGURE 5.1

The design and operation of solid oxide fuel cell (SOFC) systems requires modeling and optimization at multiple temporal and spatial scales [1–3].

layer (CCCL); (3) the thickness of the CFL and the thickness of the CCCL; and (4) the calcination of YSZ powder. The results of electrochemical measurements demonstrated that for hydrogen fuel (with 3 vol.% steam) at 700°C−900°C the LSM/YSZ mass ratio of 50/50 has the highest ratio. In addition, increasing the grain size (d_{90} of the LSM powder of 1.0 μm) of the outer CCCL further improved the electrochemical performance. A thickness of at least 10 μm for the CFL and 45−50 μm for the CCCL were recommended. Noncalcined YSZ powder was recommended for the CFL. It is notable that such configurations not only exhibit optimal electrochemical performance, but also have simplified manufacturing processes.

Andersson et al. [5] studied a single cell of a planar anode-supported SOFC. Sensitivity analysis was applied to the cathode-support thickness. The authors reported a high-temperature gradient (up to 250°C if no cathode support is used) due to high gas-phase oxygen and electron resistance. They proposed an optimized design with a wider and thinner gas channel that was more compact and, despite having slightly lower cell current density, has much higher volumetric cell current.

Li et al. [6] studied the implications of composition and microstructure for the cathode electrocatalytic activities in the case of intermediate-temperature SOFCs. The authors discussed that as the loading of SSM55 increases in the YSZ scaffold, the distribution uniformity, and hence connectivity, of SSM55 nanoparticles increases which, in turn, results in the reduction of open-circuits polarization resistance and an increase in the exchange current density. The researchers studied infiltration of 10, 15, 18, and 22 wt.% SSM55 solutions into YSZ scaffold, from which 18 wt.% was reported to have superior properties such as reduced polarization resistance within the desired range of operating temperatures.

Abdullah and Liu [7] argued that tailoring the microstructure of SOFC electrodes could enable operation at lower temperatures. They applied a multiscale polarization model in which the electrode particles were assumed to be randomly packed spheres. The authors reported superior performance for the optimized nonlinear particle-size and porosity-graded electrodes in terms of the increased power output and reduced operating temperature.

5.3 Optimization of the electrochemical performance of anodes

Cubero et al. [8] studied the optimization of the electrochemical performance of Ni−YSZ anodes through laser melting. They considered symmetrical cells with two NiO−YSZ anodes of about 20 μm thickness and a thin YSZ electrolyte of about 500 μm. Through laser-melting treatments at 100 W and processing rates of 1 mm/s a NiO−YSZ eutectic lamellar microstructure was produced on both anodes. Electrochemical impedance spectroscopy was applied to compare the

optimized eutectic and ceramic (reference) samples, which were found to be temperature dependent. While the polarization resistance was the same for both samples at 900°C, it was 1.6 and 2.9 $\Omega\,cm^2$ for the eutectic and ceramic at 800°C, respectively.

Bozorgmehri and Hamedi [9] applied a combination of black-box modeling using an artificial neural network (ANN) and a genetic algorithm to optimize the design parameters of an intermediate-temperature SOFC. Their analysis revealed that maximum power density can be achieved when the anode-support thickness is minimized, anode-support porosity is maximized, and the electrolyte thickness is minimized. The optimal value of the functional layer cathode thickness depended on multiple parameters and required optimization.

5.4 Optimization of solid oxide fuel cells

Multiscale modeling and optimization at the stack level included understanding the impact of cell geometry and dimensions on the involved electrochemical and transport phenomena, and hence the energy efficiency of the SOFC systems. Amiri et al. [10] proposed multiscale modeling and optimization in which a 0D model was developed for single compartments of an SOFC as the building blocks of a more complex model. The different flow patterns in the channels were analyzed using 1D models and 2D models were applied for analyzing the important distributed variables. The 2D model was also applied for optimization of air distribution and internal-temperature gradients.

Ji et al. [11] applied a three-dimensional model considering heat, mass, and momentum transfers as well as the thermodynamic and electrochemical aspects of an SOFC. The implications of the channel size on the performance of a thin-film SOFC were studied. The authors argued that for conventional SOFCs, increasing the inlet temperature increases the cell output and reduces the temperature gradient, but this requires more expensive materials. The application of thin-film electrolytes in miniaturized SOFCs allows operations at lower temperatures while maintaining a high-power density. It was observed that reducing the cell height (>0.5 mm) decreased the average solid temperature due to the increased mass transfer and heat transfer between the wall and flow stream, and a decrease in the current path. However, due to the smaller size the temperature gradient was also increased in the small channels, which increases the risk of thermal stress. It was also reported that a smaller ratio of the channel width to the rib width decreases the ohmic losses.

Hering et al. [12] studied the optimization of a microtubular SOFC stack integrated with a cooling system using a quasi-three-dimensional model. Their optimization methodology was based on a design of experiments (DoEs) methodology, which increased the energy efficiency from 57% (reference case) to 63% (best case) for the same power output, while the maximum occurring temperature

of the Positive-electrode/electrolyte/negative-electrode (PEN) structure was 1268K compared to 1369K for the reference case. Such improvement required an increase in the cell diameter from 2 to 3 mm. Palazzi et al. [13] conducted thermoeconomic optimization of a planar SOFC system where specific cost was minimized and efficiency was maximized. Efficiencies in the range of 34%−44% were estimated.

Bhattacharyya and Rengaswamy [14] applied simulation studies to investigate the design and operating parameters of a tubular SOFC. The authors reported that unlike cathodes, the radial variations of the species concentrations in the anode is significant when producing high currents. Similarly the pressure drop in the anode can become significant if the water is produced excessively. The authors reported that increasing the flow rate of hydrogen increases cell performance, while the effect of temperature is not monotonic and needs to be determined by optimization. It was observed that an increase in the anode thickness or anode-supported cell increases the performance, but decreases the limiting current density. Decreasing the electrolyte thickness decreases the ohmic loss and improves cell performance. Decreasing the cathode thickness resulted in overall performance loss.

Feng et al. [15] conducted structural optimization of a tubular SOFC. The power output was considered as the objective function. They reported that for fixed-volume fractions of the anode, cathode, and electrolyte there were optimal values for the thickness of the anode, cathode, and electrolyte as well as the fuel cell length, which maximized the power output by up to 18.20%.

5.5 Optimization of the manifold

In order to generate high-power outputs the cells are arranged in stacks. The role of the manifold is to ensure uniform distribution of the flow and species into the channels of the SOFCs. In addition it is desirable to reduce the pressure drop within the manifold to limit the requirements for compressors and blowers. The results suggested the value of 0.996% for the uniformity index and the value of 0.423% for the maximum standard flow deviation. Compared to the baseline the optimized manifold resulted in an 8% higher maximum-power output.

5.6 Optimization of the performance of turbomachines: compressors and turbines

Turbomachineries such as compressors and turbines consume and generate significant amounts of power. The optimal integration of turbomachines with SOFCs results in significant improvements in the overall energy conversion efficiency. Bakalis and Stamatis [16] developed an optimization methodology in which the

operating range of the SOFC−GT was assessed and the desired operating lines of the compressor and turbines were designed through the optimization of their geometries. The authors reported that such an optimization procedure not only allowed the turbomachines to operate more efficiently, but also enabled the system to operate at higher pressures, thereby enhancing the overall energy efficiency.

5.7 Optimization for solid oxide fuel cell process integration

Zhao et al. [17−19] developed a thermodynamic model for an integrated system consisting SOFCs and gas turbines (GTs) based on analyzing irreversibilities and entropy generation. They demonstrated that optimal integration and optimization allows the atmospheric SOFC system to achieve high-efficiency performance (approaching 80%) similar to pressured counterparts.

Lee et al. [20] conducted a parametric study and optimization of an SOFC system with a CO_2 adsorber placed between the reformer and stack. The authors reported that the inclusion of anode off-gas (AOG) recycling removed the need for external steam for most of the studied scenarios. The anode-gas recirculation ratio increases by increasing the steam-to-carbon ratio. Similarly the open-circuit voltage, terminal voltage, limiting current density, and the peak-power density increased with increasing the steam-to-carbon ratio, increasing the AOG recirculation, decreasing CO_2 adsorption percentage, and decreasing the SOFC temperature. The authors reported that for most scenarios the efficiency started around 70% and decreased to an average value of 50% for the peak-power density, after which it dropped sharply to zero. They reported the SOFC temperature of 900°C, steam-to-carbon ratio of 5, and no AOG recirculation for the best operating scenario.

Calise et al. [21,22] studied a hybrid GT system including an SOFC with internal reforming. The authors emphasized that isolated decision-making regarding SOFC design can result in significant inefficiencies in the turbomachinery and the balance of plant. They identified the prereforming ratio, the heat-exchange area, and the SOFC active area as the most influential decision variables.

Zhang et al. [23] studied an SOFC system integrated with a GT. In this configuration the SOFC anode-exhaust gases were burned in a combustor. The SOFC and combustor then acted as the heat reservoir for the GT. Their model included irreversibilities such as the overpotentials and heat leakage in the SOFC modules, heat transfer at finite temperature in the GT−SOFC−combustor cycle, and other irreversibilities in compression, expansion, and regeneration. Their analysis included the quantification of optimal regions for power output as well as the rates of the fuel and air flowing into the SOFC.

Joneydi Shariatzadeh et al. [24] proposed an integrated process consisting of a solar chimney, SOFCs, and solid oxide electrolysis cells (SOECs). In their proposed configuration the solar chimney converted high-intensity solar radiation to electric power, which then was partly consumed for the electricity demand while the rest was converted to hydrogen using high-temperature SOECs. The produced hydrogen was stored and converted to electricity using SOFCs overnight. The authors reported 0.28 kg/s hydrogen production at the peak, which was sufficient to meet 79.26% and 37.04% of the demand of a building complex, during summer and winter, respectively.

Zhang et al. [25] studied different configurations (Fig. 5.2) for multistage utilization of the chemical and thermal energy of SOFC exhausts in a combined heat and power (CHP) system. They observed that the recirculation of AOGs ratio allowed operational flexibility to meet heat and power demand, reaching 62.1% electrical power efficiency for low-AOG ratios ($\ll 7$) and 35.9% thermal efficiency for high-AOG ratios ($\gg 7$). The authors reported that the multistage exhaust gas combustion configuration (Fig. 5.2B) allowed a significant reduction in the operating temperature (from 1149°C to 830°C), which had significant implications for operational safety and cost of material requirements. However, the most energy-efficient system was the configuration shown in Fig. 5.2E where

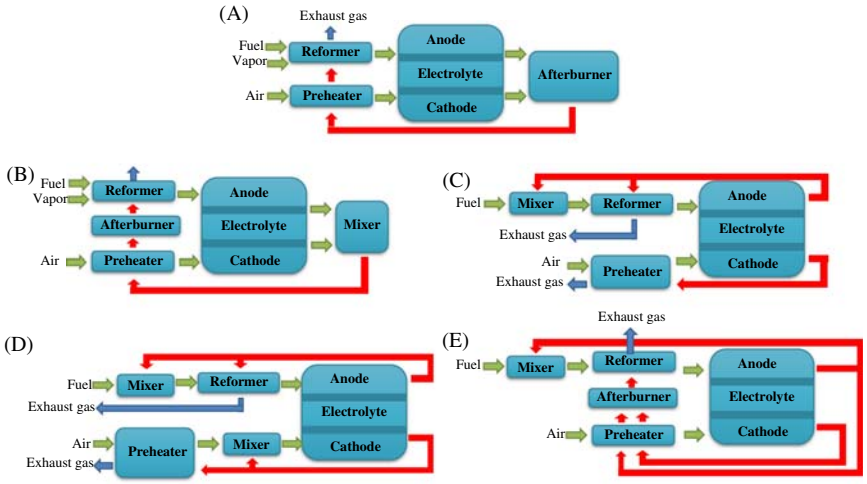

FIGURE 5.2

Various process configurations for the utilization of thermal and chemical energies of solid oxide fuel cell (SOFC) exhaust gases, including combustion of exhaust gases in a single stage (Case A), combustion of the exhaust gases in multiple stages (Case B), recovery of anode off-gases (Case C), recovery of anode off-gases and cathode off-gases (Case D), recovery of anode off-gases and combustion of the exhaust gases (Case E) [25].

the thermal energy of the cathode exhaust and chemical energy of the anode exhaust were utilized, with an overall energy efficiency of 92% (59.3% electrical efficiency and 32.8% thermal efficiency) [25].

Yi et al. [26] applied a DoEs methodology for the optimization of an internal-reforming SOFC system integrated with an intercooled GT and humidifier. They applied the DoEs method for optimization of four parameters including the moisture content, the excess air, the overall pressure ratio, and the pressure ratio of the low-pressure compressor. The authors observed that increasing the operating pressure increases the overall system efficiency. However, they indicated that this would increase the development cost and pose technical challenges. Therefore a trade-off needs to be established. For a fixed value of the overall compression ratio, decreasing the pressure ratio of the low-pressure compressor increased the overall system efficiency, however, this came at the price of higher operating temperatures at the high-pressure compressors. Decreasing excess air was reported to have a positive effect on efficiency. However, the moisture content of the fuel was reported to have bimodal effects (i.e., moisture injection increases the mass-flow rates in the expanders and lowers their inlet temperatures) but, at the same time, affects the partial pressure of reactants in the anode and the activation polarization and, therefore, requires establishing a trade-off. Through DoE-based optimization the authors reported the overall electrical efficiency (lower heating value—LHV) of 75.8% for the whole system.

Möller et al. [27] studied the optimization of a power-generation system consisting of an uncooled GT, and two SOFC stacks of 7500 cells, with tail-end CO_2 capture using a genetic algorithm. The authors reported that reducing the air flow and avoiding supplementary firing (unless necessary for combustion stability) were crucial for high efficiency. A high degree of external reforming was also recommended. The overall electrical efficiency above 60% for the SOFC−GT system with CO_2 capture was reported.

Autissier et al. [28] studied thermoeconomic optimization of a high-temperature SOFC system, integrated with a GT. Their SOFC model included detailed quantification of the electrode losses and thermal performances. A strong trade-off was observed between the cost and energy efficiency, ranging from a design with 2400 $/kW cost and 44% efficiency to another design with 6700 $/kW cost and 70% efficiency.

5.8 Optimization of solid oxide fuel cell-based systems for residential applications

Wakui and Yokoyama [29] studied the application of an SOFC-based cogeneration system integrated with battery units for residential applications. The role of the battery unit was to enhance operational flexibility. The battery charging and

discharging losses, limits, and status were incorporated into the model using mixed-integer, linear-optimization programing. The authors concluded that while the cost reduction is required for commercialization of this technology, battery-unit integration and appropriate sizing of the hot-water storage tank can increase the possibility for energy saving.

Windeknecht and Tzscheutschler [30] studied SOFC-based microcogeneration for supplying heat and electricity power in residential buildings. The authors demonstrated the impact of storage temperature on the efficiency of the CHP system.

Weber et al. [31] studied an SOFC system integrated with two absorption chillers and a heat exchanger. The design parameters and daily operation were optimized using a two-level optimization algorithm. A comparison was made to the scenario in which electricity was imported from a central-power grid. The results demonstrated that the CO_2 emissions could be reduced by 45% at the price of a 290% increase in cost.

Facchinetti et al. [32] studied small-scale SOFC−GT systems for application in residential buildings. A planar atmospheric SOFC at 5 kW was integrated with a microturbine based on an inverted Brayton cycle. The optimization and process integration enabled up to 65% exergy efficiency.

5.9 Optimization for energy performance

Sadeghi et al. [33] studied a trigeneration system including an SOFC, absorption-based refrigeration, and a supplemental heat exchanger for heating requirements. A genetic algorithm was applied for optimizing the design parameters such as SOFC-inlet temperature, fuel-utilization factor, current density, and steam-to-carbon ratio. Multiobjective optimization programing was applied in order to minimize the total product unit cost and to maximize exergy efficiency, with reported values of 25.94 $/GJ and 48.24%, respectively. The largest exergy destruction was observed in the air-heat exchanger.

Reyhani et al. [34] studied an SOFC−GT cogeneration system fueled by syngas from the gasification of heavy-fuel oil. The possibility for extra power generation in a steam turbine (ST) or producing freshwater in a multieffect distillation (MED) system were also considered. Thermodynamic and economic optimization was conducted using a genetic algorithm. The results of optimization programing suggested exergy efficiency of 40.93%, 33.62%, and 41.39% could be achieved for the SOFC−GT, SOFC−GT−ST, and SOFC−GT−MED process configurations, respectively.

Morandin et al. [35] studied a small-scale biomass gasifier integrated with an SOFC stack. Different process configurations, including a circulating, fluidized bed and downdraft gasifier, as well as a steam reformer and autothermal reformer, were considered. A bilevel optimization framework was programed. At the master

level the multiobjective optimization of cost and power generation were conducted. As the inner level, linear programing was applied in the form of pinch analysis. The analysis of optimal solutions in the form of Pareto fronts suggested that there was a strong trade-off between system efficiency and economy, especially due to the high costs of gasifiers and SOFCs at small scales. The most cost-effective configuration was 7000 $/kW.

Zhang et al. [36] studied the optimization of an SOFC integrated with an absorption-based refrigerator. The molar ratio of carbon monoxide to hydrogen (CO/H_2) was considered as the key optimization variable for which the optimal value of 0.053 resulted in an energy conversion efficiency as high as 87%.

5.10 Optimization for protecting the environment

Chitsaz et al. [37] applied multiobjective programing for an exergo-environmental comparison of internal and external reforming configurations in an SOFC-based cogeneration system for producing hot water and power. Exergy efficiency was maximized and CO_2 gas emission was minimized. The results demonstrated that the exergetic performance of the internal-reforming configuration was 9.6% higher than the process based on external reforming. This system also has superior performance by emitting 14% less CO_2.

Curletti et al. [38] studied the economic and technical optimizations of a biogas-fed SOFC power plant with CO_2 capture. The authors studied the effects of fuel utilization (FU) as well as the operating temperature and pressure of the SOFC on overall energy and economic performance using sensitivity analysis and multiobjective optimization. Electrical efficiencies in the range of 50%–62% (LHV biogas) were estimated. Increasing the FU to 90% increases the efficiency to 70%. However, if CO_2 capture is applied there will be a 10% efficiency penalty due to the energy needed for CO_2 compression and oxygen production.

5.11 Optimization of control performance

Control objectives of designing SOFC systems are diverse and include process flexibility against operational uncertainties as well as load-following capabilities. This is of particular interest when the SOFC system is integrated with other applications, as often a high degree of process integration could challenge controllability.

Nease and Adams [39] studied the load-following capabilities of an SOFC system integrated with a compressed air energy storage (CAES) system using rolling-horizon optimization (RHO) programing. The purpose of RHO programing

was to optimize the scheduling of the overall SOFC/CAES system to minimize the load-following capabilities (sum of squared errors) and maximize the process profitability. The authors applied a reduced-order model of the overall process and formulated the rolling-horizon problem as a mixed-integer, nonlinear program. White Gaussian noise and Monte Carlo simulation were applied in order to incorporate uncertainties. The results suggested that even under the worst case scenario the integrated process had 50% fewer errors in the load-following performance. The authors also observed a strong trade-off between load-following capabilities and revenue.

Zhang et al. [40] argued that ensuring fast load-following while managing fuel exhaustion and thermal transition were essential for the optimal and safe operation of integrated-SOFC systems. They proposed a control scheme in which an optimization algorithm was applied to identify optimal operating points (OOPs) with respect to efficiency. Then, in order to balance the load-following and fuel starvation, a two-stage scheme including preconditioning current strategy and feedback power-reference control was applied. In the final step the safety of thermal transition was validated.

Cheng et al. [41] also studied SOFC systems with similar concerns. They emphasized that cooperative control of the thermal and electrical performance of an SOFC is challenging due to it multitime-scale characteristics and gas-transmission delays. For optimization the authors applied an ANN system trained by the validated simulation data. The researchers conducted preliminary efficiency and thermal analyses in order to reduce the range of OOPs. Their recommended control strategy included fuel recovery to enhance the overall FU, and gas bypass to stack inlet temperature control. Current-based feedforward control and error-based feedback control systems were designed.

The commercial viability of SOFC stacks not only depends on their economic efficiency, but also their durability and reliability. Through modeling degradation processes such as the decrease in ionic conductivity of the electrolyte, metallic interconnect corrosion, anode nickel particles coarsening, and cathode chromium contamination, Nakajo et al. [42,43] investigated the distribution and evolution of faults and their interactions in stack performance. The authors suggested that under the considered operating conditions, cathode degradation was dominant, and counter-flow configuration (which results in more uniform cathode overpotential) and internal reforming with the benefit of lowered air−fuel ratio resulted in the highest lifetime. In addition, operating at lower-specific power and a higher-stack temperature improved the lifetime.

Skalar et al. [44] studied the implication of the differences in the thermal expansion coefficients of SOFC solid components for residual thermal stresses during operational variations. Using the finite element method they quantified the temperature profiles and residual stresses, and applied them for optimization of cell thickness and geometry of individual layers.

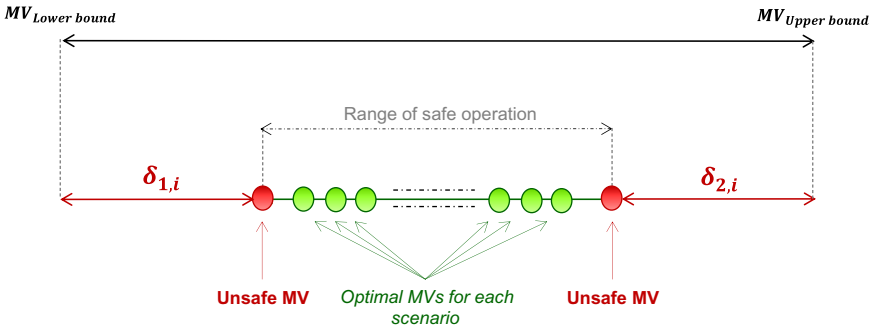

FIGURE 5.3

The range of available values for a manipulated variable, quantified as the safe (*green*) and unsafe (*red*) operating windows [1].

5.12 Optimization for operational safety

Cao et al. [45] studied the thermal management of a standalone, small-scale, SOFC system with burners and two heat exchangers. An air−bypass manifold around the heat exchangers was introduced for controlling the temperature. The researchers observed that regardless of the stack voltage value, the maximum efficiency was achieved at the inlet−outlet temperature critical points of the bypass ratio−air excess ratio (AE) plane or the plane representing the fuel utilization and the air excess ratio.

Sharifzadeh et al. [1] studied the design and operation of an SOFC-based triple combined-cycle power-generation system. The authors developed a method in which the window for safe-process operation was quantified using a bilevel optimization algorithm. The idea is shown in Fig. 5.3 for the range of values that a manipulated variable (e.g., the flow rate of the fuel) can have. The green circles refer to the values for the manipulated variable that can counteract the disturbances and operational uncertainties (change in power load) and ensure optimal performance. However, the red circles refer to the extreme operating conditions beyond which safe-process operation could not be guaranteed. The green region, therefore, quantifies the operating window in which, regardless of the values of the manipulated variables and disturbances, the operational constraints can be satisfied. The examples of the safe (*green*) and unsafe (*red*) operating windows for the air compressor, considering a 10% back-off from the surge line and stonewall, are shown in Fig. 5.4.

In order to calculate the values of the green and red circles, a method previously developed by Sharifzadeh et al. [46−49] for integrated process design and control was further extended. The process-model inversion was conducted two times; first, using the self-optimizing setpoints to quantify the green points and, then, using threshold values of the controlled variables in order to quantify the red points (Fig. 5.5).

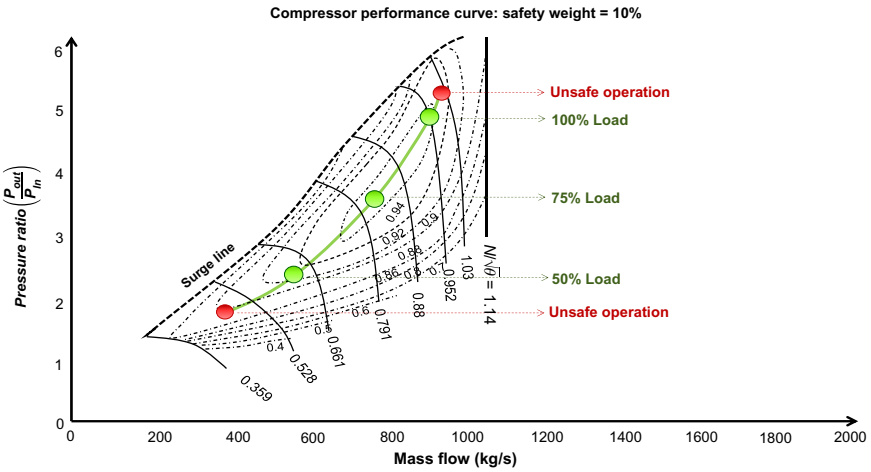

FIGURE 5.4

The safe (*green*) and unsafe (*red*) operating windows for the air compressor, considering a 10% back-off from surge line and stonewall [1].

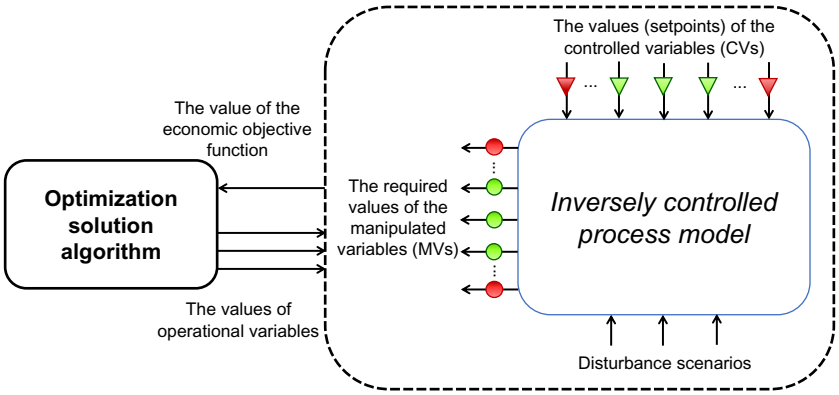

FIGURE 5.5

The inversely controlled process model applied for quantifying the optimal operating points and extreme points beyond which safe operation cannot be guaranteed [1].

5.13 Multiobjective optimization of solid oxide fuel cell-hybrid systems

The design and operation of SOFC-based systems simultaneously pursue several objectives such as economic profitability, thermodynamic (energy and exergy) performance, compliance with environmental regulations, process controllability,

and operational safety. Therefore multiobjective optimization programing is intuitively the method of choice. It should be noted that the solution of a multiobjective optimization problem is not a single point, but a set of solutions (often in the form of Pareto fronts) which quantifies the trade-off between competing and conflicting objectives, allowing decision-makers to take an informed decision by weighing the importance of each design objective.

Najafi et al. [50] studied the economic, environmental, and exergetic performance of an SOFC system integrated with a multistage flash desalination plant. Their optimization problem entailed the minimization of costs (including the greenhouse gas emission costs), and maximization of exergetic efficiency. Among the set of optimal solutions the authors chose the trade-off of 46.7% for the exergetic efficiency and 3.76 million $/year for the total cost. They stated that the calculated payback time of 9 years was associated with the high cost of the SOFC stack and was likely to be less as this technology is being commercialized.

Cheddie [51] studied the retrofit of a 10 MW power plant with an efficiency of 30%. It was posed to indirectly integrate an SOFC stack with a GT in order to enhance its energy efficiency, while minimizing the operational interruptions. The results of optimization indicated that the power output could be enhanced up to 18.9 MW at an efficiency of 48.5%, with the break-even per unit cost of 4.54 ¢/kWh (USD) for the generated electricity.

Baghernejad et al. [52] applied multiobjective programing in order to quantify the trade-off between economic, energetic, and environmental costs of a trigeneration system, in the form of Pareto front solutions. They reported that the selected solution had 13.88% lower unit-product costs, while its capital investment costs were increased by 8.03%. The authors observed 17.54%, 17.05%, and 18.22% reductions in the fuel cost, exergy destruction cost, and CO_2 emission cost, respectively.

Caliandro et al. [53] applied multiobjective optimization for small-scale and medium-scale SOFC−GT systems fed by gasified lignocellulosic biomass, with an option for CO_2 capture. The authors reported that a pressurized gasifier had the highest energy efficiency. In addition the steam-to-biomass ratio in the gasifier and the steam-to-carbon ratio in the reformer were key operating parameters to be optimized. Valorization of waste heat for cogeneration was shown to have a great economic impact. Overall energy efficiency in the range of 60%−70% was reported for most scenarios.

Khani et al. [54] studied an SOFC system indirectly coupled with a GT for power and hot-water cogeneration. Multiobjective optimization of exergy efficiency and unit costs of products was programed. The SOFC current density and the inlet-air flow of the GT had the highest effect on the trade-off between objective functions. The results suggested that it is possible to achieve 55.11% exergy efficiency, while the sum of the product unit cost was reported to be 170.5 $/GJ. Most of the exergy destruction happened in the heat recovery unit, combustion chamber, and afterburner.

Eveloy et al. [55] studied distributed power and freshwater generation through integrating a pressurized SOFC−GT system with a bottoming organic Rankine cycle and seawater reverse osmosis. Multiobjective optimization of the exergy efficiency and cost rate was programed using a genetic algorithm. The selected compromised solution had 2.4 MWe net power output and 636 m^3/day permeate. An exergy efficiency of 71.3% and cost rate of 0.0256 $/s were reported. A payback time of 6 years was estimated.

Sanaye and Katebi [56] studied the so-called 4E analysis (i.e., optimization of energy, exergy, and economic and environmental performance) of a hybrid SOFC system integrated with a micro-GT for CHP generation. The system was modeled using multiobjective optimization programing in which exergy efficiency and total-cost rate were optimized. The later was the aggregation of the capital, operational, and penalty costs of environmental emissions. The SOFC current density was reported to have the highest impact on the trade-off between the efficiency and cost rate. The total exergy efficiency of 60.7% and estimated electricity cost of 0.057 $/kW/h were reported. The payback period was estimated to be 6.3 years.

Aminyavari et al. [57] studied an internal-reforming SOFC−GT hybrid system integrated with a Rankin cycle with respect to economic, exergetic, and environmental criteria. Multiobjective optimization was programed and total order preference by similarity to an ideal solution was applied for selecting the solution from the set of the Pareto front optimal solutions. The selected solution featured 65.11% exergetic efficiency and a total-cost rate of 0.13745 €/s. Integration with the Rankin cycle resulted in 8.84% increase in the exergetic performance. This translates to 8439.2 MWh additional electricity and a reduction of about 5900 ton CO_2/year emissions.

Most of all, it is well-known that the design and operation of an industrial process are highly entangled, that is, if the process is poorly designed there might be little room left for control engineers to improve its operational performance [46]. A similar argument holds for operational safety. If the process is designed without considering safety and loss prevention criteria, it may become very difficult, if not infeasible, to ensure its operational safety (i.e., process safety should be considered at the same level as process design and be codesigned). As mentioned earlier (Figs. 5.3−5.5), Sharifzadeh et al. [1] studied the trade-off between operational safety and energy efficiency using multiobjective optimization programing. The results of the optimization were presented in the form of Pareto fronts which quantify the trade-off between process safety and economic performance. Fig. 5.6 suggests that enhancing the range of safe-process operations by 100% requires about 47% higher annual costs.

Sharifzadeh et al. [1] programed their problem in the form of optimization under uncertainty. Without loss of generality, two types of uncertainties, namely the frequent variations in the power load and gradual changes in the SOFC heat-transfer coefficients, were considered. The results demonstrated that it was possible to ensure optimal economic performance while satisfying the process safe

operation despite various uncertainties. Fig. 5.7 demonstrates that despite these variations the constraints regarding the maximum allowable temperature (1400K) were respected in all scenarios.

Fig. 5.8 demonstrate the flow of exergy using the so-called Sankey diagrams. The figures in a row show the system performance for various power loads of the same design, while the designs in each column differ according to the weight given to the safety and economic objective functions. These figures also suggest that most of the exergy destruction occurs in the SOFC stack, followed by the afterburner, the heat recovery steam generation, and the reformer.

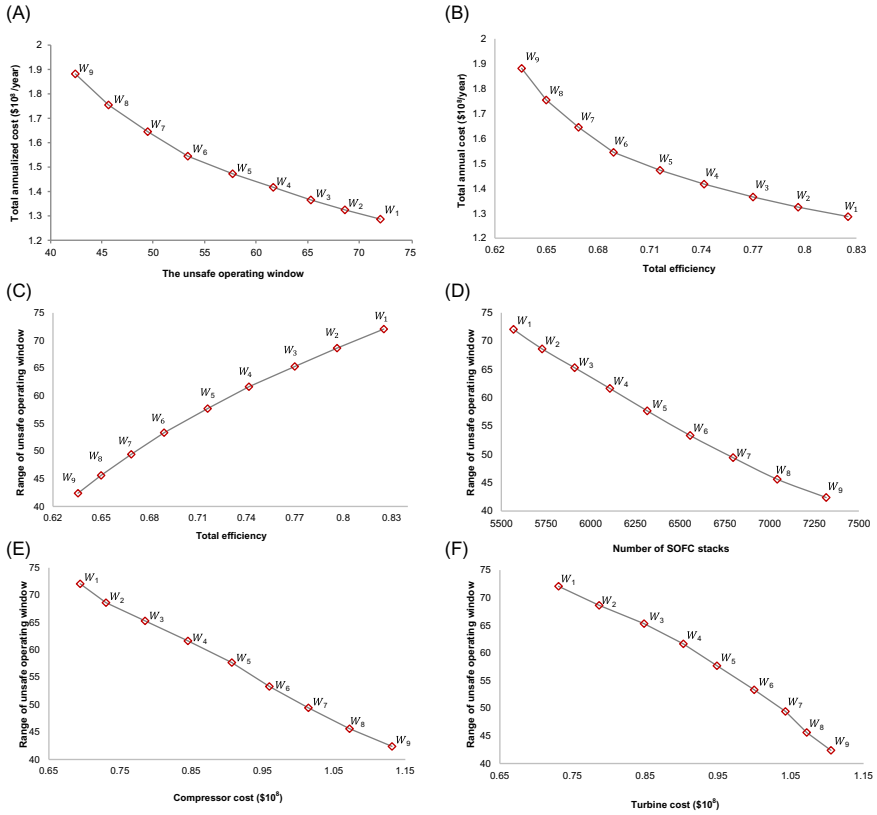

FIGURE 5.6

The solutions of multiobjective optimization in the form of Pareto fronts representing the trade-off between (A) the process economy versus safe operating window, (B) the total annual costs versus average efficiency, (C) the range of unsafe operating windows versus average efficiency, (D) the range of unsafe operating windows versus the number of SOFC stacks, (E) the range of unsafe operating windows versus the compressor cost, and (F) the range of unsafe operating windows versus the gas turbine cost [1].

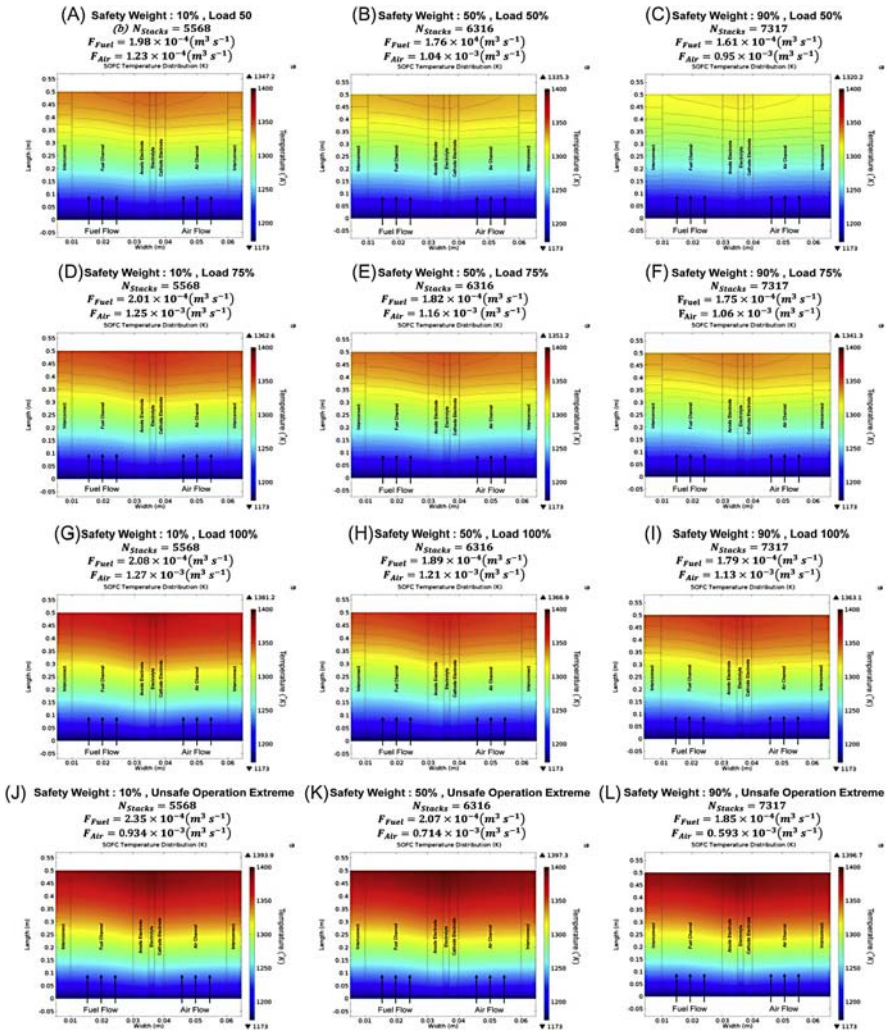

FIGURE 5.7

The two-dimensional temperature profiles for various process designs operating at different electrical power loads [1]. Figures in different columns represent the same process, operated at different loads (50%, 75%, 100%). Figures in different rows represent different designs based on different weight for process safety (10%, 50%, 90%) in the objective function.

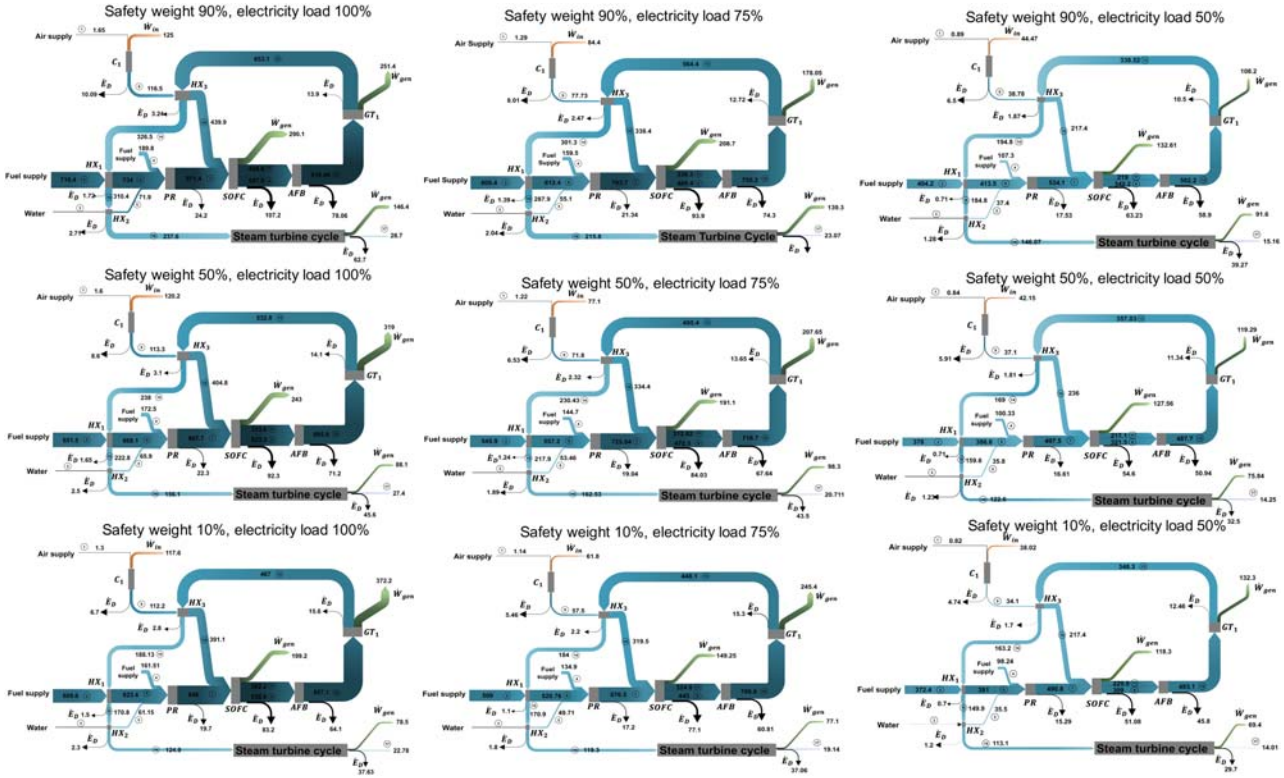

FIGURE 5.8

Sankey diagrams demonstrating the exergy flow and destruction for various process designs operating at different electricity power loads [1].

5.14 Conclusion

This chapter presents a thematic review of research into the multiscale modeling and optimization of SOFC systems. From the critical analysis of the reviewed materials, several potent directions for future research can be proposed:

1. While significant research has been conducted at different scales, their interactions in the form of multiscale optimization were rarely conducted. Therefore the multiscale nature of the involved phenomena and their exploitation for improving the key performance indicators should be further investigated.
2. Various studies reviewed in this chapter demonstrated strong trade-offs between economic, exergetic, environmental, and safety operation objectives for the design and operation of SOFC systems. Multiobjective optimization remains a research frontier.
3. Despite extensive research into the steady-state optimization of SOFC-based systems there is little literature on the dynamic optimization of these processes.
4. Modeling SOFC systems often results in a set of highly nonlinear equations. Due to the high-computational costs, systematic optimization is often replaced with sensitivity-based optimization with respect to key decision variables. Developing tailor-made solution algorithms enabling systematic decision-making for design and operational optimization variables is leading-edge research.

References

[1] M. Sharifzadeh, M. Meghdari, D. Rashtchian, Multi-objective design and operation of solid oxide fuel cell (SOFC) triple combined-cycle power generation systems: integrating energy efficiency and operational safety, Appl. Energy 185 (2017) 345–361. Available from: https://doi.org/10.1016/j.apenergy.2016.11.010.

[2] Y. Zhou, X. Guan, H. Zhou, K. Ramadoss, S. Adam, H. Liu, et al., Strongly correlated perovskite fuel cells, Nature 534 (2016) 231.

[3] D. Chen, Q. Zeng, S. Su, W. Bi, Z. Ren, Geometric optimization of a 10-cell modular planar solid oxide fuel cell stack manifold, Appl. Energy 112 (2013) 1100–1107. Available from: https://doi.org/10.1016/J.APENERGY.2013.04.035.

[4] V.A.C. Haanappel, J. Mertens, D. Rutenbeck, C. Tropartz, W. Herzhof, D. Sebold, et al., Optimisation of processing and microstructural parameters of LSM cathodes to improve the electrochemical performance of anode-supported SOFCs, J. Power Sources 141 (2005) 216–226. Available from: https://doi.org/10.1016/j.jpowsour.2004.09.016.

[5] M. Andersson, J. Yuan, B. Sundén, SOFC cell design optimization using the finite element method based CFD approach, Fuel Cells 14 (2014) 177–188. Available from: https://doi.org/10.1002/fuce.201300160.

[6] W. Li, B. Chi, C. Xiong, L. Jian, L. Jia, Q. Zhang, Composition optimization of samarium strontium manganite-yttria stabilized zirconia cathode for high performance intermediate temperature solid oxide fuel cells, Electrochim. Acta 190 (2016) 531–537. Available from: https://doi.org/10.1016/j.electacta.2016.01.035.

[7] T. Abdullah, L. Liu, Simulation-based microstructural optimization of solid oxide fuel cell for low temperature operation, Int. J. Hydrogen Energy 41 (2016) 13632–13643. Available from: https://doi.org/10.1016/j.ijhydene.2016.05.177.

[8] A. Cubero, J.I. Peña, M.A. Laguna-Bercero, Optimization of Ni-YSZ solid oxide fuel cell anodes by surface laser melting, Appl. Surf. Sci. 335 (2015) 39–43. Available from: https://doi.org/10.1016/j.apsusc.2015.01.230.

[9] S. Bozorgmehri, M. Hamedi, Modeling and optimization of anode-supported solid oxide fuel cells on cell parameters via artificial neural network and genetic algorithm, Fuel Cells 12 (2012) 11–23. Available from: https://doi.org/10.1002/fuce.201100140.

[10] A. Amiri, P. Vijay, M.O. Tadé, K. Ahmed, G.D. Ingram, V. Pareek, et al., Solid oxide fuel cell reactor analysis and optimisation through a novel multi-scale modelling strategy, Comput. Chem. Eng. 78 (2015) 10–23. Available from: https://doi.org/10.1016/j.compchemeng.2015.04.006.

[11] Y. Ji, K. Yuan, J.N. Chung, Y.C. Chen, Effects of transport scale on heat/mass transfer and performance optimization for solid oxide fuel cells, J. Power Sources 161 (2006) 380–391. Available from: https://doi.org/10.1016/j.jpowsour.2006.04.097.

[12] M. Hering, J. Brouwer, W. Winkler, Evaluation and optimization of a micro-tubular solid oxide fuel cell stack model including an integrated cooling system, J. Power Sources 303 (2016) 10–16. Available from: https://doi.org/10.1016/j.jpowsour.2015.09.036.

[13] F. Palazzi, N. Autissier, F.M.A. Marechal, D. Favrat, A methodology for thermo-economic modeling and optimization of solid oxide fuel cell systems, Appl. Therm. Eng. 27 (2007) 2703–2712. Available from: https://doi.org/10.1016/j.applthermaleng.2007.06.007.

[14] D. Bhattacharyya, R. Rengaswamy, Transport, sensitivity, and dimensional optimization studies of a tubular solid oxide fuel cell, J. Power Sources 190 (2009) 499–510. Available from: https://doi.org/10.1016/j.jpowsour.2008.12.084.

[15] H. Feng, L. Chen, Z. Xie, F. Sun, Constructal optimization for a single tubular solid oxide fuel cell, J. Power Sources 286 (2015) 406–413. Available from: https://doi.org/10.1016/j.jpowsour.2015.03.162.

[16] D.P. Bakalis, A.G. Stamatis, Optimization methodology of turbomachines for hybrid SOFC-GT applications, Energy 70 (2014) 86–94. Available from: https://doi.org/10.1016/j.energy.2014.03.093.

[17] Y. Zhao, N. Shah, N. Brandon, The development and application of a novel optimisation strategy for solid oxide fuel cell-gas turbine hybrid cycles, Fuel Cells 10 (2010) 181–193. Available from: https://doi.org/10.1002/fuce.200900127.

[18] Y. Zhao, N. Shah, N. Brandon, Comparison between two optimization strategies for solid oxide fuel cell-gas turbine hybrid cycles, Int. J. Hydrogen. Energy 36 (2011) 10235–10246. Available from: https://doi.org/10.1016/j.ijhydene.2010.11.015.

[19] Y. Zhao, J. Chen, Modeling and optimization of a typical fuel cell-heat engine hybrid system and its parametric design criteria, J. Power Sources 186 (2009) 96–103. Available from: https://doi.org/10.1016/j.jpowsour.2008.09.083.

[20] T.S. Lee, J.N. Chung, Y.C. Chen, Design and optimization of a combined fuel reforming and solid oxide fuel cell system with anode off-gas recycling, Energy Convers. Manag. 52 (2011) 3214–3226. Available from: https://doi.org/10.1016/j.enconman.2011.05.009.

[21] F. Calise, M. Dentice d'Accadia, L. Vanoli, M.R. von Spakovsky, Full load synthesis/design optimization of a hybrid SOFC-GT power plant, Energy 32 (2007) 446–458. Available from: https://doi.org/10.1016/j.energy.2006.06.016.

[22] F. Calise, M. Dentice d'Accadia, L. Vanoli, M.R. von Spakovsky, Single-level optimization of a hybrid SOFC-GT power plant, J. Power Sources 159 (2006) 1169–1185. Available from: https://doi.org/10.1016/j.jpowsour.2005.11.108.

[23] X. Zhang, Y. Wang, T. Liu, J. Chen, Theoretical basis and performance optimization analysis of a solid oxide fuel cell-gas turbine hybrid system with fuel reforming, Energy Convers. Manag. 86 (2014) 1102–1109. Available from: https://doi.org/10.1016/j.enconman.2014.06.068.

[24] O. Joneydi Shariatzadeh, A.H. Refahi, S.S. Abolhassani, M. Rahmani, Modeling and optimization of a novel solar chimney cogeneration power plant combined with solid oxide electrolysis/fuel cell, Energy Convers. Manag. 105 (2015) 423–432. Available from: https://doi.org/10.1016/j.enconman.2015.07.054.

[25] L. Zhang, Y. Xing, H. Xu, H. Wang, J. Zhong, J. Xuan, Comparative study of solid oxide fuel cell combined heat and power system with multi-stage exhaust chemical energy recycling: modeling, experiment and optimization, Energy Convers. Manag. 139 (2017) 79–88. Available from: https://doi.org/10.1016/j.enconman.2017.02.045.

[26] Y. Yi, A.D. Rao, J. Brouwer, G.S. Samuelsen, Analysis and optimization of a solid oxide fuel cell and intercooled gas turbine (SOFC-ICGT) hybrid cycle, J. Power Sources 132 (2004) 77–85. Available from: https://doi.org/10.1016/j.jpowsour.2003.08.035.

[27] B.F. Möller, J. Arriagada, M. Assadi, I. Potts, Optimisation of an SOFC/GT system with CO_2-capture, J. Power Sources 131 (2004) 320–326. Available from: https://doi.org/10.1016/j.jpowsour.2003.11.090.

[28] N. Autissier, D. Favrat, F. Marechal, J. van Herle, F. Palazzi, Thermo-economic optimization of a solid oxide fuel cell, gas turbine hybrid system, J. Fuel Cell Sci. Technol. 4 (2007) 123. Available from: https://doi.org/10.1115/1.2714564.

[29] T. Wakui, R. Yokoyama, Optimal structural design of residential cogeneration systems with battery based on improved solution method for mixed-integer linear programming, Energy 84 (2015) 106–120. Available from: https://doi.org/10.1016/j.energy.2015.02.056.

[30] M. Windeknecht, P. Tzscheutschler, Optimization of the heat output of high temperature fuel cell micro-CHP in single family homes, Energy Procedia 78 (2015) 2160–2165. Available from: https://doi.org/10.1016/j.egypro.2015.11.306.

[31] C. Weber, F. Maréchal, D. Favrat, S. Kraines, Optimization of an SOFC-based decentralized polygeneration system for providing energy services in an office-building in Tōkyō, Appl. Therm. Eng. 26 (2006) 1409–1419. Available from: https://doi.org/10.1016/j.applthermaleng.2005.05.031.

[32] E. Facchinetti, D. Favrat, F. Marechal, Design and optimization of an innovative solid oxide fuel cell-gas turbine hybrid cycle for small scale distributed generation, Fuel Cells 14 (2014) 595–606. Available from: https://doi.org/10.1002/fuce.201300196.

[33] M. Sadeghi, A. Chitsaz, S.M.S. Mahmoudi, M.A. Rosen, Thermoeconomic optimization using an evolutionary algorithm of a trigeneration system driven by a solid oxide

fuel cell, Energy 89 (2015) 191–204. Available from: https://doi.org/10.1016/j.energy.2015.07.067.

[34] H.A. Reyhani, M. Meratizaman, A. Ebrahimi, O. Pourali, M. Amidpour, Thermodynamic and economic optimization of SOFC-GT and its cogeneration opportunities using generated syngas from heavy fuel oil gasification, Energy 107 (2016) 141–164. Available from: https://doi.org/10.1016/j.energy.2016.04.010.

[35] M. Morandin, F. Maréchal, S. Giacomini, Synthesis and thermo-economic design optimization of wood-gasifier-SOFC systems for small scale applications, Biomass Bioenergy 49 (2013) 299–314. Available from: https://doi.org/10.1016/j.biombioe.2013.01.003.

[36] X. Zhang, M. Ni, F. Dong, W. He, B. Chen, H. Xu, Thermodynamic analysis and performance optimization of solid oxide fuel cell and refrigerator hybrid system based on H_2 and CO, Appl. Therm. Eng. 108 (2016) 347–352. Available from: https://doi.org/10.1016/j.applthermaleng.2016.07.096.

[37] A. Chitsaz, M. Sadeghi, M. Sadeghi, E. Ghanbarloo, Exergoenvironmental comparison of internal reforming against external reforming in a cogeneration system based on solid oxide fuel cell using an evolutionary algorithm, Energy 144 (2018) 420–431. Available from: https://doi.org/10.1016/j.energy.2017.12.008.

[38] F. Curletti, M. Gandiglio, A. Lanzini, M. Santarelli, F. Maréchal, Large size biogas-fed solid oxide fuel cell power plants with carbon dioxide management: technical and economic optimization, J. Power Sources 294 (2015) 669–690. Available from: https://doi.org/10.1016/j.jpowsour.2015.06.091.

[39] J. Nease, T.A. Adams, Application of rolling horizon optimization to an integrated solid-oxide fuel cell and compressed air energy storage plant for zero-emissions peaking power under uncertainty, Comput. Chem. Eng. 68 (2014) 203–219. Available from: https://doi.org/10.1016/j.compchemeng.2014.06.001.

[40] L. Zhang, J. Jiang, H. Cheng, Z. Deng, X. Li, Control strategy for power management, efficiency-optimization and operating-safety of a 5-kW solid oxide fuel cell system, Electrochim. Acta 177 (2015) 237–249. Available from: https://doi.org/10.1016/j.electacta.2015.02.045.

[41] H. Cheng, S. Jing, Y. Xu, Z. Deng, J. Li, X. Li, Control-oriented modeling analysis and optimization of planar solid oxide fuel cell system, Int. J. Hydrogen Energy 41 (2016) 22285–22304. Available from: https://doi.org/10.1016/j.ijhydene.2016.08.213.

[42] A. Nakajo, F. Mueller, J. Brouwer, J. Van Herle, D. Favrat, Progressive activation of degradation processes in solid oxide fuel cell stacks: Part II: Spatial distribution of the degradation, J. Power Sources 216 (2012) 434–448. Available from: https://doi.org/10.1016/j.jpowsour.2012.05.077.

[43] A. Nakajo, F. Mueller, J. Brouwer, J. Van Herle, D. Favrat, Progressive activation of degradation processes in solid oxide fuel cells stacks: Part I: Lifetime extension by optimisation of the operating conditions, J. Power Sources 216 (2012) 449–463. Available from: https://doi.org/10.1016/j.jpowsour.2012.05.078.

[44] T. Skalar, M. Lubej, M. Marinšk, Optimization of operating conditions in a laboratory SOFC testing device, Mater. Tehnol. 49 (2015) 731–738. Available from: https://doi.org/10.17222/mit.2014.209.

[45] H. Cao, X. Li, Z. Deng, J. Li, Y. Qin, Thermal management oriented steady state analysis and optimization of a kW scale solid oxide fuel cell stand-alone system for

maximum system efficiency, Int. J. Hydrogen Energy 38 (2013) 12404–12417. Available from: https://doi.org/10.1016/j.ijhydene.2013.07.052.

[46] M. Sharifzadeh, Integration of Process Design and Control: A Review, vol. 91, Institution of Chemical Engineers, 2013. Available from: https://doi.org.10.1016/j.cherd.2013.05.007.

[47] M. Sharifzadeh, Implementation of a steady-state inversely controlled process model for integrated design and control of an ETBE reactive distillation, Chem. Eng. Sci. 92 (2013) 21–39.

[48] M. Sharifzadeh, N.F. Thornhill, Optimal selection of control structure using a steady-state inversely controlled process model, Comput. Chem. Eng. 38 (2012) 126–138. Available from: https://doi.org/10.1016/J.COMPCHEMENG.2011.12.007.

[49] M. Sharifzadeh, N. Shah, MEA-based CO_2 capture integrated with natural gas combined cycle or pulverized coal power plants: Operability and controllability through integrated design and control, J. Clean. Prod. 207 (2019) 271–283. Available from: https://doi.org/10.1016/j.jclepro.2018.09.115.

[50] B. Najafi, A. Shirazi, M. Aminyavari, F. Rinaldi, R.A. Taylor, Exergetic, economic and environmental analyses and multi-objective optimization of an SOFC-gas turbine hybrid cycle coupled with an MSF desalination system, Desalination 334 (2014) 46–59. Available from: https://doi.org/10.1016/j.desal.2013.11.039.

[51] D.F. Cheddie, Thermo-economic optimization of an indirectly coupled solid oxide fuel cell/gas turbine hybrid power plant, Int. J. Hydrogen Energy 36 (2011) 1702–1709. Available from: https://doi.org/10.1016/j.ijhydene.2010.10.089.

[52] A. Baghernejad, M. Yaghoubi, K. Jafarpur, Optimum power performance of a new integrated SOFC-trigeneration system by multi-objective exergoeconomic optimization, Int. J. Electr. Power Energy Syst. 73 (2015) 899–912. Available from: https://doi.org/10.1016/j.ijepes.2015.06.017.

[53] P. Caliandro, L. Tock, A.V. Ensinas, F. Marechal, Thermo-economic optimization of a solid oxide fuel cell - gas turbine system fuelled with gasified lignocellulosic biomass, Energy Convers. Manag. 85 (2014) 764–773. Available from: https://doi.org/10.1016/j.enconman.2014.02.009.

[54] L. Khani, A.S. Mehr, M. Yari, S.M.S. Mahmoudi, Multi-objective optimization of an indirectly integrated solid oxide fuel cell-gas turbine cogeneration system, Int. J. Hydrogen Energy 41 (2016) 21470–21488. Available from: https://doi.org/10.1016/j.ijhydene.2016.09.023.

[55] V. Eveloy, P. Rodgers, A. Al Alili, Multi-objective optimization of a pressurized solid oxide fuel cell – gas turbine hybrid system integrated with seawater reverse osmosis, Energy 123 (2017) 594–614. Available from: https://doi.org/10.1016/j.energy.2017.01.127.

[56] S. Sanaye, A. Katebi, 4E analysis and multi objective optimization of a micro gas turbine and solid oxide fuel cell hybrid combined heat and power system, J. Power Sources 247 (2014) 294–306. Available from: https://doi.org/10.1016/j.jpowsour.2013.08.065.

[57] M. Aminyavari, A.H. Mamaghani, A. Shirazi, B. Najafi, F. Rinaldi, Exergetic, economic, and environmental evaluations and multi-objective optimization of an internal-reforming SOFC-gas turbine cycle coupled with a Rankine cycle, Appl. Therm. Eng. 108 (2016) 833–846. Available from: https://doi.org/10.1016/j.applthermaleng.2016.07.180.

This page intentionally left blank

CHAPTER

6 Synthesis, integration, and intensification of solid oxide fuel cell systems: process systems engineering perspective

Mahdi Sharifzadeh[1,2] **and Nilay Shah**[1]

[1]*Centre for Process Systems Engineering (CPSE), Department of Chemical Engineering, Imperial College London, London, United Kingdom*

[2]*Sharif Energy Research Institute, Sharif University of Technology, Tehran, Iran*

6.1 Introduction

The focus of *process synthesis* activities is the conceptual design of a process in terms of identifying the processing steps, their sequence, and interconnections. *Process integration* refers to the design paradigm with a holistic vision in which all the process elements work together seamlessly to achieve the design objectives. Examples of process integration are heat integration (through methodologies such as pinch) and mass integration, which have proven their utility in enhancing the economic, energetic, and environmental performances of industrial processes.

Generally speaking, all variants of solid oxide fuel cell (SOFC) technologies employ a combination of three steps, namely (1) fuel preprocessing, (2) electrochemical conversion, and (3) exhaust-energy utilization. Preprocessing strongly depends on the utilized fuel and include gasification for solid fuels such as biomass and coal, reforming for liquid and gaseous fuels, and gas cleaning, although direct fuel injection is also possible using advanced multifunctional anodes. Electrochemical conversion can happen in the anode or cathode, depending on whether the system has hydrogen proton-conducting or oxygen ion-conducting materials in the electrolytes. It is also possible to recycle the anode-exhaust gases and the cathode air for optimal fuel utilization (FU) and thermal management. The methods for fuel-exhaust utilization is much more diverse and include a variety of bottoming cycles as well as polygeneration of heating and cooling effects. These considerations are categorized and reviewed accordingly in this chapter. The diversity of fuel-cell feedstocks poses significant challenges toward process synthesis as it imposes different requirements for preprocessing, stringent criteria with respect to eliminating contaminations, and potentially vastly different

Design and Operation of Solid Oxide Fuel Cells. DOI: https://doi.org/10.1016/B978-0-12-815253-9.00006-9

integration opportunities. The first two sections of this chapter focus on the preprocessing of solid fuels such as biomass and coal, and reforming liquid and gaseous fuels such as light alcohols and hydrocarbons. Then the discussion continues with the design of SOFC stacks including the integration of high and intermediate-temperature SOFC stacks, as well as mass integration (anode- and cathode-recycle streams) and heat integration between process equipment. Next in Section 6.5, we will review the methods applied for downstream integration with gas turbines (GTs), heat recovery and steam generation (HRSG), followed by combined heat and power (CHP) cycles in Section 6.6, and carbon capture and compression in Section 6.7. The chapter concludes with key observations and the identification of potent research areas.

6.1.1 Fuel preprocessing: gasification of solid fuels

Gasification (often) refers to a high-temperature process in which carbonaceous fuels and organic solid matters are converted to a gaseous mixture of hydrogen, and carbon oxide, called synthesis gas (or syngas). Integrated gasification fuel cell technologies seem to be the only option to fulfill the economic and environmental targets of the US Department of Energy to achieve 60% energy efficiency while capturing 90% of the associated CO_2 emissions. Li et al. [1] proposed such a process (shown in Fig. 6.1) in which the SOFC was operated at high pressure. The hot-syngas generated in the gasification unit is sent for heat recovery, humidification, and gas cleaning before being fed to the SOFCS where it undergoes electrochemical reactions. The exhaust gases from the SOFC anode side go through a water−gas shift (WGS) reactor and CO_2 separation processes before they are compressed and recycled back to the hydro-gasification process. The proposed process achieved an overall energy conversion efficiency of 61.5%. The authors also considered alternative process configurations such as decarbonized exhaust gases being directly recycled to the anode so that the energy cost of recompression of the exhaust gas is less. However, in this configuration the hydrogen and CO required by the catalytic hydro-gasifier are supplied by the oxygen-blown gasifier. In addition, significantly more coal was needed to be injected to the oxygen-blown gasifier to maintain the required high temperature. As a result the overall efficiency dropped by 5%. An alternative configuration is when the SOFC was operated at a near-atmospheric pressure. This would require an ancillary compressor before the WGS reactor, which consumes a significant amount of energy. The decarbonized exhaust gases are sent for combustion. This configuration has a 9% lower energy efficiency. The latter considered configuration does not employ a methanation reactor and the efficiency was only slightly lower at 61.2%. It seems that the absence of a methanation reactor was compensated for by the WGS reactor. However, the authors suggested that the inclusion of the methanation reactor improved the quality of the SOFC composition control.

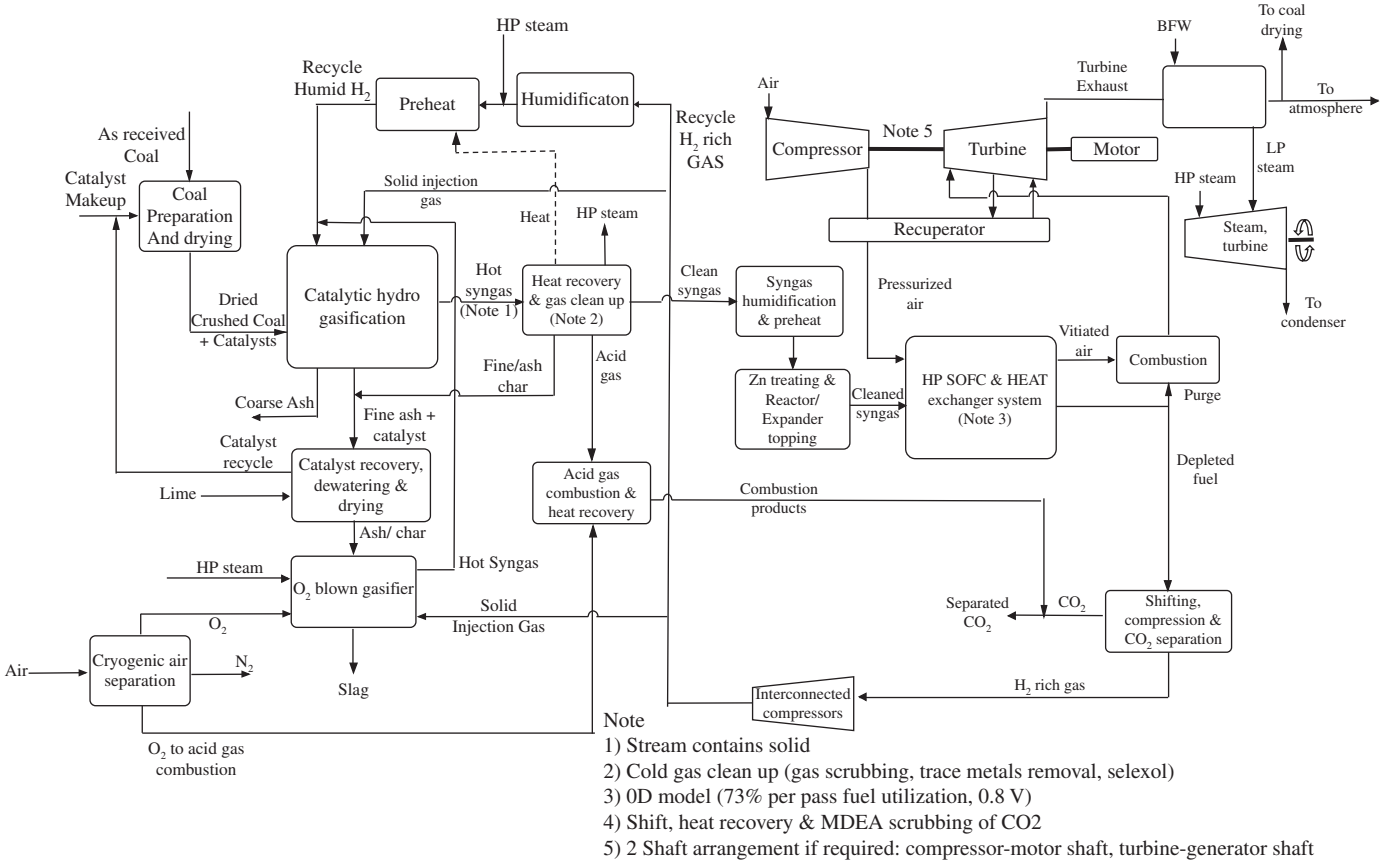

FIGURE 6.1

The integrated gasification solid oxide fuel cell process operating at a levelized pressure with two-stage gasification and anode-exhaust recycle to the gasifier [1].

The incorporation and integration of a WGS reactor is controversial. The risk of carbon deposition on the anode, decreased cell voltage, sensitivity to sulfide poisoning, efficiency loss, and capital cost are concerns that need to be overcome for large-scale commercialization implementation of these SOFC technologies [2]. Generally the WGS process includes two high and medium temperature reactors. First, most of the CO (about 80%) is converted to CO_2 in a kinetically driven, high-temperature (300°C−450°C) reactor. Then, in the second reactor that operates at a lower temperature (200°C−300°C), a near-equilibrium condition (96% of CO conversion) is achieved [2]. Nease and Adams states that an additional benefit of the WGS reactors is carbonyl-sulfide (COS) hydrolysis which results in 100% removal of this impurity [2]. They placed the WGS reactors before the H_2S removal unit (Fig. 6.2). By comparison, Li et al. [1] placed the WGS step in the anode-recycle loop (Fig. 6.1). They applied a COS hydrolysis reactor downstream from the gasifier. Li et al. [1] applied a water-wash column for the removal of particulates, chlorides, alkalis, and NH_3. In Nease and Adams' proposed structure, a Claus process was used for the separation of NH_3. Both processes applied a Selexol process for the separation of H_2S.

SOFC research is not limited to the design of new power-generation systems, but retrofitting and integration of existing ones to enhance their energy efficiency and environmental performance is also of paramount importance. Thallam Thattai et al. [3] studied retrofitting the Willem Alexander Centrale power plant—a coal-based integrated gasification combined cycle (IGCC) in the Netherlands—with SOFC technology. The aim was for the process to operate at higher efficiencies for a high degree of biomass cogasification (up to 70%). The authors concluded that no major modification was needed for the existing IGCC. They devised a control strategy in which the outlet temperature of the GT expander was controlled using variable inlet guide vanes. A booster air compressor was also required. The application of SOFC and partial oxy-combustion CO_2 capture reduced the production of low-pressure and intermediate-pressure steam. The authors reported that such a retrofit would reduce CO_2 emissions by 45%. However, full-scale CO_2 capture would require major (and costly) process retrofits.

Panopoulos et al. [4,5] studied an SOFC integrated with an allothermal biomass-gasification system for producing power and heat. As shown in Fig. 6.3 the heat of steam generation was supplied from the depleted SOFC exhaust burnt in a fluidized-combustion bed. The gasifier and fluidized-combustion bed were integrated through heat pipes with high-temperature sodium as the working fluid. The steam-to-biomass ratio was maintained at a low value (0.6) to avoid excessive-heat requirements. They reported that the process was thermally sustaining for FU (the amount of converted fuel in the fuel cell) below 75%.

Finally, Romano et al. [6] reported that including a methanation reactor and hydrogen firing could enhance the net plant efficiency by 4.5%, (under a 95% CO_2 capture scenario). The methanation reactor increases the concentration of the methane in the fuel and reduces the high air flow rates needed for cooling the SOFC. Firing hydrogen before the GT increases its inlet temperature and power output.

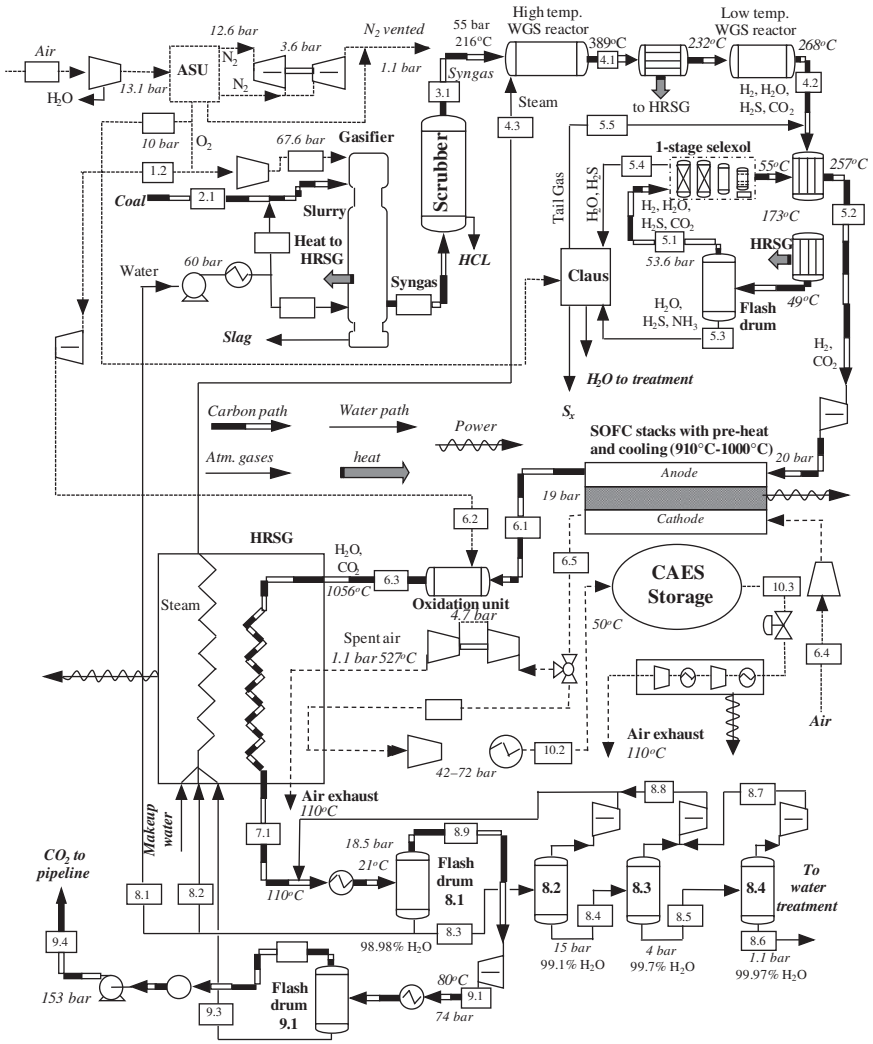

FIGURE 6.2

The integrated-gasification process proposed by Nease and Adams [2].

6.1.2 Fuel preprocessing: reforming gaseous and liquid fuels

Reforming refers to a chain of reactions where the fuel (often consisting of natural gas, light alcohols, or vaporized liquid fuels) is converted to syngas, which is a mixture of H_2, CO, and CO_2. The reforming configurations and technologies reported in the literature are highly diverse and include external reforming, internal reforming, partial reforming, combined reforming, trireforming, dry reforming, and partial oxidation, which are briefly discussed next.

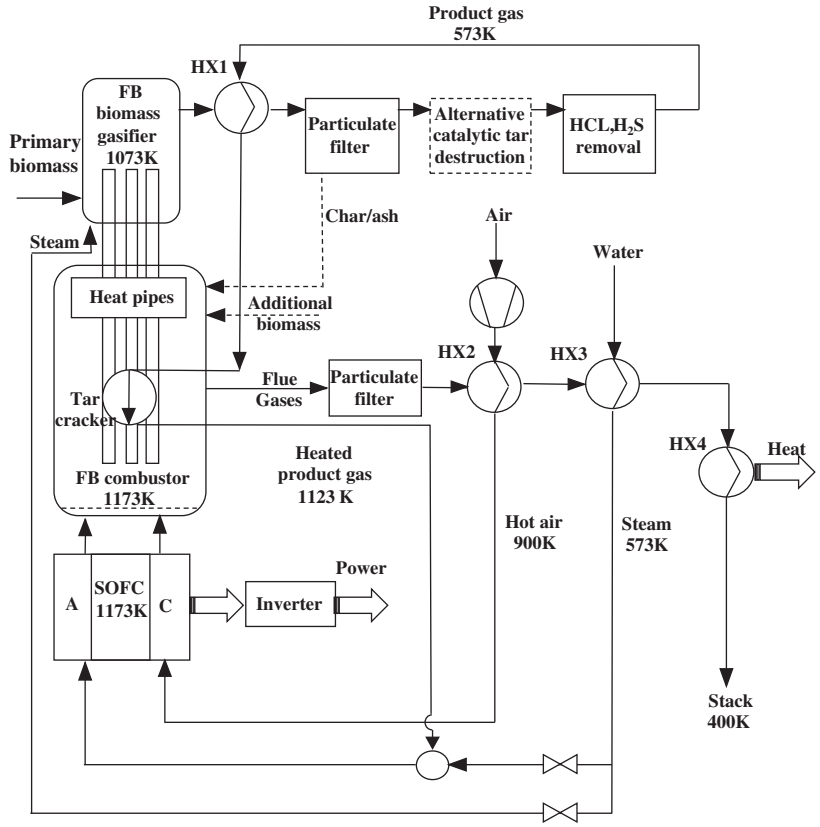

FIGURE 6.3

A flow diagram of an allothermal-biomass gasifier integrated to an solid oxide fuel cell.

External reforming has the advantage of independent and flexible operation, a schematic of which is shown in Fig. 6.4 [7]. The feedstock is converted in the reformer before being fed to the SOFC stack and the energy content of the exhaust gases is exploited in the catalytic combustor in order to supply the energy requirements of the endothermic reforming reactions. Ghang et al. [7] reported that the fuel-utilization factor has the most important influence on the reformer performance. High-temperature reforming favors fuel conversion and results in a higher H_2 yield. This requires the combustor to operate at higher temperatures. They also reported that excess air should be controlled to avoid deactivation of the combustion catalyst. These observations illustrate the interactive nature of controlling such integrated processes.

Powell et al. [8] reported the application of an adiabatic-steam reformer where the heat and water required for endothermic steam reforming were supplied by circulating anode-exhaust gases. Although the single pass fuel-utilization factor

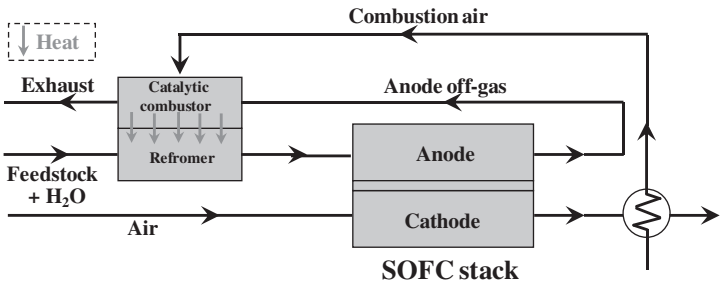

FIGURE 6.4

A schematic of an external reformer.

was only about 55%, the recycle loop enabled overall utilization of 93%. They reported an overall efficiency of over 60%.

Direct internal reforming (DIR) or internal reforming is a configuration in which the reforming reactions happen at the anode chamber. The advantage of this configuration is to avoid excessive steam concentration that would reduce the open-circuit voltage. In addition, process intensification through merging the fuel cell and reformer in a single-unit operation reduces the capital costs. This is achieved due to the nickel catalyst in the anode, which facilitates the reforming and WGS reactions to produce the H_2 required for the electrochemical reactions. The high temperature of the anode chamber also favors such reactions. If the steam required for reforming is not externally provided, but supplied by the electrochemical reactions, the internal reforming occurs at a slower rate known as *gradual internal reforming (GIR)*. Generally in the GIR configuration the steam-to-methane ratio is below 1 [9]. Alternatively, pure methane can be applied, which is known as *dry reforming*. The risk of carbon deposition remains an operational challenge in all these processes [10]. More details on internal steam reforming can be found in Ref. [11].

Klein et al. [10] reported that in the DIR configuration steam reforming occurs mostly in the inlet section of the anode electrode, while in the GIR configuration it was more homogenized. Since the produced H_2 in both configurations exceeds the requirements of electrochemical reactions, DIR and GIR were reported to have similar performances. However, the cooling effect of the endothermic reforming reactions was not observed in the GIR configuration [10]. The authors estimated that a steam-to-methane ratio below 1 could increase the risk of coke formation. Therefore catalyst dispersion and cell geometry were adjusted in the GIR configuration.

Lanzini and Leone [12] experimentally studied the application of biogases from anaerobic digestion in SOFC systems. They reported that the addition of oxidants such as air, steam, and CO_2, reduces the risk of carbon deposition. Alternatively biohydrogen could be used as an intrinsically safe fuel. The authors also suggested that a planar anode-supported SOFC is more appropriate for

DIR as more catalyst is available. Steam reforming (SR) was reported superior to dry reforming. The latter is favorable when the biogas is rich in CO_2.

Tsai et al. [13] conducted a comparative study of internal SR and dry reforming of methane. For SR they recommended a steam-to-methane ratio of 1. By comparison, for dry reforming a CO_2-to-methane ratio of 2 was suggested. For optimal results a mixture of low-steam concentration and high-CO_2concentration offered ideal operating conditions.

The choice between external and internal reforming strategies also depends on the fuel utilized. For instance, for methanol and DME reforming only low-temperature operations would suffice to improve heat recovery from the SOFC exhausts. The flexible operation of the reformer also requires the operating parameters such as temperature and the steam-to-carbon ratio to be optimally adjusted [14].

Dokamaingam et al. [15] compared conventional packed-bed and catalytic coated-wall for internal reforming of methane. They suggested that in the packed-bed−internal reformer the reforming reactions occurred rapidly at the entrance of the reformer. This resulted in a thermal mismatch between the endothermic reforming reactions and the exothermic electrochemical reactions. The coated-wall−internal reformer provided a smoother methane conversion profile, thereby avoiding local thermal effects. The authors also compared counter-flow and coflow configurations. It was observed that the coflow configuration provided a higher voltage and a smoother temperature gradient.

Fardadi et al. [16] studied the performance of a partial internal reformer integrated with a counter-flow SOFC. External reforming may suffer from transport delays and thermal fluctuations when following sharp power−load variations. The authors proposed that partial internal reforming in which a part of the methane fuel is injected directly to the anode can provide fast and reliable load-tracking capabilities, while managing thermal stresses and fatigue.

The choice between internal and external reforming is a strong function of feedstock. Laosiripojana and Assabumrungrat [17] studied the application of methane, methanol, and ethanol. They reported that if an appropriate level of steam is injected, DIR of methane does not pose any significant risk of carbon formation. The same conclusion was made for methanol if the SOFC is operated at a temperature higher than 1000°C. However, incomplete reforming of ethanol over Ni−YSZ resulted in ethane and ethylene production and indirect internal reforming where it was first converted to ethane on the Ni/Ce−ZrO_2 and then fed to the SOFC.

Janardhanan et al. [18] studied the performance of isothermal and adiabatic internal reforming in an SOFC. They reported the temperature profile to be the most influential variable on SOFC performance. They suggested that excessive use of the catalyst could have detrimental effects. The efficiency could be higher if prereforming was applied, especially if an adiabatic reformer was employed.

Wahl et al. [19] studied the internal reforming of methane in a 10 kW_e SOFC. With 65% recycling of the anode exhaust gases, an electrical efficiency of 57% was achieved. The authors observed a performance loss for high-methane concentrations (above 90%) over the SOFC's lifetime.

Recknagle et al. [20] studied the pressurized operation of SOFC stacks intensified by direct internal reforming. Increasing the cell pressure enhances the Nernst potential and reduces the polarization activation, which increase the cell voltage and power. The authors reported that increasing the pressure from 1 to 10 atm reduced the temperature by 20°C and increased cell voltage by 9%.

Georges et al. [21] studied GIR with a methane-to-steam ratio of up to 12 on a lanthanum−chromite anode. They reported 100% selectivity, suggesting no conversion via WGS reaction. Despite good oxidation−catalytic activity and no carbon deposition the current density was reported to be low.

Nikooyeh et al. [22] studied internal reforming in a coflow SOFC with 75% utilization, 0.65 A/cm^2 current density, and 0.7 V voltage. The authors explained that the large-temperature gradient is the result of relative rates of exothermic-electrochemistry and endothermic-reforming reactions. The anode recirculation ratio increases the H_2, H_2O, and CO_2 concentrations, thereby reducing the carbon deposition risk. The increase of H_2 concentration increases the electrochemistry reactions and mitigates the cooling effect of reforming reactions at the anode inlet. However, the authors suggested that there was an optimum recirculation rate to optimize the average current density.

Barelli et al. [23] studied dry external reforming using CO_2. The anode off-gases were recycled in order to supply the CO_2 for fuel reforming. The reaction of CO_2 with low-carbon fuels such as methane resulted in the production of H_2 and CO. The thermal energy of the anode exhausts supported the endothermic reforming reactions. They reported a 3.6% efficiency improvement compared to conventional reforming. The temperature increase was limited to 3°C−5°C proving the thermal safety of process operation.

Kushi [24] also investigated dry reforming of methane. The two cases of SR ($H_2O/CH_4 = 2.5$) and CO_2 reforming ($CO_2/CH_4 = 2.7$) were studied. Under low-FU the produced voltage was similar in both cases. However, for high-FU ($\sim$90%) the voltage was higher in the CO_2-reforming case. The author also compared internal and external reforming, suggesting that internal reforming requires temperature control and modification of the Ni−YSZ anode catalyst.

Lanzini et al. [25] studied direct dry reforming of methane. While thermodynamic analysis suggests that a CH_4/CO_2 ratio of 1:2 at 800°C would be sufficient to avoid carbon deposition, experimental results suggested gradual deactivation of the Ni−anode catalyst in terms of increased ohmic resistance and activation polarization, which should be attributed to accelerated coarsening. The authors suggested that the CH_4/CO_2 ratio and oxygen carrier composition must be controlled to suppress such phenomena.

Guerra et al. [26] studied dry reforming of simulated biogas ($CH_4/CO_2 = 60/40$) from anaerobic digestion. Additional CO_2 was added to prohibit carbon formation on the anode. The best performance was reported for the ratio of $CH_4/CO_2 = 50/50$. Lower methane-to-CO_2 ratios such as 30:70 or 24:76 reduced the cell efficiency (lower heating value—LHV) by 2% and 4%, respectively.

Ni [27] also studied the reforming of methane with CO_2. The author indicated that for $CH_4/CO_2 = 50/50$, methane−CO_2 reforming and reversible WGS

reactions are dominant and conversion through methane SR was negligible. An anode catalyst which promotes CO electrochemical oxidation was recommended. Operating the cell at low potentials or high temperatures enhanced the electric power output.

Alternatives to externally heated SR are *partial oxidation (POX)* and *autothermal reforming (ATR)*. POX refers to the process in which the fuel is partially combusted under substoichiometric conditions to produce H_2 and CO. ATR refers to the *process intensification* strategy in which the reformer and combustor are merged; the energy requirement of the endothermic reforming reactions is supplied through oxidizing a part of the fuel. Chiodo et al. [28] compared the performance of SR, ATR, and POX strategies for a high-temperature steam reformer. The authors attributed the lower performance of the POX configuration to the reverse WGS reaction that reduces the H_2 concentration. SR exhibited superior performance compared to ATR, as in the SR configuration part of the fuel is consumed.

Dokamaingam et al. [29] studied the effects of adding O_2 to promote the autothermal internal reformation of methane in an intermediate temperature (IT) SOFC. Adding a small amount of O_2 can avoid local cooling effects. However, high oxygen-to-carbon ratios would reduce the electrical efficiency, therefore, there is a need to establish a trade-off.

Liso et al. [30] studied the utility of an SOFC integrated with a micro-CHP (mCHP) system for residential application under SR and POX configurations with the recirculation of anode and cathode gases. They reported that SR had higher-electrical efficiency. This was associated with higher-heat recovery in SR endothermic reactions. Part-load operation reduced the efficiency due to heat losses and required additional natural-gas fuel.

Horiuchi et al. [31] studied the performance of SOFCs using *n*-butane. The in situ catalytic partial oxidation (CPOX) and anode−anode facing arrangements were exploited instead of a direct-flame configuration. Overall the performance of the system and FU were poor and the authors suggested its application for CHP systems.

A similar experiment was conducted by Lee et al. [32] using methane. They reported that CPOX could remove the risk of carbon deposition. They compared the performance of two catalysts, namely (1) Ni−gadolinium-doped ceria (GDC), and (2) Ni−yttria stabilized zirconia (YSZ). A significantly higher-power density was observed for the Ni−GDC compared to the Ni−YSZ (1.35 W/cm^2 vs 0.27 W/cm^2) for the same operating temperature. The advantage of the former system was attributed to the fact that the addition of GDC prevents oxidation of Ni, hence preventing its deactivation. In addition, stainless steel could be used for current collection.

Finally, various researchers have investigated the possibility of combining CO_2 reforming, SR, and POX in a single reactor, known as *trireforming*. Trireforming has been proven to offer flexibility in terms of H_2/CO composition in the range of 1.5−2.0 as well as eliminating the risk of carbon formation [33]. In addition, by modifying the composition of oxygen, methane and water it is possible to achieve autothermal conditions [34].

6.2 Electrochemical conversion of fuels: heat integration of solid oxide fuel cell systems

Thermal management of SOFCs and reducing the temperature gradient across the cell have important influences on its electrical efficiency, durability, and safe operation. Zeng et al. [35] proposed the application of a liquid sodium−metal heat pipe in order to "equalize" the temperature distribution. The tubular SOFC consisted of heat functional, current collector, anode, electrolyte, and cathode layers. The authors reported that the temperature gradient was reduced from 31 to 13K/cm and the power density was improved from 73 to 120 mW/cm^2.

A similar study was conducted by Dillig et al. [36] who investigated the integration of planar sodium heat pipes into an SOFC stack. The authors reported that even 1 heat pipe per 10 cells could reduce the temperature gradient by up to 50% for their hydrogen-fueled scenario. On the other hand, for methane direct internal methane reforming such integration is beneficial in terms of transferring heat from exothermic to endothermic zones, which results in a significant reduction in the cathode air and corresponding energy consumption. The authors estimated that for a methane-fed SOFC in a high-temperature (80°C−120°C) CHP plant the reduction of the electrochemically required air ratio from 5 to 1.5 would increase the thermal efficiency from 15% to 26%. For a low-temperature (<60°C) CHP plant the equivalent gain would be 16%.

Lee et al. [37] studied a planar-steam reformer thermally integrated with a catalytic burner. The unused fuel from the anode exhaust is combusted to provide the reforming energy requirements. They examined finned and unfinned configurations of the heat exchanger-steam reformer (HESR), reporting 30°C higher temperature for the finned HESR.

6.3 Electrochemical conversion of fuels: mass integration of solid oxide fuel cell systems

The recirculation of the anode and cathode exhaust gases has significant influence on power generation and thermal management. It also offers advantages in terms of FU and reducing the need for externally supplied steam [38]. These desirable features have motivated researchers to investigate their utilization for optimal and safe operations.

Peters et al. [38] studied the implication of anode off-gases recirculation. Based on 220 case studies they concluded that systems with no anode-gas recycles could have up to 16% lower electrical efficiency. They also indicated that too high-FU and recycling ratios (RR) may decrease the electrical efficiency due to higher cathode−air flow requirements and increased blower-power consumption. On the other hand, low RR and FU also could lead to carbon formation. Such trade-offs indicate the need for optimization and establishing a compromise. They recommended 60%−80% FU and 70% RR.

Similarly for the case of an SOFC integrated with an ethanol fueled reformer, Saebea et al. [39] reported that while high FU (>0.6) and anode-recirculation rate reduced the risk of carbon formation and allowed the reformer to operate at lower temperatures, they have an adverse effect on the electrical efficiency. However, for low FU (0.5−0.6) the electrical efficiency and circulation rates increased simultaneously.

Powell et al. [8] studied an SOFC stack equipped with an adiabatic reformer and anode-gas recirculation. The steam and thermal energy requirements of the endothermic reaction were supplied by the recirculated anode-gas exhausts. Although single pass-FU was estimated to be only 55%, the recirculation enhanced the overall-FU to 93%. An overall-energy efficiency above 60% was reported.

Jia et al. [40] studied the implications of internal reforming, anode off-gases recycling, and cathode-air recycling on the electrical and cogeneration energy efficiencies. They reported that 44% electrical efficiency was achievable using internal reforming and anode-exhaust recycling increased the electrical efficiency to 46%. Cathode air recycling increased the efficiency to 51%. The combined anode and cathode gas recycling increased the electrical efficiency to 52%.

Anode exhaust compression (required for recycling) could be performed using a blower or ejector. Genc et al. [41] studied an anode-cycle ejector for a mCHP. They observed that increasing the fuel-inlet temperature and its pressure ratio with respect to the anode exhaust increases the steam-to-carbon ratio and the entrainment ratio until they remain unchanged after a certain point. Under their specific case study the values of 7, and 1.159 bar were recommended for the methane and anode-exhaust pressure, respectively, which resulted in a steam-to-carbon ratio and entrainment ratio of 2.05 and 0.92, respectively.

A key advantage of SOFC technologies is their flexibility for utilizing a diverse range of fuels. Liu et al. [42] investigated the impact of fuel exchange on the anode recirculation in terms of carbon deposition and nickel oxidation. Using an experimentally validated model they concluded that the entrainment ratio of the ejector in the gasification-syngas case was smaller than in the natural-gas scenario, with a lower risk of carbon deposition.

Vincenzo et al. [43] studied the ejector design and operation for an SOFC-based mCHP, with anode-gas recirculation. The results of their analysis revealed that for a large mixing chamber diameter the entrainment ratio was higher, but the ejector efficiency was lower, indicating the need for establishing a trade-off at the design stage. They also observed that a high inlet-primary flow temperature favors entrainment and efficiency. In addition an increase in the secondary-mass flowrate increases the steam-to-carbon ratio and system efficiency.

Engelbracht et al. [44] compared the part-load operation of fuel-driven and steam-driven ejectors applied in the anode exhaust-recirculation loop (Fig. 6.5). It was observed that in both scenarios increasing FU decreased the achievable part-load. This behavior was attributed to the increased steam generation and lower oxygen-to-carbon ratio. The lower part-load limit for the configuration with the fuel-driven ejector was 78% and was constrained by the risk of carbon

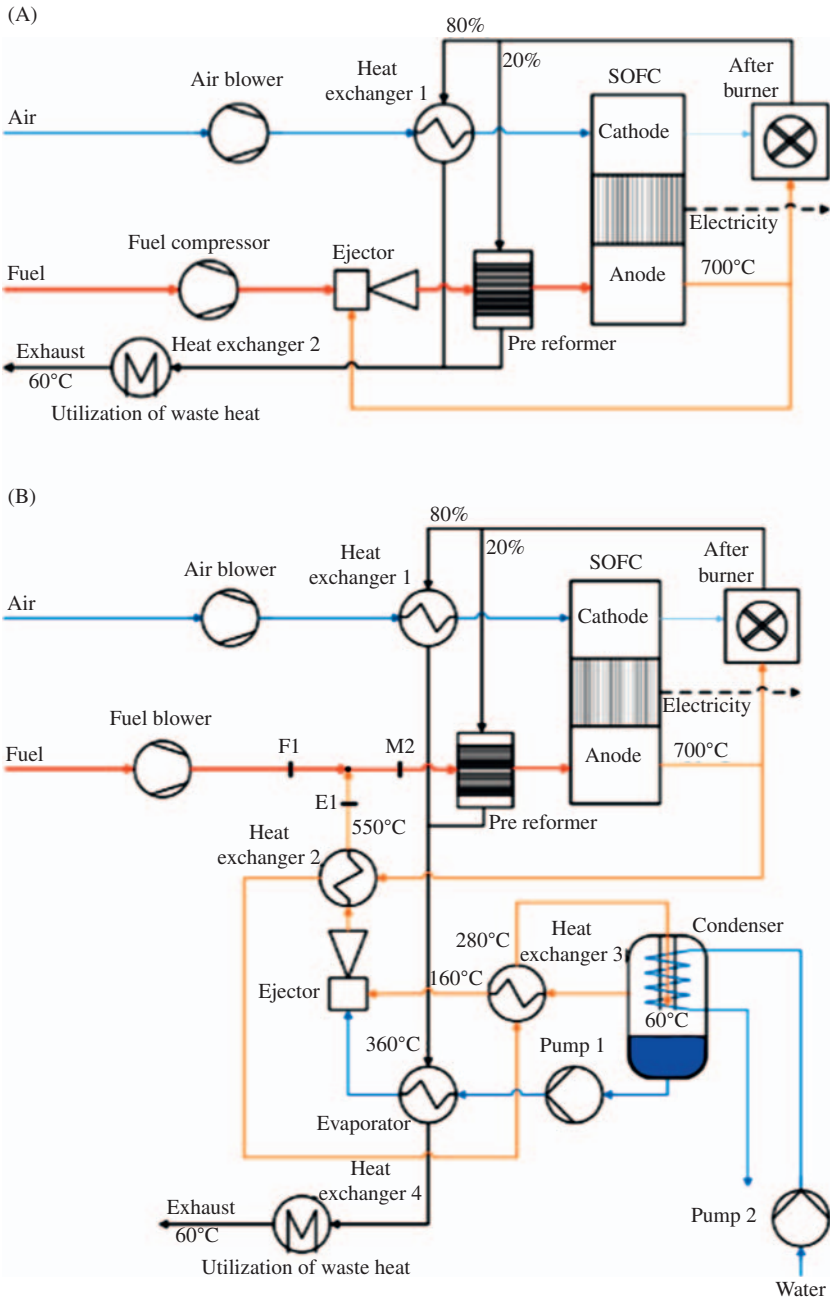

FIGURE 6.5

Process configurations with (A) a fuel-driven ejector and (B) a steam-driven ejector in the anode-recirculation loop [44].

formation. The lower limit for the configuration with the steam-driven ejector was 38% and was limited by the water balance in the system. The system with a steam ejector had an electrical efficiency of 3.2% higher than its fuel-driven counterpart due to the application of a water pump instead of a fuel compressor.

Marsano et al. [45] studied the geometric design of two ejectors for anode-gas recirculation to have either a constant pressure-mixing section or a constant area-mixing section. They observed that the performance difference between these two geometries was not significant as the flow-rate ratios of the primary and secondary fluids was very large and the pressure increase across the system was small.

Saebea et al. [46] studied the effect of the recirculation of anode and cathode gases for a hybrid SOFC−GT process. They indicated that the recirculation rates of anode- and cathode-exhaust gases had the highest impact on the turbine inlet temperature (and hence the overall energy efficiency), which should be compensated for by the addition of fuel and air to the combustion chamber. The inlet turbine temperature of the system with an anode-recycle loop was lower than the turbine requirements, necessitating additional fuel, while this parameter was higher than the suitable range for the case of cathode recycling with the need for air injection. The combined anode−cathode recirculation configuration required additional air, but less than the cathode recirculation alone. They reported the highest overall energy efficiency for the system with cathode and anode gases recirculation.

Rokni [47] studied the impact of fuel type on anode exhaust recirculation for ammonia, pure hydrogen, methanol, ethanol, DME, and biomass gasification. He reported high dependency between FU, anode recirculation, and plant efficiency. No anode-gas recirculation was recommended for the case of ammonia. When the SOFC was fed by pure hydrogen, 20% recirculation was applied for 80% FU. For the case of methanol, ethanol, and DME optimal-anode recirculation and FU had the opposite effect, that is, for high-FU low-anode recirculation rates were recommended, and vice versa.

Ferrari et al. [45] studied the implication of anode recirculation for the transient operation of a tubular SOFC integrated with a micro-GT. An ejector was applied for driving the recycled gas. The authors reported that time-dependent fluctuations of the ejector behavior had important implications for the steam-to-carbon ratio which, in turn, can push the process into unsafe operational regions if not carefully controlled.

6.4 Integration between solid oxide fuel cell stacks

As discussed by Buonomano et al. [48] a further integration opportunity exists between SOFC stacks at different temperatures. Araki et al. [49] proposed a process configuration in which a low-temperature SOFC (operating at 750°C) and a

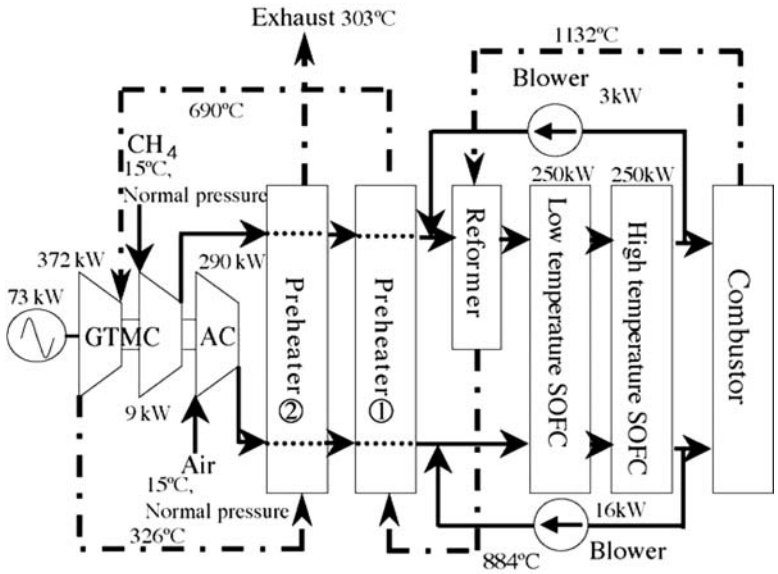

Fig. 6. Two-staged low and high temperature SOFC system.

FIGURE 6.6

The two-stage solid oxide fuel cell (SOFC) combined cycle including a low-temperature and a high-temperature SOFC stack [49].

high-temperature SOFC (operating at 884°C) were operated in series, presenting possibilities for air and fuel recirculation (Fig. 6.6). Under operating conditions of 5% FU, 30% fuel recirculation, 10% air recirculation and 100% external reforming the energy efficiencies of the SOFC stack and the combined system were reported to be 50.3% and 56.1%, respectively. By comparison for an equivalent high-temperature SOFC operating at 900°C, 50% fuel recirculation and 50% air recirculation, the stack and combined system efficiency were 45.1% and 54.7%, respectively.

Musa and De Paepe [50] studied two combined cycles including either an intermediate-temperature SOFC and a high-temperature SOFC, or two intermediate-temperature SOFCs (Fig. 6.7). The anode flow was parallel and the cathode flow was sequential. Under the considered operating conditions the process with two intermediate-temperature SOFC stacks had higher efficiency. This was expected as the energy efficiency of a single-stage (standalone) intermediate-temperature SOFC is higher. In addition, due to the IT of the second stage there is no need for preheating the cathode air, which enables a higher turbine-inlet temperature (TIT).

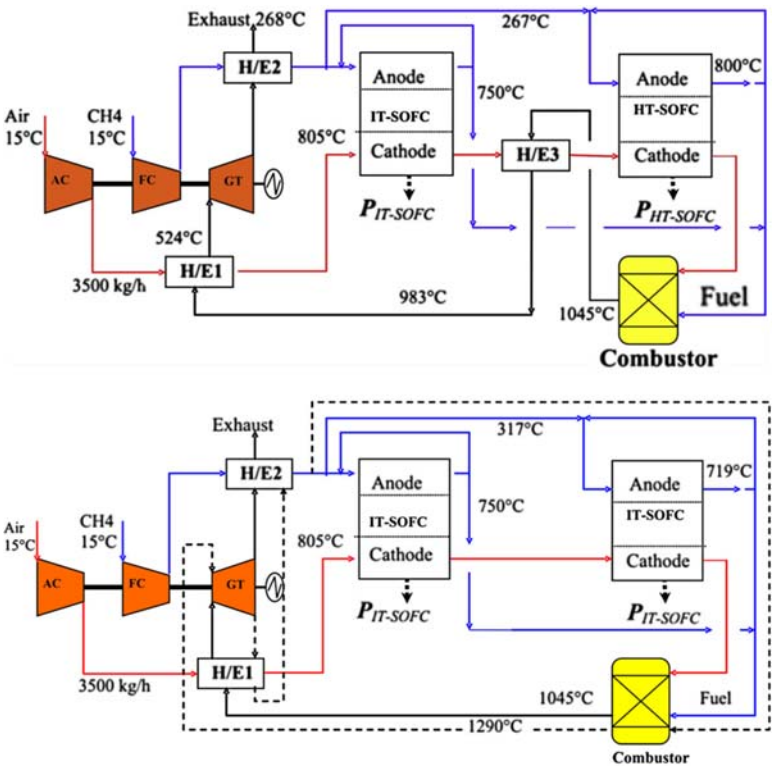

FIG. 6.7

Two process configurations for combined cycle solid oxide fuel cell systems using intermediate-temperature solid oxide fuel cells and high-temperature solid oxide fuel cells [50].

6.5 Hybrid solid oxide fuel cell-based power plants: gas turbine integration, heat recovery, and steam generation

The idea of integrating an SOFC with a GT is simply to replace the combustion section of a Brayton cycle with the SOFC stack [48]. The selection of the operating pressure has a significant influence on the overall-energy efficiency. Operating the process at atmospheric pressure results in a much simpler process, but with lower-energy efficiency. In this configuration the operation of the SOFC and turbine could be separated by an auxiliary burner applied to heat the air leaving the SOFC−cathode channel. Under this configuration it is possible to maintain the TIT and operate the turbine at its nominal design point [48]. By comparison it is evident from the Nernst equation

(as discussed in Chapter 2: Thermodynamics and energy engineering) that by increasing the stack pressure, the voltage and, consequently, the energy efficiency, improves. In addition, the heat exchange between the SOFC exhaust and air entering the turbine reduces the TIT and the expansion of the exhaust gases at the turbine, resulting in a higher efficiency of the GT (compared to the atmospheric configuration) [48]. However, as discussed extensively in this chapter, the direct pressurized coupling results in highly restricted operating conditions and reduced process flexibility.

A recuperator (heat exchanger) could be provisioned to exploit the thermal energy of the exiting exhausts for heating the air entering the SOFC stack in order to minimize the temperature gradient which, otherwise, could be detrimental to the SOFC components.

Zhao et al. [51] reported that the optimal integration between the SOFCs and GT requires optimization of the TIT. Such optimization provides the opportunity for a 19% increase in the overall-energy efficiency. The hybrid-energy efficiency was found to be insensitive to the FU, but strongly dependent on the isentropic efficiency of the turbine and compressor.

Mehrpooya et al. [52] studied SOFC−GT integration using a two-dimensional model for counter-flow and coflow configurations. They reported that increasing the temperature and pressure of the fuel cell increases the cell voltage and power output, but the extent of the increase was more in the counter-flow configuration. Increasing the FU decreased the voltage and power output, but the voltage reduction was less for the case of the coflow process. Increasing the current density also decreased the power and voltage. Overall, for the same operating conditions, the counter-flow configuration achieved higher voltage and power output, which should be attributed to lower concentration and activation polarization. The optimal values for the current density and the number of cells were estimated to be 8000 A/m^2 and 2122, respectively.

The temperature of the exhausts leaving the integrated SOFC and turbine cycle was high enough to employ Rankine cycles for HRSG. If included, it can also provide the steam needed for the reforming reactions. Otherwise anode off-gas recirculation could be the method of steam supply. While the anode-recirculation option might be cheaper it also poses difficulties in terms of controlling the steam-to-carbon ratio [48].

Yi et al. [53] compared a dual-combined cycle (i.e., SOFC−GT) and triple-combined cycle (SOFC−GT−ST). The triple cycle-power plant was found to be more effective by achieving an efficiency of 71%−74% compared to 58%−61% in the case of the dual-combined cycle. They reported that decreasing the inlet fuel and, hence, the TIT increased the efficiency at the price of a lower-power output.

Sarmah and Gogoi [54] studied an SOFC stack integrated with gas and steam turbines. The authors reported that the system efficiency would increase by increasing the compressor-pressure ratio. They compared process configurations in which the steam was reheated at a single pressure and two or three pressures in the HRSG generation section. The aim of reheating the steam is to enhance the

power output from the steam turbines. Sarmah and Gogoi [54] reported the least irreversibility (and, hence, maximum efficiency) for the configuration with single-pressure reheating.

Sharifzadeh et al. [55] studied the application of SOFCs in an integrated triple combined-cycle plant as shown in Fig. 6.8. The authors investigated the influence of the design decisions such as process equipment and nominal operating points for the flexible operation of the overall integrated process using multiobjective optimization under uncertainty. The results were quantified in the form of Pareto fronts, which demonstrated the trade-off between capital costs, energy efficiency, and the safe-operating window, quantified as the range of operating conditions that will satisfy technical and safety constraints. It was shown that enhancing the safe operating window by 100% would incur almost 47% more annual costs.

Common Rankine cycles apply water as the working fluid. Organic Rankine cycles (ORCs) by comparison apply a working fluid with a lower-boiling temperature than water, thereby enabling heat recovery at lower temperatures. Ebrahimi and Moradpoor [56] studied an SOFC stack integrated with a microturbine and an ORC that used R123 as the working fluid. They reported a high-energy efficiency of 65.7%.

Ragini Singh and Onkar Singh [57] compared the application of various working fluids (R141b, R245fa, and R236fa) in an organic-bottoming cycle integrated with an SOFC−GT system. The authors reported an 8%−13% energy-efficiency improvement compared to conventional processes. The overall system efficiency increased from 63.17% to 75.81%. R236fa was identified as the best-performing working fluid. However, R245fa was the most environment-friendly option.

Pierobon et al. [58] applied a genetic algorithm to screen more than a hundred working fluids in a hybrid plant including woodchip gasification integrated with an SOFC stack and ORCs. Propylcyclohexane at 15.9 bar was identified as the best-working fluid with efficiency in the range of 54%−56%.

An alternative is to integrate the process with a Kalina cycle that applies a mixture of two working fluids with the advantage of boiling over a range of temperatures. Gholamian and Zare [59] compared the Kalina and ORCs for waste-heat recovery from an SOFC stack. The ORC working fluid was R113, while a mixture of ammonia and water was applied in the Kalina mixture. The ORC cycle operated at a significantly lower-operating pressure and generated more power.

It was stated that the waste heat from SOFC−GT could be utilized in a HRSG section. The produced steam can be used for SR of the fuel. In addition it is known that steam injection into the GT increases the efficiency by 1%−3% [48]. This latter configuration is known as the *Cheng cycle*. The injected steam increases the mass-flow rate of the gases expanding in the GT, resulting in additional power generation [60].

Srinivas et al. [61] compared the exergy efficiency of two configurations, that is, with or without steam injection. The maximum feasible steam-to-fuel−mass ratio was estimated to be 6. It was observed that steam injection increases the efficiency of the gas cycle, but reduces the efficiency of the steam cycle. The Second Law analysis revealed that most of the exergy destruction occurred at

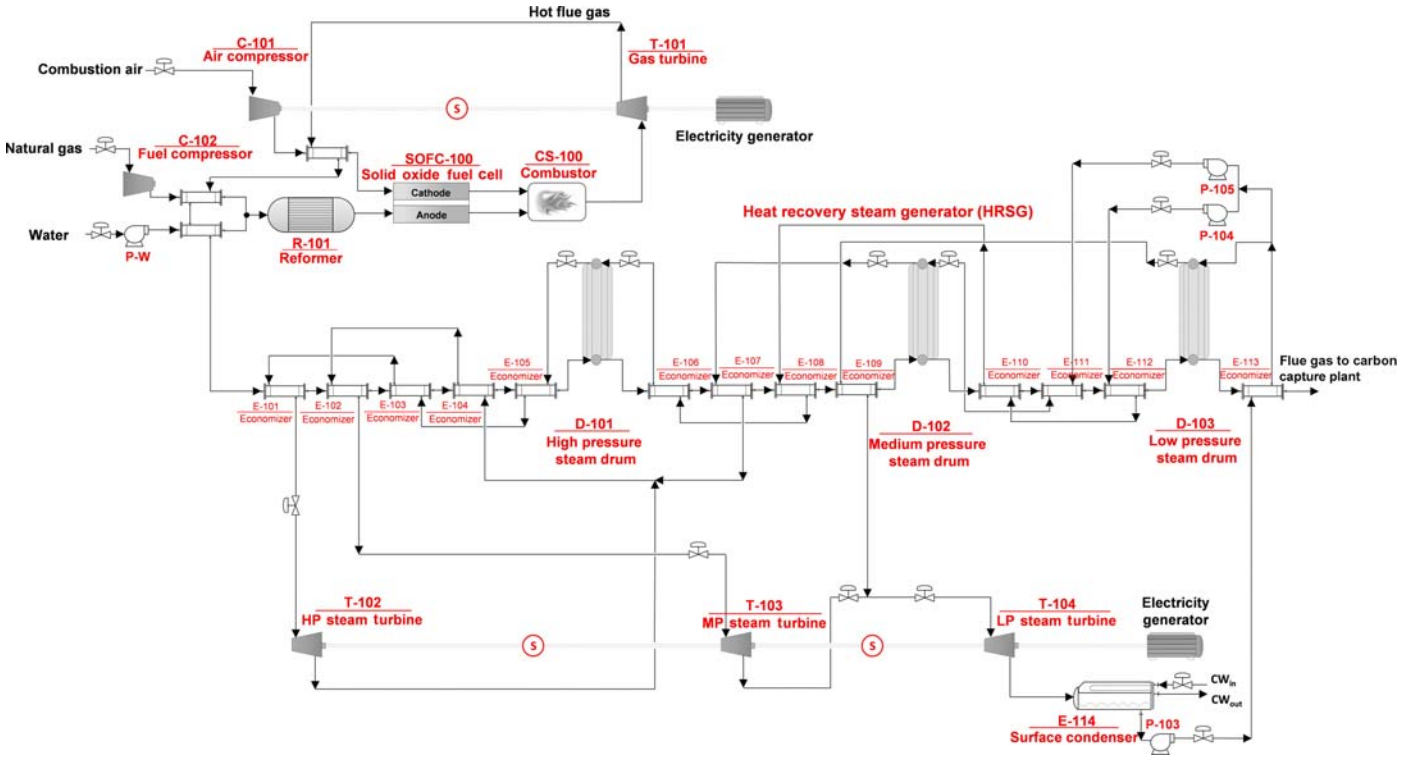

FIG. 6.8

The solid oxide fuel cell triple combined-cycle power generation system proposed by Sharifzadeh et al. [55].

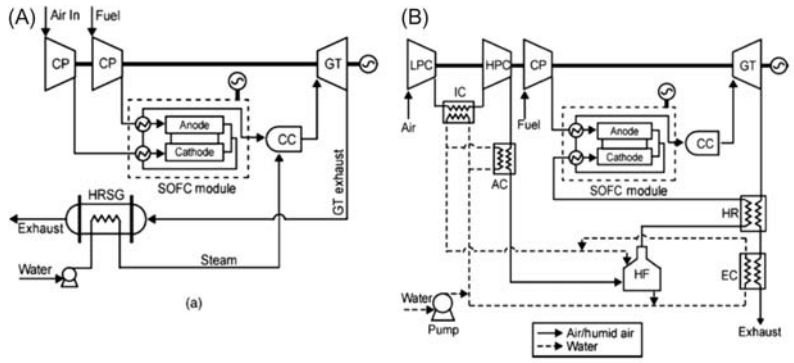

FIG. 6.9

Simplified layouts of (A) the solid oxide fuel cell–gas turbine (SOFC–GT) system with a Cheng cycle and (B) the SOFC–GT system with a humidified turbine [60].

the combustion chamber and steam injection decreases the exergy destruction from 38.5% to 36%.

Kuchonthara et al. [60] studied the effect of steam recuperation in an SOFC–GT combined cycle. It was observed that for low TITs the overall system efficiency increases with an increase in the TIT and reduction in the pressure ratio. The opposite trend was observed for high TITs.

Massardo and Lubelli [62] demonstrated that if optimally designed and operated the SOFC–GT equipped with a Cheng cycle without a steam cycle had a similar efficiency of the same process with a steam-bottoming cycle (configurations FCGT3 and FCGT4 in that publication). In fact, the Cheng cycle can be applied in a CHP cycle (to be discussed in the next section) in order to increase the operational flexibility and switching between the thermal and electrical load-following strategies [48].

While in a Cheng cycle the steam is injected into the combustion chamber, it is also possible to supply the steam by saturating the air entering the cathode channel as shown in Fig. 6.9B [60]. This figure also shows additional recuperation for cathode-air preheating. Kuchonthara et al. [60] argued that the recuperation strategy increases the TIT which, in turn, enhances the thermal and specific work of the turbine. By comparison, operating the system with the Cheng cycle with no air preheating (shown in Fig. 6.9A) at high TITs does not result in efficiency improvement.

6.6 Solid oxide fuel cell-based polygeneration systems: heating and cooling services

SOFC-based power generation systems can easily achieve energy efficiencies over 50%, which is much more than the 30%–40% conversion efficiencies of conventional combustion systems. Further improvements were reported for the

integration of CHP systems with SOFCs through which energy efficiencies as high as 90% were achievable [63]. However, the modularity of these systems makes them highly suitable for small-scale and residential applications.

Liso et al. [64] studied the effect of the heat-to-power ratio in an SOFC-based, mCHP generation system coupled with hot-water storage. Using residential data of single family households in European countries, they calculated a range of 0.5−1.5 for the heat-to-power ratio. They recommended that the power-to-heat ratio must be sized according to the summer demand and the extra energy needed for the winter-demand peak should be supplied by an auxiliary boiler and a hot-water storage.

Kupecki [65] studied the off-design operation of an SOFC-based mCHP fueled by DME. They reported electrical and overall efficiencies of more than 40% and 80%, respectively. With respect to the transient operations such as start-ups and shut-downs, the authors estimated that it will take about 10 hours for the system to achieve full-operational power from a cold state. In order to minimize the power import from the grid they recommended maximizing the electrical efficiency during transient operation for which they generated electrical and overall-efficiency maps.

Jing et al. [66] studied the application of SOFC-based−combined cooling, heating, and power (SOFC−CCHP) for public buildings in China. They applied a combination of gray relational analysis and entropy weighting in which uncertainties in information were considered. The authors reported an overall efficiency of 74% in average for various applications in the scale of 750−900 kW power generation and up to 750 kW heat generation. This performance is better than the internal combustion engine−combined cooling, heating, and power systems (ICE−CCHP) and mGT−CCHP, which have efficiencies of 66% and 60%, respectively. The authors reported even more visible environmental benefits. The carbon emission reduction was 60% for the SOFC−CCHP compared to 57% and 54% for the ICE−CCHP and mGT−CCHP systems, respectively. The air pollution−cost saving was 85% for the SOFC−CCHP compared to 25% and 56% by the ICE−CCHP and mGT−CCHP systems, respectively. The levelized cost of electricity was reported to be 0.10 $/kWh which is comparable with the average commercial price in China (0.11 $/kWh). Using a multicriteria assessment the authors concluded that SOFC−CCHP systems were more appropriate for hospitals, hotels, and supermarkets rather than office and school buildings. They identified a heat-to-power ratio of 2.6−3.8 in winter and cooling-to-power ratio of 0.1−1.9 in summer for best overall performance.

Khani et al. [67] studied a cogeneration system consisting of an SOFC fueled by hydrogen, a gas turbine, and a refrigeration cycle through exergoeconomic analysis. The authors reported a 6.5% improvement in the exergy efficiency compared to the standalone scenario. The authors found the lowest exergoeconomic factors for the burner and fuel-heat exchanger.

Chitsaz et al. [68] compared four configurations of an SOFC-based−trigeneration system based on whether anode recycling and/or cathode recycling were

applied. They identified the highest energy efficiency of 82.5% for the system with anode recycling, but the lowest total unit cost of the products (22.99 $/GJ) for the system with both anode and cathode recycles.

Hosseinpour et al. [69] studied a biomass gasification system integrated with an SOFC stack and a Goswami cycle. The Goswami cycle (i.e., bottoming cycle) is a combination of Kalina and absorption refrigeration cycles. The authors reported that upon optimization of fuel cell-operating temperature and the turbine-inlet pressure an energy efficiency of 58.5% and exergy efficiency of 33.7% were achieved. The highest exergy destruction was associated with the gasification reactor followed by the boiler and the second air−heat exchanger.

Worall et al. [63] studied a micro-SOFC−trigeneration system in which the waste heat was applied for cooling and dehumidification. They applied a membrane-separated liquid desiccant dehumidification system using a potassium formate solution. Unlike other salt-based organic solutions, potassium formate is not corrosive or harmful to health. In addition, the application of fiber membrane heat/mass exchangers eliminated the risk of liquid carry-over. A regeneration rate of up to 0.1−0.15 g/s was reported. The authors estimated that the electrical and overall efficiency of the system could achieve values of 18% and 30%, respectively.

6.7 Carbon capture from solid oxide fuel cell systems

SOFC-based−power generation technologies have great potential to reduce the carbon intensity of the generated power systems to half through enhanced energy-conversion efficiency. Furthermore, due to the application of an impervious ceramic electrolyte, nitrogen in the combustion air is not mixed with the fuel and the anode exhausts are primarily oxidation products (CO_2 and steam) and are readily amenable to compression and sequestration [70]. While the SOFC-exhaust gases often contain unconverted syngas, in order to avoid mixing with nitrogen oxyfuel combustions or chemical-looping combustion are recommended. Other configurations, including phase change and physical absorption [6], are also available in the literature.

Mahisanana et al. [71] studied two process configurations in which an SOFC system was integrated with oxyfuel combustion. One configuration applied anode-exhaust recycling and, in the other configuration, saturated steam at 60 bar was generated and recycled. Overall efficiencies of 75.6% and 67.41% were reported for the systems with anode-exhaust recycling and steam recycling, respectively. The superior performance of the first configuration was attributed to higher-FU and the possibility for fuel-turbine integration, while in the second configuration, due to the excessive energy requirements for steam generation, a fuel turbine was not implemented.

Petrakopoulou et al. [72] studied the thermodynamic performance of a large-scale SOFC-based plant with oxyfuel combustion and carbon capture and compression. An exergetic efficiency of 71.1% was estimated for the SOFC plant compared to 56.5% for the reference conventional combined-cycle power plant without carbon capture. The major sources of the exergy destruction were identified to be the fuel-cell stacks followed by the afterburner and expanders.

Nease and Adams [73] proposed to integrate an SOFC-based system with oxyfuel combustion with compressed air energy storage (CAES). The authors reported that the addition of CAES to the system significantly enhances the load-following capabilities, subject to only small efficiency penalties (1.1% HHV) and minor reductions in the levelized electricity costs (0.08−0.3 ¢/kW/h). The load-following capability, quantified in terms of the (weighted) sum of squared errors was much better than the base case with no CAES integration, and was not impacted by the inclusion of the carbon capture. The authors estimated that the proposed scheme is economical for a carbon tax above \$40 tonne^{-1} and a natural-gas price over \$7.58 G/J (\$8 MMBtu^{-1}).

Carbon capture from SOFC exhaust gases could be conducted through chemical looping combustion (CLC). The CLC unit essentially consists of dual fluidized-bed reactors, that is, a fuel reactor and an air reactor operating at mild-operating conditions (atmospheric pressures and temperatures in the range of 700°C−800°C). In the fuel reactor the unconverted syngas in the anode exhausts reduces the oxygen carrier to produce a mixture primarily consisting of CO_2 and steam [74]. The reduced oxygen carrier is then sent to the air reactor for reoxidation. The fuel oxidation is free from nitrogen and consists of steam and CO_2, and is ready for sequestration. Most of the high costs of oxygen production are avoided. Moreover the high capital and operating costs of cathode-air preheating are avoided [75].

Chen et al. [74] studied an SOFC power-generation system fueled by coal in which carbon capture was conducted through CLC as shown in Fig. 6.10. The CLC unit consisted of a fuel reactor and an air reactor. In the fuel reactor the unconverted syngas in the anode exhausts reduces the oxygen carrier to produce a mixture primarily consisting of CO_2 and steam. The reduced oxygen carrier is then sent to the air reactor for reoxidation. Under the operating conditions of the FU factor of 0.85, operating temperature of 900°C, operating pressure of 15 bar, and 100% carbon capture the net-plant efficiency was estimated to be 49.8%. The largest exergy destruction was reported to be the gasifier followed by CO_2 compression and the SOFC. NiO as the oxygen carrier resulted in the highest net-power efficiency compared to Fe_2O_3 and CuO.

Spallina et al. [75] studied CO_2 capture through CLC from a natural-gas-fueled SOFC system. They studied two scenarios of large-scale power generation (100 MW, based on the LHV) and 145 kg/h industrial CO_2 production. The authors reported an electrical efficiency exceeding 66% for both configurations. The *specific primary energy consumption for CO_2 avoided* (SPECCA) was estimated to be as low as 0.6 $MJ_{LHV}/kgCO_2$, compared to the value of 1.11 $MJ_{LHV}/kgCO_2$ for phase change−carbon capture from the literature [76].

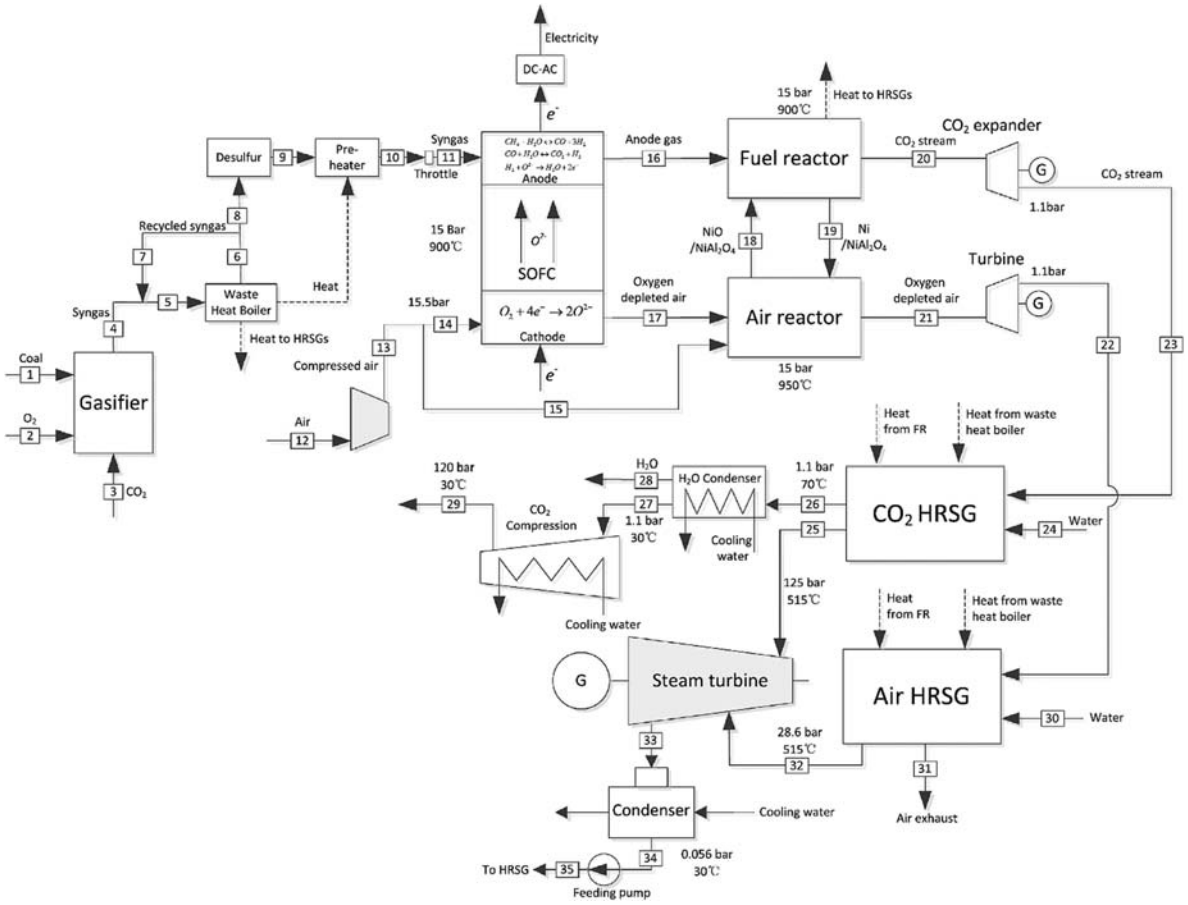

FIG. 6.10

An solid oxide fuel cell system integrated with chemical looping-carbon capture proposed by Chen et al. [74].

The SPECCA measure is defined with respect to the equivalent process with no carbon capture in order to provide a consistent measure for comparison. It is expressed in $MJ_{th}/kg\ CO_2$ and can be calculated from the relationship [75]:

$$\eta_{net} = \frac{P_{net}}{\dot{m}_{NG} \times LHV_{NG}} = \frac{P_{SOFC} - P_{SC} - P_{AUX}}{\dot{m}_{NG} \times LHV_{NG}} \tag{6.1}$$

$$E_{CO_2} = \frac{\dot{m}_{CO_2}}{P_{Net}} \times 3600 \tag{6.2}$$

$$SPECCA = \frac{Q - Q_{Ref}}{E_{Ref} - E} = \frac{\left(\frac{1}{\eta_{net}} - \frac{1}{\eta_{net\ Ref}}\right)}{E_{CO_2 Ref} - E_{CO_2}} \times 3600 \tag{6.3}$$

where Q is the ratio of the thermal energy to the heat rate (kJ_{LHV}/kWh), E is the CO_2 emission rate (kg CO_2/kWh), η is the power efficiency of the plant, and *Ref* is the reference plant without carbon capture.

Upon a wide range of sensitivity analyses on plant configuration, operating parameters, and the type of oxygen carrier the SOFC voltage was found to be the most influential variable. By increasing the voltage from 0.8 to 0.86 V the plant efficiency increased by 6%, the SPECCA decreased to 0.57 $MJ_{LHV}/kgCO_2$, and the power density increased by 80%.

6.8 Conclusion

In this chapter we provided an overview of the research in the field of SOFC process synthesis, intensification, and integration. A key feature of SOFC technologies is their high flexibility in processing various feedstocks. However, this feature also adds to their design complexity and operational difficulties. It was discussed that biomass gasification opens up a new avenue for renewable power generation, while coal gasification is the only viable pathway to achieve emission−reduction targets. On the other hand, reforming liquid and gaseous fuels offers a variety of options for process intensification and integration through internal reforming, ATR, POX, dry reforming, and others, each with significant implications for controlling fuel composition and energy management. In addition, operating SOFC stacks at different temperatures and their sequencing can enable higher electrical efficiencies. Recycling anode and cathode gases not only offers the design opportunities to adjust FU, but also provides options for energy integration. Another important consideration is the thermal management of the SOFC stack and temperature gradient within cells, which have a profound impact on the lifetime of their elements.

Moreover, the exhaust gases of the SOFC stack still have significant amounts of unexploited thermal and chemical energies. Integration with a gas turbine through a Brayton cycle enables significant energy-efficiency enhancement, but also requires optimization of the SOFC pressure and the TIT. The remaining

thermal energy of the combustion gases exiting the turbine can be further exploited in a Rankine cycle for HRSG generation. The generated steam can be exploited for controlling the SOFC steam-to-carbon ratio, be injected to the gas turbine, or be applied for the humidification of the cathode air. Each strategy has profound impacts on the operational complexity and the overall-energy efficiency of the process.

SOFC-based processes offer significant opportunities for the polygeneration of heat, power, and cooling services or even by-products, with an overall energy efficiency of up to 90%. Such flexibility and modularity have broadened the application of SOFC systems from small-scale utilities in residential buildings and remote microgrids to large-scale industrial power generation.

Last, but not least, the electrochemical nature of fuel conversion in SOFC stacks and downstream CLC or oxyfuel combustion, which avoids mixing with the nitrogen in the air, along with very high energy efficiency implies that SOFC-based-power generation may be one of the most promising technologies for the decarbonization of the power industry.

After critically considering the characteristics of the research in the field, the following research areas are recommended for future research:

1. SOFC technologies are highly flexible to process a variety of feedstocks. However, as shown by several examples in this chapter, the process design for one type of fuel may not work with another. Therefore designing processes which can handle multiple fuels is a frontier in research.
2. There are many alternative and combinatorial decisions which need to be made. Some of these decisions are structural and strategic such as the process configuration and control strategies. Some others are parametric and continuous including the size of process equipment and operating conditions (flow rates, compositions, temperatures, and pressures). As shown by many examples in this chapter, these decisions are highly interactive and influence each other differently under various configurations and operating conditions. In addition, there are often conflicts and competition between various design objectives such as economy, environmental protection, operational safety, and flexibility. A systematic framework is needed to enable optimal decision-making and establishing the trade-off between competing objectives. However, the current state-of-art for optimization programming and systematic process synthesis is far from the requirements of the scale and combinatorial design characteristics of SOFC systems. Therefore complexity reduction and developing advanced optimization algorithms remain a research frontier.
3. The design of the SOFC-based processes profoundly influences their operation. Therefore many commentators have advised that process design and control should be considered simultaneously, which is known as integrated process design and control (IPDC) [77]. As discussed by Sharifzadeh et al. [55] the IPDC paradigm is even more important for

SOFC-based processes as the high degree of process integration and intensification inherently limit the process controllability. However, little research has been performed on the interactions between the design and control of SOFC processes [55] and is critical for future studies.

References

[1] M. Li, A.D. Rao, J. Brouwer, G.S. Samuelsen, Design of highly efficient coal-based integrated gasification fuel cell power plants, J. Power Sources 195 (17) (2010) 5707–5718.

[2] J. Nease, T.A. Adams, Coal-fuelled systems for peaking power with 100% CO_2 capture through integration of solid oxide fuel cells with compressed air energy storage, J. Power Sources 251 (2014) 92–107.

[3] A. Thallam Thattai, V. Oldenbroek, L. Schoenmakers, T. Woudstra, P.V. Aravind, Towards retrofitting integrated gasification combined cycle (IGCC) power plants with solid oxide fuel cells (SOFC) and CO_2 capture – a thermodynamic case study, Appl. Therm. Eng. 114 (2017) 170–185.

[4] K.D. Panopoulos, L.E. Fryda, J. Karl, S. Poulou, E. Kakaras, High temperature solid oxide fuel cell integrated with novel allothermal biomass gasification: Part I: Modelling and feasibility study, J. Power Sources 159 (1) (2006) 570–585.

[5] K.D. Panopoulos, L. Fryda, J. Karl, S. Poulou, E. Kakaras, High temperature solid oxide fuel cell integrated with novel allothermal biomass gasification: Part II: Exergy analysis, J. Power Sources 159 (1) (2006) 586–594.

[6] M.C. Romano, V. Spallina, S. Campanari, Integrating IT-SOFC and gasification combined cycle with methanation reactor and hydrogen firing for near zero-emission power generation from coal, Energy Procedia 4 (2011) 1168–1175.

[7] T.G. Ghang, S.M. Lee, K.Y. Ahn, Y. Kim, An experimental study on the reaction characteristics of a coupled reactor with a catalytic combustor and a steam reformer for SOFC systems, Int. J. Hydrogen Energy 37 (4) (2012) 3234–3241.

[8] M. Powell, K. Meinhardt, V. Sprenkle, L. Chick, G. McVay, Demonstration of a highly efficient solid oxide fuel cell power system using adiabatic steam reforming and anode gas recirculation, J. Power Sources 205 (2012) 377–384.

[9] J.-M. Klein, M. Hénault, C. Roux, Y. Bultel, S. Georges, Direct methane solid oxide fuel cell working by gradual internal steam reforming: analysis of operation, J. Power Sources 193 (1) (2009) 331–337.

[10] J.-M. Klein, Y. Bultel, S. Georges, M. Pons, Modeling of a SOFC fuelled by methane: from direct internal reforming to gradual internal reforming, Chem. Eng. Sci. 62 (6) (2007) 1636–1649.

[11] D. Mogensen, J.-D. Grunwaldt, P.V. Hendriksen, K. Dam-Johansen, J.U. Nielsen, Internal steam reforming in solid oxide fuel cells: status and opportunities of kinetic studies and their impact on modelling, J. Power Sources 196 (1) (2011) 25–38.

[12] A. Lanzini, P. Leone, Experimental investigation of direct internal reforming of biogas in solid oxide fuel cells, Int. J. Hydrogen Energy 35 (6) (2010) 2463–2476.

[13] T.-I. Tsai, L. Troskialina, A. Majewski, R. Steinberger-Wilckens, Methane internal reforming in solid oxide fuel cells with anode off-gas recirculation, Int. J. Hydrogen Energy 41 (1) (2016) 553–561.

[14] D. Cocco, V. Tola, Externally reformed solid oxide fuel cell−micro-gas turbine (SOFC−MGT) hybrid systems fueled by methanol and di-methyl-ether (DME), Energy 34 (12) (2009) 2124−2130.
[15] P. Dokamaingam, S. Assabumrungrat, A. Soottitantawat, I. Sramala, N. Laosiripojana, Modeling of SOFC with indirect internal reforming operation: comparison of conventional packed-bed and catalytic coated-wall internal reformer, Int. J. Hydrogen Energy 34 (1) (2009) 410−421.
[16] M. Fardadi, D.F. McLarty, J. Brouwer, F. Jabbari, Enhanced performance of counter flow SOFC with partial internal reformation, Int. J. Hydrogen Energy 39 (34) (2014) 19753−19766.
[17] N. Laosiripojana, S. Assabumrungrat, Catalytic steam reforming of methane, methanol, and ethanol over Ni/YSZ: the possible use of these fuels in internal reforming SOFC, J. Power Sources 163 (2) (2007) 943−951.
[18] V.M. Janardhanan, V. Heuveline, O. Deutschmann, Performance analysis of a SOFC under direct internal reforming conditions, J. Power Sources 172 (1) (2007) 296−307.
[19] S. Wahl, et al., Modeling of a thermally integrated 10 kWe planar solid oxide fuel cell system with anode offgas recycling and internal reforming by discretization in flow direction, J. Power Sources 279 (2015) 656−666.
[20] K.P. Recknagle, E.M. Ryan, B.J. Koeppel, L.A. Mahoney, M.A. Khaleel, Modeling of electrochemistry and steam−methane reforming performance for simulating pressurized solid oxide fuel cell stacks, J. Power Sources 195 (19) (2010) 6637−6644.
[21] S. Georges, G. Parrour, M. Henault, J. Fouletier, Gradual internal reforming of methane: a demonstration, Solid State Ionics 177 (19−25) (2006) 2109−2112 (Special issue).
[22] K. Nikooyeh, A.A. Jeje, J.M. Hill, 3D modeling of anode-supported planar SOFC with internal reforming of methane, J. Power Sources 171 (2) (2007) 601−609.
[23] L. Barelli, G. Bidini, G. Cinti, F. Gallorini, M. Pöniz, SOFC stack coupled with dry reforming, Appl. Energy 192 (2017) 498−507.
[24] T. Kushi, Performance and durability evaluation of dry reforming in solid oxide fuel cells, Int. J. Hydrogen Energy 41 (39) (2016) 17567−17576.
[25] A. Lanzini, P. Leone, C. Guerra, F. Smeacetto, N.P. Brandon, M. Santarelli, Durability of anode supported solid oxides fuel cells (SOFC) under direct dry-reforming of methane, Chem. Eng. J 220 (2013) 254−263.
[26] C. Guerra, A. Lanzini, P. Leone, M. Santarelli, D. Beretta, Experimental study of dry reforming of biogas in a tubular anode-supported solid oxide fuel cell, Int. J. Hydrogen Energy 38 (25) (2013) 10559−10566.
[27] M. Ni, Modeling and parametric simulations of solid oxide fuel cells with methane carbon dioxide reforming, Energy Convers. Manag. 70 (2013) 116−129.
[28] V. Chiodo, et al., Biogas reforming process investigation for SOFC application, Energy Convers. Manag. 98 (2015) 252−258.
[29] P. Dokmaingam, J.T.S. Irvine, S. Assabumrungrat, S. Charojrochkul, N. Laosiripojana, Modeling of IT-SOFC with indirect internal reforming operation fueled by methane: effect of oxygen adding as autothermal reforming, Int. J. Hydrogen Energy 35 (24) (2010) 13271−13279.
[30] V. Liso, A.C. Olesen, M.P. Nielsen, S.K. Kær, Performance comparison between partial oxidation and methane steam reforming processes for solid oxide fuel cell

(SOFC) micro combined heat and power (CHP) system, Energy 36 (7) (2011) 4216–4226.
[31] M. Horiuchi, et al., Performance of a solid oxide fuel cell couple operated via in situ catalytic partial oxidation of *n*-butane, J. Power Sources 189 (2) (2009) 950–957.
[32] D. Lee, et al., Direct methane solid oxide fuel cells based on catalytic partial oxidation enabling complete coking tolerance of Ni-based anodes, J. Power Sources 345 (2017) 30–40.
[33] C. Song, W. Pan, Tri-reforming of methane: a novel concept for catalytic production of industrially useful synthesis gas with desired H_2/CO ratios, Catal. Today 98 (4) (2004) 463–484.
[34] F. Manenti, et al., Biogas-fed solid oxide fuel cell (SOFC) coupled to tri-reforming process: modelling and simulation, Int. J. Hydrogen Energy 40 (42) (2015) 14640–14650.
[35] H. Zeng, Y. Wang, Y. Shi, N. Cai, D. Yuan, Highly thermal integrated heat pipe-solid oxide fuel cell, Appl. Energy 216 (2018) 613–619.
[36] M. Dillig, T. Plankenbühler, J. Karl, Thermal effects of planar high temperature heat pipes in solid oxide cell stacks operated with internal methane reforming, J. Power Sources 373 (2018) 139–149.
[37] K. Lee, J. Yun, K. Ahn, S. Lee, S. Kang, S. Yu, Operational characteristics of a planar steam reformer thermally coupled with a catalytic burner, Int. J. Hydrogen Energy 38 (11) (2013) 4767–4775.
[38] R. Peters, R. Deja, L. Blum, J. Pennanen, J. Kiviaho, T. Hakala, Analysis of solid oxide fuel cell system concepts with anode recycling, Int. J. Hydrogen Energy 38 (16) (2013) 6809–6820.
[39] D. Saebea, Y. Patcharavorachot, A. Arpornwichanop, Analysis of an ethanol-fuelled solid oxide fuel cell system using partial anode exhaust gas recirculation, J. Power Sources 208 (2012) 120–130.
[40] J. Jia, Q. Li, M. Luo, L. Wei, A. Abudula, Effects of gas recycle on performance of solid oxide fuel cell power systems, Energy 36 (2) (2011) 1068–1075.
[41] O. Genc, S. Toros, B. Timurkutluk, Determination of optimum ejector operating pressures for anodic recirculation in SOFC systems, Int. J. Hydrogen Energy 42 (31) (2017) 20249–20259.
[42] M. Liu, A. Lanzini, W. Halliop, V.R.M. Cobas, A.H.M. Verkooijen, P.V. Aravind, Anode recirculation behavior of a solid oxide fuel cell system: a safety analysis and a performance optimization, Int. J. Hydrogen Energy 38 (6) (2013) 2868–2883.
[43] L. Vincenzo, N. Mads Pagh, K. S.øren Knudsen, Ejector design and performance evaluation for recirculation of anode gas in a micro combined heat and power systems based on solid oxide fuel cell, Appl. Therm. Eng. 54 (1) (2013) 26–34.
[44] M. Engelbracht, R. Peters, L. Blum, D. Stolten, Comparison of a fuel-driven and steam-driven ejector in solid oxide fuel cell systems with anode off-gas recirculation: part-load behavior, J. Power Sources 277 (2015) 251–260.
[45] M.L. Ferrari, A. Traverso, L. Magistri, A.F. Massardo, Influence of the anodic recirculation transient behaviour on the SOFC hybrid system performance, J. Power Sources 149 (2005) 22–32.
[46] D. Saebea, S. Authayanun, Y. Patcharavorachot, A. Arpornwichanop, Effect of anode–cathode exhaust gas recirculation on energy recuperation in a solid oxide fuel cell–gas turbine hybrid power system, Energy 94 (Jan. 2016) 218–232.

[47] M. Rokni, Addressing fuel recycling in solid oxide fuel cell systems fed by alternative fuels, Energy 137 (Oct. 2017) 1013–1025.
[48] A. Buonomano, F. Calise, M.D. d'Accadia, A. Palombo, M. Vicidomini, Hybrid solid oxide fuel cells–gas turbine systems for combined heat and power: a review, Appl. Energy 156 (Oct. 2015) 32–85.
[49] T. Araki, T. Ohba, S. Takezawa, K. Onda, Y. Sakaki, Cycle analysis of planar SOFC power generation with serial connection of low and high temperature SOFCs, J. Power Sources 158 (1) (2006) 52–59.
[50] A. Musa, M. De Paepe, Performance of combined internally reformed intermediate/high temperature SOFC cycle compared to internally reformed two-staged intermediate temperature SOFC cycle, Int. J. Hydrogen Energy 33 (17) (2008) 4665–4672.
[51] Y. Zhao, J. Sadhukhan, A. Lanzini, N. Brandon, N. Shah, Optimal integration strategies for a syngas fuelled SOFC and gas turbine hybrid, J. Power Sources 196 (22) (November 2011) 9516–9527.
[52] M. Mehrpooya, S. Akbarpour, A. Vatani, M.A. Rosen, Modeling and optimum design of hybrid solid oxide fuel cell–gas turbine power plants, Int. J. Hydrogen Energy 39 (36) (Dec. 2014) 21196–21214.
[53] J.H. Yi, J.H. Choi, T.S. Kim, Comparative evaluation of viable options for combining a gas turbine and a solid oxide fuel cell for high performance, Appl. Therm. Eng. 100 (2016) 840–848.
[54] P. Sarmah, T.K. Gogoi, Performance comparison of SOFC integrated combined power systems with three different bottoming steam turbine cycles, Energy Convers. Manag. 132 (2017) 91–101.
[55] M. Sharifzadeh, M. Meghdari, D. Rashtchian, Multi-objective design and operation of solid oxide fuel cell (SOFC) triple combined-cycle power generation systems: integrating energy efficiency and operational safety, Appl. Energy 185 (2017) 345–361.
[56] M. Ebrahimi, I. Moradpoor, Combined solid oxide fuel cell, micro-gas turbine and organic Rankine cycle for power generation (SOFC–MGT–ORC), Energy Convers. Manag. 116 (2016) 120–133.
[57] R. Singh, O. Singh, Comparative study of combined solid oxide fuel cell-gas turbine–Organic Rankine cycle for different working fluid in bottoming cycle, Energy Convers. Manag. 171 (2018) 659–670.
[58] L. Pierobon, M. Rokni, U. Larsen, F. Haglind, Thermodynamic analysis of an integrated gasification solid oxide fuel cell plant combined with an organic Rankine cycle, Renew. Energy 60 (2013) 226–234.
[59] E. Gholamian, V. Zare, A comparative thermodynamic investigation with environmental analysis of SOFC waste heat to power conversion employing Kalina and Organic Rankine Cycles, Energy Convers. Manag. 117 (2016) 150–161.
[60] P. Kuchonthara, S. Bhattacharya, A. Tsutsumi, Combinations of solid oxide fuel cell and several enhanced gas turbine cycles, J. Power Sources 124 (1) (2003) 65–75.
[61] T. Srinivas, A.V.S.S.K.S. Gupta, B.V. Reddy, Parametric simulation of steam injected gas turbine combined cycle, Proc. Inst. Mech. Eng. A: J. Power Energy 221 (7) (2007) 873–883.
[62] A.F. Massardo, F. Lubelli, Internal reforming solid oxide fuel cell-gas turbine combined cycles (IRSOFC-GT): Part A: Cell model and cycle thermodynamic analysis, J. Eng. Gas Turbines Power 122 (1) (2000) 27.

[63] M. Worall, T. Elmer, S. Riffat, S. Wu, S. Du, An experimental investigation of a micro-tubular SOFC membrane-separated liquid desiccant dehumidification and cooling tri-generation system, Appl. Therm. Eng. 120 (2017) 64–73.
[64] V. Liso, Y. Zhao, N. Brandon, M.P. Nielsen, S.K. Kær, Analysis of the impact of heat-to-power ratio for a SOFC-based mCHP system for residential application under different climate regions in Europe, Int. J. Hydrogen Energy 36 (21) (2011) 13715–13726.
[65] J. Kupecki, Off-design analysis of a micro-CHP unit with solid oxide fuel cells fed by DME, Int. J. Hydrogen Energy 40 (35) (2015) 12009–12022.
[66] R. Jing, et al., Economic and environmental multi-optimal design and dispatch of solid oxide fuel cell based CCHP system, Energy Convers. Manag 154 (2017) 365–379.
[67] L. Khani, S.M.S. Mahmoudi, A. Chitsaz, M.A. Rosen, Energy and exergoeconomic evaluation of a new power/cooling cogeneration system based on a solid oxide fuel cell, Energy 94 (2016) 64–77.
[68] A. Chitsaz, J. Hosseinpour, M. Assadi, Effect of recycling on the thermodynamic and thermoeconomic performances of SOFC based on trigeneration systems: a comparative study, Energy 124 (2017) 613–624.
[69] J. Hosseinpour, A. Chitsaz, B. Eisavi, M. Yari, Investigation on performance of an integrated SOFC–Goswami system using wood gasification, Energy 148 (Apr. 2018) 614–628.
[70] T.M. Gür, Comprehensive review of methane conversion in solid oxide fuel cells: prospects for efficient electricity generation from natural gas, Prog. Energy Combust. Sci. 54 (2016) 1–64.
[71] C. Mahisanana, S. Authayanun, Y. Patcharavorachot, A. Arpornwichanop, Design of SOFC based oxyfuel combustion systems with anode recycling and steam recycling options, Energy Convers. Manag. 151 (2017) 723–736.
[72] F. Petrakopoulou, Y.D. Lee, G. Tsatsaronis, Simulation and exergetic evaluation of CO_2 capture in a solid-oxide fuel-cell combined-cycle power plant, Appl. Energy 114 (2014) 417–425.
[73] J. Nease, T.A. Adams, Systems for peaking power with 100% CO_2 capture by integration of solid oxide fuel cells with compressed air energy storage, J. Power Sources 228 (2013) 281–293.
[74] S. Chen, N. Lior, W. Xiang, Coal gasification integration with solid oxide fuel cell and chemical looping combustion for high-efficiency power generation with inherent CO_2 capture, Appl. Energy 146 (2015) 298–312.
[75] V. Spallina, P. Nocerino, M.C. Romano, M. van Sint Annaland, S. Campanari, F. Gallucci, Integration of solid oxide fuel cell (SOFC) and chemical looping combustion (CLC) for ultra-high efficiency power generation and CO_2 production, Int. J. Greenh. Gas Control 71 (2018) 9–19.
[76] S. Campanari, L. Mastropasqua, M. Gazzani, P. Chiesa, M.C. Romano, Predicting the ultimate potential of natural gas SOFC power cycles with CO_2 capture – Part A: Methodology and reference cases, J. Power Sources 324 (2016) 598–614.
[77] M. Sharifzadeh, Integration of process design and control: a review, Chem. Eng. Res. Des. 91 (12) (2013) 2515–2549.

This page intentionally left blank

CHAPTER

Toward a systematic control design for solid oxide fuel cells

7

Maryam Ghadrdan

Principal Engineer Innovation, Research & Technology, Equinor ASA, Fornebu, Norway

7.1 Introduction

A solid oxide fuel cell (SOFC) is an electrochemical conversion device that produces electricity directly from fuel (hydrogen, alcohol, or other hydrocarbons) and oxidants (oxygen or air). Like most other types of fuel cells, the main attractive features of solid oxide fuel cells are high-energy efficiency and mechanical simplicity. In addition, SOFCs exhibit the following properties:

- Solid-state electrolyte can be employed.
- Water management is eliminated.
- High-fuel flexibility.
- The electrochemical reactions proceed more quickly at high temperatures and noble-metal catalysts are often not needed.
- The temperature is high enough to facilitate the extraction of hydrogen.
- High-temperature fuel cells enable combined heat and power (CHP) systems.
- High-temperature exhaust gas can be used to run a gas turbine-bottoming cycle.

The focus of this chapter is on the optimal operation of SOFCs. There are many parameters affecting the theoretical efficiency. The goal is to identify and measure or estimate these variables and control them toward the desired performance of the system. This chapter starts with a brief description on the basic operating principle of SOFCs and a discussion on the necessity of applying control. The important aspects of process design and modeling and their effect on control are discussed in Sections 7.4 and 7.5. The core of this chapter is presented in Section 7.7 where a systematic control−structure design methodology is described, which can be used both for stabilizing control and supervisory (economic) control.

7.2 Operation principle of solid oxide fuel cells

Fig. 7.1 shows the operation principle of an SOFC. The fuel is fed to the anode side where the high temperature allows it to be separated into its

Design and Operation of Solid Oxide Fuel Cells. DOI: https://doi.org/10.1016/B978-0-12-815253-9.00007-0

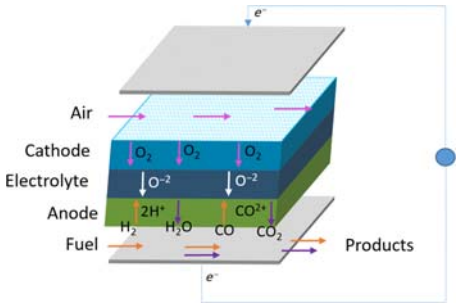

FIGURE 7.1

Operating principle of a solid oxide fuel cell [1].

constituents, hydrogen (H_2) and carbon monoxide (CO). Hydrogen reacts electrochemically to generate two electrons per molecule of hydrogen. A current is made to flow across the electrical load and reacts with oxygen at the cathode side. Every two electrons generate an oxygen ion (O^{2-}), which migrates across the electrolyte to the anode, where it reacts with the hydrogen to release again the two electrons that generate the O^{2-} ion, effectively closing the circuit. The outlet of the SOFC is a clean and a relatively pure mixture of water and carbon dioxide.

The SOFC system can provide electricity for outside devices continuously via the electrochemical reactions, namely:

$$\begin{aligned} \text{Anode reaction}: \ & 2H_2 + O^{2-} \rightarrow 2H_2O + 4e^- \\ \text{Cathode reaction}: \ & O_2 + 4e^- \rightarrow 2O^{2-} \end{aligned} \tag{7.1}$$

To turn a stack of cells to a fully functional power generating system, several auxiliary components (the balance-of-plant; BOP) must be integrated, taking care of fuel pretreatment, power management, and heat exchange. To preserve the high efficiency of the electrochemical conversion in the SOFC, the BOP often needs to be designed to optimize the integration and minimize losses. This is an important part of turning the SOFC to a real and viable end-product. When it comes to optimal operation and control, one needs to define the system and the parameters affecting the system carefully.

One of the main challenges of SOFC commercialization is their relatively short lifetime and high manufacturing costs. The cause for short life is mainly due to large temperature gradients, hot spots, interruption of supplies, impurities in fuels, catalyst poisoning, high demanding-seal material properties, and so forth. High-temperature operation also requires a higher cost of materials and manufacturing [2]. Part of these issues can be handled by advanced material technology. Some other issues should be address by process and control engineers. Optimal operation of fuel cells will result in higher efficiencies and lifetime extension.

7.3 Why should we have control of solid oxide fuel cells?

Processes are monitored and influenced with the aid of control. Fig. 7.2 shows a block diagram with feedback and feed-forward loops to control the dynamic behavior of a system. Open-loop (feed-forward) control systems utilize an actuating device to control the process directly without using feedback. Control inputs are optimized offline and are implemented with no correction. Closed-loop feedback control systems use a measurement of the output and feedback this signal to compare it with the desired output. Closed-loop control systems are more accurate even in the presence of nonlinearities, disturbances, and noise.

7.3.1 Reference following and disturbance rejection

Attenuating the effect of the disturbance on the output requires that the transfer function from disturbance to the output becomes close to zero (see Fig. 7.2). In cases when the disturbance channel has a lower gain at a given frequency, ω, than the actuator channel ($|G_d(j\omega)| < |G(j\omega)|$), satisfying this constraint would be straightforward. However, when the reverse is true ($|G_d(j\omega)| > |G(j\omega)|$), the feedback control-block must have a high gain at the given frequency. Such a high gain has several implications, including imposing large variations in the actuator command during process operation and high sensitivity to variations in the dynamic behavior of the actuated channel at high frequencies [3]. In SOFCs the process variables such as fuel flow rate, voltage, air-flow rate and fuel composition have limitations in amplitude and frequency. Dominant time constants are different, ranging from milliseconds for voltage to seconds for fuel flow. The air-flow rate has an even smaller bandwidth since the air flow primarily affects the current through a change in operating temperature. These observations indicate that disturbance−rejection control may require using multiple control layers depending on the bandwidth and amplitude of the disturbance [4]. The right choice of control structure can enhance the robustness of disturbance attenuation.

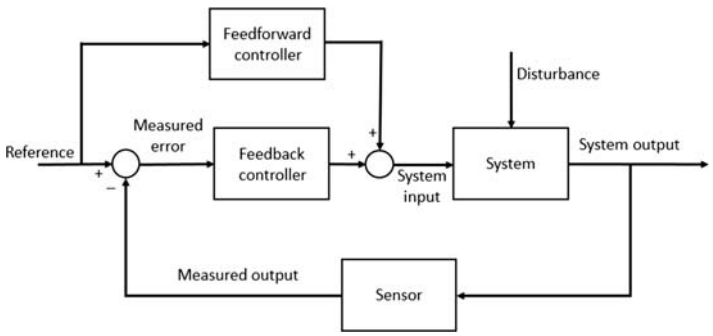

FIGURE 7.2

Control-system block diagram with feedback and feed-forward loops.

Reference following is also subject to bandwidth restrictions. Good reference following cannot be achieved unless an actuated channel is available with good actuation authority at the reference frequency. The disturbance and set-point responses cannot be designed independently due to inaccurate models and unknown disturbances. The controllers must be designed simultaneously to achieve the proper trade-off between performance and robustness.

7.3.2 Steady-state multiplicity

Multiple steady states are conditions with important consequences for the operation and control of chemical processes. From the control perspective, multiplicities (i.e., multiple steady-states) are classified into output and input multiplicities. The former refers to multiple output values for a given input, while the latter refers to the same output for multiple input values. In the case of output multiplicity, a feedback control loop ensures that the process stays at the desired steady state and does not drift to a different steady state. Input multiplicity, on the other hand, results in the possibility of "wrong" control action or steady-state transitions even with feedback control [5]. Therefore, input multiplicity can severely compromise the robustness of a control system.

Fig. 7.3 shows an example for an input–output relation that exhibits input multiplicity from a paper by Pavan Kumar and Kaistha [5]. The base-case operating condition is marked by *o* and the points where the output crosses its base-case value causing input multiplicity are marked points 1 and 2. If the input is used to control the output, the input multiplicity causes ambiguity in the control action to be taken. Close to the base-case operating condition, the controller must be direct acting. For an initial steady-state at point *a* the controller sees a positive error and so reduces the input to bring the system back to the base-case operating condition. On the other hand, for an initial steady-state at point *b* the controller sees a negative error signal and, therefore, increases the input instead of decreasing it. This leads to a wrong control action. If the input–output relation turns back again, the system would settle at the new steady state corresponding to point 3. If the

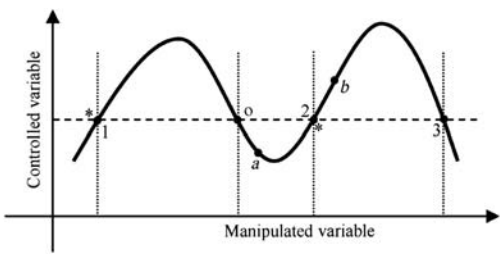

FIGURE 7.3

Typical steady-state, input–output relation with input multiplicity between manipulated and controlled variables [5].

input–output relation does not turn back the wrong control action would cause a constraint. The cause of the wrong control action is sign reversal in the error signal into the controller. This is different from process gain sign reversal corresponding to peaks and valleys in the input–output relation. Controller error sign reversal occurs at the point of crossover in the input–output relation and is marked as * in Fig. 7.3. Input multiplicity due to crossover in the input–output relation thus leads to the possibility of wrong control action and steady-state transition [5].

The existence of the multiplicity in SOFCs can make control of the fuel cells more challenging. To predict these conditions and to develop strategies for preventing unsteady states, a process model which can show the phenomena needs to be developed. Bavarian and Soroush [6] studied steady-state multiplicity in an SOFC in three modes of operation, namely constant ohmic external load, potentio-static, and galvanostatic using a first-principles-based lumped model. The effects of operating conditions such as convection heat-transfer coefficient, inlet fuel and air temperatures and velocities on the steady-state multiplicity regions were investigated. Depending on the operating conditions the cell exhibits one or three steady states. Two scenarios where the system exhibits three steady states are [7]:

- at low external load resistance values in constant ohmic external load operation,
- at low cell voltage in potentio-static operation.

Figs. 7.4 and 7.5 show output steady-state multiplicity in two different input–output relation plots for SOFCs. Output multiplicity can be tackled by closed-loop feedback control.

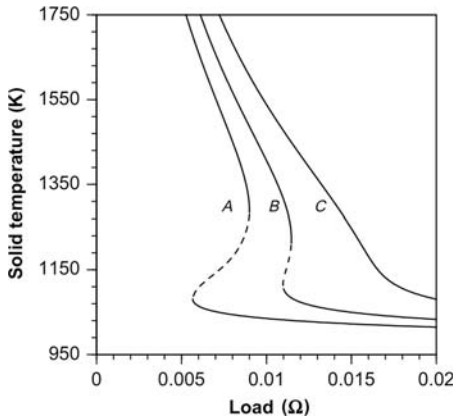

FIGURE 7.4

Output multiplicity: Solid temperature versus load resistance for different fuel and air velocities [7].

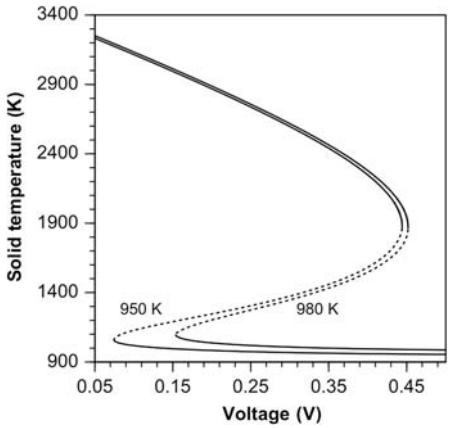

FIGURE 7.5

Output multiplicity: solid temperature versus cell voltage [7].

7.4 Effect of solid oxide fuel cell design on control

The design of SOFCs has a huge impact on how the cell is operated [8]. The ability to achieve acceptable control performance is affected by process design. Simply stated by Skogestad and Postlethwaite [9] "even the best control system cannot make a Ferrari out of a Volkswagen." The process of control-system design should in some cases also include a step zero, involving the design of the process equipment itself (see, e.g., [10–12]). Selection of cell geometry and material type (particle size and porosity distribution), sizing, bypass and recirculation loops, and integration in a Combined Heat and Power (CHP) installation are among the design concepts that affect the performance of the system.

Several extra units are added to the fuel-cell system Brown et al. [13] have studied different fuels such as methanol, gasoline or natural gas, as feed to the fuel-cell system, and the fuel pre-treatment needed for each of the cases. These units might add to the number of control degrees of freedom. The fuel pretreatment system control is a subproblem with a different objective. Temperature control in the pretreatment system becomes important as the side reactions lead to coke formation. For example, a two-input, two-output control structure was implemented for a natural gas–fuel processor system where the partial oxidation reaction temperature and the anode hydrogen mole fraction are controlled by the air blower and fuel rates in the pretreatment system [15].

SOFCs have the potential to overcome the Carnot cycle efficiency limit, if they are integrated with a conventional power plant. Developing hybrid power generation comes from the idea to exploit the exhausted heat of SOFCs [8]. An off-gas recycling approach based on the integration of waste heat is a good

example of process improvement that helps with energy integration. Each of these subsystems have different numbers of degrees of freedom, operational constraints, and objectives that are affected by the global economic objective for the whole plant.

Damping oscillations can also be addressed by process design. One example is voltage control. Any change in the load is accompanied by an instantaneous change in the stack voltage. The oscillation in the stack voltage cannot be avoided no matter what type of control is used due to the limit on the fuel and air-flow rates and their transport process to the reaction site [2]. To avoid this sudden loss in voltage and possible damage to electrical equipment, integration of SOFC with an ultracapacitor [2] or connection to a grid [16] are proposed. This gives an added boost to the control system to keep the voltage at its reference value. By avoiding a sudden drop in the voltage the controller copes with only slow changes of the voltage and can bring the voltage back to its reference value by changing fuel flow rates within its constraints relatively easily.

7.5 Modeling solid oxide fuel cells for control

Understanding SOFC dynamics is the first step in control studies. The multiphysics nature of an SOFC, where intertwined mass, heat, momentum, and charge transport phenomena take place simultaneously due to microcatalytic electrochemical reactions, is shown in Table 7.1 [1]. These phenomena occur at different scales, covering a range from the macroscopic flow of reactants within the

Table 7.1 Summary of the physical phenomena taking place within different components of an solid oxide fuel cell and their spatial scale [1].

Phenomenon	Mechanism	Layer	Spatial Scale
Mass transport	Molecular	Channels, electrodes	Macroscale
	Ionic	Electrolyte	Microscale
Momentum transport	Any	Channels, electrodes	Macroscale
Species transport	Convection	Channels, electrodes	Macroscale
	Ordinary diffusion	Channels, electrodes	Macroscale
	Knudsen diffusion	Electrodes	Mesoscale
Heat transport	Convection	Channels, electrodes	Macroscale
	Diffusion	Overall	Macroscale
	Radiation	Cell surfaces	Mesoscale
Reaction kinetics	Redox	Triple-phase boundaries	Mesoscale
	Reforming	Anode	Mesoscale
Charge transport	Ionic	Electrolyte	Microscale
	Electronics	Electrodes, interconnect	Microscale

Note: *Redox refers to reduction–oxidation reactions.*

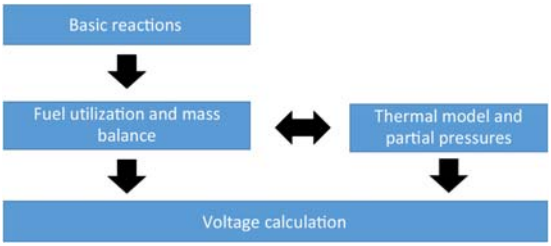

FIGURE 7.6

Solid oxide fuel modeling block diagram.

channels to the microscopic oxygen-ion dynamics through the electrolyte. One should be careful about the level of detail when it comes to modeling for control. Some of the phenomena may be ignored for simplification.

Fig. 7.6 shows the important phenomena which should be included in a simple model. More advanced dynamic models include the effects of impedance, fluid dynamics, and polarization. Bhattacharyya and Rengaswamy [17] provide a comprehensive survey of the available dynamic models of SOFCs.

Dynamic models are used to investigate responses of fuel cells under various operating conditions. The dynamic response of an SOFC is characterized by time constants ranging from milliseconds for electrical transport, tenths of seconds for mass transport, and minutes to hours for thermal transport. The model should contain multivariable interactions between manipulated and controlled variables. Real-time monitoring and control is attainable when we can have a computationally efficient model with fast-convergence time at every time step.

The open-loop dynamic response of variables provides insight into the physical phenomena associated with SOFC operation. The study by Spivey and Edgar [18] shows the open-loop behavior of all the key variables in the SOFC system. The authors have analyzed the physical phenomena behind the resulting performance plot. As an example, the effect of pressure changes of the fuel stream on power is explained here: for a step increase in fuel pressure the power quickly reaches a maximum and then decreases with a slower, first-order approach to steady-state [18]. The fast-time constant is caused by the quick response of electrochemical reactions to the changing fuel partial pressures. The slow-time constant is attributed to thermal inertia causing a longer-term drift in SOFC properties until thermal equilibrium is reached. The applied model should be able to reflect this behavior.

From the viewpoint of process control, the models should be easy to use for designing controllers and yet be detailed enough to give a sufficient account of the system dynamics [2]. Two examples are given here which show that oversimplification may have consequences.

Example 1: The ideal performance of a fuel cell is described by the fundamental laws of thermodynamics. From the First and Second Laws of thermodynamics the reversible specific work of the fuel cell (w_{rev}, per mole of reactants) is equal to the Gibbs free energy of the reaction ΔG_r [19]:

$$w_{rev} = \Delta G_r \tag{7.2}$$

The reversible power of the cell can be written as the product of the specific reversible work and the molar flow of the reactant ($\dot{n}$):

$$P_{rev} = \dot{n} w_{rev} \tag{7.3}$$

If the fuel cell is seen as an electrical device the power can be further expressed as:

$$P_{rev} = V_{rev} I \tag{7.4}$$

where V_{rev} is the reversible voltage and I is the current, which is related to the molar flow of the reactant according to the Faraday's law, as

$$I = -nF\dot{n} \tag{7.5}$$

where F is Faraday's constant and n is the number of electrons that are released during the ionization process of one fuel molecule. From the equations above, we have

$$V_{rev} = \frac{-\Delta G_r}{nF} \tag{7.6}$$

According to the Nernst equation, this equation can be rewritten in terms of the tabulated values as

$$V_{rev} = \frac{-\Delta G_r^0}{nF} - \frac{RT}{nF} \ln \frac{\prod \left(x_{pt}^{st}\right)}{\prod \left(x_{rt}^{st}\right)} \tag{7.7}$$

where x_{rt} and x_{pt} represent the molar fractions of the reactants and products at the reaction sites, respectively, and the superscript st stands for the stoichiometric coefficient. The Nernst equation relates the reduction potential of an electrochemical reaction to the standard electrode potential, temperature, and activities (often approximated by concentrations) of the chemical species undergoing reduction and oxidation.

In practice, V_{rev} represents the theoretical open-circuit voltage of the cell ($V_{rev} = V_{oc}$). However, the voltage of a real cell hardly ever meets this theoretical value, as shown in Fig. 7.7, due to the irreversibility arising in the operation. The cell voltage of a real (irreversible) fuel cell is thus estimated as

$$V = V_{oc} - \left(\eta_{act} + \eta_{con}\right)_a - \left(\eta_{act} + \eta_{con}\right)_c - \eta_{ohm} - \eta_{cross} \tag{7.8}$$

where the voltage drop ($V_{oc} - V$) should be attributed to the following major irreversibility [20]:

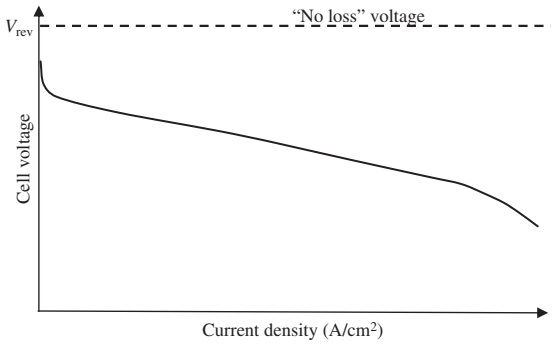

FIGURE 7.7

Typical fuel-cell performance characteristic curve [1].

- Activation overpotential (η_{act}). This is caused by the slowness of the reactions taking place on the surface of the electrodes. A proportion of the voltage generated is lost in driving the chemical reaction that transfers the electrons to, or from, the electrode.
- Crossover overpotential (η_{cross}). Although the electrolyte should only transport ions, there may be some energy losses related to the fuel passing through the electrolyte, and, to a lesser extent, due to electron conduction through the electrolyte. This source of voltage drop is usually not very important except in the case of some low-temperature fuel cells.
- Ohmic overpotential (η_{ohm}). This voltage drop is the resistance due to the flow of electrons through the material of the electrodes and the various interconnections, as well as the resistance due to the flow of ions through the electrolyte.
- Concentration overpotential (η_{con}). This results from the change in concentration of the reactants.

Cell voltage is one of the important measurements and a potential control variable in the process. Some of the control studies were performed with the focus of voltage control (see Table 7.2 for references). It is, therefore, important to accurately define this key variable and its relationship with other variables.

Example 2: Thermal analysis of SOFC is important for reliability characterization with regards to cracking and thermal fatigue. It is very common in the control literature to consider one-dimensional thermal modeling. The difference between the maximum radial−thermal gradient versus the maximum axial thermal gradient is significant, as shown in Fig. 7.8. The maximum thermal radial gradient at nominal conditions is ca. 2250K/m, whereas the maximum axial gradient remains below 750K/m. Conditions that decrease the fuel-inlet temperature and increase the air temperature near the fuel inlet will cause the radial gradient to increase

Table 7.2 Survey of control structures for solid oxide fuel cells (SOFCs).

Control objective	System	Control structure	Model	Control methodology	References	Comments
Deliver the desired power output under maximum electrical efficiency	Planar SOFC	CV: temperature, fuel utilization and power output MV: fuel and air-flow rates and the current density Constraints are related with the temperature and the fuel utilization	ODEs	NMPC + MHE	[21]	Mole fraction and temperature of exit gas are estimated using moving horizon estimator Similar control strategy: [22–24]
Keep a constant DC voltage	Standalone SOFC	MV: fuel flow and utilization CV: voltage, the only measurable variable in this study	Support Vector Machine	NMPC	[25]	To fulfill the requirement for fuel utilization and control constraints, a dynamic constraint unit plus an antiwindup scheme are adopted. A feed-forward loop is designed to deal with the current disturbance. Terminal cost is defined for control.
Voltage control	Standalone SOFC	CV: fuel utilization and voltage MV: hydrogen inlet flow	Wiener model including basic reacting, partial pressures to calculate output voltage, with constant temperature. Model consists of a linear block followed by static output nonlinearity	NMPC	[26]	Fuel utilization is held constant.
Power control	Standalone tubular SOFC	SISO version: power is controlled by H_2 flow MIMO: power and utilization factor are controlled and voltage and H_2 flow are inputs	Input–output models are identified from the data generated by a detailed dynamic model (NAARX)	MPC	[27]	In the process of model validation, it is shown that the mass transfer resistances inside the electrodes play a key role in determining the transients of the system.
Power control	SOFC system with AOR	Feed-forward control MV: natural gas, air, and recycle rates CV: stack fuel utilization and oxygen-to-carbon ratio and air flow There is a cascade temperature control using oxygen-to-carbon ratio	Algebraic deterministic relations are used to model the system, relating fuel utilization and anode recycle	PLC	[28]	The concept of AOR was tested with success for large-scale CHP units [10]

(*Continued*)

Table 7.2 Survey of control structures for solid oxide fuel cells (SOFCs). *Continued*

Control objective	System	Control structure	Model	Control methodology	References	Comments
Power control	SOFC system with AOR	CV: power, SOFC and reformer temperatures MV: cathode air, reformer air, fuel rate	Experimental setup	PID	[29]	In combination with internal reuse of waste heat the system efficiency increases compared to the usual path of partial oxidation
Stabilization and disturbance rejection	SOFC	Specific heat capacity of the system at the outlet is controlled. This is updated as a multiplication of specific heat and mass flow. Control input is a function of lie derivatives of the output.	An ODE-based thermal model is developed. The model is discretized using the finite-volume method.	Interval-based sliding mode control	[30]	Sliding mode control is a nonlinear control method that alters the dynamics of a system by application of a discontinuous control signal that forces the system to "slide" along a cross-section of the system's normal behavior
Control the voltage and guarantee the fuel utilization within a safe range	SOFC	MV: hydrogen flow rate and current CV: terminal voltage	An improved RBF neural network identification. Genetic algorithm is used to optimize the parameters of RBF NN model	MPC	[31]	The authors have compared the control structure with constant fuel usage control and concluded that voltage control performs better. See also [32].
Voltage control	SOFC + BOP	MV: natural gas input flow CV: voltage	A Hammerstein model, in which the nonlinear static part is approximated by a RBF neural network and the linear dynamic part is modeled by an ARX model.	NMPC	[33]	The fuel utilization and temperature is kept constant here. NMPC is compared to PI control using the integral of time absolute error.
Power tracking	Tubular SOFC	MV: Inlet fuel pressure and temperature, cell voltage, inlet air mass flow and temperature, and system pressure as changed by the air compressor CV: power, minimum cell temperature, maximum	DAE model for cathode-supported tubular SOFC designed by Siemens. Gas transport in the SOFC submodel is modeled as quasi-steady-state. A two-dimensional distributed parameter model provides resolution in both axial and radial directions.	MPC	[18]	The fuel and air temperatures may be changed with recuperators and bypass control valves. Fuel pressure, air mass flow, and system pressure may be changed with variable speed compressors. Cell voltage is manipulated via the electrical regulatory controls. Temperatures, utilizations, and SCR are limited by constraints.

		radial–thermal gradient, air utilization, fuel utilization, SCR, and efficiency				
Minimizing thermal stresses	SOFC with anode and cathode exhaust recirculation	CVs: power, lumped cell temperature, combustor temperature, voltage, and gas turbine shaft speed MVs: current, turbine speed set point, anode fuel flow, combustor fuel flow	Linear state-space presentation	LQR	[34]	State estimation is done via Kalman filtering. Because the LQR's state feedback is only proportional, a small tracking error will exist. Therefore, a small integral gain feedback loop on system power is added to the control design. The linear state-space representation accounts for the effect of deviations in the ambient temperature and the fuel's methane mole fraction on the system's states and outputs
Disturbance rejection and load following	Standalone SOFC	MVs: current, H_2, and O_2 flow rates CVs: power density, cell potential, and fuel utilization	Nonlinear dynamic model from [35]	Two-layer RTO + MPC	[36]	RTO + MPC with hard output constraint converges much quicker and more reliably to new optimal conditions than RTO alone. See also [37].
Track the power demand while maintaining all output variables within their allowable bounds	Standalone SOFC	CV: combination of measurements, which include output voltage, fuel and oxygen rates, current input, and pressure difference MV: fuel and oxygen flow rates	Linear model relating control inputs and disturbances to measurements	Decentralized PID	[38]	CV selection: a combination of measurements are used as control variable using self-optimizing method objectives of the SOFC closely. In terms of tracking the power demand, the performance of proposed strategies is shown to be superior than the data-driven MPC.
Power control	SOFC + fuel processing	MVs: input fuel and oxygen flow CVs: stack output voltage, fuel utilization, ratio between H_2 and O_2 flows, and fuel-cell pressure difference	First-order transfer functions are used based on experimental data	Data-driven MPC	[39]	The proposed approach can deal with systems without complete online measurement of all output variables Current demand is considered as disturbance
Minimizing total cost (capital + operating)	Tubular SOFC + ejector + prereformer	MVs: cell voltage, air mass flow, system pressure, fuel-inlet pressure, and fuel-inlet temperature CVs: power output, minimum cell temperature, radial–thermal gradient, air utilization, fuel utilization, and SCR	The system matches the tubular Siemens Power Generation design as modeled by Campanari [40]. A first-principles model was developed. The SOFC model is discretized in two dimensions, and the ejector and prereformer are modeled as lumped components.	MPC	[41]	The SOFC design is optimized for a load-following application over a power distribution subject to lifetime constraints

(*Continued*)

Table 7.2 Survey of control structures for solid oxide fuel cells (SOFCs). *Continued*

Control objective	System	Control structure	Model	Control methodology	References	Comments
Temperature control	SOFC	MV: fuel and air flow CV: SOFC temperature	Takagi–Sugeon (T–S) fuzzy model	MPC	[42]	Current is the only disturbance here A physical model (ODE) replaces the real SOFC stack to generate the simulation data required for the modified T–S fuzzy model
Load following	Bottoming planar SOFC + GT	CVs: power, voltage, SOFC temperature, and GT speed, TIT, and FU MVs: current, anode fuel flow, GT power, supplementary combustor fuel flow	Nonlinear ODEs	PID	[43]	Anode fuel flow is controlled using a feed-forward loop. Steady-state voltage is estimated.
Balancing	SOFC + BOP	Voltage, air and fuel flow outlet from BOP are controlled in the first layer. Cell current, exhaust H_2 and air exhaust temperature are controlled using the setpoints of the lower layer.	ODEs A LPV model structure is used to achieve a reduced-order model	MPC + PID	[44]	The LPV structure includes nonlinear scheduling functions that blend the dynamics of locally linear models to represent nonlinear dynamic behavior over large operating ranges
Spatial temperature control	SOFC	MVs: cathode inlet temperature, air-flow rate CVs: 5 temperature nodes in electrolyte	The fuel-cell PEN assembly temperature is solved by 1D ODEs in the flow direction capturing heat generation from electrochemistry, conduction heat transfer through the PEN assembly and metal interconnect and convection heat transfer to the fuel and air stream, and surface steam reformation and water gas shift reactions	H-infinity	[45]	This control technique is shown to be quite effective in reducing the thermal variations, due to changes in the power demand, while a variety of other disturbances (e.g., fuel variations) should also be addressed Similar studies on H-infinity: [46–48]
Stabilizing control	SOFC-grid	CV: grid bus voltage magnitude, frequency variations MV: rotor angle, phase	ODE models for swing equation, power flow equations and D/A invertor + fuel-cell equations	PID	[16]	The objective is achieved by generating appropriate switching signals to the DC–AC inverters and modulating both active and reactive powers
Disturbance rejection	SOF + fuel processor	Constant voltage and constant fuel utilization are compared	Partial pressures are calculated and substituted in the Nernst equation	PID	[24]	Focus is on introducing a feasible operating area for a SOFC power plant by establishing the relationship between the stack terminal voltage, fuel utilization, and stack current. The analysis shows that both the terminal

						voltage and the utilization factor cannot be kept constant simultaneously when the stack current changes.
Power control	SOFC–GT	MV: fuel flow, current, recycle ratio, air blow-off CV: total power, SOFC temperature, FU, and steam/methane ratio	gProms is used for modeling. ODEs for mass and energy balance for SOFC stack and use of Nernst equation + mass and energy balance for combustion chamber + power balance across the turbine shaft.	PID	[49]	Some possible choices of controlled variables were total power, SOFC temperature, FU, AU, voltage, TIT, steam/methane ratio at prereformer inlet. Results show that even though the power and temperature are controlled in a desired manner, some other system variables of interest show undesirably large deviations.
Power control	SOFC–GT + battery and anode recirculation	CV: SOFC temperature, FU, rotation speed, and system power MV: compressor outlet, bypass valve, battery state of charge, SOFC current	Models for the compressor and turbine are based on the interpolation of characteristic nondimensional curves. The recuperator model is based on a quasi-2D approach.	PID with FF	[50]	A compressor/turbine bypass valve was introduced to control the rotation speed and the SOFC temperature was controlled by adjusting the rotation speed set value. Ejector model was validated against experimental data at both steady-state and transient conditions. This plant was able to validate all the cathodic-side models at both steady-state and transient conditions against plant data. FF is used to avoid temperature oscillation. This approach can give the expected performance if load variation is smoothened by a battery or an electrical grid.
Load following and safe operation	SOFC–GT	MV: current, rotation speed, fuel flow rate CV: power, air flow, FU (SOFC temperature)	Gas flows are treated as 1D plug flow. The shaft model includes acceleration/deceleration of the shaft through moment of inertia of the moving parts. Temperature model is 2D (axial and radial directions)	PID	[23]	Focus is on part-load performance. For variable shaft speed, AU and FU as well as SOFC inlet temperatures can remain almost constant in part-load operation with only a small penalty on system efficiency. Cell temperature in controlled by

(*Continued*)

Table 7.2 Survey of control structures for solid oxide fuel cells (SOFCs). *Continued*

Control objective	System	Control structure	Model	Control methodology	References	Comments
						adjusting the air-flow set point (cascade).
Load following	SOFC–GT with cathode recirculation	MVs: current, generator load, blower power/heater bypass, guide vane angle (IGV) or Bypass (By), pre-FC fuel or post-FC fuel CVs: net power, turbine speed, cathode inlet and exhaust temperatures, turbine exhaust temperature	The model used a quasi-two-dimensional approach for simulating major components by discretizing each component in the primary flow direction and resolving important physical and chemical processes in the cross-wise direction [51]	PID	[52]	In this paper, five different control strategies for a cathode recirculation SOFC hybrid system and compared the performance of the five control strategies, while maintaining temperatures and other operating conditions within acceptable limits
Maximizing direct energy	SOFC	MVs: flow rates and splitting ratios CV: stack voltage	A set of ODEs Model 1: a "lumped model" which assumes uniform temperature throughout the cell Model 2: a "detail model" which assumes temperature distributions	NMPC	[53]	Model 1 is valid at lower current load, where the temperatures of electrode, interconnector and unreacted gases do not differ much, at higher current load, this may not be the case. Unscented Kalman filter is used for state estimation.

AU, Air Utilization*; CV,* controlled variables*; MV,* manipulated variables*; ODEs,* ordinary differential equations*; NMPC,* nonlinear model predictive controller*; MHE,* moving horizon estimation*; MPC,* model predictive control*; SISO,* single input single output*; MIMO,* multiple input multiple output*; NAARX,* nonlinear additive autoregressive with exogenous input*; PID,* proportional integral derivative*; ARX,* autoregressive with exogenous input*; RTO,* real-time optimization*; TIT,* turbine inlet temperature*; FU,* fuel utilization*; LPV,* linear parameter varying*; PEN,* positive electrode–electrolyte–negative electrode*; FF,* feed forward*; IGV,* inlet guide vane angle*; DC,* direct current*; AC,* alternate current*; AOR,* anode off-gas recycle*; CHP,* combined heat and power*; RBF,* radial basis function*; BOP,* balance-of-plant*; SCR,* steam-to-carbon ratio*; LQR,* linear quadratic regulator.*PLC,* Programmable Logic Controller; PI, Proportional Integral*; DAE,* Differential Algebraic Equation

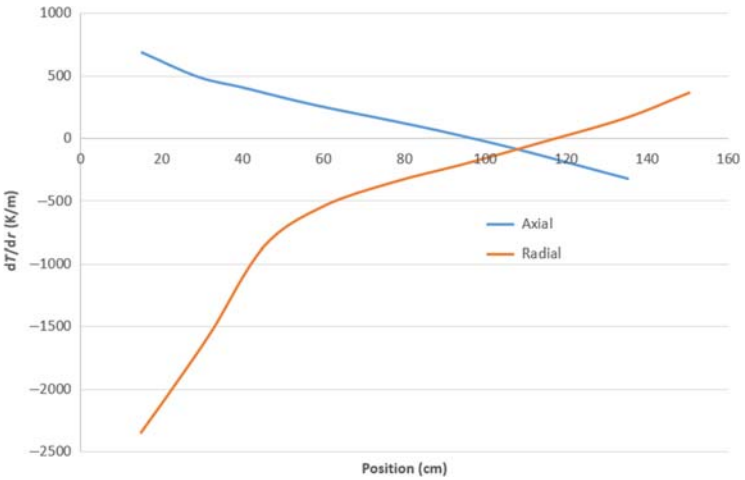

FIGURE 7.8

Axial and radial—thermal gradients along the SOFC length at nominal conditions [18].

further. This shows that 1D thermal modeling is not a good simplification when it comes to designing control for an optimal and safe operation.

Commonly, the fuel-cell thermal management system is designed based on a lumped fuel-cell temperature model for convenience, where the temperature is uniform and the anode and cathode temperatures are the same. So, there will be only one control loop to regulate the fuel-cell temperature [54].

These two examples show that accurate definition of variables and the right level of simplification is very important in the modeling step.

The choice of model structure depends on the level of understanding of the physical systems. Principle-based models have been the most used model structure in the SOFC literature (see Table 7.2). Unlike modeling from first principles, which requires an in-depth knowledge of the system, system identification methods can model different system dynamics without knowledge of the actual system physics. Generally, one can model a system using the general linear form $y(s) = G(s)u(s)$. This model can be derived by performing step tests.

Existing literature on identification of statistical models for SOFC can be divided into two categories, namely linear and nonlinear. Finite Impulse Response (FIR) [55], Auto-Regressive with eXogenous input (ARX) [56], Auto-Regressive Moving Average with eXogenous input (ARMAX) [57], Box—Jenkins (BJ) methods [58] are examples of linear data-based models for SOFCs. Artificial neural network [59] and Hammerstein model structure (a static nonlinearity followed by a dynamic linear model) [60,61] are examples of nonlinear data-based models. Bhattacharyya et al. [27] have shown that a linear model such as an ARX model is found to be satisfactory for most SISO cases. However, a nonlinear

model such as nonlinear additive auto-regressive with exogenous input (NARX) with more cross terms is found to improve the model performance significantly for the multiple-input and multiple-output (MIMO) case.

7.6 Sensing

Measurements are required to understand the physics and chemistry in the fuel-cell system, optimize system design, and apply feedback control. The life span of an SOFC stack depends on several factors. Some of them are linked to the fabrication parameters, such as materials, porosity, and other design parameters, while others depend on the operational parameters. An excessive stack temperature generally accelerates the degradation phenomena, while large temperature gradients across the stack cause thermal stresses. Too low oxygen-to-carbon (O/C) ratio cause carbon deposition, which leads to stack breakage [62]. Defects in the electrolyte thin-film cause cross-leakage of fuel and air, which deteriorates the anode-supported SOFCs [63]. These are some examples that show the importance of monitoring and control of the key variables which lead to these problems. A wide variety of sensors are developed to monitor the health and performance of SOFCs (see, e.g. [64,65]). Some examples of modern measurement devices are given next.

7.6.1 Measurements for operation and control

Temperature, pressure and flow rate measurements are the most common in the chemical industry. The conventional inlet−outlet measurements in the fuel-cell system are very useful to be integrated in control, but also fundamentally limited. Intra-fuel-cell measurements give more detailed information of the process. In this section, some examples of more recent measurements are given:

In-situ Raman spectroscopy: reduction−oxidation kinetics and local concentration variations of charge carrier across the electrode or electrolyte interface are among the key factors determining performance of SOFCs. Raman spectroscopy is a nondestructive measurement device. This method has been used in several fuel-cell systems (e.g., [66,67]). New techniques are under development to use Raman spectroscopy for the reaction zones, where charge carriers are generated, such as the triple-phase boundary area, as this area is not accessible due to low-penetration depth of the excitation radiation [68].

Distributed temperature sensors: A large gradient exists in gas concentration and temperature from the fuel-inlet to outlet as fuel is consumed across the cell. An experimental method to measure temperatures of unit cells inside SOFC stacks was developed using thin K-type thermocouples and self-developed CAS-I sealing materials in which the thin K-type thermocouple is inserted into the stack from the middle of the multilayer sealant. [69]. Another technique for measuring

the spatial distribution of temperature along an SOFC interconnect channel is to use a distributed interrogation system coupled with a single-mode fiber optic thin-film evanescent wave absorption sensor [70]. These sensors yield spatially distributed measurements with submillimeter accuracy. A review of recent advances in in-situ optical measurement devices is given by Pomfret et al. [71]

Chemical sensors: The presence of sulfur and hydrocarbons in the reformed gas can lead to degradation of nickel-based anodes [65]. Therefore measuring these impurities in the reformate gas prior to their entry in the fuel-cell stacks is needed. A chemical sensor is a device that transforms chemical information, namely the presence of a component and its concentration, into an analytically useful signal. The challenge with respect to monitoring these gaseous species is the presence of hydrogen and humidity in the reformed gases. This issue is addressed in recent research studies (e.g., [72]).

All the measurements (or combinations of them) are potential control variables. Self-optimizing control offers a systematic method (see Section 7.7.3), which is about how to choose the optimal set of measurements as control variables.

7.6.2 Soft-sensor developments for solid oxide fuel cells

Even though measuring many variables is indeed possible, implementing additional online sensors is costly and includes time delay. It also happens that some important variables are not measurable. The value of primary variables can be inferred by combining secondary variable measurements. There are several advantages of inferential sensors in comparison with traditional instrumentation, including easy implementation, no capital cost, and extraction of more information from the existing data.

Some examples of soft-sensor development for SOFCs are:

- Dynamic estimation of model parameters; for example, diffusion coefficients of the reacting species and the impedance elements, namely charge transfer capacitance and resistance, are estimated by defining an optimal input design (OID) problem in a receding-horizon framework [73]. External voltage, current, consumption rates of hydrogen and oxygen, and the production rate of water are the measured variables.
- Static estimation of process variables; for example, O/C ratio at the anode inlet is estimated based on concentration measurements at other points in the SOFC stack [62].
- Dynamic estimation of process variables; for example, unscented Kalman filter is used to estimate the states (intra-fuel-cell partial pressures and temperatures) based on measured current and input−output data [53]. This soft-sensor is used in a control problem where voltage is managed by manipulating flow rates and split ratios.
- Data-based estimation of process variables; for example, maximum stack temperature is estimated based on a multivariate linear regression of

measurement data, which are inlet gas-flow rates, temperatures, and stack current. The estimated value is controlled by manipulating a bypass valve of the air system−heat exchanger [74].

- Fault detection; for example, a fault diagnosis strategy developed by Wu and Gao [32] to classify the SOFC system faults as normal, fuel-leakage fault, air-compressor fault, or both fuel-leakage and air-compressor faults. Deviations of the estimated values for voltage and fuel utilization from the actual values confirms the faulty situation. The origin of the fault can be traced back to a few key variables. For example, since fuel utilization can be expressed as a ratio of current load and hydrogen input to the fuel cell, the fault in fuel utilization can be traced back to either a fault in the load or in the hydrogen system. The flow rate of hydrogen in the fuel cell, in turn, depends on the net-flow rate of methane in the system.

These examples suggest different types of estimations and different areas of application for the estimated values. At a very general level, these fields can be divided into three broad categories [75]:

- Process monitoring
- Process control
- Offline operation assistance

7.6.3 Theory of soft-sensors

Process data analysis is the initial step in the design of inferential sensors. The careful investigation of operational data enables us to extract relevant information contained in historical data, select influential variables, and assess data quality; that is, reliability, accuracy, completeness, and representativeness.

Principle component regression [76] and partial least squares (PLS) [77] are two of the most used data analysis tools in chemometrics. These methods are based on linear projection of the measurement space to a lower-dimensional subspace. Assume that the observations are collected in the matrices X and Y. We want to obtain a linear relationship between the data sets. $Y = XB + B0$, where B and $B0$ are optimization variables. $B0$ is normally zero if the data are centered. The least-square solution to this problem is $B = YX$.

Mathematical models are also used to design estimators. The simplest model-based static estimator is the "inferential estimator" by Brosilow and coworker [78]. A fundamental problem with the Brosilow inferential estimator is that it fails to consider the measurement noise in an explicit manner. Ghadrdan et al. [79] developed an estimation method to include the effect of measurement noise in the derivation of the optimal model-based static estimator. This means that the "high condition number problem" that has been a concern in previous works [78,80] is handled in an optimal manner. In addition, the purpose of estimation, that is-whether the estimated variable is going to be used for monitoring or control, is

taken into consideration. Ghadrdan et al. [79] derived optimal estimators for four cases:

- *Case S1*. Predicting primary variables in a system with no control, that is, the control inputs u are free variables.
- *Case S2*. Predicting primary variables in a system where the primary variables y are measured and controlled, that is, the inputs u are used to keep $y = y_s$.
- *Case S3*. Predicting primary variables in a system where the inputs u are used to control the secondary variables z, that is, $z = z_s$.
- *Case S4*. Predicting primary variables in a system where the primary variables are estimated and controlled, that is, the inputs u are used to keep $\hat{y} = y_s$.

Cases S1, S2, and S3 are practically relevant if the estimator is used for monitoring only, because the estimate $\hat{y}$ is not used for control (see Fig. 7.9). Case S4 is the relevant case when we use the estimator in closed loop (for control purposes). The optimal estimators for cases S1, S2, and S3 are least-square estimators with a similar structure to the Brosilow estimator, while the structure for case S4 is quite different and more complex. The derivation is based on results from optimal measurement combination for self-optimizing control [81]. The Y and X in Fig. 7.9 have the same nature as the input and output data for PLS method. Ghadrdan et al. [79] compared their model-based estimators with a PLS estimator. The results were similar for a large enough number of measurements, but showed better performance for the model-based estimator for a lower number of measurements. Y and X data needed for PLS are the first and second columns of Y_{all} matrix, respectively. These data are derived from the process model.

$$Y_{all} = \begin{bmatrix} Y & X \end{bmatrix} = \begin{bmatrix} G_y & 0 \\ G_x & X_{opt} \end{bmatrix} \tag{7.9}$$

Equation 7.9 shows that the quality of data is more important than the amount of data in estimators. We need to know the expected optimal variation in X as given by matrix X_{opt}. Here, optimal means that primary variable y is constant (see the second column in Y_{all}). In addition, we also need to obtain G_x and G_y from the data, which means that the data must contain nonoptimal variations in inputs u; see the first column in Y_{all} [79].

One important point in the study is to develop the estimators based on the targeted use of the estimated variables. Ghadrdan et al. [79] showed that the prediction error is the lowest when the right scenario is used; that is S1, when the estimated variable is used for monitoring and there is no control; S3, when the estimated variable is used for monitoring and there are already some stabilizing control loops in place; S4, when the estimated variables are controlled. Mathematical details on deriving the estimators and handling their dynamic behavior are skipped here as the book is intended for industrial application. The interested reader is referred to Ref. [81] for more detailed information.

The estimators explained above are in the category of static estimation. These estimators can be implemented in a dynamic setting by automating the model

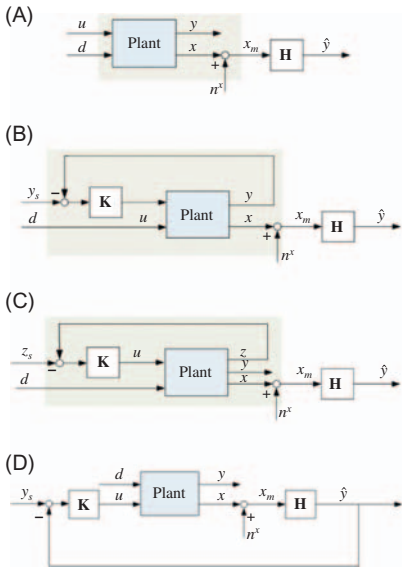

$$H_1 = Y_1 X_1^{\dagger}$$

$$Y_1 = \begin{bmatrix} G_y W_u & G_y^d W_d & 0 \end{bmatrix}$$
$$X_1 = \begin{bmatrix} G_x W_u & G_x^d W_d & W_{n^x} \end{bmatrix}$$

$$H_2 = Y_2 X_2^{\dagger}$$

$$Y_2 = \begin{bmatrix} G_y W_u & G_y^d W_d & 0 \end{bmatrix}$$
$$X_2 = \begin{bmatrix} G_x G_y^{-1} W_{y_s} & (G_x^d - G_x G_y^{-1} G_y^d) W_d & W_{n^x} \end{bmatrix}$$

$$H_3 = Y_3 X_3^{\dagger}$$

$$Y_3 = \begin{bmatrix} G_y G_z^{-1} W_{z_s} & (G_y^d - G_y G_z^{-1} G_z^d) W_d & 0 \end{bmatrix}$$
$$X_3 = \begin{bmatrix} G_x G_y^{-1} W_{z_s} & (G_x^d - G_x G_z^{-1} G_z^d) W_d & W_{n^x} \end{bmatrix}$$

$$H_{\mathrm{CL}} = \arg(\min \| H[F W_d \quad W_{n^x}] \|_F) \quad \text{s.t. } H G_x = G_y$$
$$F = \left(\frac{\partial x}{\partial d}\right)_{y=0} = G_x^d - G_x G_y^{-1} G_y^d$$

FIGURE 7.9

Block diagrams for four static estimation cases [79].
(A) S1: Monitoring case where u is a free variable; (B) S2: Monitoring case where u is used to control the primary variable y; (C) S3: Monitoring case where u is used to control the secondary variable z; and (D) S4 = CL: "closed-loop" case where u is used to control the predicted variable $\hat{y}$.

Estimator: $\hat{y} = Hx_m$, linear static models for the primary variables y, measurements x, and secondary variables z are used here:
$y = G_y u + G_y^d d$
$x = G_x u + G_x^d d$
$z = G_z u + G_z^d d$
u: inputs (degrees of freedom); these may include setpoints to lower-layer controllers
d: disturbances, including parameter changes
x: all available measured variables
n^x: measurement noise (error) for x
y: primary variables that we want to estimate
z: secondary variables, which we may control, dim(z) = dim(u)
W: expected magnitudes.

updating and calculation of sensitivities (F matrix). This method has much less computational cost compared to other dynamic methods, such as Kalman filter or moving horizon estimator, and guarantees convergence as it is based on estimation of the final steady-state values.

7.7 Control

Implementation of a control system is necessary to operate chemical plants safe, stable, and economically optimal in the presence of disturbances, which may frequently occur during operation. To achieve desired performance and long durability in an SOFC, it is needed to carefully balance the fuel and air with specific flow rates, compositions, and temperatures. Such operation requires a control system to regulate the SOFC and BOP components. Several control objectives have been used in the literature [4,21,82,83]:

- Follow the load demand; that is, provide desired electrical power.
- Regulate disturbances such as handling the abrupt change of the fuel-cell voltage during transient operations.
- Maximize efficiency; that is, maximize the ratio of produced power and chemical potential of the fuel.
- Satisfy the constraints on input and output variables; that is, assure that the SOFC and BOP are not damaged.

Examples of control systems that tackle one or more of the objectives can be found in the literature. Representative examples are presented in Table 7.2. The existing literature include studies on single-loop (SISO— single-input and single-output) and multiloop (MIMO) control, decentralized (PID—proportional integral derivative) and multivariable control, a single SOFC unit and hybrid systems. Model predictive controllers (MPCs) have been used in many control studies for SOFC, both model-based (e.g., [60]) and data-driven (e.g., [39]). Choice of decentralized versus multivariable control is the answer to "how" a system should be controlled. However, there is one important question to answer before taking this decision; it is about "what" to control. The next section presents the systematic control problem definition and control−structure design.

7.7.1 Control−structure design

Control−structure design includes the design of controllers as well as selecting the potential control and manipulated variables and decide on the way they should be connected. There is generally a time-scale separation between different control layers, which are connected through control variables; i.e., regulatory control is in the scale of seconds, while the supervisory control is in the scales of minutes [84]. At each layer the set point for controlled variables is given by the upper layer and implemented by the lower layer. The control−structure design procedure includes a top-down analysis to optimize the process for various disturbances and to identify primary self-optimizing controlled variables (economic control layer), and a bottom-up analysis to build up the control system from the bottom layer, study the dynamics, and decide on pairings. The procedure is shown in

Table 7.3 Systematic control—structure design strategy [84].

Top-down (focus on steady-state economics)	Bottom-up (focus on dynamics)

• Define operational objectives (optimal operation):
  • Scalar cost function J (to be minimized)
  • Constraints
• Objective: Find regions of active constraints
  • Identify steady-state degrees of freedom and
  • Expected disturbances
  • Optimize the operation with respect to the degrees of freedom for the expected disturbances (offline analysis)
• Select location of throughput manipulator (TPM) (Decision 3)
  • Some plants, for example, with parallel units, may have more than one TPM
  • One may consider moving the TPM depending on the constraint region
	• Select structure of regulatory control layer (including inventory control):
	  • Select "stabilizing" controlled variables CV2 (Decision 2)
	  • Select inputs (valves) and "pairings" for controlling CV2 (Decision 4)
	  – Stabilizes the process and avoids drift
	  – If possible, use same regulatory structure for all regions
	• Select structure of supervisory control
	  • Controls primary CV1s
	  • Supervises regulatory layer
	  • Performs switching between CV1s for different regions
	• Select structure of (or evaluate the need for) optimization layer (RTO)
	Update setpoints for CV1 (if necessary)

TPM, throughput manipulator*; RTO,* real-time *optimization*.

Table 7.3. Self-optimizing control is a method to choose the best control variables from measurements (or as a combination of measurements).

The top-down analysis focuses on steady-state economics, where an economical optimization problem is formulated. It starts with defining an objective function. Optimization is performed both at the nominal-operation point and for important disturbances to calculate the sensitivities. Based on the optimization results, a self-optimizing control strategy analysis is performed to select the best controlled variables in different active-constraint regions. These regions are calculated by optimizing the system for a large range of disturbances, and track the constraints. Having a new constraint in the active set (or losing one constraint from the active set) means that the system has entered another active-constraint region. Control variable selection procedure should be done separately for each active-constraint region. Selection of the throughput manipulation (TPM) point is important for inventory control. Throughput bottleneck dictates where the TPM point should be located [85].

The bottom-up analysis focuses on dynamics and control of the process. A dynamic model is necessary to validate the proposed control structure and analyze the dynamic behavior of the closed-loop system. In this part, stabilizing control variables (secondary CVs) are selected and paired with the proper manipulated variables, and then the structure of the supervisory control layer is determined.

One example of applying this systematic method for SOFC control is presented by Chatrattanawet et al. [86]:

Step 1: Define cost and constraints. With a given load (current density), the cost function to be minimized is the cost of the fuel feed minus the value of the power, subject to satisfying constraints on the cell temperature kept at a specific value.
Step 2: Identify optimal operation as a function of disturbances. At steady-state, there are two operational degrees of freedom, the inlet molar flow rate of air and fuel, MV = $[\dot{n}_{\text{air,in}}, \dot{n}_{\text{fuel,in}}]$. The current density is the main disturbance. The fuel-cell temperature constraint is assumed to be always active. There is then one remaining unconstrained degree of freedom, namely excess air.
Step 3: Identify economic control variables. CV = $\begin{bmatrix} T_{\text{FC}} & x_{\text{CH4}} \end{bmatrix}$. Fuel-cell temperature is the active constraint. As a "self-optimizing" variable for the unconstrained degree of freedom, the fraction of unconverted methane in the exhaust gas (x_{CH4}) was chosen, which was found to result in a small economic loss.
Step 4: The throughput manipulator is the current density.
Step 5: Regarding the structure of the stabilizing control layer, an important decision is to select the "stabilizing" controlled variables CV2, which include inventories and other drifting variables that need to be controlled on a short-time scale. It is necessary to control temperature tightly to avoid material stresses and to prevent cell voltage drop due to the depletion of fuel. In this study, the economic controlled variables (CV1) were considered to be acceptable as stabilizing variables (CV2 = CV1), so a separate regulatory layer is not considered in this study.
Step 6: Select structure for control of CV1 (pairing).

7.7.2 What to control?

A control system makes use of sensor measurements to command actuation of input variables. One of the first tasks in controller design is to decide which measurements to use as control variables. In some cases, the choice of control variables may not be clear a priori. To meet the requirements by the solid-state energy conversion alliance, the fuel-cell community recognizes the importance of fuel-cell dynamics regarding the operability of critical-to-quality variables, including steam-to-carbon ratio, thermal gradients, local temperatures, and fuel or air utilizations [17,18]. Table 7.2 lists the signals which have been used as CVs in SOFC control studies in the literature. Every measurement in the process (or combination of all or a subset of measurements) can be used as a control variable. Selection of optimal control variables depends on the control objective, sensitivity of the measurements to the expected disturbances and control inputs, dynamic

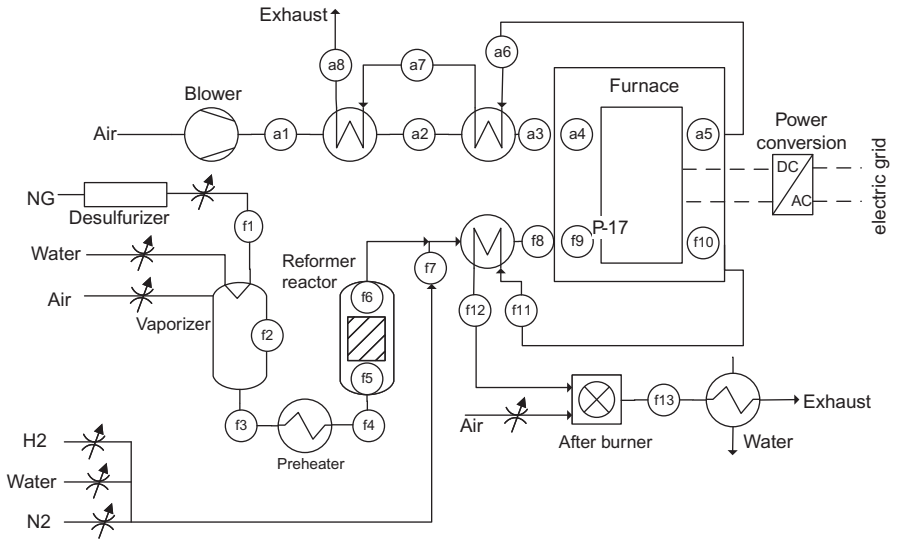

FIGURE 7.10

Input–output measurements in an solid oxide fuel process [87].

behavior of the closed-loop system, and process limitations. Fig. 7.10 provides an example flowsheet that shows the measurements to be used for control. Intra-fuel-cell measurements are not shown in this figure. Some of these variables are limited by process or safety constraints; for example:

- Minimum O/C ratio to avoid carbon deposition.
- Maximum rates due to pump limitation and pressure limitation.
- Maximum air utilization to ensure that enough oxygen is always supplied to the cathode during power generation.
- Maximum fuel utilization to avoid possible degradation and local-fuel starvation.
- Air-to-fuel ratio should be kept in a defined range to ensure that combustion can be sustained. Too low oxygen means that only a fraction of the fuel will be burnt, leading to high CO concentrations in the exhaust gas. Too much air will lead to temperature decrease in the combustion chamber, forcing the combustion to be stopped.
- Maximum cell temperature and temperature gradients to avoid degradation.
- To prevent damage to the electrolyte, the fuel-cell pressure difference between the hydrogen and oxygen passing through the anode and cathode gas compartments should have small deviations from normal operation under transient conditions.

7.7.3 Self-optimizing control

Self-optimizing control is a systematic method for finding the appropriate set of controlled variables from a set of process measurements. It is assumed that the economics of the plant are characterized by the scalar objective function $J(u, d)$, where u and d represent the inputs (or unconstrained degrees of freedom) and the disturbances, respectively. When the disturbances change from nominal values, the optimal operation policy is to update the control input accordingly. This usually requires using an online optimizer that provides the optimal value of the objective function [88]. A simpler strategy results when the control input u can be indirectly adjusted using a feedback controller. In this case, the feedback controller manipulates u to hold the CVs close to their specified setpoints. It is important to note that self-optimizing is not a property of the controller itself. Rather the term self-optimizing control has been used for describing a strategy for designing the control structure where the aim is to achieve close-to-optimal operation by (constant) set-point control [84].

Fig. 7.11 shows the feedback diagram for a linearized model. The diagonal matrices W_d and W_n contain the magnitudes of expected disturbances and implementation errors associated with the individual measurements, respectively. The matrices G_x and G_x^d are the steady-state gains from inputs and disturbances to measurements, which are obtained by linearizing the system around the operating point.

The self-optimizing control variables will be found by minimizing a loss which is defined as [9]:

$$\text{Loss} = J(u, d) - J_{opt}(d) = \frac{1}{2} z^T z \tag{7.10}$$

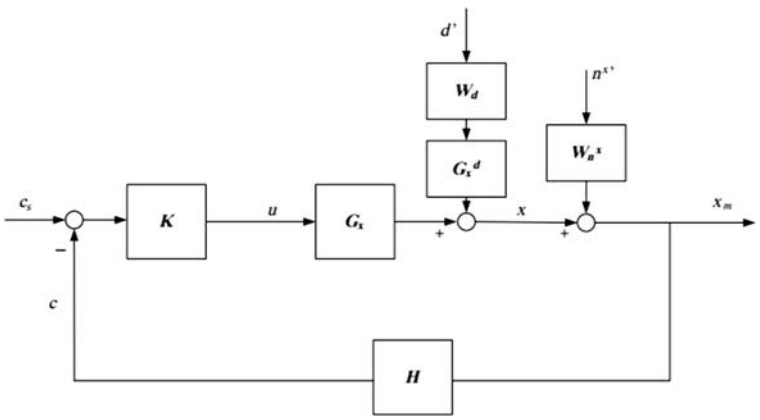

FIGURE 7.11

Feedback diagram for a linearized model [89].

where

$J_{opt}(d)$ is the optimized objective function at a given disturbance, and

$$z = J_{uu}^{1/2}(u - u_{opt}) \tag{7.11}$$

$u_{opt}(d)$ is obtained by expanding the gradient of the objective function around the nominal point

$$J_u = \underbrace{J_u^*}_{=0} + \begin{bmatrix} J_{uu}^* & J_{ud}^* \end{bmatrix} \begin{bmatrix} u \\ d \end{bmatrix} \tag{7.12}$$

To remain optimal, we must have $J_u = 0$, so

$$u_{opt} = -J_{uu}^{-1} J_{ud} d \tag{7.13}$$

A linear relation is assumed between inputs, disturbances, and outputs. So,

$$x_{opt} = G_x u_{opt} + G_x^d d = \underbrace{\left(-G_x J_{uu}^{-1} J_{ud} + G_x^d\right)}_{F} d \tag{7.14}$$

F is defined as the optimal sensitivity matrix. The main objective in self-optimizing control is to find a linear combination of measurements, $c = Hx$, such that control of these indirectly leads to close-to-optimal operation with a small loss despite unknown disturbances and measurement noise.

$$c = Hx = HG_x u + HG_x^d d \tag{7.15}$$

$$c_{opt} = Hx_{opt} = HG_x u_{opt} + HG_x^d d \tag{7.16}$$

$$u - u_{opt} = \left(\underbrace{HG_x}_{G}\right)^{-1} (c - c_{opt}) \tag{7.17}$$

We need to write $c - c_{opt}$ as a function of d and n^x.

$$H(x + n^x) = \underbrace{c_s}_{0} \tag{7.18}$$

We also have $c_{opt} = HFd$. So,

$$c - c_{opt} = H(Fd + n^x) = H\left(FW_d d' + W_{n^x} n^{x'}\right) = H[FW_{d\ Wn^x}] \begin{bmatrix} d' \\ n^{x'} \end{bmatrix} \tag{7.19}$$

The final loss term will be

$$L = \frac{1}{2} J_{uu}^{1/2} (HG_x)^{-1} H[FW_d\ W_{n^x}] \begin{bmatrix} d' \\ n^{x'} \end{bmatrix} \tag{7.20}$$

Optimization of the loss function L is done after deciding on the structure of H matrix:

- Single measurements; that is, only one nonzero element in every row of H matrix

- Combination of all measurements; that is, all the H elements are considered as nonzero
- Combination of subset of measurements; that is, some of the elements in every row of H are nonzero

Solutions of the optimization problem for different H structures are discussed in Refs. [80,90–92]. Better self-optimizing abilities can be shown with controlled variables as combination of measurements [81,92]. As an example, a combination of multiple temperature measurements along a process unit can give a better estimate of the composition in the outlet flow compared to a single-point measurement. Dynamic properties of the control loops should be studied and in some cases corrected (see [93]), before taking the final decision on the best control structure.

7.7.4 Controllability

The controllability of a process is the ability to achieve acceptable control performance; that is, to preserve the outputs within specified bounds. Controllability analysis offers a numerical indication, which provides a qualitative assessment of the control properties of the alternative designs. Relative gain array (RGA) is one of the popular controllability indices for the selection of control pairing and to describe the interactions between inputs and outputs. Generally, RGA close to the unity matrix are preferred. RGA of a nonsingular square complex matrix (G) is defined as indicated in the equation below, where $\times$ denotes element by element multiplication (the Schur product).

$$\mathrm{RGA}(G) = G \times (G^{-1})^T \tag{7.21}$$

Chatrattanawet et al. [86] have used RGA to perform the controllability analysis of DIR–SOFC. They have considered lumped parameter models with the inlet molar flow rates of air ($u1$) and fuel ($u2$). The fuel-cell temperature ($y1$) and the fraction of methane ($y2$) are selected as outputs. The steady-state RGA for the diagonal pairings ($u1-y1$, $u2-y2$) is close to 1, as desired. This pairing is also reasonable from a dynamic point of view because the molar flow rate of fuel at inlet ($u2$) has a direct effect on the fraction of methane ($y2$).

One important point is that modeling has a big effect on controllability analysis. Radisavljevic [94] has shown that the linear models of SOFCs, commonly used in the literature, are not controllable. The source of uncontrollability is the equation for the pressure of the water vapor that is only affected by the fuel-cell current, which, in fact, is a disturbance in this system and cannot be controlled by the given model inputs, that is, inlet molar flow rates of hydrogen and oxygen. Being uncontrollable, such models are not good candidates for studying control of dynamic processes in SOFCs.

7.7.5 Controllers

Various controllers including traditional PID controllers and linear and nonlinear MPCs have been applied for control of fuel cells. Model predictive control is formulated to solve a finite horizon open-loop optimal control problem in real time, subject to system dynamics and constraints. The controller predicts the dynamic behavior of the system over a prediction horizon and determines the input such that the "open-loop" performance is optimized (Fig. 7.12). In general, the system behaves quite differently from the prediction due to the disturbance and the mismatching between the dynamic model and the plant. The input value is calculated according to the open-loop input and the feedback mechanism. The control input is implemented only for one time step. When the new measurements are available, the whole procedure is repeated to find the next input with the control and prediction horizon moving forward.

More than 95% of the controller in industry are still PID control. Multivariable control is normally recommended when the control loops are highly interactive (based on controllability analysis). It should be remembered that the optimization is for open-loop case; that is, the control input is optimal for the open-loop process.

There have been several studies on performance comparison of PI controllers and model predictive controllers (see, e.g., [95,96]), which reported the efficiency of either of the controllers for the applications under study. The conclusion depend on control structure, existence of interactive control loops, and controller tuning (see, e.g., [97,98]).

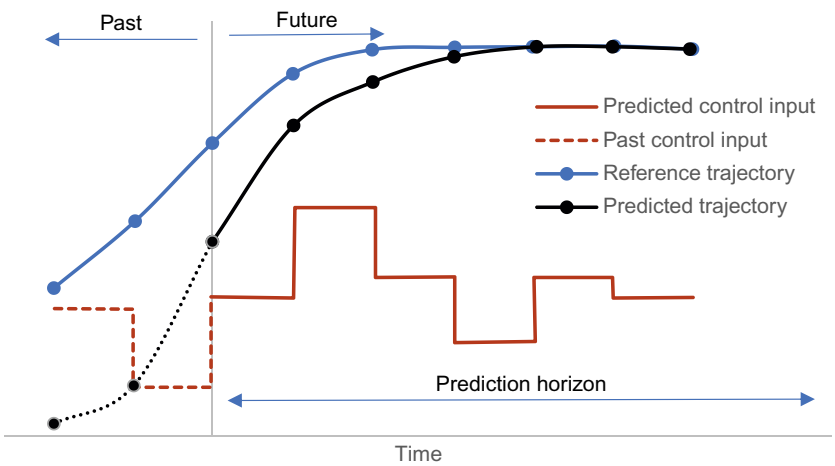

FIGURE 7.12

Model predictive control for an single-input and single-output system.

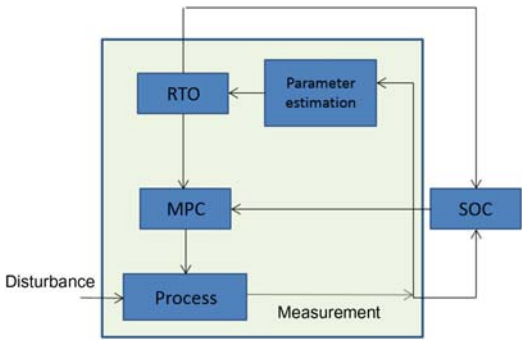

FIGURE 7.13

Integration of model predictive control (MPC) and self-optimizing control (SOC) strategies [99].

7.7.6 Model predictive control–self-optimizing control strategy

Control systems based on self-optimizing variables have low sensitivity toward disturbances and are always convergent. MPC works best for interactive control loops. High actuation usage may be an issue for MPCs, if the control structure is not selected wisely. Integration of self-optimizing control with MPC is probably the best solution to achieve optimal performance. Merging the two methods will help to get rid of the drawbacks of the two methods, while the actuator usage will be minimized. This has been tested on a case study by Graciano et al. [99]. They noted that set-point updates computed by the real-time optimization were not frequent enough to capture all disturbances. This leads to suboptimal process operation because the system is not reoptimized after a disturbance until it has reached its new (suboptimal) steady state. An efficient way to handle this issue is to include economic considerations in the design of the lower MPC layer. Fig. 7.13 shows the suggested structure.

7.8 Conclusion

This section summarizes the most important points which are discussed in this chapter on the optimal operation of SOFCs. These points include potential research directions.

- Different modeling paradigms have been suggested in the literature. The level of simplification depends on the control objective. The important point is that there should be a link between the key variables in the objective function and control inputs in the model, reflecting the reality of the system. In addition, the variables in the fuel-cell system have different dynamics. The model should be able to show this.

- Many decisions that affect the operation of the plant are made during the plant-design phase. To reach the maximum potential in a process, it is necessary to study how the design will affect performance during operation. A process design may lead to a robust control structure, for example, by adding additional load-shaping devices to compensate for the disturbances in the electrical load demands, while another process design leads to active-constraint control where there is no place for optimization. Although there have been some studies on integrating process control and design, there is no research on systematically integrating self-optimizing control concepts into the plant-design phase.
- Systematic control−structure design is missing in many of the control studies in the literature. Defining a clear control objective, dividing the stabilizing and economic control layers based on time-scale separation, selection of control variables and CV−MV pairings are some of the important decisions. Deciding on "what to control" has not been a part of most research studies. The systematic control variable selection presented in this chapter is based on offline optimization of steady-state simulation models and is easy to implement. An important potential research activity is to design a control structure for an SOFC system and its integration with other chemical processes based on self-optimizing control strategy. Decentralized or multivariable control should be chosen based on controllability analysis.
- Measuring or estimation of key variables in an SOFC system is important for monitoring and control. Each of the measurements, or a combination of them (which may be an estimate for another process variable), are potential control variables. An estimation problem should be formulated based on the application of the estimated variable, that is, whether it's going to be used for monitoring or in a closed-loop control structure. A static-estimation method is presented in this chapter, which covers four different cases. Extension of these estimators to be applied in a dynamic setting is a potential research direction.

References

[1] M.G. García-Camprubí, Multiphysics models for the simulation of solid oxide fuel cells (PhD Dissertation), 2012. Retrieved from http://citeseerx.ist.psu.edu/viewdoc/download?doi = 10.1.1.726.8398&rep = rep1&type = pdf.

[2] B. Huang, Y. Qi, M. Murshed, Solid oxide fuel cell: perspective of dynamic modeling and control, J. Process Control 21 (10) (2011) 1426−1437.

[3] K. Sundmacher, Advances in Chemical Engineering: Fuel cell Engineering, Academic Press, 2012.

[4] R.J. Braun, T.L. Vincent, H. Zhu, R.J. Kee, Analysis, optimization, and control of solid-oxide fuel cell systems, *Advances in Chemical Engineering: Fuel* Cell Engineering, vol. 41, Academic Press, Burlington, 2012, pp. 383−446.

[5] M.V. Pavan Kumar, N. Kaistha, Steady-state multiplicity and its implications on the control of an ideal reactive distillation column, Ind. Eng. Chem. Res. 47 (8) (2008) 2778–2787.
[6] M. Bavarian, M. Soroush, Steady-state multiplicity in a solid oxide fuel cell, 2011. Proceedings of the American Control Conference. 1506–1511. 10.1109/ACC.2011.5991053
[7] M. Bavarian, M. Soroush, Steady-state multiplicity in a solid oxide fuel cell: practical considerations, Chem. Eng. Sci. 67 (1) (2012) 2–14.
[8] F. Ramadhani, M.A. Hussain, H. Mokhlis, S. Hajimolana, Optimization strategies for solid oxide fuel cell (SOFC) application: a literature survey, Renew. Sustain. Energy Rev. 76 (2017) 460–484.
[9] S. Skogestad, I. Postlethwaite, Multivariable Feedback Control: Analysis and Design, Wiley, 2005.
[10] J.F. Pierre, Siemens SOFC Test Article and Module Design (Technical report), Prepared under DOE Co-Operative Agreement No. DE-FE0000781, Retrieved from https://www.osti.gov/servlets/purl/1052995, 2011.
[11] M. Xu, T. Li, M. Yang, M. Andersson, Solid oxide fuel cell interconnect design optimization considering the thermal stresses, Sci. Bull. 61 (17) (2016) 1333–1344.
[12] M. Sharifzadeh, Integration of process design and control: a review, Chem. Eng. Res. Des. (2013).
[13] L.F. Brown, A comparative study of fuels for on-board hydrogen production for fuel-cell-powered automobiles, Int. J. Hydrogen Energy 26 (2001) 381–397.
[14] S. Birch, Ford's focus on the fuel cell (Technical report), Automotive Engineering International, 2001, pp. 25–28.
[15] J.T. Pukrushpan, A.G. Stefanopoulou, H. Peng, Control of Fuel Cell Power Systems: Principles, Modeling, Analysis and Feedback Design, Springer, London, 2013.
[16] K. Ro, S. Rahman, Control of grid-connected fuel cell plants for enhancement of power system stability, Renew. Energy 28 (3) (2003) 397–407.
[17] D. Bhattacharyya, R. Rengaswamy, A review of solid oxide fuel cell (SOFC) Dynamic models, Ind. Eng. Chem. Res. 48 (13) (2009) 6068–6086.
[18] B.J. Spivey, T.F. Edgar, Dynamic modeling, simulation, and MIMO predictive control of a tubular solid oxide fuel cell, J. Process Control 22 (8) (2012) 1502–1520.
[19] S.C. Singhal, K. Kendall, High Temperature Solid Oxide Fuel Cells: Fundamentals, Design and Applications, Elsevier, 2003.
[20] J. Larminie, A. Dicks, Fuel Cell Systems Explained, second ed., Wiley, 2003.
[21] X.W. Zhang, S.H. Chan, H.K. Ho, J. Li, G. Li, Z. Feng, Nonlinear model predictive control based on the moving horizon state estimation for the solid oxide fuel cell, Int. J. Hydrogen Energy 33 (9) (2008) 2355–2366.
[22] R. Roberts, et al., "Control design of an atmospheric solid oxide fuel cell/gas turbine hybrid system: variable versus fixed speed gas turbine operation, J. Power Sources 161 (1) (2006) 484–491.
[23] C. Stiller, B. Thorud, O. Bolland, R. Kandepu, L. Imsland, Control strategy for a solid oxide fuel cell and gas turbine hybrid system, J. Power Sources 158 (1) (2006) 303–315.
[24] Y.H. Li, S.S. Choi, S. Rajakaruna, An analysis of the control and operation of a solid oxide fuel-cell power plant in an isolated system, IEEE Trans. Energy Convers. 20 (2) (2005) 381–387.
[25] Y. Li, J. Shen, J. Lu, Constrained model predictive control of a solid oxide fuel cell based on genetic optimization, J. Power Sources 196 (14) (2011) 5873–5880.

[26] T.H. Lee, J.H. Park, S.M. Lee, S.C. Lee, Nonlinear model predictive control for solid oxide fuel cell system based on Wiener model, Int. J. Comput. Electr. Autom. Control Inf. Eng. 4 (12) (2011) 137–142.
[27] D. Bhattacharyya, R. Rengaswamy, C. Finnerty, Dynamic modeling and validation studies of a tubular solid oxide fuel cell, Chem. Eng. Sci. 64 (9) (2009) 2158–2172.
[28] M. Carré, R. Brandenburger, W. Friede, F. Lapicque, U. Limbeck, P. Da Silva, "Feed-forward control of a solid oxide fuel cell system with anode offgas recycle, J. Power Sources 282 (2015) 498–510.
[29] R.U. Dietrich, et al., Efficiency gain of solid oxide fuel cell systems by using anode offgas recycle - results for a small scale propane driven unit, J. Power Sources 196 (17) (2011) 7152–7160.
[30] T. Dötschel, A. Rauh, H. Aschemann, Reliable control and disturbance rejection for the thermal behavior of solid oxide fuel cell systems, IFAC Proc. 45 (2012) 532–537.
[31] X.J. Wu, X.J. Zhu, G.Y. Cao, H.Y. Tu, Predictive control of SOFC based on a GA-RBF neural network model, J. Power Sources 179 (1) (2008) 232–239.
[32] X. Wu, D. Gao, Fault tolerance control of SOFC systems based on nonlinear model predictive control, Int. J. Hydrogen Energy 42 (4) (2017) 2288–2308.
[33] H.-B.B. Huo, X.-J.J. Zhu, W.-Q.Q. Hu, H.-Y.Y. Tu, J. Li, J. Yang, Nonlinear model predictive control of SOFC based on a Hammerstein model, J. Power Sources 185 (1) (2008) 338–344.
[34] F. Mueller, F. Jabbari, J. Brouwer, S.T. Junker, H. Ghezel-Ayagh, Linear quadratic regulator for a bottoming solid oxide fuel cell gas turbine hybrid system, J. Dyn. Syst. Meas. Control. 131 (5) (2009) 51002.
[35] A. Marchetti, Modifier-Adaptation Methodology for Real-Time Optimization, EPFL, 2009.
[36] G.A. Bunin, G. François, D. Bonvin, Two-layered real-time optimization of a solid oxide fuel cell stack, IFAC Proc. 9 (Pt 1) (2010) 847–852.
[37] G.A. Bunin, Z. Wuillemin, G. François, A. Nakajo, L. Tsikonis, D. Bonvin, Experimental real-time optimization of a solid oxide fuel cell stack via constraint adaptation, Energy 39 (1) (2012) 54–62.
[38] A.Y. Sendjaja, V. Kariwala, Decentralized control of solid oxide fuel cells, IEEE Trans. Ind. Inform. 7 (2) (2011) 163–170.
[39] X. Wang, B. Huang, T. Chen, Data-driven predictive control for solid oxide fuel cells, J. Process Control 17 (2) (2007) 103–114.
[40] S. Campanari, Thermodynamic model and parametric analysis of a tubular SOFC module, J. Power Sources 92 (2001) 26–34.
[41] B.J. Spivey, J.D. Hedengren, T.F. Edgar, Constrained control and optimization of tubular solid oxide fuel cells for extending cell lifetime, in: Proc. Am. Control Conf., 2012.
[42] J. Yang, X. Li, H.G. Mou, L. Jian, Predictive control of solid oxide fuel cell based on an improved Takagi-Sugeno fuzzy model, J. Power Sources 193 (2) (2009) 699–705.
[43] F. Mueller, F. Jabbari, J. Brouwer, R. Roberts, T. Junker, H. Ghezel-Ayagh, Control design for a bottoming solid oxide fuel cell gas turbine hybrid system, J. Fuel Cell Sci. Technol. 4 (3) (2007) 221.
[44] B.M. Sanandaji, T.L. Vincent, A.M. Colclasure, R.J. Kee, Modeling and control of tubular solid-oxide fuel cell systems: II. Nonlinear model reduction and model predictive control, J. Power Sources 196 (1) (2011) 208–217.
[45] M. Fardadi, F. Mueller, F. Jabbari, Feedback control of solid oxide fuel cell spatial temperature variation, J. Power Sources 195 (13) (2010) 4222–4233.

[46] K. Sedghisigarchi, A. Feliachi, H-infinity controller for solid oxide fuel cells, in: Proceedings of the 35th Southeastern Symposium on System Theory, 2003, pp. 464–467.
[47] A. Tsai, L. Banta, D. Tucker, R. Gemmen, Multivariable robust control of a simulated hybrid solid oxide fuel cell gas turbine plant, J. Fuel Cell Sci. Technol. 7 (4) (2010) 0410081–0410089.
[48] V. Knyazkin, L. Söder, C. Canizares, Control challenges of fuel cell-driven distributed generation, in: 2003 IEEE Bol. PowerTech - Conf. Proc., vol. 2, pp. 564–569, 2003.
[49] R. Kandepu, L. Imsland, B.A. Foss, C. Stiller, B. Thorud, O. Bolland, Modeling and control of a SOFC-GT-based autonomous power system, Energy 32 (4) (2007) 406–417.
[50] M.L. Ferrari, Advanced control approach for hybrid systems based on solid oxide fuel cells, Appl. Energy 145 (2015) 364–373.
[51] D. McLarty, Y. Kuniba, J. Brouwer, S. Samuelsen, Experimental and theoretical evidence for control requirements in solid oxide fuel cell gas turbine hybrid systems, J. Power Sources 209 (2012) 195–203.
[52] D. McLarty, J. Brouwer, S. Samuelsen, Fuel cell–gas turbine hybrid system design part II: dynamics and control, J. Power Sources 254 (2014) 126–136.
[53] A.K.M.M. Murshed, B. Huang, K. Nandakumar, Estimation and control of solid oxide fuel cell system, Comput. Chem. Eng. 34 (1) (2010) 96–111.
[54] J. Chen, M. Liang, H. Zhang, S. Weng, Study on control strategy for a SOFC-GT hybrid system with anode and cathode recirculation loops, Int. J. Hydrogen Energy 42 (49) (2017) 29422–29432.
[55] B. Kwon, S. Han, K. Lee, Robust estimation and tracking of power system harmonics using an optimal finite impulse response filter, Energies 11 (7) (2018) 1811.
[56] H.B. Huo, X.H. Kuang, H.E. Huo, X.J. Zhu, Dynamic modeling of SOFC stack using ARX identification algorithm, in: Proc. 2012 Int. Conf. Model. Identif. Control, 2012, pp. 647–652.
[57] Q. Song, F. Liu, The direct approach to unified GPC based on ARMAX/CARIMA/CARMA model and application for pneumatic actuator control, in: First International Conference on Innovative Computing, Information and Control (ICICIC'06), vol. 1, 2006, pp. 336–339.
[58] F. Jurado, Modeling SOFC plants on the distribution system using identification algorithms, J. Power Sources 129 (2004) 205–215.
[59] H. Cheng, S. Jing, Y. Xu, Z. Deng, J. Li, X. Li, Control-oriented modeling analysis and optimization of planar solid oxide fuel cell system, Int. J. Hydrogen Energy 41 (47) (2016) 22285–22304.
[60] F. Jurado, A method for the identification of solid oxide fuel cells using a hammerstein model, J. Power Sources 154 (1) (2006) 145–152.
[61] F. Jurado, M. Valverde, M. Gómez, Identification of hammerstein model for solid oxide fuel cells, in: Can. Conf. Electr. Comput. Eng., 2007, pp. 442–445.
[62] B. Dolenc, D. Vrecko, D. Juricic, A. Pohjoranta, J. Kiviaho, C. Pianese, Soft Sensor Design for estimation of SOFC stack temperatures and oxygen-to-carbon ratio, ECS Trans. Adv. Solid State Electrochem. Sci. Technol. 68 (1) (2015) 2625–2636.
[63] H. Sumi, H. Shimada, K. Sato, T. Hashida, Estimation of micro-size defects in electrolyte thin-film by X-ray stress measurement for anode-supported solid oxide fuel cells, Adv. Technol. Exp. Mech. 3 (6) (2016) 16–00177.

[64] JENTEK Sensors, Characterization of Solid Oxide Fuel Cell Components Using Electromagnetic Model-Based Sensors (Technical report), Prepared for Department of Energy under Phase I SBIR Contract No. DE-FG02-03ER83690, 2004, Retrieved from https://pdfs.semanticscholar.org/b222/7f5e87c57fa75ec61748c971bbfb63f75e49.pdf.

[65] A. Azad, C. Holt, S. Swartz, Development of chemical sensors for PEM and SOFC systems, (Technical report), 2003, Retrieved from https://pdfs.semanticscholar.org/40e2/7d3526371159423942ff7337e68d343ea355.pdf.

[66] J. Yarwood, R. Douthwaite, S. Duckett, Spectroscopic Properties of Inorganic and Organometallic Compounds: Techniques, Materials and Applications, Royal Society of Chemistry, Cambridge, 2012.

[67] H. Kishimoto, et al., In situ analysis on the electrical conductivity degradation of NiO doped yttria stabilized zirconia electrolyte by micro-Raman spectroscopy, Electrochim. Acta 82 (2012) 263−267.

[68] D.A. Agarkov, I.N. Burmistrov, F.M. Tsybrov, I.I. Tartakovskii, V.V. Kharton, S.I. Bredikhin, In-situ Raman spectroscopy analysis of the interfaces between Ni-based SOFC anodes and stabilized zirconia electrolyte, Solid State Ionics 302 (2017) 133−137.

[69] W.B. Guan, H.J. Zhai, L. Jin, C. Xu, W.G. Wang, Temperature measurement and distribution inside planar SOFC stacks, Fuel Cells 12 (1) (2012) 24−31.

[70] M. Buric, P. Ohodnicki, A. Yan, S. Huang, K.P. Chen, Distributed fiber-optic sensing in a high-temperature solid-oxide fuel cell, in: Proceedings of the SPIE, vol. 9977, 2016, p. 997708.

[71] M.B Pomfret, J. Owrutsky, R.A Walker, In Situ Optical Studies of Solid-Oxide Fuel Cells, Annual Review of Analytical Chemistry vol. 3, pp. 151−174, 2010, doi: 10.1146/annurev.anchem.111808.073641.

[72] B. Urasinska-Wojcik, J.W. Gardner, H_2S sensing in dry and humid H_2 environment with p-type CuO thick film gas sensors, IEEE Sensors J. 18 (9) (2018) 3502−3508.

[73] B. Ram, J. Biao, H. Amos, Receding horizon experiment design with application in SOFC parameter estimation, Dycops 2010, Leuven, Belgium, July 5−7, 2010, pp. 541−546, 2011.

[74] M. Halinen, A. Pohjoranta, J. Pennanen, J. Kiviaho, Application of multivariable regression model for SOFC stack temperature estimation in system environment A1306 application of multivariable regression model for SOFC stack temperature estimation in system environment, In: Proceedings of 11th European SOFC & SOE Forum, pp. 183−191, 2014.

[75] S. Khatibisepehr, B. Huang, S. Khare, Design of inferential sensors in the proess industry: a review of bayesian methods, J. Process Control 23 (2013) 1575−1596.

[76] W.F. Massy, Principal component regression in exploratory statistical research, J. Am. Stat. Assoc. 60 (1965) 234−246.

[77] H. Wold, 11 - Path Models with Latent Variables: The NIPALS Approach, Quantitative Sociology, International Perspectives on Mathematical and Statistical Modeling, 1975, pp. 307-357.

[78] B. Joseph, C.B. Brosilow, Inferential control of processes: Part I. Steady state analysis and design, AIChE J. 24 (3) (1978) 485−492.

[79] M. Ghadrdan, C. Grimholt, S. Skogestad, A new class of model-based static estimators, Ind. Eng. Chem. Res. 52 (35) (2013) 12451−12462.

[80] E.S. Hori, S. Skogestad, V. Alstad, Perfect steady-state indirect control, J. Ind. Eng. Chem. Res. 44 (2005) 863–867.
[81] M. Ghadrdan, Optimal Operation of Kaibel Columns, Norwegian University of Science and Technology, 2014.
[82] J. Padulles, G. Ault, J. McDonald, An integrated sofc plant dynamic model for power systems simulation, J. Power Resour. 86 (2000) 495–500.
[83] Y. Zhu, K. Tomsovic, Development of models for analyzing the load-following performance of microturbines and fuel cells, Electr. Power Syst. Res. 62 (1) (2002) 1–11.
[84] S. Skogestad, Near-optimal operation by self-optimizing control: From process control to marathon running and business systems, Comput. Chem. Eng. 29 (1) (2004) 127–137.
[85] E.M.B. Aske, S. Skogestad, Consistent inventory control, Ind. Eng. Chem. Res. 48 (24) (2009) 10892–10902.
[86] N. Chatrattanawet, S. Skogestad, A. Arpornwichanop, Control structure design and controllability analysis for solid oxide fuel cell, Chem. Eng. Trans. 39 (2014) 1291–1296 (Special issue).
[87] M. Halinen, Improving the Performance of Solid Oxide Fuel Cell Systems, VTT Technical Research Centre of Finland, 2015.
[88] T. Marlin, A.N. Hrymak, Real-time operations optimization of continuous processes, in: International Conference in Process Control, 1996.
[89] M. Halinen, J. Saarinen, M. Noponen, I.C. Vinke, J. Kiviaho, Experimental analysis on performance and durability of SOFC demonstration unit, Fuel Cells 10 (2010) 440–452.
[90] I. Halvorsen, S. Skogestad, J. Morud, V. Alstad, Optimal selection of controlled variables, Ind. Eng. Chem. Res. 42 (2003) 3273–3284.
[91] V. Alstad, S. Skogestad, Self-optimizing control: optimal measurement selection, AIChE Annual Meeting, Austin, Texas, Nov. 2004, Poster 403e.
[92] R. Yelchuru, Quantitative Methods for Controlled Variables Selection, Norwegian University of Science and Technology, 2012.
[93] M. Ghadrdan, I.J. Halvorsen, S. Skogestad, Dynamic compensation of static estimators from Loss method, in: IFAC Proceedings Volumes (IFAC-PapersOnline), vol. 10, 2013, no. Part 1.
[94] V. Radisavljevic, On controllability and system constraints of the linear models of proton exchange membrane and solid oxide fuel cells, J. Power Sources 196 (20) (2011) 8549–8552.
[95] M. Panahi, S. Skogestad, Economically efficient operation of CO_2 capturing process. Part II. Design of control layer, Chem. Eng. Process. Process Intensif. 52 (2012) 112–124.
[96] F. Salem, M.I. Mosaad, A comparison between MPC and optimal PID controllers: case studies, in: Michael Faraday IET International Summit 2015, 2015, pp. 59–65.
[97] C. Grimholt, S. Skogestad, Optimal PI-*Control* and *Verification* of the SIMC *Tuning Rule*, vol. 2, no. PART 1, IFAC, 2012.
[98] J.L. Garriga, M. Soroush, Model predictive control tuning methods: a review, Ind. Eng. Chem. Res. 49 (8) (2010) 3505–3515.
[99] J.E.A. Graciano, J. Jäschke, G.A.C. Le Roux, L.T. Biegler, Integrating self-optimizing control and real-time optimization using zone control MPC, J. Process Control 34 (2015) 35–48.

This page intentionally left blank

CHAPTER

8

Fault detection, loss prevention, hazard mitigation, and safe operation of solid oxide fuel cell systems

Mahdi Sharifzadeh[1] **and Davood Rashtchian**[2]

[1]*Sharif Energy Research Institute, Sharif University of Technology, Tehran, Iran*

[2]*Chemical and Petroleum Engineering Department, Sharif University of Technology, Tehran, Iran*

8.1 Introduction

Solid oxide fuel cells (SOFCs) offer several advantages including high-energy efficiency, fuel flexibility, tolerance of minor fuel contaminations, and the possibility of being integrated with a diverse array of applications. However, these advantages come at the price of a highly interactive operation and more extreme operating conditions. This chapter provides an overview of the research in the field of fault detection, loss prevention, and operational safety concerning SOFC technologies. First, the mechanisms that cause equipment faults and their diagnostic procedures are discussed. Then the explosive and electrical hazards associated with installation, operation, and handling of SOFC systems are reviewed. The next theme is concerned with operational safety and interactions between various SOFC system components. Finally the interactions of process design and safety are demonstrated by using an example of a hybrid SOFC, triple combined-cycle power generation system. The chapter concludes with a summary of the findings in the research field and recommendations of potent areas for future research.

8.2 Solid oxide fuel cell fault mechanisms

As discussed briefly in previous chapters, there are risks associated with thermal stress, carbon formation, and catalyst poisoning that could result in sudden failure of an SOFC stack and its components. The performance degradation could be due to the deterioration of a single component or the interactions with other process-unit operations. Broadly speaking the degradation mechanisms could lead to

Design and Operation of Solid Oxide Fuel Cells. DOI: https://doi.org/10.1016/B978-0-12-815253-9.00008-2

reversible or irreversible performance degradations, which demonstrate themselves as the loss of potential for a constant-current load [1]. The examples of reversible-performance loss are early carbon deposition and sulfur poisoning, which are associated with minor and reversible thermochemical changes. However, most of the thermomechanical damages including electrode delamination and electrolyte cracking cause irreversible failure and would require the replacement of the damaged component.

A thorough review of the diagnostic methods for SOFC failures was presented by Barelli et al. [1]. They classified the degradation mechanism into those resulting in ohmic resistance or the faults that degrade the microstructure of the electrode. Electrode delamination, anode reoxidation, oxide-layer growth, and rib detachment are the mechanisms that increase the ohmic resistance. By comparison, electrode microstructure sintering, cathode-microstructure poisoning, carbon deposition on the anode, anode sulfur-poisoning, and cathode boron-poisoning are responsible for the microstructure degradation faults. These will be briefly discussed next.

The *electrode delamination* refers to a phenomenon in which an electrode is detached from the electrolyte. Thermal cycling due to the load variations from ambient temperature to extreme operating conditions is the main cause of this failure and could result in the detachment of the adjacent layers due to the differences in the thermal-expansion factors of the metal and ceramic SOFC components. The open gaps act as barriers to the electric current and result in the deactivation of the electrochemical reactions in the areas below and above delamination [1]. Frequent and rapid load-cycling could also result in *thermal stress*, which could degrade the material and detachments due to thermal-expansion differences of the cell components. *SOFC seal failure* could result in leakage of the fuel and air, the local shortage of fuel, as well as anode reoxidation. It is crucial that the seal can tolerate the frequent heating and cooling procedures between the high-operating temperature and the ambient temperature, and do not degrade other cell materials with which it is in contact [1]. Another important failure mechanism is the *oxide-layer growth* when oxidation results in a less electrically conducting layer covering the interface of the interconnect and electrode, which increases the overall resistance [1]. *Rib detachment* can disconnect the local, electrical-current flow. The change in the electron pathways may overheat and oxidize the adjacent connect ribs, increasing the resistance and causing degradation. All these failures contribute to an increase in *ohmic resistance* [1].

Fuel contamination could cause *microstructure degradation* of the electrode-porous materials at elevated temperatures. The electrode-porous structure provides the active sites for electrochemical reactions and the transport of gaseous materials. Its degradation deteriorates the cell performance. *Sintering and coarsening* of the nickel−YSZ cermet microstructures of the anode occur due to the agglomeration of Ni due to its weak-adhesion properties, resulting in the reduction of chemically active sites, uneven electrode-porosity distribution, and reduced electrical pathways. Such failure would be detected as increased overpotentials and reduced

power outputs [1]. The application of stainless-steel interconnectors results in the outgas of *chromium* products that deposit on the electrochemically active sites and *poison* the electrode microstructure [1]. *Carbon deposition* is an undesirable side reaction that is catalyzed by the Ni active sides on the anode, which affects the electrochemical activity and the species transport rate. Early carbon deposition could be reversibly removed by adjusting the operating conditions. However, at temperatures above 923K the deposited carbon dissolves in the Ni particles and degrades the structural integrity [1]. The adsorption of a molecular monolayer of sulfur compounds as a fuel contaminant blocks the active sides and poisons the anode materials. This phenomenon is, to a large extent, reversible at low concentrations and short-exposure durations [1]. However, it should be strictly avoided as it greatly reduces cell performance. In addition the presence of boron compounds results in cathode degradation due to agglomeration and grain-size growth.

Liu et al. [2] studied the interfacial shear stress and peeling stress of two common SOFC configurations, namely electrolyte-supported and anode-supported SOFCs, during thermal cycling. The authors reported that the interfacial shear and peeling stress were intense near the electrode free-edge areas. The authors reported that the anode−electrolyte interface was at a high risk of delamination under thermal stresses. In electrolyte-supported SOFCs the electrolyte is relatively thicker than the anode electrode (100 μm vs 50 μm). In anode-supported SOFCs the electrolyte is much thinner (<20 μm); the cathode thickness is larger (50 μm), but still much less than the anode electrode (0.3−1.5 mm). As a result of the thickness differences, anode-supported SOFCs can operate at a much lower temperatures (700°C−800°C compared to 1000°C in the former configuration). Liu et al. [2] reported that for both configurations the number of thermal cycling before failure decreases as the electrode porosity increases (the anode electrode in the case of electrolyte-supported SOFCs or the electrolyte electrode in the case of anode-supported SOFCs). The authors reported that anode off-gas recirculation can enhance the net-electrical efficiency up to 160%.

Zaccaria et al. [3] studied the degradation of a syngas-fed SOFC over an operational period of 12,000 hours. The degradation was monitored by observing the ohmic resistance as functions of the current density, fuel utilization, and temperature. They observed that at the beginning of the operation duration the degradation starts at the cell inlet where the fuel utilization and current density is higher and the temperature is lower. However, by increasing the resistance at the inlet the current density peak shifts toward the center (around 50 hours operational time).

8.3 Solid oxide fuel cell fault diagnosis

It is notable that most of the abovementioned fault mechanisms do not exhibit themselves as a unique symptom. Therefore sophisticated diagnostic procedures are under development. Electrochemical impedance spectroscopy methods are

recommended as noninvasive procedures for the detection of delamination. Thermodynamic equilibrium calculations allow detection of the operating conditions which would lead to oxidation. For high-fuel utilization the partial pressure of the fuel drops very low and the reductive-reaction environment changes to an oxidative environment. The increased polarization resistance of anode and cathode electrodes with no corresponding changes in the peak frequency, accompanied by a proportional rise in series resistance, is the diagnostic feature of delamination [1].

Anode reoxidation also depends on the temperature, and for a certain temperature and fuel flow rate there is a maximum fuel-utilization limit that should not be exceeded in order to avoid locally, lean-fuel concentrations. Since anode reoxidation results in the expansion of the anode bulk materials, anode-volume expansion is considered as a diagnostic feature [1].

Although SOFC stacks capable of multiple reduction−oxidation (redox) cycles are developed, for thick anode-supported SOFCs, the volume change causes small cracks and leakage, with the detrimental consequence of the combustion of air and fuel. The mitigation strategy is often to use a reducing, purge gas. The reducing gas can be supplied from the gas storage tank, reducing hydrogen from prereformer catalyst oxidation, or a separate catalytic partial oxidation reformer. Alternatively a reverse potential could be applied to the stack [4].

Impedance analysis is the method of choice for detecting the chromium-oxide layer formed between the interconnect rib and cathode. A slight increase in the polarization resistance, with a constant characteristic frequency, is the diagnostic signature of this failure [1]. Rib detachment causes less severe damage compared to delamination, which should be associated with the mobility of electrons [1]. Barelli et al. [1] emphasized that despite the great importance of microstructural degradation mechanisms there are no global diagnostic methods available for them.

Thermal stresses cause discontinuities across the electrode and electrolyte interfaces. Acoustic emission is recognized as a useful indicator for diagnosing such failures. Even small differences in the thermal-expansion coefficients could result in large mechanical stress between cell components due to rapid thermal cycles (start-up or shut-downs) and temperature gradients. Functionally graded materials are developed to limit the changes in the composition of the contact layers between two cell components with different properties. Saied et al. [5] reported that a functionally graded electrode offers 23% higher power density at the voltage of 0.6 V, with much better yields.

Yan et al. [6] studied an SOFC stack consisting of 10 anode-supported cells with an external manifold structure. The external manifold allowed uniform flow with differences less than 0.1%. The system was examined with respect to degradation after 700 hours. The degradation rate was reported to be 17.6% per 1000 hours. Minor microstructure changes in the material and increase in area-specific resistance was observed. Stainless-steel interconnect oxidation and small leakages were also observed.

Wu and Gao [7] reported the design of a fault tolerant-control system for heat management and load tracking of an SOFC system. The control system consisted

of a fault-diagnosis module, a decision-making part, and four backup nonlinear model predictive controllers corresponding to the four modes of normal operation, namely operation with the fuel-leakage fault, operation with the air-compressor fault, or operation with both fuel-leakage and air-compressor faults. The authors applied a model-based classifier to detect the occurring fault type. The NMPCs were based on back propagation neural network models. The authors reported enhancements in the lifetime and performance of the SOFC system.

Esposito et al. [8] applied continuous wavelet transform to detect the failure signature in the voltage signal for anode reoxidation due to higher-than-normal fuel utilization. The authors reported a success rate of 6% for fault detection.

Wu and Ye [9] studied the diagnosis of anode poisoning and cathode humidification in an SOFC system. They applied the least squares support vector machine classifier to detect the faults, and the hidden semi-Mark models to estimate the remaining useful life. They reported a 97% success rate for fault detection and the estimation of the SOFC lifetime drop was in the range of $\pm 20\%$ error.

Polverino et al. [10,11] applied a fault signature matrix analysis based on a fault-tree analysis. The considered fault scenarios included the increase in air-blower mechanical losses, leakage in the manifold, temperature-controller failure, corrosion of the prereformer heat-exchange surface, and increase in stack-polarization losses. The stack power, air-blower power, and stack temperature were applied for monitoring and fault isolation.

8.4 Solid oxide fuel cell hazards and their risk-control strategies

The Great Britain Health and Safety Executive (HSE) issued a guideline in 2004 on the safe installation of fuel cells, as well as controlling the operational risk, which is summarized here [12]. Broadly speaking the SOFC installation and operation hazards can be classified into the three categories of fire and explosion, electric shocks, and the exposure to harmful materials, as discussed next.

For fire or explosion to occur three elements are needed, namely a fuel with high-energy content, an oxidant, and a source of ignition. SOFC systems have a high potential to operate flexibly with various fuels, including hydrogen, natural gas and biogas, methanol, ethanol, dimethyl ether, liquid hydrocarbons, and synthesis gases from biomass and coal sources. Among these, hydrogen liquefied petroleum gas (LPG) is the most dangerous fuel due to its very wide flammability range, low-ignition energy, the possibility of detonation, and the possibility of causing embrittlement of some metals. Hydrogen burns with an almost invisible flame. Its lower explosion limit (LEL) is 4% v/v with an upper limit of 75% v/v. The ignition energy for a 2:1 hydrogen−oxygen mixture is 0.02 mJ, which is one-tenth of other fuels such as methane. Even small sparks from wearing some cloths can ignite the hydrogen−air mixture [12]. The detonation of the hydrogen

flammable mixtures creates a supersonic exothermic front and is much more dangerous than other types of explosion such as deflagrations. The low viscosity of hydrogen requires more stringent consideration to make the equipment "leak-tight" compared to other gases such as nitrogen. This is an important consideration when designing SOFC systems using multiple fuels [12].

Various fuels have different densities compared to air and, therefore, show different leakage behaviors. Compressed hydrogen is much lighter than air and quickly moves upward due to its buoyancy and diffusivity. This helps with its discharge if appropriate ventilation is in place. However, if it accumulates in an enclosed area its concentration may build up quickly in the higher regions and unprotected electrical equipment could be the source of ignition, with a high risk of explosion. By comparison, liquid hydrogen boils at $-253^{\circ}C$ and, immediately after leakage, would create a very cold sinking gas, heavier than air. This gas layer forms a flammable atmosphere at a low level. In addition the low temperature of hydrogen storage often induces an oxygen-rich liquid air, which upon leakage could result in a severe cold burn on the unprotected pipework [12]. Natural gas is lighter than air, but much heavier than hydrogen, and diffuses upward much more slowly. LPG vapors are heavier than air and may permeate downward onto the floor or accumulate in sumps.

In addition to flammability concerns some fuels such as methanol may also be toxic by inhalation, adsorption on the skin, or digestion. The safety measures include prevention from spillage and accumulation through containment and ventilation [12]. The ignition sources could be naked flame or hot surfaces, sparks from welding or grinding, as well as the electrostatic sparks from motors, mobile phones, switches, and mechanical devices.

The other important hazard in working with SOFCs is electrical shock. The voltage and current of individual cells are often small, but the output from the stack could be in the order of 200−400 V. A short circuit across the output busbars could result in a sharp temperature increase and potentially a shower of sparks [12]. The risk-control strategies recommended by the HSE include designing inherently safer processes by substituting hydrogen with safer fuels, preventing the formation of flammable mixtures, eliminating the sources of ignition, and suppression, mitigation, and containment of the explosion. The containment, segregation, separation, and ventilation strategies are applied to avoid the formation of flammable mixtures [12].

SOFCs and other fuel cells employ harmful chemicals in their components. These are often in closed systems with minimal risk of exposure. However, it is important to safeguard personnel from potential exposures during disposal or in the case when the fuel cell is damaged. Some fuels could be poisonous or cancerogenic. Methanol−air mixture is harmful to the health of personnel at concentrations (the time-weighted average of 200 ppm) much lower than its flammability limit (LEL 6% v/v) [12]. General safety considerations regarding manual handling, training personnel, and emergency procedures are strictly required [12].

Lanzini et al. [13] reported the safety design of the DEMOSOFC plant, which is planned to be the first biogas-fueled, industrial-size SOFC installation in Europe. In their design the highest priority was given to eliminating the explosion risk. The combustible streams are present in the process and stack modules. In their analysis the process module was divided into cold and hot areas, separated by an insulating wall, with appropriate ventilation. A gas detector monitors the risk of leakage. Differential pressure control ensures proper negative-pressure inside the process module. A cooling system was provided to cool the ventilation air in the hot area. In the case of (emergency) shut-downs, the fuel-feed valve is closed and the pipelines and vessels containing combustible fuel are flushed with nitrogen. In addition the DC/AC converter and the fuel cells are disconnected and shut down by the means of safety relays [13].

8.5 Loss prevention during solid oxide fuel cell fuel transition

Harun et al. [14] studied the impact of fuel composition on the safety of transient operations. The research motivation was the significant capability of SOFCs for fuel flexibility. Safety constraints such as compressor surge or stall and the thermal stresses of process equipment were considered. They observed that in the first milliseconds of the transition from a coal-based syngas to humidified methane (14% CH_4) the thermal effluent of the fuel cell increased by 17% as the result of the conversion of the stack thermal energy into chemical energy. After 250 seconds the temperature gradient across the fuel cell was increased by 39%, which could be attributed to the cooling effect of reforming reactions. They recommended thermal management using the cathode air flow to mitigate the undesirable effects of the fuel transition. In another study, Harun et al. [15] investigated the role cathode air plays for the transition from a lean-methane syngas to a rich-methane fuel. The authors reported significant air-flow fluctuations (up to 8%) in less than a minute after fuel-composition change.

Liu et al. [16] studied an SOFC system with anode-exhaust recirculation and its ejector applied for recycling gas compression. The focus of their study was the behavior of the ejector that was originally designed for natural-gas compression when syngas derived from biomass gasification is applied. The safety issues such as carbon deposition, anode Ni oxidation, as well as the cell performance were investigated. They observed that the entrainment ratio of the biomass gasification syngas was significantly less than the natural-gas scenario (i.e., 0.71 vs 8.9). Under the studied operating conditions, no carbon deposition or Ni oxidation was observed for the biomass-derived fuel. However, the electrical efficiency was reported to be 15% lower than the natural-gas scenario.

Lv et al. [17] studied the application of four gasified biomass gases from wood chips, cottonwood, corn stalks, and grape-seed gas. The authors reported

the risk of overheating of the turbine and the SOFC system for gasified wood chips. By comparison, low turbine-inlet temperature and compressor surge was reported for cottonwood gas and corn-stalk gas. The electrical efficiency was the highest for the wood-chip gas, followed by the grape-seed gas, cottonwood gas, and corn-stalk gas.

8.6 Safe operation of solid oxide fuel cell systems

Zhang et al. [18] emphasized the complications associated with the safe and efficient operation of SOFC systems. They proposed to add a second, air-bypass manifold (Fig. 8.1) to control the temperature and enable smooth, safe, and resilient load-tracking. Three load-tracking strategies were investigated. The external power load was almost doubled and the implemented changes in the excess-air ratio, bypass-opening ratio, and fuel utilization was the same in all these scenarios. However, the stack output current was changed with the three strategies of (1) a step change, (2) multistep change, and (3) parabolic power-switching. By studying the concertation of hydrogen, they concluded that the parabolic gradual change of the current is the most effective strategy to avoid fuel exhaustion that could be the result of gas transmission delays.

During the starting up of SOFC systems, electrical heaters or start-up burners are applied for heating up the system. By comparison, cooling down during shutdown operations is done passively through production discontinuation or, if needed, could be accelerated by an air blower [4]. Peksen [19] studied the rapid heating up of SOFC systems using electrical heaters integrated into the stack (Fig. 8.2). The electrically heated cartridges were programmed to increase the temperature from the room conditions to 900°C in 6600 seconds. In order to avoid tensile stress a minimal temperature gradient is desirable. The authors optimized

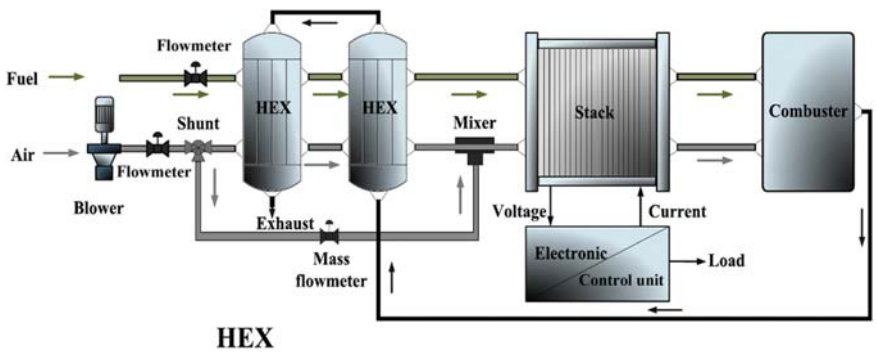

FIGURE 8.1

A solid oxide fuel cell (SOFC) system with cathode-air bypass for safe and efficient transient operation [18].

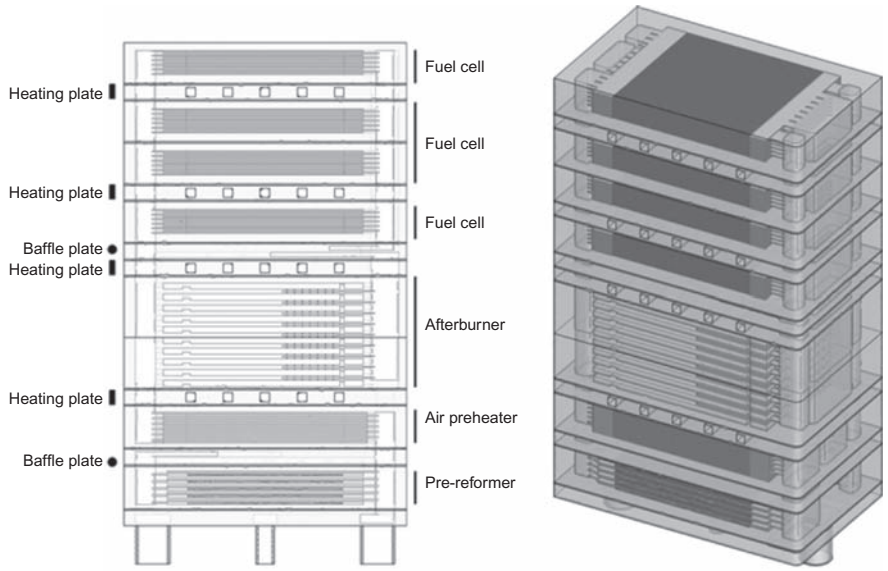

FIGURE 8.2

An integrated fuel cell system module including prereformer, air preheater, fuel cells, and heating plates studied by Peksen [19].

the location of the heating plates to minimize the temperature gradient during the heating-up operation.

In order to protect the anode from reoxidation during start-up operations, premixed reducing gases are applied. Halinen et al. [20] studied the application of prereformer and anode off-gas recycling instead of reducing gas. The authors reported that the oxygen presence (e.g., through air leakage in the recycled anode off-gases) would hinder reforming reactions at low temperatures and increase the light-off temperature (start of reforming reactions) by 200°C. In this scenario, hydrogen needs to be injected. While the SOFC stack itself is capable of producing hydrogen at temperatures above 400°C, due to the catalytically active Ni particles in the anode, this strategy is not recommended as anode oxidation can start at temperatures as low as 350°C. Therefore the reducing hydrogen gas must be injected at such temperatures or lower. The recommended start-up procedure was to apply electrical or other heating systems to increase the temperature to 400°C to enable reformer light-off and then to 500°C to shift the hydrogen production from the stack to the reformer. This operational strategy allows the application of fuel gas and steam instead of a reducing gas and could also ensure anode protection while not resulting in any significant performance loss.

Engelbracht et al. [21] proposed an on-demand safety-gas generator consisting of an evaporator and a reformer. To start the reducing gas generation, two electrical heating elements increase the temperature of the evaporator and steam

reformer to 100°C and 400°C, respectively. Then water is pumped and evaporated and then mixed with the natural gas to start the reforming reactions. Increasing the temperature or steam concentration will favor hydrogen and carbon-monoxide generation, and improves the reducing properties of the generated syngas. The authors reported the successful application of the system to SOFC and electrolyzer systems with no need for storage systems.

Li et al. [22] emphasized that operating the anode at a high pressure requires the cathode to operate at an elevated pressure too as the thin, SOFC elements cannot tolerate high-pressure differences. They suggested that transient fluctuations in pressure on one side can damage the fuel cell. Thermal management requires the minimum air flow to be regulated so that the maximum safe-temperature is not exceeded.

Stiller et al. [23] studied the safe dynamic operation of an solid oxide fuel cells−gas turbine (SOFC−GT) system. They studied a range of operating conditions, quantified as RFF (fuel flow relative to design point), and RSS (shaft speed relative to design point) in the ranges of 65%−105% and 15%−110%, respectively. It was observed that an operating line with constant mean SOFC temperature could be applied for the load range of 80%−100%. However, below 80% the temperature should be decreased due to instability issues. The authors developed a feasible control scheme in which the set-point of the shaft speed was directly coupled with the power output in order to ensure that the system is on the appropriate operating line. This scheme has a better performance compared to the scenario in which the shaft speed is directly used. However, they emphasized the most effective control strategy was to apply the fuel-flow rate in a feedback control configuration that compares the actual-power output and the load demand. In addition they suggested that unlike the grid-connected scenario, the remote application of an SOFC−GT system required a swift transition between steady-state operations and load-compensating equipment, therefore, batteries and capacitors are recommended.

An important feature of SOFC operation is the change of its characteristics due to degradation mechanisms. Therefore constant control strategies, such as maintaining the stack temperature and air flow fixed at their setpoints, could potentially result in the stack failure. In addition, the direct estimation of the stack temperature is challenging as the application of a high number of thermocouples could compromise the stack's reliability due to the risk associated with the gas leaks and short circuits. Halinen et al. [24] applied multivariate regression models and the design of experimental (full factorial) methods in order to estimate the maximum internal stack temperature from the stack current, air flow, and air-inlet temperature.

Zaccaria et al. [25,26] studied various operational strategies in order to minimize the degradation of SOFCs and to enhance their lifetime and durability. Two systems of an atmospheric standalone stack and a pressurized SOFC−GT hybrid configuration were studied using distributed models, where the latter was coupled with hardware components in the National Energy Technology Laboratory (NETL) facility. Three operational strategies of constant current, constant voltage,

and constant stack power were compared. The authors argued that the hybridization enhances the flexibility of the SOFCs system and allows more control options, extending the operational lifetime by an order of magnitude. They reported that maintaining a constant voltage at constant total power was the most efficient strategy. They also suggested that allowing the power output to degrade would increase the lifetime of the standalone stack by 70%. After 2000 hours the overpotential and heat generation were maximum at the outlet. The cell voltage was 12% lower after 12,000 hours. The authors also reported that although the average cell temperature was relatively constant, the temperature gradient increased from 170°C to 230°C after 120,000 hours.

Lv et al. [27] studied the safe operational zones of an intermediate-temperature SOFC−GT, fueled by biomass gasification. They studied the unsafe characteristics of various process components such as the SOFC temperature gradient (<10K/cm), SOFC working temperature (873K−1123K), compressor surge margin (>12%), turbine-inlet temperature (1023K−1223K), and the compressor chocking flow (<0.2 kg/s), which constrain the process operation. Based on these constraints the authors proposed a calculation flowchart that iteratively explores the operational regions and creates a map of the safe, operational zones. The authors identified two unbalanced (i.e., unsafe) energy operational zones where (1) the air flow relative to fuel and the rotational speed of the gas turbine (GT) are low and (2) the fuel-flow rate is low. The former zone corresponds to the risk of thermal stress of the SOFC and too-high turbine-inlet temperature, while the latter scenario corresponds to the risk of carbon deposition in the SOFC and excessively low turbine-inlet temperature. The authors reported that in the safe, operational zone, decreasing the turbine shaft rotational speed decreases the load, but enhances the efficiency up to 63.43%.

Campanari et al. [28,29] discussed the risk of forming a flammable mixture upon leakage in the exchanger, where the thermal energy of the anode exhaust is transferred to the cathode air. They proposed an inert CO_2 heat-transferring loop for indirect heat exchange between the anode exhaust and air.

Ferrari and Massardo [30] studied the interactions between anode and cathode for part-load operation. They applied an emulator rig consisting of software (model) and hardware coupling at the University of Genoa. The authors studied two configurations with different control strategies. In the first the microgas turbine was connected to the electricity grid with a constant turbine-outlet temperature. In the second configuration the microgas turbine was operated in a standalone mode with a constant rotational speed. Different trends were reported for the anode recirculation ratio, for the gird-connected scenario the recirculation ratio was increased with an increase in the load, and for the standalone scenario it showed a decrease. The authors also reported that in the standalone scenario the injection of air into the anodic side increased the compressor-outlet pressure, which could violate the surge margin. In the grid-connected mode an increase in the load also increased the anode−cathode pressure differential significantly, which was not the case for the standalone

scenario. However, a decrease in the primary mass-flow rate of the ejector would induce a significant differential pressure in both scenarios, which could, in turn, create mechanical stresses.

8.7 Integrated design for inherently safer solid oxide fuel cell processes

Energy efficiency is the design objective of most solid-oxide technologies as it directly influences their economic and environmental performance. However, as extensively discussed in this chapter, enhancing energy efficiency poses significant challenges toward operational safety in terms of equipment degradation and avoiding hazardous situations. Moreover, energy efficiency and operational safety strongly depend on design decisions such as process configuration, equipment size, and the nominal-operating point. These observations suggest that the integration between process design and operational safety is the key enabler to unlock energy efficiency while meeting the safety criteria.

The interactions between process design and control design, known as integrated process design and control, is broadly recognized in the literature for which a comprehensive review was presented by Sharifzadeh [31] and was demonstrated on a wide spectrum of industrial applications (e.g., [32–36]). However, this methodology has not yet fully been adopted for operational safety. More recently Sharifzadeh et al. [37] proposed a multiobjective optimization framework to incorporate safety aspects into the design of a hybrid SOFC triple combined-cycle power generation system. The process is shown in Fig. 8.3 and consists of an SOFC, GT, and a heat-recovery and steam-generation system at three pressure levels.

Sharifzadeh et al. [31] proposed a methodology for simultaneously considering the process design and operational safety. The concept is shown schematically in Figs. 8.4 and 8.5. The proposed optimization framework applies an *inversely controlled process model* in order to estimate the values of manipulated variables (control inputs such as the fuel flow rate) in the presence of various disturbances imposed to the system (e.g., the external load), given the desired values of controlled variables (set points, such as the turbine-inlet temperature). This enables the optimizer to quantify the safe, operational window as shown in Fig. 8.5. The *green circles* refer to the optimal value of the manipulated variables for each disturbance scenario. The *red circles* specify the extreme operational points beyond which the safety of the process and the satisfaction of constraints cannot be guaranteed. The values of the *green points* along with other process variables are utilized to estimate the value of the economic objective function, while the length of the safe operational points (the distance of the *red points*) scaled by the whole operating region is applied as the measure for operational safety and flexibility.

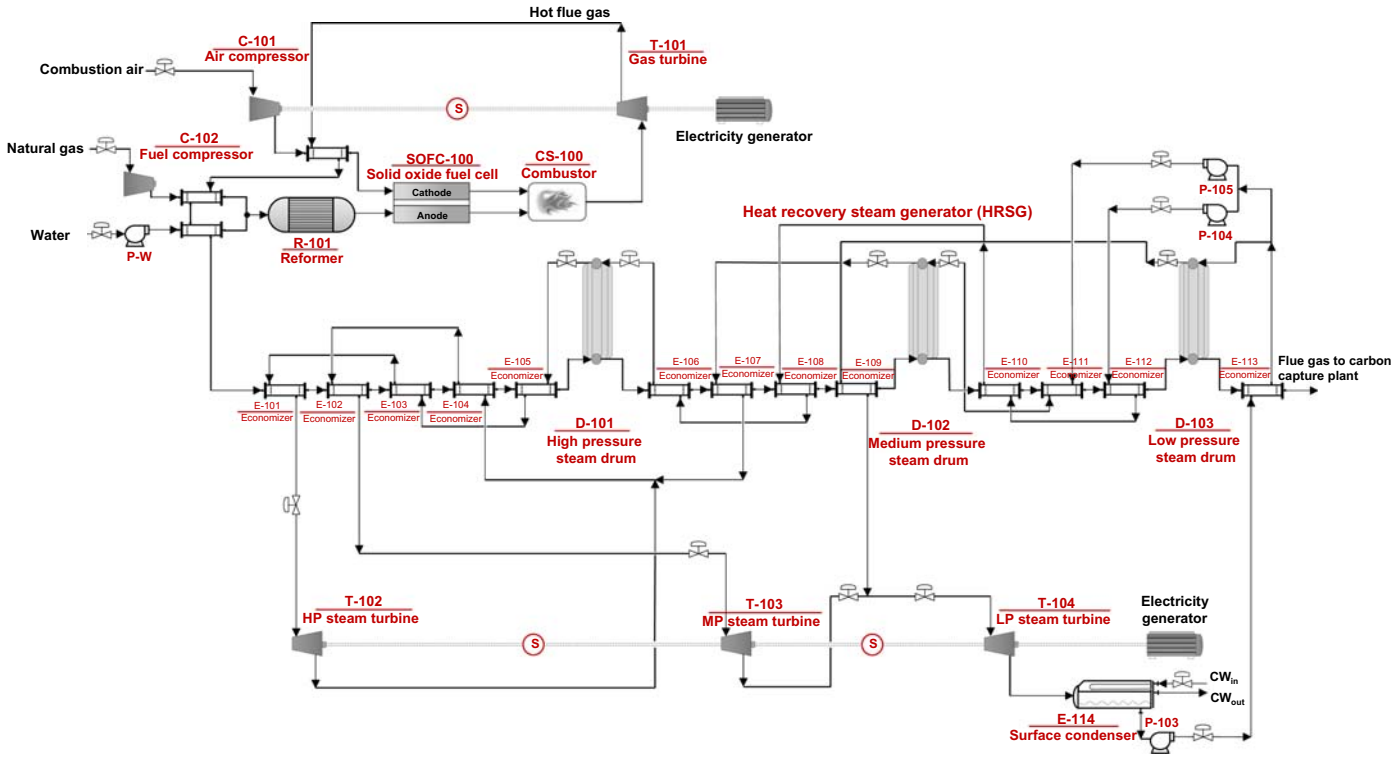

FIGURE 8.3

The solid oxide fuel cell (SOFC) triple combined-cycle power generation system proposed by Sharifzadeh et al. [37].

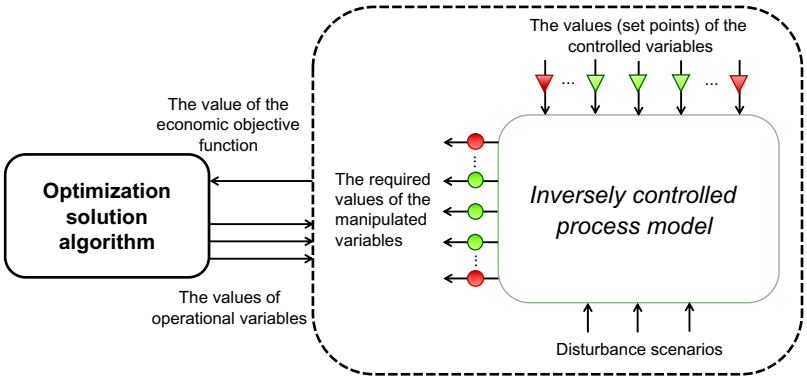

FIGURE 8.4

Optimization framework proposed by Sharifzadeh et al. [37].

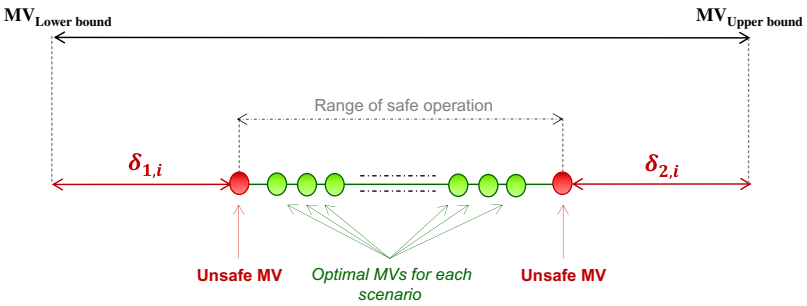

FIGURE 8.5

Safe and unsafe operating windows as quantified by Sharifzadeh et al. [37].

The optimization framework was formulated using a simulation−optimization program developed by linking Aspen Plus (Power plant model), COMSOL (SOFC model), and a genetic algorithm. In terms of optimization programming this was a multiobjective, stochastic optimization with implicit constraints. The solution of a multiobjective optimization problem is not a single point but a Pareto front which demonstrates the trade-off between competing objectives. For instance, as shown in Fig. 8.6A, enhancing the safe, operating window by 100% would incur almost 47% more annualized costs, demonstrating the strong trade-off between the economy and operational safety factors. Figs. 8.7 and 8.8 show the safe operating regions for various manipulated variables and their corresponding operating points on a compressor map, respectively.

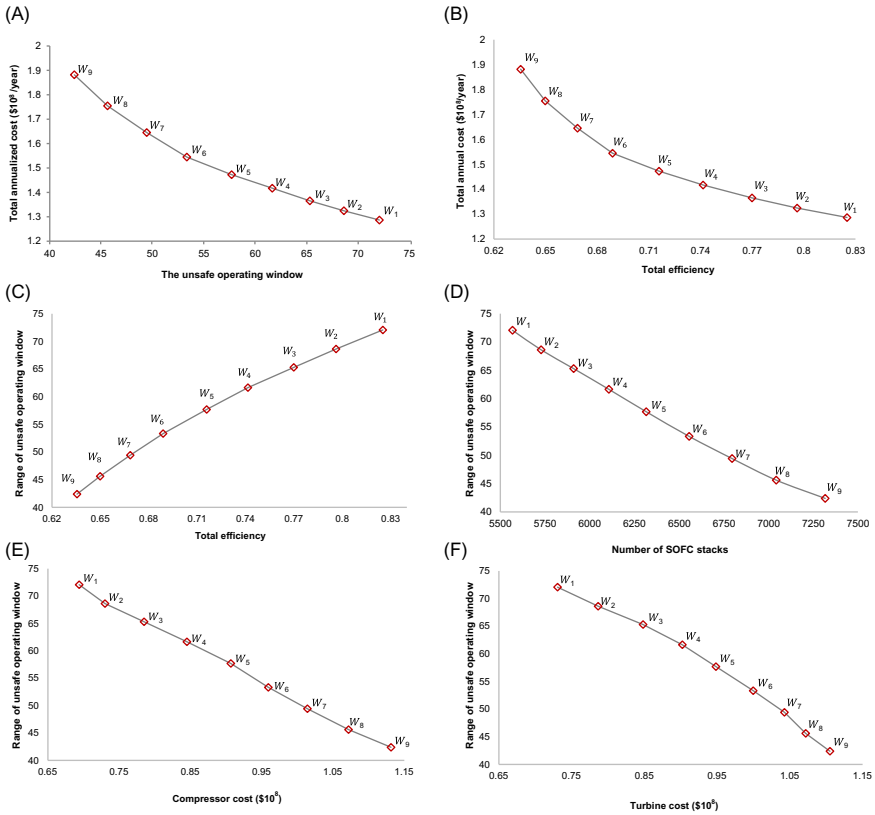

FIGURE 8.6

(A) The Pareto front demonstrating the trade-off between the process economy and safe, operating window. (B) Total annual costs versus average efficiency for all scenarios. (C) The range of unsafe, operating windows versus average efficiency for all scenarios. (D) The trade-off between the range of unsafe, operating windows and the number of solid oxide fuel cell stacks. (E) The trade-off between the range of unsafe, operating windows and the compressor cost. (F) The trade-off between the range of unsafe, operating windows and the gas turbine cost. See Sharifzadeh et al. [37].

8.8 Conclusion

This chapter presents a survey of the research into the safe design and operation of SOFC technologies. The presented materials are diverse and include the mechanisms of fault detection and their diagnostic procedures, hazard risk mitigation, and operational safety considerations. The final part of this chapter illustrates

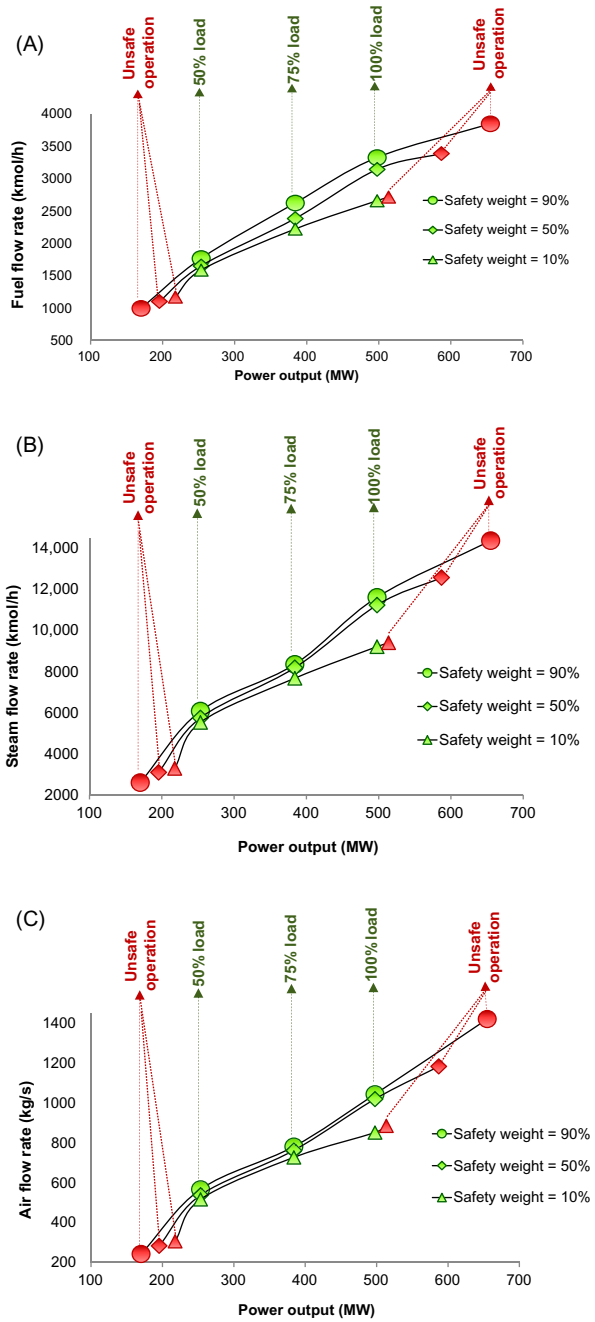

FIGURE 8.7

(A) The safe range of fuel-flow rate. (B) The safe range of steam flow rate. (C) The safe range of air flow rate [37].

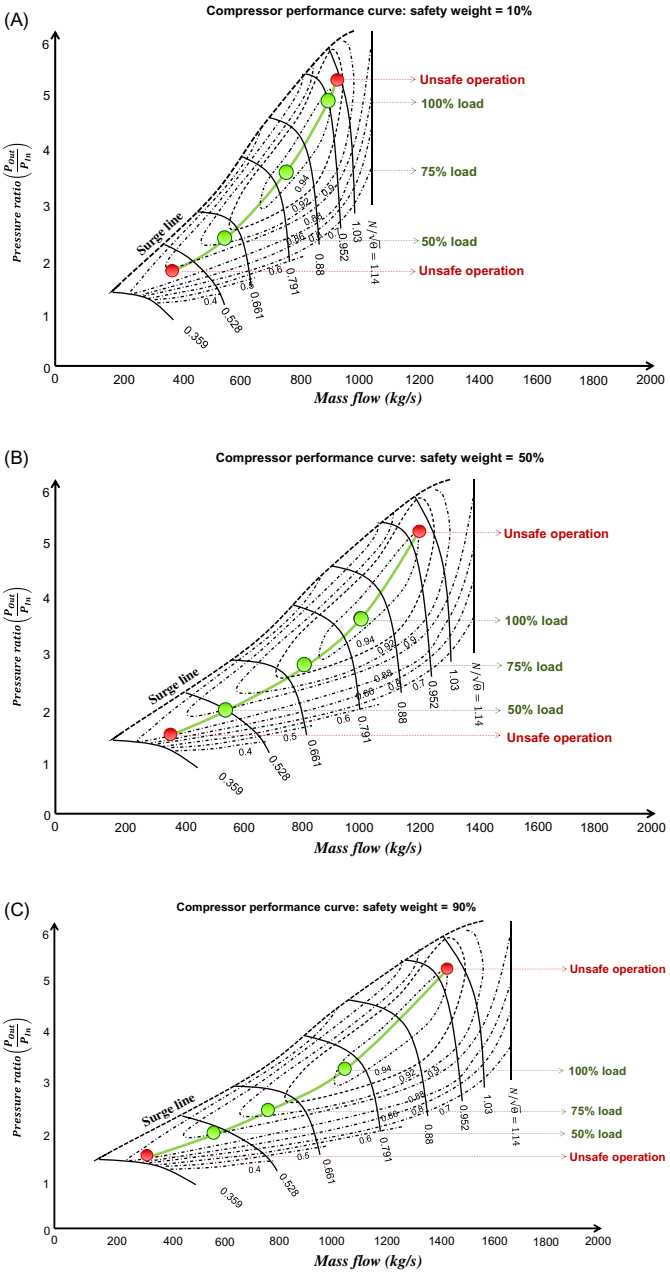

FIGURE 8.8

The safe range of air flow rate: (A) $W_{\text{Safety}} = 10\%$, (B) $W_{\text{Safety}} = 50\%$, and (C) $W_{\text{Safety}} = 90\%$ [37].

the necessity for considering safety aspects at the process design stage. Considering our critical review of the literature, the following points are noted:

1. Degradation of SOFC process equipment has a significant impact on the economic performance and durability of this technology. Nevertheless, most of the reviewed fault mechanisms are irreversible and do not exhibit a unique symptom. Development of noninvasive monitoring methods that enable real-time condition-based monitoring is a research frontier.
2. Fuel variability is one of the greatest advantages of SOFC systems. However, it also poses a significant challenge toward process safety as different fuels exhibit very different hazardous properties and very different failure mechanisms and, therefore, would require significantly different strategies for mitigating the associated risks.
3. SOFCs and associated processes are subject to many variabilities including the external load, but also the change in the behaviors of the fuel cell itself during its lifetime. Designing control strategies that dynamically adapt to the process conditions and devise appropriate safety measures to protect the process equipment from premature degradations can deliver great economic impact.
4. Finally, and most importantly, safe process operations strongly depend on SOFC design. Ignoring safety aspects at the design stage would require expensive modifications at the operational stage or may even render the process operation unsafe. Therefore the safety aspect should be systematically applied in the design of SOFC processes.

References

[1] L. Barelli, E. Barluzzi, G. Bidini, Diagnosis methodology and technique for solid oxide fuel cells: a review, Int. J. Hydrogen Energy 38 (12) (2013) 5060–5074.
[2] L. Liu, G.-Y. Kim, A. Chandra, Modeling of thermal stresses and lifetime prediction of planar solid oxide fuel cell under thermal cycling conditions, J. Power Sources 195 (8) (2010) 2310–2318.
[3] V. Zaccaria, D. Tucker, A. Traverso, A distributed real-time model of degradation in a solid oxide fuel cell, part II: analysis of fuel cell performance and potential failures, J. Power Sources 327 (2016) 736–742.
[4] M. Halinen, Improving the Performance of Solid Oxide Fuel Cell Systems, Aalto University, 2015.
[5] M. Saied, K. Ahmed, M. Ahmed, M. Nemat-Alla, M. El-Sebaie, Investigations of solid oxide fuel cells with functionally graded electrodes for high performance and safe thermal stress, Int. J. Hydrogen Energy 42 (24) (2017) 15887–15902.
[6] D. Yan, et al., Performance degradation and analysis of 10-cell anode-supported SOFC stack with external manifold structure, Energy 125 (2017) 663–670.
[7] X. Wu, D. Gao, Fault tolerance control of SOFC systems based on nonlinear model predictive control, Int. J. Hydrogen Energy 42 (4) (2017) 2288–2308.

[8] A. Esposito, L. Russo, C. Kändler, C. Pianese, B. Ludwig, N.Y. Steiner, High fuel utilization in solid oxide fuel cells: experimental characterization and data analysis with continuous wavelet transform, J. Power Sources 317 (2016) 159–168.
[9] X. Wu, Q. Ye, Fault diagnosis and prognostic of solid oxide fuel cells, J. Power Sources 321 (2016) 47–56.
[10] P. Polverino, A. Esposito, C. Pianese, B. Ludwig, B. Iwanschitz, A. Mai, On-line experimental validation of a model-based diagnostic algorithm dedicated to a solid oxide fuel cell system, J. Power Sources 306 (2016) 646–657.
[11] P. Polverino, C. Pianese, M. Sorrentino, D. Marra, Model-based development of a fault signature matrix to improve solid oxide fuel cell systems on-site diagnosis, J. Power Sources 280 (2015) 320–338.
[12] HSE, Fuel *Cells*: Understand the *Hazards*, *Control* the *Risks*, Great Britain Health and Safety Executive, 2004.
[13] A. Lanzini, et al., DEMOnstration of large SOFC system fed with biogas from WWTP, 2016.
[14] N.F. Harun, D. Tucker, T.A. Adams, Impact of fuel composition transients on SOFC performance in gas turbine hybrid systems, Appl. Energy 164 (2016) 446–461.
[15] N.F. Harun, D. Tucker, T.A. Adams II, Technical challenges in operating an SOFC in fuel flexible gas turbine hybrid systems: coupling effects of cathode air mass flow, Appl. Energy 190 (2017) 852–867.
[16] M. Liu, A. Lanzini, W. Halliop, V.R.M. Cobas, A.H.M. Verkooijen, P.V. Aravind, Anode recirculation behavior of a solid oxide fuel cell system: a safety analysis and a performance optimization, Int. J. Hydrogen Energy 38 (6) (2013) 2868–2883.
[17] X. Lv, C. Lu, X. Zhu, Y. Weng, Safety analysis of a solid oxide fuel cell/gas turbine hybrid system fueled with gasified biomass, J. Fuel Cell Sci. Technol. 12 (1) (2018) 011008–011008-6.
[18] L. Zhang, X. Li, J. Jiang, S. Li, J. Yang, J. Li, Dynamic modeling and analysis of a 5-kW solid oxide fuel cell system from the perspectives of cooperative control of thermal safety and high efficiency, Int. J. Hydrogen Energy 40 (1) (2015) 456–476.
[19] M. Peksen, Safe heating-up of a full scale SOFC system using 3D multiphysics modelling optimisation, Int. J. Hydrogen Energy 43 (1) (2018) 354–362.
[20] M. Halinen, O. Thomann, J. Kiviaho, Experimental study of SOFC system heat-up without safety gases, Int. J. Hydrogen Energy (2014).
[21] M. Engelbracht, R. Peters, W. Tiedemann, I. Hoven, L. Blum, D. Stolten, An on-demand safety gas generator for solid oxide fuel cell and electrolyzer systems, Fuel Cells 17 (6) (2017) 882–889.
[22] M. LI, A.D. Rao, J. Brouwer, G.S. Samuelsen, Design of highly efficient coal-based integrated gasification fuel cell power plants, J. Power Sources 195 (17) (2010) 5707–5718.
[23] C. Stiller, B. Thorud, O. Bolland, Safe dynamic operation of a simple SOFC/GT hybrid system, J. Eng. Gas Turbines Power 128 (3) (2006) 551.
[24] M. Halinen, A. Pohjoranta, J. Pennanen, J. Kiviaho, Stack temperature estimation in system environment by utilizing the design of experiments methodology, ECS Trans. 57 (1) (2013) 205–214.
[25] V. Zaccaria, D. Tucker, A. Traverso, Operating strategies to minimize degradation in fuel cell gas turbine hybrids, Appl. Energy 192 (2017) 437–445.
[26] V. Zaccaria, D. Tucker, A. Traverso, A distributed real-time model of degradation in a solid oxide fuel cell, part I: model characterization, J. Power Sources 311 (2016) 175–181.

[27] X. Lv, X. Liu, C. Gu, Y. Weng, Determination of safe operation zone for an intermediate-temperature solid oxide fuel cell and gas turbine hybrid system, Energy 99 (2016) 91–102.
[28] S. Campanari, L. Mastropasqua, M. Gazzani, P. Chiesa, M.C. Romano, Predicting the ultimate potential of natural gas {SOFC} power cycles with {CO_2} capture – Part B: applications, J. Power Sources 325 (2016) 194–208.
[29] S. Campanari, L. Mastropasqua, M. Gazzani, P. Chiesa, M.C. Romano, Predicting the ultimate potential of natural gas SOFC power cycles with CO_2 capture – Part A: Methodology and reference cases, J. Power Sources 324 (2016) 598–614.
[30] M.L. Ferrari, A.F. Massardo, Cathode–anode side interaction in SOFC hybrid systems, Appl. Energy 105 (2013) 369–379.
[31] M. Sharifzadeh, Integration of process design and control: a review, Chem. Eng. Res. Des. 91 (12) (2013) 2515–2549.
[32] M. Sharifzadeh, Implementation of a steady-state inversely controlled process model for integrated design and control of an ETBE reactive distillation, Chem. Eng. Sci. 92 (2013) 21–39.
[33] M. Sharifzadeh, N. Shah, Carbon capture from natural gas combined cycle power plants: solvent performance comparison at an industrial scale, AIChE J. 62 (1) (2016) 166–179.
[34] M. Sharifzadeh, P. Bumb, N. Shah, Carbon capture from pulverized coal power plant (PCPP): solvent performance comparison at an industrial scale, Appl. Energy 163 (2016) 423–435.
[35] S. Mahdi, X. Wang, N. Shah, Interactions between the design and operation of shale gas networks, including CO_2 sequestration, Engineering 3 (2) (2017) 244–256.
[36] M. Sharifzadeh, N. Shah, MEA-based CO_2 capture integrated with natural gas combined cycle or pulverized coal power plants: operability and controllability through integrated design and control, J. Clean. Prod. 207 (2019) 271–283.
[37] M. Sharifzadeh, M. Meghdari, D. Rashtchian, Multi-objective design and operation of solid oxide fuel cell (SOFC) triple combined-cycle power generation systems: integrating energy efficiency and operational safety, Appl. Energy 185 (2017) 345–361.

PART

2

Economic and Environmental Perspectives for Potential Application Areas

This page intentionally left blank

CHAPTER

Fuel variability and flexible operation of solid oxide fuel cell systems

9

Mahdi Sharifzadeh[1,2] **and Nilay Shah**[1]

[1]*Department of Chemical Engineering, Centre for Process Systems Engineering (CPSE), Imperial College London, London, United Kingdom*

[2]*Sharif Energy Research Institute, Sharif University of Technology, Tehran, Iran*

9.1 Introduction

Table 9.1 summarizes representative research in the field of the application of various fuels to feed solid oxide fuel cells (SOFCs). This table suggests that SOFCs offer a high degree of flexibility for using various feedstocks including biorenewables as well as conventional fuels for stationary and mobile applications. The flexibility of SOFCs to accept a variety of fuels has important implications for the diversification of their applications. In addition it opens up new avenues to enhance the sustainability of energy infrastructure and mitigate greenhouse-gas emissions. Liquid and solid fuels facilitate energy storage for remote applications. Such flexibility, of course, comes at the price of dealing with a more complex range of fuel contaminants that can cause poisoning or performance degradation of the fuel-cell stacks. In addition it has implications for the process configurations and their operating conditions. These complications are the focus of this chapter.

9.2 Synthesis gas, carbon oxides, and hydrogen as solid oxide fuel cell fuels

Synthesis gas (syngas), which is a mixture of carbon oxides (CO and CO_2) hydrogen, and water, is perhaps the most studied fuel for SOFCs. This observation should be attributed to the fact that most of the reforming and gasification technologies produce mixtures with similar compositions. However, the high variability of contaminants in various syngas compositions has implications for SOFC performance and will be discussed in this section.

Nagel et al.[24] studied the interactions between heat transfer, mass transfer, and charge within SOFCs for various compositions of syngases. They observed

Design and Operation of Solid Oxide Fuel Cells. DOI: https://doi.org/10.1016/B978-0-12-815253-9.00009-4

Table 9.1 Representative studies on fuel variabilities in solid oxide fuel cell technologies.

Contributor	Feedstock	Focus	Refs.
Stoeckl et al.	Humidified methane and carbon monoxide	Carbon deposition in auxiliary power units (APUs)	[1]
Lo Faro et al.	Methanol, ethanol, propane, glycerol	Fuel flexibility for remote and distributed or portable applications	[2]
Lanzini et al.	Biogas	Internal reforming and inhibiting carbon deposition/dealing with contaminants	[3,4]
Kim et al.	Dual-fuel (natural gas and liquefied petroleum gas)	Prereformer to convert C_2^+ to a CH_4-rich fuel stream	[5]
Kupecki	Dimethyl ether (DME)	Performance analyzing by variation of electrical load, fuel, and oxidant utilization	[6]
Cocco and Tola	Methanol and DME	Lower temperature reforming; enhancing energy efficiency	[7]
Saunders et al.	Liquid hydrocarbon fuels such as ethanol or isooctane	Carbon deposition on microtubular SOFC for hybrid vehicle applications	[8]
Yi et al.	Natural gas, biogas, the products of biomass and coal gasification, and distillate fuel	Thermodynamic analysis of fuel variability	[9]
Stelter et al.	Diesel reformate	A thermally self-sustaining APU applied in a vehicle	[10]
Doherty et al.	Biomass gasification	Investigating operating conditions and integration method	[11]
Cocco and Tola	Methane, methanol, ethanol, and DME	Low-temperature reforming and enhanced energy-conversion efficiency	[12]
Xu et al.	Diesel and jet fuels	Small-scale autothermal reforming, steam reforming, and partial oxidation reforming	[13]
Cinti and Desideri	Urea	Energy efficiency analysis	[14]
Harun et al.	Syngas	The implications of SOFC fuel variation on the constant-speed operation of the integrated gas turbine	[15]
Recalde et al.	Fecal-sludge	Superheated steam-dryer and multistage gasifier to overcome challenges of energy generation from fecal-sludge using SOFCs	[16]
Aravind and de Jong	Biomass	High-temperature cleaning of biomass gasification products	[17]

(*Continued*)

Table 9.1 Representative studies on fuel variabilities in solid oxide fuel cell technologies. *Continued*

Contributor	Feedstock	Focus	Refs.
Colpan et al.	Humidified hydrogen	Transient heat transfer during heat-up and transient operations	[18]
Schluckner et al.	Diesel reformat	Mobile applications	[19]
Ozcan and Dincer	Biomass	Products of various biomass gasification technologies, namely bubbling fluidized bed, circulating fluidized bed, and dual fluidized bed gasifiers	[20]
Santin et al.	Methanol and kerosene	Four process configurations taking required processing steps into account	[21]
Rokni	Ammonia, hydrogen, methanol, ethanol, DME and biogas	Anode off-gas recirculation for various fuels	[22]
Horiuchi et al.	*n*-Butane	In situ catalytic partial oxidation	[23]

that considerable amounts of methane promote steam reforming−reaction pathways, which additionally disturb the mass and energy balances of the system. They reported that the effect of fuel variations is more significant than geometrical or material-related phenomena.

Zabihian and Fung [25] reported efficiencies of 74.6% and 73.9% for a hybrid SOFC power plant with and without anode circulation for pure methane fuel. Compared to the base case of pure methane the performance of the SOFC decreases when other syngas compounds such as H_2, CO_2, CO, and N_2 were introduced.

The application of carbonaceous fuels can result in carbon deposition on anodes. Stoeckl et al. [1] studied such degradation effects by measuring the electrochemical impedance, gas composition, and temperature in the anodes. They reported that while a fuel mixture containing methane, steam, and nitrogen offers better performance compared to a syngas consisting of carbon monoxide, steam, and nitrogen, the former also resulted in sharp cell degradation. Methane cracking was blamed for carbon deposition and high-polarization resistance.

While the high-operating temperature of SOFCs allows decomposition of hydrocarbons and minimizes the capital costs and process complexities, such benefits come at the price of higher carbon decomposition risk. Baldinelli et al. [26] reported that regulating the oxygen-to-carbon ratio through air addition and partial CO_2 separation is efficient in preventing such degradation.

Homel et al. [27] studied the application of CO as the primary fuel of SOFCs. They reported a power density of 0.67 W/cm^2, which is comparable with hydrogen-fed SOFCs.

Li and Weng [28] studied the operation of a methane-based SOFC with pure hydrogen and ethanol. They reported an electrical efficiency of 62.29% for methane, 56.59% for hydrogen, and 60.5% for ethanol. Since the methane-based SOFC was designed for internal reforming of methane, in the absence of such endothermic reactions significantly higher radial temperatures were observed for nondesign fuels. Therefore thermal management has an important role in multiple fuel operation. Li and Weng [28] reported that the lost output power can be compensated by using auxiliary fuel and bypassing the exhaust gases around the fuel preheater. However, such strategies would reduce the overall net energy efficiency to 45%.

9.3 Biogas as solid oxide fuel cell fuel

Biogas, which is generally a mixture of methane, CO_2, and small amounts of hydrogen sulfide, is produced through anaerobic digestion or fermentation of biodegradable materials such as agricultural and municipal wastes [29]. Biogas as a renewable fuel has shown promise in enhancing the sustainability of energy infrastructure. Moreover, due to the similarity of biogas with natural gas (NG) and syngas components, it is highly compatible with existing SOFC technologies.

Chiodo et al. [30] studied biogas reforming processes through steam reforming, autothermal reforming, and partial oxidation (POx). They reported an overall efficiency in the range of 62%−52% with steam reforming as the best option and followed by autothermal reforming. The poor performance of POx was due to the reverse gas-shift reaction.

De Lorenzo et al. [31] studied the application of dry biogas in an intermediate-temperature SOFC. In this configuration, methane is consumed through partial and total oxidation reactions without the need for a reforming gas such as steam, oxygen, or CO_2. The anode was protected by a Ni−Fe/CGO layer and was applied in a cogenerative configuration with anode-exhaust recirculation. Three compositions ranging from methane-rich to CO_2-rich biogas were considered. The biogas with high or intermediate-methane content showed the risk of carbonation at the fuel-cell inlet due to cracking chemical reactions. However, the CO_2-rich biogas did not suffer from the risk of carbon deposition as the Boudouard chemical reaction was dominant.

Papurello et al. [32] studied the technical feasibility of power generation from biogas using a lab-scale test rig, including a cleaning unit, reformer (at 700°C), and short SOFC stack. They applied a mixture of 60% methane, 40% carbon dioxide, and 30 ppmv of hydrogen sulfide in order to simulate biogas conditions. A moderate

amount of steam was added to inhibit carbon deposition. The process showed stability against H_2S contamination and with a performance comparable to hydrogen fuel.

Chatrattanawet et al. [33] compared internal and external reforming of biogas using thermodynamic analysis. The chemical equilibrium conditions were calculated by minimizing the mixture's Gibbs free energy. They identified the optimal reformer temperature to be 973K with a steam-to-carbon ratio of 0.5. The optimal operating conditions of the SOFC that established a good compromise between power density and electrical efficiency was 173K, 3 atm, and 5000 A/m^2 for internal and external reforming configurations.

9.4 Biomass as solid oxide fuel cell fuel

Biomass is a renewable source of energy that is more geographically dispersed than fossil fuels. The diversified and abundant biomass resources promote it as a promising renewable fuel. The integration of biomass technologies with SOFCs for power generation offers an alternative and highly efficient pathway to electricity that does not involve direct combustion, with potentially positive economic and environmental impacts. However, such application requires biomass gasification and gas treatment in order to suppress contaminants such as H_2S, HCl, and alkali components like tar and particulates [34].

Jia et al. [35] studied the operating conditions of a downdraft gasifier integrated with SOFCs and a gas turbine (GT). They reported that char conversion increases with a decrease in biomass moisture content and increasing the equivalence ratio (the ratio of airflow rate to its stoichiometric value), which could be attributed to the higher temperature at the reduction zone. Although decreasing the biomass flowrate is favorable for char conversion and overall system efficiency it comes at the price of higher capital costs.

Wongchanapai et al. [36] studied the influence of decision variables such as the steam-to-biomass ratio (STBR), SOFC inlet temperatures, fuel utilization, and anode-recirculation rate on system performance and the number of cells in the SOFC stack. They observed that the STBR improves the SOFC performance while deteriorating the gasifier performance, where a trade-off was established for STBR around the value of 1.5. Increasing the SOFC temperature showed a negative impact on the gasifier performance, but a slight improvement on the SOFC performance was observed, and it would require a smaller number of cells. They reported 0.75 and 0.6 for the fuel utilization factor and anode off-gas recirculation rate, respectively.

Pieratti et al. [37] studied a biomass gasification process with a catalytic filter to purify syngas. A hydrogen concentration of up to 60% was reported. They emphasized the need for gas cleaning to remove tar and H_2S.

Hosseinpour et al. [38] proposed an integrated system for the cogeneration of electricity and a cooling service that consisted of a downdraft fixed-bed wood gasifier integrated with SOFCs. The exhaust gases were applied in a Goswami

cycle, which is a combination of a Kalina cycle and ammonia–water absorption refrigeration. They reported that the bottoming cycle (Goswami) increased the overall power output with an additional cooling effect. The values of 58.5% and 33.7% were reported for the overall energy and exergy efficiencies, respectively. The authors reported the highest exergy destruction in the gasification reactor, boiler, and second air–heat exchanger. Increasing the boiler and rectifier temperatures improved the system efficiencies, but increasing the SOFC current density adversely affected them.

Doherty et al. [11] applied process simulation to study an integrated biomass gasifier–SOFC system for combined heat and power (CHP) generation. They recommended that the steam-to-carbon ratio and moisture content should be as low as possible. The fuel utilization factor is a key decision variable for switching between heat and electricity-generation modes.

Gadsbøll et al. [39] studied a Topsoe SOFC integrated with a commercial two-stage gasifier. The gas-cleaning unit was equipped with a bag filter, carbon filters, and humidification and desulfurization units. They did not detect any tar, but small amounts of sulfur compounds were found. They reported a biomass-to-electricity efficiency of 43%. Part-load operation down to 55% flowrate did not cause any loss in efficiency.

9.5 Coal as solid oxide fuel cell fuel

Coal as a fossil fuel with a low hydrogen to carbon content, is less favorable from the environmental perspective. However, there are abundant coal resources in some countries such as China, and there are already extensive coal-based power generation infrastructure. Therefore, retrofitting such existing facilities with high-efficiency low-emission technologies offers an alternative pathway for the decarbonization of energy industry. While such integrated designs seem essential to achieve ambitious decarbonization targets [40] the key challenge here is to treat the coal contaminations poisonous to SOFC materials.

Kuramoto et al. [41] studied the effects of a coal-based syngas contaminated with trace species such as S, Cl, and Si, on an SOFC with an anode made of NiO and yttria-stabilized zirconia (YSZ). They conducted experiments using a post-CCS, hydrogen-enriched coal syngas with trace amounts of H_2S, HCl, and tetraethylorthosilicate (TEOS). The latter represented Si vapors and could cause performance degradation in the form of increases in the ohmic and polarization resistances. The deposition of Si compounds was observed on the surface and diffusion layers of the anode. The underlying mechanism was attributed to thermal polymerization of TEOS and the formation SiO from SiO_2 under the hydrogen-rich environment. The injection of H_2S resulted in an immediate modest performance degradation. However, long-run H_2S up to 10 ppm was reported to

be tolerable. The HCL impurities up to 10 ppm did not result in appreciable performance loss.

9.6 Methanol, ethanol, dimethyl ether, and butanol as solid oxide fuel cell fuels

Motivation for the application of light alcohols such as methanol, ethanol, and dimethyl ether (DME) to fuel SOFCs is the possibility for external reforming at lower temperatures, which enables better utilization of waste heat in the process. Furthermore, some of alcohols such as ethanol and butanol can be produced from renewable pathways such as fermentation, which improves their environmental footprint. Methanol can also be produced from NG offering a gas-to-liquid path for otherwise difficult-to-transport NG. Finally the ease of storing liquid fuels allows remote and auxiliary applications [42].

Cocco and Tola [7] studied external reforming of DME and methanol in an SOFC system, integrated with a microgas turbine. They identified the steam-to-carbon ratio and reforming temperature as the key influencing parameters on the overall efficiency. The optimum reforming temperature for methanol and DME were reported to be 240°C and 280°C, respectively. Since a low steam-to-carbon ratio can result in carbon deposition, practical values of 1 for methanol and 1.5−2 for DME were chosen. Under these conditions the methanol-fed SOFC gained energy efficiency of 67% and 73%, respectively, for the operating temperatures of 900°C and 1000°C. Similar values were 65% and 69% for the case of DME fuel.

Lo Faro et al. [2] studied a perovskite composite containing dispersed Ni particles for anode electrodes, which enables direct utilization of a range of fuels including methane, methanol, propane, and glycerol. They reported a power density in the range of 250−400 mW/cm^2.

Kupeck [6] studied the off-design operation of a micro-CHP incorporated to an SOFC fed by DME. They reported that air recirculation-blowers had the highest energy consumption within the system. The values of 44% and 80% (lower heating value-based) were estimated for the electrical and overall efficiencies, respectively.

Tippawan et al. [43] studied a trigeneration system providing electricity, heating, and cooling services fueled by ethanol. They estimated at least 32% energy efficiency and 10% exergy efficiency gains compared to conventional power-only systems. They reported fuel utilization in the SOFC as an important parameter, which was sensitive to the trigeneration product ratio. The SOFC and afterburner were reported to be the most important sources of exergy destruction.

Laosiripojana and Assabumrungrat [44] studied the application of methane, methanol, and ethanol for direct internal reforming in an SOFC by employing Ni−YSZ. They reported that methane could be applied for internal reforming

with no risk of carbon deposition. However, for the case of ethanol, even with high-steam-to-carbon ratios, internal reforming was not feasible due to carbon formation. In addition significant amounts of ethane and ethylene were detected due to incomplete reforming. They proposed an indirect internal-reforming configuration in which ethanol was first reformed in a reformer in thermal contact with the anode side of the SOFC. In this configuration the overall system acts as an "autothermal" unit. This configuration offers the option to optimize the catalyst for the SOFC and reformer separately. The reformer temperature was reported to be more than 850°C. Finally, they reported that methanol could be applied even in a direct internal-reforming configuration, if the inlet of the anode chamber had enough space for its homogenous conversion to syngas.

Horiuchi et al. [23] studied in situ catalytic POx in an SOFC system fueled by *n*-butane. In the proposed configuration two anodes were facing each other. The POx of fuel by the heterogeneous reactions taking place in the porous anode provided the SOFC's energy requirements.

Farrell and Linic [45] studied the application of ethanol as a more carbon-neutral fuel from renewable resources. However, oxygenated biofuels put Ni-based anodes at the risk of carbon formation. The authors suggested that introducing a small amount of Sn to the electrocatalyst improved the performance of the anode.

Saebea et al. [46] studied an SOFC system fed by ethanol. They reported that for similar operating conditions, partial anode-exhaust gas recirculation improves the overall electric and thermal efficiencies. They reported that a high circulation ratio and fuel utilization reduce the risk of carbon formation in the reformer and it could be operated at a lower temperature. The trade-off is that the recirculation and fuel utilization variables also affect the electrical efficiency and should be optimized accordingly. The complication is that these variables have a highly nonlinear relationship. For low fuel utilization in the range of 0.5−0.6 the electrical efficiency improves with the recirculation ratio, while for fuel utilization values higher than 0.6 it had the opposite effect.

9.7 Liquid hydrocarbons as solid oxide fuel cell fuel

Liquid fuels are of great interest for utilization in SOFCs due to their high-volumetric energy density and ease of storage, thereby offering new opportunities for mobile and remote applications. Saunders and Kendall [8] studied a range of liquid fuels including methanol, methanoic acid, ethanol, ethanoic acid, butanoic acid, and iso-octane for direct injection into an SOFC system. Using temperature-programmed oxidation they concluded that only methane and methanoic acid could be directly injected into the nickel cermet anode. Even for such fuels a small addition of steam or air was recommended. They also reported that a mixture of iso-octane, water, alcohol, and surfactant lowered the carbon-deposition risk significantly.

Yi et al. [9] studied NG, biogas, syngas from coal-driven sources, and syngas from diesel reformate applied in SOFCs. Although they observed that an SOFC is capable of dealing with a range of syngas compositions, such flexible operation would require a significant change in its operating conditions.

Stelter et al. [10] studied the operation of an auxiliary SOFC with diesel reformate for application in vehicles. Electrolyte supported cells (ESC) were employed and operated at 800°C and a power density of 0.2 kW/L. The process was designed for low-pressure drop at the anode and cathode sides in order to simplify the layout. They reported the technical feasibility of such mobile and modular applications under a thermally, self-sustaining, operating strategy.

Schluckner et al. [19,47] applied three-dimensional computational fluid dynamics (3D-CFD) to study the application of diesel in planar industrial-sized ($100 \times 100\ mm^2$) SOFCs. They justified their choice of modeling method by the complexities associated with simultaneous electrochemical and gas-phase reactions. Their model was validated with in-house experimental data. A key challenge was identified to be the deposition of carbon on the Ni/YSZ anode structure, especially on the anode-inlet region.

Santin et al. [21] compared methanol and kerosene for SOFC−GT hybrid applications. The methanol-fuel system showed better performance due to lower capital and fuel costs.

9.8 Ammonia and urea as solid oxide fuel cell fuels

Ammonia dissociates into N_2 and H_2, and can be applied as a fuel for solid oxide fuels with the advantage of being a carbon-free operation. The decomposition of ammonia is endothermic and enables heat absorption and better control of stack temperature [48]. Cinti et al. studied the application of pure and diluted ammonia. They reported a higher-energy efficiency for the ammonia-fueled SOFC compared to the scenario where pure hydrogen was applied. The higher performance was attributed to the cooling effect of internal ammonia decomposition which reduced the need for the ancillary cooling of the airflow on the cathode side [48].

Urea is widely used as a fertilizer with the advantage of ease of storage and handling. As a low-cost product with a high-energy density it can be retrieved as the by-product of biorefineries and wastewater-treatment facilities. Alternatively it can be produced from hydrogen and captures CO_2 through renewable and environment-friendly technologies, offering a sustainable fuel for SOFCs [14]. Urea can be converted to ammonia and carbon dioxide through thermohydrolysis. Nonetheless it does pose safety concerns associated with the direct use of hydrogen and ammonia [49].

Cinti and Desideri [14] studied urea reforming to feed SOFCs experimentally and then through optimization and modeling. For the operating condition of 800°C and 0.8 fuel utilization, they reported an energy efficiency of 55%.

Abraham and Dincer [49] compared the thermodynamic performance of the direct injection of urea into oxygen ion-conducting SOFCs and hydrogen proton-conducting SOFCs. The process consisted of a SOFC integrated with a GT for CHP generation. They reported the SOFC and combustion chamber as the key points of exergy destruction. The oxygen ion-conducting solid oxide fuel cell (SOFC-O) offered better performance. The lower performance of the hydrogen proton-conducting solid oxide fuel cell (SOFC-H) was attributed to the detrimental influence of inverse water−gas-shift reaction for CO consumption on the anode side.

9.9 Contamination and its implication for fuel flexibility of solid oxide fuel cells

A key challenge for operating SOFCs using various feedstocks is the trace amounts of contaminating materials that could poison the SOFC anode and electrolyte or provoke their degradation. For instance, the application of biomass for fueling SOFCs requires the produced gases to be treated in order to minimize tar formation and remove HCl, H_2S, and alkali materials [17]. In the case of biogas, H_2S needs to be removed. On the other hand, the existence of phosphine in coal-based syngas promotes degradation through the formation of nickel phosphides and surface diffusion of phosphorus that increases electrodic resistance or migration of Ni from the active layer of the anode [50,51].

Rasmussen and Hagen [52] studied the impact of H_2S on Ni−YSZ anodes. Under the operating condition of 850°C and 1 A/cm^2 (current density), they reported the effects of H_2S contamination (2−100 ppm) to be reversible. It was concluded that the poisoning effect was of a chemisorption nature by blocking the Ni particles. However, irreversible changes in the anode microstructure were not detected.

Lanzini et al. [4] discussed that although sulfur-tolerant anodes such as Cu-based electrodes, Ce-based electrodes, and perovskite and double-perovskite anodes were being developed, reduction of SO_x emissions eventually requires the deep removal of sulfur. From the various contaminants present in biogases derived from anaerobic digestion and landfills, siloxanes (organic silicone polymers) showed the most severe and irreversible effects on the reformer and SOFC catalysts. H_2S was blamed for the temporary deactivation of electrocatalysts, while HCl had the least impact.

Nagel et al. [53] studied the impact of thiophene (C_4H_4S) contamination (up to 400 ppm) on SOFC performance. The reductions in the catalyst activity for steam reforming and POx were identified as the underlying mechanism for degradation.

Bao et al. [54,55] studied the effects of coal contaminations such as CH_3Cl, HCl, arsenic (As), phosphorus (P), zinc (Zn), mercury (Hg), cadmium (Cd), and

antimony (Sb) elements on an anode made of nickel, YSZ, and lanthanum strontium manganese oxide over the temperature range of 750°C−850°C. They reported that the arsenic and phosphorous elements resulted in severe degradation of the power density at concentrations over 10 and 35 ppm, respectively. The degradation mechanism of As was to attack the Ni current collector and cause electrical connectivity problems. The phosphorous species caused a significant change in the surface morphology of the anode. CH_3Cl and Cd only resulted in power density loss when the temperature was above 800°C. Other vaporized elements resulted in degradations of less than 1%.

Coyle et al. [56] studied the effect of arsenic contamination in a coal-driven syngas on a nickel/zirconia SOFC anode. The concentration of arsenic species was up to 10 ppm and the SOFC was operated in temperatures in the range of 700°C−800°C. They observed that strong interactions between nickel and arsenic resulted in nickel−arsenic solid solutions, namely Ni_5As_2 and $Ni_{11}As_8$. The main mode of degradation was the loss of electrical connectivity, which occurs well before the entire anode converts to nickel arsenide. The rate of degradation was not dependent on the current density or fuel utilization. The time to failure was proportional to the reciprocal square root of arsenic partial pressure, suggesting a diffusion-based, rate-limiting step.

Although the integration of biomass gasification with SOFCs offers a renewable pathway to sustainable power generation, complications also arise from its product contaminants. In addition to sulfur compounds, there are also concerns regarding particulate matters and tar. It is recommended that particles should be reduced to a few ppmw as their size matches with the anode pores and can potentially block them [34]. Although tar is not poisonous it may result in carbon formation and anode catalyst deactivation, which is also a function of operating conditions such as steam-to-carbon ratio, current density, and temperature. Hot cleaning of particulate matter or separation using ceramic and sintered filters are recommended. Otherwise, when particle removal is conducted below 450°C, tar should be removed first as it will condense [34].

9.10 The implications of fuel variability for fuel-cell materials

Conventionally the SOFC electrolytes are made of oxygen ion-conducting ceramics. The application of proton-conducting materials in the electrolyte relocates the place of water formation from the anode electrode to the cathode electrode, thereby allowing high fuel utilization. In addition, high-hydrogen concentration allows a higher Nernst potential in the new configuration [57]. For methane fuel, Ni [57] demonstrated that oxygen ion-conducting SOFCs generally have superior performance compared to proton-conducting SOFCs, which could be attributed to the electrochemical oxidation of CO in the former type. However, for high-

operating potential, when the contribution of CO fuel is smaller, proton-conducing SOFCs outperform [57]. The implication of an electrolyte-type option for other fuel types is yet to be investigated.

Hou et al. [58] studied the direct application of (premium) gasoline in SOFCs without external reforming. They applied an MoO_2-based anode for a range of operating conditions including an open-cell voltage of 0.94 V and maximum power density of 31 mW/cm^2 at 0.45 V. The key feature of molybdenum dioxide is its metallic-like conductivity leading to high-catalytic activity for POx of liquid fuels such as jet-A fuel, iso-octane, and *n*-dodecane. In addition its selective transport properties reduce the risk of carbon formation.

9.11 The implications of fuel variability for process configuration

The high-operating temperature (800°C−900°C) of SOFCs enables internal reforming of fuels at the stack. However, it has been widely observed that reforming the fuel at a lower temperature could result in higher overall energy-conversion efficiency [12]. For instance, the reforming temperature of methanol and DME is in the range of 250°C−350°C, which enables the use of waste heat.

Kim et al. [5] applied a prereformer to enable dual-fuel operation of a 1 kW SOFC power package by using NG and liquefied petroleum gas (LPG). They reported that for the proposed process configuration, the NG:LPG ratio did not have a significant effect on the stable performance of the SOFC stack.

Manenti et al. [59] proposed the application of a trireforming process for a biogas-driven SOFC. The trireformer supports all the three reactions of dry reforming, steam reforming, and POx. Their developed model showed good agreement with experimental data at microscales.

Anode recirculation and fuel utilization have profound implications for the energy efficiency of SOFCs. Rokni studied anode off-gas recirculation for various fuels including ammonia, hydrogen, methanol, ethanol, DME, and biogas. It was observed that fuel recycling strongly depends on the utilized fuel. No recycling was recommended for ammonia, while 20% recycling was beneficial for pure hydrogen. For the cases of methanol, ethanol, and DME fuels high fuel utilization requires low-anode recirculation, and vice versa [22].

Toonssen et al. [60] studied alternative system configurations for integrating biomass gasification and SOFCs. The options for biomass gasifiers were atmospheric indirect-steam gasification and pressurized direct-air gasification. Gasification products were cleaned in low-temperature and high-temperature units. Two scales of 100 kW_e and 30 MW_e were studied. The results suggested that a large-scale process system consisting of pressurized direct-air gasification and high-temperature gas-cleaning units gained a high exergy efficiency of 49.9%. The large-scale process had a better efficiency compared to small-scale

systems. In addition, high-temperature gas cleaning had slightly better performance (0.5%).

To achieve high efficiency for coal utilization in SOFC systems, Li et al. [40] proposed a process configuration including a catalytic hydro-gasifier, low-temperature gas cleaning, and an integrated SOFC−turbine section. In the proposed process, humidified decarbonized anode exhaust was recycled back to the gasification unit. The SOFC was operated at the pressure of 10 bars. This also required the cathode to operate at a similar pressure, as thin SOFCs cannot tolerate higher pressure differences. The authors emphasized that achieving electrical efficiencies as high as 60% (HHV basis) required the gasification unit to produce a syngas containing at least 35% (dry-molar basis) methane, low-exit temperature for syngas, free of tar and oil, and with a carbon conversion of 90% or more. They reported the requirements for SOFCs to operate at 10 bars, separated anode and cathode flows, and application of internal reforming to minimize the excess air.

Saebea et al. [61] studied an integrated SOFC−GT hybrid system fed by ethanol. Two alternative heat recovery strategies were studied, that is, using a recuperative heat exchanger (RHE) or through cathode-exhaust recirculation. They reported that cathode-exhaust recirculation minimized the need for fresh-air compression. In addition, the heat recovered from the SOFC was sufficient for preheating the air and the fuel-preprocessing unit. By comparison the configuration using RHE required an external source of energy. Increasing the SOFC pressure and fuel utilization increased the efficiency of the process with cathode recirculation, while decreasing that in the configuration utilizing RHE. The reason for the lower performance of the RHE process was the need to increase airflow to control the SOFC temperature. In addition the inlet temperature of the turbine decreases, which affects overall energy efficiency.

Recalde et al. [16] studied fecal-sludge gasification to fuel SOFCs. The challenge is to treat the involved contaminants such as tar and overcome intensive energy requirements due to endothermic gasification reactions as well as water-content removal. Their proposed process included a superheated steam-dryer combined with an indirectly heated multistage gasifier. The required heat was supplied from a microwave plasma torch and heat integrated with the existing process streams. An overall efficiency of 65% was reported. The authors suggested that the proposed integrated gasification-SOFC process offers a more energy-efficient pathway compared to rival technologies such as biochar production through pyrolysis, with additional sanitation application.

9.12 The implication of fuel variability for process control

Harun et al. [15] studied the transient operation of fuel change from a coal-derived syngas to methane fuel. They analyzed the technical feasibility of a swift

fuel switch and the interactions between the operating variables. They reported that a step-change switch between syngas and a humidified methane (14% CH_4) to reach a new steady-state within 2 hours was feasible, with no risk of violating SOFC safety constraints, compressor surge, or stall. They observed that such transition resulted in 17% thermal release in a timespan of milliseconds. They suggested that thermal management by air recirculation in the cathode could mitigate undesirable transient effects.

Zhou et al. [62] studied the effect of fuel composition for cathode airflow regulation. The cathode airflow is often applied as a manipulated variable for thermal management of an SOFC−GT. They observed that controllability and observability are strong functions of the fuel composition. Therefore constant values for controller gain could result in operational instability. They observed that the estimated values of the gain and poles for the transfer functions differ up to 20% for syngas and humidified hydrogen. They also reported two-way disturbance propagation between cathode airflow and turbine speed. The authors recommended advanced control strategies such as gain scheduling and adaptive control, although further investigation was called for.

Li et al. [40] studied integrated coal gasification with a hybrid SOFC/turbine system. They suggested that adding a methanation reactor operating at an elevated pressure in the reactor/expander cycle path gave good control of the syngas composition. Another consideration is that in coal-based processes similar to their methane counterparts, exhaust gas expanders do not produce enough power to completely cover the energy consumption in the air compressor. The power deficit requires a motor and complicates the transient operation. The authors suggested that separate shafts would ease process control, especially for off-design operations and start-up or shut-downs.

Kupecki [6] studied the off-design operation of a micro-CHP integrated with an SOFC stack fueled by DME. They reported that for the SOFC stack comprising two 1.3 kW (each cell), 10 hours was needed to reach the full-power capacity from a cold state. In order to maximize energy efficiency and minimize the need for power import, low-oxidant utilization was recommended. Manipulation of fuel utilization was reported less important. This observation was attributed to the high power consumption of the air blower.

Santin et al. [21] compared the application of methane, methanol, and kerosene under four process configurations. On the cathode (air) side, one layout employed a high-temperature heat exchanger and the other the recirculation of the burner exhaust to achieve the required air temperature at the cathode inlet. Similarly for the anode side, the fuel processing (reforming) was either in the anode recycle path or external to it. They reported that the process fuel by methanol offered better economics. The external reformer showed a higher efficiency, but both internal and external reforming had similar economic performance. Overall, between the four process configurations and three considered fuels, the methanol-fueled process with an external reformer and high-temperature heat exchanger offered the best option.

9.13 Conclusion

Fuel diversity and flexibility are the key advantages of SOFCs to promote their commercialization, especially for small-to-medium size applications. In particular, they can play an important role in the transition from fossil fuels to more sustainable and renewable options. However, this opportunity comes at the price of more complicated processing requirements. Based on the critical review presented in this chapter, the following potent research directions are recommended:

1. Contaminations are the key challenge for flexible fueling SOFC systems. The diversity of alternative feedstock options adds to this complexity. The impacts of many of these associated impurities on the SOFC's material lifetime, corresponding degradation mechanism and detection signature, and required loss-prevention procedure remain as research frontiers.
2. Evidenced by various studies reviewed in this chapter, fuel transition may require significant changes in the operating conditions and potentially may require the inclusion of auxiliary process equipment. Developing process systems capable of utilizing multiple fuels requires methodologies that enable the quantification of various performance metrics (energetic, environmental, economic, etc.) and systematic decision-making regarding the design and operation of SOFC technologies.
3. Regardless of the effects of contaminants on SOFC operation and lifetime, meeting environmental protection targets would require significant fuel preprocessing and remains a research frontier.

References

[1] B. Stoeckl, V. Subotić, D. Reichholf, H. Schroettner, C. Hochenauer, Extensive analysis of large planar SOFC: operation with humidified methane and carbon monoxide to examine carbon deposition based degradation, Electrochim. Acta 256 (2017) 325–336.

[2] M. Lo Faro, V. Antonucci, P.L. Antonucci, A.S. Aricò, Fuel flexibility: a key challenge for SOFC technology, Fuel 102 (2012) 554–559.

[3] A. Lanzini, P. Leone, Experimental investigation of direct internal reforming of biogas in solid oxide fuel cells, Int. J. Hydrogen Energy 35 (6) (2010) 2463–2476.

[4] A. Lanzini, et al., Dealing with fuel contaminants in biogas-fed solid oxide fuel cell (SOFC) and molten carbonate fuel cell (MCFC) plants: degradation of catalytic and electro-catalytic active surfaces and related gas purification methods, Prog. Energy Combust. Sci 61 (2017) 150–188.

[5] Y. Kim, S.-A. Hong, S. Nam, S.-H. Seo, Y.-S. Yoo, S.-H. Lee, Development of 1 kW SOFC power package for dual-fuel operation, Int. J. Hydrogen Energy 36 (16) (2011) 10247–10254.

[6] J. Kupecki, Off-design analysis of a micro-CHP unit with solid oxide fuel cells fed by DME, Int. J. Hydrogen Energy 40 (35) (2015) 12009–12022.

[7] D. Cocco, V. Tola, Externally reformed solid oxide fuel cell−micro-gas turbine (SOFC−MGT) hybrid systems fueled by methanol and di-methyl-ether (DME), Energy 34 (12) (2009) 2124−2130.
[8] G. Saunders, J. Preece, K. Kendall, Formulating liquid hydrocarbon fuels for SOFCs, J. Power Sources 131 (1) (2004) 23−26.
[9] Y. Yi, A.D. Rao, J. Brouwer, G.S. Samuelsen, Fuel flexibility study of an integrated 25 kW SOFC reformer system, J. Power Sources 144 (1) (2005) 67−76.
[10] M. Stelter, A. Reinert, B.E. Mai, M. Kuznecov, Engineering aspects and hardware verification of a volume producable solid oxide fuel cell stack design for diesel auxiliary power units, J. Power Sources 154 (2) (2006) 448−455.
[11] W. Doherty, A. Reynolds, D. Kennedy, Process simulation of biomass gasification integrated with a solid oxide fuel cell stack, J. Power Sources 277 (2015) 292−303.
[12] D. Cocco, V. Tola, Use of alternative hydrogen energy carriers in SOFC−MGT hybrid power plants, Energy Convers. Manag. 50 (4) (2009) 1040−1048.
[13] X. Xu, P. Li, Y. Shen, Small-scale reforming of diesel and jet fuels to make hydrogen and syngas for fuel cells: a review, Appl. Energy 108 (2013) 202−217.
[14] G. Cinti, U. Desideri, SOFC fuelled with reformed urea, Appl. Energy 154 (2015) 242−253.
[15] N.F. Harun, D. Tucker, T.A. Adams, Impact of fuel composition transients on SOFC performance in gas turbine hybrid systems, Appl. Energy 164 (2016) 446−461.
[16] M. Recalde, T. Woudstra, P.V. Aravind, Renewed sanitation technology: a highly efficient faecal-sludge gasification−solid oxide fuel cell power plant, Appl. Energy 222 (2018) 515−529.
[17] P.V. Aravind, W. de Jong, Evaluation of high temperature gas cleaning options for biomass gasification product gas for solid oxide fuel cells, Prog. Energy Combust. Sci 38 (6) (2012) 737−764.
[18] C.O. Colpan, F. Hamdullahpur, Transient heat transfer modeling of a solid oxide fuel cell operating with humidified hydrogen, Int. J. Hydrogen Energy 36 (17) (2011) 11488−11499.
[19] C. Schluckner, V. Subotić, V. Lawlor, C. Hochenauer, Three-dimensional numerical and experimental investigation of an industrial-sized SOFC fueled by diesel reformat − Part II: detailed reforming chemistry and carbon deposition analysis, Int. J. Hydrogen Energy 40 (34) (2015) 10943−10959.
[20] H. Ozcan, I. Dincer, Performance evaluation of an SOFC based trigeneration system using various gaseous fuels from biomass gasification, Int. J. Hydrogen Energy 40 (24) (2015) 7798−7807.
[21] M. Santin, A. Traverso, L. Magistri, A. Massardo, Thermoeconomic analysis of SOFC−GT hybrid systems fed by liquid fuels, Energy 35 (2) (2010) 1077−1083.
[22] M. Rokni, Addressing fuel recycling in solid oxide fuel cell systems fed by alternative fuels, Energy 137 (2017) 1013−1025.
[23] M. Horiuchi, et al., Performance of a solid oxide fuel cell couple operated via in situ catalytic partial oxidation of *n*-butane, J. Power Sources 189 (2) (2009) 950−957.
[24] F.P. Nagel, T.J. Schildhauer, S.M.A. Biollaz, S. Stucki, Charge, mass and heat transfer interactions in solid oxide fuel cells operated with different fuel gases—a sensitivity analysis, J. Power Sources 184 (1) (2008) 129−142.
[25] F. Zabihian, A.S. Fung, Performance analysis of hybrid solid oxide fuel cell and gas turbine cycle (part II): effects of fuel composition on specific work and efficiency, J. Energy Inst. 87 (1) (2014) 28−34.

[26] A. Baldinelli, L. Barelli, G. Bidini, A. Di Michele, R. Vivani, SOFC direct fuelling with high-methane gases: optimal strategies for fuel dilution and upgrade to avoid quick degradation, Energy Convers. Manag. 124 (2016) 492–503.
[27] M. Homel, T.M. Gür, J.H. Koh, A.V. Virkar, Carbon monoxide-fueled solid oxide fuel cell, J. Power Sources 195 (19) (2010) 6367–6372.
[28] Y. Li, Y. Weng, Performance study of a solid oxide fuel cell and gas turbine hybrid system designed for methane operating with non-designed fuels, J. Power Sources 196 (8) (2011) 3824–3835.
[29] Wikipedia, Biogas. <https://en.wikipedia.org/wiki/Biogas>, 2018 (accessed: 20.11.18).
[30] V. Chiodo, et al., Biogas reforming process investigation for SOFC application, Energy Convers. Manag. 98 (July 2015) 252–258.
[31] G. De Lorenzo, et al., Thermoelectric characterization of an intermediate temperature solid oxide fuel cell system directly fed by dry biogas, Energy Convers. Manag. 127 (2016) 90–102.
[32] D. Papurello, et al., Performance of a solid oxide fuel cell short-stack with biogas feeding, Appl. Energy 125 (2014) 254–263.
[33] N. Chatrattanawet, D. Saebea, S. Authayanun, A. Arpornwichanop, Y. Patcharavorachot, Performance and environmental study of a biogas-fuelled solid oxide fuel cell with different reforming approaches, Energy 146 (2018) 131–140.
[34] Z. Ud Din, Z.A. Zainal, Biomass integrated gasification–SOFC systems: technology overview, Renew. Sustain. Energy Rev. 53 (2016) 1356–1376.
[35] J. Jia, A. Abudula, L. Wei, B. Sun, Y. Shi, Effect of operating parameters on performance of an integrated biomass gasifier, solid oxide fuel cells and micro gas turbine system, Biomass Bioenergy 75 (2015) 35–45.
[36] S. Wongchanapai, H. Iwai, M. Saito, H. Yoshida, Performance evaluation of an integrated small-scale SOFC-biomass gasification power generation system, J. Power Sources 216 (2012) 314–322.
[37] E. Pieratti, M. Baratieri, S. Ceschini, L. Tognana, P. Baggio, Syngas suitability for solid oxide fuel cells applications produced via biomass steam gasification process: experimental and modeling analysis, J. Power Sources 196 (23) (2011) 10038–10049.
[38] J. Hosseinpour, M. Sadeghi, A. Chitsaz, F. Ranjbar, M.A. Rosen, Exergy assessment and optimization of a cogeneration system based on a solid oxide fuel cell integrated with a stirling engine, Energy Convers. Manag. 143 (2017) 448–458.
[39] R.Ø. Gadsbøll, J. Thomsen, C. Bang-Møller, J. Ahrenfeldt, U.B. Henriksen, Solid oxide fuel cells powered by biomass gasification for high efficiency power generation, Energy 131 (2017) 198–206.
[40] M. LI, A.D. Rao, J. Brouwer, G.S. Samuelsen, Design of highly efficient coal-based integrated gasification fuel cell power plants, J. Power Sources 195 (17) (2010) 5707–5718.
[41] K. Kuramoto, S. Hosokai, K. Matsuoka, T. Ishiyama, H. Kishimoto, K. Yamaji, Degradation behaviors of SOFC due to chemical interaction between Ni-YSZ anode and trace gaseous impurities in coal syngas, Fuel Process. Technol. 160 (2017) 8–18.
[42] D. Saebea, L. Magistri, A. Massardo, A. Arpornwichanop, Cycle analysis of solid oxide fuel cell-gas turbine hybrid systems integrated ethanol steam reformer: energy management, Energy 127 (2017) 743–755.

[43] P. Tippawan, A. Arpornwichanop, I. Dincer, Energy and exergy analyses of an ethanol-fueled solid oxide fuel cell for a trigeneration system, Energy 87 (2015) 228–239.
[44] N. Laosiripojana, S. Assabumrungrat, Catalytic steam reforming of methane, methanol, and ethanol over Ni/YSZ: the possible use of these fuels in internal reforming SOFC, J. Power Sources 163 (2) (2007) 943–951.
[45] B. Farrell, S. Linic, Direct electrochemical oxidation of ethanol on SOFCs: improved carbon tolerance of Ni anode by alloying, Appl. Catal. B Environ. 183 (2016) 386–393.
[46] D. Saebea, Y. Patcharavorachot, A. Arpornwichanop, Analysis of an ethanol-fuelled solid oxide fuel cell system using partial anode exhaust gas recirculation, J. Power Sources 208 (2012) 120–130.
[47] C. Schluckner, V. Subotić, V. Lawlor, C. Hochenauer, Three-dimensional numerical and experimental investigation of an industrial-sized SOFC fueled by diesel reformat – Part I: creation of a base model for further carbon deposition modeling, Int. J. Hydrogen Energy 39 (33) (2014) 19102–19118.
[48] G. Cinti, U. Desideri, D. Penchini, G. Discepoli, Experimental analysis of SOFC fuelled by ammonia, Fuel Cells 14 (2) (2014) 221–230.
[49] F. Abraham, I. Dincer, Thermodynamic analysis of direct urea solid oxide fuel cell in combined heat and power applications, J. Power Sources 299 (2015) 544–556.
[50] O.A. Marina, C.A. Coyle, E.C. Thomsen, D.J. Edwards, G.W. Coffey, L.R. Pederson, Degradation mechanisms of SOFC anodes in coal gas containing phosphorus, Solid State Ionics 181 (8) (2010) 430–440.
[51] O. Demircan, W. Zhang, C. Xu, J. Zondlo, H.O. Finklea, The effect of overpotential on performance degradation of the solid oxide fuel cell Ni/YSZ anode during exposure to syngas with phosphine contaminant, J. Power Sources 195 (10) (2010) 3091–3096.
[52] J.F.B. Rasmussen, A. Hagen, The effect of H_2S on the performance of Ni–YSZ anodes in solid oxide fuel cells, J. Power Sources 191 (2) (2009) 534–541.
[53] F.P. Nagel, T.J. Schildhauer, J. Sfeir, A. Schuler, S.M.A. Biollaz, The impact of sulfur on the performance of a solid oxide fuel cell (SOFC) system operated with hydrocarboneous fuel gas, J. Power Sources 189 (2), (2009) 1127–1131.
[54] J. Bao, G.N. Krishnan, P. Jayaweera, K.-H. Lau, A. Sanjurjo, Effect of various coal contaminants on the performance of solid oxide fuel cells: Part II. ppm and sub-ppm level testing, J. Power Sources 193 (2) (2009) 617–624.
[55] J. Bao, G.N. Krishnan, P. Jayaweera, J. Perez-Mariano, A. Sanjurjo, Effect of various coal contaminants on the performance of solid oxide fuel cells: Part I. accelerated testing, J. Power Sources 193 (2) (2009) 607–616.
[56] C.A. Coyle, et al., Interactions of nickel/zirconia solid oxide fuel cell anodes with coal gas containing arsenic, J. Power Sources 193 (2) (2009) 730–738.
[57] M. Ni, The effect of electrolyte type on performance of solid oxide fuel cells running on hydrocarbon fuels, Int. J. Hydrogen Energy 38 (6) (2013) 2846–2858.
[58] X. Hou, O. Marin-Flores, B.W. Kwon, J. Kim, M.G. Norton, S. Ha, Gasoline-fueled solid oxide fuel cell using MoO_2-based anode, J. Power Sources 268 (5) (2014) 546–549.
[59] F. Manenti, et al., Biogas-fed solid oxide fuel cell (SOFC) coupled to tri-reforming process: modelling and simulation, Int. J. Hydrogen Energy 40 (42) (2015) 14640–14650.

[60] R. Toonssen, S. Sollai, P.V. Aravind, N. Woudstra, A.H.M. Verkooijen, Alternative system designs of biomass gasification SOFC/GT hybrid systems, Int. J. Hydrogen Energy 36 (16) (2011) 10414−10425.
[61] D. Saebea, S. Authayanun, Y. Patcharavorachot, A. Arpornwichanop, Effect of anode−cathode exhaust gas recirculation on energy recuperation in a solid oxide fuel cell-gas turbine hybrid power system, Energy 94 (2016) 218−232.
[62] N. Zhou, V. Zaccaria, D. Tucker, Fuel composition effect on cathode airflow control in fuel cell gas turbine hybrid systems, J. Power Sources 384 (2018) 223−231. Available from: https://doi.org/10.1016/j.envsci.2007.07.001. 5−37.

This page intentionally left blank

CHAPTER

Renewable power generation

10

Meysam Qadrdan[1], Xiandong Xu[1], Ehsan Haghi[2] and Christopher Williams[1]
[1]*Cardiff University, United Kingdom*
[2]*University of Waterloo, Canada*

10.1 Renewable power generation technologies

10.1.1 Wind

Wind is an intermittent source of energy and therefore the power generated by wind turbines and wind farms is highly variable. The relationship between electric power and wind speed for a single typical turbine and a wind farm are shown in Fig. 10.1. A typical wind turbine starts generating electricity at wind speeds of around 4 m/s. Between 4 and 12 m/s, the power output rapidly increases to the rated generating capacity of the turbine and remains constant for wind speeds between 12 and 25 m/s. For wind speeds above 25 m/s the turbine is shut down to avoid mechanical damage. After shut-down a wind turbine typically restarts after 3 minutes of the wind speed being below 20 m/s.

As can be observed from the wind turbine power curve in Fig. 10.1, at wind speeds of 4−12 m/s and also around 25 m/s, small variations in wind speed result

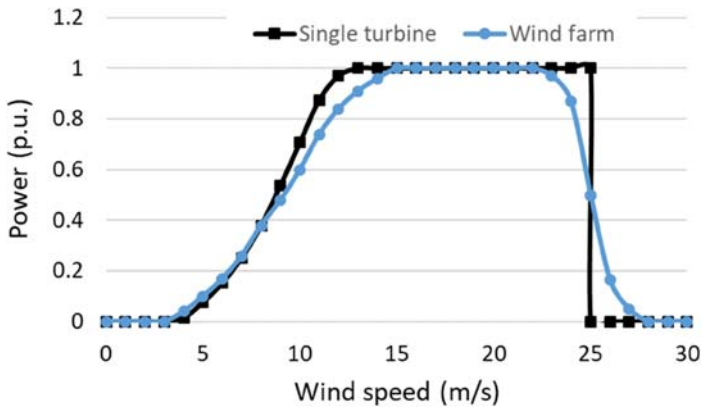

FIGURE 10.1

Power curve for a single wind turbine and a wind farm.

Design and Operation of Solid Oxide Fuel Cells. DOI: https://doi.org/10.1016/B978-0-12-815253-9.00010-0

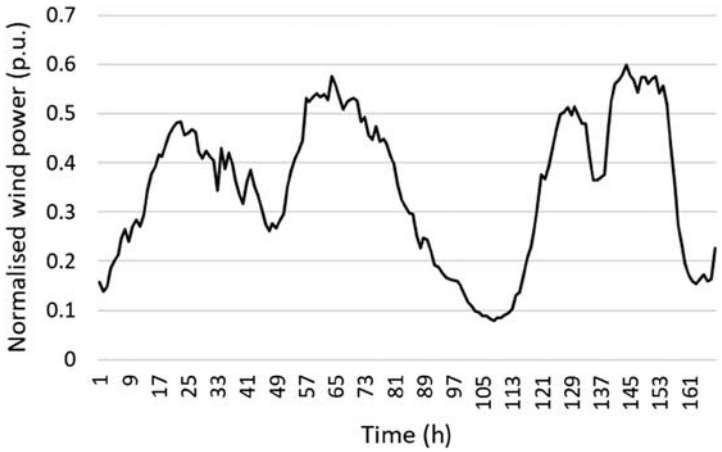

FIGURE 10.2

Hourly real wind power generation in Great Britain during January 10–16, 2015, normalized by total-installed wind generating capacity [1].

in large changes in the power output. With many turbines connected in a wind farm, the aggregate power output of the farm is smoother than the output from a single turbine. Although the aggregate power generation from wind farms dispersed across a wide geographical region is less sensitive to the wind speed in any one area, it still shows a significant degree of hourly variation.

Fig. 10.2 shows the hourly historical wind power generation in Great Britain from January 10 to 16 in 2015, normalized by the total-installed wind generation capacity, which was approximately 12 GW. This figure demonstrates the short-term variation of aggregated electricity generation by wind farms across the country. The power generated from wind varied between 10% and 60% of the installed wind capacity within the week and includes significant and abrupt increases and reductions.

Depending on the climate, wind power generation could have seasonal variation too. Fig. 10.3 shows half-hourly wind power generation injected to Great Britain's high-voltage electricity transmission system in 2018. As can be seen, wind power generation has a higher capacity factor (i.e., average generated power/installed capacity) in winter.

10.1.2 Solar

Energy from the sun is a renewable source of energy that has been widely exploited through different technologies such as concentrating solar power plants and photovoltaic panels (PVs). Currently PVs are widely used in energy systems. The continuous decrease in the cost of solar PV technologies as well as the

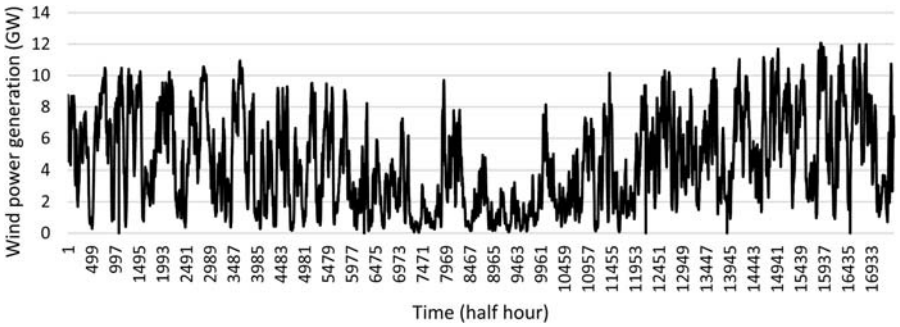

FIGURE 10.3

Half-hourly wind power generation injected to Great Britain's high-voltage electricity transmission system in 2018.

Data from [1].

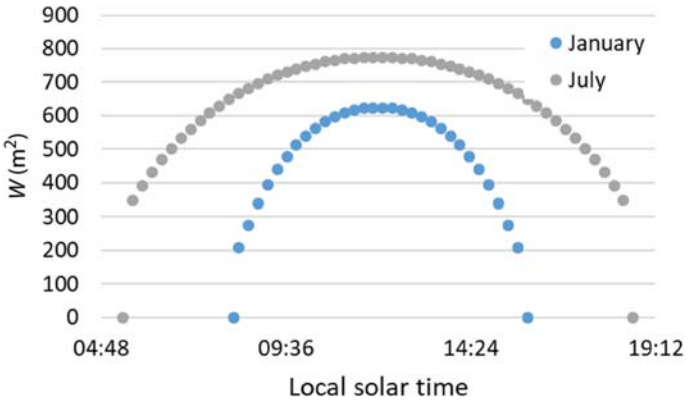

FIGURE 10.4

Average clear sky direct normal irradiance in Oxfordshire, United Kingdom.

Data from [2].

applicability of PV systems for installation on rooftops has made them a promising alternative electricity generation technology.

Fig. 10.4 shows the average clear sky direct normal irradiance in January and July for a site in Oxfordshire, United Kingdom. In the United Kingdom the peak demand for electricity usually occurs in winter from around 6 p.m. to 8 p.m.; however, the solar irradiance is zero during these hours and therefore solar energy cannot contribute to meeting the peak electricity demand.

Fig. 10.5 compares the potential of monthly electricity generation with a 1 kW photovoltaic panel (PV) system located in Oxfordshire. As can be seen in Fig. 10.5, solar energy generation is higher in summer compared to spring and

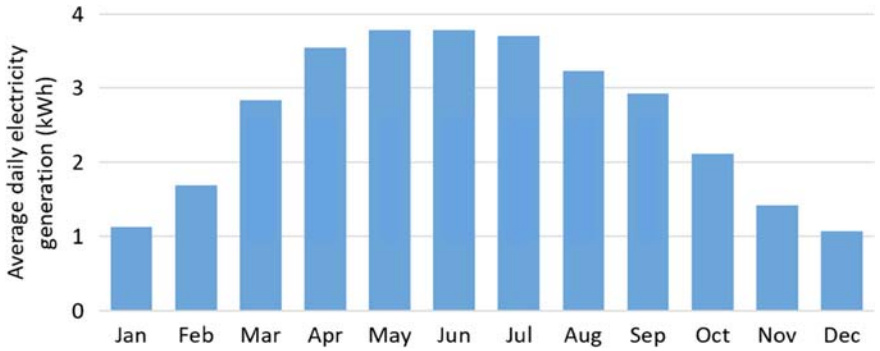

FIGURE 10.5

Average daily electricity generation from a typical 1 kW PV system in Oxfordshire, United Kingdom.

Figure created using data from [2].

winter. The solar resource in winter in the United Kingdom makes only a small contribution to the supply of electrical energy. The summer daytime electrical demand is relatively constant and a large capacity of PV generation can cover a significant portion of the demand on clear days around noon.

10.1.3 Tidal

10.1.3.1 Tides and currents

Tidal energy systems are in early stages of development (in terms of their share in the global electricity generation mix) compared to wind and solar energy systems. However, due to their predictability, tidal energy is an interesting option for renewable generation of electricity.

Tides are mainly governed by the gravitational attraction of the moon and sun. Since the moon is closer to the Earth, it has a greater effect. This gravitation causes the water on the near side to be attracted toward the moon, causing a bulge. The Earth is also spinning on its axis, which creates an inertial force and as the gravitational attraction is weaker on the far side of the Earth, the inertial force is dominant and therefore causes another bulge on that side (Fig. 10.6). On the remaining areas of the Earth the inertia and gravity forces are relatively balanced. Water is a fluid, therefore, the bulges caused by gravity and inertia will stay in line with the moon as the Earth rotates. This produces the variation in tides over a day.

In addition to the gravitational attraction from the moon, the sun also affects tides. These so-called solar tides can either work in the same direction as the moon or against it.

FIGURE 10.6

Influence of the moon on tides.

Figure reproduced from [3].

10.1.3.2 Structure of a tidal lagoon

A tidal lagoon or barrage is designed to use the movement of the oceans to create energy. As the tides rise and fall, water is channeled through turbines whose rotation generates power. This is a simple concept that only requires a few main parts to operate:

- Embankments are an essential component for a tidal lagoon. The main role of this structure it to provide a watertight seal to hold the water in, or prevent it from entering the lagoon. This is important as any leakage would reduce the capacity of the lagoon because there would be a reduction in the head difference either side of the wall. The embankment also provides safe housing for the power cables connecting the turbines to the grid.
- The turbines are submerged in water and located in the walls of the lagoon. They extract the potential energy of the difference in height between the water on either side of the lagoon. The water rushes through the turbines forcing them to rotate creating kinetic energy, which the turbines then convert into electric energy by moving generators.
- Sluices are another important feature of a tidal lagoon. Sluices are openings in the lagoon's wall, can be opened or closed, and are designed to allow large volumes of water to pass into, or out of, the lagoon in a short period of time.

10.1.3.3 Operation of a tidal lagoon power scheme

A tidal lagoon can operate in three main modes, namely ebb generation, flood generation, and two-way generation [4].

Ebb generation is the method of operation that generates electricity when the tide is going out of the lagoon. During flood tide the lagoon is filled through the sluice gates until high tide. The gates are then closed and as the tide goes back out it creates a head difference across the lagoon. The water is released through the turbines going in the same direction as the ebb tide.

The number of turbines installed determines how quickly the water is released from the lagoon. If there are too few turbines then the level of water inside the

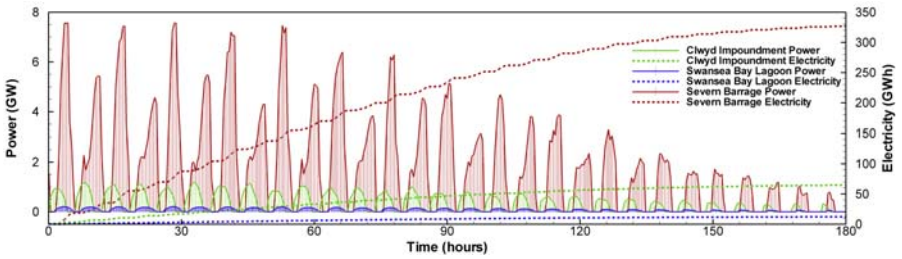

FIGURE 10.7

Power and electrical energy production by three proposed tidal schemes in the United Kingdom [5].

lagoon will hardly change between the tides. A large number of turbines would allow the basin to be drained quickly and maximum energy will be produced from the water flow. However, if there are too many turbines then the power generated will be over a short period.

In *flood generation* the turbines are used when the tide is coming in and the sluices are opened when the tide is going out. However, this process is less efficient compared to ebb generation because flood generation operates between low-tide and mid-tide, which has significantly lower volume compared to mid-tide to high-tide. Thus the flood generation scheme is less effective in generating energy compared to ebb generation.

In a *two-way generation* mode, electricity is generated during ebb and flood tides. Although this operation looks like the best option as the energy produced could theoretically be twice as much as a single operation on its own, this is not the case. The sluices need to be opened during flood and ebb tides, therefore leading to a reduction in the energy produced for both operations as there will be a significant volume of water that will not flow through the turbines. As the turbines are optimized to flow in a specific direction the efficiency in the reverse direction is reduced.

10.1.3.4 Electricity generation profiles

Fig. 10.7 shows electricity produced by a two-way generation tidal scheme. Although electricity production is highly predictable, it varies periodically and there are periods of no electricity production.

10.2 Need for flexibility

10.2.1 The challenge of balancing electricity supply and demand

The high penetration of variable renewable generation in power systems leads to an increased need for flexibility and ancillary services. A few examples are provided here to demonstrate the emerging need for flexibility in various energy systems.

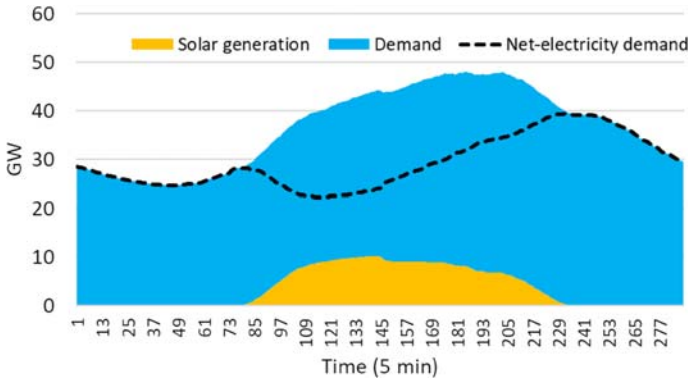

FIGURE 10.8

Electricity demand and generation by solar PV on August 16, 2018, in California, United States.

Figure created using data from [6].

California: The increasing PV generation capacity in California, United States, is significantly affecting the net-electricity demand and makes it more variable. Electricity demand and solar power generation on August 16, 2018, in California are shown in Fig. 10.8. The net-electricity demand during days when the sun is shining is reduced to a great extent. In the late afternoon when the sunset coincides with peak electricity demand a significant ramp-up in the net-electricity demand occurs. Therefore alternative energy sources that are capable to ramp-up/down quickly are required to compensate for the variation of the solar energy.

Germany: The large-scale integration of wind and solar generation in the German power system has caused challenges in balancing electricity demand and supply. The German power generation mix in 2018 consisted of 46 GW solar and 60 GW wind, which accounted for more than 50% of the total electricity generation capacity. The high penetration of variable renewable generation in the electricity mix has led to power curtailment and is one of the reasons behind negative electricity prices in some hours of a year in Germany. For example, Germany had 134 hours of negative electricity prices on the wholesale market in 2018, while this number was 146 hours in 2017, 97 hours in 2016, and 126 hours in 2015 [7].

Ontario: In Ontario, Canada, 3.33 TWh of wind and solar generation was curtailed in 2017 due to the supply exceeding the electricity demand [8]. In 2018 the Ontario electricity market had negative prices on the wholesale market for more than 360 hours (data from [9]).

10.2.2 Options for providing flexibility to low-carbon power systems

Energy storage systems are efficient options to balance electricity supply and demand in the presence of variable renewable generation. Energy storage devises absorb surplus electricity generated by renewable sources during low-demand

periods and inject this electricity back to the grid when the demand rises. Various energy storage technologies and systems are currently under development. A vast amount of funding is annually spent on research and development of energy-storage technologies. Pumped hydro, batteries, flywheels, compressed air, and hydrogen are among the most noted storage systems. These systems have unique characteristics in terms of cost, capacity potential, storage time, efficiency, and end-use applications.

A system including an electrolyzer, hydrogen storage, and a fuel cell can act as energy storage by using excess electricity from renewables and converting it into hydrogen. The hydrogen then can be stored and used in a fuel cell to generate electricity when the demand is high. A hydrogen-based storage system reduces renewable power curtailment. Hydrogen produced by renewable energy can be used in a solid oxide fuel cell (SOFC), which operates as a combined heat and power (CHP) system. As a result the renewable electricity that would be otherwise curtailed is used to reduce greenhouse gas emissions in the power and heat sectors. By using technologies such as polymer electrolyte membrane electrolyzers for hydrogen production, it is possible to provide fast response ancillary services to power systems.

Hydrogen produced by electrolyzers can also be injected in existing natural gas pipeline systems to form hydrogen-enriched natural gas. This option provides a significant storage capacity in countries and regions that have developed natural gas infrastructure. In those regions, hydrogen can be used to provide seasonal storage for renewable energy.

10.3 Solid oxide fuel cells for distributed power generation

SOFCs are increasingly used as distributed power generation technologies due to their high efficiency and multifuel capability. SOFCs have four main applications which are discussed in Sections 10.3.1–10.3.4.

10.3.1 Residential applications

Their low noise and emission characteristics make SOFCs ideal for home installations. The ability to provide heat and power simultaneously makes them a promising option for use as distributed generations. Additionally, SOFCs can contribute to peak-load shaving and reduce home bills for residential buildings when a difference in peak and off-peak tariffs are in place. Through integration with battery banks and/or hydrogen storage, SOFCs can be used in remote areas to provide electric and thermal energy to local consumers.

The application of fuel cells as residential CHP systems is demonstrated in Japan's ENE-FARM program [10]. Through this program the government of

Japan has set a target of installing 5.3 million residential fuel cell CHP systems in Japan by 2030. This number of systems equals 10% of households in Japan [10].

Several studies (i.e., [11]) investigated the thermal and electrical behavior of SOFCs. Ullah et al. [11] carried out experiments and demonstrated that by increasing the operating temperature of an SOFC from 650°C to 750°C, the maximum electrical power generation and overall efficiency (electrical plus thermal efficiency) can be increased, while the electrical efficiency drops slightly.

There are, however, three main challenges in the widespread deployment of SOFC systems in the residential sector. First, highly variable residential power demands require SOFCs to operate with high flexibility. Second, SOFC systems have higher capital and operating costs compared to other energy conversion technologies used in residential buildings such as conventional CHPs and boilers. Finally, limited experience is available in installing, maintaining, and supporting the use of SOFC systems in residential systems. This lack of experience is a crucial challenge for the widespread introduction of SOFCs in the residential sector.

10.3.2 Commercial applications

Reliable power and heat supply is a requirement for commercial and public sites such as office buildings, large hotels, schools, and shopping malls. These sites provide great opportunities for SOFCs to be used for distributed generation of heat and electricity. Moreover, dispatchable SOFCs enable operators to provide grid support to a local utility or an independent system operator, which will help to avoid investments into reinforcing electricity networks and new generation capacities.

10.3.3 Industrial applications

Main applications of SOFCs in industries include backup power generating unit, CHP, and trigeneration in a range of different industries such as data centers, wood processing and steel works. In the EU-funded GrinHy project [12] onsite tests of reversible SOFCs were conducted in a steel works aimed at exploiting the high-temperature waste heat. Palomba et al. [13] investigated the use of a 630 kWe SOFC for trigeneration of heat, cooling, and electricity in an industrial site. The SOFC was fed by syngas produced through gasification of lignocellulosic biomass. It was demonstrated that using SOFC for trigeneration could reduce the primary energy consumption of the industrial site by about 15 GWh/year (about 50% less than a traditional system with separate energy production) with a significant amount of avoided CO_2 emissions of about 5000 tonnes/year. As SOFCs perform well using light hydrocarbon fuels, Lackey et al. [14] investigated the use of SOFC fueled by biogas produced by anaerobic digestion in a wastewater treatment plant. The study showed that reductions of 2400 tonnes CO_2, 60 kg CH_4, and 18 kg N_2O emission from the wastewater treatment plant could be achieved through using biogas in SOFCs.

Using SOFCs as a distributed generation technology can also provide peak-shaving capability for grid support and to avoid high demand charges in industries, such as in the case of TRIAD in the Great Britain.

10.3.4 Military and transport applications

SOFCs can provide electricity for propulsion and service of navy ships, supply energy to the tent-city of a bare base, and act as a flight-line generator in air force applications. For army and marine applications the use of SOFCs may include an auxiliary power unit and propulsion of armored vehicles, mobile power station, military communication stations, underwater vehicles, and so forth. Since SOFCs are silent, reliable, resilient, and uninterruptible they are an ideal option for energy supply in military applications. Moreover the good heat rejection capability makes it possible for an SOFC propulsion system to have high-power density and being suitable for long-term use.

Strazza et al. [15] adopted a life cycle assessment approach to evaluate the performance of SOFCs as auxiliary power systems for commercial ships. It was shown that the fuel production phase has a significant effect on the life cycle performance of SOFCs. From the life cycle point of view, biomethanol was identified as an environment-friendly fuel for SOFCs.

10.4 Integrated solid oxide fuel cells and renewable power generations

The basic idea of a hybrid, renewable, SOFC power-generation system is to use the surplus electricity from renewable energy sources such as solar and wind to produce hydrogen. The hydrogen is stored and used to generate electricity when required. During the electricity generation process via an SOFC the cogenerated heat can be used to supply heat demand locally or through a district heating system. It should be noted that the high-electrical efficiency indicates less heat supply ability of the SOFCs.

Concerning the connection mode to the power grid, the hybrid system can be divided into two categories, namely grid-connected and standalone. Usually in the grid-connected mode the operation of an SOFC (i.e., power generation) is determined to maximize the profit of the hybrid system considering electricity prices. Therefore SOFCs are mainly used for generating electricity during peak hours when electricity prices are high.

In the standalone mode the SOFCs need to work together with other renewable technologies to meet the local demand for electricity. The availability of hydrogen storage ensures SOFCs are able to generate electricity to fill the gap between electricity demand and renewable generation.

Hydrogen storage is crucial in order to maximize the flexibility of a hybrid energy system including SOFCs. Hydrogen storage is one of the most flexible energy storage solutions for power grids. Hydrogen can be stored as high-pressure gas, low-temperature liquid, and physically or chemically bonded to hydride complexes. To support the energy storage process, fuel cells for electricity generation and electrolyzers for hydrogen generation are interfaces between the electricity system and the hydrogen system. With these interfaces the hydrogen storage operator will be able to use renewable energy to reduce the cost and emission of the produced hydrogen.

The reversible solid oxide cell (ReSOC) is an electrochemical energy conversion technology that operates at high temperatures (600°C−1000°C) and can be used either as an SOFC to generate electricity or as a solid oxide electrolyzer cell (SOEC) to produce H_2. This is an interesting feature that encourages the use of ReSOCs in hybrid energy systems (Fig. 10.9).

Perna et al. [17] assessed the performance (e.g., round-trip efficiency) of an ReSOC as electric energy storage. In the SOFC mode, electricity is generated by converting the reactant gas, which is mainly composed of CH_4 and H_2, into a mixture of H_2O and CO_2. During the electrolysis process, CH_4 can also be produced due to the methanation reaction that, under proper operating conditions, occurs at the cathode of the solid oxide cell. It was shown that a stack round-trip efficiency of about 70% can be achieved when the ReSOC operates at low temperature (700°C). Frank et al. [16] designed and carried out an experiment on an ReSOC system as energy storage that can be upscaled to provide flexible services to power grids. In fuel cell mode the ReSOC showed an efficiency of up to 67.1% and in the electrolysis mode it was 76% efficient, which gave a round-trip efficiency of 51%.

Nease et al. [18] analyzed the performance of an integrated SOFC and compressed air energy storage system for supplying zero-emission electricity during peak demand hours in Ontario, Canada. Sadeghi [19] proposed a hybrid energy system including an SOFC, solar panels, and flow batteries to meet varying electricity loads.

The use of bioenergy as a fuel for SOFCs is an environment-friendly option for electricity generation. A hybrid SOFC and micro gas turbine fueled by biogas

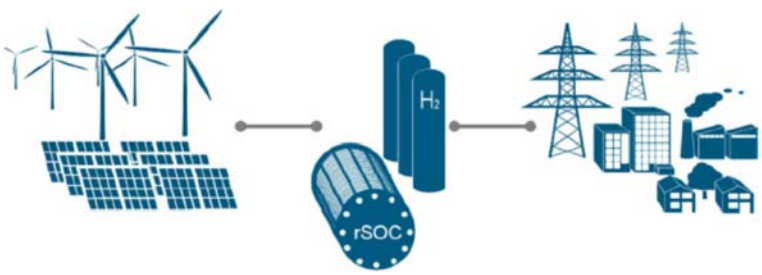

FIGURE 10.9

Reversible solid oxide cell as a large-scale energy storage system to provide flexibility to power grids [16].

was analyzed by Perna et al. [20] for the distributed generation of electricity and heat. Zabaniotou [21] studied the use of various agricultural residues in a decentralized CHP system based on SOFCs. Mehr et al. [22] studied a power and heat cogeneration system consisting of a biogas-fed SOFC and a concentrating solar thermal system for a wastewater treatment plant in Italy. The biogas was produced onsite from the anaerobic digestion of collected sludge. The thermal power recovered from the SOFC exhaust stream was used to meet part of the digester thermal load, with concentrated solar thermal and an auxiliary boiler supplying the rest of the heat load.

10.5 Conclusion

Traditionally different energy systems of electricity, gas, district heating/cooling, and hydrogen had relatively few interactions and were designed and operated independently of each other. Currently, however, there is significant interest in exploring the synergies between energy networks through coupling components such as power-to-gas [23], fuel cells, and thermal energy storage. Interactions take place through energy conversion between different energy carriers and its storage to provide services and ensure that each is managed optimally. Numerous possible interactions between the various energy systems are shown in Fig. 10.10.

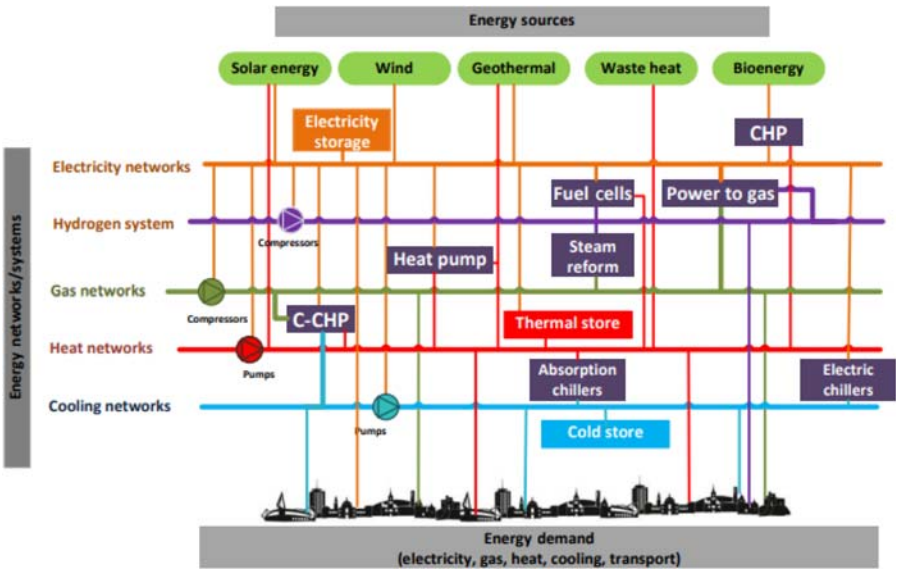

FIGURE 10.10

Potential interactions between hydrogen and other energy-carrier systems [24].
CHP: Combined heating and power.

From the technical viewpoint the integration of multi-vector energy systems increases the difficulties of managing and operating complex energy systems. In order to analyze the interactions and interdependencies among different energy systems at different spatial and temporal scales, enhanced modeling tools are required to study the impact of cascading failures affecting the reliability of energy supplies. Moreover, more software tools (planning, simulation, and operational control) are needed to quantify the performance of the integrated energy systems under different scenarios. Additionally, assessment methodologies and evaluation criteria are required to quantify the techno-economic performance of the integrated energy systems. Based on the evaluation criteria, standard test networks need to be designed to support the relevant studies and validate the developed models.

References

[1] ELEXON, https://www.bmreports.com/bmrs/?q = generation/fueltype/current (accessed February 2019).

[2] European Union Joint Research Centre, http://re.jrc.ec.europa.eu/pvgis/apps4/pvest.php (accessed March 2019).

[3] National Oceanic and Atmospheric Administration, U.S. Department of commerce, https://oceanservice.noaa.gov/education/tutorial_tides/tides03_gravity.html (accessed March 2019).

[4] N. Yates, I. Walkington, R. Burrows, J. Wolf, Appraising the extractable tidal energy resource of the UK's western coastal waters, Phil. Trans. R. Soc. A 371 (1985) (2013). 20120181.

[5] A. Angeloudis, R.A. Falconer, S. Bray, R. Ahmadian, Representation and operation of tidal energy impoundments in a coastal hydrodynamic model, Renew. Energy 99 (2016) 1103−1115.

[6] California ISO Website, http://www.caiso.com/TodaysOutlook/Pages/supply.aspx (accessed February 2019).

[7] Clean Energy Wire, https://www.cleanenergywire.org/news/german-wholesale-power-prices-turn-negative-less-often-2018 (accessed March 2019).

[8] Independent Electricity System Operator, http://www.ieso.ca/en/Corporate-IESO/Media/Year-End-Data, Accessed January 2019.

[9] Independent Electricity System Operator, http://reports.ieso.ca/public/PriceHOEPPredispOR/ (accessed February 2019).

[10] Government of Japan, https://www.gov-online.go.jp/eng/publicity/book/hlj/html/201706/201706_10_en.html (accessed February 2019).

[11] K.R. Ullah, R.K. Akikur, H.W. Ping, R. Saidur, S.A. Hajimolana, M.A. Hussain, An experimental investigation on a single tubular SOFC for renewable energy based cogeneration system, Energy Convers. Manage. 94 (2015) 139−149.

[12] GrinHy Project, http://www.green-industrial-hydrogen.com/home/ (accessed March 2019).

[13] V. Palomba, M. Prestipino, A. Galvagno, Tri-generation for industrial applications: development of a simulation model for a gasification-SOFC based system, Int. J. Hydrogen Energy 42 (2017) 27866−27883.

[14] J. Lackey, P. Champagne, B. Peppley, Use of wastewater treatment plant biogas for the operation of solid oxide fuel cells (SOFCs), J. Environ. Manage. 203 (2017) 753–759.
[15] C. Strazza, A. Del Borghi, P. Costamagna, A. Traverso, M. Santin, Comparative LCA of methanol-fuelled SOFCs as auxiliary power systems on-board ships, Appl. Energy 87 (2010) 1670–1678.
[16] M. Frank, R. Deja, R. Peters, L. Blum, D. Stolten, Bypassing renewable variability with a reversible solid oxide cell plant, Appl. Energy 217 (2018) 101–112.
[17] A. Perna, M. Minutillo, S.P. Cicconardi, E. Jannelli, S. Scarfogliero, Performance assessment of electric energy storage (EES) systems based on reversible solid oxide cell, in: 71st Conference of the Italian Thermal Machines Engineering Association, ATI2016, 14–16 (2016), Turin, Italy.
[18] Jake Nease, Nina Monteiro, Thomas A. Adams, Application of a two-level rolling horizon optimization scheme to a solid-oxide fuel cell and compressed air energy storage plant for the optimal supply of zero-emissions peaking power, Comput. Chem. Eng. 94 (2016) 235–249.
[19] S. Sadeghi, Study using the flow battery in combination with solar panels and solid oxide fuel cell for power generation, Sol. Energy 170 (2018) 732–740.
[20] A. Perna, M. Minutillo, E. Jannelli, V. Cigolotti, S.W. Nam, K.J. Yoon, Performance assessment of a hybrid SOFC/MGT cogeneration power plant fed by syngas from a biomass down-draft gasifier, Appl. Energy 227 (2018) 80–91.
[21] A. Zabaniotou, Agro-residues implication in decentralized CHP production through a thermochemical conversion system with SOFC, Sustain. Energy Technol. Assess. 6 (2014) 34–50.
[22] A.S. Mehr, M. Gandiglio, M. MosayebNezhad, A. Lanzini, S.M.S. Mahmoudi, M. Yari, et al., Solar-assisted integrated biogas solid oxide fuel cell (SOFC) installation in wastewater treatment plant: energy and economic analysis, Appl. Energy 191 (2017) 620–638.
[23] A. Maroufmashat, M. Fowler, Transition of future energy system infrastructure; through power-to-gas pathways, Energies 10 (8) (2017) 1089.
[24] M. Abeysekera, J. Wu, N. Jenkins, Integrated energy systems: an overview of benefits, analysis methods, research gaps and opportunities, HubNET position paper series, 2016.

CHAPTER

Energy storage 11

Tohid N. Borhani
School of Water, Energy and Environment, Cranfield University, Bedford, United Kingdom

11.1 Introduction

Energy-storage technologies can be classified as mechanical, chemical, electrochemical, thermal, and electrical [1]. Among different types of energy-storage systems, the chemical-based storage methods offer enduring storage and a manageable discharge according to the energy demand. Chemical-based storage systems are not site-specific and can operate with high efficiency by producing hydrogen or syngas. One of the most important technologies among chemical-based energy storage systems are reversible (or regenerative) solid oxide cells (ReSOCs or rSOCs) [1].

ReSOCs are systems that can be used in two different operating modes, namely fuel cells and electrolysis. In the solid oxide fuel cell (SOFC) mode, electricity is generated by the electrochemical reaction of a fuel (e.g., hydrogen and natural gas) with air. In the electrolysis mode [solid oxide electrolyzer cell (SOEC) or solid oxide steam electrolyzer (SOSE)] the hydrogen or syngas is produced using electricity when coupled with an energy source. Therefore it could be said that the ReSOC is both the SOFC and SOEC incorporated in a single unit, and the SOEC is an SOFC that works in the opposite manner [2]. SOFC, and SOEC, have the potential to show considerably lower electrochemical losses than the other type of methods [3]. The idea of ReSOCs utilization for energy storage returns to pioneering research in 1987 [4] when Bents presented the design of the system and described the forward and reverse operating cycles. He also reported that for solar photovoltaic (PV) applications the ReSOC system was better than an alkaline regenerative fuel cell system.

Although the concept of using ReSOCs for electricity production and storage is promising, the technology is not yet commercially competitive with the other technologies. The main issues are the high cost and the short lifetime of the cells [5]. In addition, the round-trip efficiency of ReSOC for energy storage is not at the level of batteries [6]. Therefore development in materials and system design is required for ReSOCs to make this technology competitive with the other common energy-storage technologies to result in efficient and economical operation. In addition, process optimization also can be useful to reduce the stresses and

Design and Operation of Solid Oxide Fuel Cells. DOI: https://doi.org/10.1016/B978-0-12-815253-9.00011-2

optimize the performance of the system. ReSOCs can potentially offer a low-cost approach to support a hydrogen economy in the future [7].

As ReSOCs can operate over a varied range of energy-to-power ratios it is appropriate for energy management applications. In addition to the traditional energy-storage scenario, the ReSOC system is very beneficial for energy sustainability when the electrical energy is produced from renewable energies such as wind or PV energy [8]. This technology is helpful for stabilization of the grid and can be considered a useful alternative to shutting down renewable energies during production peaks. A schematic diagram of the combination of an ReSOC energy-storage system with renewable energies is presented in Fig. 11.1. As can be seen these renewable energies could be solar, wind, and biomass-sourced energy.

The characteristics of ReSOCs are described in Section 11.2. This includes a discussion on two features of the system. Commonly utilized materials in ReSOC systems are reviewed in Section 11.3. The process configuration and units required for ReSOC systems are explained in Section 11.4. The strategies to manage the thermal aspects of the process are presented in Section 11.5. As the efficiency of the system is important, this parameter is defined and discussed in Section 11.6. Section 11.7 is devoted to economic aspects and the techno-economic assessment

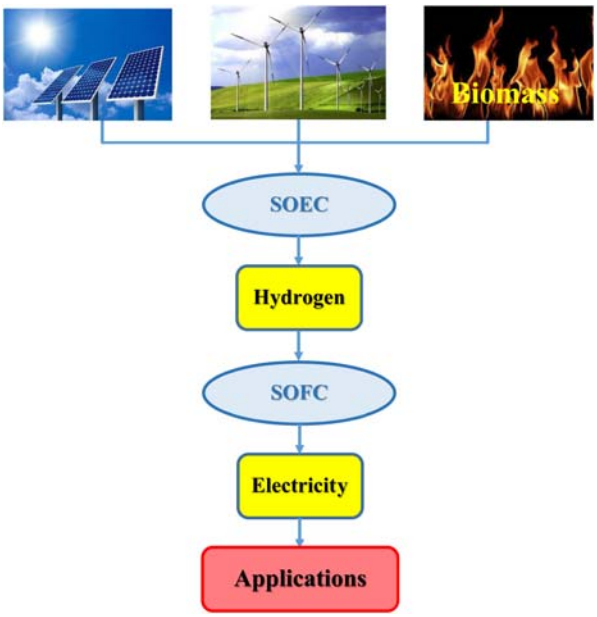

FIGURE 11.1

Reversible solid oxide cell system application using various renewable energy sources. *SOEC*, solid oxide electrolyzer cell; *SOFC*, solid oxide fuel cell.

Adapted from L. Bi, S. Boulfrad, E. Traversa, Steam electrolysis by solid oxide electrolysis cells (SOECs) with proton-conducting oxides, Chem. Soc. Rev. 43 (24) (2014) 8255–8270.

(TEA) of the ReSOC operation. Finally, in Section 11.8, the conclusions of the chapter are drawn and directions for future research in this subject are listed.

11.2 Characteristics of reversible solid oxide cells

Minh and Mogensen [2] considered five features for ReSOCs, namely compatibility, flexibility, capability, adaptability, and affordability. It is required that ReSOCs have two important features, in addition to those belongings to SOFC and SOEC modes. These two features are reversibility of the electrode operation and efficient cyclic operation, which cause complexity in the technical aspect of electrode development. These two important features and reactions in ReSOC systems are discussed by more detail in the following subsections.

11.2.1 Reversibility of the electrode operation

The fuel electrode in ReSOCs must show proper performance reversibility between the SOFC and SOEC modes. It is also necessary for the oxygen electrode to have performance reversibility at low-current densities. However, in practice, the SOEC mode depends on different parameters such as microstructure of the electrodes, type of materials used in the system, and operating parameters the system may utilize irreversibly. Microstructures of the electrodes have a high influence on the performance stability of the electrodes. During electrolysis the microstructures of an oxygen electrode need to be engineered to overcome the oxygen pressure build-up problem at the electrode−electrolyte interfaces. On the other hand, the fuel electrode microstructures are required to be designed to simplify the transport of water and fuel to and from reaction sites.

11.2.2 Efficient cyclic operation

A cyclic operation with high efficiency and stability is a very important feature that must be considered for ReSOCs. Single-cell and multicell stacks have been constructed and examined by considering their cyclic operation [9]. The cyclic operation is related to the capability of the anode or hydrogen electrode for internal reforming. It has been shown that a higher degradation rate is usually reported for cell and stack performance in the SOEC mode than those in the SOFC mode [9].

11.2.3 Reactions and other characteristics

Overall, reactions in ReSOCs include electrochemical fuel oxidation (or reduction), fuel reforming, and water−gas shift (or reverse shift) as shown in the equations:

$$H_2 + \frac{1}{2}O_2 \rightleftarrows H_2O, \quad \Delta H = -248\text{kJ/mol} \tag{11.1}$$

$$CH_4 + H_2O \rightleftarrows 3H_2 + CO, \quad \Delta H = 226 kJ/mol \tag{11.2}$$

$$H_2O + CO \rightleftarrows H_2 + CO_2, \quad \Delta H = -34 kJ/mol \tag{11.3}$$

The forward reactions are for the SOFC mode and the backward reactions belong to the SOEC mode. The ΔH is the molar heat of reaction of the forward reaction at 800°C [10]. A schematic diagram of two operation modes of ReSOC, diffusion of species and reaction chemistry, is illustrated in Fig. 11.2.

According to Fig. 11.2 the positive–electrolyte–negative structure could be a coated ceramic and metal structure including: (1) a fuel electrode that is considered as the anode and cathode in the SOFC and SOEC modes, respectively; (2) a tiny solid electrolyte; and (3) an oxygen electrode which is considered as the cathode and anode in the SOFC and SOEC modes, respectively. As can be seen, there is a channel for fuel near the fuel electrode in which the reactant elements flow. It must be mentioned that these reactant elements may be any type of fuel in the SOFC mode. In the SOEC mode the reactant species are H_2O and/or CO_2. The process is known as electrolysis if the only reactant in the system is steam.

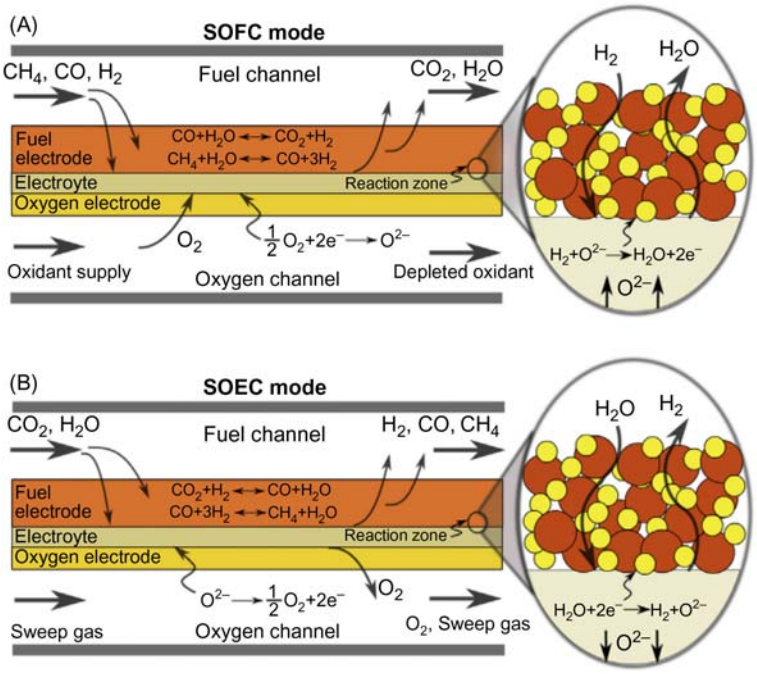

FIGURE 11.2

Schematic diagram of two different operation modes of reversible solid oxide cells: (A) SOFC mode and (B) SOEC mode [11]. *SOFC*, solid oxide fuel cell; *SOEC*, solid oxide electrolyzer cell.

The term coelectrolysis is utilized to express the utilization of water and carbon dioxide to produce syngas. In the SOFC mode an oxygen supply in the form of pure oxygen or air is necessary for the oxygen electrode to operate as a reactant in the electrochemical conversion. There is oxygen generation at the air electrode in the SOEC operation. The typical operation voltage for a single ReSOC is 0.5−2.0 V and cell stacking is necessary to obtain the suitable voltage output from the device. In addition, cell staking has two more important duties. In order to eliminate the excess heat generated by oxidation reactions in the SOFC mode, cooling airflow is needed for the stack. Internal reforming reactions can also act as a thermal energy sink. In contrast, additional heat is necessary in the reduction reactions in the SOEC mode, which is provided either from an external source or by having a less efficient operation of the cell in that the waste-heat generation provides the required thermal energy shortage.

There is an important challenge for the integration of the two different modes of the ReSOC system due to the different thermal behavior of each mode. Cell performance degradation is another significant challenge in ReSOCs. As the cell has to work in both oxidizing and reducing situations, it is critical to have electrode components that are stable in both conditions [12].

It was reported that severe degradation of oxygen electrodes in the SOEC mode is a critical issue in ReSOCs [13,14]. Graves et al. [13] found that at high-current densities the ReSOC showed insufficient long-term stability and, hence, this problem limited its application in the past. The authors showed that similar to a rechargeable battery, the serious degradation problem of electrolysis can be entirely removed by reversible cycling between SOEC and SOFC modes. It must be mentioned that it was believed previously that this degradation problem was not reversible. Chen et al. [14] considered the stability of ReSOCs (the performance of oxygen electrodes in the SOEC mode) as the most critical issue that had to be solved to have a high-performance system. In their study they found that the deterioration of a lanthanum strontium manganite (LSM)—was oxygen electrode caused by anodic polarization. They suggested a solution to this problem by introducing cathodic polarization.

11.3 Common materials in reversible solid oxide cells

The materials for ReSOCs are similar to the materials commonly used in SOFC systems. Three main physical items in ReSOCs that construct a membrane electrode assembly are a solid electrolyte, oxygen electrode, and fuel electrode. A comprehensive review of the different types of electrolytes, fuel electrodes, and oxygen electrodes and their manufacturing was presented [15]. The authors categorized electrolytes as zirconia-based, ceria-based, lanthanum gallates based, and proton conducting; fuel electrodes as conventional cermets, lanthanum strontium chromium manganites, titanate composites, and lanthanum chromium ferrites; and

Table 11.1 Common materials utilized in reversible solid oxide cells [15].

Application	Family	Material	Abbreviation
Solid electrolyte	Zirconia-based	Yttria-stabilized zirconia	YSZ
		Scandia-stabilized zirconia	ScSZ
	Ceria-based	Samaria-doped CeO_2	SDC
		Gadolinia-doped CeO_2	GDC
	Lanthanum gallates-based	Lanthanum strontium gallium magnesium oxide lanthanum gallium oxide	LSGMLM
	Proton conducting	Barium zirconate cerates	–
Oxygen electrode	Lanthanum strontium-based	Lanthanum strontium manganite	LSM
	Perovskites	Lanthanum strontium cobalt iron oxide	LSCF
	Ruddlesden–Popper series	$A_2NiO_{4+\delta}$ (A = Nd, La or Pr)	–
	Double perovskites	$GdBaCO_2O_{5+\delta}$	GBCO
		$PrBaCO_2O_{5+\delta}$	PBCO
		$Sr_2Fe_{1.5}Mo_{0.5}O_{6-\delta}$	SMFO
Fuel electrode	Conventional cermets	Nickel-impregnated, yttria-stabilized zirconia cermet	Ni–YSZ
		Copper-impregnated, yttria-stabilized zirconia cermet	Cu–YSZ
	Lanthanum strontium-based	Lanthanum strontium chromium manganite	LSCM
	Titanate composites	Lanthanum strontium titanate	LST
		Yttrium strontium titanate	YST
	Lanthanum chromium ferrite	Lanthanum strontium chromium ferrite	LSCrF
		Lanthanum calcium chromium ferrite	LCaCrF

oxygen electrodes as LSMs, perovskites, Ruddlesden–Propper series, and double perovskites. The list of common materials utilized in ReSOCs is provided in Table 11.1.

More and more studies are being conducted on the development of materials for ReSOCs over the past few years. These new materials improved the performance of the ReSOC system considerably. Bi et al. [16] investigated the utilization of proton-conducting oxides as a chemically stable material for the SOFC and SOEC modes of ReSOC. They also found that these materials could reduce the operating temperature of the ReSOC system because they have better ionic conductivity compared with common oxygen-ion conducting conductors. An oxygen electrode free of strontium and ornamented using $Er_{0.4}Bi_{1.6}O_3$ is produced

and used on a barrier-layerfree YSZ electrolyte film [17]. The newly designed oxygen electrode showed a peak-power density of 1.81 and 0.58 W/cm^2 at 750°C and 650°C, respectively. In addition the operating stability obtained for the SOFC mode was 600°C for about 500 hours and 750°C for the SOEC mode for more than 200 hours. Huan et al. [18] developed a stable and efficient air electrode, $SrEu_2Fe_{1.8}Co_{0.2}O_{7-\delta}$ (SEFC), in a proton-conducting ReSOC (P-ReSOC). The authors reported that by applying this air electrode the system operated and easily switched between the SOFC and the SOEC modes without degradation for 135 hours.

11.4 Process configuration and unit operations

A typical ReSOC system involves pumps, tanks, compressors, and heat exchangers and the complete system should be designed and established to work with appropriate efficiency [19]. There are different challenges in the design of ReSOC systems that must be managed prior to the adaption of the system. These challenges include control of cell performance and system stability, system integration, and effective thermal establishment in the two operating modes [11]. In general the challenges in designing ReSOC systems can be summarized as [10]:

1. The challenge related to how to overcome the thermal difference between the SOFC mode (exothermic) and the SOEC mode (endothermic or near thermoneutral)—it must be mentioned that both SOFC and SOEC modes are considered as exothermic in some cases [20]—utilizing a unitized cell-stack and common hardware.
2. The challenge of selecting configurations and operating conditions (temperature, pressure, utilization, composition) that result in high efficiency in both operating modes.
3. The challenge of thermal integration between high-temperature stack operation and lower temperature, pressurized storage.
4. The challenge related to the required process of reaction products (such as economical compression to the storage pressure) that are tanked and need to be used in the opposite modes of operation.

An example of the energy-storage concept using ReSOC technology is presented in Fig. 11.3.

The device presented in Fig. 11.3 runs successively between the two distinct modes, namely discharging (SOFC) and charging (SOEC). In the SOFC operation a fuel stream contains a mixture of gases transferred from a fuel-storage tank to the ReSOC stack. By electrochemical oxidation of the fuel species in the stack, electrical power will be generated. The exhaust components from the stack are water and carbon dioxide with some amount of unreacted fuel that is collected in a separate tank to be utilized in the SOEC mode. The stack is operated as an

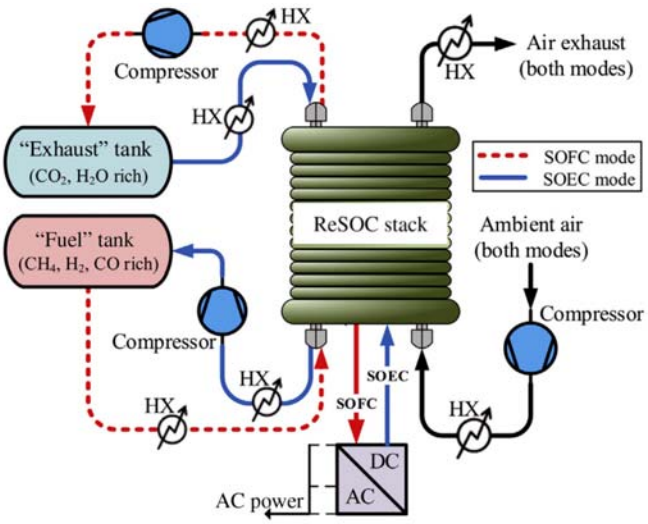

FIGURE 11.3

A schematic diagram of the unit operations in reversible solid oxide cell system [11]. *SOFC*, solid oxide fuel cell; *SOEC*, solid oxide electrolyzer cell; *ReSOC*, reversible solid oxide cell.

electrolyzer in the SOEC mode in which the reactant and product flow in opposite directions to provide the mixture of gases comes from the exhaust tank for the stack.

The extra energy from renewable methods or in the off-peak hours is sent to the SOEC system to generate hydrogen. The required water can be provided by different methods. The water can come from a power plant, sea, or industrial water supply [21]. It must be noted that a portion of the required water in the SOEC mode can be supplied by storing the water generated in the SOFC reactions. In the SOFC mode the compressed hydrogen that was stored in the gas-storage tubes is used to generate energy for the grid in the peak hours or any time when necessary.

Some new designs and configurations for ReSOC systems have been presented in recent years. Mermelstein and Posdziech [21] reported the collaboration between Boeing and Sunfire companies in the design of a fully integrated, automated, and grid-tied ReSOC system that includes two identical submodules with 60 kWDc SOEC power and 25 kWDC SOFC power each. Di Giorgio and Desideri [22] presented two different storage concepts for ReSOCs in which the produced thermal energy during the SOFC mode is stored as sensible heat in a material with high density and high-specific heat or is stored as latent heat in a phase-change material. The sensible or latent heat is used in the SOEC mode. Lou et al. [23] used gPROMS to develop a dynamic model containing an ReSOC,

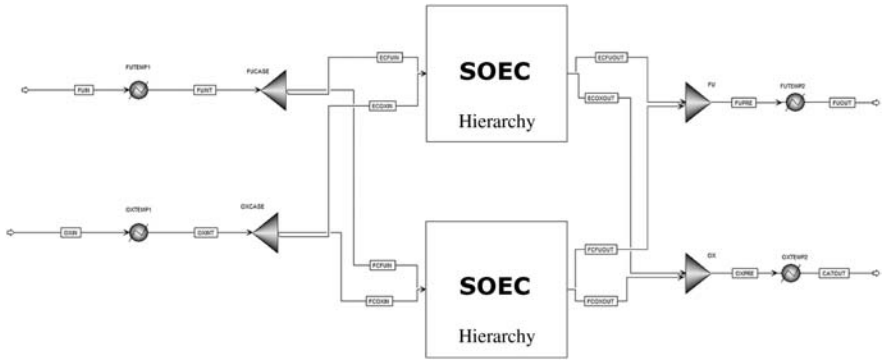

FIGURE 11.4

The reversible solid oxide cell model developed using Aspen Plus simulation [24]. *SOFC,* solid oxide fuel cell; *SOEC,* solid oxide electrolyzer cell.

Li-ion batteries, internal combustion engine, heat exchangers, and other equipment. They simulated a distributed system combining renewable energy (RE), natural gas (NG), and energy storage. The authors considered different scenarios to comprise the power quality, efficiency, RE penetration, and device cost and size. They reported that the optimal strategy of the RE−NG distributed system was achieved when no more than 36% of the maximum renewable power was supplied to users. Hauck et al. [24] investigated the impact of inlet-gas composition, temperature, and pressure on the performance of an ReSOC using Aspen Plus simulation (see Fig. 11.4). Their parametric study showed that the increase of hydrogen content and decrease of steam content can improve the performance of the system in the SOEC mode. The authors also evaluated the pressurized operation, which increased the operational voltage and reduced the diffusion losses.

Giap et al. [25] integrated an ReSOC system with waste steam (see Fig. 11.5). They considered three different round-trip efficiencies to evaluate the performance of the system. A parametric study was also performed by considering the effects of fuel composition, waste-steam temperature, and steam-conversion ratio on the system. The calculation for the base case of the ReSOC working at 750°C and 1.1 bar, resulted in 37.9% as the reference system of round-trip efficiency, 53.8% as the electrical round-trip efficiency, and 49.6% as the exergy round-trip efficiency.

Perna et al. [26] proposed and analyzed an ReSOC system fed by a mixture of methane, carbon monoxide, water, and hydrogen. They investigated the behavior of the system under different operating conditions by considering a thermo-electrochemical model. In order to produce power and hydrogen, the biomass-based ReSOC was integrated with a gas turbine by considering different gases as the gasification agents [27] (see Fig. 11.6). The authors evaluated the system in terms of energy, exergy, exergoeconomic, and environmental impact using a

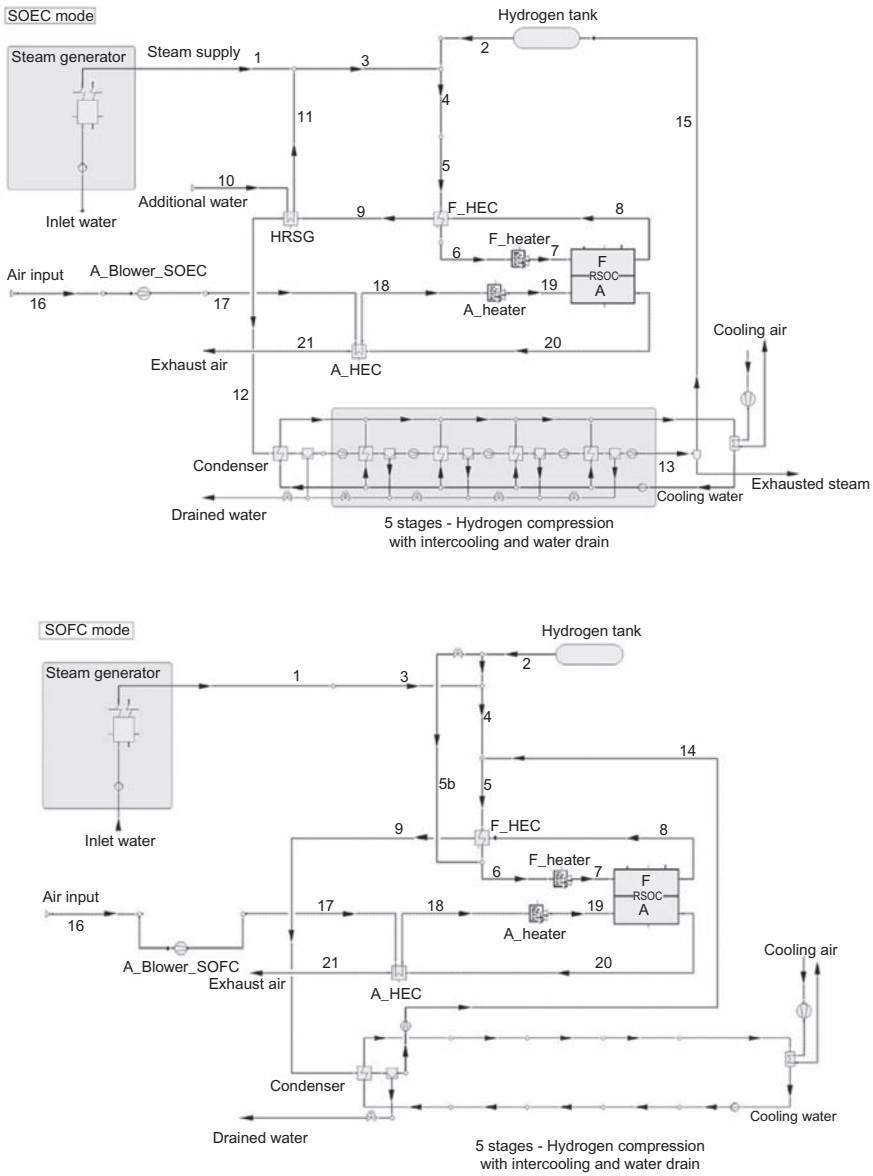

FIGURE 11.5

Integration of reversible solid oxide cell system with waste steam [25].

parametric study. They also optimized the system using a multiobjective optimization method by considering different objectives when CO_2 was a gasification agent. The exergy efficiency and total product cost under optimum operating conditions were 45.25% and 16.21 $/GJ, respectively.

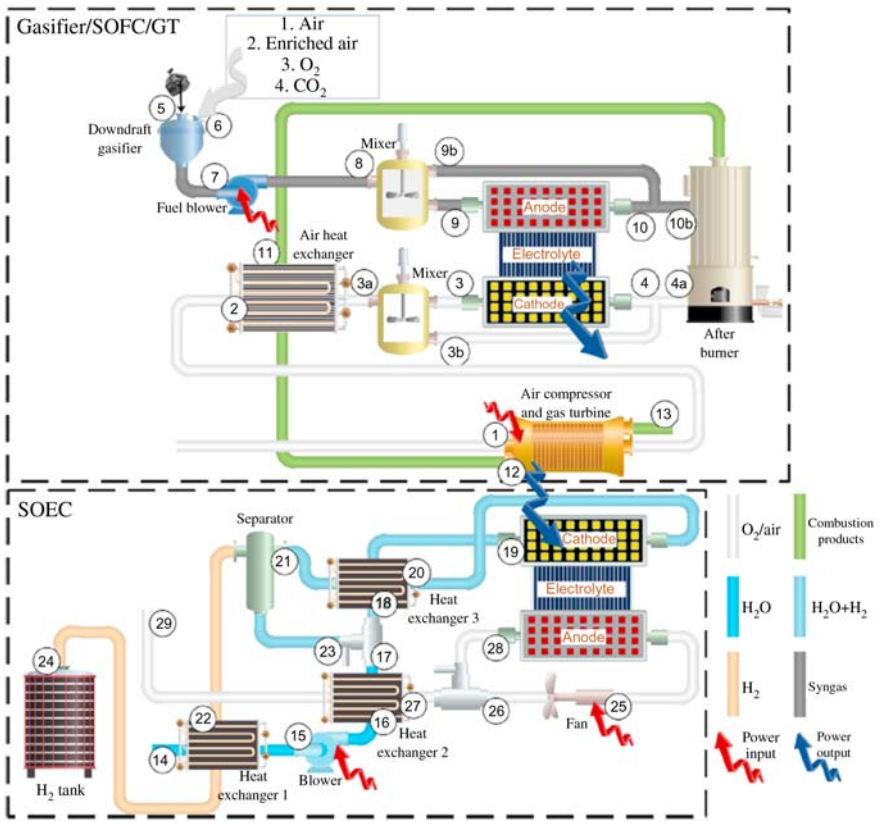

FIGURE 11.6

Integration of a biomass-based solid oxide fuel cell, gas turbine, and solid oxide electrolyzer cell [27].

11.5 Thermal management

Similar to SOFCs, ReSOCs operate in a temperature range of 600°C−1000°C. Their operating temperature is higher than other types of electrolyzers such as alkaline or PEM electrolyzers because the efficiency of the ReSOCs was significantly influenced by cell temperature [28]. In general the operating temperature of an ReSOC is related to the cell and stack designs, selected components, and the high-operating temperature resulting in cell and stack design flexibility, multiple fabrication options, high-electrolysis efficiency, multifuel capability, lower electrochemical loss, and operating temperature choices [29]. The advantages and disadvantages of the high-temperature operation of ReSOCs are summarized in Table 11.2. It should be noted that in recent years the utilization of intermediate temperature electrolyte in ReSOCs also attracted considerable attention [30].

Table 11.2 Advantages and disadvantages of high-temperature operation of ReSOCs.

Advantage	Disadvantage
• The high temperature causes the mobility of oxygen ions in the solid electrolytes and consequently resulted in an efficient ReSOC operation. • Ability to use carbonaceous reactants without risk of CO catalyst poisoning. • Precious-metal catalysts are not required for the oxidation or reduction reactions. • Even without precious-metal catalysts, the activation losses are relatively small, which is particularly important for reversible energy-storage applications. • High-system efficiencies are possible for combined heat and power generation.	• Material durability issues with thermal expansion compatibility and durability in an extreme operating environment. • The expensive balance of plant components to handle high-temperature gas processing. • High-temperatures heat must be provided to a solid-oxide electrolyzer to allow higher efficiency.

Decreasing the ReSOC temperature to an intermediate value (500°C−700°C) allows the use of more economical components, more simple design of the process, shorter start-up time, and increased durability [31].

Thermal management has high importance in ReSOCs. As mentioned before, in the SOFC mode the ReSOC is exothermic, but in the SOCE mode it could be endothermic. Therefore a proper strategy is required to balance between the exothermic and endothermic characteristics in ReSOCs. However, it must be notes that Wendel and Braun [20] considered ReSOCs as mildly exothermic in both operation modes and reported this characteristic as a point which simplifies the balance of plant integration and thermal management. Bierschenk et al. [32] coupled methanation (which is an endothermic reaction) with an endothermic electrolysis reaction inside an ReSOC and obtained a thermal balance.

As can be seen in Fig. 11.7, the electrical energy is stored by electrolyzing a mixture of water and carbon monoxide (dashed arrows) and electricity is produced (solid arrows) in the SOFC mode utilizing the resulting fuel containing methane and hydrogen. Pure oxygen is produced during the SOEC mode and is stored for use during the SOFC mode.

Similar methods were also utilized by different researchers [19,33]. It must be mentioned that the methanation method needs to be performed at lower temperatures and higher pressures. Therefore ReSOC should work with low-electrochemical losses at those reaction temperatures and high pressures [34]. Commercially available ReSOCs operate at high temperatures [21]. Santhanam et al. [35] presented another type of thermal strategy by integrating the heat storage with an ReSOC. In this method the heat produced during the exothermic

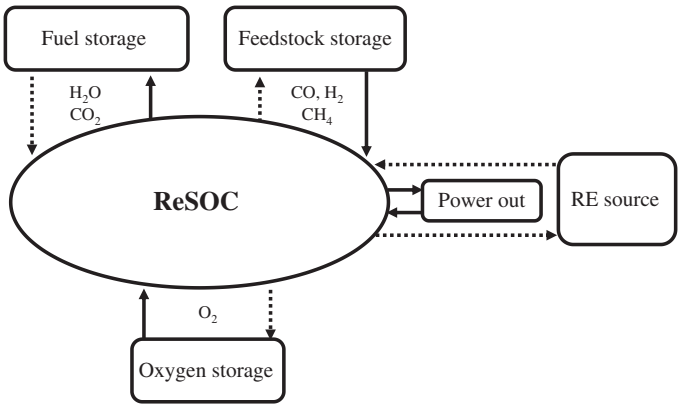

FIGURE 11.7

Integration of methanation and reversible solid oxide cell system. *ReSOC*, reversible solid oxide cell.

Adopted from D.M. Bierschenk, J.R. Wilson, S.A. Barnett, High efficiency electrical energy storage using a methane–oxygen solid oxide cell, Energy Environ. Sci. 4 (3) (2011) 944–951.

operation of ReSOC will be stored and then can be used during the endothermic operation of ReSOC. The heat also can be used as a heat supply to other processes.

11.6 Efficiency of the system

Energy and entropy balances over the ReSOC can be used in order to calculate the production of electrical energy during the SOFC mode and the consumption of electrical energy during the SOEC mode. The irreversible entropy generation denotes the internal-energy losses of the system. Even for an ideal ReSOC, which operates isothermally, there is still energy losses due to unavoidable thermodynamic irreversibility because of the changes in compositions, mixing of products, electrochemical and chemical reactions, and unconverted reactants leaving the system in the fuel stream. Therefore for an ideal ReSOC, in addition to ideal required work, some energy is necessary to overcome such losses.

Inevitable loss can be considered as thermodynamic loss and should be accounted for in addition to the ideal working state of the ReSOC [36]. There are different methods to calculate the ideal voltage and work of ReSOCs. They can be calculated using the Nernst equation with either inlet or outlet compositions, or by studying the difference between the Gibbs function at the outlet and inlet of the ReSOC [35].

The most significant factor that must be estimated for electrical energy-storage systems is the round-trip efficiency that is defined as the "overall

round-trip efficiency" and "stack round-trip efficiency" in literature. The overall round-trip efficiency of the system that depends on the efficiency of the stack and the auxiliary power required for the system is the ratio of the net-energy generated in the SOFC mode to the total-energy supplied in the SOEC mode, and can be calculated by:

$$\eta_{\text{roundtrip,overall}} = \frac{E_{\text{SOFC}}}{E_{\text{SOEC}}} = \frac{E_{\text{el,out,stack}} - W_{\text{AUX,SOFC}}}{E_{\text{el,in,stack}} - W_{\text{AUX,SOEC}}} = \frac{Q_{\text{SOFC}} V_{\text{SOFC}} - W_{\text{AUX,SOFC}}}{Q_{\text{SOEC}} V_{\text{SOEC}} - W_{\text{AUX,SOEC}}} \tag{11.4}$$

where E is the electrical energy delivered or recovered by the system over some charge and discharge duration, Q is the total-electrical charge associated with a charge or discharge process. W is the energy consumed by the auxiliary systems. V is the operating nominal cell voltage. When considering only the stack, the round-trip efficiency will be:

$$\eta_{\text{roundtrip,stack}} = \frac{E_{\text{el,out,stack}}}{E_{\text{el,in,stack}}} = \frac{Q_{\text{SOFC}} V_{\text{SOFC}}}{Q_{\text{SOEC}} V_{\text{SOEC}}} \tag{11.5}$$

To fully recharge the system, the charge transfer in each operating mode is required to be equal over a certain time interval ($Q_{\text{SOFC}} = Q_{\text{SOEC}}$). Therefore:

$$\eta_{\text{roundtrip,stack}} = \frac{E_{\text{el,out,stack}}}{E_{\text{el,in,stack}}} = \frac{V_{\text{SOFC}}}{V_{\text{SOEC}}} \tag{11.6}$$

The stack's round-trip efficiency is a useful measure to understand the performance of the system by quantifying the efficiency impact of the ReSOC stack and the auxiliary power. The efficiency of the system implementation considered in different studies is shown to be highly dependent on the ReSOC operating conditions, notably temperature, pressure, and reactant composition.

According to the literature, high-temperature ReSOC systems have high round-trip efficiency (more than 70%) and higher energy density than batteries [37]. This higher round-trip efficiency in comparison with typical low-temperature fuel cells is related to the unique characteristics of solid oxide cells namely high temperatures and carbonaceous reactants [20]. It must be mentioned that the low-temperature ReSOC systems obtain lower round-trip efficiencies (about 20%−55%) [38,39]. Xu et al. [40] proposed a novel system consisting of an SOEC integrated with a redox-cycle unit. The charge−discharge characteristics were explicitly observed by operating between the SOFC and SOEC modes. The authors reported that by using Fe or FeO as the redox materials, the new storage battery could produce an energy capacity of 348 Wh/kg−Fe and round-trip efficiency of 91.5% over 20 stable charge−discharge cycles. Mottaghizadeh et al. [41] presented an improved process design for ReSOCs in Aspen Plus with a system round-trip efficiency of 60.4% at 25 bar. The authors found that the system behavior was dependent on the design and performance of the ReSOC reactor and that the efficiency of the reactor and system had a direct relation to each other (Fig. 11.8).

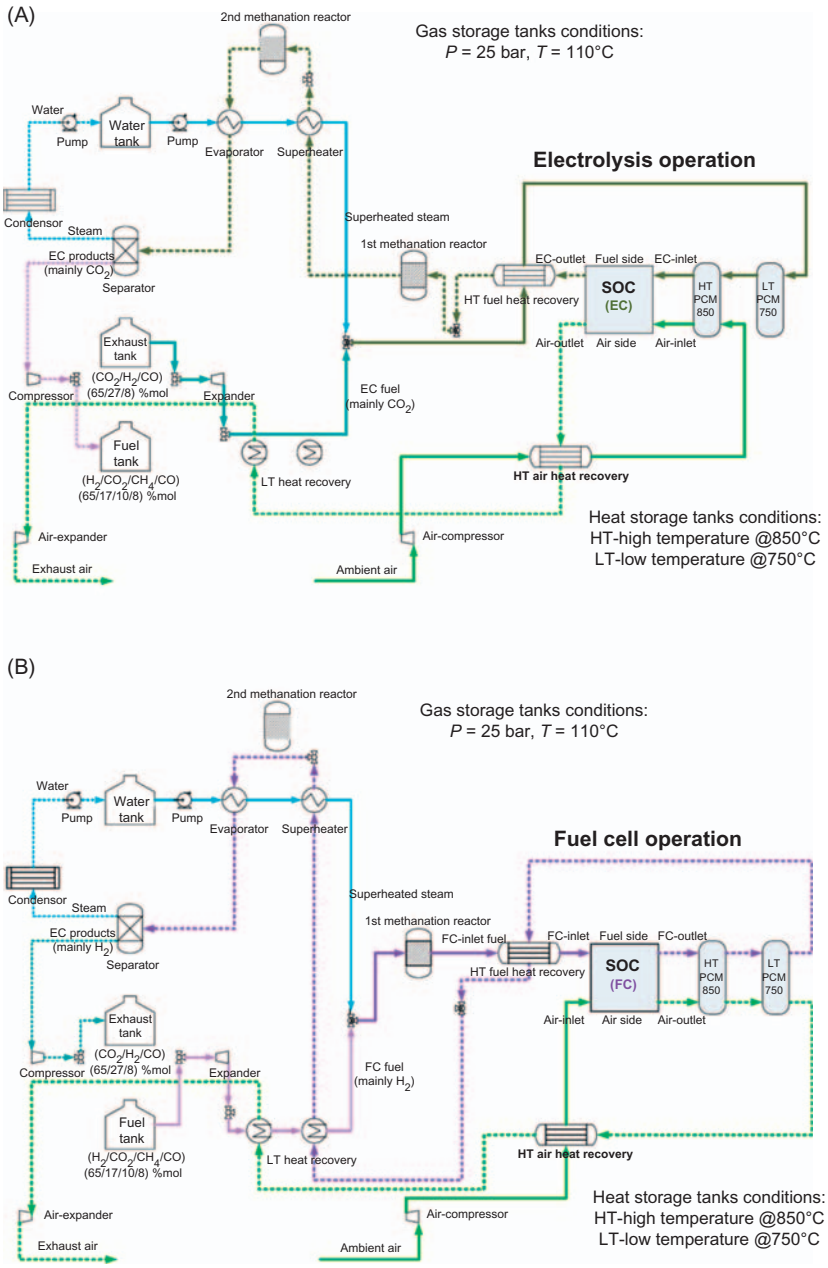

FIGURE 11.8

Reversible solid oxide cell system in (A) solid oxide electrolyzer cell mode and (B) solid oxide fuel cell mode [41].

Santhanam et al. [35] performed a theoretical study on ReSOC energy systems by experimental analysis of an ReSOC reactor under different pressures. The authors reported that a system round-trip efficiency of 55%−60% with existing ReSOC technology could be achieved. They also found that increasing the pressure could increase the round-trip efficiency. They determined the maximum theoretical limit for round-trip efficiency to be about 98% at 1 bar and 99% at 30 bar and mentioned that by using thinner electrolysis and application of better materials, even higher round-trip efficiency is possible. Kazempoor and Braun [42] showed that by operating the ReSOCs at relatively low temperatures and high pressures the produced CO and H_2 could be catalytically converted into a CH_4-rich gas inside the cell. The heat generated by the exothermic CH_4 formation could be used by the endothermic CO and H_2 formation, thereby minimizing heat losses and optimizing round-trip efficiency.

Lototskyy et al. [43] combined a solar power system as the primary energy source and utilized R-SOFC for producing hydrogen and generating electricity in the SOEC and SOFC modes, respectively. The system used metal hydride for storage of both hydrogen and heat in high temperature and metal hydride in low temperature for additional heat management, which was composed of hot-water supply, residential heating during winter, or cooling/air conditioning during summer. The energy efficiencies are reported as 69.4% and 72.4% in the SOEC and SOFC modes, respectively. Butera et al. [44] proposed a large-scale electricity storage system that was obtained by integration of a pressurized ReSOC system and catalytic reactors to store electricity as synthetic natural gas (SNG). An energy efficiency of 89% was achieved by storing SNG. They reported that gas-to-electricity efficiency was equally high and a round-trip storage efficiency of 80% was obtained in their study.

11.7 Cost and economic performance

Cost and economics studies on ReSOC systems are less than studies performed on cost and economic aspects of standalone SOFC and SOEC systems. Ni et al., [7] found that the capability of dual functions, namely work in the SOEC and SOFC modes, makes ReSOCs economically sound. Guan et al. [9] proposed a high-performance ReSOC system. They examined 10 ReSOC stacks for 1000 hours while alternating the modes. The proposed process showed highly efficient production of hydrogen and electricity. Akikur et al. [45] modeled the combination of a solar energy system and an ReSOC. The overall system efficiency achieved for the solar-SOFC mode was 23%, for the solar-SOEC mode it was 20%, and for the standalone-SOFC mode it was 83.6%. They also performed an economic analysis on an ReSOC for the cyclic duration of one year, where the SOEC and SOFC modes operated for 2920 and 2815.2 hours, respectively. The results showed the electricity cost of 0.068 US$/kWh. Jensen et al. [33] proposed

an ReSOC in combination with subsurface storage of CO_2 and CH_4 (gas-storage technology) in which the system had a high capacity for electricity storage (about 3 months), the round-trip efficiency was reported to be over 70%, and the estimated storage cost was about 0.03 $ kW/h. The authors stated that their proposed system was a modification of the system proposed by Bierschenk et al. [32]. The study showed the importance of NG for power generation and energy storage. They also illustrated that in the future, through the development of renewable electricity and energy systems, the production of electricity using the ReSOC system could be more economical. Sigurjonsson and Clausen [46] integrated a gasification system with an ReSOC system. As can be seen in the integrated system shown in Fig. 11.9A, syngas is produced in the gasifier and sent to the ReSOC, which works in SOFC mode to produce electricity. The gas engine utilized increased the electricity production by conversion of the extra fuel from the SOFC. As can be seen in Fig. 11.9B, hydrogen was mixed with syngas from the

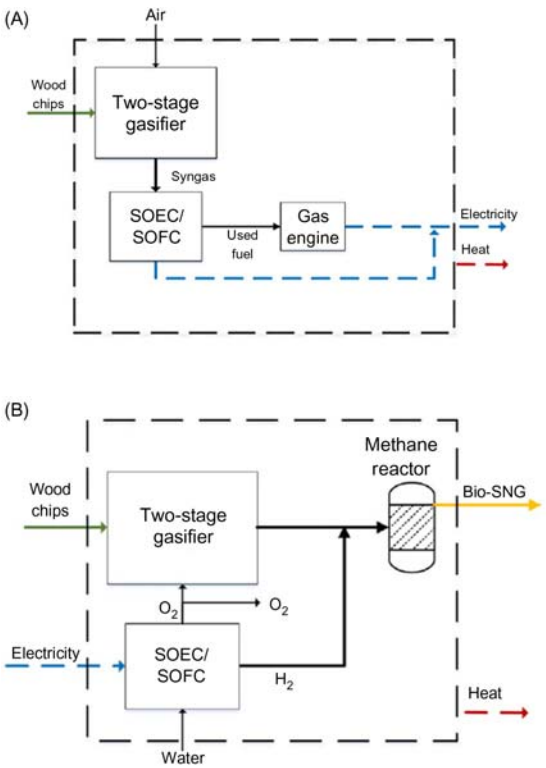

FIGURE 11.9

The integrated system proposed by Sigurjonsson and Clausen [46] in (A) electricity-production mode, and (B) electricity-storage mode. *SOFC*, solid oxide fuel cell; *SOEC*, solid oxide electrolyzer cell.

gasifier and converted into SNG in a methane reactor. Significant heat was also generated in this operation mode and used to produce district heat, as in the electricity-production mode. The authors reported that in the electricity production mode, the efficiency of the system without and with considering the heat production are 46% and 90%, respectively. In the reverse mode, the efficiency of the system without and with including the heat production are 69% and 85%, respectively.

The main part of the study by Sigurjonsson and Clausen [46] was related to a TEA of the proposed system. The TEA showed that the investment cost is high, owing to the gasifier and ReSOC costs. The analysis also indicated that district, heating sales were important for the economic feasibility of the proposed system. Analysis of the marginal cost and mode of operation demonstrated that the operational time in each mode varied significantly depending on future electricity and bio-SNG prices. A design and techno-economic study was done by Wendel and Braun [20]. They evaluated different system configurations based on round-trip efficiency, tanked energy density, and capital cost. The authors reported that the cost of energy storage using an ReSOC system was influenced by two important parameters, namely stack power and system-energy density.

11.8 Conclusion

The development of ReSOCs strongly depends on improvement of SOEC and SOFC technologies. This development is limited more by the SOEC technology in which the constraints are more critical and further due to there being fewer studies in comparison with those on SOFCs. There are several issues that are only related to an ReSOC (not SOEC and SOFC), namely the oxygen-electrode performance, set of materials, design of cell and stack, operating conditions appropriate for reversible operation, and design and integration of the system to determine the possibility of the technology. The main concerns to overcome the drawbacks and improve the performance of ReSOCs are related to reliability, new materials, performance, stability, and reduced production costs [15].

In order to improve the ReSOC system, various research scenarios are proposed:

- A single-step cofiring process, which is the manufacture of several green layers of the materials and sintering them, is one scenario to reduce the steps and energy of production of the entire cell [47].
- The next scenario, which is common in SOFCs and just developing for SOECs and ReSOCs, is using alternative metal-supported cells because of their low-cost, manufacturability, and mechanical strength [48].
- Pressurized operation is another research scenario in ReSOCs. In this type of process, the ReSOC can operate at high pressure due to the required compression of hydrogen for storage and high-pressure operation necessary

for catalysts. Utilization of high pressure showed the same benefit for the SOEC and SOFC by increasing the limited current density (which means fewer over-potentials) [49].

- Although there have been exergy and heat integration studies for the SOEC system [50], there are only a few studies on this aspect for ReSOCs [27]. This indicates a research frontier.
- More investigations are required to address the transient operation of ReSOC systems.
- TEA of different configurations can be useful for different aspects of ReSOC systems.

References

[1] F. José, A. Moreno, Reversible Solid Oxide Cell as Energy Storage System, University of Perugia, 2016.

[2] N.Q. Minh, M.B. Mogensen, Reversible solid oxide fuel cell technology for green fuel and power production, Electrochem. Soc. Interface 22 (4) (2013) 55–62.

[3] T.A. Adams, J. Nease, D. Tucker, P.I. Barton, Energy conversion with solid oxide fuel cell systems: a review of concepts and outlooks for the short-and long-term, Ind. Eng. Chem. Res. 52 (9) (2012) 3089–3111.

[4] D.J. Bents, High temperature solid oxide regenerative fuel cell for solar photovoltaic energy storage, in: 22nd Intersociety Energy Conversion Engineering Conference, 1987, p. 9203.

[5] O.Z. Sharaf, M.F. Orhan, An overview of fuel cell technology: fundamentals and applications, Renew. Sustain. Energy Rev. 32 (2014) 810–853.

[6] V.N. Nguyen, L. Blum, 5 - Reversible fuel cells, in: F. Barbir, A. Basile, T. Nejat Veziroğlu TNBT-C of HE, (Eds.), Woodhead Publishing Series in Energy. Compendium of Hydrogen Energy, Woodhead Publishing, Oxford, 2016, pp. 115–145.

[7] M. Ni, M.K.H. Leung, D.Y.C. Leung, A modeling study on concentration overpotentials of a reversible solid oxide fuel cell, J. Power Sources 163 (1) (2006) 460–466.

[8] L. Bi, S. Boulfrad, E. Traversa, Steam electrolysis by solid oxide electrolysis cells (SOECs) with proton-conducting oxides, Chem. Soc. Rev. 43 (24) (2014) 8255–8270.

[9] J. Guan, B. Ramamurthi, J. Ruud, J. Hong, P. Riley, D. Weng, N. Minh, High performance flexible reversible solid oxide fuel cell, GE Global Research Center Report DE-FC36e04GO14351, 2007.

[10] C.H. Wendel, P. Kazempoor, R.J. Braun, A thermodynamic approach for selecting operating conditions in the design of reversible solid oxide cell energy systems, J. Power Sources 301 (2016) 93–104.

[11] C.H. Wendel, Z. Gao, S.A. Barnett, R.J. Braun, Modeling and experimental performance of an intermediate temperature reversible solid oxide cell for high-efficiency, distributed-scale electrical energy storage, J. Power Sources 283 (2015) 329–342.

[12] D. Penchini, G. Cinti, G. Discepoli, U. Desideri, Theoretical study and performance evaluation of hydrogen production by 200 W solid oxide electrolyzer stack, Int. J. Hydrogen Energy 39 (17) (2014) 9457–9466.

[13] C. Graves, S.D. Ebbesen, S.H. Jensen, S.B. Simonsen, M.B. Mogensen, Eliminating degradation in solid oxide electrochemical cells by reversible operation, Nat. Mater. 14 (2) (2015) 239.
[14] K. Chen, S.-S. Liu, N. Ai, M. Koyama, S.P. Jiang, Why solid oxide cells can be reversibly operated in solid oxide electrolysis cell and fuel cell modes? Phys. Chem. Chem. Phys. 17 (46) (2015) 31308–31315.
[15] S.Y. Gómez, D. Hotza, Current developments in reversible solid oxide fuel cells, Renew. Sustain. Energy Rev. 61 (2016) 155–174.
[16] L. Bi, S. Boulfrad, E. Traversa, Reversible solid oxide fuel cells (R-SOFCs) with chemically stable proton-conducting oxides, Solid State Ionics 275 (2015) 101–105.
[17] N. Ai, M. Chen, S. He, K. Chen, T. Zhang, S.P. Jiang, High performance nanostructured bismuth oxide–cobaltite as a durable oxygen electrode for reversible solid oxide cells, J. Mater. Chem. A 6 (15) (2018) 6510–6520.
[18] D. Huan, et al., New, efficient, and reliable air electrode material for proton-conducting reversible solid oxide cells, ACS Appl. Mater. Interfaces 10 (2) (2018) 1761–1770.
[19] P. Kazempoor, R.J. Braun, Model validation and performance analysis of regenerative solid oxide cells: electrolytic operation, Int. J. Hydrogen Energy 39 (6) (2014) 2669–2684.
[20] C.H. Wendel, R.J. Braun, Design and techno-economic analysis of high efficiency reversible solid oxide cell systems for distributed energy storage, Appl. Energy 172 (2016) 118–131.
[21] J. Mermelstein, O. Posdziech, Development and demonstration of a novel reversible SOFC system for utility and micro grid energy storage, Fuel Cells 17 (4) (2017) 562–570.
[22] P. Di Giorgio, U. Desideri, Potential of reversible solid oxide cells as electricity storage system, Energies 9 (8) (2016).
[23] Y. Luo, Y. Shi, Y. Zheng, N. Cai, Reversible solid oxide fuel cell for natural gas/renewable hybrid power generation systems, J. Power Sources 340 (2017) 60–70.
[24] M. Hauck, S. Herrmann, H. Spliethoff, Simulation of a reversible SOFC with Aspen Plus, Int. J. Hydrogen Energy 42 (15) (2017) 10329–10340.
[25] V.-T. Giap, S. Kang, K.Y. Ahn, High-efficient reversible solid oxide fuel cell coupled with waste steam for distributed electrical energy storage system, Renew. Energy 144 (2018) 129–138.
[26] A. Perna, M. Minutillo, S.P. Cicconardi, E. Jannelli, S. Scarfogliero, Performance assessment of electric energy storage (EES) systems based on reversible solid oxide cell, Energy Procedia 101 (2016) 1087–1094.
[27] A. Habibollahzade, E. Gholamian, A. Behzadi, Multi-objective optimization and comparative performance analysis of hybrid biomass-based solid oxide fuel cell/solid oxide electrolyzer cell/gas turbine using different gasification agents, Appl. Energy 233–234 (2019) 985–1002.
[28] D. Ferrero, A. Lanzini, M. Santarelli, P. Leone, A comparative assessment on hydrogen production from low- and high-temperature electrolysis, Int. J. Hydrogen Energy 38 (9) (2013) 3523–3536.
[29] S.C. Singhal, K. Kendall, High-temperature Solid Oxide Fuel Cells: Fundamentals, Design and Applications, Elsevier Science, 2003.

[30] C.H. Wendel, P. Kazempoor, R.J. Braun, Novel electrical energy storage system based on reversible solid oxide cells: system design and operating conditions, J. Power Sources 276 (2015) 133–144.
[31] J. Huang, F. Xie, C. Wang, Z. Mao, Development of solid oxide fuel cell materials for intermediate-to-low temperature operation, Int. J. Hydrogen Energy 37 (1) (2012) 877–883.
[32] D.M. Bierschenk, J.R. Wilson, S.A. Barnett, High efficiency electrical energy storage using a methane–oxygen solid oxide cell, Energy Environ. Sci. 4 (3) (2011) 944–951.
[33] S.H. Jensen, et al., Large-scale electricity storage utilizing reversible solid oxide cells combined with underground storage of CO_2 and CH_4, Energy Environ. Sci. 8 (8) (2015) 2471–2479.
[34] M. Lo Faro, D. La Rosa, V. Antonucci, A.S. Arico, Intermediate temperature solid oxide fuel cell electrolytes, J. Indian Inst. Sci 89 (4) (2012) 363–380.
[35] S. Santhanam, M.P. Heddrich, M. Riedel, K.A. Friedrich, Theoretical and experimental study of reversible solid oxide cell (r-SOC) systems for energy storage, Energy 141 (2017) 202–214.
[36] S.L. Miller, M.N. Svrcek, K.Y. Teh, C.F. Edwards, Requirements for designing chemical engines with reversible reactions, Energy 36 (1) (2011) 99–110.
[37] C.H. Wendel, Design and analysis of reversible solid oxide cell systems for electrical energy storage, Colorado School of Mines, Arthur Lakes Library, 2015.
[38] E. Varkaraki, N. Lymberopoulos, E. Zoulias, D. Guichardot, G. Poli, Hydrogen-based uninterruptible power supply, Int. J. Hydrogen Energy 32 (10) (2007) 1589–1596.
[39] A. Doddathimmaiah, J. Andrews, Theory, modelling and performance measurement of unitised regenerative fuel cells, Int. J. Hydrogen Energy 34 (19) (2009) 8157–8170.
[40] N. Xu, X. Li, X. Zhao, J.B. Goodenough, K. Huang, A novel solid oxide redox flow battery for grid energy storage, Energy Environ. Sci. 4 (12) (2011) 4942–4946.
[41] P. Mottaghizadeh, S. Santhanam, M.P. Heddrich, K.A. Friedrich, F. Rinaldi, Process modeling of a reversible solid oxide cell (r-SOC) energy storage system utilizing commercially available SOC reactor, Energy Convers. Manag 142 (2017) 477–493.
[42] P. Kazempoor, R.J. Braun, Model validation and performance analysis of regenerative solid oxide cells for energy storage applications: Reversible operation, Int J Hydrogen Energy 39 (11) (2014) 5955–5971.
[43] M. Lototskyy, et al., A concept of combined cooling, heating and power system utilising solar power and based on reversible solid oxide fuel cell and metal hydrides, Int. J. Hydrogen Energy 43 (40) (2018) 18650–18663.
[44] G. Butera, S.H. Jensen, L.R. Clausen, A novel system for large-scale storage of electricity as synthetic natural gas using reversible pressurized solid oxide cells, Energy 166 (2019) 738–754.
[45] R.K. Akikur, R. Saidur, H.W. Ping, K.R. Ullah, Performance analysis of a co-generation system using solar energy and SOFC technology, Energy Convers. Manag. 79 (2014) 415–430.
[46] H.Æ. Sigurjonsson, L.R. Clausen, Solution for the future smart energy system: a polygeneration plant based on reversible solid oxide cells and biomass gasification producing either electrofuel or power, Appl. Energy 216 (2018) 323–337.

[47] K.J. Yoon, G. Ye, S. Gopalan, U.B. Pal, Cost-effective single step cofiring process for manufacturing solid oxide fuel cells using HSC anode, J. Fuel Cell Sci. Technol. 7 (2) (2010) 21010.
[48] M.C. Tucker, Progress in metal-supported solid oxide fuel cells: a review, J. Power Sources 195 (15) (2010) 4570–4582.
[49] L. Bernadet, G. Gousseau, A. Chatroux, J. Laurencin, F. Mauvy, M. Reytier, Influence of pressure on solid oxide electrolysis cells investigated by experimental and modeling approach, Int. J. Hydrogen Energy 40 (38) (2015) 12918–12928.
[50] Y. Luo, X. Wu, Y. Shi, A.F. Ghoniem, N. Cai, Exergy analysis of an integrated solid oxide electrolysis cell-methanation reactor for renewable energy storage, Appl. Energy 215 (2018) 371–383.

CHAPTER

Mobile applications: cars, trucks, locomotives, marine vehicles, and aircraft

12

Wenqian Chen

Imperial College London, Department of Chemical Engineering, London, United Kingdom

12.1 Introduction

A vehicle is an entity designed for the transportation of people or materials. Vehicles require energy for propulsion and auxiliary operations such as lighting and air conditioning, all of which can be supplied by fuel cells (FCs). Table 12.1 summarizes the key performance metrics of an solid oxide fuel cell (SOFC) as the power source for a vehicle.

SOFCs have clear advantages over conventional energy generation systems in terms of energy efficiency and power density. The typical energy efficiency of an SOFC ($>50\%$) is significantly higher than that of a conventional diesel engine (approximately 35%) [1], and the power density of an SOFC is superior in comparison to internal combustion engines [2]. Due to its high energy efficiency, an SOFC consumes much less fuel than internal combustion engines and emits significantly less CO_2.

In comparison with other fuel-cell technologies such as alkaline, direct methanol, molten carbonate, and phosphoric acid fuel cells, proton exchange membrane fuel cells (PEMFCs) and SOFCs are the most suitable for vehicle applications [3]. Although much development work has been conducted on PEMFCs as the power source for fuel cell electric vehicles (FCEVs) due to its low operation temperature (approximately 80°C) and short response time, its application is limited by the lack of an extensive hydrogen fuel distribution network and the safety concerns about the storage of hydrogen. SOFCs are considered as a viable energy source for FCEVs due to its fuel flexibility, as it can consume a wide range of hydrocarbons such as diesel and gasoline. Furthermore, the high operating temperature of SOFCs enable internal reforming of hydrocarbon fuels and the consumption of the resulting reformate [4–6]. This removes the necessity of a fuel reformer, which is of paramount importance for PEMFCs.

The high operating temperature of SOFCs means the excess heat produced by the cell can be partially recovered by a heat engine such as a gas turbine (GT) or Stirling engine (Fig. 12.1) [7,8]. In a SOFC–GT system (Fig. 12.2A), the flue gas of the SOFC heats up the air and fuel gas in heat exchangers before they enter

Design and Operation of Solid Oxide Fuel Cells. DOI: https://doi.org/10.1016/B978-0-12-815253-9.00012-4

Table 12.1 Key considerations for solid oxide fuel cell (SOFC) as a power source for vehicles.

Performance metric	Note
Power density	Tubular SOFC has higher power density than the planar configuration
Energy efficiency	SOFCs have the highest energy efficiency among all types of fuel cells
Fuel flexibility	SOFCs can use a wide range of hydrocarbons as fuels
Safety	High operating temperature of SOFCs can be a safety concern
Emission	SOFCs have low emission of CO_2 due to high energy efficiency
Cost	Significant cost reduction is needed for SOFCs to be competitive

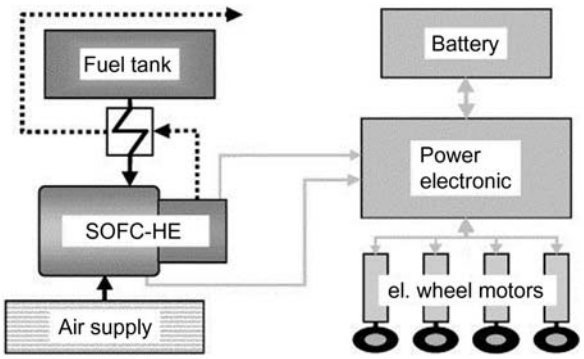

FIGURE 12.1

Vehicle system with an solid oxide fuel cell as the energy source for propulsion [8].

the cathode and anode chambers. Leaving the heat exchangers with a lower temperature, the flue gas is then heated by the integrated cooler of the SOFC before its expansion in the GT. On the other hand, the cooling and reaction loops in the SOFC−Stirling engine system are separated (Fig. 12.2B). The working fluid of the Stirling engine (usually helium) serves as the coolant of the SOFC section.

The SOFC−GT system is particularly interesting as it has been implemented for stationary power generation to achieve high overall-energy efficiencies [9]. For instance, Siemens Westinghouse Power has developed a number of SOFC−GT systems that have an overall energy efficiency of approximately 75% [10]. Its 100 kW system was installed in Arnhem, the Netherlands, and consisted of two 576 cell substacks in an SOFC generator. The diameter and length of each tubular cell were 22 mm and 1500 mm, respectively. The 220 kW system installed in the University of California, Irvine, as well as the 300 kW system tested in Pittsburgh had similar designs as the 100 kW system. Mitsubishi Heavy Industries

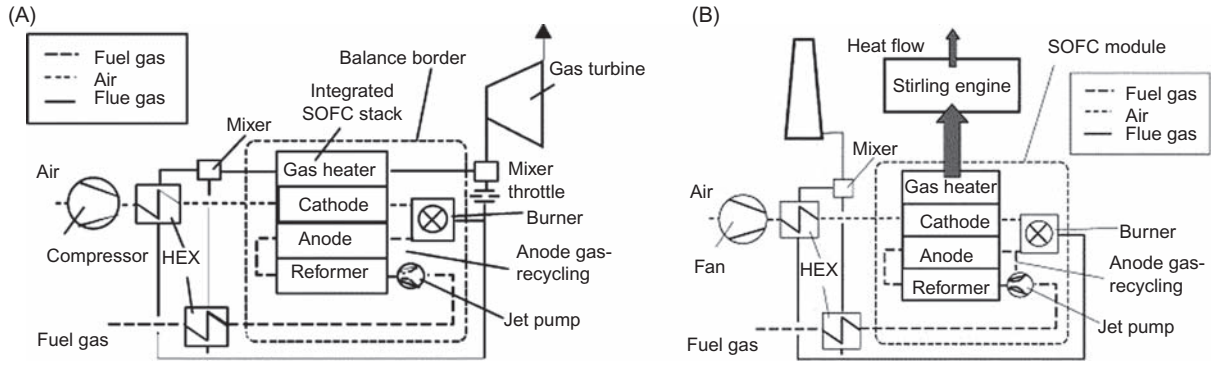

FIGURE 12.2

(A) Solid oxide fuel cell (SOFC)—gas turbine and (B) SOFC—Stirling engine systems [8].

has also developed a 200 kW SOFC−GT system that comprised tubular SOFC cells [11]. Similar to the Siemens Westinghouse systems, the tubular cells were 1500 mm in length and 28 mm in diameter. The reported electric efficiency was 50%, which was higher than the reported value for the 100 kW Siemens Westinghouse system (46%). While these systems demonstrate the feasibility of SOFC−GT systems for achieving high energy efficiency, they also serve as the basis for many simulation studies on the design and operation of SOFC−GT systems [12−16].

A typical SOFC−GT system for stationary-power generation is too large for the direct application in a land FCEV. For example, the dimension of the 200 kW Siemens Westinghouse Power system was 7.4 m × 2.8 m × 3.9 m [10]. The development of microtubular SOFC (MT-SOFC) (Fig. 12.3) and microgas turbines enables the miniaturization of the SOFC−GT system, which is vital for its vehicle applications [8,17−20].

An MT-SOFC typically has a single-cell diameter less than 3−5 mm, which is a significant reduction from the case of stationary power generation (e.g., 22 mm for the Siemens Westinghouse Power system) [21]. The development of MT-SOFCs started in the early 1990s [22]. The first prototypes of cell stacks reported in 1997 and 1998 consisted of 200 and 1000 yttria-stabilized zirconia (YSZ) tubes, whose diameter and wall thickness were 2.4 and 0.2 mm, respectively [23−25]. These tubes could survive 50 thermal cycles between 400°C and 800°C with a rate of 200°C/min, demonstrating their excellent thermal shock resistance due to the large surface-area-to-volume ratio.

In order to further improve the performance of MT-SOFCs, the anode-supported and cathode-supported versions have been developed to significantly reduce the thickness of the electrolyte and the related ohmic loss [26−28].

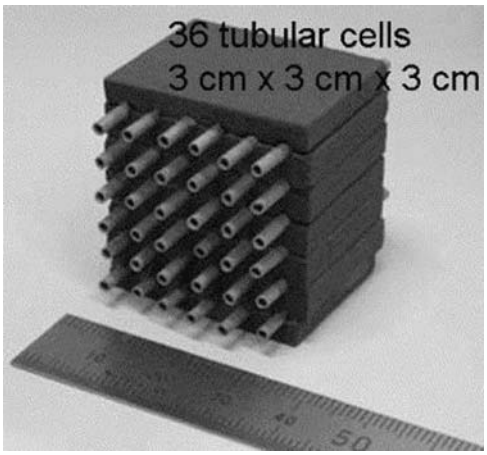

FIGURE 12.3

Microtubular solid oxide fuel cell stack [19].

Table 12.2 List of commercial microgas turbines [31].

Manufacturer	Power (kWe)	Efficiency (%)
Nissan	3	8 – 10
MTT BV	3	16
Bladon jets	12	–
Capstone turbine corporation	30	26
	65	29
	200	33
ET group	45	28
Elliott energy system	45	30
	80	
	200	
Ingersoll-Rand	70	33
Honeywell (allied signal)	75	29
Bowman	80	27

Nanodynamics Energy has developed anode-supported MT-SOFCs that have excellent thermal shock resistance and stability [29]. Experimental data show that its anode-supported MT-SOFCs could survive thermal cycles between 200°C and 850°C with a heating rate of 350°C/min and a cooling rate of 550°C/min. In addition, they showed no power degradation after 2000 hours of long-term load cycling.

A microgas turbine has a typical power range less than 500 kW [30]. Its compact design is achieved by assembling a permanent magnet of the generator, turbine, and compressor on the same shaft. Table 12.2 summarizes the power output and efficiency of some commercial microgas turbines showing the general trend that efficiency decreases with power output, which is directly proportional to size [31]. The recuperator is one of the most important components in a microgas turbine as it enables the heat exchange between the exhaust gas and the compressed air before the combustor. The thermal-hydraulic performance of the recuperator has a significant effect on the efficiency of the microgas turbine [32]. The recuperator should have a heat-transfer effectiveness higher than 90%, while having good oxidation resistance at temperatures higher than 650°C and a relative pressure loss less than 3% [31].

12.2 Solid oxide fuel cells for vehicle propulsion

Energy storage is necessary in the power generation system of SOFCs for handling peak power and absorbing the regenerative energy from the deceleration of the vehicle. The most commonly used energy storage systems are rechargeable

Table 12.3 List of rechargeable batteries for electric vehicles [34].

Type	Specific energy (Wh/kg)	Specific power (W/kg)	Cycle life (cycles)
Lithium-ion	120–130	1500	–
Lead-acid	30–50	200–400	400–600
Nickel-metal hydride	80	1000	–

batteries and supercapacitors [33]. There are various types of rechargeable batteries, including lead-acid, lithium-ion, and nickel-based types (Table 12.3) [34]. Although lithium-ion battery is by far the best option in terms of durability and energy density, it is also much more costly than its lead-acid and nickel-based counterparts [35].

In general a rechargeable battery has higher energy density but lower power density than a supercapacitor. In addition, the charging time of a supercapacitor is significantly shorter in comparison to a rechargeable battery as the supercapacitor can tolerate a larger charging current. Coupling a FC with a supercapacitor can be more advantageous than the FC–battery combination as the former produces smaller power variations during operations where the vehicle is accelerated and decelerated regularly [33]. This also means the power supply by FC is more consistent, leading to a longer cycle life.

12.2.1 Propulsion of land vehicles

Various major automakers have commercialized electric vehicles as cleaner alternatives to traditional automotives that are based on the combustion of fossil fuels, paving the way for the introduction of FCEVs in the near future. For land automotives, the typical power output requirements for propulsion and auxiliary operations are 75 and 2–20 kW, respectively [3,8,36].

One prototype of SOFC-based FCEVs is the ZEBRA battery-intermediate-temperature SOFC hybrid vehicles (Fig. 12.4) [37–41]. The system consists of a power generation section, which includes fuel tank, fuel processor, SOFC, ZEBRA battery, motor, auxiliary units, and control system. The vehicle management unit is the interface between the hardware and control system. At the center of the control system is the power controller, which manages the power flow among the various components of the system. The fuel cell management interface controls the operations of the energy generation section, whereas the battery management interface controls the operation of the ZEBRA battery.

Unlike the high temperature SOFC in the Siemens Westinghouse Power system, the intermediate-temperature SOFC in this system operates between 500°C and 850°C. Lowering the operation temperature of SOFCs has several advantages. First, it reduces the manufacturing cost as economical materials can be used for

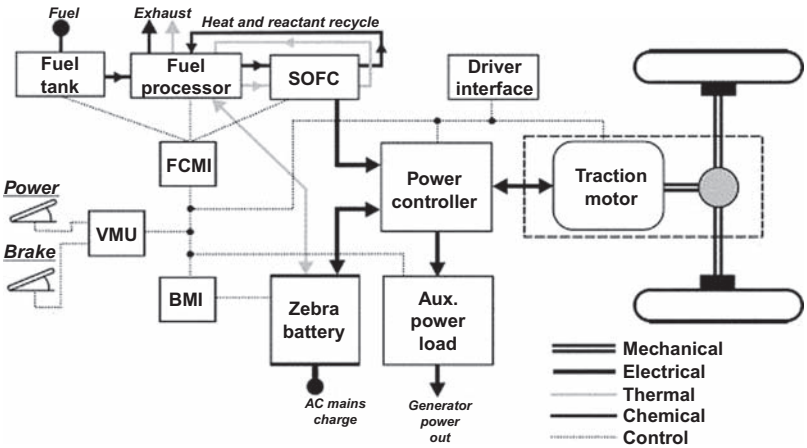

FIGURE 12.4

ZEBRA battery-intermediate-temperature solid oxide fuel cell system [37].

making components such as interconnects. Second, the cell has a longer cycle life due to the slower corrosion rate at lower temperature. Third, the overall system requirements are significantly simpler, leading to lower cost of the vehicle.

Two types of planar intermediate-temperature SOFCs were tested in this system. The first was a metal-supported low-temperature model that operated between 500°C and 650°C, and the second was an anode-supported high-temperature model with direct internal reforming that operated between 700°C and 850°C [38,42–44]. With a cell dimension of 10 cm × 10 cm, both models could generate a net-electrical direct current power of 5 kW with similar net-system efficiencies (48%). Clean methane and air were the fuel and oxidant, respectively.

The ZEBRA battery (Fig. 12.5) investigated was a sodium–nickel–chloride battery that was designed as the main power source for electric vehicles [45]. At the charged state the cathode is nickel–nickel chloride and the anode contains molten sodium. The current collectors at the cathode and anode are a copper-cored nickel wire and a cell case, respectively. The ceramic electrolyte is β-alumina, which is a dense non-porous material that allows the passage of the Na^+ ions at high temperature, but not the electrons. For example, the resistivities of β-alumina for Na^+ ions and electrons at 350°C are 5.5 Ω cm and 10^{12} Ω cm, respectively.

Unlike the SOFC–GT system, the ZEBRA intermediate-temperature SOFC hybrid system does not have a gas turbine. The hybrid system is "battery dominant", where the immediate and intermediate power requirement of the vehicle are supplied by the battery. The intermediate-temperature SOFC operates in a "always-on" mode to supply energy to the battery. The economic analysis of the hybrid system in comparison with the internal combustion engine only, battery only, and SOFC only systems is presented in Fig. 12.6 based on the parameters

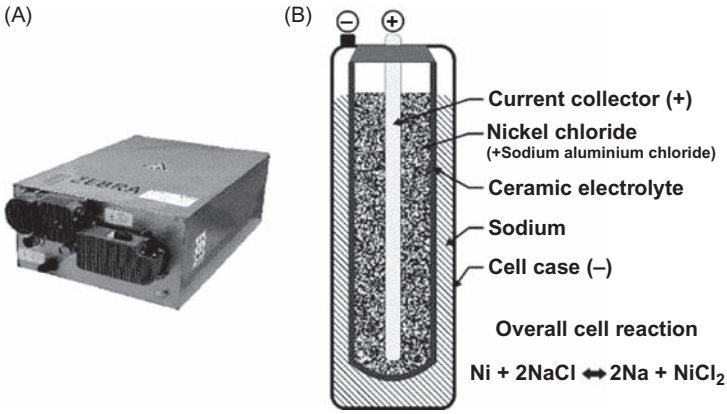

FIGURE 12.5

ZEBRA (A) battery and (B) cell [37].

summarized in Table 12.4 [39]. It was found that the hybrid system could be economically viable if the fuel-cell price could be reduced to less than £400/kW and the hybrid system would be more cost effective for commercial vehicles than private vehicles due to their longer driving time per day.

In a simulation study a 3.5 kW SOFC−GT system was modeled as the range extender of an electric vehicle powered by a 19 kWh lithium-ion battery [46]. Unlike the "always-on" mode in the ZEBRA intermediate-temperature SOFC system, the SOFC in this case operated in the "on/off" mode. The simulated SOFC was turned on to charge the battery once the charge fell below a certain level and then turned off when the maximum-charge level was reached. The integration of the SOFC−GT system dramatically increased the autonomy of the vehicle from 151 km to more than 600 km, while the total mass only increased marginally by approximately 5%. The SOFC−GT system increased the capital investment from €24,000 to €30,000. The resulting tank-to-wheel emission of CO_2 was only 30 g/km, which was significantly lower than the value of a typical internal combustion engine vehicle (115 g/km).

Several simulation studies demonstrated the feasibility of using the SOFC−GT system to power locomotives, which require a maximum power of approximately 4 MW [47−51]. In one case the SOFC−GT system was coupled with the reformation of biodiesel (Fig. 12.7). Four stacks of 1 MW SOFCs were required and each had a dimension of 0.33 m × 0.33 m × 20.46 m based on the planar membrane configuration. Table 12.5 presents the cost breakdown of the SOFC−GT powered locomotive in comparison to the case of a conventional diesel internal combustion engine over 40 years with an internal rate of return of 8%. Biodiesel was the fuel in both cases. Although the SOFC−GT system had a higher power weighted average efficiency than the diesel internal combustion engine (48% vs 35%), the significantly higher capital cost of the SOFC−GT system

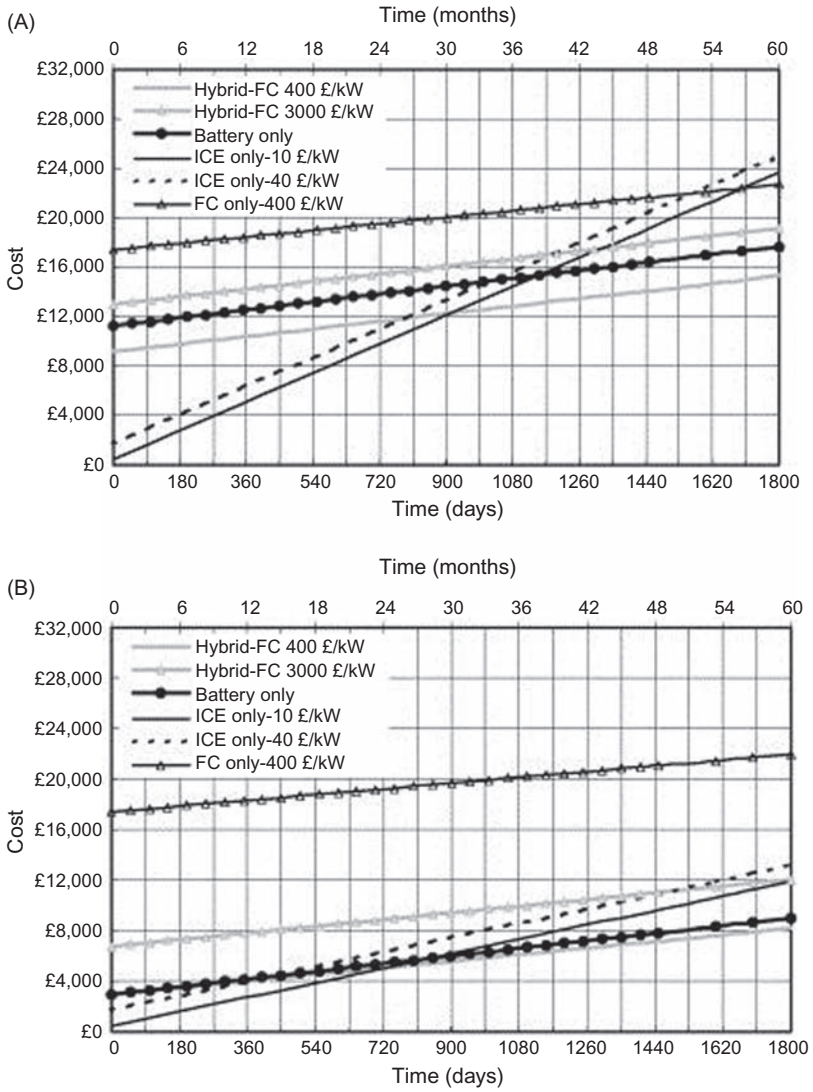

FIGURE 12.6

Capital and running costs for systems with different power supplies: (A) current battery price and taxed fuels; (B) volume manufacture battery price and untaxed fuels [39].

meant that an annual fuel cost increase higher than 9% would be required for it to be more cost-effective than the conventional diesel internal combustion engine.

Another simulation study showed that natural gas could be a better fuel than diesel for SOFC−GT systems [51]. Although the SOFC−GT system that used diesel had significant CO_2 and NO_x emission reduction compared to the

Table 12.4 Parameters for the economic analysis of ZEBRA battery, intermediate-temperature, SOFC system [39].

Parameter	Value[a]
CNG price	£0.50 $kg^{-}1$
CNG fuel duty	£0.07 kg^{-1}
Methane energy	9 kWh m^{-3}
Methane density (1 bar)	0.645 kg m^{-3}
Methane consumption	0.230 m^3 h^{-1} kW^{-1}
Gasoline price	£0.754 L^{-1}
Gasoline duty	£0.3826 L^{-1}
Gasoline fuel economy	15.4 km L^{-1}
Electricity price	£0.08 kWh^{-1}
Electricity VAT	5%
Fuel cell efficiency	48.4%
Battery efficiency	89%
Fuel cell price range	£305 – 2287 kWh^{-1}
Battery price range	£53 – 233 kWh^{-1}
ICE price range	£7.6 – 30 kW^{-1}
Power electronics and electric motor price	£8.4 kW^{-1}
ICE power	42.3 kW
Average traction power required	5.10 kW
Average speed for NEDC drive cycle	33.6 km h^{-1}
Auxiliary power requirement	800 W
Maximum power requirement	42.3 kW
Battery power to energy ratio	1.8 W Wh^{-1}

CNG, Compressed natural gas*; FC,* fuel cell*; ICE,* internal combustion engine*; NEDC,* New European Driving Cycle.
[a]*British pound converted to US dollars based on the average yearly rates of 2017 and 2018 (£1 = US $1.312).*

conventional internal combustion engine, the heat integration of the diesel reformer was difficult to control. In addition, the reformation of diesel consumed a large quantity of water that exceeded the storage quantity in a typical locomotive. The use of natural gas as fuel removed the necessity of the reformer and, hence, all the technical issues involved.

The control problem created by the use of diesel was echoed by two other simulation studies in which the use of hydrogen, natural gas, and diesel was considered [49,50]. Although the use of these fuels led to high-system efficiency (65%−70%) the case of diesel took a significantly longer time to reach steady-state in response to the dynamic changes of power requirement. This was caused by the difficulty in the control of fuel utilization. Therefore, the use of natural gas as fuel can enhance the competitiveness of the SOFC−GT system for powering locomotives.

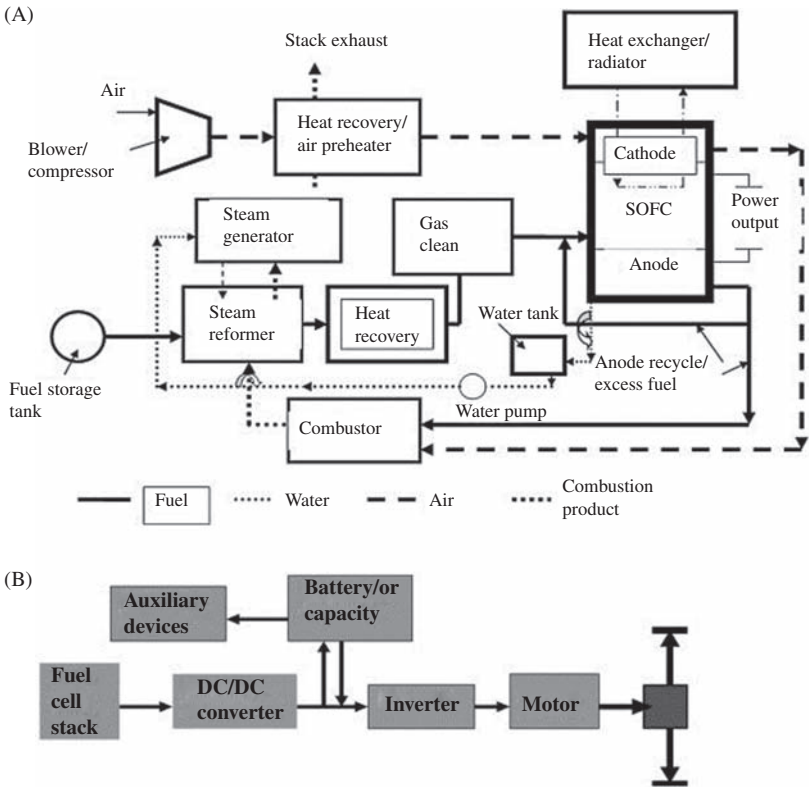

FIGURE 12.7

(A) Proposed system consisting of solid oxide fuel cell (SOFC)–gas turbine and fuel gasification unit. (B) SOFC powered train [47].

Table 12.5 Cost breakdown of the solid oxide fuel cell (SOFC)–gas turbine and diesel internal combustion engine cases over 40 years in millions [47].

	Diesel IC (no fuel-cost increases)	SOFC (no fuel-cost increases)	Diesel IC (9% annual fuel-cost increase)	SOFC (9% annual fuel-cost increase)
Capital cost	$1.0	$2.7	$1.0	$2.7
Maintenance cost	$0.014	$0.046	$0.014	$0.046
Fuel cost	$2.0	$1.4	$7.3	$5.3
Total	$3.0	$4.2	$8.3	$8.1

IC, *Internal combustion.*

12.2.2 Propulsion of aerial and water vehicles

There is a strong interest in the use of SOFCs for powering aerial and water vehicles, especially unmanned aerial vehicles (UAVs) and unmanned underwater vehicles (UUVs), which have been frequently used for surveillance and communication in the civilian and military domains [52–57]. The key-performance metric for UAVs and UUVs is endurance (i.e., maximum operating time), which is heavily dependent on the specific energy of the power system. On the other hand, fuel efficiency and emissions into the environment are the focus of the applications of SOFCs in airliners and ships [58–61].

Fig. 12.8 is the typical power profile for a high-altitude long-endurance UAV, showing that the peak power requirement for the SOFC-based power system is approximately 140 kW [52]. The conventional lithium-based batteries in UAVs have specific energies between 150 Wh/kg and 250 Wh/kg, which limits the endurance of the vehicles to 60–90 minutes [62–65]. This problem can be overcome by FCs such as PEMFCs and SOFCs, which have significantly higher specific energies. While most of the commercial fuel-cell systems for UAVs are based on PEMFC (Table 12.6), the low volumetric energy densities of compressed hydrogen and liquid hydrogen in comparison with common hydrocarbon fuels such as kerosene and propane (Table 12.7) have encouraged the adoption of the SOFC-based system due to its fuel flexibility.

In a simulation study, kerosene was used as the fuel for SOFC in an UAV and the system allowed the recirculation of anode and cathode exhausts [66]. The overall efficiency was 64%, which was better than most existing UAV systems. The simulation results showed a compromise between efficiency and current density, as higher current density would result in higher polarization loss and lower efficiency.

A number of prototypes have been developed for SOFC-powered UUVs [57]. For example, API Engineering LLC and Nextech Materials were tasked with the development of a 2.5 kW SOFC-power system for a UUV with a length of 54 cm,

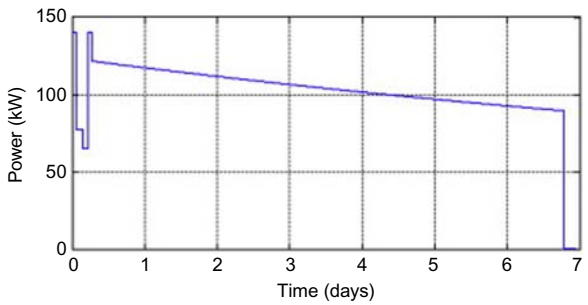

FIGURE 12.8

Power profile of a typical high-altitude long-endurance unmanned aerial vehicle [52].

Table 12.6 Commercial fuel-cell systems for the propulsion of unmanned aerial vehicles (UAVs) [56].

Manufacturer/ model	Type	Power (W)	Specific power (W/kg)	Power density (W/L)
Ultra Elec. AMI Roamio D245	SOFC	245	96.1	–
BCS FC	PEMFC	500	52	–
Energyor EPOD EO-210-XLE	PEMFC	210	57.5	–
Energyor EPOD EO-310-XLE	PEMFC	310	78.5	–
Energyor EPOD 410-LE	PEMFC	410	120.6	–
Horizon AeroStack A-200	PEMFC	200	400	278
Horizon AeroStack A-500	PEMFC	500	434	162
Horizon AeroStack A-1000	PEMFC	1000	571	224
Lynntech Gen IV	PEMFC	5000	250	263
Protonex ProCore	PEMFC	200	74	71.5
Protonex ProCore VI	PEMFC	800	1961	–
Protonex UAV C-250	PEMFC	250	208	185
Protonex Ion Tiger	PEMFC	550	550	–
Spectronik FLY-150	PEMFC	150	326.1	–
Spectronik FLY-200	PEMFC	200	400	–
Spectronik FLY-300	PEMFC	300	545.5	320.7
UTRC Rotorcraft	PEMFC	1200	675	–

whereas FC energy was to develop an SOFC−battery system that could provide 1800 kWh electricity with liquid fuels over 70 days without using any external air. Like UAVs, the specific energy of the SOFC system is the most important design parameter due to the limited space available inside UUV as well as the neutral buoyancy requirement for the vehicle.

For surface ships the typical power requirement for propulsion is between 5 and 50 MW [67]. The high cost of SOFC systems relative to conventional diesel internal combustion engines makes it difficult to propel a surface ship solely with an SOFC system. In a simulation study, an SOFC was hybridized with the conventional diesel internal combustion engine to power a platform supply vessel (PSV) (Fig. 12.9), which is commonly used for supporting various activities on offshore platforms [68]. Two modules of 250 kW SOFC were installed to provide up to 20% of the total power requirement of the PSV, whose power requirement was between 2.5 and 5 MW. The SOFC modules consumed methanol as the fuel

Table 12.7 Energy density of hydrogen and hydrocarbon fuels [52].

Fuel	Gravimetric density (MJ/kg)	Volumetric density (MJ/L)
Kerosene	43	35
Hydrogen (350 bar)	120	1.7
Hydrogen (650 bar)	120	3.6
Liquid hydrogen	120	8.4
Methanol	20	16
Propane	46	25

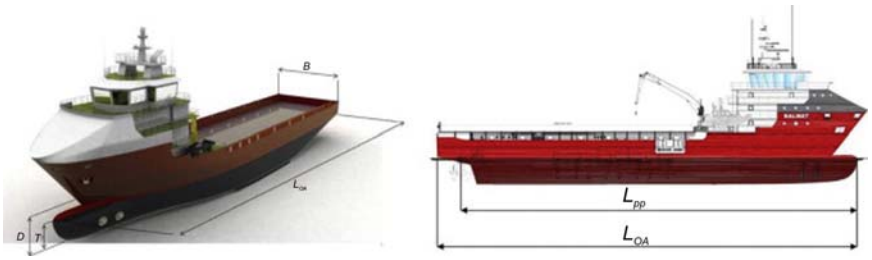

FIGURE 12.9

Platform supply vessel powered by solid oxide fuel cell and diesel internal combustion engine [68].

and the total efficiency was between 80% and 85%. Powering a PSV with this hybrid system could achieve more than 50% reduction in exhaust gas emission and more than 30% reduction in fuel cost.

12.3 Solid oxide fuel cell for auxiliary power supply

The high cost of an SOFC hinders its immediate adoption as the main power source for vehicles despite its high energy efficiency and low environment damaging emissions. The auxiliary operations of the vehicle such as lighting and air conditioning provide comfort and ease of operation to the operator during travel. As the corresponding power requirement is significantly lower than propulsion (e.g., 2−5 kW vs 75 kW for land automotives) [7], various SOFC-based auxiliary power units (APUs) have demonstrated the operational feasibility and potential of cost saving due to their high energy efficiency and low environment damaging emission.

12.3.1 Auxiliary power for land vehicles

The proof of concept SOFC-APU developed by Delphi Automotive Systems and BMW was designed for automotive applications [69,70]. It comprised mainly a

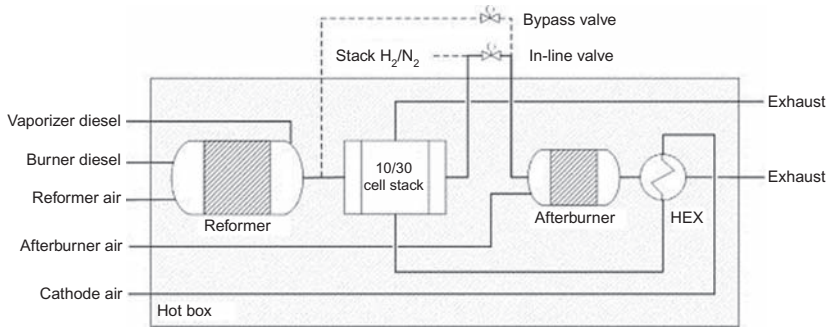

FIGURE 12.10

Solid oxide fuel cell-based auxiliary power unit prototype produced by Webasto AG [71].

fuel reformer system, four stacks of SOFCs, and a lithium ion battery. The SOFC consumed gasoline as the fuel and was operated at 750°C. The successful development of this SOFC-APU led to more advanced generations that could produce 3−10 kW power and use gasoline and diesel as fuels.

The SOFC-APU prototype produced by Webasto AG comprised mainly a fuel reformer, SOFC stack, and an afterburner (Fig. 12.10) [71]. The fuel was diesel with low sulfur content and the power generation target was 1 kW with the 60-cell stack. In the reformer the diesel was partially oxidized by the catalyst. The SOFC was electrolyte-supported and operated at 850°C. Experimental data showed that the demonstration systems with 10-cell and 30-cell stacks had no degradation over 4 hours of operation and no soot was formed. The 30-cell stack system could generate over 360 W electricity.

The DESTA project recently developed an SOFC-APU for a heavy-duty long-haul truck [72]. During the nights of the multiple-day journey, the internal combustion engine of the truck is usually run at low power relative to the rated power to meet the auxiliary power requirements. The resulting efficiency is less than 10%, while the engine generates disproportionately large emissions into the environment. The developed SOFC-APU consumed ultra low sulfur diesel as fuel to supply approximately 3 kW power. The system comprised mainly a fuel reformer, an SOFC stack, and an off-gas burner. The operating temperature was 800°C. The SOFC-APU was installed in a Volvo class 8 heavy-duty truck for road testing (Fig. 12.11). Experimental data showed that the electrical efficiency was 29% and the CO_2 emission was reduced by 73% relative to the internal combustion engine truck. The start-up time was less than 70 minutes from cold state and 30 minutes from warm state.

12.3.2 Auxiliary power for aerial and water vehicles

The conventional APU in aircraft is a small gas turbine system that provides pneumatic and electrical power for various operations such as starting the main

FIGURE 12.11

Demonstration truck with the DESTA solid oxide fuel cell-based auxiliary power unit [72].

engines, lighting, and air conditioning. An SOFC-APU can overcome the problems of conventional aircraft APU including low efficiency (20% on land and 40% in air) and high level of noise and pollution. For long-range traveling the target power generation capacity is between 400 and 977 kW [73].

Due to high cost the development of an aircraft SOFC-APU has been limited to simulations, which showed that the SOFC−GT system (Fig. 12.2A) could be a suitable configuration [55,74−78]. One of the simulation studies showed that the SOFC−GT system could achieve an overall-thermal efficiency of 62%. The model also showed that high turbine inlet temperature and low pressure ratio could lead to high thermal efficiency.

In another simulation study an SOFC−GT system (Fig. 12.12) was designed to produce a net electrical power of 440 kW for a long-range aircraft with a capacity of 300 passengers [76]. The operations at sea level and cruise level (12,500 m) were considered to account for the changes in the ambient temperature and pressure. The mass of the SOFC−GT system was significantly higher at sea level than at cruise level (1912 kg vs 1396 kg) because a larger SOFC was needed to meet the higher power requirement at sea level as the turbine could not expand the gas as much under ambient pressure. The system designed for operating at sea level also had a significantly lower thermal efficiency than at cruise level (42% vs 73%) as the pre-compressed air from the environmental control system could be utilized at cruise level.

Another simulation study investigated two configurations of an SOFC−GT system (Fig. 12.13) as the APU of a 300-passenger long-range aircraft [78]. Similar to the study mentioned above, the target electrical power requirement was 440 kW. At similar operating conditions, configuration 1 resulted in a slightly higher cycle efficiency than configuration 2 (58% vs 54%) as the operating temperature of the SOFC in configuration 1 was higher than configuration 2 (944°C vs 832°C) and the performance of the SOFC increased with temperature. The higher operating temperature of the SOFC in configuration 1 was the result of enhanced fuel heating by the low mass flow rate steam (Fig. 12.13A). Sensitivity analysis (Fig. 12.14) shows that high overall heat transfer coefficient and low air flow rate could lead to high cycle efficiency.

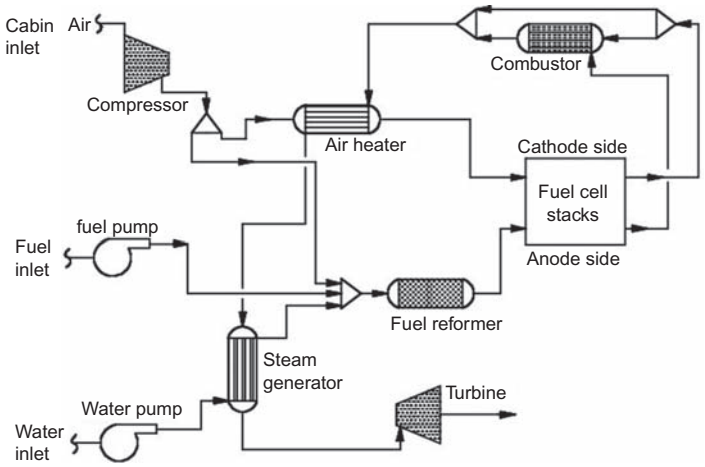

FIGURE 12.12

Solid oxide fuel cell–gas turbine system as an aircraft auxiliary power unit [76].

Although one prototype has been launched, the development of an SOFC-APU for marine applications is largely simulation-based [79–82]. One simulation study investigated the SOFC–GT tri-generation system where the power output of the SOFC–GT unit was 250 kW [79]. Also known as combined heating, cooling and power, tri-generation is an integrated energy system where the exhaust provides heating and desiccant provides cooling. Modeling results show that the SOFC–GT system with a double effect adsorption chiller, desiccant wheel, heating ventilation, and air conditioning (HVAC) (Fig. 12.15) had the highest overall system efficiency (68%) among the different configurations. This system could produce 25%–47% more electricity than the SOFC–GT system with heating ventilation and air conditioning only. This improvement of performance is attributed to the absorption chiller, which can make use of the waste heat from the SOFC–GT system. Furthermore, more cooling is available by using a double effect absorption chiller and, hence, less electricity was used by the HVAC for cooling.

In another simulation study a diesel-fueled SOFC system was designed to provide 120 kW auxiliary power for a naval surface ship [80]. With a target electrical power output of 120 kW, the net efficiency of the diesel-fueled SOFC system was significantly higher than the marine diesel engine (55% vs 25%). The CO_2 mission of the SOFC system was less than half of that of the marine diesel engine (423 gCO_2/kW h vs 890 gCO_2/kW h). In addition, the SOFC system was significantly lighter than the marine diesel engine (520 kg vs 3400 kg) and produced much less noise (50 dB vs 100 dB).

One important breakthrough for SOFC-APUs is the 50 kW prototype developed by sunfire GmbH in the SchiffsIntegration BrennstoffZelle (SchiBZ) project [81–83]. The initial simulation study suggests that the SOFC system (Fig. 12.16)

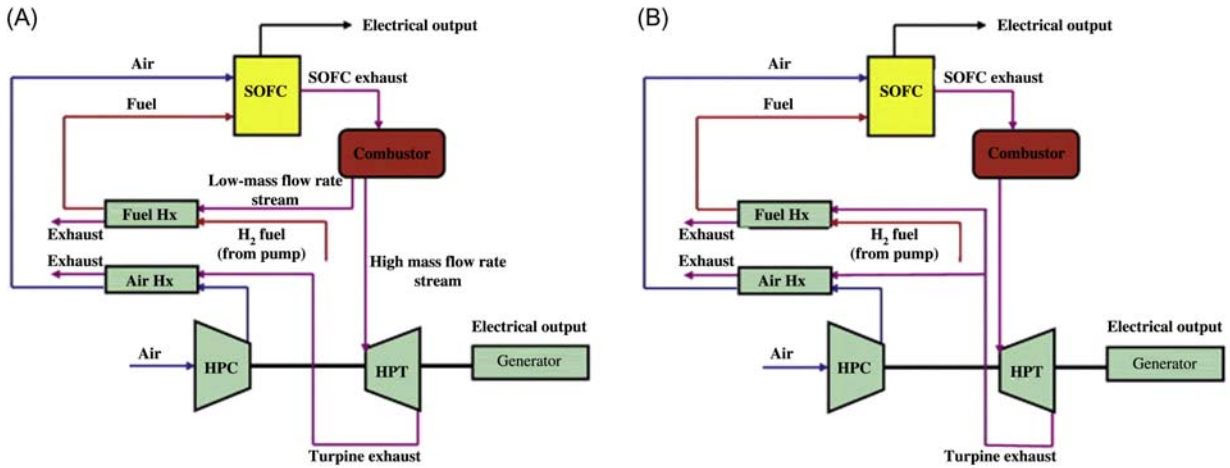

FIGURE 12.13

Solid oxide fuel cell–gas turbine systems as an aircraft auxiliary power unit: (A) configuration 1; (B) configuration 2 [78].

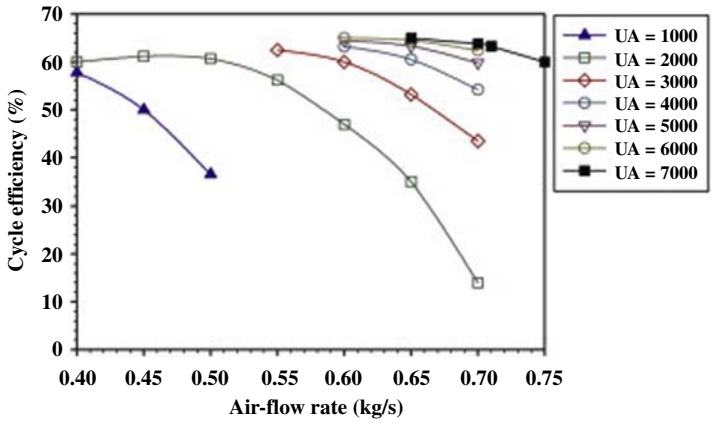

FIGURE 12.14

Effect of air flow rate and overall heat transfer coefficient (UA) on cycle efficiency [78].

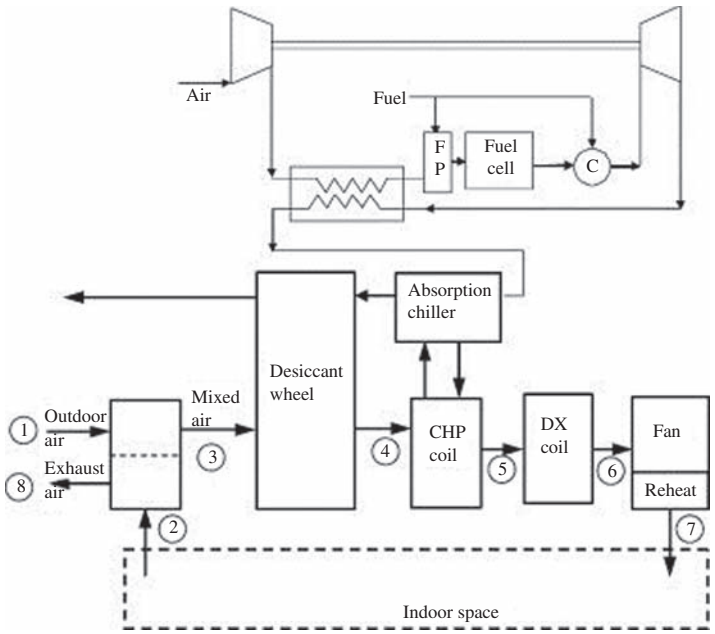

FIGURE 12.15

Solid oxide fuel cell–gas turbine absorption chiller, desiccant wheel, heating, ventilation, and air conditioning system [79].

is advantageous over other FC systems in terms of investment cost and system efficiency [81]. Later experiments demonstrated the robustness of a similar sunfire SOFC system with smaller power output (3.8 kW) as the voltage degradation

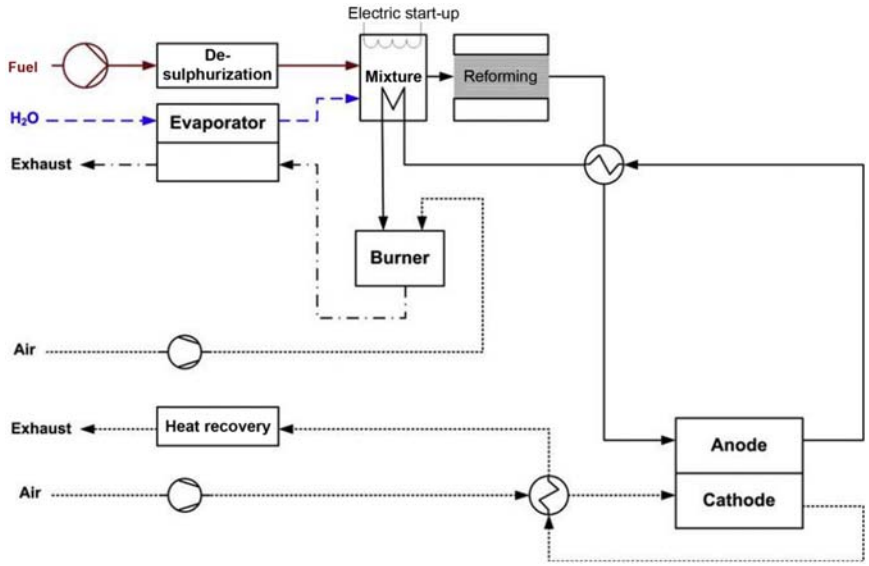

FIGURE 12.16

Diesel-fueled solid oxide fuel cell system [81].

over 1000 hours of operation was insignificant [83]. The 50 kW prototype was installed on a test ship from Reederei Braren to provide 25% − 50% of the onboard power [82]. The electrical and overall efficiencies of the prototype were claimed to be over 50% and 90%, respectively.

12.4 Outlook for mobile applications of solid oxide fuel cells

The application of SOFCs in transportation represents an important milestone in the movement toward clean energy. An SOFC offers fuel flexibility, which allows the use of common hydrocarbon fuels such as diesel and makes SOFC an important player in the transition to a hydrogen economy where PEMFC uses hydrogen to produce energy with zero emission of CO_2. In recent years the development of SOFC-APU for land, aerial, and marine vehicles have several breakthroughs such as the 3 kW DESTA SOFC-APU for heavy-duty long-haul trucks and the 50 kW sunfire SOFC-APU for naval surface ships. They can lead to the wider adoption of SOFC-APUs in the foreseeable future. On the other hand, the use of an SOFC as the sole energy source for propelling vehicles still has a long way to go, as the cost of an SOFC unit is significantly higher than the conventional internal combustion engine. Substantial cost reduction of SOFC units can be achieved by the

development of more effective materials and economy of scale for production. To promote the adoption of SOFCs in vehicles, governmental incentives will play an important role before the economy of scale is realized.

Abbreviations

APU	auxiliary power unit
FC	fuel cell
FCEV	fuel cell electric vehicle
GT	gas turbine
HVAC	heating, ventilation, and air conditioning
IC	internal combustion
MT-SOFC	microtubular SOFC
PEMFC	proton exchange membrane fuel cell
PSV	platform supply vessel
SOFC	solid oxide fuel cell
UAV	unmanned aerial vehicle
UUV	unmanned underwater vehicle
YSZ	yttria stabilized zirconia

References

[1] A. Kirubakaran, S. Jain, R.K. Nema, A review on fuel cell technologies and power electronic interface, Renew. Sustain. Energy Rev. (2009) 2430–2440.
[2] E.D. Wachsman, K.T. Lee, Lowering the temperature of solid oxide fuel cells, Science (80-.) 334 (6058) (2011) 935–939.
[3] C. Bernay, M. Marchand, M. Cassir, Prospects of different fuel cell technologies for vehicle applications, J. Power Sources 108 (1–2) (2002) 139–152.
[4] P.K. Cheekatamarla, C. Finnerty, J. Cai, Internal reforming of hydrocarbon fuels in tubular solid oxide fuel cells, ECS Trans. 12 (1) (2008) 439–448.
[5] P.K. Cheekatamarla, C.M. Finnerty, Y. Du, J. Jiang, J. Dong, P.G. Dewald, et al., Advanced tubular solid oxide fuel cells with high efficiency for internal reforming of hydrocarbon fuels, J. Power Sources 188 (2) (2009) 521–526.
[6] O. Smorygo, V. Mikutski, A. Marukovich, Y. Vialiuha, A. Ilyushchanka, N. Mezentseva, et al., Structured catalyst supports and catalysts for the methane indirect internal steam reforming in the intermediate temperature SOFC, Int. J. Hydrogen Energy 34 (23) (2009) 9505–9514.
[7] W. Winkler, H. Lorenz, The design of stationary and mobile solid oxide fuel cell-gas turbine systems, J. Power Sources 105 (2) (2002) 222–227.
[8] W. Winkler, H. Lorenz, Design studies of mobile applications with SOFC-heat engine modules, J. Power Sources (2002).
[9] A. Buonomano, F. Calise, M.D. d'Accadia, A. Palombo, M. Vicidomini, Hybrid solid oxide fuel cells–gas turbine systems for combined heat and power: a review, Appl. Energy (2015) 32–85.

[10] S.E. Veyo, L.A. Shockling, J.T. Dederer, J.E. Gillett, W.L. Lundberg, Tubular solid oxide fuel cell/gas turbine hybrid cycle power systems: status, J. Eng. Gas Turbines Power 124 (4) (2002) 845.
[11] T. Gengo, Y. Kobayashi, Y. Ando, N. Hisatome, T. Kabata, K. Kosaka, Development of 200 kW class SOFC combined cycle system and future view, Mitsubishi Heavy Ind. Ltd. Tech. Rev. 45 (1) (2008) 33–36.
[12] P. Costamagna, L. Magistri, A.F. Massardo, Design and part-load performance of a hybrid system based on a solid oxide fuel cell reactor and a micro gas turbine, J. Power Sources 96 (2) (2001) 352–368.
[13] R. Roberts, J. Brouwer, F. Jabbari, T. Junker, H. Ghezel-Ayagh, Control design of an atmospheric solid oxide fuel cell/gas turbine hybrid system: variable versus fixed speed gas turbine operation, J. Power Sources 161 (1) (2006) 484–491.
[14] C. Stiller, B. Thorud, O. Bolland, R. Kandepu, L. Imsland, Control Strategy for a solid oxide fuel cell and gas turbine hybrid system, J. Power Sources 158 (1) (2006) 303–315.
[15] F. Mueller, R. Gaynor, A.E. Auld, J. Brouwer, F. Jabbari, G.S. Samuelsen, Synergistic integration of a gas turbine and solid oxide fuel cell for improved transient capability, J. Power Sources 176 (1) (2008) 229–239.
[16] C. Bao, Y. Shi, C. Li, N. Cai, Q. Su, Multi-level simulation platform of SOFC-GT hybrid generation system, Int. J. Hydrogen Energy 35 (7) (2010) 2894–2899.
[17] V. Lawlor, S. Griesser, G. Buchinger, A.G. Olabi, S. Cordiner, D. Meissner, Review of the micro-tubular solid oxide fuel cell: part I. Stack design issues and research activities, J. Power Sources 193 (2) (2009) 387–399.
[18] V. Lawlor, Review of the micro-tubular solid oxide fuel cell (part II: cell design issues and research activities), J. Power Sources 240 (2013) 421–441.
[19] Y. Funahashi, T. Shimamori, T. Suzuki, Y. Fujishiro, M. Awano, Fabrication and characterization of components for cube shaped micro tubular SOFC bundle, J. Power Sources 163 (2) (2007) 731–736.
[20] M. Cadorin, M. Pinelli, A. Vaccari, R. Calabria, F. Chiariello, P. Massoli, et al., Analysis of a micro gas turbine fed by natural gas and synthesis gas: MGT test bench and combustor CFD analysis, J. Eng. Gas Turbines Power 134 (7) (2012) 71401.
[21] B. Timurkutluk, C. Timurkutluk, M.D. Mat, Y. Kaplan, A review on cell/stack designs for high performance solid oxide fuel cells, Renew. Sustain. Energy Rev. 56 (2016) 1101–1121.
[22] K. Kendall, Progress in microtubular solid oxide fuel cells, Int. J. Appl. Ceram. Technol. 7 (1) (2010) 1–9.
[23] M. Prica, T. Alston, K. Kendall, Mechanical and thermal properties of a 200 tube SOFC reactor, ECS Proc. 1997 (1997) 619–625.
[24] K. Kendall, M. Palin, A small solid oxide fuel cell demonstrator for microelectronic applications, J. Power Sources 71 (1–2) (1998) 268–270.
[25] T. Alston, K. Kendall, M. Palin, M. Prica, P. Windibank, A 1000-cell SOFC reactor for domestic cogeneration, J. Power Sources 71 (1–2) (1998) 271–274.
[26] S.M. Jamil, M.H.D. Othman, M.A. Rahman, J. Jaafar, A.F. Ismail, K. Li, Recent fabrication techniques for micro-tubular solid oxide fuel cell support: a review, J. Eur. Ceram. Soc. 35 (1) (2015) 1–22.
[27] X. Meng, N. Yang, X. Gong, Y. Yin, Z.-F. Ma, X. Tan, et al., Novel cathode-supported hollow fibers for light weight micro-tubular solid oxide fuel cells with an active cathode functional layer, J. Mater. Chem. A 3 (3) (2015) 1017–1022.

[28] T. Liu, Y. Wang, C. Ren, S. Fang, Y. Mao, F. Chen, Novel light-weight, high-performance anode-supported microtubular solid oxide fuel cells with an active anode functional layer, J. Power Sources 293 (2015) 852–858.
[29] Y. Du, C. Finnerty, J. Jiang, Thermal stability of portable microtubular SOFCs and stacks, J. Electrochem. Soc. 155 (9) (2008) B972–B977.
[30] D. Aquaro, M. Pieve, High temperature compact heat exchangers: performance of advanced metallic recuperators for power plants, in: Proceedings of Enhanced, Compact and Ultra-Compact Heat Exchangers: Science, Engineering and Technology, 2005.
[31] G. Xiao, T. Yang, H. Liu, D. Ni, M.L. Ferrari, M. Li, et al., Recuperators for micro gas turbines: a review, Appl. Energy 197 (2017) 83–99.
[32] C.F. McDonald, D.G. Wilson, The utilization of recuperated and regenerated engine cycles for high-efficiency gas turbines in the 21st century, Appl. Therm. Eng. 16 (8–9) (1996) 635–653.
[33] Q. Xun, Y. Liu, E. Holmberg, A comparative study of fuel cell electric vehicles hybridization with battery or supercapacitor, in: 2018 International Symposium on Power Electronics, Electrical Drives, Automation and Motion (SPEEDAM), 2018, pp. 389–394.
[34] Z. Rao, S. Wang, A review of power battery thermal energy management, Renew. Sustain. Energy Rev. 15 (9) (2011) 4554–4571.
[35] L. Gaines, R. Cuenca, Costs of lithium-ion batteries for vehicles (No. ANL/ESD-42). Argonne National Lab., IL (US), 2000.
[36] A. Elleuch, K. Halouani, Y. Li, Bio-methanol fueled intermediate temperature solid oxide fuel cell: a future solution as component in auxiliary power unit for eco-transportation, Mater. Des. 97 (2016) 331–340.
[37] D.J.L. Brett, P. Aguiar, N.P. Brandon, R.N. Bull, R.C. Galloway, G.W. Hayes, et al., Concept and system design for a ZEBRA battery--intermediate temperature solid oxide fuel cell hybrid vehicle, J. Power Sources 157 (2) (2006) 782–798.
[38] D.J.L. Brett, P. Aguiar, N.P. Brandon, System modelling and integration of an intermediate temperature solid oxide fuel cell and ZEBRA battery for automotive applications, J. Power Sources 163 (1) (2006) 514–522.
[39] P. Aguiar, D.J.L. Brett, N.P. Brandon, Feasibility study and techno-economic analysis of an SOFC/battery hybrid system for vehicle applications, J. Power Sources 171 (1) (2007) 186–197.
[40] D.J.L. Brett, P. Aguiar, N.P. Brandon, R.N. Bull, R.C. Galloway, G.W. Hayes, et al., Project ABSOLUTE: a ZEBRA battery/intermediate temperature solid oxide fuel cell hybrid for automotive applications, J. Fuel Cell Sci. Technol. 3 (3) (2006) 254–262.
[41] D.J. Brett, P. Aguiar, N.P. Brandon, I. Coop, J. Dueck, R.C. Galloway, et al., Operational experience of an IT-SOFC/battery hybrid system for automotive applications, ECS Trans 7 (1 Pt 1) (2007) 113–122.
[42] R.T. Leah, N.P. Brandon, P. Aguiar, Modelling of cells, stacks and systems based around metal-supported planar IT-SOFC cells with CGO electrolytes operating at 500 − 600°C, J. Power Sources 145 (2) (2005) 336–352.
[43] P. Aguiar, C.S. Adjiman, N.P. Brandon, Anode-supported intermediate temperature direct internal reforming solid oxide fuel cell. I: Model-based steady-state performance, J. Power Sources 138 (1–2) (2004) 120–136.
[44] P. Aguiar, C.S. Adjiman, N.P. Brandon, Anode-supported intermediate-temperature direct internal reforming solid oxide fuel cell: II. Model-based dynamic performance and control, J. Power Sources 147 (1–2) (2005) 136–147.

[45] J.L. Sudworth, The sodium/nickel chloride (ZEBRA) battery, J. Power Sources 100 (1–2) (2001) 149–163.
[46] Z. Dimitrova, F. Maréchal, Environomic design for electric vehicles with an integrated solid oxide fuel cell (SOFC) unit as a range extender, Renew. Energy 112 (2017) 124–142.
[47] D.J. Schroeder, P. Majumdar, Feasibility analysis for solid oxide fuel cells as a power source for railroad road locomotives, Int. J. Hydrogen Energy 35 (20) (2010) 11308–11314.
[48] L. Guo, K. Yedavalli, D. Zinger, Design and modeling of power system for a fuel cell hybrid switcher locomotive, Energy Convers. Manag. 52 (2) (2011) 1406–1413.
[49] A.S. Martinez, J. Brouwer, G.S. Samuelsen, Feasibility study for SOFC-GT hybrid locomotive power: Part I. Development of a Dynamic 3.5 MW SOFC-GT FORTRAN model, J. Power Sources 213 (2012) 203–217.
[50] A.S. Martinez, J. Brouwer, G.S. Samuelsen, Feasibility study for SOFC-GT hybrid locomotive power part II. System packaging and operating route simulation, J. Power Sources 213 (2012) 358–374.
[51] A.S. Martinez, J. Brouwer, G.S. Samuelsen, Comparative analysis of SOFC-GT freight locomotive fueled by natural gas and diesel with onboard reformation, Appl. Energy 148 (2015) 421–438.
[52] P. Aguiar, D.J.L. Brett, N.P. Brandon, Solid oxide fuel cell/gas turbine hybrid system analysis for high-altitude long-endurance unmanned aerial vehicles, Int. J. Hydrogen Energy 33 (23) (2008) 7214–7223.
[53] A. Fernandes, T. Woudstra, P.V. Aravind, System simulation and exergy analysis on the use of biomass-derived liquid-hydrogen for SOFC/GT powered aircraft, Int. J. Hydrogen Energy 40 (13) (2015) 4683–4697.
[54] G. Giacoppo, O. Barbera, N. Briguglio, F. Cipitì, M. Ferraro, G. Brunaccini, et al., Thermal study of a SOFC system integration in a fuselage of a hybrid electric mini UAV, Int. J. Hydrogen Energy 42 (46) (2017) 28022–28033.
[55] T. Choudhary, S. Krishna, Thermodynamic analysis of solid oxide fuel cell gas turbine hybrid system for aircraft power generation, in: SAE Aerospace Congress and Exhibition 2017, 2017.
[56] A. Gong, D. Verstraete, Fuel cell propulsion in small fixed-wing unmanned aerial vehicles: current status and research needs, Int. J. Hydrogen Energy 42 (33) (2017) 21311–21333.
[57] A. Mendez, T.J. Leo, M.A. Herreros, Current state of technology of fuel cell power systems for autonomous underwater vehicles, Energies 7 (7) (2014) 4676–4693.
[58] P. Ryabov, S. Kalenskiy, Y. Khaletskiy, A. Mirzoyan, Efficiency assessment of HPS for advanced airliners using different fuels, Aircr. Eng. Aerosp. Technol. 86 (6) (2014) 494–500.
[59] K. Okai, H. Nomura, T. Tagashira, A. Nishizawa, Effects of Fuel Type on Aircraft Electric Propulsion with SOFC/GT Hybrid Core, in: 53rd AIAA/SAE/ASEE Joint Propulsion Conference, 2017.
[60] G. Genç, S. Sarikoç, Energy and exergy analysis of a solid-oxide fuel cell power generation system for an aerial vehicle (ISSA- 2015–139), Int. J. Green Energy 15 (3) (2018) 151–160.
[61] L. van Biert, M. Godjevac, K. Visser, P.V. Aravind, A review of fuel cell systems for maritime applications, J. Power Sources 327 (September) (2016) 345–364.

[62] J.P. Thomas, M.A. Qidwai, J.C. Kellogg, Energy scavenging for small-scale unmanned systems, J. Power Sources 159 (2) (2006) 1494–1509.
[63] G.D. Rhoads, N.A. Wagner, B. Taylor, D. Keen, T.H. Bradley, Design and flight test results for a 24 hour fuel cell unmanned aerial vehicle, in: Proceedings of Proceedings of the 8th Annual International Energy Conversion Engineering Conference, July 2010.
[64] T. Kim, S. Kwon, Design and development of a fuel cell-powered small unmanned aircraft, Int. J. Hydrogen Energy 37 (1) (2012) 615–622.
[65] D. Verstraete, K. Lehmkuehler, K.C. Wong, Design of a fuel cell powered blended wing body UAV, in: Advances in Aerospace Technology, vol. 1, 2012.
[66] Z. Ji, J. Qin, F. Guo, C. Dang, S. Zhang, P. Dong, Effect of operating parameters on a hybrid propulsion system with high efficiency fueled by kerosene for high altitude long endurance unmanned aerial vehicles, in: 2018 Joint Propulsion Conference, 2018, p. 4583.
[67] G. Sattler, Fuel cells going on-board, J. Power Sources 86 (1) (2000) 61–67.
[68] M.C. Díaz-de-Baldasano, F.J. Mateos, L.R. Núñez-Rivas, T.J. Leo, Conceptual design of offshore platform supply vessel based on hybrid diesel generator-fuel cell power plant, Appl. Energy 116 (2014) 91–100.
[69] J. Zizelman, S. Shaffer, S. Mukerjee, Solid oxide fuel cell auxiliary power unit - a development update, SAE Technical Paper 2002-01-0411, 2002.
[70] P. Lamp, J. Tachtler, O. Finkenwirth, S. Mukerjee, S. Shaffer, Development of an auxiliary power unit with solid oxide fuel cells for automotive applications, Fuel Cells 3 (3) (2003) 146–152.
[71] J. Lawrence, M. Boltze, Auxiliary power unit based on a solid oxide fuel cell and fuelled with diesel, J. Power Sources 154 (2) (2006) 479–488.
[72] J. Rechberger, A. Kaupert, J. Hagerskans, L. Blum, Demonstration of the first European SOFC APU on a heavy duty truck, in: Transportation Research Procedia, 2016.
[73] M.D. Fernandes, S.T. de, V.N. Bistritzki, R.M. Fonseca, L.G. Zacarias, H.N.C. Gonçalves, et al., SOFC-APU systems for aircraft: a review, Int. J. Hydrogen Energy 43 (33) (2018) 16311–16333.
[74] S. Eelman, T. Krieg, Fuel cell APU's in commercial aircraft – an assessment of SOFC and PEMFC concepts, in: 24th International Congress of the Aeronautical Sciences, 2004, pp. 1–10.
[75] R. Tornabene, X. Wang, C.J. Steffen, J.E. Freeh, Development of parametric mass and volume models for an aerospace SOFC/gas turbine hybrid system, in: ASME Turbo Expo 2005: Power for Land, Sea, and Air, 2005, pp. 135–144.
[76] J.E. Freeh, C.J. Steffen, L.M. Larosiliere, Off-design performance analysis of a solid-oxide fuel cell/gas turbine hybrid for auxiliary aerospace power, in: 3rd International Conference on Fuel Cell Science, Engineering and Technology, vol. 2005, 2005, pp. 265–272.
[77] J. Dollmayer, N. Bundschuh, U.B. Carl, Fuel mass penalty due to generators and fuel cells as energy source of the all-electric aircraft, Aerosp. Sci. Technol. 10 (8) (2006) 686–694.
[78] P. Chinda, P. Brault, The hybrid solid oxide fuel cell (SOFC) and gas turbine (GT) systems steady state modeling, Int. J. Hydrogen Energy 37 (11) (2012) 9237–9248.

[79] L.K.C. Tse, S. Wilkins, N. McGlashan, B. Urban, R. Martinez-Botas, Solid oxide fuel cell/gas turbine trigeneration system for marine applications, J. Power Sources 196 (6) (2011) 3149–3162.
[80] C. Ezgi, M. Turhan Çoban, Ö. Selvi, Design and thermodynamic analysis of an SOFC system for naval surface ship application, J. Fuel Cell Sci. Technol. 10 (3) (2013) 031006.
[81] K. Leites, A. Bauschulte, M. Dragon, S. Krummrich, P. Nehter, SchIBZ-design of different diesel based fuel cell systems for seagoing vessels and their evaluation, ECS Trans. 42 (1) (2012) 49–58.
[82] Sunfire 50 KW SOFC for Ship-Integrated Fuel Cell Project in Germany, Fuel Cells Bull. 2015 (11) (2015) 3–4.
[83] N. Kleinohl, J.B. Hansen, P. Nehter, H. Modarresi, A. Bauschulte, J. vom Schloß, et al., Results for a fuel cell system consisting of an SOFC fed by an adiabatic pre-reforming fuel processor with european standard road diesel, Mater. Perform. Charact. 4 (1) (2015) 245–261.

CHAPTER

13 Feasibility of solid oxide fuel cell stationary applications in China's building sector and relevant progress

Yingru Zhao, Rui Jing and Zhihui Zhang
College of Energy, Xiamen University, Xiamen, P.R. China

Abbreviations

CHP	combined heat and power
DG	distributed generation
ICE	internal combustion engine
(m)GT	(micro)gas turbine
SOFC	solid oxide fuel cell
SOEC	solid oxide electrolyzer

13.1 Introduction

13.1.1 Various scales of microgrids

In contrast with the traditional, centralized electricity grid (macrogrid), the microgrid is a modern, localized, small-scale energy grid with a group of interconnected loads and distributed energy resources incorporating the storage. Microgrids can operate in island mode or interact with the centralized grid, which strengthen the utility grid resilience and help mitigate grid disturbances. Microgrids employ various distributed energy resources, such as solar and wind power, which reduce carbon emissions significantly. The basic framework of a microgrid is shown in Fig. 13.1.

The scale of a microgrid can be evaluated based on the size of the distributed generation (DG) system that is the core of microgrid. DG (also known as onsite generation, embedded generation or decentralized generation) refers to relatively small-scale energy generation systems that are installed and operated close to end users, producing several kilowatts (kW) to less than 6 MW of power. According to the scale of DG power, microgrids can be divided into four categories, as shown in Table 13.1.

Design and Operation of Solid Oxide Fuel Cells. DOI: https://doi.org/10.1016/B978-0-12-815253-9.00013-6

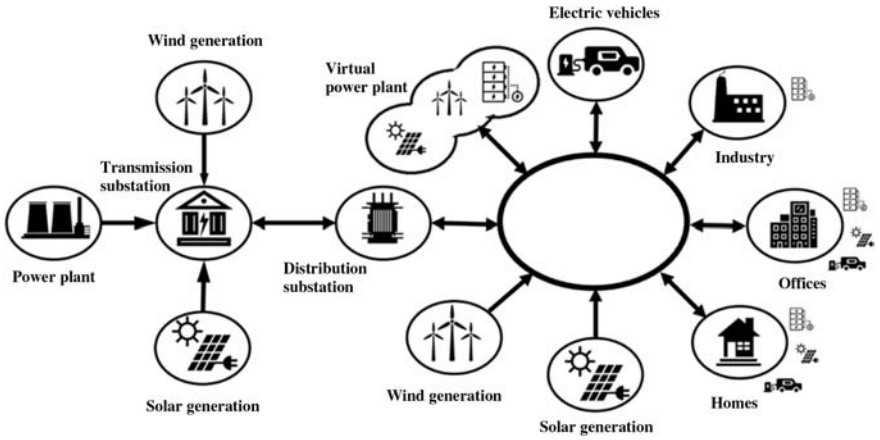

FIGURE 13.1 THE B

asic framework of a microgrid [1].

Table 13.1 Microgrid classification according to distributed generation scale.

Scale	Capacity
Small	<10 kW
Medium–small	10–100 kW
Medium	100 kW–1 MW
Large	1–6 MW

13.1.2 Comparison of full cell–combined heat and power with other combined heat and power technologies

As the core of a microgrid, onsite DG units utilize a wide range of technologies to generate power, including gas turbines, solar photovoltaic, wind turbines, fuel cells (FCs), biomass, and others. Among various onsite generation technologies, combined heating and power (CHP) technology can recover waste heat from the power-generation process, produce space heating, hot water, and low-pressure steam to end users, which greatly improves the energy conversion efficiency of microgrids. Currently the main devices that can be used as prime movers for CHP systems include the reciprocating engine, internal combustion engine (ICE), microgas turbine (mGT), FC, and others. Among these, SOFCs have been increasingly deployed for CHP systems due to their high efficiency, good reliability, fuel flexibility, and good part-load performance. When an SOFC is used as the prime mover of a cogeneration system, the CHP efficiency can exceed 80%. Table 13.2

Table 13.2 Performance comparison of various CHP prime-mover technologies.

Technology	Reciprocating engine	Steam turbine	Gas turbine	Microgas turbine	Fuel cell
Power (MW)	0.005–10	0.5–hundreds MW	0.5–300	0.03–1.0	0.2–2.8
Electrical efficiency	27%–41%	5%–40%	27%–39%	22%–28%	30%–63%
Overall efficiency of CHP	~80%	~80%	~80%	~70%	55%–90%
Heat-to-power ratio	0.83–2.0	10–14	0.9–1.7	1.4–2.0	0.5–1.0
Installation cost of CHP ($/$kW_e$)	1500–2900	670–1100	1200–3300	2500–4300	5000–6500
Maintenance cost excluding fuel ($/$kW_{he}$)	0.009–0.025	0.006–0.01	0.009–0.013	0.009–0.013	0.032–0.038
Lifetime (h)	30,000–60,000	>50,000	25,000–50,000	40,000–80,000	32,000–64,000
Start-up time	10 s	1 h–1 day	10 min/h	60 s	3 h–2 day
NO_x (kg/MWht)	0.027	0.18–0.36	0.24–0.59	0.06–0.22	0.005–0.007

CHP, *combined heating and power.*
US Environmental Protection Agency (EPA) Catalog of CHP Technologies, March 2015 [2].

summarizes the performance of various prime-mover technologies for CHP systems. By comparing FCs with the other types, it can be seen that:

1. In terms of electrical efficiency, the FC is the highest (up to 63%) compared to that of other CHP prime movers, which are generally between 30% and 63%.
2. Fuel cells have the highest CHP efficiency, which can exceed 90%, representing the most effective way to utilize primary energy.
3. Since FC technology is still in the early stage of commercialization, its manufacturing and maintenance costs are the highest. The initial investment cost is around 5000−6500 \$/kW_e, which entails a long payback period and is therefore unattractive from an investment point of view.
4. From the perspective of environmental protection, FC technology has the lowest NO_x emission and best environmental friendliness.

Due to the advantages of excellent electrical efficiency, flexible scale, and environmental friendliness, FC−CHP has drawn growing attention in developed countries. A series of research studies have been carried out and a number of demonstration projects have been built around the world. However, in China there is no stationary FC−CHP demonstration project. Several representative demonstration projects from more advanced countries (United States, European Union, Japan, South Korea, etc.) are introduced as follows.

13.1.3 Stationary applications of fuel cells in public buildings

13.1.3.1 Medium scale (100 kW_e− 1 MW_e) fuel cell stationary applications

A capacity from 100 kW_e to 1 MW_e is suitable for building-level energy demands. Therefore a large number of building energy-supply projects using various types of FCs have been demonstrated worldwide. These projects include various types of buildings such as office buildings, hospitals, supermarkets, factories, residential buildings, and others. A selection of these demonstration projects are described in Table 13.3.

From above FC−CHP demonstration projects, it is seen that the actual operating electrical efficiency exceeds 40% and the total efficiency exceeds 80%. They can meet the electricity and heating demands of industrial or commercial users and can be applied to supply energy for the residential sector as well.

13.1.3.2 Large-scale (10− 100 MWe) fuel cell stationary applications

Large-scale FC−CHP demonstration projects (above 1 MW_e) are still relatively rare. Developed countries such as Japan, South Korea, and the United States are currently the leaders in this industry. Some examples of demonstration projects are listed in Table 13.4.

Table 13.3 Demonstration projects of medium scale FC stationary applications.

Source	Capacity	Efficiency	Remarks
Beacon Capital Partners, LLC [3]	400 kW_e	• NM[a]	• Power, heating, and hot-water services for the Fox News office building • Government subsidy: $2 M; Tax deduction: $1.1 M; Net cost: $1.0 M; Total cost: $4.1 M
Fuel Cell Energy [4]	230 kW_e, 170 kW_{th}	• Electrical efficiency: 42% • Total efficiency: 80%	• Natural gas + desulfurization • Operation started in 2010, with plans to run for 12 years
Doosan PureCell [5]	400 kW_e	• Electrical efficiency: 40% • CHP efficiency: 90%	• St. Helena Hospital, 35,000 m^2 and 180 beds, California, United States • Meets 63% of electricity demand and 50% of heating demand • Designed lifetime: 10 years
Doosan PureCell [6]	400 kW_e	• Electrical efficiency: 40% • CHP efficiency: 90%	• Natural gas drive • Energy-supply area: 6900 m^2 • Meeting 60% electricity and heating demand of Price Chopper supermarket • Steady output/load following mode
Doosan PureCell [7]	400 kW_e	• Electrical efficiency: 40% • CHP efficiency: 90%	• Meeting 35% electricity and heating demand of Elmsford, New York, United States • Steady output/load following mode
Bloom Energy [8]	100 kW_e	• Electrical efficiency: 50% • CHP efficiency: 95%	• Success case: eBay, Google, Yahoo, Walmart, FedEx • Operating temperature: 980°C • Total cost: $0.8 M
Fuel Cell Energy Solutions [7]	300 kW_e, 235 kW_{th}	• NM	• Low-temperature type: 350°C • Total cost: $5 M • Meeting the electricity and heating demand of about 235 average US households
Beratung Renz Consulting [5]	200 kW_e, 400 kW_{th}	• Electrical efficiency: 42%	• Total designed lifetime: 80,000 h • Initial investment: €1.1 M

[a]NM, *not mentioned.*
CHP, *combined heating and power.*

Table 13.4 Demonstration projects of large-scale FC stationary applications.

Source	Capacity	Electrical efficiency	Remarks
Fuel Cell Energy [7]	58.8 MW_e	40%	• Annual power production capacity: 464 million kWh/year • Annual heat production capacity: 195 billion kcal/year • Supplying power for 140,000 households • 60,000 tons of greenhouse gas emissions per year
US Department of Energy [8]	1.4 MW_e	NM[a]	• Consists of seven 200 kW_e batteries • Total cost: $11.8 M • Collecting lithium bromide absorption chillers to form CCHP • Meeting 33% of the cooling demand and 75% heating demand
POSCO Energy [9]	2.5 MW_e	47%	• Output of hot water: 2000 L/h • Heating production: 1.0 Gcal/h • Gas consumption: 507 Nm^3/h • Output voltage: 13.8 kV (22.9 kV)

[a]NM, *not mentioned.*
FC, *fuel cell;* CCHP, *combined cooling, heating, and power.*

Developed countries such as Europe, America, Japan, and South Korea are at the forefront of the world in terms of large-scale FC applications. In addition to providing efficient and clean power and heat supply to the city, FCs can also provide pure hydrogen. As a result, this technology can be the solid foundation for clean transportation in the future. Furthermore, FC−CHP is also a hot spot in university research activities. A number of research FC−CHP demonstration projects from US universities are summarized in Table 13.5.

China only launched FC related research relatively late and there are no stationary FC−CHP demonstration projects in China at present. It has been proven that FC−CHP technology has a bright future for building energy supply from the representative case analysis in the tables. Therefore it is advantageous to learn from the advanced experience from the leading countries to explore the feasibility of applying FC−CHP technology in China's building sector.

13.1.4 Research progress of solid oxide fuel cell applications

As a high-temperature FC, solid oxide fuel cells (SOFCs) have several advantages such as an all-solid structure, convenient maintenance, and fuel flexibility. Suitable fuels include methane, hydrogen, biogas, digester gas, and landfill gas,

Table 13.5 FC–CHP demonstration projects undertaken at American universities.

List of fuel cell installations at universities[a]				
Location	**Power**	**City**	**State**	**Year**
Michigan Alternative and Renewable Energy Center at Grand Valley University	250 kW	Muskegon	Michigan	2004
Alcorn State University	200 kW	Lorman	Mississippi	2000
Alcorn State University-ROTC facility	5 kW	Lorman	Mississippi	2006
The College of New Jersey	600 kW	Ewing Township	New Jersey	2004
Ocean County College	250 kW	Toms River	New Jersey	2003
Ramapo College	400 kW	Mahwah	New Jersey	2002
Richard Stockton College of New Jersey	200 kW	Pomona	New Jersey	2003
Hofstra University	15 kW	Hempstead	New York	2002
Nassau Community College	10 kW	Garden City	New York	2004
Southampton College	10 kW	Southampton	New York	2003
SUNY College of Environmental Science and Forestry	250 kW	Syracuse	New York	2006
Union College	5 kW	Schenectady	New York	2009
North Carolina State Agricultural and Technical University-ROTC facility	5 kW	Greensboro	North Carolina	2003
Portland Community College	10 kW	Sylvania	Oregon	2011
University of South Carolina Scoreboard	5 kW	Columbia	South Carolina	2011
University of South Carolina Scoreboard, West Quad Residential Complex	5 kW	Columbia	South Carolina	N/a
University of Tennessee Chattanooga (UTC) SimCenter	5 kW	Chattanooga	Tennessee	2006
Old Dominion University	40 kW	Norfolk	Virginia	1980s
Central Washington University	1 kW	Ellensburg	Washington	2004

[a]*Some fuel cells have been decommissioned; N/a, information not available.*
U.S. Department of Energy, The Business Case for Fuel Cells, 2014 [10].

with little or no impact on performance or emissions after gas clean-up processes [11]. With the rapid development of SOFC stack and assembling technologies, increasing attention has been paid on system integrations [12]. Different kinds of system configurations have been proposed, including hydrogen-fueled SOFC systems, SOFC co/trigeneration systems, SOFC–GT (gas turbine) hybrid systems, and SOFC/solid oxide electrolyzer (SOEC) systems [13]. The hydrogen-fueled SOFC systems have ultra-low emissions and a simple system layout [14]. The corresponding operation control scheme was analyzed by Jiang et al. [15]. As for

SOFC co/trigeneration systems, both external and inner reforming are available with high flexibility [16,17]. A completely external reforming SOFC system needs to run at steady conditions, and control and fault diagnoses issues are analyzed as well [18]. Based on these analyses, several studies investigated the technical and economical feasibilities of SOFC co/tri-generation systems by mathematic programming and multiobjective optimization [19,20]. The results indicate that although high capital cost is currently a barrier for market penetration, it has a potentially bright future. The hybrid system of a SOFC−GT has also drawn great attention. The system is integrated with various kinds of bottom cycles and the thermal-dynamic, technical, and economical features have been widely analyzed [21,22]. SOFC/SOEC combined systems are a relatively new application that can capture CO_2 and produce H_2 as an energy storage alternative. The thermal-dynamic model of the stack and electrochemical activities have been developed and further verified by Drach et al. [23].

Although in-depth research on thermal-dynamic applications of typical SOFC systems has been conducted, market penetration feasibility and sufficient policy support research are relatively few. The application is case specific and therefore more efforts are needed to identify the reasonable system configurations for different scenarios, and to highlight the unique merits and features of SOFC.

13.2 Feasibility of implementing solid oxide fuel cell−combined heating and power systems in public buildings in China

13.2.1 Load characteristics of public buildings in China's different climate zones

Various kinds of climate exist in China since the latitude of major cities varies from 20° North to 50° North. According to the thermal design code for buildings, the entire country can be categorized into five climate zones, namely severely cold, cold, hot summer−cold winter, hot summer−warm winter, and mild (see Fig. 13.2 [24]). Five representative cities (i.e., Changchun, Dalian, Shanghai, Hong Kong, Kunming) were selected for each climate zone. The different energy consumption characteristics of the representative cities are reported in Table 13.6.

In this study, one year is subdivided into three seasons, namely winter, summer, and transition. Furthermore, five public building categories, that is, hotel, office, hospital, school and supermarket, in each representative city were chosen for analysis. The 24-hour energy demand profiles including electricity, heating, and cooling of each building type located in different cities have been modeled (as shown in Figs. 13.3−7 [25−32]).

For each building at each location, the electricity demand during the three seasons is assumed to be similar within 5% fluctuation, while heating or cooling

FIGURE 13.2

The five different climate zones in China.

Table 13.6 Five representative cities in China's five climate zones.

Climate zone	Energy consumption characteristics	Representative city
Severely cold	Extremely large heating demand in winter; less cooling demand in summer	Changchun
Cold	Large heating demand in winter; little cooling demand in summer	Dalian
Hot summer—cold winter	Large heating demand in winter; little cooling demand in summer	Shanghai
Hot summer—warm winter	Little heating demand in winter; extremely high cooling demand in summer	Hong Kong
Mild	Little heating demand in winter; large cooling demand in summer	Kunming

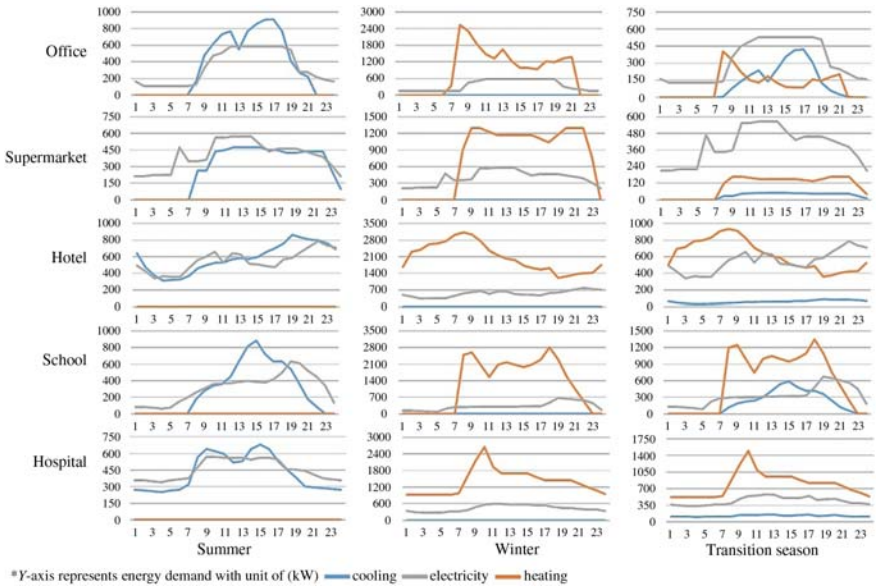

FIGURE 13.3

Typical weekday electricity heating and cooling demand profiles of Changchun.

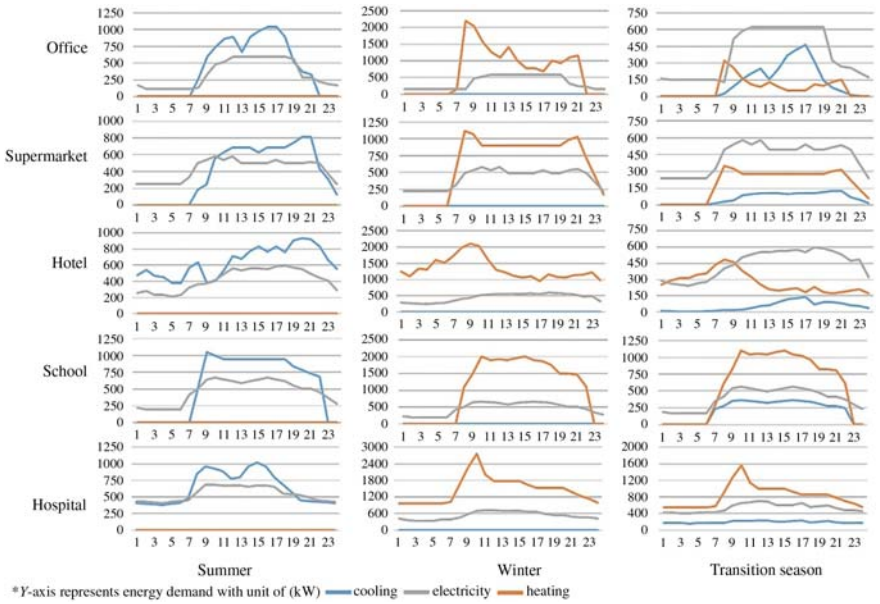

FIGURE 13.4

Typical weekday electricity heating and cooling demand profiles of Dalian.

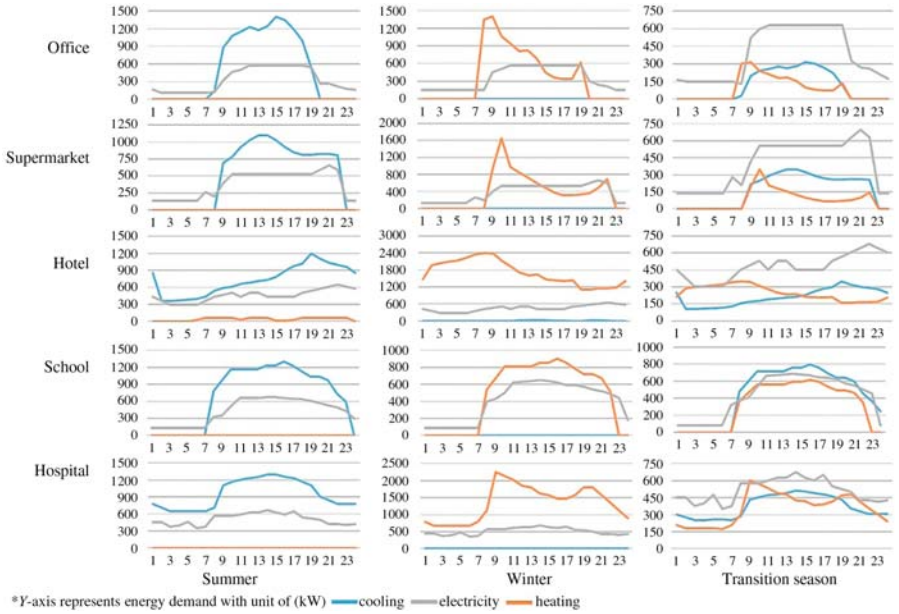

FIGURE 13.5

Typical weekday electricity heating and cooling demand profiles of Shanghai.

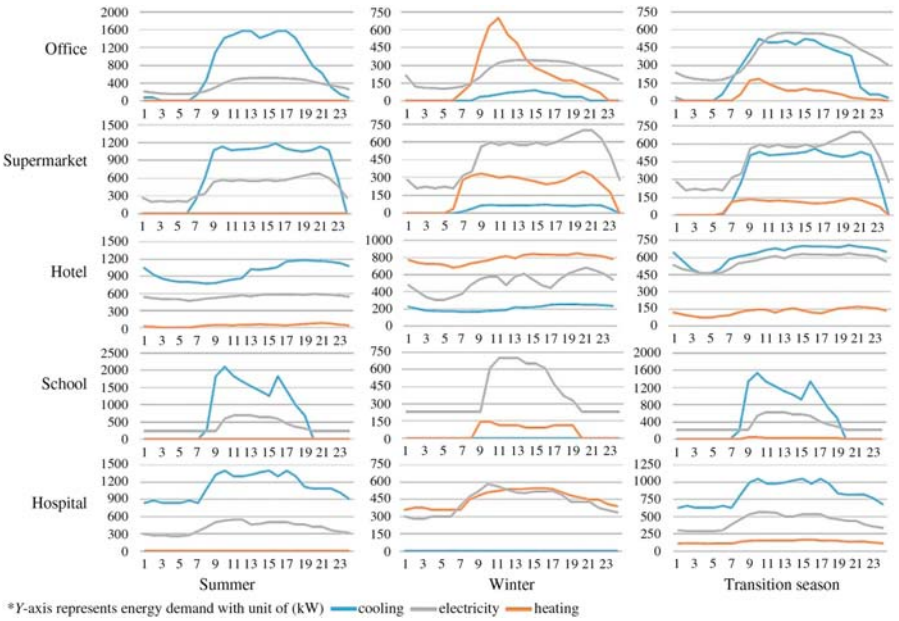

FIGURE 13.6

Typical weekday electricity heating and cooling demand profiles of Hong Kong.

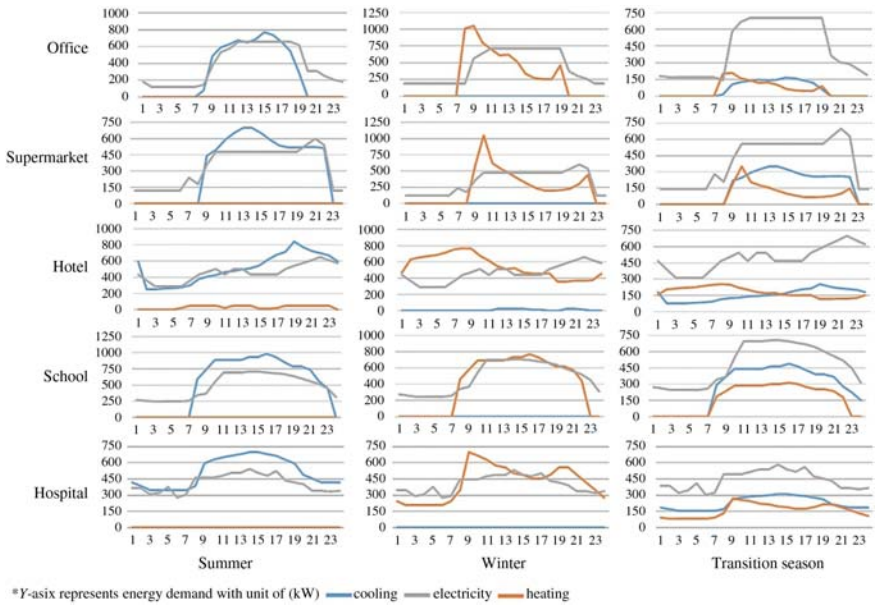

FIGURE 13.7

Typical weekday electricity heating and cooling demand profiles of Kunming.

demand varies significantly according to the climate zones and building categories. Electricity is required for 24 hours for every kind of public building in different zones, while heating is only required during winter and cooling is required during summer. As for the transitional period, heating or cooling supply depends on the building category. Weekday and weekend energy demands are different for each type of building. For supermarkets and hospitals, weekend energy load is 1.2-times that of weekday energy loads. By contrast, only a basic load is applied for office and school buildings during the weekend period, while the hotel energy demand is regarded to be the same on weekdays and weekends.

In general, different types of public buildings have different electricity and heating demands during the different seasons. High-temperature SOFC−CHPs can supply power for buildings while fulfilling heating demands by making use of waste heat. In section 13.2.2, more details of simulation analyses for SOFC−CHP systems applied in various public buildings in China are provided.

13.2.2 Application analysis of using fuel cells in public buildings

13.2.2.1 Operation strategies of fuel cells

Typically there are four operation strategies for SOFC−CHP systems [33], namely: (1) following thermal load, (2) following electrical load, (3) following

Table 13.7 Characteristics of four operation strategies.

Operation strategies	Advantage	Disadvantage
Following thermal load	• Simple operation • Effective use of waste heat with the highest system efficiency • Operation can be loaded the following/day−night modulation/ segment modulation, etc.	• Not optimal for electricity generation • Not optimal for economy • Need better instrument control system
Following electrical load	• Optimum economy • Meets electrical demand well • Operation can be loaded the following/day−night modulation/ segment modulation, etc.	• Complete operation may bring additional operating cost • Excess heat may be generated • Need better instrument control system
Following the grid	• As a mean of steady energy supply • Be profitable with subsides	• Grid operators are required to have remote control over fuel cell • Not optimal for the efficiency of fuel cells
Constant output	• Simple control • Surplus generation can be sold back to grid	• Inflexible operation • Have to consider the use of waste heat • Not optimal for economy and efficiency

the grid, and (4) constant output. Their advantages and disadvantages are summarized in Table 13.7.

In order to improve the economic performance of SOFC−CHP system, following electrical load mode is selected considering the load characteristics as mentioned above. In following the electrical load mode, it is assumed that the SOFC−CHP system is operated to meet the electricity demand as much as possible, and the insufficient electricity demand is covered by purchased electricity from the grid. Since the system is operated referring to the electrical load, the recovered heat may not fulfill the heating demand. If the recovered heat is more than the heating demand, the excess heat is discharged into atmosphere without costs, otherwise if the recovered heat is insufficient to cover the heating demand, a natural gas boiler will have to be adopted.

13.2.2.2 Energy supply analysis of different building types in the same area

Fully combining the operation strategy of SOFC−CHP and the load conditions of various public buildings in China, the hot summer−cold winter zone (Shanghai)

is taken as an example. A hotel, office building, supermarket, school, and hospital were selected as research objects. For comparison, the traditional energy system (i.e., purchasing electricity and gas to meet electricity and heating demands, respectively) is considered as the baseline, with other control groups including simulations of the economic and environmental performance of mGT−CHP and ICE−CHP. Relevant system parameter assumptions are shown in Table 13.8 [34−37]. The operating efficiency and fuel consumption of mGT, ICE, and SOFC are simulated with reference to Innovus Power's MVS series of prime movers [38], the MTU 4000 series [39], and FuelCell Energy's DFC series product parameters [5,40].

Based on the assumptions in Table 13.8, the scenarios of energy supply for five buildings using the traditional energy supply method, mGT−CHP, ICE−CHP, and SOFC−CHP systems were simulated. First, the basic information of the five buildings, initial investment, annual energy consumption, and carbon emissions for baseline conditions are given in Table 13.9. Second, the simulation results are compared according to three evaluation indicators (i.e., energy consumption cost reduction rate, carbon emission reduction rate, and simple payback period). A detailed comparison of the results are provided in Table 13.10.

Compared with mGT−CHP and ICE−CHP technologies, SOFC−CHP systems provide better energy saving and emission reduction effects, and can achieve 23%−36% energy cost saving and 52%−59% carbon emission reduction. However, its payback period is the longest. From the view of various building types, hotels and hospitals have the most significant energy saving and emission reduction effects, and their payback periods are relatively short. This is due to the fact that the energy demand of hospitals and hotels are relatively stable and

Table 13.8 Relevant system parameters of different technologies.

Parameters	Value	Unit/note
Average electricity price	0.17	USD/kWh
Natural gas price	0.49	USD/m^3
Capital cost of mGT−CHP	2400−3300	USD/kW
Capital cost of ICE−CHP	3000−3800	USD/kW
Capital cost of SOFC−CHP	5000−6000	USD/kW
Capital cost of traditional power supply	300	USD/kW
Capital cost of traditional heating supply	100	USD/kW
Annual maintenance cost	6%	6% of the annual fuel cost
Heat value of CH_4	10	kWh/m^3
Efficiency of boiler	85%	
Discount rate	4%	
CO_2 emission factor of gas	0.2	kgCO_2/kWh
CO_2 emission factor of electricity	1.1	kgCO_2/kWh

mGT, *microgas turbine;* ICE, *internal combustion engine;* SOFC, *solid oxide fuel cell;* CHP, *combined heating and power.*

Table 13.9 Detailed information of five public building categories.

Type	Working time	Building area (m^2)	Annual electricity consumption (MWh)	Annual heating demand (MWh)	Initial cost ($\times 10^6$ RMB)	Annual energy cost ($\times 10^6$ RMB)	CO_2 emission ($\times 10^3$ ton)
Hotel	24 h	15,000	4072	3329	2.56	6.26	5.26
Office	7:30–19:30	15,000	3110	1370	2.66	4.30	3.74
Supermarket	8:00–21:30	13,000	3760	1340	3.05	4.60	4.03
School	7:00–10:00	19,000	3690	2330	2.28	5.40	4.61
Hospital	24 h	18,000	4490	4206	3.15	7.13	5.94

Table 13.10 Analysis of the economic and environmental friendliness of different buildings' energy supply in Shanghai.

Type	Technology	Energy cost reduction rate (%)	CO_2 emission reduction rate (%)	Simple payback period (year)
Hotel	mGT–CHP	21	49	4–7
	ICE–CHP	27	53	3–5
	SOFC–CHP	36	59	6–9
Office	mGT–CHP	17	49	5–10
	ICE–CHP	21	51	4–8
	SOFC–CHP	23	52	15–20
Supermarket	mGT–CHP	16	48	6–14
	ICE–CHP	22	52	6–10
	SOFC–CHP	23	53	15–22
School	mGT–CHP	22	51	6–9
	ICE–CHP	29	55	4–6
	SOFC–CHP	35	59	9–12
Hospital	mGT–CHP	22	49	4–7
	ICE–CHP	29	54	3–5
	SOFC–CHP	34	58	9–12

mGT, *microgas turbine;* ICE, *internal combustion engine;* SOFC, *solid oxide fuel cell;* CHP, *combined heating and power.*

uninterrupted, which allows the CHP units to continue working at higher load rates while the energy supply efficiency is higher and, thereby, achieving better economy.

13.2.2.3 Energy supply analysis of the same building type in different areas

Considering that hotels and hospitals have the best energy saving and emission reducing effects, hotels are selected as research objects. Hotels in the five climate zones in China with similar conditions and system configurations were compared,

and the results are shown in Table 13.11. In addition, Table 13.12 lists the energy saving and emission reducing effects and simple payback period from using different kinds of CHP technologies.

Table 13.11 The basic situation of hotel energy supply in China's five climate zones using traditional energy supply technology.

Climate zone	Initial cost ($\times 10^6$ RMB)	Annual energy cost ($\times 10^6$ RMB)	CO_2 emission ($\times 10^3$ ton)	Annual electricity consumption (MWh)	Annual heating demand (MWh)
Severely cold	4.69	9.59	7.46	4799	9316
Cold	3.31	6.97	5.58	3864	5651
Hot summer–cold winter	2.56	6.26	5.26	4072	3329
Hot summer–warm winter	2.12	6.61	5.75	4756	2204
Mild	2.17	5.85	5.07	4172	2051

Table 13.12 Simulation results of buildings' energy supply.

climate zone	Technology	Energy cost reduction rate (%)	CO_2 emission reduction rate (%)	Simple payback period (year)
Severely cold	mGT–CHP	18	45	6–9
	ICE–CHP	24	49	4–7
	SOFC–CHP	32	53	8–11
Cold	mGT–CHP	18	46	5–8
	ICE–CHP	24	50	5–6
	SOFC–CHP	34	56	7–10
Hot summer–cold winter	mGT–CHP	21	49	4–7
	ICE–CHP	27	53	3–5
	SOFC–CHP	36	59	6–9
Hot summer–warm winter	mGT–CHP	18	49	5–8
	ICE–CHP	26	53	4–5
	SOFC–CHP	34	58	7–10
Mild	mGT–CHP	19	49	7–11
	ICE–CHP	25	53	5–8
	SOFC–CHP	33	58	10–14

mGT, *microgas turbine;* ICE, *internal combustion engine;* SOFC, *solid oxide fuel cell;* CHP, *combined heating and power.*

As can be seen from Table 13.12, although hotels are located in different climate zones, the adoption of CHP technologies can still achieve energy and emission savings. Compared with three other types of the CHP technologies, SOFC−CHP systems have better energy saving and emission reducing effects in all the regions, but their payback period is relatively long (7−14 years). From the perspective of different climate zones, the same CHP technology in each climate zone has different energy saving and emission reducing effects. The effects obtained in the hot summer−cold winter regions are the most significant, and the corresponding payback period is relatively short compared to that in a milder area, which is relatively long. It is possible that the climate conditions determine a smaller heating demand, which leads to the failure of SOFC−CHP technologies to offer advantages. Overall, the application of SOFC−CHP systems in hotels in all climate zones can allow for superior energy saving and emission reduction effects to other technologies, and the simple payback period is longer because of the higher investment cost.

13.2.2.4 Capacity selection of solid oxide fuel cells

In the previous sections, we discussed the economic and environmental performance of various types of CHP technologies for powering buildings in different regions assuming the systems are working at their rated efficiency. However, in the case of large changes in electric load, there is a possibility that the system will experience a drop in efficiency. The electrical efficiency of an SOFC−CHP system under partial load conditions is generally maintained at a high level, but it will be slightly reduced under low-load conditions. As shown in Fig. 13.8, in general, the load rate will be higher when the system efficiency is higher, and it achieves the highest value at rated power. For SOFC−CHP systems, when the load rate is greater than 30% the efficiency of the FC−CHP will exceed 40% and remain relatively stable, which is higher than the ICE−CHP and mGT−CHP systems. When the load rate is less than 10% the units will cut out and stop running. As for ICE−CHP and mGT−CHP systems, the units will stop when the load rate is less than 25%. Therefore the SOFC−CHP system can operate continuously at a low-load rate with high power-generation efficiency, which makes it more flexible in terms of equipment selection.

In order to compare SOFC−CHP with ICE−CHP and mGT−CHP systems and to avoid ICE−CHP and mGT−CHP systems from working at too-low load rates (load rate below 25%), this study uses multiple small prime mover combination systems to supply energy for buildings. For example, when the peak load of a hotel is about 2000 kW, three 700 kW small prime movers are used to supply energy. When the load drops to a lower level, some units will shut down so that the remaining units keep working at a higher efficiency. At the same time it is convenient to provide a stable energy supply during maintenance of individual units.

In addition, high-quality intermittent renewable energy can also be fully utilized in a microgrid. For example, during the daytime, the electricity load is high

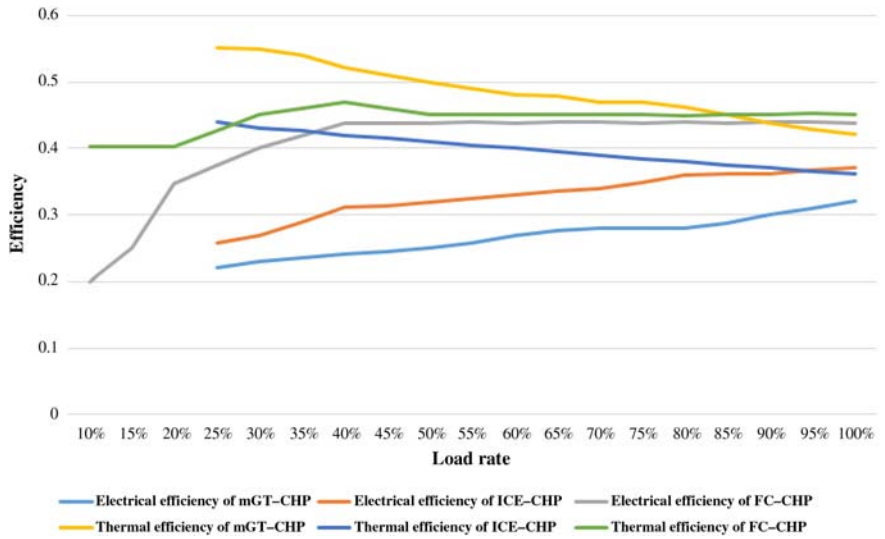

FIGURE 13.8

Efficiency of FC−CHP, mGT−CHP, and ICE−CHP systems at different load rates. *FC−CHP*, fuel cell−combined heating and power; *mGT−CHP*, microgas turbine−combined heating and power; *ICE−CHP*, internal combustion engine−combined heating and power.

and solar energy is sufficient during this period. Therefore we can consider introducing solar photovoltaic power generation and making a joint system with a SOFC−CHP system to supply energy. By choosing a smaller SOFC−CHP, we can not only save on the initial investment cost, but also maintain high-system efficiency. Further discussion will be conducted in future work.

13.2.2.5 Capital cost variations of solid oxide fuel cells

Seen from the analyses presented in this chapter thus far, the installation cost of SOFC−CHP is still high. Considering the cost of an SOFC−CHP system in 2013 (23,500−43,000 RMB/kW_e) the median value of 37,000 RMB/kW_e was selected, 50% of which is the cost of the FC itself, with the remaining 50% being the cost of the other units of the system [21,35,41].

With the development of SOFC−CHP technology, the initial investment cost is expected to decline. Meanwhile, government policies for encouraging distributed energy and advanced technologies like SOFC−CHP will provide support for market penetration, such as investment subsidies, tax reductions, gas price discount, promising feed-in tariffs, and so forth. As shown in Table 13.13, the following assumptions have been made for the initial cost changes of SOFC−CHP systems according to predictions from relevant institutions [33,42].

Table 13.13 Settings of initial cost reduction.

Scenario	Cost reduction/proportion of government subsidy (%)	Initial cost after the change (RMB/W)
Baseline	0	37.5
Scenario 1	10	33.8
Scenario 2	20	30
Scenario 3	30	26.3
Scenario 4	40	22.5
Scenario 5	50	18.8

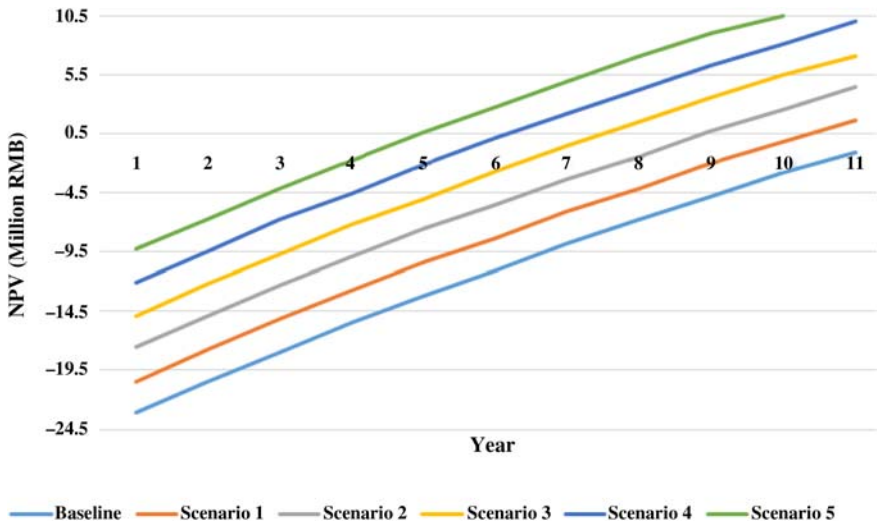

FIGURE 13.9

Net percent value under six different initial cost scenarios.

On the basis of the six scenarios listed in Table 13.13, the energy supply of a hotel in Shanghai by using FC−CHP is simulated and analyzed. The discount rate was 4% and the corresponding net percent value was calculated for each scenario (as shown in Fig. 13.9).

As shown in Fig. 13.9, due to the combined effect of SOFC cost reductions and government subsidies, when the initial cost of the FC reaches 80% of the current level (about 30 RMB/W_e), the simple payback period (SPP) of the project will be 9 years. When the initial cost is 60% of the current level (about 23 RMB/W_e), the SPP will be 5 years, and the internal rate of return (IRR) will be about 10%. However, when the capital cost is 50% of the current level (about 19 RMB/

W_e), the SPP will be less than 4 years, and IRR will be over 15%. At this trajectory, the project has good investment attractiveness.

Therefore further reducing the cost of FC−CHPs and increasing their service life are crucial for the market penetration of this technology. Meanwhile, the Chinese government's development of a medium/long-term policy roadmap as well as subsidies and incentives for promoting new low-carbon energy technologies also play an important role for the popularization of new technologies. When the joint action of two aspects makes the initial cost reach 50% of the current level, it can achieve a rewarding payback period.

Besides the costs and government subsidies, changes in fuel prices will have a certain impact on the economics of the technology. In section 13.2.2.6 the impact of fuel price changes on the popularity of FC−CHP systems will be analyzed further.

13.2.2.6 Life cycle levelized cost of energy

Apart from the simple payback period, the life cycle levelized cost of energy (LCOE) and power-generation cost of SOFC−CHPs are also key indicators for market competitiveness. When applying SOFC−CHPs in hotels in a hot summer−cold winter zone (like Shanghai), the energy and emission reduction performance is the best and the payback period is short. Thus the costs of energy supply for hotels in the hot summer−cold winter zone are compared with different energy-supply technologies. The results are shown in Fig. 13.10.

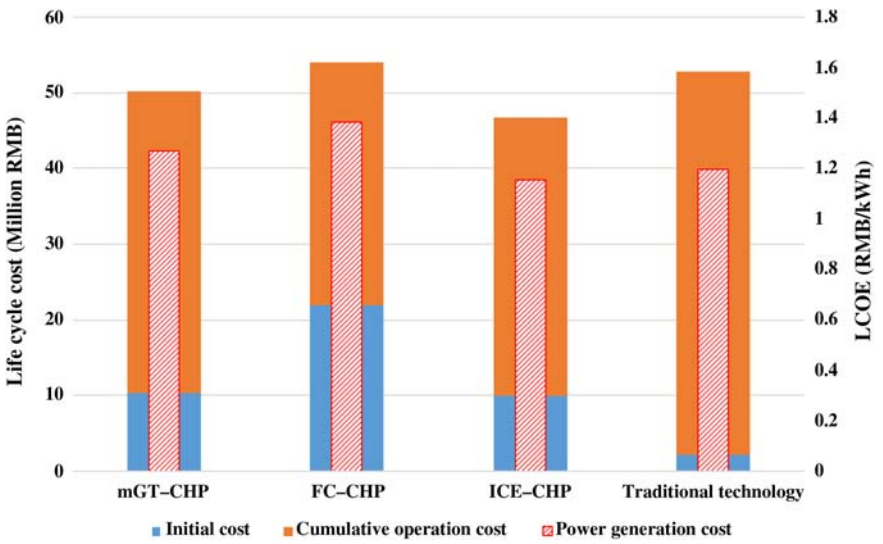

FIGURE 13.10

Comparison of life cycle levelized cost of energy analyses of different technologies.

As shown in Fig. 13.10 the difference of the life cycle LCOE analyses among various energy-supply technologies is within 10%, but the ratio of initial cost to cumulative operation cost is significantly different. Among them, the cumulative operation cost of the traditional technology accounts for more than 90%, while the initial cost ratio of mGT−CHP and ICE−CHP is about 20% and SOFC−CHP accounts for more than 40%. The relatively large proportion of capital investment represents a larger investment risk. By means of calculating the life cycle LCOE and power-generation cost, it is seen that the life cycle LCOE of FC−CHP, mGT−CHP, and ICE−CHP are 1.34 RMB/kWh, 1.24 RMB/kWh, and 1.15 RMB/kWh, respectively, which is close to the average commercial electricity price in China in 2014 (1.2 RMB/kWh). However, considering that CHP technology can recover heat energy while generating electricity, it saves heating cost compared with traditional energy systems. If the recovered heat is taken into account, the energy-supply cost is greatly reduced, making SOFC−CHP more competitive in market.

13.3 Applications of fuel cell in residential buildings

The tech-economic-environment performance of SOFC−CHP applications in various public buildings in different regions in China have been reported in Section 13.2. This section focuses on the feasibility of applying micro-FC−CHP in residential buildings in China.

Residential buildings are gradually becoming one of the main contributors of global energy demands as estimated by the International Energy Agency. Considering an expected increase in the population, along with the growing trend of urbanization and comfort level improvement, the energy demands in buildings will keep rising. The leading countries in applications of FC−CHP in residential buildings are Japan and EU member states, where the heating demand is very large. Therefore this section will introduce demonstrations of FC−CHP projects in Japan and the EU, and then analyze these taking into account the energy consumption characteristics of residential buildings in China.

13.3.1 Japan

Japan is the leading country in terms of research, development, and demonstration of FC-based mCHP systems, in particular, the ENE−FARM demonstration project which was initialized in 2009 with an accumulated installation number of residential FC stacks over 154,000 in 2016. The proton exchange membrane fuel cells developed by Toshiba and Panasonic, and the SOFCs from Aisin Seiki are the main products. The commercialization of these products has been established, and the relevant product parameters are provided in Table 13.14 [43].

Table 13.14 Product parameters of ENE−FARM.

	PEMFC		SOFC	
Manufacturer	Panasonic	Toshiba	JX	Osaka Gas/ Aisin/Kyocera
Date of launch	April 1, 2014	April 1, 2014	October 27, 2011	April 1, 2014
Fuel	NG	NG/LPG	NG/LPG	NG/LPG
Rate electrical power	750 W	700 W	700 W	700 W
Max. electricity efficiency	39% LHV	39% LHV (NG) 38% LHV (LPG)	45% LHV	46.5% LHV
Max. efficiency	95% LHV	95% LHV	87% LHV	90% LHV
Price (excluding tax and installation)	1,900,000 yen	1,944,000 yen	Open price	2,150,000 yen

PEMFC, *proton exchange membrane fuel cells;* SOFC, *solid oxide fuel cell;* NG, *natural gas;* LPG, *liquefied petroleum gas;* LHV, *lower heating value.*

The ENE−FARM system utilizes FCs as the core and combines them with other equipment (heat storage tank, auxiliary heater, etc.) to build a household cogeneration system with simultaneous heating and electricity outputs. With fast system response and various operating modes, a significant amount of CO_2 emissions and fuel consumptions can be saved, namely by 50% and 37%, respectively. The energy cost savings can reach 60,000−70,000 yen/year and have a life expectancy of 50,000−90,000 hours. Meanwhile, it can effectively avoid long-distance transmission loss of utility grid and improve the safety of the transmission and distribution systems. It also has the potential to integrate with various intermittent energy sources in the future.

The target of the Japanese government for 2020 is to reduce the initial cost of FC−mCHP systems to as low as 700,000−800,000 yen/unit. Furthermore, the Japanese government aims to shorten the payback period of ENE−FARM products to 7−8 years by 2020 and 5 years by 2030 by capital subsidies for consumers.

13.3.2 European Union

The European Union is also invested in the FC industry by the 2012 launch of field trials for a residential FC−mCHP demonstration program named ENE. FIELD (as shown in Fig. 13.11). The project is Europe's largest demonstration project for FC−mCHP systems. The project has demonstrated more than 1000 small, stationary, fuel-cell systems for residential and commercial applications in 10 countries [44]. The ENE.FIELD program successfully came to an end in October 2017. Its successor, the PACE project, is a five-year project that will deploy more than 2800 next generation Fuel Cell micro-Cogeneration units in 10

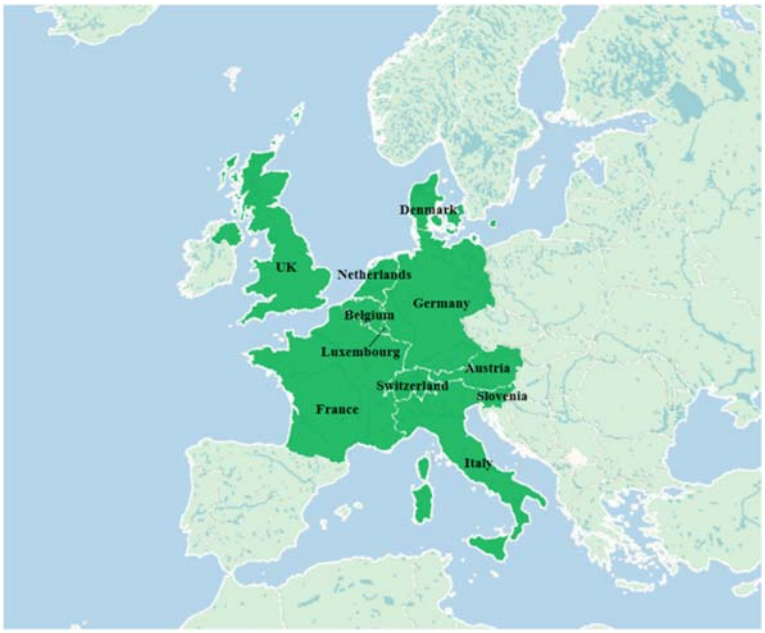

FIGURE 13.11

Countries involved in ENE.FIELD.

European countries by 2021. The project brings together five leading European suppliers (BDR Thermea, Bosch, SOLIDpower, Sunfire, and Viessmann) and will focus on households and small enterprises [45].

13.3.3 Energy usage characteristics of residential buildings in China

Based on the US Energy Information Administration's Shanghai Statistical Yearbook, the average electricity consumption of Shanghai households per annum was 2508 kWh_e/year in 2013. This data will continue to rise with rising living standards. Heating demand of Shanghai households are mainly fulfilled by split units (air-source heat pumps). According to the survey, about one-third of household electricity consumption in Shanghai is for cooling and heating [46]. Assuming electricity consumption of air conditioning in the summer is approximately the same as that for heating in winter, then annual electricity consumption of cooling and heating is both 418 kWh_e/year. Therefore the total electricity consumption for meeting the heating and electricity demand is about 2090 kWh_e/year per household for Shanghai, including 1670 kWh_e/year for electricity and 419 kWh_e/year for heating. Supposing air-source heat pumps are used for heating

in winter, whose coefficient of performance takes the value of 3, the average annual heating demand of Shanghai households is then calculated to be 1257 kWh_h/year.

As a representative city of the cold region, Beijing's average household electricity consumption is roughly 2000 kWh_e/year, including consumption for lighting, home appliances, air conditioners, and others, in which air-conditioning electricity consumption in summer accounts for 25%. Meanwhile, the average household heating energy consumption in winter is about 3500 kWh_h/year, which is generally in the form of district heating and regional boiler plants. Therefore for Beijing households the energy required to meet the heating demand is about 3500 kWh_h/year and 1500 kWh_e/year for other electrical appliances.

At present, the electricity price in different parts of China is not uniform. In general, the electricity price in China's cities is about 0.52−0.62 RMB/kWh_e. Therefore we take the median value of 0.57 RMB/kWh_e for simplification in this analysis. For heating, the northern part of China adopts the method of central heating, while the south decide on their own whether they require heating or not. Heating in the northern region is usually charged according to the space area. The price fluctuates between 23 and 32 RMB/m^2 (median value is 27.5 RMB/m^2). With each household assumed to be around 70 m^2, the annual heating cost is about 1610−2240 RMB (median value is 1925 RMB).

According to the household energy consumption in Shanghai and Beijing, the average annual cost of households on meeting total heating and electricity demands can be calculated. As shown in Fig. 13.12, this is roughly 1086−1295 RMB/year (median value is 1191 RMB/year) in Shanghai, and 2390−3170 RMB/year (median value is 2780 RMB/year) in Beijing.

After dividing the residential buildings by district, we select a representative city for each climate zone as the research object, as shown in Table 13.15.

It is assumed that heating demand occurs when the average outdoor temperature per day is lower than 18°C, and cooling demand occurs in when the average outdoor temperature is higher than 26°C. Each household is assumed to be a single family residing in an area of 70 m^2. Based on these assumptions, with data cited from Thematic Database for Human−Earth System and data sharing infrastructure, the monthly load bar graph of cooling, heating, and electricity consumption of the five representative cities can be obtained. Fig. 13.13 illustrates the relationship between month and energy consumption (kWh/day). As can be seen from the figure, there are significant differences in energy demand as a result of the climatic conditions. Heating demand accounts for a large part of the residential energy consumption in the cold winter region, while cooling demand does this in the hot summer region. In the mild region, residential cooling, heating, and electricity demand are more balanced, and the total energy consumption is lower than for other regions. Different residential buildings in different climate regions have different cooling, heating, and heating demands, while an FC-based microgrid can provide heat and electricity to nearby end users in an efficient way. This makes it possible to apply FC−CHP systems in

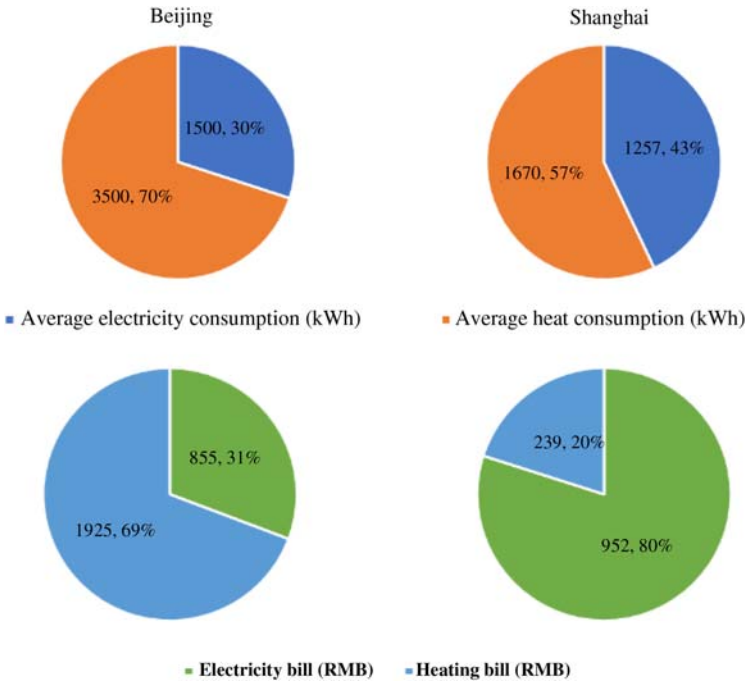

FIGURE 13.12

Annual average heat and electricity consumption and expenditure of households in Beijing and Shanghai.

Table 13.15 Climate division and representative cities.

Climate Zone	Representative City
Severely cold	Harbin
Cold	Beijing
Hot summer–cold winter	Shanghai
Hot summer–warm winter	Xiamen
Wild	Kunming

Chinese residential buildings. Further analysis of this feasibility is provided in section 13.3.4.

13.3.4 Application analysis of fuel cell in Chinese residential buildings

Considering the operating experience on household FC–CHP systems in Japan and the EU in Sections 13.3.1 and 13.3.2, as well as the energy usage

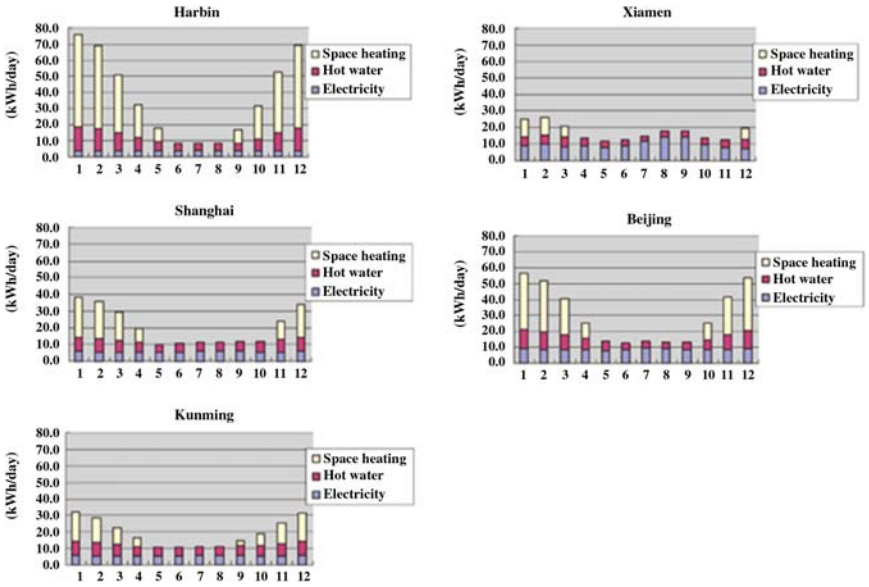

FIGURE 13.13

Residential energy demand of a 70 m^2 single-family household.

Table 13.16 Energy mix of urban residents in China.

Energy	East (%)	Center (%)	West (%)	Northeast (%)
Heat	16	20	25	60
Electricity	64	65	30	25
Gas (natural gas/coal gas)	20	15	25	15
Coal	–	–	20	–

characteristics of Chinese residential buildings described in Section 13.3.3, the feasibility of applying ENE−FARM products in Chinese households is analyzed next. The following section will analyze the application of SOFC−mCHP systems in Chinese residential buildings from the perspectives of the energy structure, emissions, and economy/cost.

13.3.4.1 Changes in household energy consumption

The energy structure of Chinese urban residents (data for 2011) is shown in Table 13.16 [38]. Among them, the most important energy source for urban residents in east China is electricity, accounting for about 64%, natural gas accounts for about 20% of total energy consumption, and the remaining 16% is mainly for

Table 13.17 Energy mix of urban residents in China (completely SOFC−mCHP).

Energy	East (%)	Center (%)	West (%)	Northeast (%)
Heat	–	–	–	–
Electricity	26	26	12	10
Gas (natural gas/coal gas)	74	74	88	90
Coal	–	–	–	–

heating or hot water demands. The electricity consumption in central China is almost as same as that in east China, although the heating demand is slightly larger. Energy consumption in west China is relatively average, roughly 30% electricity, 25% gas, and 20% coal. Due to the cold winter in northeast China, heating/living hot water accounts for the majority of the energy demand at about 60%, followed by 25% electricity and 15% gas consumption, without the direct use of coal.

Supposing a natural gas/coal gas-driven SOFC−mCHP system is used to supply the total heating and electricity demands in Chinese residential buildings with assistance of gas boilers, the energy structure of such a system may change as shown in Table 13.17.

As seen in Table 13.17, natural gas/coal gas consumption will be greatly increased, while electricity demand will be partially provided by SOFC−mCHP systems and the rest being satisfied by grid purchases. At the same time, heating/hot water is fully satisfied by the SOFC−mCHP, which effectively realize energy saving and avoids device installations like water heaters to supply domestic hot water.

13.3.4.2 Changes in emission and economy

The cost of the Japanese household SOFC−mCHP system under government subsidies is about 65,000 RMB/set, with annual energy consumption savings of 37% (electricity bill of around 4600 RMB/ year). According to the average annual electricity bill of households in Beijing and Shanghai (about 2390−3170 RMB/year and 1086−1295 RMB/year, respectively) and the annual energy consumption rate (calculated as 37%), the payback period is not as competitive as it currently is. However, with the development of SOFCs and improvement of emission criteria in China, energy consumption per capita will increase and the cost of SOFC−mCHP can be further reduced with technological progress and government support. In the near future the simple payback period is expected to be within 10 years. Therefore in order to promote stationary applications of SOFCs in China's building sector, it not only relies on technological advancement, which reduces the equipment cost, but also government subsidies.

13.4 Other applications of solid oxide fuel cells

13.4.1 Energy storage by solid oxide electrolyzer cells

A SOEC is the reverse operation of an SOFC in regenerative mode. By the electrolysis of water, hydrogen can be produced. This way of producing pure hydrogen is promising as hydrogen is a clean fuel and is a potential alternative for large-scale and long-term energy storage [47]. Although there are some disadvantages, for example, the high-operating temperature may increase corrosion, long start-up time, and costly materials, great efforts are spent to improve the performance of such promising long-term energy storage and hydrogen-production solutions [48]. A typical SOFC−SOEC stack layout is presented in Fig. 13.14. The system can be further integrated with mGT and biomass gasification devices so as to improve the energy and environment-friendly performances [49]. Different gasification agents can be compared, such as air, O_2-enriched air, O_2 and CO_2, and by multiobjective optimization techniques, energy, exergy, and exergoeconomic performance can be optimized simultaneously [48].

13.4.2 Applications of solid oxide fuel cell with biomass

In addition to buildings' energy applications, small/medium scale SOFCs are also excellent solutions for remote area applications (e.g., telecommunication, by coupled with CHP and thermal driven cooling supplier−adsorption chiller) [50]. By

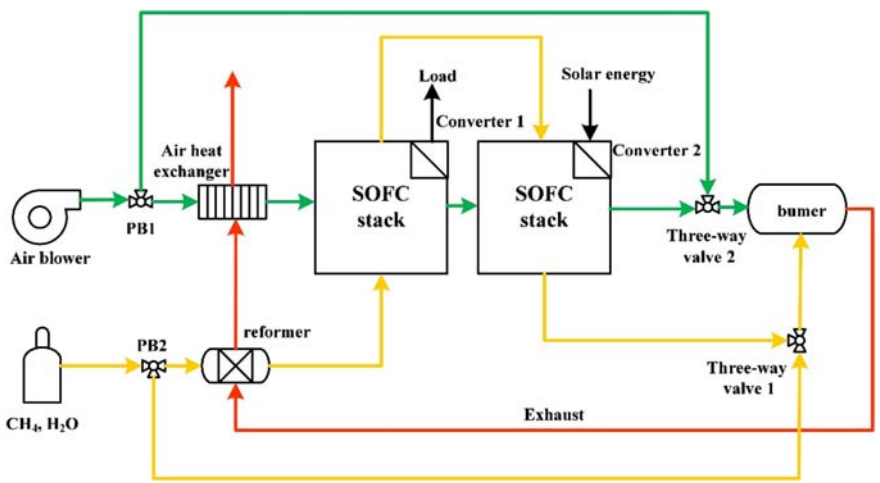

FIGURE 13.14

Typical layout of a combined SOFC−SOEC system. *SOFC*, solid oxide fuel cell; *SOEC*, solid oxide electrolyzer.

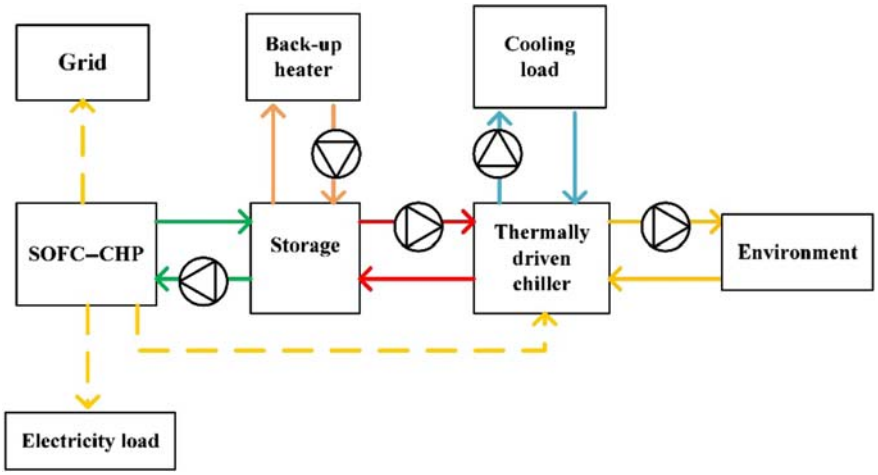

FIGURE 13.15

Typical layout of an SOFC–CHP with a thermally driven cooling system for telecommunication applications. *SOFC*, solid oxide fuel cell; *CHP*, combined heating and power.

integration with a $NaNiCl_2$ battery, constant power can be provided by an SOFC, which is beneficial to peak shaving as well. The stack life cycle can reach 30,000 hours and the single cell's life cycle is up to 90,000 hours, with a 16% lifetime growing rate [51]. A typical layout of an SOFC–CHP with a thermally driven cooling system for telecommunication applications is presented in Fig. 13.15 [50]. Current research has demonstrated its benefits both from energy and environment-friendly perspectives compared to standard grid-connected systems [50].

SOFCs are also good candidates to utilize biomass gas to achieve near-zero emissions with stable power output [52]. Through a gasifier, biomass can be utilized to produce syngas for SOFC utilizations. The typical process of combining biomass with an SOFC system is presented in Fig. 13.16 [53].

By multistage preheating the biomass-generated syngas can be fed into the SOFC cathode to generate power and heat [54]. A further highly integrated system was developed by Behzadi et al. to provide electricity, cooling, heating, and desalinate water simultaneously [55]. A biomass-based SOFC was combined with a GT, chiller, and desalination devices. Through the multiobjective optimization technique, the integrated system was compared from exergy or exergoeconomic viewpoints. An optimal exergy efficiency of 38.16% and cost of 69.47 $/GJ can be achieved at optimum output. Perna et al. proposed an SOFC–mGT cogeneration power plant fed by syngas from a biomass down-draft gasifier [56]. The hybrid BG–SOFC/MGT plant, based on a simplified configuration and realized

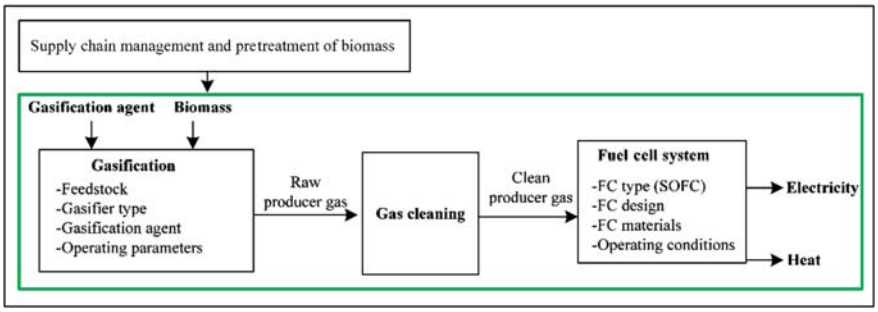

FIGURE 13.16

Typical process of biomass gas treatment for solid oxide fuel cell use.

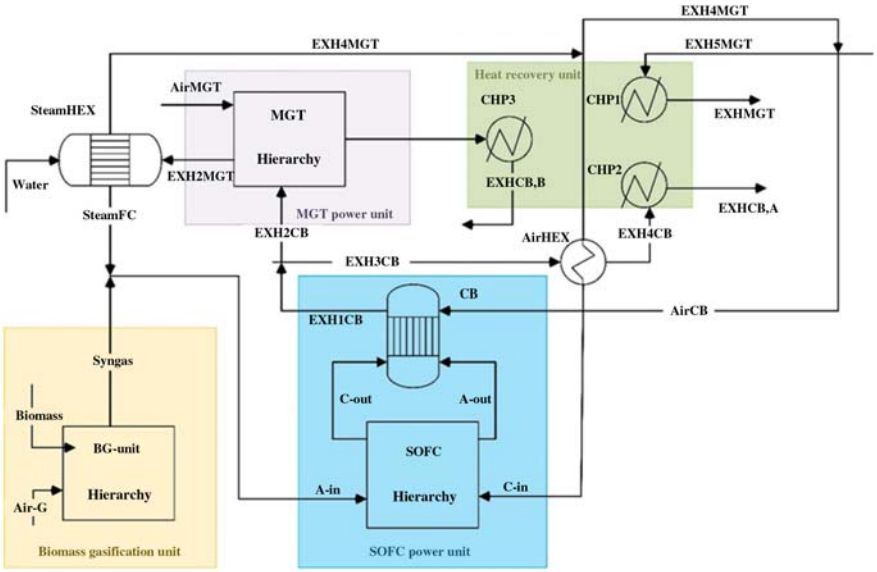

FIGURE 13.17

Typical layout of biomass-based SOFC−mGT−CHP system. *SOFC*, solid oxide fuel cell; *mGT*, microgas turbine; CHP, combined heating and power.

considering commercially available components, was designed to optimize not only the electric power generation, but also the thermal power production. The results indicate that the system's power output can reach 262 kW (SOFC provides 180 kW) with thermal power of 405 kW. The electrical and cogeneration efficiencies can reach 35% and 88%, respectively. The typical layout of a biomass-based SOFC−mGT−CHP system is presented in Fig. 13.17 [56].

13.5 Risk analysis

13.5.1 Market demand

Although SOFCs are proven to have great marketing potential in the near future, development risk still exists. For example, the overinvestment on fossil fuel power-generation in Europe increased the production capacity by 16% in 2000. However, electrical demand did not increase due to the recession. As a result, energy enterprises, especially renewable energy companies, suffered in difficult times and hindered the development of new technologies. The development of SOFC−CHP systems is no exception. The implementation of SOFC-based-CHP technology has made remarkable progress, especially in the residential sector. Thanks to subsidy policies of government on fuel cells and tax increase for traditional power companies, SOFC−CHP systems have shown a good development according to the ENE−FIELD plan in Europe.

13.5.2 Alternative technologies

The competition from other alternative technologies cannot be neglected. Progress on various technologies of gas-fired CHPs, as well as variations of electricity price caused by renewable energy (e.g., solar or wind), will have a significant impact on the development of SOFCs' stationary applications.

The performance and lifespan of SOFCs should be further improved to meet various types of requirement. Meanwhile, reducing cost and shortening payback are the keys to improve their market competitiveness as the government subsidy in Europe is gradually decreasing. Overall, it can be expected that with the further development of SOFC systems more suppliers will gain access to this industry to fulfill the growing market demand.

13.6 Conclusion

With the continuous development of the Internet and alternative energy sources, SOFC−CHP hybrid systems have the potential to be the core of microgrids due to their high-energy efficiency, cascade utilization of energy, and stable power output. The SOFC is a power supplier which converts the chemical energy of fuel directly into electricity. Combined SOFC with CHP technology will significantly increase electrical efficiency and overall efficiency. Besides, it has other advantages, for example, a wide range of fuel selection, flexible capacity range, environment friendliness, and low noise. However, SOFC technology is still in the early stage of commercialization, thus its durability is relatively poor combined with high initial capital cost.

This chapter introduces several cases worldwide of the implementation of FC−CHP systems in commercial buildings. Then the performance of

implementing SOFC−CHP systems in five types of commercial buildings located in five climate zones of China were modeled and evaluated. The selected commercial buildings are hotels, offices, supermarkets, schools, and hospitals. Three criteria of operation cost saving, carbon emission reduction rate, and simple payback were adopted for evaluation. Furthermore, parallel simulations of a combustion-based CHP system and conventional energy system were conducted for comparison. Meanwhile, the LCOE for the case of implementing an SOFC-based CHP system at a hotel in Shanghai was calculated and compared to the state-of-art energy price in China. Furthermore, a sensitivity analysis of the capital costs was also conducted.

In terms of environment protection, compared with the traditional energy system, all three cogeneration systems can achieve significant carbon emission reduction. Among them, the SOFC−CHP has better technical and environmental performance than mGT−CHP and ICE−CHP, where the hot summer−cold winter zone (e.g., Shanghai) is the best demonstration site with an emission reduction rate as high as 59%. In terms of project economics, all three cogeneration systems can significantly reduce operating costs. Among them, SOFC−CHP has achieved the best fuel cost savings for hotel buildings in the hot summer−cold winter zone of roughly 36%. Meanwhile, the life cycle LCOE of SOFC−CHP is about 1.34 RMB/kWh, which is slightly higher than other technologies. However, as SOFC−CHP is a technology in the rapid developing stage, its capital cost is expected to be further reduced which will allow better market competitiveness in the near further. The payback period of an SOFC−CHP system is not attractive due to its current high investment cost. However, as seen from the sensitivity analysis, it will attract strong investment attention when the initial investment cost drops by 50%.

In addition, this chapter introduces demonstration projects of implementing FC−CHP systems for residential buildings in Japan and the Europe Union. Further, the feasibility of implementing SOFC−CHP systems in the Chinese residential sector have been assessed from the energy structure, emission reduction, and project economy perspectives. In addition, case studies of Beijing and Shanghai has been conducted with more detail.

In general, SOFCs have high-energy efficiency, few mechanical components in the generation units, and low-working noise. The emissions are mainly water vapor and a small amount of carbon dioxide, which have little impact on environment. Furthermore, SOFCs can be integrated with other devices to act as a hybrid system and can produce hydrogen when operating in reverse mode. SOFCs can operate with a wide varieties of fuels, including natural gas, coal gas, biomass gas, and so forth. Therefore SOFC−CHP technology has a bright future for application and development prospects. Further research in two aspects is required to improve its market competitiveness, namely, (1) further reduction in the cost of FC−CHP and improving its service life, and (2) promoting and utilizing government subsidies for low-carbon technologies.

References

[1] Eurelectric, 10 Steps to Smart Grids, 2011.
[2] U.S. Environmental Protection Agency, Catalog of CHP Technologies, 2015.
[3] A.B. Scaramelli, Fuel Cells in Commercial Office Buildings - Why and How It Makes Sense, Beacon Capital Partners, LLC, 2012.
[4] Fuel Cell Energy Solution. http://www.fuelcellenergy.com/.
[5] ＜A study of energy performance of hotel buildings in Hong Kong.pdf＞.
[6] Bloom Energy. http://www.bloomenergy.com/.
[7] Fuel Cell Energy. http://www.fuelcellenergy.com/.
[8] U.S. Department of Energy, Fuel Cell Technologies Program, 1-877-EERE-INFO, 2010.
[9] POSCO Energy. http://eng.poscoenergy.com/.
[10] U.S. Department of Energy, The Business Case for Fuel Cells, 2014.
[11] M. Fardadi, D.F. McLarty, F. Jabbari, Investigation of thermal control for different SOFC flow geometries, Appl. Energy 178 (2016) 43−55.
[12] S.Y. Gómez, D. Hotza, Current developments in reversible solid oxide fuel cells, Renew. Sustain. Energy Rev. 61 (2016) 155−174.
[13] T. Cheng, J. Jiang, X. Wu, X. Li, M. Xu, Z. Deng, et al., Application oriented multiple-objective optimization, analysis and comparison of solid oxide fuel cell systems with different configurations, Appl. Energy 235 (2019) 914−929.
[14] H. Cheng, X. Li, J. Jiang, Z. Deng, J. Yang, J. Li, A nonlinear sliding mode observer for the estimation of temperature distribution in a planar solid oxide fuel cell, Int. J. Hydrogen Energy 40 (2015) 593−606.
[15] J. Jiang, T. Shen, Z. Deng, X. Fu, J. Li, X. Li, High efficiency thermoelectric cooperative control of a stand-alone solid oxide fuel cell system with an air bypass valve, Energy 152 (2018) 13−26.
[16] R. Jing, M. Wang, N. Brandon, Y. Zhao, Multi-criteria evaluation of solid oxide fuel cell based combined cooling heating and power (SOFC-CCHP) applications for public buildings in China, Energy 141 (2017) 273−289.
[17] D. Papurello, C. Iafrate, A. Lanzini, M. Santarelli, Trace compounds impact on SOFC performance: experimental and modelling approach, Appl. Energy 208 (2017) 637−654.
[18] X. Wu, D. Gao, Fault tolerance control of SOFC systems based on nonlinear model predictive control, Int. J. Hydrogen Energy 42 (2017) 2288−2308.
[19] O. Joneydi Shariatzadeh, A.H. Refahi, M. Rahmani, S.S. Abolhassani, Economic optimisation and thermodynamic modelling of SOFC tri-generation system fed by biogas, Energy Convers. Manag. 105 (2015) 772−781.
[20] R. Jing, M. Wang, N.P. Brandon, N. Li, J. Chen, Y. Zhao, Economic and environmental multi-optimal design and dispatch of solid oxide fuel cell based CCHP system, Energy Convers. Manag. 154 (2017) 365−379.
[21] M.A. Azizi, J. Brouwer, Progress in solid oxide fuel cell-gas turbine hybrid power systems: System design and analysis, transient operation, controls and optimization, Appl. Energy 215 (2018) 237−289.
[22] J. Wang, C. Yang, F. Liu, X. Meng, J. Wang, J. Liu The development and utilization of new clean energy, in: 2016 IEEE International Conference on Power and Renewable Energy (ICPRE), 2016, pp. 639−643.

[23] Z. Drach, S. Hershkovitz, D. Ferrero, P. Leone, A. Lanzini, M. Santarelli, et al., Impedance spectroscopy analysis inspired by evolutionary programming as a diagnostic tool for SOEC and SOFC, Solid State Ionics 288 (2016) 307–310.
[24] W. Yang, Y. Zhao, V. Liso, N. Brandon, Optimal design and operation of a syngas-fuelled SOFC micro-CHP system for residential applications in different climate zones in China, Energy Build. 80 (2014) 613–622.
[25] H. Ren, W. Zhou, Ki Nakagami, W. Gao, Q. Wu, Multi-objective optimization for the operation of distributed energy systems considering economic and environmental aspects, Appl. Energy 87 (2010) 3642–3651.
[26] G. Mavromatidis, S. Acha, N. Shah, Diagnostic tools of energy performance for supermarkets using Artificial Neural Network algorithms, Energy Build. 62 (2013) 304–314.
[27] S. Acha, Y. Du, N. Shah, Enhancing energy efficiency in supermarket refrigeration systems through a robust energy performance indicator, Int. J. Refriger. 64 (2016) 40–50.
[28] M. Li, H. Mu, N. Li, B. Ma, Optimal design and operation strategy for integrated evaluation of CCHP (combined cooling heating and power) system, Energy 99 (2016) 202–220.
[29] M. Chung, H.-C. Park, Comparison of building energy demand for hotels, hospitals, and offices in Korea, Energy 92 (2015) 383–393.
[30] J. Jiang, W. Gao, Y. Gao, X. Wei, S. Kuroki, Performance analysis of CCHP system for University Campus in North China, Proc. – Soc. Behav. Sci. 216 (2016) 361–372.
[31] M. Abbasi, M. Chahartaghi, S.M. Hashemian, Energy, exergy, and economic evaluations of a CCHP system by using the internal combustion engines and gas turbine as prime movers, Energy Convers. Manag. 173 (2018) 359–374.
[32] P.J. Mago, L.M. Chamra, J. Ramsay, Micro-combined cooling, heating and power systems hybrid electric-thermal load following operation, Appl. Therm. Eng. 30 (2010) 800–806.
[33] R. Napoli, M. Gandiglio, A. Lanzini, M. Santarelli, Techno-economic analysis of PEMFC and SOFC micro-CHP fuel cell systems for the residential sector, Energy Build. 103 (2015) 131–146.
[34] L. Kang, J. Yang, Q. An, S. Deng, J. Zhao, H. Wang, et al., Effects of load following operational strategy on CCHP system with an auxiliary ground source heat pump considering carbon tax and electricity feed in tariff, Appl. Energy 194 (2017) 454–466.
[35] D. McLarty, J. Brouwer, C. Ainscough, Economic analysis of fuel cell installations at commercial buildings including regional pricing and complementary technologies, Energy Build. 113 (2016) 112–122.
[36] X. Xu, B. Xu, J. Dong, X. Liu, Near-term analysis of a roll-out strategy to introduce fuel cell vehicles and hydrogen stations in Shenzhen China, Appl. Energy (2016).
[37] M. Moradi, M. Mehrpooya, Optimal design and economic analysis of a hybrid solid oxide fuel cell and parabolic solar dish collector, combined cooling, heating and power (CCHP) system used for a large commercial tower, Energy 130 (2017) 530–543.
[38] Ltd. IP. http://www.innovus-power.com/, 2018.
[39] Engines MA. http://www.mtu.de/, 2017.

[40] E. Rillo, M. Gandiglio, A. Lanzini, S. Bobba, M. Santarelli, G. Blengini, Life cycle assessment (LCA) of biogas-fed solid oxide fuel cell (SOFC) plant, Energy 126 (2017) 585–602.
[41] M. Wei, S.J. Smith, M.D. Sohn, Experience curve development and cost reduction disaggregation for fuel cell markets in Japan and the US, Appl. Energy 191 (2017) 346–357.
[42] S. Pellegrino, A. Lanzini, P. Leone, Techno-economic and policy requirements for the market-entry of the fuel cell micro-CHP system in the residential sector, Appl. Energy 143 (2015) 370–382.
[43] O. Nishimura, AISIN SOFC–update information, 2016.
[44] ene.field, Fuel Cell micro-CHP in the Context of EU's Energy Transition Policy Analysis & Recommendations, 2016.
[45] Market PtaCEFCm-C. http://www.pace-energy.eu/, 2016.
[46] W. Zhou, B. Zhu, D. Chen, C. Griffy-Brown, Y. Ma, W. Fei, Energy consumption patterns in the process of China's urbanization, Popul. Environ. 33 (2011) 202–220.
[47] F. Ramadhani, M.A. Hussain, H. Mokhlis, S. Hajimolana, Optimization strategies for solid oxide fuel cell (SOFC) application: a literature survey, Renew. Sustain. Energy Rev. 76 (2017) 460–484.
[48] A. Habibollahzade, E. Gholamian, A. Behzadi, Multi-objective optimization and comparative performance analysis of hybrid biomass-based solid oxide fuel cell/solid oxide electrolyzer cell/gas turbine using different gasification agents, Appl. Energy 233–234 (2019) 985–1002.
[49] J. Milewski, M. Wołowicz, J. Lewandowski, Comparison of SOE/SOFC system configurations for a peak hydrogen power plant, Int. J. Hydrogen Energy 42 (2017) 3498–3509.
[50] V. Palomba, M. Ferraro, A. Frazzica, S. Vasta, F. Sergi, V. Antonucci, Experimental and numerical analysis of a SOFC-CHP system with adsorption and hybrid chillers for telecommunication applications, Appl. Energy 216 (2018) 620–633.
[51] V. Antonucci, L. Branchini, G. Brunaccini, A. De Pascale, M. Ferraro, F. Melino, et al., Thermal integration of a SOFC power generator and a Na–$NiCl_2$ battery for CHP domestic application, Appl. Energy 185 (2017) 1256–1267.
[52] H. Ozcan, I. Dincer, Performance evaluation of an SOFC based trigeneration system using various gaseous fuels from biomass gasification, Int. J. Hydrogen Energy 40 (2015) 7798–7807.
[53] Z. Ud Din, Z.A. Zainal, Biomass integrated gasification–SOFC systems: technology overview, Renew. Sustain. Energy Rev. 53 (2016) 1356–1376.
[54] J. Hosseinpour, A. Chitsaz, B. Eisavi, M. Yari, Investigation on performance of an integrated SOFC-Goswami system using wood gasification, Energy 148 (2018) 614–628.
[55] A. Behzadi, A. Habibollahzade, V. Zare, M. Ashjaee, Multi-objective optimization of a hybrid biomass-based SOFC/GT/double effect absorption chiller/RO desalination system with CO_2 recycle, Energy Convers. Manag. 181 (2019) 302–318.
[56] A. Perna, M. Minutillo, E. Jannelli, V. Cigolotti, S.W. Nam, K.J. Yoon, Performance assessment of a hybrid SOFC/MGT cogeneration power plant fed by syngas from a biomass down-draft gasifier, Appl. Energy 227 (2018) 80–91.

This page intentionally left blank

CHAPTER

Waste management 14

Majid Saidi and Aliakbar Ghaffari
School of Chemistry, College of Science, University of Tehran, Tehran, Iran

14.1 Introduction

Solid oxide fuel cells (SOFCs) have proven to be one of the long-range, continuously developed systems in chemical energy conversion to heat and electrical energy. Provided that the fuel used to supply fuel cell-derived electricity is renewable, it could be categorized as a renewable technology. Biofuel (e.g., biogas) is widely produced from processed municipal solid waste (MSW) in anaerobic digesters or is combusted. Fortunately the direct injection of biogas as a renewable energy source into an SOFC not only makes it a renewable energy resource, but also assists in reducing the greenhouse-gas (GHG) emission and the release of hazardous compounds. Thus by combining the existing anaerobic decomposition/digestion (AD) technology with SOFCs toward constructing a power plant fueled by organic wastes has emerged as a promising approach to address energy, waste management, and environmental concerns. Therefore the integration of AD and SOFC fields is highly recommended. In order to combine these two technologies for further development the feasibility of different SOFC configurations including single cell and/or stacked (short stacked) SOFCs have been investigated [1–3].

Due to escalating waste production worldwide at domestic and industrial levels the issue of waste management has become an emergent research field in various domains over the past 20 years. However, cities that are unable to effectively manage their urban waste production are rarely able to manipulate more necessary services like electricity, health, education, or transportation. Waste management in this regard is a necessity in urban infrustructure.

In the past waste incineration was the main method of diminishing harmful substances in order to prevent threats to human health [4,5]. Currently waste is no longer regarded as a useless by-product and efforts have been made to treat it via more environmental-friendly methods that eliminate the production of NO_x, SO_x, and hydrocarbon pollutants in the routine combustion processes. On the other hand, conventional energy generation (i.e., nonrenewable resources) could lead to drastic environmental problems due to the associated GHG emissions, and so forth [6]. Therefore the development of wastewater and MSW disposal processes capable of exploiting the potential energy of organic wastes is highly favorable.

Design and Operation of Solid Oxide Fuel Cells. DOI: https://doi.org/10.1016/B978-0-12-815253-9.00014-8

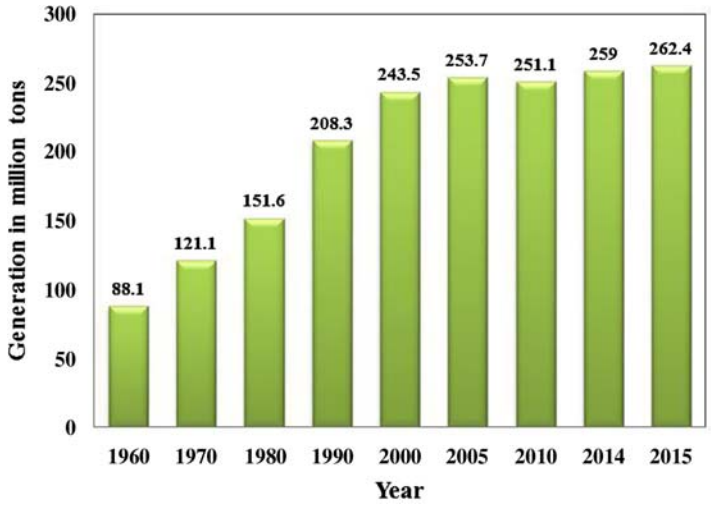

FIGURE 14.1

Municipal solid wastes generation rates in the United States from 1960 to 2015 [7].

The MSW generated by most households such as paper, cardboard, metals, textiles, organics (food and garden waste), and wood debris accounts for approximately 262 million tons (US short tons unless specified) of the wastes generated in the United States in 2015 (Fig. 14.1) [7]. The majority of the waste disposal is assigned to landfilling operations. Due to statistical analyses about 15% of MSW in Asia and 52% in North America is deposited in landfills; the latter is illustrated in Fig. 14.2 [9]. Landfill gas (LFG) is the by-product of the bacterial activities via AD and contains about 50% − 55% methane and 40% − 45% carbon dioxide. AD produces LFG through four main reaction phases, namely hydrolysis, acidogenesis, acetogenesis, and methanogenesis [10,11].

The first, leading AD operation on the organic fraction of municipal solid waste (OFMSW) was in Europe at the beginning of the 1980s in research pilot plants [12]. SOFC systems running on a wide compositional range of biogas derived from agricultural residue and industrial waste (IW) have been studied in the relevant literature [13−17]. Among them, the response of SOFCs toward waste ammonia has been studied. Siavashi et al. [18] investigated the recovery process of the purging gas stream of ammonia synthesis plant in the Razi petrochemical complex by an integrated configuration of catalytic hydrogen-permselective membrane reactor and SOFCs. Their reported results confirmed the high potential of this novel approach to improve the power generation and GHG emission control. Saidi et al. [19] applied an SOFC for flare-gas recovery. Their case study demonstrated that using SOFC technology for the flare-gas recovery of the Asalouyeh gas processing plant not only generates about 1200 MW electrical energy, but also it reduces the equivalent mass of GHG emission from 1700 kg/s

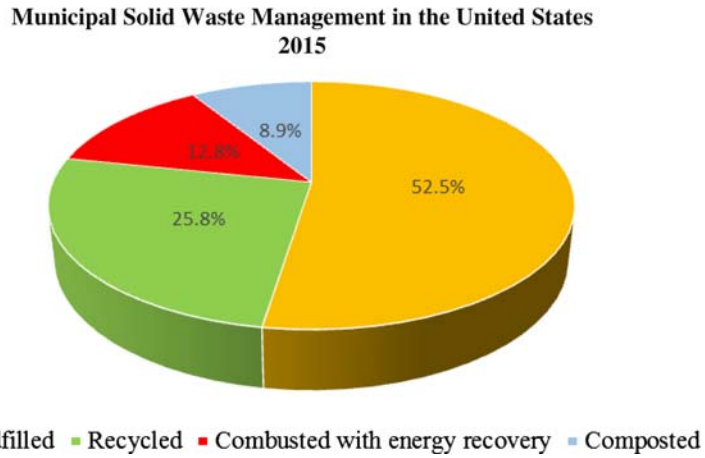

FIGURE 14.2

Management of municipal solid wastes in North America in 2015 [8].

to 68 kg/s. However, the idea of an anaerobic digestion−solid oxide fuel cell (AD−SOFC) system has rarely been scrutinized thoroughly. In one case study the process of generating electrical power using biogas derived from Tehran's MSW fed into an SOFC was investigated in detail and it was shown that recycling parts of the MSW reduced the power-generation capability of the proposed method [20]. Papurello et al. [21] established a successful AD−SOFC waste-to-energy (WtE) pilot plant system featuring a 500Wel SOFC stack in which an overall electrical efficiency of 17% was achieved. They also proposed concerns and suggestions about the optimization of these systems whether on the AD section or SOFC stack, which included increasing the biogas pressure from 2 to 4 mbar, enhancing the electrical efficiency, and future works on the CO_2 sequestration from the plant using algae growth through a photo-bioreactor. Besides these studies, several modeling and experimental evaluations about the feasibility and performance of the combined AD−SOFC system have been conducted using simulation/modeling software UniSIM [22], BELSIM [23], and Aspen Plus [24−26].

Another dominant waste-derived renewable source that has the potential to be utilized as a fuel for SOFCs is "bioalcohol" (i.e., bioethanol and biomethanol). Generally the application of biofuels (mostly biogas and bioethanol) in term of fuel can be conducted in two ways, namely direct combustion to gain thermal energy, and reforming it into hydrogen for clean-energy production in a fuel cell. The alcohol-based biofuel, after processing, either undergoes external reforming to produce syngas or is directly injected to the SOFC stack where the internal reforming along with the electrochemical reactions involved therein takes place simultaneously. In 2016 the Japanese automaker Nissan Motor Company developed an SOFC-powered system running on bioethanol reformed onboard the

vehicle. Nissan has claimed that it was the world's first automotive use of a system featuring a bioelectric fuel cell with an SOFC power generator [27].

Compared to natural gas (NG), biofuels offer the advantages of being indigenous and renewable, free from nonmethane hydrocarbons excluding LFG. However, biofuels have lower efficiency and lower fuel-utilization factors [23,28]. In a comparison between various biofuels in the temperature range of 700°C − 800°C it was demonstrated that direct feeding of biodiesel fuels caused carbon deposition, while biogas obtained by anaerobic fermentation of garbage was more suitable for SOFC operation because it contains a natural reforming agent (CO_2) [29]. Utilizing the exhaust heat from the high-temperature SOFC stack to convert methane-rich biogas to a hydrogen-rich gas mixture (i.e., internal reforming) could lead to a significant reduction in GHG emissions and enhancement in air quality. Different SOFC waste management pathways, namely hybrid systems, might be the key to address future challenges in their application in different biofuel-based power plants.

The main focus of the research presented in this chapter was to investigate the novel approaches of renewable-energy production using wastes as feedstocks. In this regard, a detailed review on the feasibility of SOFC systems in waste-management disciplines is provided. Waste-processing techniques with the capability to be integrated with SOFC stacks were reviewed and compared with other state-of-the-art technologies pioneering in waste-management fields from various criteria. Different challenges and opportunities of utilizing various types of waste-derived fuels as a feed to SOFCs were elaborated on. Finally, a brief overlook of the management of SOFC exhaust gases (i.e., SOFC hybrid systems configurations as well as carbon capture methods) were investigated. The environmental impacts and the economic sustainability of SOFC hybrid−power plants through life cycle assessment (LCA) studied in the literature were reported.

14.2 Waste: challenges and opportunities

Broadly speaking, MSW could be produced in different forms and compositions depending on economic development, climate, culture, and energy sources in the countries and, thus, various disposal methods are utilized including landfilling, incineration, and composting [30]. According to the World Bank estimation the current amount of 1.3 billion tons of waste per year will increase to 2.2 billion tons per year by 2025 [31]. These factors make MSW management a challenging issue in obtaining other kinds of stuff like recycling materials, heat, or energy [32]. As proposed by Morris and Waldheim [33] for successful waste management some considerations should be taken to account such as preventing waste generation, recycling waste materials, minimizing landfilling disposal, incineration with a conventional energy recovery at efficiencies comparable with alternative technologies and advanced equipment for purifying exhaust gases and the

gasification process. By employing MSW in a power plant some advantages are achievable, among which the most important ones are the reduction in pollutants and GHG emissions as well as allocating the spaces occupied by landfills to other human activities. Generators and types of solid waste are reported in Table 14.1.

Waste landfilling should preferably be avoided not only due to its negative effects on public health and the environment, but also because the energy and recycling potential of the wastes are unexploited. Combustion processes, generally incineration, are the most frequently used treatment method applied to different types of waste including MSW, solid-refuse fuels, IW, and industrial-hazardous waste [34]. Thermal treatment of wastes and further energy production in standard utility systems would lead to reaping the benefits of renewable energy by making the waste a stock fuel source rather than being a problem. This means that waste management and energy production are highlighted at the same time. Thermal-treatment plants associated with energy and further fuel production are commonly referred to as WtE or waste-to-fuel plants [35]. The main advantage of employing MSW as a fuel feedstock is that its low-cost availability (it is often supplied for free by waste management companies) might offset the relatively high capital cost investment required for an integrated gasification and/or downstream fuel or chemical production system such as Fischer–Tropsch (FT) or catalytic biosyngas conversion to biodiesel, jet fuel, or bioethanol installations [36].

Selecting the type of WtE technology would largely depend on the origin and volume of the incoming waste stream. A key factor is the energy content (calorific value) of the waste, which determines the energy content extractable from it. Approximate net-calorific values for common fractions of MSW are presented in Table 14.2. The majority fraction of solid waste includes paper, organic material, plastics, glass, metal, and textiles [8]. It is generally accepted that if the incoming waste stream has an average net-calorific value of at least 7 MJ/kg, WtE incineration might be regarded as a self-sustaining technique [37].

14.3 Waste processing

The methodology behind waste management is principally based on enhancing energy recovery (ER) from waste and, consequently, reducing landfilling disposal. WtE technologies aim to recover energy from the organic fraction of waste through biochemical or thermochemical processes. By moving away from incineration since the 1970s, other MSW processing technologies including pyrolysis, gasification, and plasma-based methods have been studied and developed [40]. Higher added-value gaseous or liquid fuels such as ethanol, syngas, and refuse-derived fuel are attainable via three different trajectories schematically depicted in Fig. 14.3. General WtE conversion technologies are classified into three major processes, namely thermochemical, biochemical, and mechanical/physical. The process type and the final product extractable from MSW processing largely

Table 14.1 The sources and types of solid wastes.

Food waste (garbage)	
Sources	Households, institutions, and commercial such as hotels, stores, restaurants, markets, etc.
Description	• Wastes from preparation, cooking and serving of food. Market reuse, waste from the handling storage, etc.
Rubbish	
Description	• Combustible (primary organic): paper, cardboard, cartons, plastics, rubber, leather, yard trimmings • Noncombustible (inorganic): metal foils, tin cans, ceramics, bricks, glass bottles, other mineral metal reuse
Ashes and residues	
Description	• Residues from fires used for cooking and for heating buildings, clinkers and thermal power plants
Street waste	
Source	Construction and demolition
Description	• Street sweepings, dirt, leaves, catch basin dirt, contents of receptacles
Dead animals	
Source	Aviculture and slaughterhouses
Description	• Small animals: cats, dogs, poultry, etc. large animals: horses, cattle, pigs, cows, etc.
Construction and demolition waste	
Source	Construction and demolition sites, repairing and remodeling sites
Description	• Lumber, roofing and sheathing scraps, broken concrete, plaster, wire, etc.
Industrial waste and sludge	
Source	Factories, power plants, treatment plants, etc.
Description	• Solid waste resulting from industry processes and manufacturing operations: food processing waste, boiler house cinders, wood, plastic and metal scraps, etc. • Effluent treatment plant sludge of industries and sewage treatment plant sludge and coarse and screening, grit, and septic tank
Agricultural waste	
Source	Crops, orchards, vineyards, dairies, feedlots, farms
Description	• Degasses, ground nut shell, maize cobs, straw of cereals, etc.
Hazardous wastes	
Source	Hospitals, nuclear plants, chemical industries, or institutions
Description	• Pathological wastes, explosives, radioactive metals, toxic wastes, etc.

Table 14.2 The approximate net-calorific values of common fractions of municipal solid wastes [37–39].

Fraction	Net-calorific value (MJ/kg)
Paper	16
Organic material	14
Plastics	35
Glass	0
Metals	0
Textiles	19
Other materials	11

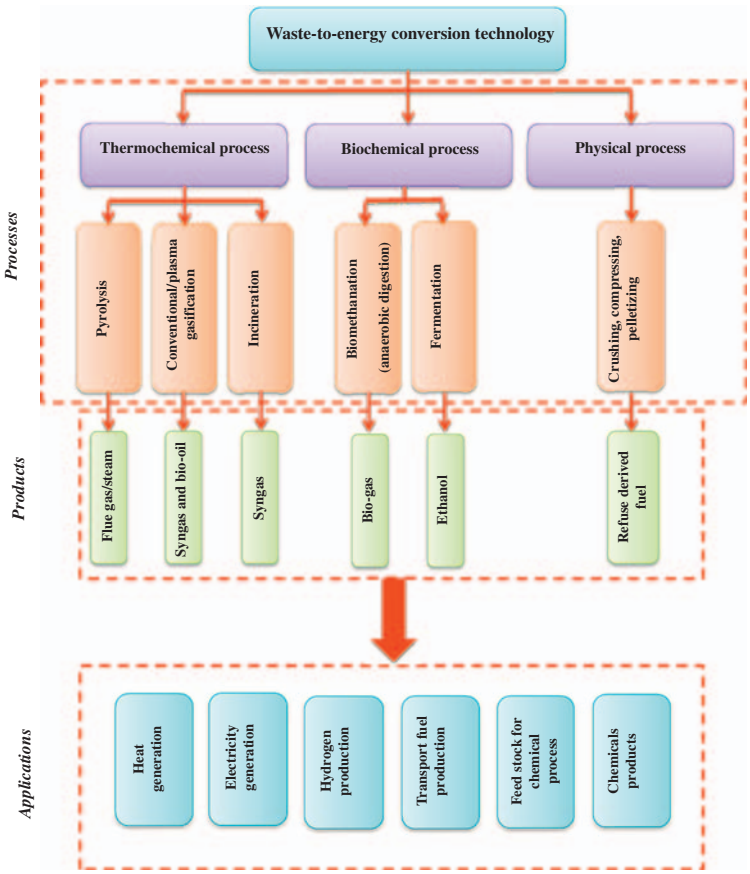

FIGURE 14.3

Technologies for the conversion of waste-to-energy.

depend on the type of solid waste and its contamination level. Pretreatment techniques (i.e., shredding, screening, sorting, drying, or palletization) are also influential on the solid-waste feedstock characteristics. Thermochemical processes usually operate at higher temperatures and, thus, have higher conversion in comparison with biochemical processes [41].

Incineration as an ancient thermochemical process, involves combustion of waste at very high temperatures in the presence of excess oxygen and results in the production of ash, flue gas/steam, and thermal energy. It is feasible for unprocessed or minimally processed refuse alongside the segregated fraction of the high-calorific waste.

Pyrolysis, another efficient thermochemical process, is a thermal degradation process of organic materials at elevated temperatures that takes place in the absence of oxygen and generally produces gaseous, liquid, and solid products. Pyrolysis oils/biooils have received much attention due to their high potential to be alternative precursors for the synthesis of renewable fuels and chemicals necessary to limit the use of those produced from fossil fuels [36].

Gasification is the thermochemical conversion of a carbonaceous fraction of the waste into syngas (CO, H_2,) and smaller amounts of CO_2 and CH_4 as coproducts in an oxygen-deficient environment and in the presence of steam or CO_2 as the gasification agents at high temperatures (650°C−1600°C) [42]. Inorganic fractions present in the waste are converted to ash and can be safely landfilled. Syngas could also be utilized for several applications such as the generation of electricity, Fischer−Tropsch fuels, and chemicals and hydrogen production [43].

Among the gasification technologies, thermal-plasma gasification has been investigated as the most efficient and environment-friendly technique for waste treatment [44−47]. Plasma is an ionized gas where the atoms of the gas have lost one or more electron/s and have become electrically charged. Waste is introduced into the plasma field where intense heat breaks down the waste molecules into simple compounds and are converted into a tar-free syngas, whereas the inorganic matters are melted and converted into a dense, inert, nonleachable slag and, ultimately, fuel gases with high-calorific value and inert, solid slag in the temperature range of 1200°C−2000°C. The main characteristics of thermochemical treatment processes of MSW as well as their major advantages and challenges are listed in Table 14.3.

Biomethanation as a biochemical process is the AD of biodegradable organic waste in an enclosed container under controlled conditions of temperature, moisture, pH, and others. Organic fractions present in the waste undergo decomposition, thereby generating biogas comprising mainly of methane and carbon dioxide. The remaining material (digestate) is nutrient-rich and can be used as fertilizer. AD has alternatively been suggested as a cost-effective and cutting-edge technology to circumvent negative environmental impacts of the traditional disposal methods in the renewable energy generation as well as waste treatment of MSW. AD is commonly employed in many wastewater treatment plants (WWTP) for biochemical stabilization of the sludge before final treatment and disposal

Table 14.3 Main characteristics of thermochemical treatment processes of municipal solid wastes.

Pyrolysis		
Air supply	No air	
Products	Gas	CO, H_2, CH_4, Hydrocarbons
	Liquid	Pyrolysis/bio-oil, H_2O
	Solid	Ash, coke
Advantages	• Immediate reduction in volume and weight and less space requirement • Stabilization of waste • Easy to operate	
Challenges	• Pyrolysis oil is unstable and needs further processing • Energy is distributed in three fractions	
Gasification		
Air supply	Partial amount of air	
Products	Gas	CO, H_2, CO_2, H_2O, CH_4, N_2
	Liquid	–
	Solid	Slag, ash
Advantages	• Immediate reduction in volume and weight & less space requirement • Stabilization of waste • Easy to operate	
Challenges	• Higher initial cost compared to incineration • Skilled labor is required	
Plasma gasification		
Air supply	Partial air	
Products	Gas	CO, CO_2, H_2, H_2O, CH_4
	Liquid	–
	Solid	Slag
Advantages	• Tar/ash absence • A smaller installation • Size for a given waste throughput • Using electricity as a source and the possibility of treating wide range of wastes	
Challenges	• Initial cost and return on investment • Lack of standards • Uncertainty on environmental effects	
Incineration		
Air supply	Excess or stoichiometric amount of air	
Products	Gas	CO_2, H_2O, O_2, N_2
	Liquid	–
	Solid	Slag and ash
Advantages	• Immediate reduction in volume and weight by about 90% and 75%, respectively • Stabilization of waste • Energy recovery	
Challenges	• Management of dioxins and furans formed in incineration	

[48,49]. Invaluable chemicals (e.g., bioplastic, furans, organic acids, etc.) and fuels (e.g., biodiesel, biogas, bioalcohols, etc.) could be produced through the AD or biochemical routes. However, the AD as a relatively developed and widely established treatment method in the wastewater, effluent, and animal dung, still encounters a number of technical, economic, and social constraints such as the volatile fatty-acid accumulation and process instability, and the high cost of transportation and operation. Besides these issues, biomethanation or AD is suitable only for wet biodegradable wastes. There are two main types of AD processes for treatment of biodegradable wastes, namely wet AD systems operating at low-total organic solids (TOS) ($<10\%-20\%$ TOS) and dry systems possessing high-operating solids ($>20\%-40\%$ TOS). In an overall comparison between the two processes, dry AD plants offered several benefits including flexibility in using various types of feedstocks, reduced water usage, as well as lower required heat and power [10,50]. Recently Xu et al. [51] reviewed the challenges and opportunities of the AD of food wastes in case of generation, availability, and utilization as well as composition and methane potential of food waste from different sources. Codigestion by using different micronutrient additives, biochar, and multistage process designs could be promising candidates for improving AD optimization to overcome these challenges [52,53].

In hydrolysis and fermentation as a category of biochemical treatment of MSW, the first step is the conversion of cellulosic fractions of waste to ethanol in which cellulose and hemicellulose would be hydrolyzed into simple sugars using chemicals or enzymes. The second step is fermentation of sugars into ethanol followed by distillation that produces lignin as a by-product. The major challenges in hydrolysis and fermentation are their integration into a single step and the availability of low-cost enzymes.

Biogas obtained via AD or biomass gasification is a high-potential raw material that can be employed in SOFCs or other kinds of loading fuel cells for generating power or electricity. It can be injected into an SOFC directly as a source of fuel or further be processed, and the resulting H_2 enters for the same purpose. The combination of biogas reforming processes, as an alternative CH_4 source, with the fuel cell using H_2 (especially for SOFCs) has attracted much attention among researchers as an important route for generating clean energy with high-added efficiency (up to 60%) [54,55]. H_2 possesses the largest amount of energy density [121 MJ/kg (LHV—lower heating value)] among other known fuels and SOFCs are excellent candidates to exploit it [56]. Methane, the major biogas component, is mainly converted through reforming in order to obtain H_2. However, the production of H_2 mixed with CO (i.e., syngas) has been widely developed in various industries. It is a great challenge toward the application of H_2 because CO is recognized as a contaminant for fuel cells and has to be removed mainly via catalysts [57]. Ni-based catalysts are the most widely used in the reforming processes. However, cells with higher temperatures such as SOFCs, in addition to higher electrical efficiency, represent a higher tolerance to CO (50 ppm). Moreover, the remarkable advantage of SOFCs is that different fuels other than

H_2 (e.g., biogas, gasoline, NG, and ethanol) could possibly be utilized [58]. It should also be noted that corrosive species such as H_2S have to be eliminated in all processes. A brief overview of the conventional processes used for generating hydrogen from methane and biogas is presented. Each system has a different fuel-processing method to prevent carbon deposition over the anode catalyst under biogas fueling. Other nonconventional processes have also been reported in the literature for the production of H_2 from methane, such as solar reforming, thermal-plasma reforming with/without catalyst, and direct electro-catalytic oxidation [59–64]. Table 14.4 presents the chemical reactions involved in the conventional methane reforming processes as well as their advantages and challenges.

Steam reforming (SR) is the conversion of methane in the presence of water steam in a highly endothermic reaction and over a catalyst, thereby producing CO and H_2 (60%–70% yield of H_2) [65,71,72]. The water–gas-shift reaction is often carried out to eliminate CO. Catalysts based on noble metals (e.g., Pd, Pt, Ru, Rh) and base metals (e.g., Co, Ni, Cu) are also widely used in the catalytic steam-reforming reaction [73–75]. Conventional SR processes to produce H_2 include reformer, conversion reactor (shift reaction) and separating. In the latter, the CO and CO_2 are efficiently separated for attaining high-purity H_2 [66].

Partial oxidation reforming (POR) is an alternative method (exothermic) in which methane is partially oxidized to syngas. It is operated at atmospheric pressure, but needs elevated temperatures up to 900°C to complete conversion (i.e., H_2/CO ratio ≈ 2). It was also found in a study that the O_2/CH_4 feed ratio to the reactor was more influential than temperature increase on CH_4 conversion [76].

Autothermal reforming (ATR) involves the combination of these two reforming techniques [67,68,77]. This system benefits from the advantages of both POR and SR in that partial oxidation reaction of methane with SR takes place simultaneously under autothermal conditions making the process self-sustaining with reduced energy costs and a higher H_2/CO ratio.

Dry reforming (DR) occurs when CH_4 reacts with CO_2 to produce CO and H_2. This system is a highly favored reaction type from environment-sustaining and industrial points of view since it consumes two GHGs (CH_4 and CO_2) and provides a synthetic platform of FT synthesis for producing syngas with an H_2/CO ratio close to 1 [78]. According to the literature, competing reactions also accompany the main reactions, which are reverse gas–water shift, the disproportionation of CO, and decomposition of methane [79]. In summary, the DR of methane forms substantial amounts of water at high pressure and is not a practical method for hydrogen production [78].

Trireforming (TR) is a novel process of methane reforming by carbon dioxide, steam, and oxygen simultaneously in one reactor which, thus, involves three reforming reactions, namely endothermic SR, endothermic DR, and exothermic POR. In an investigation of a biogas-fed SOFC coupled with an external trireforming system over Ni/CeO_2 catalyst, the results indicated that utilizing biogas TR and SOFC was a promising process for application in small and medium-size stationary power systems [69].

Table 14.4 Conventional methane reforming processes, the reactions involved, and the main challenges and advantages of each process [65–70].

Steam reforming (SR)	
Reaction	Main reaction: $C_nH_m + nH_2O \leftrightarrow nCO + (n + m/2)H_2$ Water–gas-shift reaction: $CO + H_2O \leftrightarrow CO_2 + H_2$
Advantages	• High H_2/CO ratio produced (≈ 3)
Challenges	• Forming water at high pressures • Requiring external power supply
Partial oxidation reforming (POR)	
Reaction	$C_nH_m + (n/2)O_2 \leftrightarrow nCO + (m/2)H_2$
Advantages	• Reduced energy costs (exothermic reaction)
Challenges	• Forming hotspots in the reactor bed and forming coke on the catalyst surface • Generating a lower H_2/CO ratio
Autothermal reforming (ATR)	
Reaction	$C_nH_m + (m/4)O_2 + 2(n - m/4)H_2O \leftrightarrow nCO + 2nH_2$ $C_nH_m + ((n-1)/2)O_2 + CO_2 \leftrightarrow (n+1)CO + (m/2)H_2$
Advantages	• Possibility of controlling the reactor speed and temperature • Capacity to produce higher amounts of H_2 with lower O_2 consumption
Challenges	• Requires conditions of autothermal and adiabatic in SR and POR together
Dry reforming (DR)	
Reaction	$C_nH_m + nCO_2 \leftrightarrow 2nCO + (m/2)H_2$
Advantages	• Environment-friendly (reducing GHG effect) • Industrial Fischere-Tropsch synthesis route
Challenges	• Higher tendency to form coke and catalyst deactivation
Tri-reforming (TR)	
Reaction	SR + DR + POR
Advantages	• Higher resistance against coke deactivation • Yield a syngas with a H_2/CO molar ratio around 2
Challenges	• Scarcity of the feasible catalysts in the reforming process

14.4 Waste-derived fuels

Recovery of energy from waste and biomass has a number of environmental benefits such as the retrieval of energy from a low-carbon source. Once waste has been recycled the residual waste that remains can be a source of this low-carbon energy. Biomass has been considered as the fourth greatest renewable resource for biofuel and biochemical production. Industrially, it is defined as an organic matter used as fuel or for the production of other chemicals. Some examples of materials that make up biomass fuels are scrap lumber, agricultural residues or forest debris, terrestrial and aquatic crops, the organic component of municipal and IWs, and oil-rich algae such as microalgae. Biomass can be converted to various products that could be used as a fuel for fuel cells (more suitably for SOFCs), technically referred to as biomass-derived fuels. Most biomass-derived fuels, in either liquid or gas form, are easy to transport and cost-effective for industrial use [58].

Bioalcohol products such as biomethanol and bioethanol obtained from biomass fermentation processes are considered as a promising fuel for SOFCs due to their high-hydrogen content and heating value [80–82]. Researches revealed that bioethanol could be obtained via animal manure waste, MSW, and waste by saccharification and fermentation [83,84]. For example, a 1 kW SOFC stack has been successfully operated with fermentation gas for over 5000 h with steam reforming employed for the conversion of ethanol to hydrogen [85].

Biodiesel is another waste-derived fuel and is produced from monoalkyl esters of long chain-fatty acids derived from renewable feedstock like vegetable oils and animal fats. It is nonpoisonous and biodegradable. Biodiesel is produced by transesterification in which oil or fat is reacted with an alcohol (e.g., methanol or ethanol) or a metallic base (e.g., sodium or potassium hydroxide) in the presence of a catalyst. The reaction produces methyl or ethyl ester (biodiesel) and glycerol as a by-product. Biodiesel is easier than the original oils to reform to high-quality, hydrogen-rich gas due to its shorter carbon chains and, thus, is a promising feedstock for fuel-cell applications. However, only a few reports have shown successful reforming of biodiesel with high efficiency and stability as a feedstock in SOFCs, in which they indicated that the content of unsaturated fatty acid methyl esters in biodiesel fuel and the operational temperatures should be, respectively, as low and as high as possible [29,86].

Bioglycerol is a by-product of biodiesel production with a theoretical mole ratio of 3 to 1 (bioglycerol/biodiesel). Most importantly it is produced in a renewable, environment-friendly, and cost-effective way. Some studies have been done on steam reforming and ATR of glycerol to produce hydrogen-rich gas for fuel cells [87,88]. In a recent work [89], Ni-based perovskite catalysts were prepared by two different methods and used as selective catalysts for hydrogen production from glycerol via steam reforming in a fixed bed down flow reactor at atmospheric pressure. Under optimized reaction conditions the $LaNiO_3$ catalyst exhibited 72% glycerol conversion with 70% hydrogen selectivity [89].

Table 14.5 Approximate composition of biogas.

Compound	Percentage (vol.%)
CH_4	55 – 70
CO_2	30 – 45
H_2S	500 – 4000 ppm
NH_3	100 – 800 ppm
H_2	Trace (<1)
N_2	Trace
O_2	Trace
H_2O	Trace

Biogas typically refers to a mixture of different gases produced by the breakdown of organic matter in the absence of oxygen. Biogas can be produced from raw materials such as agricultural waste, manure, municipal waste, plant material, sewage, and green or food waste. It is produced through the AD process of the OFMSWs and/or residual biomass and is composed of mainly methane and carbon dioxide and a trace of other volatile (gas) compounds. The generic chemical composition of biogas is presented in Table 14.5 [90,91]. A possible alternative for production of energy with biomass is AD. AD not only allows material recovery, but also generates heat and energy from biowaste. Due to the presence of CO_2 most of the biogas is abused in inefficient ways such as combustion in internal combustion engines or burning for heat. The versatility of biogas to be used in power plants has attracted scientists all over the world to see biogas as a precious high-potential fuel source because it could be utilized for cogeneration of thermal energy and water through high-temperatures engines (e.g., SOFCs), be flared to generate heat energy in boilers, and employed as fuel for automotive and stationary engines [92,93].

14.4.1 Biogas resources characteristics

A major challenge that stands in the way of local biogas resources (i.e., MSWs or those from farms or landfills) is their low-power houses in the range of 5−100 kWe (kilowatt electric). Another specific problem concerning the present biogas installations (mainly LFG representing 80% of the world's biogas production) is the leftover gas by-products. The chemical composition as well as the energy content of biogas is spontaneously influenced by the origin and quality of the used biomass, the digester type, and the AD management system process. As there are variant possible resources in abundance for biogas production, detailed characterization and evaluation of each specific feedstock type is necessary. To decide on the suitability of a particular feedstock one first should have a thorough understanding of the biogas generation methods, especially AD. Convenient

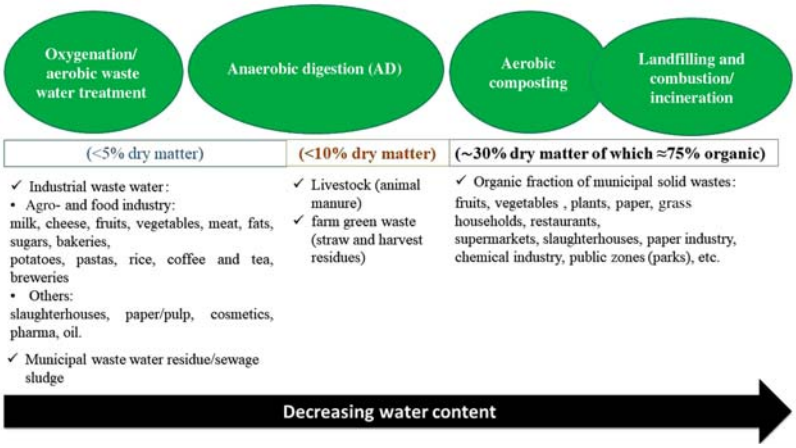

FIGURE 14.4

Various biogas resources and their suitable treatment technologies.

biogas resources must comply with degradability and sufficient water content as well as a low amount of fibrous material (e.g., lignocellulosic material). Crucial characteristics of a biogas to be analyzed for power-generation applications are pH, total solids/dry matter, volatile solids (VS)/organic dry matter, chemical oxygen demand (COD), ammonia nitrogen, and biochemical methane potential. In most cases, the evaluation of VS and COD could be good enough to determine the energy content of a feedstock [94]. Water content and the amount of bulky/fibrous or inorganic materials are determinative criteria for deciding on the suitability of different treatment technologies. Fig. 14.4 depicts biogas sources ranging from a more liquid to more solid nature and, by order of decreasing water content, the treatment technologies that would be preferred. Feedstock possessing considerable water content and a low amount of organic matter or bulky/fibrous material are ideal for AD. As an alternative to AD, for a very high water content feedstock, the oxygenation and/or aerobic wastewater treatment is generally applied. On the other hand, an increase in the amount of organic matter or bulky/fibrous material and decrease in water content, aerobic composting, landfilling, and/or incineration are generally preferred, with regard to the associated costs.

14.4.2 Biogas impurities

The presence of impurity species in fuel feeds highly affects the performance and durability of SOFCs. Preprocessing of the fuel is a necessity for their practicability in high-temperature fuel cells such as SOFCs. In fact, complex hydrocarbons break down into a reformate containing light hydrocarbons, hydrogen, and carbon oxides. This could be accomplished via an appropriate fuel processor and includes

unit operations and processes for enhancing the concentration of H_2 and reducing the impurities. Moisture, heavy hydrocarbons, aromatics, alcohols, and others also exist in the biogas, but do not directly damage the fuel cell or diminish its performance. In this regard impurities are defined as the chemical species that do not participate in the electrochemical oxidation reaction for electric-power generating. However, waste-derived fuels such as biogas contain several trace contaminants, some of which are generated at the biological digestion and others are volatilized from the waste stream being digested [95]. Variant factors including the type and age of waste, temperature and pressure, and the stage of the decomposition process determine the amount and specification of these trace contaminants [48,95]. According to Papadias and Ahmed's database for classification of the impurities found in the biogas [96], three major classes including sulfur, siloxanes, and VOCs (volatile organic compounds) are of special concern when applied in fuel cells or combined heat and power (CHP) systems.

14.4.2.1 Sulfur

Biogas contains a significant amount of sulfur compounds, often as hydrogen sulfide (H_2S), which needs to be stripped off due to its highly corrosive nature. It could lead to deactivation of the fuel processing catalysts used in prereforming and of the fuel-cell anode and, in most cases, the poisoning is irreversible. H_2S is also found in several other gas streams in addition to the streams from biogas digesters, such as LFG, NG, and syngas. Therefore it must be eliminated before it is used in different applications for energy generation. The impact of sulfur impurities on the yttria-stabilized zirconia anode (Ni−YSZ) has been investigated by associated researchers [97,98]. The Ni−YSZ cermet is very susceptible to even low amounts of H_2S in the fuel. Under typical conditions, H_2S will dissociate into elemental hydrogen and sulfur, of which the latter is strongly absorbed on the surface of the anode blocking the active sites on the nickel and prevent the electrochemical oxidation of the fuel cell. This mechanism is depicted in Fig. 14.5 [97]. The organic sulfur is usually present as mercaptans (thiols), disulfides, and dimethyl sulfide (DMS). Compared to the biogas from AD, organic sulfur (mostly DMS) is found in higher concentrations (> 10 ppm) in LFG. Organic sulfur species react with hydrogen and carbon oxides to form H_2S and COS, especially at elevated temperatures.

14.4.2.2 Siloxanes

The second-largest family of biogas contaminants is volatile organic silicon compounds, known as silanes and siloxanes. The latter are organic silicon compounds typically used in industrial processes and are frequently added to consumer products such as hygiene products, cosmetics, detergents, pharmaceuticals, paper coatings, and textiles [99]. The most conventional ones in biogases are the linear and cyclic species. In WWTP with anaerobic digesters and landfills, siloxanes are volatilized into biogas, which is affected by numerous factors, including temperature. LFG may also contain significant quantities of other siloxanes such as

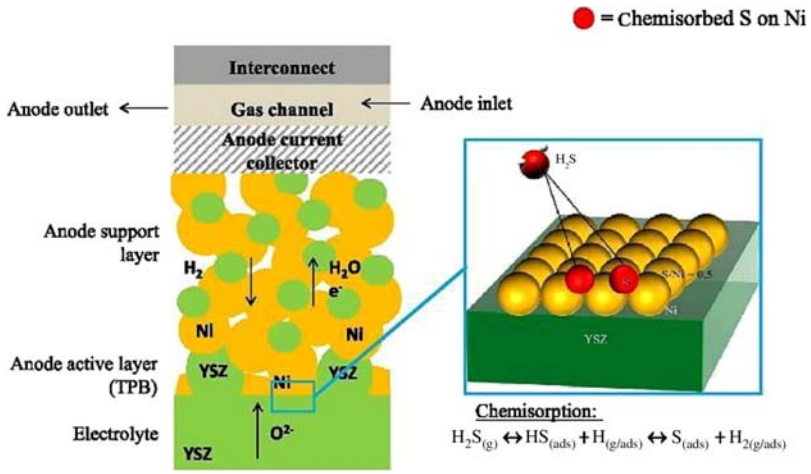

FIGURE 14.5

The chemisorption mechanism of Ni-based anode deactivation in solid oxide fuel cells resulting from the presence of H_2S as an impurity in biogas fuels [97]. *TPB*, Triple phase boundary.

trimethylsilanol (TMS). Siloxanes in fuel gas can lead to the formation and deposition of SiO_2 that would affect many instruments of the fuel cell system, such as heat exchangers, catalysts, and sensors [100]. In a study by Haga et al. [101], they showed that 10 ppm of D5 led to a total SOFC failure in 30 h at 1000°C.

14.4.2.3 Volatile organic compounds

Other gas trace compounds (i.e., alkanes, alcohols, aromatics, halogenated hydrocarbons) typically found in waste-derived fuels are also known to cause detrimental effects on fuel-cell catalysts [23,102]. Chlorine is the most abundant form of halogens, whereas bromine and fluorine-containing hydrocarbons generally occur in lower concentrations. Paraffinic and aromatic hydrocarbons are usually found in higher concentrations in LFG compared to the biogas from the AD of WWTPs. Among the aromatic species, benzene, toluene, and xylene are typically found at high concentrations. Although the amount of hydrocarbons commonly found in waste-derived fuels may not be hazardous to the fuel cell, their presence reduces the capacity of the adsorbents that are typically utilized to capture the more deleterious species from the biogas (e.g., siloxanes).

14.4.3 Impurity removal

For deep treatment and gas cleaning to be installed at a pilot-plant level in a WWTP and for integration opportunities with SOFC technologies, one has to evaluate the tolerance limit, power output capacity and the balance between the

costs of impurity removal and so on. In order to determine the specific tolerance limits of a certain impurity, the type and origin of the impurity as well as its interaction with the materials in the anode chamber including the electrocatalyst and the electrolyte should be considered. Impurity levels allowable in the biogas fed to the SOFC anode reported in the literature are: $H_2S \leq 1$ ppm, HCl few or trace, NH_3 5000 ppm, halogens 1 ppm, and total silicon < 0.01 ppm [103,104].

H_2S elimination techniques from gas streams are mainly categorized as biological, physical, and chemical processes. Biological treatments are cost-effective and typical environment-friendly processes that have been implemented for biogas treatment [105]. The other two classes defined as physicochemical processes can be classified as chemical absorption (reactive or chemical oxidation) and physical adsorption (iron adsorbents, activated carbon) techniques, and their application largely depends on H_2S feed−gas flow rates [106].

Since the chemical backbone of siloxanes (Si-O-Si) is very stable and its chemical reaction with the surface is unexpected, the most frequently used method for elimination of siloxanes is physical adsorption on activated carbons [107]. The temperature and moisture of the gas affect the efficiency of activated carbon performance; thus, before activated carbon filtration, the gas should be dried otherwise the filter quickly saturates with water. Likewise the removal of other gas trace compounds is also accomplished by adsorption systems.

Adsorption is likely the only technique capable of reducing the concentration of contaminants to the stringent extent of a fuel cell's specifications [108]. Due to the biogas resources' versatility the requirements and aims of each gas purification project has been engineered by different methods. Instead of utilizing a standalone adsorption system, researches have come to the breakthrough of a combination of impurity removal methods to ensure fulfilling the desired quality of a biogas for utilization in SOFCs. These gas-cleaning strategies involve a primary clean-up, followed by a gas-polishing step prior to entering the fuel-cell system [96,109]. The first step in the clean-up system in the biogas purification unit is the primary H_2S abatement. Desulfurization is recognized by the reaction with mixed-metal oxides forming a stable metal sulfide. Conventional examples of media options for H_2S removal include an impregnated activated carbon and iron sponge, which are catalytic processes for H_2S removal from biogas [110,111]. The latter involves the chemical reaction on the adsorbent surface typically using ferric oxide coated onto a supporting material. The adsorption removal mechanism for H_2S chemisorption is by flowing the biogas through the iron sponge, the hydrated iron oxide reacts with H_2S forming iron sulfide, which leads to the removal of H_2S from the gas [112]. Activated carbon (AC) does not show selectivity by itself; however, it could be achieved against certain compounds and adsorption capacities may be enhanced by impregnating the carbon with certain caustics (KOH, NaOH, or other modifying reagents) [113]. A thin basic layer present on the pore surface of the impregnated AC functional groups is believed to dissolve the slightly acidic H_2S gas and oxygen, then O_2 would break down into radicals reacting with the dissolved hydrosulfide ions.

Before entering the polisher unit the biogas from the sulfur removal beds needs to be dried to remove moisture through refrigeration or condensation. The capacity of adsorbents such as AC, silica gel, and zeolites is significantly reduced by the existing moisture, especially at relative humidity of exceeding 40% and less than 10%, respectively [114]. For instance, Arespacochaga et al. [96] designed and implemented a three-stage polishing system based on adsorption which consisted of a regenerable iron-based adsorbent unit to remove H_2S, a biogas drying unit to remove moisture, and an activated carbon unit to remove the remaining trace components (siloxanes, linear, and aromatic hydrocarbons). They achieved over 99% removal efficiency and 21%wt. adsorption capacity by iron-based adsorbent. From the economic point of view, they concluded that combining upstream H_2S abatement followed by downstream adsorption technologies, in comparison with standalone adsorption systems (i.e., either standalone chemisorption or physical adsorption) significantly reduces the overall treatment costs and aids the development of biogas-fueled fuel cell projects.

14.5 Direct waste to solid oxide fuel cell systems: case study for flare gas recovery

Utilizing the flare gas as a feed of SOFC is regarded as a novel approach to recovery of flare gas. In the study by Saidi et al. [19] an electrochemical model was developed for a steady-state, planar SOFC by considering the direct internal methane steam reforming. NG and flare gas which contain mainly methane (i.e., 80%−95%) is the most appealing fuel for SOFCs. In the new configuration the sweetened flare gas was fed to the SOFC directly without any need for prereforming. One of the main problems of internal steam reforming is carbon deposition on the Ni-based anode which leads to catalyst deactivation and the reduction of cell performance and lifetime. They also referred to the research by Rahimpour and Jokar [115] where they proposed electricity production from the flare gas from the Asalouyeh gas processing plant by gas turbine (GT) technology. Fig. 14.6 represents a comparison between the generated electrical power by their approach and an SOFC. As depicted, the generated electrical power in GT and SOFC technologies is 2130 MW and 1200 MW, respectively, which are significant amounts.

For a comparison between the feasible pathways of flare-gas recovery, Viswanathan et al. [116] studied material and device targets for a flare-gas recovery system including gas-to-liquid (GTL), gas compression system, and electricity generation via SOFC or GT. According to the scales adopted in their study [117], capital investment of the SOFC system (about 67.7 million $) was the least among the flare gas recovery systems. In Fig. 14.7 the capital investment of SOFC, GT, GTL, and gas compression approaches are compared.

However, the main drawback of SOFCs was that the generated electricity needs to be consumed instantly and, thus, such a system often requires energy

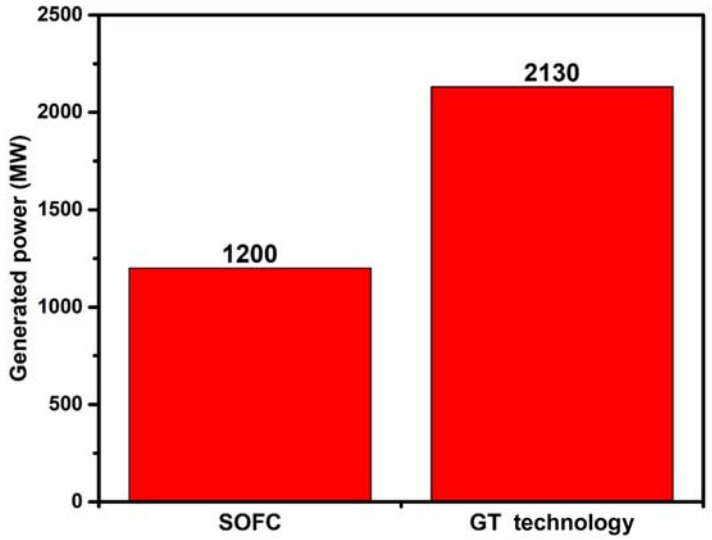

FIGURE 14.6

A comparison between total-generated power by solid oxide fuel cell and gas-turbine technology. *SOFC*, Solid oxide fuel cell; *GT*, gas turbine.

(electricity) storage. It has been shown that the total cost of energy storage (e.g., lithium-ion batteries) could be as high as the cost of electricity-generation systems.

In a similar study [18], ammonia and methane as the main GHGs in the purge gas were converted to pure hydrogen through methane-steam reforming and ammonia-decomposition reactions over nickel-based catalyst in the membrane reactor. The produced hydrogen is permeated through the Pd−Ag membrane and sent to the SOFC as feed. The modeling results demonstrated that increasing temperature and pressure of the reactor up to 873 K and 35 bar, respectively, through 0.6 length of the reactor, enhanced the conversion of methane and ammonia to 100%. Besides these results the parametric analysis of SOFC revealed that the cell had superior performance at higher temperature and hydrogen composition and fuel utilization of about 8 MW power was generated via the designed configuration.

14.6 Internal versus external biogas reforming

Fuel external-reforming processes are commercialized technologies for efficiently converting H_2 into electrical energy and to the desired power levels. Meanwhile, a great deal of attempts has been paid to the direct use of biogas in the fuel cells

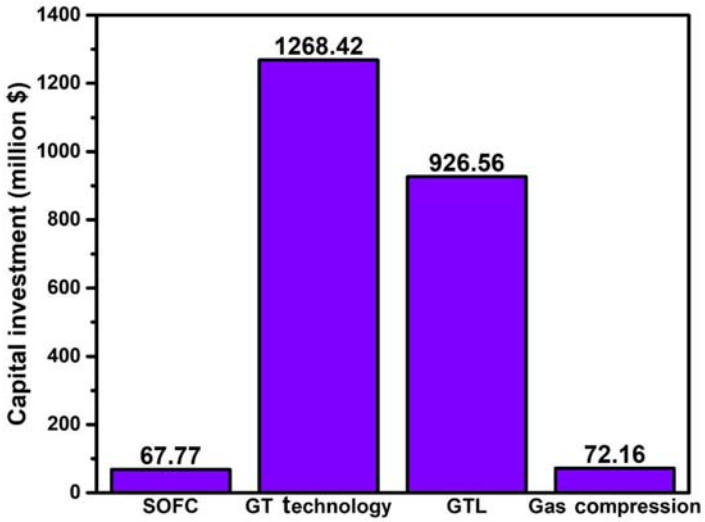

FIGURE 14.7

A comparison between total-capital investments for no-flare approaches.

referred to as internal reforming [68]. Due to the high operating temperature of SOFCs and steam produced during the chemical process, SOFCs can be used to internally reform methane to hydrogen. This means that methane fuel enters directly into the SOFC and hydrogen is extracted simultaneously. On the one hand, conventional thermochemical treatment processes (i.e., types of biomass gasification) in which the biogas is obtained usually require elevated operating temperatures and coupling these technologies to the SOFCs operating in the same temperature range is of great attractiveness and advantage. On the other hand, high-temperature SOFC fuel cells are best-suited for the direct use of biogas because they have a greater capacity to thermally integrate internal reforming and have an increased tolerance against contaminants while preserving high-electrical efficiency (up to 50%). In an internal reforming SOFC (IR−SOFC) most of the fuel reformation takes place in a passage prior to entering the anode. In a planar stack of cells, internal reforming passages would be located in between the cells (electrodes). Furthermore, an SOFC in a direct internal reforming configuration benefits from the direct heat exchange between the exothermic electrochemical reactions and the endothermic reforming reactions taking place in an individual device. Because the amount of heat generated by the fuel cell is beyond that necessary for reforming, excess air in the cathode might act as the SOFC coolant [118]. Conventionally, in an external reforming SOFC (ER−SOFC) configuration the location of reformer is most likely before the anode [119]. Overall the concepts of SOFCs running on biogas with external and internal reforming are schematically represented in Fig. 14.8A and B, respectively.

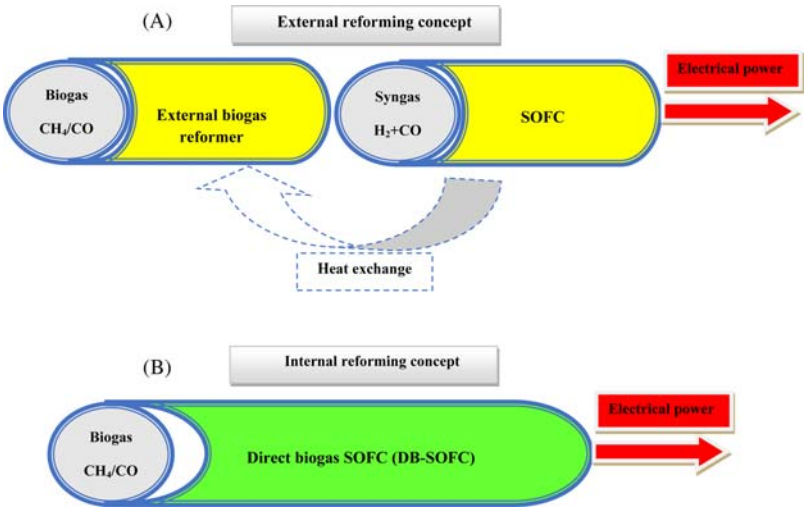

FIGURE 14.8

General concept of solid oxide fuel cells running on biogas with (A) external reforming and (B) internal reforming. *SOFC*, solid oxide fuel cell; *DB-SOFC*, direct biogas-SOFC.

Several studies have been reported in the literature on the use of various types of biogas as a direct feed in high-temperature SOFCs. Typically the electrodes in SOFC cells also exhibit catalytic activities which comprise anode and support including Ni−YSZ (yttria-stabilized zirconia) or Ni−ScSZ (scandia-stabilized zirconia), cathode including LSM (lanthanum strontium doped manganate) or composite as well as electrolyte including YSZ−TiO_2, ZEI−MgO, Y_2O_3, CeO_2, MnO − CeO_2, and GdO_2−CeO_2 [120,121]. Shiratori et al. [122] evaluated the feasibility of direct biogas to an SOFC using Ni−ScSZ cermet as an anode material. It was demonstrated that cell voltage over 0.9 V (at 200 $mAcm^{-2}$) was stably obtained over 50 h without carbon deposition at the operating temperature of 1000°C. Internal dry reforming of methane was progressed on the Ni-based anode which provided advantages such as performing the role of catalyst necessary for the reforming process as well as enabling the internal reforming utilizing CO_2 present at the biogas feed while avoiding the external reforming and the requisite of precious metal catalysts thereof. In another investigation on direct feeding of biogas to SOFC by the same authors [123], using anode-supported button cells, stable operation of biogas-fueled SOFC with cell voltage above 0.8 V was achieved over 800 h at 200 mA cm^{-2} through the IR mode at 800°C. Both studies revealed that air addition to actual biogas reduced the risk of carbon formation and led to a more stable operation. However, investigations of biogas-fueled SOFC systems are limited to small-scale, proof-of-concept projects. Tjaden et al. [70] investigated the technical analysis and assessment of a small-scale (25 kW), biogas-fueled SOFC model operated on various biogas feedstocks. From their

comprehensive energy and electrochemical model of the SOFC stack, which included different gas reforming options, it was concluded that ATR did not have a high performance. Also from the system analysis, it yielded to an electric efficiency of 56.55% based on lower heating value (LHV) under steam reforming (SR). In a study by Omosun et al. [124] the integration of an SOFC with biomass gasification technique for a CHP system was investigated using the gPROMS modeling tool. Two situations, a cold process involving gas cleaning at a reduced temperature versus a hot process involving gas cleaning at a high temperature, were modeled and compared. The hot process was found to be superior to the cold process with respect to the electrical and total system efficiency, but required a higher capital costs. In another study, Trendewicz et al. [24] evaluated biogas-fueled SOFC systems for CHP applications in WWTPs with electric power capacities ranging from 300 kW to 6 MW in terms of their performance and life-cycle costs. They developed an SOFC−CHP system model with Aspen Plus for integration with small, medium, and large biogas resources characterized by 640 kW_{LHV}, 2.97 MW_{LHV}, and 11.92 MW_{LHV}, respectively, and included anode gas recirculation, a biogas pretreatment system, and a waste heat-recovery unit. Their model predicted a net electrical efficiency of 51.6% LHV and net−CHP efficiency of 87.5% LHV. In a parametric case study the leveled costs of electricity (COE) and heat (COH) in economic evaluation was comparable with those from reciprocating engines, GTs, microturbines, and molten carbonate fuel cell (MCFC) technologies with grid electricity prices at 5−8 $/kWh. Wheeldon et al. [125] modeled the assessment of recoverable energy from biogas generated in AD units of three various WWTPs in the Canadian province of Ontario and their utility as inputs for process flow simulation of a biogas-fueled SOFC system. Based on HHV, overall efficiencies of 55%, 58%, and 60% for the three plants were calculated, respectively. They also pointed out that if all the wastewater sludge in Ontario was processed through AD, the biogas produced could theoretically provide approximately 1.51 GWh/d of electrical energy.

However, the main problems that the internal reforming process in direct biogas-fueled SOFC systems commonly encountered were with the biogas composition variability and the poisoning of the catalysts of the fuel cell by carbon deposition (coke) by CO disproportionation and the presence of sulfur traces [126]. The diagram of C−H−O ternary phase depicted in Fig. 14.9 has been adopted by numerous researchers to represent the zone with the greatest tendency to the carbon deposition when biogas internal reforming is used in SOFCs [68,120,122,123]. As proposed by Lanzini and Leone [120] a significant operational improvement of an SOFC system is achieved since carbon deposition at a certain threshold-hydrogen content was completely avoided by enriching biogas with hydrogen. In a related work by Guerra et al. [127] the catalytic properties of Ni−YSZ anodes as electrodes of SOFCs to be operated under direct DR of methane was investigated. At 800°C the best performances were for the volumetric ratios of carbon dioxide/methane between 1.5 and 2, while the conversion was

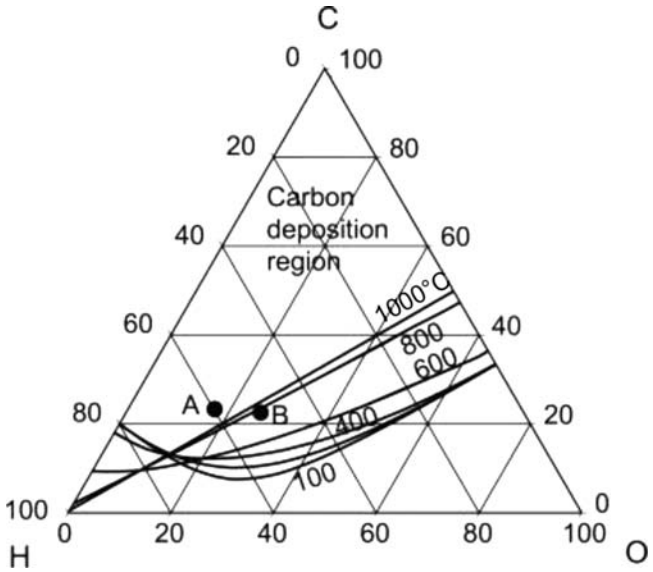

FIGURE 14.9

Ternary C–H–O diagram showing the possibility of coke formation in the related temperature for biogas internal reforming in solid oxide fuel cell.

Adapted from Y. Shiratori, T.Q. Tran, Y. Takahashi, K. Sasaki, Application of biofuels to solid oxide fuel cell, ECS Trans. 35 (2011) 2641–2651.

poor for both $T < 450^{\circ}C$ and carbon dioxide/methane ratio <1 at 800°C. Stable conversion performance was maintained over a test period of 70 h.

Novel approaches have been conducted to address the carbon deposition and the consequent coke formation through the addition of variant promoters such as Sr, Ce, Ru, Rh, Pd, and Pt to the Ni–YSZ anode and also adding water and air to the fuel [121]. Air addition to biogas is one of the most effective ways to solve this problem. In a related study it was stated that the strong temperature gradient generated in the cell caused by ER reaction could lead to drastic cell failure [128]. Air addition to biogas resulted in the temperature homogenization in SOFC in which air/biogas ratio of 0.7 was found to be optimum in terms of reforming efficiency. In another related study, Farhad et al. [129] predicted the performance of three SOFC systems fueled by biogas produced through the AD process for CHP generation in WWTPs by a UniSIM™ simulation. Testing was also performed with humidified dilute hydrogen fuel and various gas diluents and successful biogas reformate tests were achieved with up to 20 mol% humidification. Moreover, they employed different fuel-processing methods to prevent carbon deposition over the anode catalyst including AGR, SR, and partial oxidation (POX) in the three systems, where the AGR and SR based systems yielded electrical efficiency of 45.1% and 43%, respectively.

14.7 Comparison of cogeneration technologies for biogas utilization

Biogas in its raw and upgraded forms can be utilized via various pathways. Its utility addresses the necessity for developing ecofriendly production of sustainable energy and added-value chemicals. Different technologies can be employed for converting biogas as an energy carrier into final products. Growing interests have been focused on biogas upgrading, biogas CHP, and biogas-fueled SOFCs [130]. Yentekakis and Goula projected two main avenues for advanced biogas utilization regarding research and development, technology, and implementation [131]. However, from the commercial standpoint, feasible biogas utilization methods include: (1) electricity generation with CHP or fuel cells; (2) multigeneration of heat, steam, electricity, and cooling in industry; (3) injection in the gas grids; (4) transport fuel; (5) production of chemicals and other energy-associated operations such as (6) energy storage applications and (7) stabilizing intermittent wind and solar renewable energy systems [132,133]. The digestate from anaerobic fermentation is also a valuable fertilizer due to the increased availability of nitrogen, minimized survival of pathogens, and the better short-term fertilization effect.

Biogas-to-CHP represents one the most common utilizations worldwide. Biogas is mostly applied for providing electricity and is generally obtained by the small to medium-scale installation on farms in the agricultural sectors as well as in larger AD plants for waste digestion. Based on local energy renewable policies and regulations, biogas plants of each country are different. For example, Sweden uses biogas plants in which the biogas is directly used as a vehicle fuel after a filtration process, while in Germany the biogas plant usually is integrated with gas engines or gas turbines to provide heat and electricity [134–136]. Table 14.6 summarizes the results obtained from a survey of biogas plant operators in Germany in 2016 regarding the kind and amount of biogas production. According to Daniel-Gromke et al. [135], in 2016 more than 95% of biogas plants were assigned to the biomethane-CHP plants. Also, 17.2% of renewable energy–based electricity was generated from biogas, which is about 32.37 TWh_e [135]. Although lots of biomethane-CHP plants have been established in developed countries, recent studies show that the technology still faces major problems. For example, Wu et al. [134] assessed a biogas system with three utilization pathways from the energetic-environmental-economic point of view. The assessment results indicated that biomethane-CHP plants have lower systematic energy efficiency than a biogas plant integrated with SOFCs or biogas upgrading pathway, while for biogas SOFC pathways the green degree (gd) production is the highest (21.77 gd/day). Energy efficiencies of a biogas system with three utilization pathways are presented in Table 14.7. Based on reported data in this table, although the utilization of biogas as the fuel for gas grid or in vehicle industry is preferred relative to other pathways, there are still some concerns hindering its wide usage.

Table 14.6 Types and number of biogas production plants in Germany in 2016 [135].

Type of biogas production plants	Value
Agricultural biogas plants	~8200
Thereof manure-based small-scale plants (≤75 kW)	560
Biowaste digestion plants (share of organic waste larger than 90%)	~135
AD plants based on organic waste and manure/energy crops (share of waste smaller than 90%)	200
Biogas upgrading plants (biomethane)	196
Biogas production plants	~8700

Table 14.7 Energy efficiency of three biogas utilization systems [134].

Systems	Net electricity output (MJ/day)	Net heat recovery (MJ/day)	Net electric efficiency (%)	Net heat efficiency (%)	Energy efficiency (%)
Biogas upgrading	–	–	–	–	46.5
Biomethane–CHP plants	4139.8	5202.5	13.8	16.6	30.4
Biogas at SOFCs	5286.5	3530.6	20.4	12.5	32.9

Furthermore it should be noted that the energy efficiency of the biogas upgrading system was calculated by the output–input ratio method. This method relies solely on the LHV of feedstock and methane, different from the method used in assessing other technologies. Nevertheless, there are commercial biogas plants based on biogas upgrading. In this technology the purification system is of prime importance. The methods of biogas impurity removal have been briefly discussed in the Sections 14.4.2 and 14.4.3 and various types of technologies are summarized in Fig. 14.10 [137–139].

In a wider perspective, the results of energy-efficiency evaluation of various biogas production and utilization pathways by Poeschl et al. [140] who indicated that primary energy input to output (PEIO) ratio for small and large-scale biogas utilization methods ranges between about 4%–46% and 1%–34%, respectively. For the calculation of the energy efficiency of the biogas utility pathways especially biomethane–CHP plants and biogas–SOFCs, LHV–based net electric efficiency and heat are also important factors. State-of-the-art technologies play a key role to ensure energy efficiency enhancement and economic viability of the biogas utilization systems by suggesting process and infrastructure innovations.

In most commercially power plants running on biogas, internal combustion engines (ICE) such as gas engines have emerged as the standard technology. Dual fuel engines involving the co-combustion of biogas with usually very small

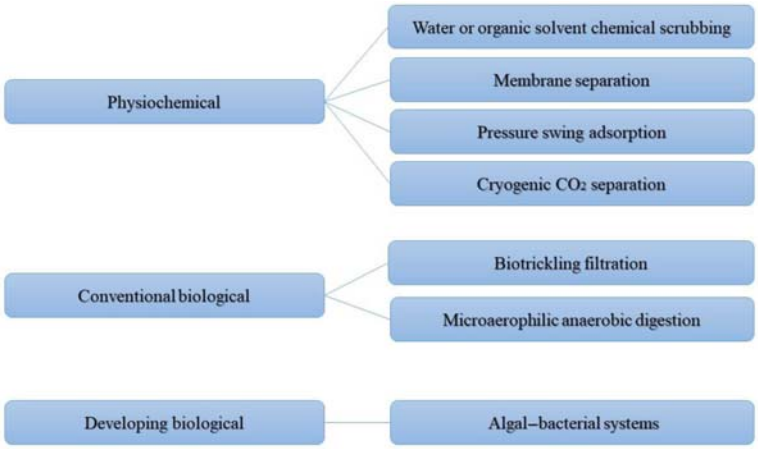

FIGURE 14.10

Biogas upgrading technologies.

proportion of, for example, biodiesel, bioethanol, microgas turbines, and Stirling engines (SE) are also other innovative options [141–144]. Although micro–GTs and SEs are available on the market they are rarely utilized due to their high cost and maintenance requirements as well as lower electricity production than other state-of-the-art engines. Typical electricity production efficiencies range from about 20% for SE to 45% or more for gas engines and micro–GTs. Flameless combustion, commonly known as diluted or mild combustion, is a combustion technique with potential to alleviate unwanted emissions and improve fuel conversion efficiency. Hosseini and Wahid [145] investigated biogas flameless combustion and claimed that for flameless biogas combustion in a furnace based system, electrical efficiency of 53% and CHP efficiency of 82% together with low–NO_x emissions were possible.

The organic Rankine cycle (ORC) process, as another biogas utility option, converts thermal energy from low-temperature heat sources to electricity using organic fluids of high molecular mass. Organic waste integrated aerobic/anaerobic system for ORC fueling has been investigated by Di Maria et al. [146]. Therein an AD system was integrated to the 1–25 kW ORCs that resulted in higher than 20% energy conversion efficiency. In a related work by Dumont et al. [147] the authors focused on the thermoeconomic optimization of an ORC waste heat recovery unit for a 500 kW biogas power plant located in a detailed regional market. By means of a genetic algorithm a methodology was adopted to optimize and compare subcritical, transcritical, and wet expansion cycle architectures and different types of expanders from technical and economic standpoints. The results demonstrated that optimal ORC solutions with a potential of energy savings up to 600 MWh per year and with a payback period lower than 3 years were achievable

in the regional market analyzed. In general, modest thermodynamic efficiencies of ORC typically lower than 20% (approximately 9%) seem to limit their commercialization potential [148]. Nevertheless, ORCs could be applied in biogas engines including power plants, biorefineries, and industrial systems involving AD where their efficiencies would improve.

14.8 Waste utilization in other types of fuel cells

A proton exchange membrane fuel cell (PEMFC) as another type of fuel cell with the distinguishing feature of lower operational temperature/pressure ranges (50°C−100°C) uses a special proton-conducting polymer electrolyte membrane. PEMFCs are less suitable for biogas utilization because they are less tolerant to other biogas compositions (especially CO) and usually require clean fuels enriched with hydrogen. Of the pioneering works, biogas processing and its utility in PEMFCs was experimentally studied by Schmersahl et al. [149]. The biogas was processed in a steam reformer to produce hydrogen having over 50% purity, which was sufficient for an efficient and stable operation of the PEMFC stack. They also concluded that power generation via biogas and fuel cells from agricultural residues such as wheat straw can provide a constant power of up to 0.5 kW per hectare of acreage. The thermodynamic analysis of a biogas reforming process and PEMFC integrated system for hydrogen and power generation using Aspen Plus simulator was performed by Authayanun et al. [150]. The effect of key parameters on the yields of H_2 and carbon in the biogas reformer as well as the performance of PEMFC systems with different H_2 purification methods (conventional and membrane-based technologies) were analyzed. Increases in the H_2O/CH_4 ratio and reformer temperatures enhanced the hydrogen yield and reduced the carbon formation. However, the conventional PEMFC system represented low-system efficiency when operated at high-operating pressures because of the high-power requirement in auxiliary units. In a project dealing with a design study for the decentralized conversion of 1 m^3 h^{-1} biogas to electricity, a high temperature polymer-electrolyte membrane fuel cell (HT−PEMFC) with modular prototype design was proposed by Birth et al. [151]. The simulation results revealed the full conversion of methane with a maximum yield of hydrogen and a low concentration of carbon monoxide. The calculated electrical efficiency of the process was approximately 40%, thus making it suitable for HT−PEMFC applications.

AD and gasification (GF), as the two developed conversion technologies for liquid and solid biomass, respectively, were employed to investigate biomass-fueled PEMFCs for different raw materials using simulation methods by Guan et al. [152]. Hence the product gas of the mentioned methods (i.e., biogas in the AD) underwent reforming and was utilized in an AD−PEMFC system and GF−PEMFC system for residential applications. The GF−PEMFC system yielded

a 20% electric efficiency and 57% thermal efficiency, whereas the AD−PEMFC system showed only a 9% electric efficiency and 13% thermal efficiency. In a discussion of the environmental performances of these two systems in terms of CO_2 emission offset and land-use efficiency, the GF−PEMFC system had a high CO_2 emission offset factor.

Molten carbonate fuel cell (MCFC) is considered as one of the most promising power generation systems owing to their high efficiency, low emissions, and wide-ranging fuel possibility [153,154]. There are several good reasons to select the MCFC for CHP systems. High-temperature fuel cells are better suited for biogas operation since their components are tolerant toward several components of the biogas that are harmful for low-temperature fuel cells. However, H_2S must be removed from raw biogas. Due to its high-operating temperatures, MCFC can employ conventional steam reforming catalysts based on Ni, which is cheaper than noble metals [155]. Furthermore, MCFCs have the advantage that CO is not only a poisoning element for them, but also (mostly present as CO_2 in the high-operating temperature) is a reactant in the process, increasing the electrical efficiency by approximately 2% [156]. Hamad et al. [157] discussed the design of combined hydrogen, heat, and power (CHHP) system in which biogas produced by AD of local resources supplied fuel for commercial DFC1500MCFC unit. The CHHP system were able to provide electricity to power the university campus, thermal energy for heating the anaerobic digester, hydrogen for transportation, back-up power, and other requirements. After further validation by experimental demonstration the commercial deployment is yet to be achieved. Economic evaluations represent the current challenges for MCFCs systems. A techno-economical comparison between conventional CHP technologies (reciprocating engines and gas turbines) and innovative solutions comprising MCFCs fed with biogas produced in wastewater plants has successfully been accomplished by Chacartegui et al. [158]. The thermodynamic and environmental analyses were focused on the CHP facility. The hybrid systems exhibited the best thermodynamic and environmental performances. It was shown that a hybrid MCFC−gas engine with CO_2 sequestration by simple water condensation could achieve direct CO_2 emissions between 374 and 567 kg/MWh in specific terms.

The combination of the conventional AD and a microbial fuel cell (MFC) is considered as an innovative pathway for further biogas utilization towards electricity. Some specific advantages of MFC technology such as its applicability for the treatment of low-concentration substrates at temperatures below 20°C provides specific application niches where it does not compete with, but complements, the AD technology [159]. Ge et al. [160] investigated the long-term operation of MFC for treating primary and digested sludge. The results suggested that total-energy production in MFCs could be comparable to anaerobic digesters, while direct electricity generation had a minor contribution to total energy production. A LCA was conducted by Foley et al. [161] to compare the environmental impact of three IW-water treatment options including an anaerobic treatment with biogas generation, a MFC treatment with direct electricity generation, and a

microbial electrolysis cell (MEC) with hydrogen peroxide production. Their analysis indicated that an MEC could provide significant environmental benefits relative to the conventional anaerobic treatment and MFC treatment options through the displacement of chemical production by conventional means. Generally, MFCs can rarely achieve interesting PEIO and, thus, further innovative approaches and basic researches are required to shift to WtE technology. Building an energy balance is a key and necessary step to understanding energy issues and will provide valuable information to optimize MFC operation [162].

14.9 Solid oxide fuel cell waste management

The recirculation of SOFC exhaust gases has also received great emphasis among the systems studied, in that it highly affects the waste management and production of heat and power as well as capital costs within the system. By utilizing the exhaust heat from the high-temperature SOFC stack to convert methane-rich biogas to a hydrogen-rich gas mixture (i.e., internal reforming) a significant reduction in GHG emissions and enhancement in air quality would be achieved. In the SOFC, anode waste gases containing hydrogen and carbon dioxide are separated from the waste gas stream by means of, for example, a scrubbing step and/or an adsorption system, and the resulted hydrogen is recycled to the anode. Solid-state conduction within the SOFC structure selectively enables the transport of oxygen ions toward the anode (fuel) electrode and prevents that of other gaseous species such as hydrogen, carbon, nitrogen, and so forth [163]. All of the fuel electrochemical oxidation reactions take place at the triple-phase boundary on the anode side exclusively and, thus, for hydrocarbon feeds, the anode exhaust contains primarily water, carbon dioxide, and unreacted fuel (H_2 and CO due to concentration losses). Utilizing seals is another way to ensure that the anode exhaust (spent fuel) and cathode exhaust (spent air) are not mixed and results in two separate exhaust streams. The residual fuel can be oxy-combusted in an afterburner to achieve a H_2O-O_2 stream only. With the use of an SOFC arrangement, no external conversion of CO to CO_2 is required since the CO is converted in the fuel cells properly and the thus-formed CO_2 is exhausted with the anode waste gas. The high-operating temperature of SOFCs have facilitated variant pathways for treatment and downstream utilization of the anode and cathode waste/exhaust streams in a wide variety of research studies, institutions, and power plants across the globe [164–174]. A simple schematic of CO_2 capture from the exhaust at low cost is shown in Fig. 14.11. The exhaust CO_2 is eventually cooled and water is separated via condensation. CO_2 recovery and sequestration from the SOFC anode exhaust is, thus, relatively straightforward.

Complementing plants capable of exploiting local energy sources coupled with an efficient CO_2 separation and carbon reuse/recycling are of prime interest from environmental standpoint, that is, CO_2 emission abatement. Nevertheless the recycling of the anode exhaust gas in an integrated SOFC system is considered to improve its performance. For instance, the performance of an SOFC system fueled

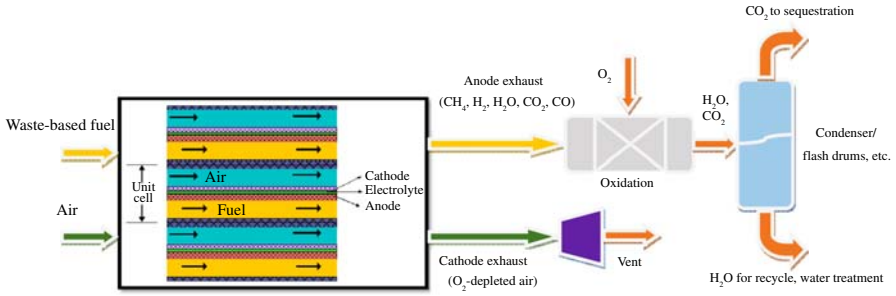

FIGURE 14.11

Schematic of CO_2 capture from the exhaust stream.

by syngas derived from an ethanol-reforming process with nonrecycling and recycling of the anode exhaust gas was investigated by Saebea et al. [175]. The results indicated that anode exhaust gas recycling operated at a higher recirculation ratio and fuel utilization could lead to reduction of carbon formation. In addition the results showed that the electrical efficiency depends on the fuel utilization of the SOFC. In another related study, Saidi et al. [19] found that decreasing the recirculation ratio from 0.6 to 0.2 increases the electrical efficiency of the cell and increasing the fuel utilization ratio improves the cell performance. In a related research by Lackey et al. [22] the performance of tubular SOFCs operated on AD derived biogas was examined with different H_2 fuel dilutions. Also, a model using UniSIM was developed to predict system efficiency and GHG emissions and the results estimated a higher electrical system efficiency for a steam/carbon ratio of 2 compared to 1, and reductions in GHG emissions at 2400 tones CO_2, 60 kg CH_4 and 18 kg N_2O. A comparative study on thermoeconomic analysis of four different configurations of biogas-fed SOFC power plants focusing on anode and cathode recycling was conducted by Mehr et al. [176]. Results indicated that when the current density is low there is an optimum anode recycling ratio at which the thermal efficiency is maximized. In addition an increase in the anode recycling ratio increases the unit product cost of the system while an increase in the cathode recycling ratio has a reverse effect. At the same working conditions, the SOFC anode and cathode recycling system is superior to the other configurations and its thermal efficiency is calculated as 46.09% which is 6.81% higher than that of the simple SOFC fed by NG. Different configurations of SOFC waste management based on exhaust gas recovery are schematically depicted in Fig. 14.12 [177].

14.10 Hybrid solid oxide fuel cell energy systems

Hybrid energy systems are capable of exploiting the advantages of two or more energy technologies simultaneously. The SOFC as a high-temperature technology can be combined with bottoming cycles such as gas turbines and steam turbines

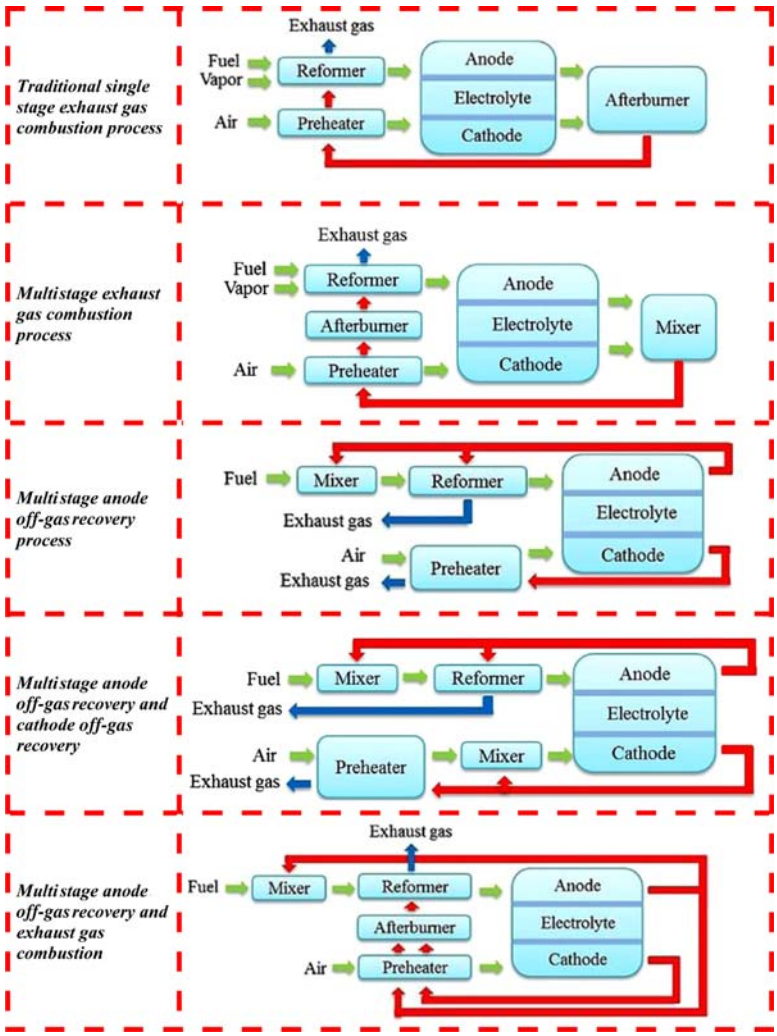

FIGURE 14.12

Different configurations of solid oxide fuel cell waste management based on exhaust gas recovery [177].

in cascade to meet higher efficiency suggesting great potential as a green decentralized CHP system. SOFC offers high WtE or fuel-to-electricity ratios and, on the other hand, GT improves the utility of thermal energy of exhaust/flue gases derived from high-temperature SOFCs. Accordingly, SOFC−GT hybrid systems have attracted much attention in recent literature [178−183]. A 5 kW planar SOFC module integrated with a microgas turbine unit including two radial

FIGURE 14.13

Block scheme of the municipal solid wastes gasification with solid oxide fuel cell and Stirling engine plant hybrid systems. *SOFC*, solid oxide fuel cell.

turbines and one radial compressor was thermodynamically optimized by Facchinetti et al. [178]. Sensitivity analyses on the more influential parameters were also carried out. The optimization results indicated the existence of optimal designs achieving exergy efficiency higher than 65%. Wongchanapai et al. [179] evaluated the combination of direct-biogas SOFC with an MGT−CHP system. The effect of key parameters such as SOFC reforming agent, SOFC fuel utilization factor (U_f), turbine inlet temperature, and compression ratio on system performance was examined. The results showed the feasibility of 55% electrical and more than 80% overall CHP efficiency. An integrated MSW gasification combined with SOFC and stirling engine for decentralized CHP plant of 120 kW electricity power was presented and thermodynamically studied by Rokni [180]. A block schematic of the utilized plant is depicted in Fig. 14.13. Plant electrical efficiency up to 48% and CPH efficiency up to 95% was possible, depending on the plant design and MSW composition.

On the other hand, the high-temperature exhaust gas from SOFC have high exergy that can be exploited in other cycles for additional power generation or for heating and cooling purposes (cogeneration/trigeneration) with different configurations [184]. These systems are referred to as SOFC hybrid systems. The basic idea of an SOFC/GT hybrid cycle is quite simple. Overall, SOFC/GT layouts are classified to two sections due to the applied pressure: SOFC/GT pressurized and atmospheric cycles. Furthermore, the SOFC/GT pressurized cycles differ due to internal reforming operation which includes anode gas recirculation or heat recovery steam generator and external reforming operation. Different bottoming cycles have also been considered, such as Rankine cycles which this configuration means hybrid SOFC/ORC or SOFC/GT−ORC [182,185−187] and also novel hybrid layout of a trigeneration system based on SOFC, ORC, solar collectors, and absorption chillers [188]. In addition, innovative hybrid SOFC based system in research and development projects with high potentials for commercialization involve: SOFC-GT hybrid desalination plants for freshwater power generation [183,189], SOFC−combined cooling and powers hybrid systems (SOFC-CCP)

[190], photovoltaics (PV)-coupled SOFC, and GT-(electrolyzer) hybrid power generation systems [191,192], and others [181].

However, highly efficient electrochemical reactions of SOFCs when running on biogas possess the desired characteristic that the exhausts of the plant are pure CO_2 and water which makes biogas one of the best candidates for hybrid SOFC-based applications. A comprehensive study on the utility of gasified biomass in a hybrid SOFC/GT power plant was presented by Toonssen et al. [193]. The authors investigated the effect of gasification technology, gas-cleanup technology, and system scale on the overall performance of the system considering four different systems. All these systems were based on a recuperated internally reformed SOFC/GT hybrid system equipped with anode and cathode recirculation arrangements in which the former was used to provide the steam required for the internal SR reaction, and the latter was utilized for air preheating. The lignocellulosic biomass conversion process into electricity using integrated gasification and SOFC/GT systems was studied in small and medium-scale applications (100 kW and 8 MW of dry-biomass input) by Caliandro et al. [194]. They conducted multiobjective optimization for maximizing the efficiency and minimizing the capital investment costs. The overall energy efficiency for converting woody biomass into electricity was up to 70%. The economic analysis of the optimal configurations showed the great impact of the fuel cell cost on the total cost. The analyses showed the promising potential of the economic and thermodynamic feasibility of such plants.

In the framework of the European project SOFCOM, a 2 kW SOFC based demonstration plant was installed in Torino, Italy, in 2013 within one of the largest WWTP in Europe [195,196]. The design of the main plant sections included the gas cleaning unit, fuel processor, SOFC "hot-box," oxycombustor, CO_2/H_2O condensation unit and photobioreactors further utilized for algal growth. Later in a similar work about the context of carbon recovery and utilization, the results of EU-funded SOFCOM project on the performance of the proof-of-concept plant units were investigated [172]. The main outcomes from the general environmental perspective were: microalgae are a fast-growing biomass and thus an effective solution; the SOFCOM system was successful in complete abolishing of CO_2 emission from an SOFC; and carbon capture from biogas power plants contributed to an overall emissions cut-off. Nevertheless, photobioreactors faced technological problems which require further considerations and solutions for operation enhancement.

14.11 Life-cycle assessment of hybrid solid oxide fuel cell systems for waste minimization

LCA (also known as life-cycle analysis) is an environmental management tool that enables quantification of environmental burdens accompanied with the life cycle of renewable and fossil fuel based systems [197]. It can help avoid a narrow outlook on environmental concerns by evaluating the potential impacts associated

with identified inputs and releases and interpreting the results to assist in a rational choice of technical solutions for power generation. LCA of SOFC systems studied in the literature lacks an all-round overview and often life cycle phases of which are declined due to simplification needs. Therefore these assessments differ widely owing to the selected perspectives and indicators such as size, fuel type (i.e., NG or biofuel), applications, system boundaries (i.e., cradle-to-gate or cradle-to-grave), decommissioning indicators, global warming (GWP100), Eutrophication (EP), energy and resources demand, LCA software, and others [15,198–202].

Strazza et al. [203] evaluated the potential environmental impacts and potential costs of the operation of a 230 kW SOFC system. Combined LCA–life cycle costs (LCC) methodologies were applied to compare SOFC with a microgas turbine as well as different SOFC configurations fueled with biogas from sewage sludge or NG. The findings revealed that the biogas-to-SOFC provides environmental advantages with respect to the NG case considering an average European power grid mix for energy demand for digestion. It was conclusively proved that the investigated SOFC system was preferable to the conventional micro-GT technology by the sustainability of investment cost, environmental performance, as well as the life time. Lin et al. [200] proposed and developed a methodology that integrates LCA with thermodynamic analysis for evaluating the environmental impacts of producing biofuels from waste biomass, including biodiesel from waste cooking oil, ethanol from a corn stover, and compressed NG from MSWs. Results showed that the latter was an optimal biofuel option for SOFC–auxiliary power unit applications in terms of energy consumption and GHG emissions in New York State. The application of biogas for distributed microgeneration through SOFCs was evaluated by Sadhukan [15] through the life cycle of sewage sludge and comparison of alternative uses. An integrated Monte Carlo simulation and LCA framework was proposed for sensitivity analysis of biogas yields on the environmental impact characterizations and to determine the sensitive, primary-impact characterizations. The results based on avoided impacts ranked as follows: PEMFC < micro-GT < SOFC. Rillo et al. [204] evaluated the environmental performance of a sewage biogas-fueled SOFC integrated with a CO_2 recovery system in which CO_2 recovery was performed through a tubular photo-bioreactor, fixing the recovered carbon in the form of a microalgae. Three different scenarios were analyzed through life cycle impact assessment and life cycle inventory. They were also compared with traditional technologies (internal combustion engines and microturbines) using the same fuel. The results demonstrated that SOFCs can be a high potential method for future electricity generation applications in biogas plants.

14.12 Conclusion

In primary sections of this study, challenges and opportunities of the waste-processing technologies including thermochemical and biological with looking

forward to their potential for coupling with SOFC stacks were presented and compared. The process type and the final product extractable from MSW processing largely depend on the solid-waste type and its contamination level. AD was demonstrated as a promising candidate to be integrated to an SOFC, known as an AD−SOFC. Biogas is the main product of AD and its high-methane content is an excellent feature that makes them more suitable for SOFC application. Various conventional reforming processes for injection of biogas and biofuels to SOFC including SR, POR, ATR, DR, and TR were compared and the results were tabulated. Variant impurities stemming from biogas resources affecting the performance of biogas−SOFC were classified. Conventional adsorption methods as well as recent innovations to remove these anode-poisoning materials known as biogas upgrading techniques were discussed. Consequently, biogas-fueled SOFC systems and the modeling and simulation software utilized for evaluation and assessment of these systems from different standpoints and worthy results were indicated. In addition, the comparison of these systems with other biogas utilization pathways in terms of efficiency, environmental impact, and payback duration were conducted. The reported results showed that SOFCs can be a good potential method for future electricity generation application in biogas plants. SOFC waste/exhaust gases management is also of paramount importance because it highly affects their environmental and economic (and thus commercial) viability due to the CO_2 emission and energy-loss issues. The SOFCs can be combined with bottoming cycles such as gas turbines and steam turbines in cascade to have higher efficiency and be utilized in CHP plants. Besides these, possible hybrid SOFC-based configuration of power plants studied in the relevant literature with the feasibility of cogeneration and trigeneration could successfully address these challenges. The results indicate that power generation using SOFCs coupled with WtE and hybrid technologies can make a significant contribution to a green-energy future.

14.13 Future prospects and outlook

- The utility of SOFCs due to their modularity and high efficiency at small-scale for carbon capture and utilization at the distributed generation plants.
- *Making zero-CO_2 emission feasible*: coupling SOFCs to convenient CO_2 utilization and optimization of this polygeneration plant to attain near-zero emissions.
- *Materials engineering*: more considerations on the manufacturing of materials with improved tolerance against waste contamination and economically viable fabrication techniques of lightweight cells, employing cheap and reliable cells and the infrastructures involved.
- *Turning an environmental problem to an opportunity*: biomass, not only as a feed to energy production plants, but also to be treated for fabrication of

electrodes applied in energy storage devices, like Li-ion batteries and supercapacitors, thus addressing the storage challenges of SOFC generated electricity (for further study refer to: [205,206]).

Abbreviations

AC	activated carbon
AD	anaerobic digestion
AGR	anode gas recirculation
ATR	autothermal reforming
CHHP	combined heat, hydrogen and power
CHP	combined heat and power
COD	chemical oxygen demand
DR	dry reforming
FT	Fischer−Tropsch
GHG	greenhouse gas
GT	gas turbine
$\mathbf{g_d}$	green degree
HHV	higher heating value
IW	industrial waste
ICE	internal combustion engines
kWhe	kilowatt hours of energy
LCA	life-cycle assessment
LFG	landfill gas
LHV	lower heating value
MSW	municipal solid waste
MCFC	molten carbonate fuel cell
MEC	microbial electrolysis cell
NG	natural gas
Ni−YSZ	yttria-stabilized zirconia
OFMSW	organic fraction of municipal solid waste
ORC	organic Rankine cycles
PEIO	Primary energy input to output
POR	partial oxidation reforming
SE	Stirling engines
SOFC/CCP	Solid oxide fuel cell/combined cooling and powers systems
SOFC/GT	Solid oxide fuel cell/gas turbine
SR	steam reforming
TR	trireforming
$\boldsymbol{U_f}$	fuel utilization
VOC	volatile organic compound
VS	volatile solids
WtE	waste-to-energy
WWTP	wastewater treatment plants

References

[1] D. Papurello, R. Borchiellini, P. Bareschino, V. Chiodo, S. Freni, A. Lanzini, et al., Performance of a solid oxide fuel cell short-stack with biogas feeding, Appl. Energy 125 (2014) 254–263.

[2] L. Barelli, G. Bidini, G. Cinti, F. Gallorini, M. Pöniz, SOFC stack coupled with dry reforming, Appl. Energy 192 (2017) 498–507.

[3] T. Pröll, H. Hofbauer, Development and application of a simulation tool for biomass gasification based processes, Int. J. Chem. Reactor Eng. 6 (2008).

[4] T. Sabbas, A. Polettini, R. Pomi, T. Astrup, O. Hjelmar, P. Mostbauer, et al., Management of municipal solid waste incineration residues, Waste Manage. 23 (2003) 61–88.

[5] C.R. Brunner, Hazardous Waste Incineration, McGraw-Hill, Inc, New York, NY (United States), 1993.

[6] L. Otten, Wet dry composting of organic municipal solid waste: current status in Canada, Can. J. Civil Eng. 28 (2001) 124–130.

[7] Z.P. Shiner, An Investigation of Wood and Wood Packaging Waste in the United States, Virginia Tech, 2018.

[8] D. Hoornweg, P. Bhada-Tata, (Urban Development Series Knowledge Papers) What A Waste: A Global Review of Solid Waste Management., World Bank, 2012.

[9] H. Jouhara, D. Czajczyńska, H. Ghazal, R. Krzyżyńska, L. Anguilano, A.J. Reynolds, et al., Municipal waste management systems for domestic use, Energy 139 (2017) 485–506.

[10] Y. Li, S.Y. Park, J. Zhu, Solid-state anaerobic digestion for methane production from organic waste, Renew. Sustain. Energy Rev. 15 (2011) 821–826.

[11] F. Khan, Effect of Hydrogen Sulfide in Landfill Gas on Anode Poisoning of Solid Oxide Fuel Cells, Youngstown State University, 2012.

[12] A. Confalonieri, Technologies and trends for anaerobic digestion across Europe: a survey, Gruppo di Studio sul Compostaggio e la Gestione Integrata dei Rifiuti Scuola Agraria del Parco di Monza. III Conferenza Internazionale ATIA-ISWA (International Solid Waste Association) ITALIA sul Trattamento Biologico, Perugia, 2010, pp. 15–16.

[13] F. Maréchal, S. Leuenberger, D. Favrat, Energy balance model of a SOFC cogenerator operated with biogas, J. Power Sources 118 (2003) 375–383.

[14] F. Maréchal, S. Leuenberger, Y. Membrez, O. Bucheli, D. Favrat, Process flow model of solid oxide fuel cell system supplied with sewage biogas, J. Power Sources 131 (2004) 127–141.

[15] J. Sadhukhan, Distributed and micro-generation from biogas and agricultural application of sewage sludge: comparative environmental performance analysis using life cycle approaches, Appl. Energy 122 (2014) 196–206.

[16] J. Staniforth, R.M. Ormerod, Running solid oxide fuel cells on biogas, Ionics 9 (2003) 336–341.

[17] M. Plochl, M. Heiermann, Biogas farming in central and northern Europe: a strategy for developing countries? Invited overview, CIGR E-J 8 (2006).

[18] F. Siavashi, M. Saidi, M.R. Rahimpour, Purge gas recovery of ammonia synthesis plant by integrated configuration of catalytic hydrogen-permselective membrane reactor and solid oxide fuel cell as a novel technology, J. Power Sources 267 (2014) 104–116.

[19] M. Saidi, F. Siavashi, M. Rahimpour, Application of solid oxide fuel cell for flare gas recovery as a new approach: a case study for Asalouyeh gas processing plant, Iran, J. Nat. Gas Sci. Eng. 17 (2014) 13–25.
[20] M. Moulod, A. Jalali, R. Asmatulu, Biogas derived from municipal solid waste to generate electrical power through solid oxide fuel cells, Int. J. Energy Res. 40 (2016) 2091–2104.
[21] D. Papurello, A. Lanzini, L. Tognana, S. Silvestri, M. Santarelli, Waste to energy: exploitation of biogas from organic waste in a 500 Wel solid oxide fuel cell (SOFC) stack, Energy 85 (2015) 145–158.
[22] J. Lackey, P. Champagne, B. Peppley, Use of wastewater treatment plant biogas for the operation of solid oxide fuel cells (SOFCs), J. Environ. Manage. 203 (2017) 753–759.
[23] Y. Membrez, O. Bucheli, Biogas as a fuel source for SOFC co-generators, J. Power Sources 127 (2004) 300–312.
[24] A. Trendewicz, R. Braun, Techno-economic analysis of solid oxide fuel cell-based combined heat and power systems for biogas utilization at wastewater treatment facilities, J. Power Sources 233 (2013) 380–393.
[25] R.S. Kempegowda, Ø. Skreiberg, K.-Q. Tran, P. Selvam, Techno-economic assessment of thermal co-pretreatment and co-digestion of food wastes and sewage sludge for heat, power and biochar production, Energy Proc. 105 (2017) 1737–1742.
[26] A. Galvagno, V. Chiodo, F. Urbani, F. Freni, Biogas as hydrogen source for fuel cell applications, Int. J. Hydrogen Energy 38 (2013) 3913–3920.
[27] S. Barrett, Nissan SOFC powered vehicle system runs on bioethanol, Fuel Cells Bull. 2016 (2016) 2–3.
[28] J. Milewski, J. Lewandoski, Biofuels as fuels for high temperature fuel cells, J. Power Technol. 93 (2013) 347–353.
[29] Y. Shiratori, T.Q. Tran, Y. Takahashi, K. Sasaki, Application of biofuels to solid oxide fuel cell, ECS Trans. 35 (2011) 2641–2651.
[30] C.S.K. Lin, L.A. Pfaltzgraff, L. Herrero-Davila, E.B. Mubofu, S. Abderrahim, J.H. Clark, et al., Food waste as a valuable resource for the production of chemicals, materials and fuels, Curr. Situat. Glob. Persp. Energy Environ. Sci. 6 (2013) 426–464.
[31] D. Hoornweg, P. Bhada-Tata, What a waste: a global review of solid waste management, World Bank's Urban Development and Local Government Unit of the Sustainable Development Network, Washington DC (2012).
[32] J. Portugal-Pereira, L. Lee, Economic and environmental benefits of waste-to-energy technologies for debris recovery in disaster-hit Northeast Japan, J. Clean. Prod. 112 (2016) 4419–4429.
[33] M. Morris, L. Waldheim, Energy recovery from solid waste fuels using advanced gasification technology, Waste Manage. 18 (1998) 557–564.
[34] M. Pavlas, M. Touš, L. Bébar, P. Stehlík, Waste to energy – an evaluation of the environmental impact, Appl. Therm. Eng. 30 (2010) 2326–2332.
[35] L. Lombardi, E. Carnevale, A. Corti, A review of technologies and performances of thermal treatment systems for energy recovery from waste, Waste Manage. 37 (2015) 26–44.
[36] A. Bosmans, I. Vanderreydt, D. Geysen, L. Helsen, The crucial role of waste-to-energy technologies in enhanced landfill mining: a technology review, J. Clean. Prod. 55 (2013) 10–23.

[37] O. Ellabban, H. Abu-Rub, F. Blaabjerg, Renewable energy resources: current status, future prospects and their enabling technology, Renew. Sustain. Energy Rev. 39 (2014) 748–764.
[38] A. Soltani, R. Sadiq, K. Hewage, Selecting sustainable waste-to-energy technologies for municipal solid waste treatment: a game theory approach for group decision-making, J. Clean. Prod. 113 (2016) 388–399.
[39] J. Twidell, T. Weir, Renewable Energy Resources, Routledge, 2015.
[40] F. Fava, G. Totaro, L. Diels, M. Reis, J. Duarte, O.B. Carioca, et al., Biowaste biorefinery in Europe: opportunities and research & development needs, N. Biotechnol. 32 (2015) 100–108.
[41] I.S. Pieta, W.S. Epling, A. Kazmierczuk, P. Lisowski, R. Nowakowski, E.M. Serwicka, Waste into fuel—catalyst and process development for MSW valorisation, Catalysts 8 (2018) 113.
[42] H. De Lasa, E. Salaices, J. Mazumder, R. Lucky, Catalytic steam gasification of biomass: catalysts, thermodynamics and kinetics, Chem. Rev. 111 (2011) 5404–5433.
[43] D.L. Carpenter, R.L. Bain, R.E. Davis, A. Dutta, C.J. Feik, K.R. Gaston, et al., Pilot-scale gasification of corn stover, switchgrass, wheat straw, and wood: 1. Parametric study and comparison with literature, Ind. Eng. Chem. Res. 49 (2010) 1859–1871.
[44] G. Galeno, M. Minutillo, A. Perna, From waste to electricity through integrated plasma gasification/fuel cell (IPGFC) system, Int. J. Hydrogen Energy 36 (2011) 1692–1701.
[45] F. Fabry, C. Rehmet, V. Rohani, L. Fulcheri, Waste gasification by thermal plasma: a review, Waste Biomass Valoriz. 4 (2013) 421–439.
[46] M. Materazzi, P. Lettieri, R. Taylor, C. Chapman, Performance analysis of RDF gasification in a two stage fluidized bed-plasma process, Waste Manage. 47 (2016) 256–266.
[47] M. Pourali, Application of plasma gasification technology in waste to energy—challenges and opportunities, IEEE Trans. Sustain. Energy 1 (2010) 125–130.
[48] L. Appels, J. Baeyens, J. Degrève, R. Dewil, Principles and potential of the anaerobic digestion of waste-activated sludge, Prog. Energy Combust. Sci. 34 (2008) 755–781.
[49] A.S. Stillwell, C.W. King, M.E. Webber, I.J. Duncan, A. Hardberger, The energy-water nexus in Texas, Ecol. Soc. 16 (2011).
[50] E. Angelonidi, S.R. Smith, A comparison of wet and dry anaerobic digestion processes for the treatment of municipal solid waste and food waste, Water Environ. J. 29 (2015) 549–557.
[51] F. Xu, Y. Li, X. Ge, L. Yang, Y. Li, Anaerobic digestion of food waste–challenges and opportunities, Bioresour. Technol. 247 (2018) 1047–1058.
[52] M.S. Romero-Güiza, J. Vila, J. Mata-Alvarez, J.M. Chimenos, S. Astals, The role of additives on anaerobic digestion: a review, Renew. Sustain. Energy Rev. 58 (2016) 1486–1499.
[53] M.O. Fagbohungbe, B.M. Herbert, L. Hurst, C.N. Ibeto, H. Li, S.Q. Usmani, et al., The challenges of anaerobic digestion and the role of biochar in optimizing anaerobic digestion, Waste Manage. 61 (2017) 236–249.
[54] D.B. Levin, R. Chahine, Challenges for renewable hydrogen production from biomass, Int. J. Hydrogen Energy 35 (2010) 4962–4969.
[55] D. Hotza, J.C. Diniz da Costa, Fuel cells development and hydrogen production from renewable resources in Brazil, Int. J. Hydrogen Energy 33 (2008) 4915–4935.

[56] G. Thomas, Overview of Storage Development DOE Hydrogen Program, vol. 9, Sandia National Laboratories, 2000.
[57] J. Li, K.J. Smith, Methane decomposition and catalyst regeneration in a cyclic mode over supported Co and Ni catalysts, Appl. Catal. A: Gen. 349 (2008) 116–124.
[58] J. Xuan, M.K.H. Leung, D.Y.C. Leung, M. Ni, A review of biomass-derived fuel processors for fuel cell systems, Renew. Sustain. Energy Rev. 13 (2009) 1301–1313.
[59] A. Faghri, Z. Guo, Challenges and opportunities of thermal management issues related to fuel cell technology and modeling, Int. J. Heat Mass Transfer 48 (2005) 3891–3920.
[60] Z. Chen, J.R. Grace, C. Jim Lim, A. Li, Experimental studies of pure hydrogen production in a commercialized fluidized-bed membrane reactor with SMR and ATR catalysts, Int. J. Hydrogen Energy 32 (2007) 2359–2366.
[61] L. Bromberg, D.R. Cohn, A. Rabinovich, N. Alexeev, Plasma catalytic reforming of methane, Int. J. Hydrogen Energy 24 (1999) 1131–1137.
[62] A. Gutsol, A. Rabinovich, A. Fridman, Combustion-assisted plasma in fuel conversion, J. Phys. D Appl. Phys. 44 (2011) 274001.
[63] J.M. Cormier, I. Rusu, Syngas production via methane steam reforming with oxygen: plasma reactors versus chemical reactors, J. Phys. D Appl. Phys. 34 (2001) 2798.
[64] D.J. Moon, J.W. Ryu, Electrocatalytic reforming of carbon dioxide by methane in SOFC system, Catal. Today 87 (2003) 255–264.
[65] A. Boyano, A. Blanco-Marigorta, T. Morosuk, G. Tsatsaronis, Exergoenvironmental analysis of a steam methane reforming process for hydrogen production, Energy 36 (2011) 2202–2214.
[66] A. Iulianelli, P. Ribeirinha, A. Mendes, A. Basile, Methanol steam reforming for hydrogen generation via conventional and membrane reactors: a review, Renew. Sustain. Energy Rev. 29 (2014) 355–368.
[67] S.C. Dantas, J.C. Escritori, R.R. Soares, C.E. Hori, Effect of different promoters on $Ni/CeZrO_2$ catalyst for autothermal reforming and partial oxidation of methane, Chem. Eng. J. 156 (2010) 380–387.
[68] H.J. Alves, C. Bley Junior, R.R. Niklevicz, E.P. Frigo, M.S. Frigo, C.H. Coimbra-Araújo, Overview of hydrogen production technologies from biogas and the applications in fuel cells, Int. J. Hydrogen Energy 38 (2013) 5215–5225.
[69] M.L. Faro, A. Vita, L. Pino, A.S. Aricò, Performance evaluation of a solid oxide fuel cell coupled to an external biogas tri-reforming process, Fuel Process. Technol. 115 (2013) 238–245.
[70] B. Tjaden, M. Gandiglio, A. Lanzini, M. Santarelli, M. Järvinen, Small-scale biogas-SOFC plant: technical analysis and assessment of different fuel reforming options, Energy Fuels 28 (2014) 4216–4232.
[71] X. Zhu, H. Wang, Y. Wei, K. Li, X. Cheng, Hydrogen and syngas production from two-step steam reforming of methane using CeO_2 as oxygen carrier, J. Nat. Gas Chem. 20 (2011) 281–286.
[72] X. Zhai, S. Ding, Z. Liu, Y. Jin, Y. Cheng, Catalytic performance of Ni catalysts for steam reforming of methane at high space velocity, Int. J. Hydrogen Energy 36 (2011) 482–489.
[73] P. Kolbitsch, C. Pfeifer, H. Hofbauer, Catalytic steam reforming of model biogas, Fuel 87 (2008) 701–706.

[74] S. Jafarian, A. Tavasoli, A. Karimi, O. Norouzi, Steam reforming of bagasse to hydrogen and synthesis gas using ruthenium promoted NiFe/γAl_2O_3 nano-catalysts, Int. J. Hydrogen Energy 42 (2017) 5505–5512.
[75] J. Nishikawa, K. Nakamura, M. Asadullah, T. Miyazawa, K. Kunimori, K. Tomishige, Catalytic performance of Ni/CeO_2/Al_2O_3 modified with noble metals in steam gasification of biomass, Catal. Today 131 (2008) 146–155.
[76] V. Liso, A.C. Olesen, M.P. Nielsen, S.K. Kær, Performance comparison between partial oxidation and methane steam reforming processes for solid oxide fuel cell (SOFC) micro combined heat and power (CHP) system, Energy 36 (2011) 4216–4226.
[77] M. Simeone, L. Salemme, C. Allouis, Reactor temperature profile during autothermal methane reforming on Rh/Al_2O_3 catalyst by IR imaging, Int. J. Hydrogen Energy 33 (2008) 4798–4808.
[78] S.T. Oyama, P. Hacarlioglu, Y. Gu, D. Lee, Dry reforming of methane has no future for hydrogen production: comparison with steam reforming at high pressure in standard and membrane reactors, Int. J. Hydrogen Energy 37 (2012) 10444–10450.
[79] O. Bereketidou, M. Goula, Biogas reforming for syngas production over nickel supported on ceria–alumina catalysts, Catal. Today 195 (2012) 93–100.
[80] S. Douvartzides, F. Coutelieris, P. Tsiakaras, Exergy analysis of a solid oxide fuel cell power plant fed by either ethanol or methane, J. Power Sources 131 (2004) 224–230.
[81] M. Saidi, Performance assessment and evaluation of catalytic membrane reactor for pure hydrogen production via steam reforming of methanol, Int. J. Hydrogen Energy 42 (2017) 16170–16185.
[82] M. Saidi, A. Jahangiri, Theoretical study of hydrogen production by ethanol steam reforming: Technical evaluation and performance analysis of catalytic membrane reactor, Int. J. Hydrogen Energy 43 (2018) 15306–15320.
[83] T. Foyle, L. Jennings, P. Mulcahy, Compositional analysis of lignocellulosic materials: evaluation of methods used for sugar analysis of waste paper and straw, Bioresour. Technol. 98 (2007) 3026–3036.
[84] R. Lal, Crop residues as soil amendments and feedstock for bioethanol production, Waste Manage. 28 (2008) 747–758.
[85] P. Tsiakaras, A. Demin, Thermodynamic analysis of a solid oxide fuel cell system fuelled by ethanol, J. Power Sources 102 (2001) 210–217.
[86] W.A. McPhee, M. Boucher, J. Stuart, R.S. Parnas, M. Koslowske, T. Tao, et al., Demonstration of a liquid-tin anode solid-oxide fuel cell (LTA-SOFC) operating from biodiesel fuel, Energy Fuels 23 (2009) 5036–5041.
[87] S. Adhikari, S.D. Fernando, A. Haryanto, Hydrogen production from glycerin by steam reforming over nickel catalysts, Renew. Energy 33 (2008) 1097–1100.
[88] B. Zhang, X. Tang, Y. Li, Y. Xu, W. Shen, Hydrogen production from steam reforming of ethanol and glycerol over ceria-supported metal catalysts, Int. J. Hydrogen Energy 32 (2007) 2367–2373.
[89] S. Ramesh, N. Venkatesha, Template free synthesis of Ni-perovskite: an efficient catalyst for hydrogen production by steam reforming of bioglycerol, ACS Sustain. Chem. Eng. 5 (2017) 1339–1346.
[90] C.S. Lau, A. Tsolakis, M.L. Wyszynski, Biogas upgrade to syn-gas (H_2–CO) via dry and oxidative reforming, Int. J. Hydrogen Energy 36 (2011) 397–404.

[91] S. Rasi, Biogas Composition and Upgrading to Biomethane, University of Jyväskylä, 2009.
[92] S. Swami Nathan, J.M. Mallikarjuna, A. Ramesh, An experimental study of the biogas–diesel HCCI mode of engine operation, Energy Convers. Manage. 51 (2010) 1347–1353.
[93] E.C. Vagia, A.A. Lemonidou, Hydrogen production via steam reforming of bio-oil components over calcium aluminate supported nickel and noble metal catalysts, Appl. Catal. A: Gen. 351 (2008) 111–121.
[94] B. Drosg, R. Braun, G. Bochmann, T. Al Saedi, 3 - Analysis and characterisation of biogas feedstocks, in: A. Wellinger, J. Murphy, D. Baxter (Eds.), The Biogas Handbook, Woodhead Publishing, 2013, pp. 52–84.
[95] D.D. Papadias, S. Ahmed, R. Kumar, Fuel quality issues with biogas energy–An economic analysis for a stationary fuel cell system, Energy 44 (2012) 257–277.
[96] N. De Arespacochaga, C. Valderrama, C. Mesa, L. Bouchy, J. Cortina, Biogas deep clean-up based on adsorption technologies for solid oxide fuel cell applications, Chem. Eng. J. 255 (2014) 593–603.
[97] D. Papurello, A. Lanzini, S. Fiorilli, F. Smeacetto, R. Singh, M. Santarelli, Sulfur poisoning in Ni-anode solid oxide fuel cells (SOFCs): deactivation in single cells and a stack, Chem. Eng. J. 283 (2016) 1224–1233.
[98] C.J. Laycock, J.Z. Staniforth, R.M. Ormerod, Biogas as a fuel for solid oxide fuel cells and synthesis gas production: effects of ceria-doping and hydrogen sulfide on the performance of nickel-based anode materials, Dalton Trans. 40 (2011) 5494–5504.
[99] R. Dewil, L. Appels, J. Baeyens, Energy use of biogas hampered by the presence of siloxanes, Energy Convers. Manage. 47 (2006) 1711–1722.
[100] T. Matsui, S. Imamura, Removal of siloxane from digestion gas of sewage sludge, Bioresour. Technol. 101 (2010) S29–S32.
[101] K. Haga, S. Adachi, Y. Shiratori, K. Itoh, K. Sasaki, Poisoning of SOFC anodes by various fuel impurities, Solid State Ionics 179 (2008) 1427–1431.
[102] K. Sasaki, K. Haga, T. Yoshizumi, D. Minematsu, E. Yuki, R. Liu, et al., Chemical durability of solid oxide fuel cells: influence of impurities on long-term performance, J. Power Sources 196 (2011) 9130–9140.
[103] G. Krishnan, P. Jayaweera, J. Bao, J. Perez, K. Lau, M. Hornbostel, et al., Effect of Coal Contaminants on Solid Oxide Fuel System Performance and Service Life, Sri International, 2008.
[104] S. Veyo, Evaluation of fuel impurity effects on solid oxide fuel cell performance, Final Report, US Dept. of Energy, 1998, 2.1–2.9.
[105] M. Fortuny, J.A. Baeza, X. Gamisans, C. Casas, J. Lafuente, M.A. Deshusses, et al., Biological sweetening of energy gases mimics in biotrickling filters, Chemosphere 71 (2008) 10–17.
[106] A.B. Baspinar, M. Turker, A. Hocalar, I. Ozturk, Biogas desulphurization at technical scale by lithotrophic denitrification: Integration of sulphide and nitrogen removal, Process Biochem. 46 (2011) 916–922.
[107] M. Ajhar, M. Travesset, S. Yüce, T. Melin, Siloxane removal from landfill and digester gas – a technology overview, Bioresour. Technol. 101 (2010) 2913–2923.
[108] N. Abatzoglou, S. Boivin, A review of biogas purification processes, Biofuels Bioprod. Biorefining 3 (2009) 42–71.

[109] M. Arnold, Reduction and monitoring of biogas trace compounds, VTT Tiedotteita−Res. Notes 2496 (2009) 27.
[110] D.-Y. Choi, J.-W. Lee, S.-C. Jang, B.-S. Ahn, D.-K. Choi, Adsorption dynamics of hydrogen sulfide in impregnated activated carbon bed, Adsorption 14 (2008) 533−538.
[111] R. Yan, T. Chin, Y.L. Ng, H. Duan, D.T. Liang, J.H. Tay, Influence of surface properties on the mechanism of H_2S removal by alkaline activated carbons, Environ. Sci. Technol. 38 (2004) 316−323.
[112] P. Cherosky, Y. Li, Hydrogen sulfide removal from biogas by bio-based iron sponge, Biosyst. Eng. 114 (2013) 55−59.
[113] R. Yan, D.T. Liang, L. Tsen, J.H. Tay, Kinetics and mechanisms of H_2S adsorption by alkaline activated carbon, Environ. Sci. Technol. 36 (2002) 4460−4466.
[114] M. Arnold, T. Kajolinna, Development of on-line measurement techniques for siloxanes and other trace compounds in biogas, Waste Manage. 30 (2010) 1011−1017.
[115] M.R. Rahimpour, S.M. Jokar, Feasibility of flare gas reformation to practical energy in Farashband gas refinery: no gas flaring, J. Hazard. Mater. 209−210 (2012) 204−217.
[116] P. Promoppatum, V. Viswanathan, Identifying material and device targets for a flare gas recovery system utilizing electrochemical conversion of methane to methanol, ACS Sustain. Chem. Eng. 4 (2016) 1736−1745.
[117] M.R. Rahimpour, Z. Jamshidnejad, S.M. Jokar, G. Karimi, A. Ghorbani, A.H. Mohammadi, A comparative study of three different methods for flare gas recovery of Asalooye gas refinery, J. Nat. Gas Sci. Eng. 4 (2012) 17−28.
[118] E.A. Liese, R.S. Gemmen, Performance comparison of internal reforming against external reforming in a SOFC, gas turbine hybrid system, ASME Turbo Expo 2003, collocated with the 2003 International Joint Power Generation Conference, American Society of Mechanical Engineers, 2003, pp. 305−310.
[119] A. Chitsaz, M. Sadeghi, M. Sadeghi, E. Ghanbarloo, Exergoenvironmental comparison of internal reforming against external reforming in a cogeneration system based on solid oxide fuel cell using an evolutionary algorithm, Energy 144 (2018) 420−431.
[120] A. Lanzini, P. Leone, Experimental investigation of direct internal reforming of biogas in solid oxide fuel cells, Int. J. Hydrogen Energy 35 (2010) 2463−2476.
[121] M. Benito, S. García, P. Ferreira-Aparicio, L.G. Serrano, L. Daza, Development of biogas reforming Ni−La−Al catalysts for fuel cells, J. Power Sources 169 (2007) 177−183.
[122] Y. Shiratori, T. Oshima, K. Sasaki, Feasibility of direct-biogas SOFC, Int. J. Hydrogen Energy 33 (2008) 6316−6321.
[123] Y. Shiratori, T. Ijichi, T. Oshima, K. Sasaki, Internal reforming SOFC running on biogas, Int. J. Hydrogen Energy 35 (2010) 7905−7912.
[124] A.O. Omosun, A. Bauen, N.P. Brandon, C.S. Adjiman, D. Hart, Modelling system efficiencies and costs of two biomass-fuelled SOFC systems, J. Power Sources 131 (2004) 96−106.
[125] I. Wheeldon, C. Caners, K. Karan, B. Peppley, Utilization of biogas generated from Ontario wastewater treatment plants in solid oxide fuel cell systems: a process modeling study, Int. J. Green Energy 4 (2007) 221−231.

[126] A. Effendi, K. Hellgardt, Z.G. Zhang, T. Yoshida, Optimising H_2 production from model biogas via combined steam reforming and CO shift reactions, Fuel 84 (2005) 869–874.
[127] C. Guerra, A. Lanzini, P. Leone, M. Santarelli, N.P. Brandon, Optimization of dry reforming of methane over Ni/YSZ anodes for solid oxide fuel cells, J. Power Sources 245 (2014) 154–163.
[128] Y. Takahashi, Y. Shiratori, S. Furuta, K. Sasaki, Thermo-mechanical reliability and catalytic activity of Ni–zirconia anode supports in internal reforming SOFC running on biogas, Solid State Ionics 225 (2012) 113–117.
[129] S. Farhad, Y. Yoo, F. Hamdullahpur, Effects of fuel processing methods on industrial scale biogas-fuelled solid oxide fuel cell system for operating in wastewater treatment plants, J. Power Sources 195 (2010) 1446–1453.
[130] R. Cozzolino, L. Lombardi, L. Tribioli, Use of biogas from biowaste in a solid oxide fuel cell stack: application to an off-grid power plant, Renew. Energy 111 (2017) 781–791.
[131] I.V. Yentekakis, G. Goula, Biogas management: advanced utilization for production of renewable energy and added-value chemicals, Front. Environ. Sci. 5 (2017) 7.
[132] J.B. Holm-Nielsen, T. Al Seadi, P. Oleskowicz-Popiel, The future of anaerobic digestion and biogas utilization, Bioresour. Technol. 100 (2009) 5478–5484.
[133] W.M. Budzianowski, Sustainable biogas energy in Poland: prospects and challenges, Renew. Sustain. Energy Rev. 16 (2012) 342–349.
[134] B. Wu, X. Zhang, D. Shang, D. Bao, S. Zhang, T. Zheng, Energetic-environmental-economic assessment of the biogas system with three utilization pathways: combined heat and power, biomethane and fuel cell, Bioresour. Technol. 214 (2016) 722–728.
[135] J. Daniel-Gromke, N. Rensberg, V. Denysenko, W. Stinner, T. Schmalfuß, M. Scheftelowitz, et al., Current developments in production and utilization of biogas and biomethane in Germany, Chemie Ingenieur Technik 90 (2018) 17–35.
[136] M. Lantz, The economic performance of combined heat and power from biogas produced from manure in Sweden – a comparison of different CHP technologies, Appl. Energy 98 (2012) 502–511.
[137] R. Kadam, N.L. Panwar, Recent advancement in biogas enrichment and its applications, Renew. Sustain. Energy Rev. 73 (2017) 892–903.
[138] Q. Sun, H. Li, J. Yan, L. Liu, Z. Yu, X. Yu, Selection of appropriate biogas upgrading technology-a review of biogas cleaning, upgrading and utilisation, Renew. Sustain. Energy Rev. 51 (2015) 521–532.
[139] A. Toledo-Cervantes, J.M. Estrada, R. Lebrero, R. Muñoz, A comparative analysis of biogas upgrading technologies: photosynthetic vs physical/chemical processes, Algal Res. 25 (2017) 237–243.
[140] M. Pöschl, S. Ward, P. Owende, Evaluation of energy efficiency of various biogas production and utilization pathways, Appl. Energy 87 (2010) 3305–3321.
[141] D. Barik, S. Murugan, Investigation on combustion performance and emission characteristics of a DI (direct injection) diesel engine fueled with biogas–diesel in dual fuel mode, Energy 72 (2014) 760–771.
[142] G. Li, C. Zhang, Y. Li, Effects of diesel injection parameters on the rapid combustion and emissions of an HD common-rail diesel engine fueled with diesel–methanol dual-fuel, Appl. Therm. Eng. 108 (2016) 1214–1225.

[143] M. Renzi, C. Brandoni, Study and application of a regenerative Stirling cogeneration device based on biomass combustion, Appl. Therm. Eng. 67 (2014) 341–351.
[144] H. Nikpey Somehsaraei, M. Mansouri Majoumerd, P. Breuhaus, M. Assadi, Performance analysis of a biogas-fueled micro gas turbine using a validated thermodynamic model, Appl. Therm. Eng. 66 (2014) 181–190.
[145] S.E. Hosseini, M.A. Wahid, Biogas utilization: experimental investigation on biogas flameless combustion in lab-scale furnace, Energy Convers. Manage. 74 (2013) 426–432.
[146] F. Di Maria, C. Micale, A. Sordi, Electrical energy production from the integrated aerobic-anaerobic treatment of organic waste by ORC, Renew. Energy 66 (2014) 461–467.
[147] O. Dumont, R. Dickes, M. De Rosa, R. Douglas, V. Lemort, Technical and economic optimization of subcritical, wet expansion and transcritical Organic Rankine Cycle (ORC) systems coupled with a biogas power plant, Energy Convers. Manage. 157 (2018) 294–306.
[148] A. Bryszewska-Mazurek, T. Świeboda, W. Mazurek, Performance analysis of a solar-powered organic rankine cycle engine, J. Air Waste Manage Assoc. 61 (2011) 3–6.
[149] R. Schmersahl, J. Mumme, V. Scholz, Farm-based biogas production, processing, and use in polymer electrolyte membrane (PEM) fuel cells, Ind. Eng. Chem. Res. 46 (2007) 8946–8950.
[150] S. Authayanun, P. Aunsup, Y. Patcharavorachot, A. Arpornwichanop, Theoretical analysis of a biogas-fed PEMFC system with different hydrogen purifications: conventional and membrane-based water gas shift processes, Energy Convers. Manage. 86 (2014) 60–69.
[151] T. Birth, W. Heineken, L. He, Preliminary design of a small-scale system for the conversion of biogas to electricity by HT-PEM fuel cell, Biomass Bioenergy 65 (2014) 20–27.
[152] T. Guan, B. Chutichai, P. Alvfors, A. Arpornwichanop, Biomass-fuelled PEMFC systems: evaluation of two conversion paths relevant for different raw materials, Energy Convers. Manage. 106 (2015) 1183–1191.
[153] V. Cigolotti, E. Massi, A. Moreno, A. Polettini, F. Reale, Biofuels as opportunity for MCFC niche market application, Int. J. Hydrogen Energy 33 (2008) 2999–3003.
[154] S. Trogisch, J. Hoffmann, L.D. Bertrand, Operation of molten carbonate fuel cells with different biogas sources: a challenging approach for field trials, J. Power Sources 145 (2005) 632–638.
[155] J. Milewski, G. Discepoli, U. Desideri, Modeling the performance of MCFC for various fuel and oxidant compositions, Int. J. Hydrogen Energy 39 (2014) 11713–11721.
[156] S. Trogisch, Potential applications and synergies of biogas fuel cells as an efficient alternative energy conversion technology, in: IEA, Conference: Hydrogen and Fuel Cell Based Energy Systems, Vienna, Austria, 2004.
[157] T.A. Hamad, A.A. Agll, Y.M. Hamad, S. Bapat, M. Thomas, K.B. Martin, et al., Study of combined heat, hydrogen and power system based on a molten carbonate fuel cell fed by biogas produced by anaerobic digestion, Energy Convers. Manage. 81 (2014) 184–191.

[158] R. Chacartegui, B. Monje, D. Sánchez, J.A. Becerra, S. Campanari, Molten carbonate fuel cell: towards negative emissions in wastewater treatment CHP plants, Int. J. Greenhouse Gas Control 19 (2013) 453–461.
[159] T. Pham, K. Rabaey, P. Aelterman, P. Clauwaert, L. De Schamphelaire, N. Boon, et al., Microbial fuel cells in relation to conventional anaerobic digestion technology, Eng. Life Sci. 6 (2006) 285–292.
[160] Z. Ge, F. Zhang, J. Grimaud, J. Hurst, Z. He, Long-term investigation of microbial fuel cells treating primary sludge or digested sludge, Bioresour. Technol. 136 (2013) 509–514.
[161] J.M. Foley, R.A. Rozendal, C.K. Hertle, P.A. Lant, K. Rabaey, Life cycle assessment of high-rate anaerobic treatment, microbial fuel cells, and microbial electrolysis cells, Environ. Sci. Technol. 44 (2010) 3629–3637.
[162] Z. He, Microbial Fuel Cells: Now Let Us Talk About Energy, ACS Publications, 2012.
[163] M.C. Williams, J.P. Strakey, W.A. Surdoval, U.S. Department of Energy's solid oxide fuel cells: technical advances, Int. J. Appl. Ceram. Technol. 2 (2005) 295–300.
[164] S. Campanari, L. Mastropasqua, M. Gazzani, P. Chiesa, M.C. Romano, Predicting the ultimate potential of natural gas SOFC power cycles with CO_2 capture – Part A: methodology and reference cases, J. Power Sources 324 (2016) 598–614.
[165] S. Campanari, L. Mastropasqua, M. Gazzani, P. Chiesa, M.C. Romano, Predicting the ultimate potential of natural gas SOFC power cycles with CO_2 capture – Part B: applications, J. Power Sources 325 (2016) 194–208.
[166] R.K. Akikur, R. Saidur, H.W. Ping, K.R. Ullah, Performance analysis of a cogeneration system using solar energy and SOFC technology, Energy Convers. Manage. 79 (2014) 415–430.
[167] M. Liu, A. Lanzini, W. Halliop, V.R.M. Cobas, A.H.M. Verkooijen, P.V. Aravind, Anode recirculation behavior of a solid oxide fuel cell system: a safety analysis and a performance optimization, Int. J. Hydrogen Energy 38 (2013) 2868–2883.
[168] D. Saebea, S. Authayanun, Y. Patcharavorachot, A. Arpornwichanop, Effect of anode–cathode exhaust gas recirculation on energy recuperation in a solid oxide fuel cell-gas turbine hybrid power system, Energy 94 (2016) 218–232.
[169] A. Chitsaz, J. Hosseinpour, M. Assadi, Effect of recycling on the thermodynamic and thermoeconomic performances of SOFC based on trigeneration systems: a comparative study, Energy 124 (2017) 613–624.
[170] S. Wahl, A.G. Segarra, P. Horstmann, M. Carré, W.G. Bessler, F. Lapicque, et al., Modeling of a thermally integrated 10 kWe planar solid oxide fuel cell system with anode offgas recycling and internal reforming by discretization in flow direction, J. Power Sources 279 (2015) 656–666.
[171] R. Torii, Y. Tachikawa, K. Sasaki, K. Ito, Anode gas recirculation for improving the performance and cost of a 5-kW solid oxide fuel cell system, J. Power Sources 325 (2016) 229–237.
[172] M. Santarelli, L. Briesemeister, M. Gandiglio, S. Herrmann, P. Kuczynski, J. Kupecki, et al., Carbon recovery and re-utilization (CRR) from the exhaust of a solid oxide fuel cell (SOFC): analysis through a proof-of-concept, J. CO_2 Utiliz. 18 (2017) 206–221.

[173] M.L. Ferrari, A. Traverso, L. Magistri, A.F. Massardo, Influence of the anodic recirculation transient behaviour on the SOFC hybrid system performance, J. Power Sources 149 (2005) 22–32.
[174] J. Jia, Q. Li, M. Luo, L. Wei, A. Abudula, Effects of gas recycle on performance of solid oxide fuel cell power systems, Energy 36 (2011) 1068–1075.
[175] D. Saebea, Y. Patcharavorachot, A. Arpornwichanop, Analysis of an ethanol-fuelled solid oxide fuel cell system using partial anode exhaust gas recirculation, J. Power Sources 208 (2012) 120–130.
[176] A. Mehr, S. Mahmoudi, M. Yari, A. Chitsaz, Thermodynamic and exergoeconomic analysis of biogas fed solid oxide fuel cell power plants emphasizing on anode and cathode recycling: a comparative study, Energy Convers. Manage. 105 (2015) 596–606.
[177] L. Zhang, Y. Xing, H. Xu, H. Wang, J. Zhong, J. Xuan, Comparative study of solid oxide fuel cell combined heat and power system with multi-stage exhaust chemical energy recycling: modeling, experiment and optimization, Energy Convers. Manage. 139 (2017) 79–88.
[178] E. Facchinetti, D. Favrat, F. Maréchal, Design and optimization of an innovative solid oxide fuel cell–gas turbine hybrid cycle for small scale distributed generation, Fuel Cells 14 (2014) 595–606.
[179] S. Wongchanapai, H. Iwai, M. Saito, H. Yoshida, Performance evaluation of a direct-biogas solid oxide fuel cell-micro gas turbine (SOFC-MGT) hybrid combined heat and power (CHP) system, J. Power Sources 223 (2013) 9–17.
[180] M. Rokni, Municipal solid waste gasification with solid oxide fuel cells and stirling engine, in: Proceedings of the International Conference on Clean Energy, 2014, pp. 2431–2445.
[181] Y. Kobayashi, Y. Ando, H. Kishizawa, K. Tomida, N. Matake, Recent progress of SOFC-GT combined system with tubular type cell stack at MHI, ECS Trans. 51 (2013) 79–86.
[182] M. Ebrahimi, I. Moradpoor, Combined solid oxide fuel cell, micro-gas turbine and organic Rankine cycle for power generation (SOFC–MGT–ORC), Energy Convers. Manage. 116 (2016) 120–133.
[183] M. Meratizaman, S. Monadizadeh, M. Amidpour, Introduction of an efficient small-scale freshwater-power generation cycle (SOFC–GT–MED), simulation, parametric study and economic assessment, Desalination 351 (2014) 43–58.
[184] A. Buonomano, F. Calise, M.D. d'Accadia, A. Palombo, M. Vicidomini, Hybrid solid oxide fuel cells–gas turbine systems for combined heat and power: a review, Appl. Energy 156 (2015) 32–85.
[185] L. Pierobon, M. Rokni, U. Larsen, F. Haglind, Thermodynamic analysis of an integrated gasification solid oxide fuel cell plant combined with an organic Rankine cycle, Renew. Energy 60 (2013) 226–234.
[186] H. Tuo, Energy and exergy-based working fluid selection for organic Rankine cycle recovering waste heat from high temperature solid oxide fuel cell and gas turbine hybrid systems, Int. J. Energy Res. 37 (2013) 1831–1841.
[187] F.A. Al-Sulaiman, I. Dincer, F. Hamdullahpur, Thermoeconomic optimization of three trigeneration systems using organic Rankine cycles: Part I – Formulations, Energy Convers. Manage. 69 (2013) 199–208.

[188] H. Ozcan, I. Dincer, Thermodynamic analysis of an integrated SOFC, solar ORC and absorption chiller for tri-generation applications, Fuel Cells 13 (2013) 781–793.
[189] B. Najafi, A. Shirazi, M. Aminyavari, F. Rinaldi, R.A. Taylor, Exergetic, economic and environmental analyses and multi-objective optimization of an SOFC-gas turbine hybrid cycle coupled with an MSF desalination system, Desalination 334 (2014) 46–59.
[190] A. Al-Qattan, A. ElSherbini, K. Al-Ajmi, Solid oxide fuel cell application in district cooling, J. Power Sources 257 (2014) 21–26.
[191] S. Sadeghi, M. Ameri, Exergy analysis of photovoltaic panels-coupled solid oxide fuel cell and gas turbine-electrolyzer hybrid system, J. Energy Resour. Technol. 136 (2014) 031201.
[192] J. Sanz-Bermejo, J. Muñoz-Antón, J. Gonzalez-Aguilar, M. Romero, Optimal integration of a solid-oxide electrolyser cell into a direct steam generation solar tower plant for zero-emission hydrogen production, Appl. Energy 131 (2014) 238–247.
[193] R. Toonssen, S. Sollai, P.V. Aravind, N. Woudstra, A.H.M. Verkooijen, Alternative system designs of biomass gasification SOFC/GT hybrid systems, Int. J. Hydrogen Energy 36 (2011) 10414–10425.
[194] A. Di Carlo, D. Borello, E. Bocci, Process simulation of a hybrid SOFC/mGT and enriched air/steam fluidized bed gasifier power plant, Int. J. Hydrogen Energy 38 (2013) 5857–5874.
[195] A. Surjosatyo, F. Vidian, Y.S. Nugroho, A review on gasifier modification for tar reduction in biomass gasification, Jurnal Mekanikal 31 (2010).
[196] M. Gandiglio, A. Lanzini, M. Santarelli, P. Leone, Design and balance-of-plant of a demonstration plant with a solid oxide fuel cell fed by biogas from waste-water and exhaust carbon recycling for algae growth, J. Fuel Cell Sci. Technol. 11 (2014) 031003.
[197] E. Santoyo-Castelazo, L. Stamford, A. Azapagic, Environmental implications of decarbonising electricity supply in large economies: the case of Mexico, Energy Convers. Manage. 85 (2014) 272–291.
[198] I. Staffell, A. Ingram, K. Kendall, Energy and carbon payback times for solid oxide fuel cell based domestic CHP, Int. J. Hydrogen Energy 37 (2012) 2509–2523.
[199] Varun, I.K. Bhat, R. Prakash, LCA of renewable energy for electricity generation systems—a review, Renew. Sustain. Energy Rev. 13 (2009) 1067–1073.
[200] J. Lin, C.W. Babbitt, T.A. Trabold, Life cycle assessment integrated with thermodynamic analysis of bio-fuel options for solid oxide fuel cells, Bioresour. Technol. 128 (2013) 495–504.
[201] C. Strazza, A. Del Borghi, P. Costamagna, A. Traverso, M. Santin, Comparative LCA of methanol-fuelled SOFCs as auxiliary power systems on-board ships, Appl. Energy 87 (2010) 1670–1678.
[202] S. Evangelisti, P. Lettieri, R. Clift, D. Borello, Distributed generation by energy from waste technology: a life cycle perspective, Process Saf. Environ. Protect. 93 (2015) 161–172.
[203] C. Strazza, A. Del Borghi, P. Costamagna, M. Gallo, E. Brignole, P. Girdinio, Life Cycle assessment and life cycle costing of a SOFC system for distributed power generation, Energy Convers. Manage. 100 (2015) 64–77.

[204] E. Rillo, M. Gandiglio, A. Lanzini, S. Bobba, M. Santarelli, G. Blengini, Life cycle assessment (LCA) of biogas-fed solid oxide fuel cell (SOFC) plant, Energy 126 (2017) 585–602.

[205] P. Salimi, S. Javadian, O. Norouzi, H. Gharibi, Turning an environmental problem into an opportunity: potential use of biochar derived from a harmful marine biomass named Cladophora glomerata as anode electrode for Li-ion batteries, Environ. Sci. Pollut. Res. 24 (2017) 27974–27984.

[206] S.E.M. Pourhosseini, O. Norouzi, P. Salimi, H.R. Naderi, Synthesis of a novel interconnected 3D pore network algal biochar constituting iron nanoparticles derived from a harmful marine biomass as high-performance asymmetric supercapacitor electrodes, ACS Sustain. Chem. Eng. 6 (2018) 4746–4758.

CHAPTER

15 Design and operation of solid oxide fuel cell systems: challenges and future research directions

Mahdi Sharifzadeh[1,2], Wenqian Chen[3], Giorgio Triulzi[4,5], Mirko Hu[6], Tohid N. Borhani[7], Majid Saidi[8], Venkatesan Krishnan[9], Maryam Ghadrdan[10], Meysam Qadrdan[11], Yingru Zhao[12], Alireza Mohammadzadeh[2,13], Seyedeh Kiana Naghib Zadeh[2,13], Mohammad Hassan Saidi[2,13], Davood Rashtchian[14] and Nilay Shah[1]

[1]*Department of Chemical Engineering, Centre for Process Systems Engineering, Imperial College London, London, United Kingdom*

[2]*Sharif Energy Research Institute (SERI), Sharif University of Technology, Tehran, Iran*

[3]*Department of Chemical Engineering, Imperial College London, London, United Kingdom*

[4]*School of Management, Universidad de los Andes, Bogotá, Colombia*

[5]*Sociotechnical Systems Research Center, Massachusetts Institute of Technology, MA, United States*

[6]*IMT School for Advanced Studies, Lucca, Italy*

[7]*School of Water, Energy and Environment, Cranfield University, Bedford, Bedfordshire, United Kingdom*

[8]*School of Chemistry, College of Science, University of Tehran, Tehran, Iran*

[9]*School of Science, Engineering and Design, Teesside University, Middlesbrough, United Kingdom*

[10]*Research & Technology, Equinor ASA, Fornebu, Norway*

[11]*Cardiff University, United Kingdom*

[12]*College of Energy, Xiamen University, Xiamen, P.R. China*

[13]*Department of Mechanical Engineering, Sharif University of Technology, Tehran, Iran*

[14]*Department of Chemical & Petroleum Engineering, Sharif University of Technology, Tehran, Iran*

15.1 Introduction

The chapters of this book explored various aspects of solid oxide fuel cell (SOFC) technologies. Our discussions began by investigating the technological growth of SOFC systems among other fuel-cell technologies, followed by a thermodynamic analysis of SOFC-based systems, the mechanical engineering of SOFCs, material engineering for them, their process synthesis and integration,

Design and Operation of Solid Oxide Fuel Cells. DOI: https://doi.org/10.1016/B978-0-12-815253-9.00015-X

computer-aided engineering and optimization, as well as control engineering and the safe operation of SOFC systems. The second part of the book is more application-oriented and offers a divergent perspective with respect to the fuel variability of SOFC technologies, their capability in the utilization of renewable energies, energy storage through reversible SOFC systems, various mobile and stationary applications of SOFC systems, and their application for waste minimization. This concluding chapter integrates these discussions by providing a summary of these analyses and articulating suggestions for future research directions.

15.2 Challenges and future research directions in quantifying the technological improvement of solid oxide fuel cell technologies

Chapter 1, Technological change in fuel cell technologies, quantified the technological growth of SOFCs and other fuel-cell technologies. Our research methodology included collecting patent data about several technological subdomains of fuel-cell technologies, and transforming this information into valuable quantitative knowledge of their technical improvement rates. There are several research directions for further investigation:

- Our research relied on scientometrics tools. Even though the accuracy of the forecast is already high, it is very likely that finding new predictors and using different tools for patent network analysis could improve the prediction quality.
- Our present analysis relied on patent and nonpatent data. As fuel-cell technologies advance into the commercialization stage, it will be also possible to collect actual performance data that can be used to validate and improve the forecast rates.
- Besides empirical analysis, the first-principles analysis could be applied for the identification of technological barriers and physical constraint that limit the growth of a certain technology.
- Last, the combination of cost analyses and the identification of the life-cycle stage of these technologies should guide investment planning as well as research and development activities.

15.3 Challenges and future research directions in the thermodynamic analysis and energy engineering of solid oxide fuel cell-based systems

In Chapter 2, Thermodynamics and energy engineering, the underlying thermodynamic principles that affect SOFC-based systems were reviewed. Beginning with a preliminary introduction to the classic thermodynamic analysis applied

to heat engines, the differences between cyclic engines and fuel-cell engines were illustrated.

The inapplicability of the Carnot engine (for thermodynamic cycles) to fuel cells (not a cycle, but a steady-state process) was emphasized. Therefore the required approach followed was to first formulate the efficiency of conversion from chemical energy to electrical power for cyclic engines and then to fuel cells. In the classic way of defining efficiency, the First Law of thermodynamics was used, and this is applicable for fuel cells. In both cases, there is a maximum limit on the efficiency (i.e., the Carnot engine limit is $1-T_c/T_H$, whereas the fuel cell limit is $\Delta G/\Delta H$) and is shown to be the case when the process is reversible. Once the fuel cell or the cyclic engine is operated under irreversible conditions, the efficiency is primarily given by work done/heat supplied, which is a First Law representation.

For fuel cells the actual performance efficiency was, and to an extent continues to be defined by the First Law, but there is now increasing awareness toward a more effective and meaningful representation of energy usable for work; hence the term exergy and exergetic efficiency.

Many process flow diagrams and configurations were assessed in Chapter 2, Thermodynamics and energy engineering, whereby it was shown how exergy (which is a representation of the potential of a system to do work, due to its physical and chemical departure from an unchangeable environmental state) varies across the various processes in a hybrid gas turbine/steam turbine−SOFC stack power plant. The strategy for estimating the exergetic efficiency of a power plant, is to carry out exergy balance for each element of the power plant (e.g., SOFC stack, stack off-gas combustor, gas turbines, steam turbines, fuel/air compressors, and heat exchangers) observes the losses in exergy at each stage (termed exergy destruction) and eventually determine the cumulative exergy destruction for the whole process. Not only is the irreversibility and consequently the exergetic efficiency estimated for the full plant, but also the individual exergy destructions for each process unit is estimated. Not surprisingly, the maximum exergy destruction occurs at the SOFC stack in many of the examples. Therefore the exergy approach is useful in directing research efforts toward enhancing cell performance, which can include the electrode/electrolyte materials, electrode microstructure, and multifunctional electrocatalysts in the anode (to handle the complex fuel compositions in the feedstock), enumerated, as:

1. Advanced cathodes (materials) to lower cathodic overpotentials, for example, higher ionic conductivities, higher electronic conductivities.
2. Multifunctional anodes that can absorb a higher degree of internal fuel reformation. To facilitate this catalytic functionalities, which are more effective towards CO oxidation, and water−gas-shift reaction are of interest. Most Ni−anodes are sufficient for hydrogen oxidation reactions, but the multifunctionality of the anode electrocatalyst makes the SOFC stack very versatile and ensures heat balancing in the stack.

3. Advanced microstructures for both cathodes and anodes that enhance three-phase boundaries, thereby leading to lower polarization.
4. Thinner and dimensionally stable electrolytes in addition to combinations with higher ionic conduction leading to lower ohmic polarization. To achieve this there needs to be advanced manufacturing processes that offer precision in dimension, in addition to materials compatibility and dimensional stability.

Other major challenges relating to SOFCs, include:

5. Lowering the degradation of electrodes by effects such as chromium poisoning; stable and conductive interconnect coatings offer longer lifetimes.
6. Cost reductions are independent of thermodynamics/systems analysis, for example, metal-supported cells that offer significant lowering of materials cost, but still face manufacturing challenges.

15.4 Challenges and future research directions in the mechanical engineering of solid oxide fuel cell-based systems

SOFCs are highly efficient energy conversion technologies, benefiting from low-carbon intensity and flexibility to employ a variety of fuels. However, they often operate at temperatures as high as 800°C and suffer from a slow start-up. The latter problem as well as lower-produced voltage limit the application of SOFCs especially for mobile applications. Basically there are two main types of geometries for SOFCs, planar and tubular, which both have some pros and cons. For instance, planar SOFCs offer a higher-power density. On the other hand, tubular SOFCs benefit from a tighter sealing. It is desirable to benefit from the advantages of both geometries and to overcome their limitations. Several geometries combining planar and tubular geometries have been introduced by different research groups. The most important examples are integrated planar (IP) or segmented in series, cone-shaped, flat tube (FT), honeycomb, and microtubular (MT) SOFCs. The main achievement of these designs is the improvement of the power density. IP-SOFCs have a smaller number of interconnectors, but their integrity and sealing of the cell is a drawback. The interconnector in FT-SOFCs is a challenging part of its mechanical design. Interconnectors in this geometry not only connect cells electronically, but are also barriers between the fuel and oxidant. The start-up time of all macrosized SOFCs is about one or more hours; however, MT-SOFCs' startup time is as short as a few minutes. Such low-startup time should be attributed to their microsize and, consequently, high resistance to thermal shocks. For increasing the output voltage and power of the cell, the concept of an SOFC stack for collecting current from single cells was introduced. Our critical analysis suggests that although significant improvement is made through the introduction of various geometries and stack configurations, currently there is no such design that satisfies all the requirements.

The next step after choosing the geometry is the selection of the fabrication method. SOFCs contain different thin layers, supporting layers, and functional layers within their elements, namely the anode, cathode, and electrolyte. The microstructure of these layers and their thickness are the main design parameters affecting the performance and durability of the cell. The common methods of fabrication include screen printing, tape casting, and dip coating. The first two are usually used for fabrication of the functional layers. Other parts of the cell can be produced using different methods of fabrication. For MT-SOFCs, however, usually, the phase inversion is the method of choice. Extrusion is another method that is used for producing cells that have channels in their geometry (i.e., honeycomb and flat-tube geometries). Many fabrication methods employ a slurry mixture, whose exact composition and viscosity have a direct influence on the microstructure and properties of the layer. Fabricating a cell using these methods of fabrication is a time-consuming procedure, thus studying different methods that are fast enough to ensure the cell quality for mass production is a frontier in research.

Nevertheless, SOFCs, similar to other process equipment, face malfunctioning and failure scenarios, for example due to asymmetry and concentration of stress in some parts of the cell, propagation of defects, or irregular operating condition. Most of the defects are chemical and related to the microstructure of electrodes or electrolyte layers. The malfunctions that are studied in the third chapter included redox, delamination, and degradation. Redox is the reduction−oxidation of the anode which occurs in Ni-based anodes due to fuel depletion and, as a result, Ni is oxidized instead of the fuel. Delamination refers to a phenomenon in which gaps appear between the electrode and electrolyte layers, for which analyzing the electrochemical impedance of a cell is a diagnostic method. Finally, degradation refers to a wide range of malfunctions in SOFCs. Degradation means the change in the microstructure of a cell. It can occur due to the fuel shortage or impurities (especially sulfur) in the fuel. Some early-stage defects are reversible and repairable. However, if some failures occur, the damaged piece of the cell must be replaced.

Another prominent aspect of SOFCs is the thermal analysis which aims at predicting SOFC's performance under various operational conditions. Since various chemical and transport phenomena occur in SOFCs simultaneously, a comprehensive thermal analysis of SOFCs would require the consideration of various coupled physics. These include mass transfer, fluid flow, charge transport, electrochemical reactions, and species transport. The analyses should solve species-transport equations, momentum equations, electrical-field equations as well as heat-transfer equations in a coupled manner. The outputs of such analyses include temperature distribution, which should be used to calculate thermal stresses through structural analysis. Finding the maximum-principal stress provides designers a better understanding of the structural design of the system. Thermal-transient modeling of SOFCs is another important consideration, whose significance is due to the long time required by SOFCs to reach the desired operating

temperature during start-up and shut-down operations. Thermal modeling can provide a deep understanding of the time-constant of different process transitions as well as the dominant phenomena. Furthermore, cell configurations can reduce the temperature gradients in the SOFC stacks, which can consequently reduce the thermal stresses. Therefore the effect of the configuration on the SOFC's performance remains a research focus. Finally, thermal management is required to ensure safe-process operation and the maintenance planning for SOFC-based systems. Proper thermal management of the system becomes more prominent when the SOFC is needed to start-up instantly, especially for portable applications. This can be achieved by keeping the temperature as close as possible to the operating temperature while considering maintenance aspects. Integrating an SOFC with another thermal system such as heat pipes is another main research area.

15.5 Challenges and future research directions in engineering the materials for solid oxide fuel cells

The general direction for innovation in SOFC materials is to develop materials and fabrication techniques that can produce SOFCs for the efficient operation at reduced temperatures (i.e., $<800^{\circ}C$). Although the components of SOFC have different performance requirements, they must be physically and chemically compatible with their neighbors (e.g., the electrolyte and electrodes must have compatible thermal-expansion coefficients). The developments of new materials for these components will hence continue to be closely intertwined.

For electrolyte the pursuit of more ionic-conductive materials at reduced temperature will continue with promising candidates that are derived from ceria, bismuth oxide, pyrochlore, perovskite, apatite, and LAMOX [1–7]. The general issues to be overcome are electronic conductivity and stability. A good example is bismuth (III) oxide: despite its significantly higher conductivity than ceria and zirconia at reduced temperature, it has stability issues under low oxygen-partial pressure [8]. The intrinsic limitations of materials can be partly overcome by various engineering methods, such as reducing electrolyte thickness to lower its ohmic resistance, improving the homogeneity of the ceramic particles to produce electrolyte via various wet-chemistry routes, as well as making bi-layer composite electrolytes [9–11]. In particular, various wet-chemistry routes such as sol–gel and co-precipitation can produce ceramic particles with high homogeneity in particle size as well as high phase purity, which eventually contributes to the good performance of the electrolyte thin film. Therefore, future research efforts should focus on the optimization of these wet-chemistry routes for large scale production.

For cathodes the challenge is to overcome the low ionic conductivity of $La_{1-x}Sr_{x-}MnO_{3\pm\delta}$ ($x \leq 0.5$) at reduced temperatures. Novel materials such as ferro-cobalites, manganites and nikelates should be further optimized in terms of

electrical and ionic conductivities at reduced temperatures, while having thermal expansion coefficients and chemical properties that are compatible with the electrolytes [12–18]. For example, the lanthanum in LSM can be substituted with neodymium, samarium, or praseodymium to produce $Ln_{0.7}Sr_{0.3}MnO_3$, where Ln is the substituted component, for enhancing their ionic and electrical conductivities. In terms of fabrication the performance of cathode can be enhanced by improving the quality of the starting particles, which can be synthesized with wet-chemistry routes. Similar to the electrolytes, these wet-chemistry routes should be further investigated for optimization.

For anodes the suitable materials must have resistance to sulfur poisoning and carbon deposition in addition to high ionic and electrical conductivities, high activities for fuel oxidation, and thermal expansion coefficients that are compatible with the electrolyte and interconnect at reduced temperatures. The conventional Ni–YSZ can be modified to increase its resistance against carbon deposition and sulfur poisoning, whereas novel materials such as noble-metal-based materials and perovskites have been developed [19–22]. For instance, copper and cobalt can be impregnated into the matrix of samaria-doped ceria to improve its resistance to carbon deposition. Similar to electrolytes and cathodes, the fabrication of anodes can be improved by utilizing the wet-chemistry routes for making the starting particles.

The interconnect and sealant are important in the practical application of SOFC. The main requirements are stability, compatible thermal expansion coefficient with respect to electrodes, and the costs. Metallic alloys are used to make the interconnect for reduced-temperature operation in order to lower the manufacturing cost of SOFCs. In particular, various chromium-based alloys can be further optimized as they have high electrical conductivity, high oxidation resistance, and compatible thermal expansion coefficients with common electrode materials [23–25]. For compressive sealants, iron and chromium-based alloys are economical materials that can be further optimized [23]. For rigid sealants, glass–ceramics such as aluminosilicate are attractive in terms of cost and can be further optimized in the future [26–29].

15.6 Challenges and future research directions for computer–aided multiscale modeling and optimization of solid oxide fuel cell-based systems

The design and operation of SOFC-based systems involves decisions that are spread over a very diverse range of temporal and spatial scales, which were extensively discussed in Chapter 6, Synthesis, integration, and intensification of solid oxide fuel cell systems: process systems engineering perspective. This involves the design of SOFC materials at molecular and nanoscales to cell geometries of SOFC stacks, expanding further to the process synthesis, and integration

and energy network optimization. The design decisions for the cathode, anode, and electrolyte include compositions, grain size, and microstructures of their materials, the thickness of their functional and supporting layers, and the required manufacturing methods. These considerations profoundly influence the electrochemical performance of the cells as well as their thermal behavior and lifetime. Further optimization is possible through the arrangement of the cells and stacks as well as the flow distribution through the manifold. Nonetheless the operating conditions of an SOFC stack not only influences the electrochemical conversion efficiency, but significantly influences the operational optimality of the integrated turbomachines. The overall performance optimization should systematically consider such interactions. The range of downstream integration is highly diverse and includes various steam cycles, carbon capture and compression, and reverse operation in electrolysis mode (solid oxide electrolysis cells—SOECs). Moreover, it was discussed that the optimization objectives may include competing metrics such as environmental footprint, controllability, operational safety, as well as economic performance, requiring multiobjective optimization programming. Upon critical analysis of the research in the field the following research areas can be identified for further investigation:

1. Despite intensive research at various scales, there is little integration between them. Modeling and optimization of key performance indicators considering the multiscale nature of the problem remain a frontier in research.
2. The multifaceted nature of the design and operation of SOFC systems requires quantitative evaluation of various indicators and their multiobjective optimization.
3. Industrial-scale application of multiscale modeling and optimization of SOFC systems requires advanced solution algorithms for large-scale optimization problems.

15.7 Challenges and future research directions for the process synthesis, intensification, and integration of solid oxide fuel cell-based systems

Process synthesis refers to the design activities in which the configuration of the process flow diagram and the involved processing steps are decided. Considering the adaptability of SOFC technologies for integration with a variety of power-generation technologies, process integration and intensification of process equipment have great potential for energy saving and environmental protection. Chapter 6, Synthesis, integration, and intensification of solid oxide fuel cell systems: process systems engineering perspective, extensively discusses these topics.

Generally speaking, SOFC-based power generation technologies include a preprocessing section, electrochemical conversion section, and energy recovery and utilization section, which depends on the utilized fuel and required generation services. Nevertheless, a key feature of SOFC technologies is their high flexibility in

processing various feedstocks. Solid fuels can be gasified in order to produce a mixture of carbon oxides and hydrogen, called synthesis gas (syngas). The method of preprocessing for gaseous and liquid fuels is reforming, which can be conducted in a variety of configurations including external reforming, direct or gradual internal reforming, dry reforming, partial reforming, and auto-thermal reforming. The key design considerations are the energy intensity of the process, mitigation of carbon deposition, and handling contaminations. Heat integration is often applied to mitigate the temperature gradient which otherwise would result in cell material degradation. Moreover, recirculation of anode-exhaust gases can reduce the need for an external supply of steam and enhances fuel utilization. On the other hand, cathode-air recirculation is applied for thermal management and has energetic implications with respect to the blower-power requirements. A further integration opportunity is between SOFC stacks at different temperatures, which could be in parallel or series. Most of all, the exhaust gases from the fuel cell have high thermal and chemical energy contents which can be extracted for further power generation using combustion, expansion, heat recovery, and steam generation. Such combinatorial integration opportunities open up avenues to polygeneration of electricity power as well as heating and cooling services. Moreover, the unmixed nature of electrochemical reactions within SOFCs offers one of the most viable options for carbon capture.

Upon careful investigation of the research in the field, the following potent research directions are recommended:

1. Utilization of various fuels requires different considerations in terms of preprocessing and syngas cleaning. Design of flexible processes capable of processing multiple fuels remains a frontier in research.
2. The highly combinatorial, interactive, and multicriteria nature of the decisions involved in the design and operation of SOFC-based process systems requires systematic, decision-making algorithms. Advanced frameworks capable of establishing the trade-off between the competing design and operational objectives are highly desirable.
3. The design and operation of SOFC-based process systems are highly interactive. The high degree of applied process integration and intensification adds to the problem complexity. The implication is that if the process is poorly designed, the process operation may become very challenging. Therefore it is highly recommended that process design and operational decisions are made at the same level, known as integrated process design and control (IPDC).

15.8 Challenges and future research directions for the control of solid oxide fuel cells

Many decisions that affect the operation of the plant are made during the plant-design phase. To reach the maximum potential, it is necessary to study how the

design will affect later performance during operation. While a process design may lead to a robust control structure, for example, by adding additional load-shaping devices to compensate for the disturbances in the electrical-load demands, while another process design leads to active constraint control where there is no place for optimization. Although there have been some studies on integrating process control and design, there is no research on systematically integrating self-optimizing control concepts into the plant-design phase.

Control is dependent on the information from the system. Chapter 5, gives a review of many model and data-based models used to control SOFC systems. The level of modeling simplification depends on the control objective. The objective function is dependent on some key variables. The relation of those variables and the control inputs should be reflected accurately in the model. MIMO and SISO, linear and nonlinear models with different levels of simplification have been suggested in the literature. The choice of the right model depends on the control problem definition. In addition the variables in the fuel-cell system have different dynamics. The model should be able to show the right time constants for the transients.

Systematic control structure design is missing in many of the control studies in the literature (see the review in Chapter 8). Defining a clear control objective, dividing the stabilizing and economic control layers based on their time scale, selection of "self-optimizing" control variables and CV-MV pairings are some of the important decisions. Deciding on "what to control" has not been a part of most research studies. Systematic control variable selection, described in chapter 8, is based on offline optimization of steady-state simulation models and is easy to implement. An important potential research activity is to design a control structure for the SOFC system and its integration with other chemical processes based on a self-optimizing control strategy. Decentralized or multivariable control should be chosen based on controllability analysis.

Measuring or the estimation of key variables in n SOFC system is important for monitoring and control. Each of the measurements, or combination of them (which may be an estimate for another process variable), are potential control variables. An estimation problem should be formulated based on the application of the estimated variable, that is, whether it's going to be used for monitoring or in a closed-loop control. A static estimation method was presented in Chapter 8, Toward a systematic control design for solid oxide fuel cells, and offers the optimal estimator for a given application. Extension of these estimators to be applied in a dynamic setting is a potential research direction.

15.9 Challenges and future research directions for the safe design and operation of solid oxide fuel cell-based systems

While SOFC systems experience a wide range of fluctuations and uncertainties, their operation is subject to significant risks associated with thermal stresses,

carbon deposition, and catalyst poisoning, which could affect the system reversibly or irreversibly. Such faults result in performance degradation in a single component or through interactions with other parts. These failures may result in ohmic resistance and degradation of the electrode microstructure. Electrode delamination, anode reoxidation, oxide-layer growth, and rib detachment are the mechanisms that increase the ohmic resistance. By comparison, electrode microstructure sintering, cathode-microstructure poisoning, carbon deposition on the anode, anode sulfur-poisoning, and cathode boron-poisoning are responsible for the microstructure degradation faults. Chapter 8, Fault detection, loss prevention, hazard mitigation, and safe operation of solid oxide fuel cell systems, extensively discusses these phenomena. This chapter also discusses the health and safety concerns and argues that since different fuels exhibit different fire and explosion behaviors, fuel variability calls for more intense consideration of the safety aspects.

Upon careful analysis of the research in the field the following directions are recommended for further investigation:

1. While degradation of the SOFC process equipment has a significant impact on the economic performance and durability of this technology, many fault mechanisms do not exhibit a unique symptom. Development of noninvasive monitoring methods that enable real-time, condition-based, monitoring is at the research frontier.
2. However, it also poses a significant challenge toward process safety, as different fuels exhibit very different hazardous properties and very different failure mechanisms and, therefore, would require significantly different strategies for mitigating the associated risks.
3. Finally, and most importantly, the safe process operation strongly depends on its design. Therefore the safety aspect should be systematically applied in the design of SOFC processes.

15.10 Challenges and future research directions for the fuel variability in solid oxide fuel cell-based systems

The flexibility of SOFCs to accept a variety of fuels offers great potential for the diversification of their applications. In addition, it opens up avenues to the application of renewable resources and reducing environmental footprints. However, such great advantages come at the price of more convoluted process configurations and operating conditions, as well as the treatment of a more diverse range of contaminants. Chapter 9, Fuel variability and flexible operation of solid oxide fuel cell systems, discusses these complexities.

Syngas (a mixture of hydrogen, carbon oxides, and water) is perhaps the most-studied fuel for SOFCs. This observation should be attributed to the fact

that most reforming and gasification technologies produce a mixture with similar compositions. Biogas (a mixture of methane, CO_2 and small amounts of hydrogen sulfide) is a renewable fuel produced through anaerobic digestion or fermentation of biodegradable materials. It offers a promising option as an SOFC fuel, because not only it is produced from renewable resources, but also its similarity with natural gas and syngas components makes it highly compatible with existing SOFC technologies. Biomass is another synergistic renewable fuel that requires gasification and gas treatment. Considering its low hydrogen-to-carbon content, coal is less desirable for utilization in SOFCs. However, the abundance of its resources suggests that retrofitting its existing infrastructure with highly efficient SOFC technologies, could contribute to the decarbonization of the coal industry. The motivation for the application of light alcohols such as methanol, ethanol, dimethyl ether, and butanol as the SOFC fuel is the possibility for external reforming at lower temperatures, resulting in the better utilization of waste heat an integrated process. In addition, some of the light alcohols such as methanol and ethanol can be produced from renewable resources offering an alternative path to renewable-power generation. Generally speaking, liquid fuels are of great interest to be utilized in SOFCs due to their high volumetric-energy density and ease of storage, offering new opportunities for mobile and remote applications. An alternative fuel for SOFCs is ammonia which dissociates into N_2 and H_2 with the added advantage of being a carbon-free operation. On the other hand, urea can be converted to ammonia and carbon dioxide through thermohydrolysis. Utilization of urea in SOFCs bypasses the safety concerns associated with the application of ammonia and hydrogen. In addition, it can be produced from wastewater treatment or carbon-capture technologies offering a pathway for environment protection. Nonetheless, the commercial application of these fuels requires removal of contaminants which, otherwise, could result in poisoning and degradation of the SOFC materials. The main contaminant of biogas is H_2S. For utilizing biomass, HCl, H_2S, and alkali materials should be removed from the gasification products. The existence of phosphine in coal-based syngas promotes degradation too, and should be removed.

Upon careful investigation of the research in the field, the following potent research areas were identified:

1. Contamination is the key challenge against flexible fuel operation in SOFC systems. The impact of various fuels on the lifetime of SOFC materials, and developing flexible fuel processing schemes to prevent adverse effects remain a frontier in research.
2. Fuel transition may require significant changes in the operating conditions. Nevertheless, the design and operation of industrial processes are highly interactive, and design and operational decisions should be considered at the same level. Therefore the methodology of IPDC is the enabler for fuel variability [30,31].
3. An additional benefit of the treatment of contamination is environment protection, which should be considered at the same level.

15.11 Challenges and future research directions for the application of renewable energies in solid oxide fuel cells

Chapter 11, Energy storage, provided an overview of the characteristics of main renewable sources for electrical-power generation. First, three forms of renewable sources for electric power generation (wind, solar and tidal) are reviewed to show their intermittent characteristics. Second, the challenge resulting from high penetration of variable renewable-power generation was discussed. Flexibility in the power grid is thus required for balancing the electricity supply and demand. Third, the integration of SOFCs with renewable power-generation technologies is investigated to show how SOFCs could support the transition to a low-carbon power system. SOFCs have the potential to contribute to achieving a low-carbon power system. This contribution is mainly implemented via two ways. The first is to generate electricity using renewable gases such as hydrogen or biogas. The second is to provide flexibility to the power grid such as providing ancillary services. This flexibility is able to facilitate the large-scale integration of renewable power-generation technologies in power systems. SOFCs can also play a role as backup generation for local-energy systems.

It has been pointed out that the synergies among different energy vectors through coupling components is a potent research area. The following aspects should be investigated further:

- Spatial−temporal modeling tools are required to analyze the interactions and interdependencies among different energy systems and to study the impact of cascading failures affecting the reliability of energy supply.
- Assessment methodologies and evaluation criteria are required to quantify the techno-economic performance of energy-system integration.

15.12 Challenges and future research directions for the application of reversible solid oxide cells for energy storage

Chapter 11, Energy storage, discusses the application of SOFCs for energy storage. Upon careful evaluation of research in the field the following research directions are identified:

- One of the methods for chemical-based energy storage that has attracted considerable attention is using reversible solid oxide cells (ReSOCs).
- ReSOC systems can be used in two different modes. A SOFC in which electricity is generated through the electrochemical reactions of a fuel with the oxygen in air, and a solid oxide steam electrolyzer in which the hydrogen or syngas is produced using electricity.

- ReSOCs have two important features, namely reversible operation of the electrode and efficient cyclic operation.
- Due to the fluctuating and unpredictable demand for energy and the intermittency of renewable energy resources, the energy-storage systems play an important role in our future energy infrastructure.
- The important characteristics of ReSOCs, their optimal configurations and integration methods, as well as their economic aspects are research frontiers.

15.13 Challenges and future research directions for the application of solid oxide fuel cells in mobile devices

For land vehicles, SOFC can be an attractive source of auxiliary power for hybrid models. In general the high energy efficiency and low emission of SOFC are more beneficial for commercial applications than private ones [32]. The SOFC-based auxiliary power units designed by Delphi Automotive Systems, Webasto, and the DESTA project have demonstrated the technical feasibility of these units in mobile applications [33–36]. In addition to high energy efficiency and low emission, these units are compatible with common fuels such as gasoline and diesel, significantly lowering the barrier for technology adoption. The prototype recently developed by the DESTA project for long-distance heavy-duty trucks is especially promising as it can reduce up to 75% of the fuel consumption during the idling period of the truck, which costs between US$5000 and US$9000 per truck per year. The prototype was integrated into a demonstration vehicle from Volvo for successful road testing with more than 2500 km covered on public roads.

The use of SOFC for auxiliary-power generation in aircraft and ships will take more time to materialize than in land vehicles, but various simulation studies have shown the benefits of such technology adoption [37–42]. One prototype of an SOFC-based auxiliary power unit for marine vessels has been recently developed by the SchiBZ project [43]. The prototype was installed on a test ship to deliver 25%–50% of the total power requirements with an overall energy efficiency above 90%, demonstrating the promising prospect of SOFC-based auxiliary power units for marine applications.

In the foreseeable future, SOFCs can be used as the main power source for propelling unmanned aerial and underwater vehicles due to its high-specific energy. A commercial example of an unmanned aerial vehicle propelled by SOFC is the Stalker XE developed by Lockheed Martin [44]. This model runs on conventional hydrocarbon fuel (i.e., propane) and can be operational up to 13 hours. It was successfully tested for combat missions.

On the other hand, using SOFCs to propel land vehicles requires more research and development. The main challenge is to reduce the size of the SOFC

systems, while ensuring high energy efficiency. Further development of MT-SOFCs and micro-gas turbines are desirable in the foreseeable future [45,46]. The development of MT-SOFCs can benefit from the development of more efficient and stable materials. For example, the anode-supported MT-SOFC developed by Nanodynamics Energy can endure rapid heating and cooling within a large temperature range (i.e., 200°C−850°C) without performance degradation [47]. Another area for further development is the energy storage system for handling the regenerative energy during deceleration and peak power. For example, the pairing of a rechargeable battery or supercapacitor with an SOFC can be optimized for specific applications [48,49].

The development of SOFC-propelled land vehicles will also benefit from the further development of reduced-temperature SOFCs as they have simpler overall system requirements, a longer fuel-cell life, and lower manufacturing costs. A prototype was developed by the ZEBRA system, whose SOFC operates within the temperature range of 500°C−850°C [50,51]. The reduced-temperature SOFC continuously supplied energy to the sodium−nickel−chloride battery, which was the main power source for propulsion and auxiliary requirements. Due to the continuous operation of the reduced-temperature SOFC, this system was more cost-efficient for commercial vehicles. It was found that the cost of fuel cells attributed to a significant portion of the manufacturing cost and reducing it to less than £400/kW could make this system economically viable.

15.14 Challenges and future research directions in the stationary application of solid oxide fuel cells

Chapter 13 conducted a feasibility analysis of SOFC-based CHP (combined heating and power) applications in commercial and residential buildings in China. Meanwhile, relevant research progress of SOFC stationary application is also presented, for example, SOFC/SOEC for power-to-gas energy storage as well as combined with biomass applications.

The performance of an SOFC-based CHP system in the public and residential building sector are comprehensively investigated from technical, economic, and environment perspectives. The results show that a significant amount of emissions can be saved by SOFCs compared to traditional energy systems and other CHP prime movers. In addition, SOFCs have better part-load performance than other CHP prime movers. From the cost perspective, the payback duration of SOFC is not economically attractive so far due to the high-capital cost and relatively short lifetime compared to other CHP prime movers, which suggests further development is needed.

From the end-use perspective, the application of SOFC-based CHP in commercial buildings shows better economic performance than in residential buildings. Among five investigated commercial buildings, hotels show the best overall

performance than other categories of buildings. Meanwhile, the hot-summer cold-winter-climate zone with large heating demand in winter and large cooling demand in summer turns out to be the best demonstration site for SOFC stationary applications. In terms of SOFC applications in the residential sector, due to the high-capital cost of SOFC and relatively low price of electricity, it is still a relatively large gap to wide market penetration.

From the application perspective, future efforts would be undertaken to improve the lifetime of SOFC stacks and further reduce the capital cost so as to make it more attractive for investment. Government subsidies on sustainable-energy technologies should be better utilized to promote the market penetration of SOFCs, which also contributes to their price reduction. Meanwhile, better integration of SOFCs with other systems, for example, combined with a gas turbine, utilizing biomass fuel, and reverse operation as SOECs for energy storage, demonstrates their outstanding potential and could play a vital role in future energy systems.

15.15 Challenges and future research directions in the application of solid oxide fuel cell-based systems for waste minimization

Chapter 14, Waste management, provides an overview of the research into waste minimization using SOFC technologies. Upon careful investigation of the state-of-the-art, the following potent research areas were identified:

- Utility of the SOFCs due to their modularity and high efficiency at the small-scale for carbon capture and utilization at the distributed generation plants.
- *Making zero-CO_2 emission feasible*: Coupling SOFC to convenient CO_2 utilization and optimization of this polygeneration plant to attain near-zero emissions.
- *Materials engineering*: more considerations on the manufacturing of materials with improved tolerance against waste contamination and economically viable fabrication techniques of lightweight cells, employing cheap and reliable cells, and the infrastructures involved.
- *Turning an environmental problem into an opportunity*: biomass to not only as a feed to energy production plants, but also to be treated for fabrication of electrodes applied in energy storage devices, like Li-ion batteries and super-capacitors, and thus addressing the storage challenges of SOFC-generated electricity.

15.16 Conclusion and final remarks

The present chapter summarized the key findings and articulated the future research challenges of the design and operation of SOFC-based systems. The key

observation emphasized in various of chapters of the present book is the flexibility and adaptability of solid oxide fuel cells (SOFCs) for a diverse range of industrial application spanning from modular and small-scale systems to maga-scale processes, and from stationary to mobile applications. Moreover, SOFCs are capable of processing a diverse range of fuels, opening new avenues to renewable power generation and decarbonization of existing infrastructure. However, as discussed extensively in various chapters, exploiting such great opportunities poses a multi-scale systems engineering problem which requires a diverse range of expertise at the interface of multiple engineering disciplines. The present contribution made endeavours to offer a panoramic overview of this cross-disciplinary research, and to provide insights into potent research areas. We hope that the current contribution will motivate and promote such multidisciplinary research.

References

[1] B.C.H. Steele, Oxygen ion conductors, High Conductivity Solid Ionic Conductors: Recent Trends and Applications, World Scientific, 1989, pp. 402–446.

[2] H. Inaba, Ceria-based solid electrolytes, Solid State Ionics 83 (1–2) (1996) 1–16.

[3] B. Dalslet, P. Blennow, P.V. Hendriksen, N. Bonanos, D. Lybye, M. Mogensen, Assessment of doped ceria as electrolyte, J. Solid State Electrochem. 10 (8) (2006) 547–561.

[4] T. Ishihara, H. Matsuda, Y. Takita, Doped $LaGaO_3$ perovskite type oxide as a new oxide ionic conductor, J. Am. Chem. Soc. 116 (9) (1994) 3801–3803.

[5] H. Arikawa, H. Nishiguchi, T. Ishihara, Y. Takita, Oxide ion conductivity in Sr-doped $La_{10}Ge_6O_{27}$ apatite oxide, Solid State Ionics 136–137 (2000) 31–37.

[6] P. Lacorre, F. Goutenoire, O. Bohnke, R. Retoux, Y. Lallgant, Designing fast oxide-ion conductors based on $La_2Mo_2O_9$, Nature 404 (6780) (2000) 856–858.

[7] R. Subasri, H. Näfe, F. Aldinger, On the electronic and ionic transport properties of $La_2Mo_2O_9$, Mater. Res. Bull. 38 (15) (2003) 1965–1977.

[8] N. Jiang, E.D. Wachsman, Structural stability and conductivity of phase-stabilized cubic bismuth oxides, J. Am. Ceram. Soc 82 (11) (2004) 3057–3064.

[9] M. Cassidy, Trends in the processing and manufacture of solid oxide fuel cells, Wiley Interdiscipl. Rev.: Energy Environ. 6 (5) (2017).

[10] Z. Shao, W. Zhou, Z. Zhu, Advanced synthesis of materials for intermediate-temperature solid oxide fuel cells, Prog. Mater. Sci. 57 (4) (2012) 804–874.

[11] J.Y. Park, H. Yoon, E.D. Wachsman, Fabrication and characterization of high-conductivity bilayer electrolytes for intermediate-temperature solid oxide fuel cells, J. Am. Ceram. Soc. 88 (9) (2005) 2402–2408.

[12] R. Pelosato, G. Cordaro, D. Stucchi, C. Cristiani, G. Dotelli, Cobalt based layered perovskites as cathode material for intermediate temperature solid oxide fuel cells: a brief review, J. Power Sources 298 (2015) 46–67.

[13] S.P. Jiang, Development of lanthanum strontium manganite perovskite cathode materials of solid oxide fuel cells: a review, J. Mater. Sci. 43 (21) (2008) 6799–6833.

[14] T. Ishiham, T. Kudo, H. Matsuda, Y. Takita, Doped perovskite oxide, $PrMnO_3$, as a new cathode for solid-oxide fuel cells that decreases the operating temperature, J. Am. Ceram. Soc. 77 (6) (1994) 1682–1684.

[15] T.L. Wen, H. Tu, Z. Xu, O. Yamamoto, A study of (Pr, Nd, Sm)$_{1-x}$Sr$_x$MnO$_3$ cathode materials for solid oxide fuel cell, Solid State Ionics 121 (1−4) (1999) 25−30.
[16] R. Chiba, F. Yoshimura, Y. Sakurai, An investigation of LaNi$_{1-x}$Fe$_x$O$_3$ as a cathode material for solid oxide fuel cells, Solid State Ionics 124 (3) (1999) 281−288.
[17] R. Chiba, F. Yoshimura, Y. Sakurai, Properties of La$_{1-y}$Sr$_y$Ni$_{1-x}$Fe$_x$O$_3$ as a cathode material for a low-temperature operating SOFC, Solid State Ionics 152−153 (2002) 575−582.
[18] H. Orui, K. Watanabe, R. Chiba, M. Arakawa, Application of LaNi(Fe)O$_3$ as SOFC cathode, J. Electrochem. Soc. 151 (9) (2004) A1412−A1417.
[19] A. Yan, M. Phongaksorn, D. Nativel, E. Croiset, Lanthanum promoted NiO-SDC anode for low temperature solid oxide fuel cells fueled with methane, J. Power Sources 210 (2012) 374−380.
[20] S.H. Choi, J.H. Wang, Z. Cheng, M. Liu, Surface modification of Ni-YSZ using niobium oxide for sulfur-tolerant anodes in solid oxide fuel cells, J. Electrochem. Soc. 155 (5) (2008) B449−B454.
[21] F.S. Silva, T.M. Souza, Novel materials for solid oxide fuel cell technologies: a literature review, Int. J. Hydrogen Energy 42 (41) (2017) 26020−26036.
[22] N. Mahato, A. Banerjee, A. Gupta, S. Omar, K. Balani, Progress in material selection for solid oxide fuel cell technology: a review, Prog. Mater. Sci. 72 (2015) 141−337.
[23] Z. Yang, K.S. Weil, D.M. Paxton, J.W. Stevenson, Selection and evaluation of heat-resistant alloys for SOFC interconnect applications, J. Electrochem. Soc. 150 (9) (2003) A1188.
[24] W.Z. Zhu, S.C. Deevi, Opportunity of metallic interconnects for solid oxide fuel cells: a status on contact resistance, Mater. Res. Bull. 38 (6) (2003) 957−972.
[25] J. Wu, X. Liu, Recent development of SOFC metallic interconnect, J. Mater. Sci. Technol. 26 (4) (2010) 293−305.
[26] S.-B. Sohn, S.-Y. Choi, G.-H. Kim, H.-S. Song, G.-D. Kim, Stable sealing glass for planar solid oxide fuel cell, J. Non. Cryst. Solids 297 (2−3) (2002) 103−112.
[27] S.B. Sohn, S.Y. Choi, G.H. Kim, H.S. Song, G.D. Kim, Suitable glass-ceramic sealant for planar solid-oxide fuel cells, J. Am. Ceram. Soc 87 (2) (2004) 254−260.
[28] C. Lara, M.J. Pascual, M.O. Prado, A. Durán, Sintering of glasses in the system RO-Al$_2$O$_3$-BaO-SiO$_2$(R = Ca, Mg, Zn) studied by hot-stage microscopy, Solid State Ionics 170 (3−4) (2004) 201−208.
[29] C. Lara, M.J. Pascual, A. Durán, Glass-forming ability, sinterability and thermal properties in the systems RO-BaO-SiO$_2$ (R = Mg, Zn), J. Non Cryst. Solids 348 (2004) 149−155.
[30] M. Sharifzadeh, Integration of process design and control: a review, Inst. Chem. Eng. (2013).
[31] M. Sharifzadeh, M. Meghdari, D. Rashtchian, Multi-objective design and operation of solid oxide fuel cell (SOFC) triple combined-cycle power generation systems: integrating energy efficiency and operational safety, Appl. Energy 185 (2017) 345−361.
[32] P. Aguiar, D.J.L. Brett, N.P. Brandon, Feasibility study and techno-economic analysis of an SOFC/battery hybrid system for vehicle applications, J. Power Sources 171 (1) (2007) 186−197.
[33] J. Zizelman, S. Shaffer, S. Mukerjee, Solid oxide fuel cell auxiliary power unit - a development update, SAE Technical Paper 2002-01-0411, 2002. Avaliable from: https://doi.org/10.4271/2002-01-0411.

[34] P. Lamp, J. Tachtler, O. Finkenwirth, S. Mukerjee, S. Shaffer, Development of an auxiliary power unit with solid oxide fuel cells for automotive applications, Fuel Cells 3 (3) (2003) 146–152.
[35] J. Lawrence, M. Boltze, Auxiliary power unit based on a solid oxide fuel cell and fuelled with diesel, J. Power Sources 154 (2) (2006) 479–488.
[36] J. Rechberger, A. Kaupert, J. Hagerskans, L. Blum, Demonstration of the first European SOFC APU on a heavy duty truck, in: Transportation Research Procedia, 2016.
[37] S. Eelman, T. Krieg, Fuel cell APU's in commercial aircraft – an assessment of SOFC and PEMFC concepts, in: 24th International Congress of the Aeronautical Sciences (IC), 2004, pp. 1–10.
[38] R. Tornabene, X. Wang, C.J. Steffen, J.E. Freeh, Development of parametric mass and volume models for an aerospace SOFC/gas turbine hybrid system, in: ASME Turbo Expo 2005: Power for Land, Sea, and Air, 2005, pp. 135–144.
[39] J.E. Freeh, C.J. Steffen, L.M. Larosiliere, Off-design performance analysis of a solid-oxide fuel cell/gas turbine hybrid for auxiliary aerospace power, in: 3rd International Conference on Fuel Cell Science, Engineering and Technology, vol. 2005, 2005, pp. 265–272.
[40] P. Chinda, P. Brault, The hybrid solid oxide fuel cell (SOFC) and gas turbine (GT) systems steady state modeling, Int. J. Hydrogen Energy 37 (11) (2012) 9237–9248.
[41] L.K.C. Tse, S. Wilkins, N. McGlashan, B. Urban, R. Martinez-Botas, Solid oxide fuel cell/gas turbine trigeneration system for marine applications, J. Power Sources (2011).
[42] C. Ezgi, M. Turhan Çoban, Ö. Selvi, Design and thermodynamic analysis of an SOFC system for naval surface ship application, J. Fuel Cell Sci. Technol. (2013).
[43] Sunfire 50 kW SOFC for ship-integrated fuel cell project in Germany, Fuel Cells Bull. 2015 (11) (2015) 3–4.
[44] A. Gong, D. Verstraete, Fuel cell propulsion in small fixed-wing unmanned aerial vehicles: current status and research needs, Int. J. Hydrogen Energy 42 (33) (2017) 21311–21333.
[45] Y. Funahashi, T. Shimamori, T. Suzuki, Y. Fujishiro, M. Awano, Fabrication and characterization of components for cube shaped micro tubular SOFC bundle, J. Power Sources 163 (2) (2007) 731–736.
[46] D. Aquaro, M. Pieve, High temperature compact heat exchangers: performance of advanced metallic recuperators for power plants, Applied Thermal Engineering 27 (2) (2005) 389–400.
[47] Y. Du, C. Finnerty, J. Jiang, Thermal stability of portable microtubular SOFCs and stacks, J. Electrochem. Soc. 155 (9) (2008) B972–B977.
[48] Q. Xun, Y. Liu, E. Holmberg, A comparative study of fuel cell electric vehicles hybridization with battery or supercapacitor, in: 2018 International Symposium on Power Electronics, Electrical Drives, Automation and Motion (SPEEDAM), 2018, pp. 389–394.
[49] L. Gaines, R. Cuenca, Costs of lithium-ion batteries for vehicles. United States Department of Energy, 2000. Avaliable from: https://doi.org/10.2172/761281.
[50] J.L. Sudworth, The sodium/nickel chloride (ZEBRA) battery, J. Power Sources 100 (1–2) (2001) 149–163.
[51] D.J.L. Brett, et al., Concept and system design for a ZEBRA battery--intermediate temperature solid oxide fuel cell hybrid vehicle, J. Power Sources 157 (2) (2006) 782–798.

This page intentionally left blank

A visual tutorial on the modeling of a planar solid oxide fuel cell using COMSOL multiphysics

A

Mojtaba Meghdari[1], Mohsen Foroughi Doust[1,2] and Mahdi Sharifzadeh[2]

[1]*Chemical & Petroleum Engineering Department, Sharif University of Technology, Tehran, Iran*

[2]*Sharif Energy Research Institute (SERI), Sharif University of Technology, Tehran, Iran*

A.1 Introduction

This Appendix provides tutorials on modeling a planar solid oxide fuel cell (SOFC) using the COMSOL multiphysics software tool. The physical elements of a planar SOFC are shown in Fig. A.1. The planar SOFC model is developed to simulate the mass transport, energy transport, and electrochemical phenomena that take place in the fuel and air channels, porous electrodes, electrolyte, and interconnects of an SOFC. The model computes 2D species composition profiles at the anode and cathode sides, temperature profiles in the SOFC, electric potential, and current distributions at the electrodes and electrolyte. A gaseous mixture of H_2 and H_2O is used as the fuel in the anode side, while at the cathode side the gaseous mixture is composed of O_2 and N_2 [1].

The presented materials are supplied with screenshots of the software tool to facilitate reproduction of the simulation by the user. The required procedure can be divided into six main steps:

1. Model initialization: selecting the appropriate application mode in the *Model Navigator*.
2. Creating the *Model Geometry* using the *Geometry* tab, and specifying the domains.
3. Setting up the *Subdomain Equations* and *Boundary* conditions using the *Physics* tab.
   a. Mass transfer for each domain.
   b. Momentum transfer for each domain.
   c. Heat transfer for each domain.
4. Geometrical discretization using the *Mesh* tab.
5. Simulation execution in the *Study* tab.
6. Analyzing the results in the *Result* tab.

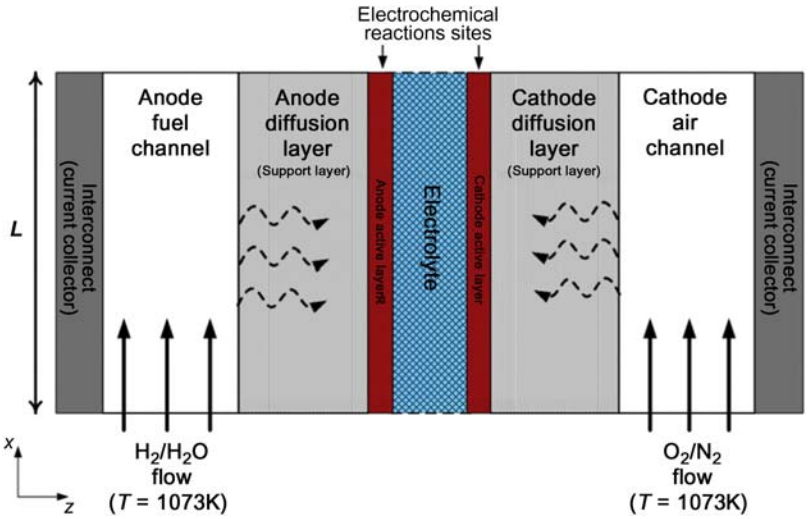

FIGURE A.1

The elements of a planar solid oxide fuel cell (from left): anode interconnect, anode porous electrode, anode active layer, electrolyte, cathode active layer, cathode porous electrode, and cathode interconnect [1].

The main assumptions of the simulation are listed below:

1. The gaseous mixtures are assumed to consist of ideal gases.
2. The electrochemical reactions take place at the electrode layer boundary−interfaces.
3. The porous electrodes are assumed to be isotropic and macrohomogeneous.
4. The electrolyte is assumed to be impermeable to mass transport.
5. Ohmic heating of the interconnects is neglected because they are considered to be excellent conductors.
6. The heat capacity of the gas mixtures is considered to be temperature-independent.
7. The SOFC voltage is equal to the voltage difference between the anode and cathode.
8. The heat transferred through the radiation mechanism is negligible in interconnects [1].

A.2 Initialization of the program (model navigator)

In the model navigator window of COMSOL multiphysics shown in Fig. A.2, there are two options for starting the modeling activities; they are *Model Wizard* and *Blank Model*. *Model Wizard* initializes the model using a prespecified template.

FIGURE A.2

Model navigator window.

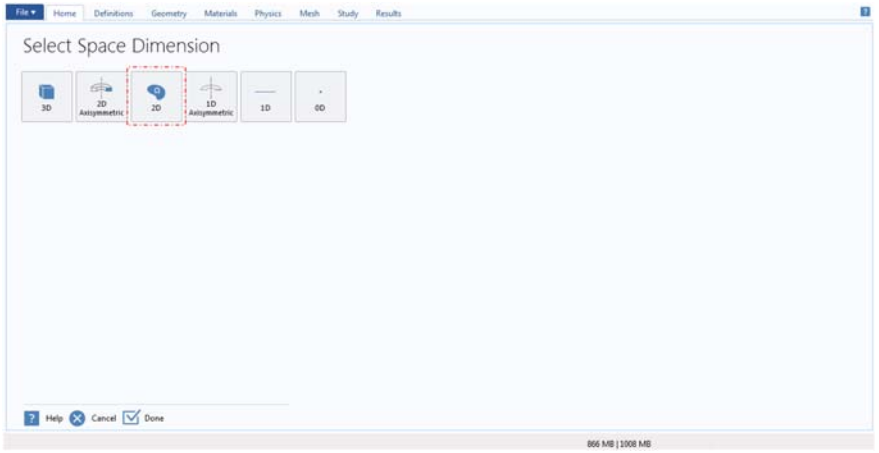

FIGURE A.3

Dimension selection.

Click on the *Model Wizard* option will open the next window as shown in Fig. A.3. This window is related to *Space Dimension* specifications. On this page, click on the *2D* option as shown by the red dots.

The next step is to go to the *Physics Selection* window and specify the physics involved in the modeling of SOFCs as shown in Fig. A.4.

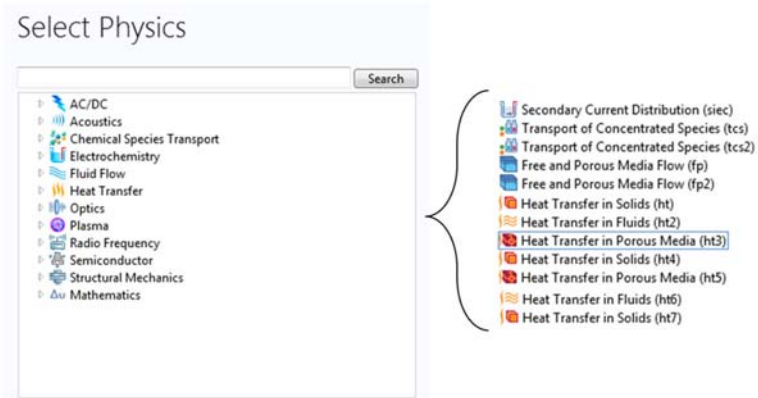

FIGURE A.4

Physics selection.

The required physics are listed below:

- *Secondary Current Distribution* physics is applied for generic modeling of electrochemical cells. The relation between charge transfer and overpotential can be described using arbitrary kinetic expressions such as Butler–Volmer and Tafel equations.
- *Transport of Concentrated Species* physics is applied for multicomponent diffusion, where the diffusive driving force of each species depends on the mixture composition, temperature, and pressure. This physics is used for modeling mass transport phenomena between a free channel (e.g., anode channel) and a porous media (anode itself) in a fuel cell.
- *Free and Porous Media Flow* physics is applied to compute the fluid velocity and pressure fields of single-phase flow where the free flow is connected to a porous media. In SOFCs the anode and cathode are integrated with fuel and air-free channels.
- *Heat Transfer in Solids* physics is used to model heat transfer by conduction, convection, and radiation in solids. In SOFCs the heat transfer calculations of the anode and cathode interconnect and the solid electrolyte are conducted using this physics.
- *Heat Transfer in Fluids* physics is applied to model heat transfer by the conduction, convection, and radiation mechanisms in fluid or free channels. In SOFCs the heat transfer of fuel and air-free channels are simulated using this physics.
- *Heat Transfer in Porous Media* physics is used to model heat transfer in the porous media domains (anode and cathode porous electrodes). This physics corresponds to the convection and diffusion equations, and the thermodynamic properties are averaged for both *Solid Matrix* and *Fluid* sections [2].

The underlying assumption of each physics approach is summarized in Table A.1.

Table A.1 Map of the involved physics and solid oxide fuel cell domains.

Physics	Geometric domain	Application [2]
Secondary current distribution	Anode porous electrode Electrolyte Cathode porous electrode	• Applied for defining activation overpotentials • Applied for describing the relation between charge transfer and overpotential • Applied for generic modeling of electrochemical cells • Applied for combining with mass transport interfaces • Applied for describing conduction of currents in the electrodes and electrolytes using Ohm's Law
Transport of Concentrated Species	Anode-free channel Anode porous electrode Cathode porous electrode Cathode-free channel	• Applied for gaseous and liquid mixtures • Applied for species concentration with the same order of magnitude • Applied for a solution which none of the species can be identified as a solvent • Applied for the mixture which properties depend on the composition • Applied for multicomponent diffusion • Applied for transport modeling through convection, diffusion, and migration in an electric field
Free and Porous Media Flow	Anode-free channel Anode porous electrode Cathode porous electrode Cathode-free channel	• Applied for computing fluid velocity and pressure fields of single-phase flow where the free flow is connected to porous media • Applied for at least two different domains: a free channel and a porous medium • Applied for coupling between slow flow in porous media and fast flow in channels • Applied for fluids with Mach numbers below 0.3
Heat Transfer in Solids	Anode interconnect Electrolyte Cathode interconnect	• Applied for modeling heat transfer by conduction, convection, and radiation in solids • Applied for defining the temperature equation in solid domains with the differential form of Fourier's law
Heat Transfer in Fluids	Anode-free channel Cathode-free channel	• Applied for modeling heat transfer by conduction, convection, and radiation in fluids • Applied for defining the temperature profile in fluid domains with the convection–diffusion equation
Heat Transfer in Porous Media	Anode porous electrode Cathode porous electrode	• Applied for modeling heat transfer by conduction, convection, and radiation in porous media • Applied for defining the temperature equation in porous, media domains with the convection–diffusion equation

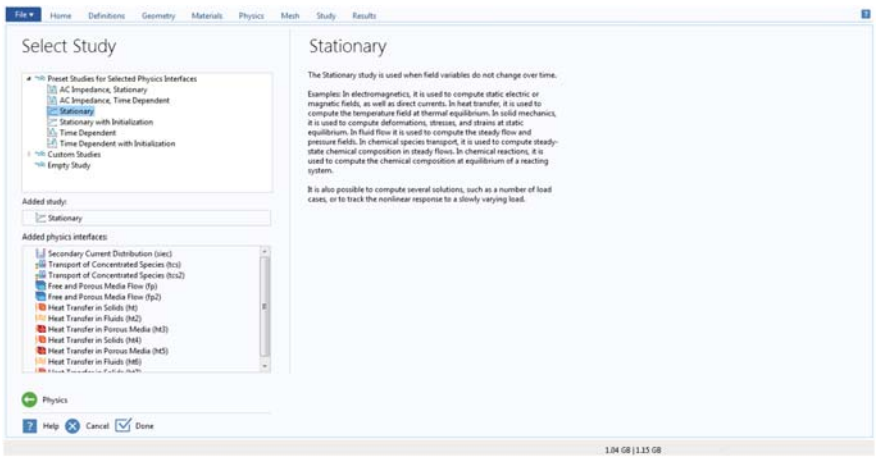

FIGURE A.5

Study selection.

On the *Select Study* page, click to select the type of study to perform. The available options depend on the set of physics interfaces included in the model. However, it should be noted that a study type may be applicable to all physics interfaces, while others have limitations. You can select the study type from one of the following branches as seen in Fig. A.5:

- *Preset studies for selected physics interfaces*: studies applicable to all physics interfaces that you have chosen for your model.
- *Custom studies*: in some study types, not all physics interfaces can be applied.

Stationary and time-dependent studies generate equations without time derivatives and transient (time-dependent) simulations, respectively. In this simulation, the *Stationary* mode is used.

Fig. A.6 shows the *Model Builder* hierarchical tree. It is composed of four main domains, namely *Global Definitions*, *Component*, *Study*, and *Results*, as discussed next:

- The *Global Definitions* section allows specification of the model geometry, material properties, parameters, variables, and functions. This information is accessible in any domain of the model. For adding *Parameters* and *Variables* you need to right-click on *Global Definition* and select the corresponding option.
- The *Component* section is the main domain of the modeling that contains *Definitions*, *Geometry*, *Dependent variables*, and *Physics*. Each of these will be discussed later in Section A.3, A.4, A.5, and A.6.
- In the *Study* section it possible to conduct either *stationary* (i.e., steady-state) or *time-dependent* (dynamic) simulation.
- Finally, the *Results* section reports the numerical values of the solution and postprocessing computation.

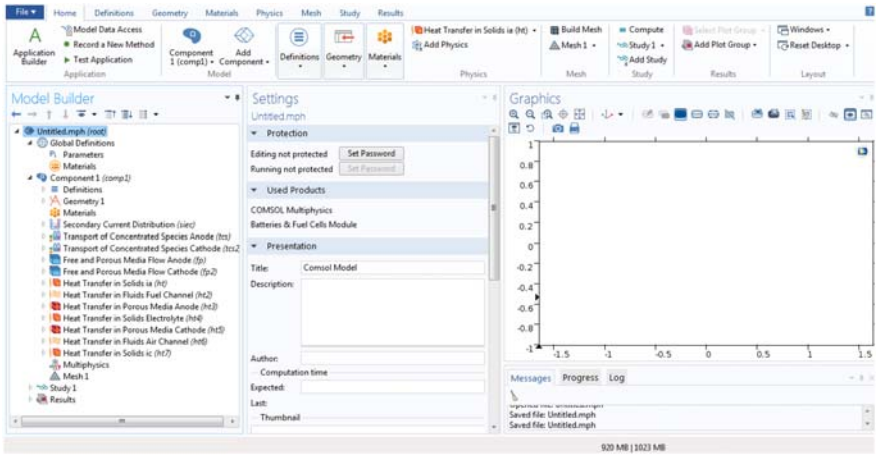

FIGURE A.6

The model builder hierarchical tree.

A.3 Defining the required parameters and variables

The required parameters for the modeling of an SOFC must be specified in the *Global Definitions* section. Right-click on *Global Definitions*, select *Parameters*, and enter all the parameters based on Table A.2 and Fig. A.7.

Table A.3 shows the correlations and parametric values applied for modeling heat transfer phenomena [1,3].

Fig. A.8 Shows the entered *Heat Capacities* for using *Heat Transfer* physics. These variables can be defined using three methods, namely typing and inserting .txt or excel files.

Table A.4 shows the current density parameters and coefficients, the cell-voltage value to calculate the Bulter–Volmer equation, and the current densities of the anode, cathode, and electrolyte.

The reaction rate of hydrogen is computed using the Faraday constant based on the number of released electrons as shown in Table A.5. It is also used for the calculation of the heat-flux rate caused by the electrochemical reactions through the electrolyte boundaries to the electrodes (Fig. A.9).

A.4 Constructing the geometry

In the *Geometry* section the model's geometry is constructed using the recommended methods in COMSOL multiphysics. The planar SOFC system has seven rectangular domains, namely *anode interconnect*, *fuel channel*, *anode*, *electrolyte*,

Table A.2 Parameters required for modeling planar solid oxide fuel cell systems.

Parameter	Value	Unit	Description
patm	1	atm	Atmospheric pressure
T	1123	K	Temperature
ssa	5e15	1/m	Specific surface area, anode
ssc	5e15	1/m	Specific surface area, cathode
mu	2.01e−5	(N s)/(m^2)	Viscosity, air
perma	1.98e−10	m^2	Anode permeability
permc	1.98e−10	m^2	Cathode permeability
Eeq_a	0	V	Equilibrium voltage, anode
Eeq_c	1	V	Equilibrium voltage, cathode
ec	$33{,}400 \times \exp(-10300/T)$	1/(ohm m)	Electrolyte conductivity
sea	$(9.5 \times (10^7)/T) \times \exp(-1150/T)$	1/(ohm m)	Solid effective conductivity, anode
sec	$(4.2 \times (10^7)/T) \times \exp(-1200/T)$	1/(ohm m)	Solid effective conductivity, cathode
eea	ec	1/(ohm m)	Electrolyte effective conductivity, the anode
eec	ec	1/(ohm m)	Electrolyte effective conductivity, cathode
vh2	7.07		Kinetic volume, H_2
vo2	16.6		Kinetic volume, O_2
vn2	17.9		Kinetic volume, N_2
vh2o	12.7		Kinetic volume, H_2O
Mh2	2	g/mol	Molar mass, H_2
Mo2	32	g/mol	Molar mass, O_2
Mn2	28	g/mol	Molar mass, N_2
Mh2o	18	g/mol	Molar mass, H_2O
kd	0.00143	m^2/s	Reference diffusivity
epor	0.46		Porosity
to	4.5		Tortuosity

Dh2h2o	$kd \times (T^{1.75})/(patm \times (vh2^{(1/3)} + vh2o^{(1/3)})^2) \times (1/Mh2 + 1/Mh2o)^{0.5}$	m^2/s	Diffusivity, H_2-H_2O
Do2h2o	$kd \times (T^{1.75})/(patm \times (vo2^{(1/3)} + vh2o^{(1/3)})^2) \times (1/Mo2 + 1/Mh2o)^{0.5}$	m^2/s	Diffusivity, O_2-H_2O
Do2n2	$kd \times (T^{1.75})/(patm \times (vo2^{(1/3)} + vn2^{(1/3)})^2) \times (1/Mo2 + 1/Mn2)^{0.5}$	m^2/s	Diffusivity, O_2-N_2
Dn2h2o	$kd \times (T^{1.75})/(patm \times (vh2o^{(1/3)} + vn2^{(1/3)})^2) \times (1/Mh2o + 1/Mn2)^{0.5}$	m^2/s	Diffusivity, N_2-H_2O
Dh2h2oeff	$Dh2h2o \times (epor/to)^{1.5}$	m^2/s	Effective diffusivity, H_2-H_2O
Do2h2oeff	$Do2h2o \times (epor/to)^{1.5}$	m^2/s	Effective diffusivity, O_2-H_2O
Do2n2eff	$Do2n2 \times (epor/to)^{1.5}$	m^2/s	Effective diffusivity, O_2-N_2
Dn2h2oeff	$Dn2h2o \times (epor/to)^{1.5}$	m^2/s	Effective diffusivity, N_2-H_2O
xh2ref	0.95		Inlet weight fraction, H_2 at the anode
xo2ref	0.21		Inlet weight fraction, O_2 at the cathode
Wel	2e−4	m	Electrolyte channel width
W	2e−3	m	Gas flow channel width
Wadl	5e−4	m	Anode porous electrode width
Wcdl	3e−4	m	Cathode porous electrode width
L	5e−2	m	Flow channel length
F	96485.3365	C/mol	Faraday constant
Rg	8.314	J/(mol K)	Gas constant
gamaA	7.55E + 09	$A/(m^2)$	Anode preexponential coefficient
gamaC	6.91E + 08	$A/(m^2)$	Cathode preexponential coefficient
EA	1.20E + 05	J/(mol)	Anode activation energy
EC	1.10E + 05	J/(mol)	Cathode activation energy
Vair	0.6	m/s	Air velocity
Vfuel	0.4	m/s	Fuel velocity
Wai	0.001	m	Anode interconnect width
Wci	0.001	m	Cathode interconnect width

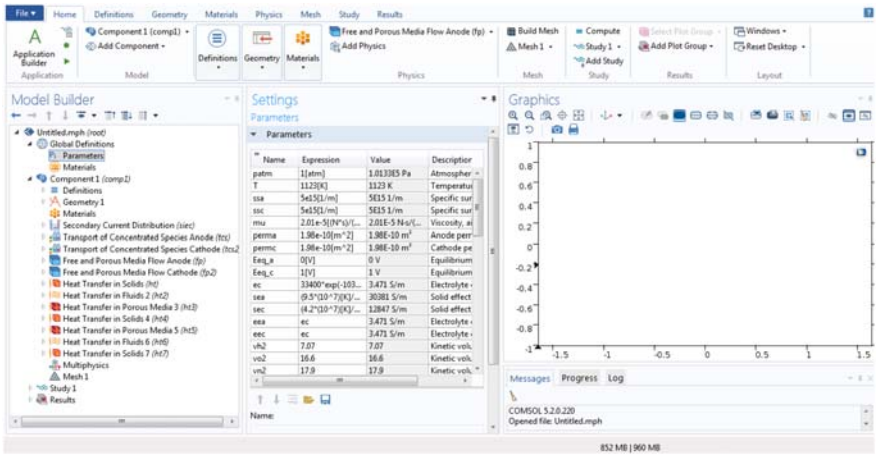

FIGURE A.7

Entered parameters in COMSOL.

Table A.3 The parameters applied for modeling heat transfer phenomena.

Parameter	Value	Unit	Description
hH2	$(-667.75 + 29.806 \times T3)$	J/(mol)	Enthalpy
hH2O	$(-3510.07 + 39.316 \times T3)$	J/(mol)	Enthalpy
hO2	$(-2673.58 + 34.026 \times T3)$	J/(mol)	Enthalpy
hN2	$(-1664.96 + 31.754 \times T3)$	J/(mol)	Enthalpy
ka	10	W/(m K)	Anode thermal conductivity
kc	11	W/(m K)	Cathode thermal conductivity
ke	2	W/(m K)	Electrolyte thermal conductivity
Ca	0.65	J/(kg K)	Anode-specific heat
Cc	0.9	J/(kg K)	Cathode-specific heat
Ce	0.3	J/(kg K)	Electrolyte-Specific Heat
roa	6200	kg/(m^3)	Anode density
roc	6000	kg/(m^3)	Cathode density
roe	5560	kg/(m^3)	Electrolyte density
kH2	$(0.08525 + 2.964e{-}4 \times T)$	W/(m K)	Hydrogen thermal conductivity
kH2O	$(-0.01430 + 9.782e{-}5 \times T)$	W/(m K)	Water thermal conductivity
kO2	$(0.01569 + 5.690e{-}4 \times T)$	W/(m K)	Oxygen thermal conductivity

(*Continued*)

Table A.3 The parameters applied for modeling heat transfer phenomena. *Continued*

Parameter	Value	Unit	Description
kN2	$(0.01258 + 5.444e{-}5 \times T)$	W/(m K)	Nitrogen conductivity
CpH2	$(12986 + 5.421 \times T{-}0.0045 \times (T^2)$	J/(kg K)	Specific-heat capacity
CpH2O	$(1672 + 0.477 \times T + 0.00019 \times (T^2))$	J/(kg K)	Specific-seat capacity
CpO2	$(896 + 0.0115 \times T + 0.00026 \times (T^2))$	J/(kg K)	Specific-heat capacity
CpN2	$(1070{-}0.198 \times T + 0.00034 \times (T^2))$	J/(kg K)	Specific-heat capacity
hH21	$CpH2 \times T3$	J/(kg)	Hydrogen-heat capacity
hH2O1	$CpH2O \times T3$	J/(kg)	Water-heat capacity
hO21	$CpO2 \times T3$	J/(kg)	Oxygen-heat capacity
Ci	0.8	J/(kg K)	Interconnect-heat capacity
roi	7700	kg/(m^3)	Interconnect density
ki	6	W/(m K)	Interconnect thermal conductivity

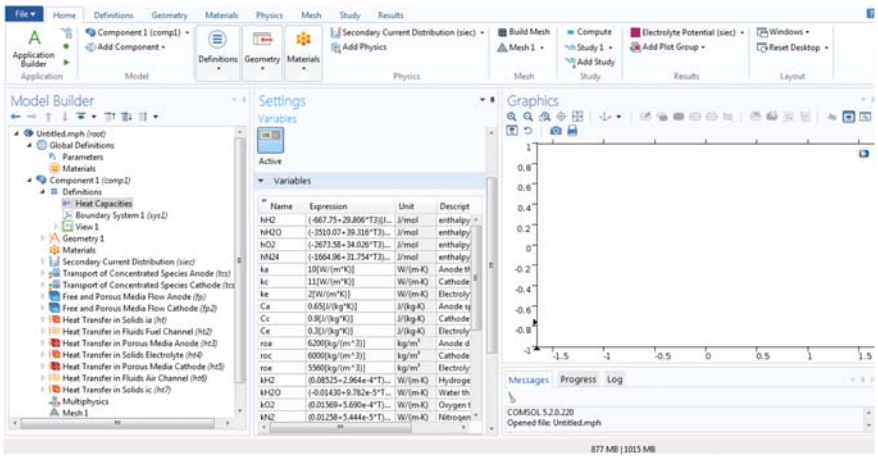

FIGURE A.8

Entered variables (heat capacities) in COMSOL.

Table A.4 Current density and cell-voltage variables.

Parameter	Value/expression	Unit	Description
i0aa	6000	A/m^2	Exchange current density of anode
i0cc	1500	A/m^2	Exchange current density of cathode
i0a	$gamaA \times (xh2ref) \times (1-xh2ref) \times \exp(-EA/(Rg \times T))$	A/m^2	Current density of anode
i0c	$gamaC \times ((xo2ref)^{0.25}) \times \exp(-EC/(Rg \times T))$	A/m^2	Current density of cathode
Vcell	0.5	V	Cell voltage

Table A.5 Reaction rate of hydrogen.

Parameter	Value/expression	Unit	Description
RH2	$siec.Normll/(2 \times F)$	mol/(m^2 s)	Reaction rate

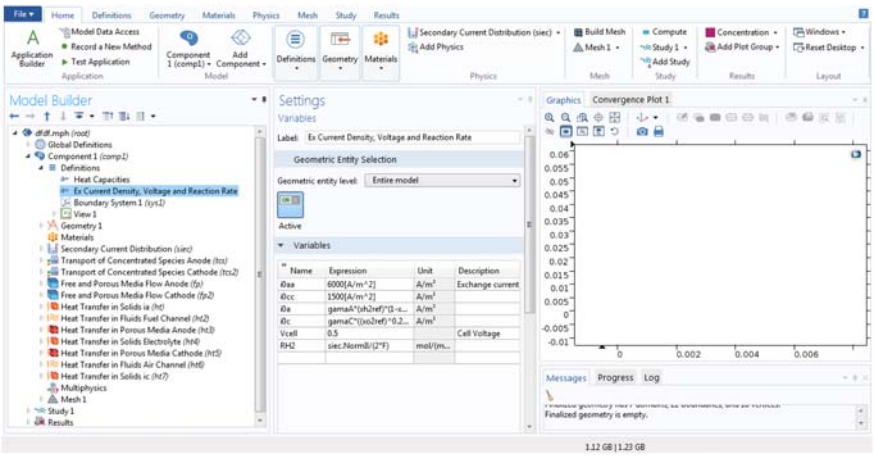

FIGURE A.9

Entered variables (excurrent density, voltage, and reaction rate) in COMSOL.

cathode, *air channel*, and *cathode interconnect* as shown in Fig. A.1. The corresponding geometries are created by right-clicking on *Geometry* and selecting rectangular for each domain. Table A.6 lists the dimensions of these seven domains in parametric terms.

Table A.6 Geometry dimensions.

Domains	Width	Height	X-corner position
Anode interconnects	*Wai*	*L*	0
Fuel channel	*W*	*L*	*Wai*
Anode electrode	*Wadl*	*L*	*Wai* + *W*
Electrolyte	*Wel*	*L*	*Wai* + *W* + *Wadl*
Cathode electrode	*Wcdl*	*L*	*Wai* + *W* + *Wadl* + *Wel*
Air channel	*W*	*L*	*Wai* + *W* + *Wadl* + *Wel* + *Wcdl*
Cathode interconnect	*Wci*	*L*	*Wai* + *W* + *Wadl* + *Wel* + *Wcdl* + *W*

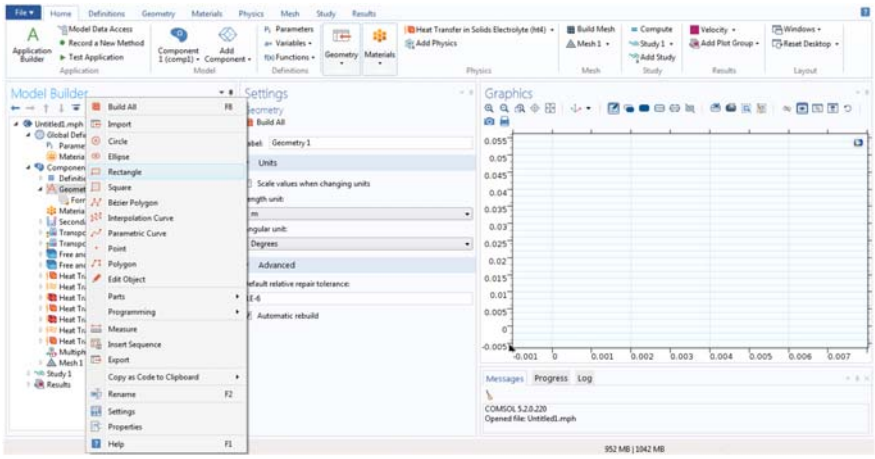

FIGURE A.10

Specifying rectangular geometry.

In order to specify the rectangular elements of the planar SOFC as shown in Fig. A.1, right-click on *Geometry* and then choose the *Rectangle* option based on Fig. A.10.

As shown in Fig. A.11 under the *Rectangle* setting it is necessary to specify the value of the width and height of the rectangle (*L* and *W* parameters in Table A.6). The *Position* section is used to define the corner point of the rectangle as the base for drawing. The anode interconnect rectangle has *Wai* width and *L* height, and the position of its lower-left corner is the point (0,0). A similar procedure can be applied for constructing the other six elements of the planar SOFC as shown in Figs. A.12–A.17.

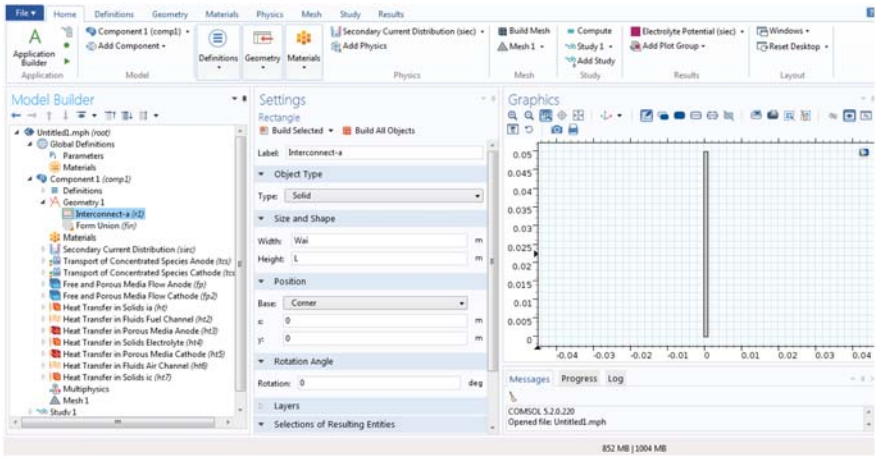

FIGURE A.11

Anode interconnect geometry.

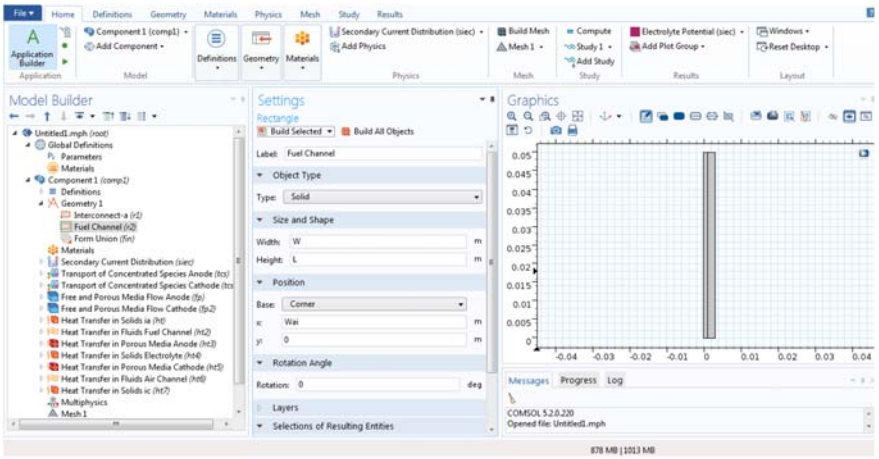

FIGURE A.12

Fuel channel geometry.

A.5 Specifying dependent variables

For specifying the dependent variables such as *electrolyte potential* and *electric potential*, click on the *Dependent Variables* section in the setting window of each physics option and enter the related variables using a red-dotted envelope as shown in Fig. A.18.

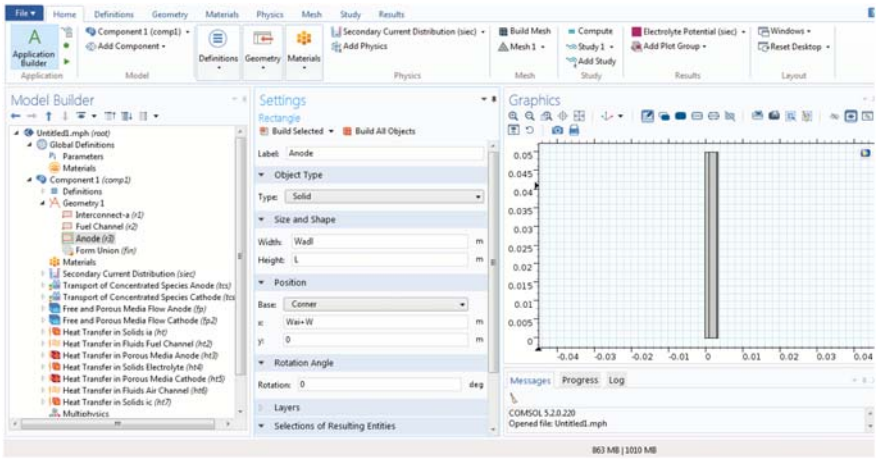

FIGURE A.13

Anode porous electrode geometry.

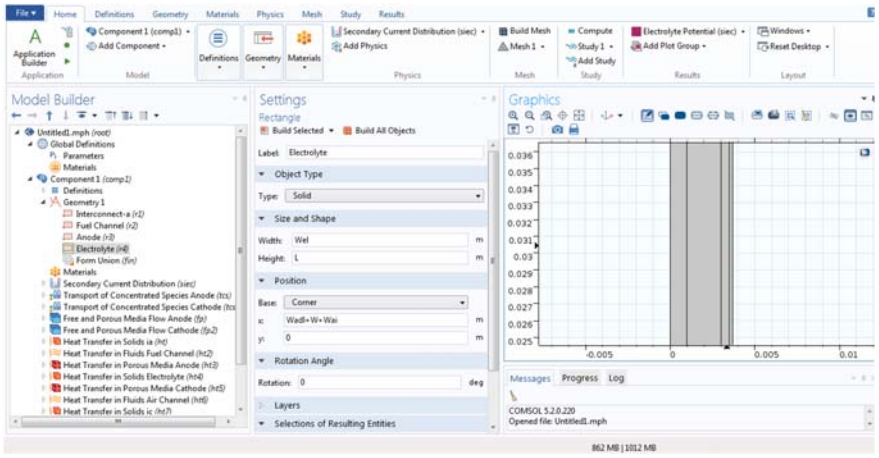

FIGURE A.14

Electrolyte geometry.

The *Secondary Current Distribution* in Fig. A.18 has two *dependent variables* for calculating the *electrolyte potential* and the *electric potential* of anode and cathode due to the electrochemical reaction. The variables *phil* and *phis* are defined as *electrolyte potential* and *electric potential* and can be calculated and used by the *Secondary Current Distribution* physics. Their calculated values will be reported in the *Result* section.

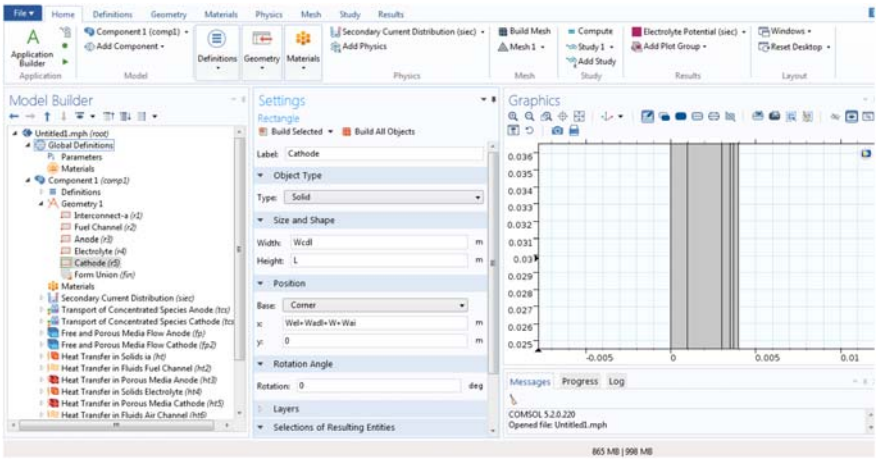

FIGURE A.15

Cathode porous electrode geometry.

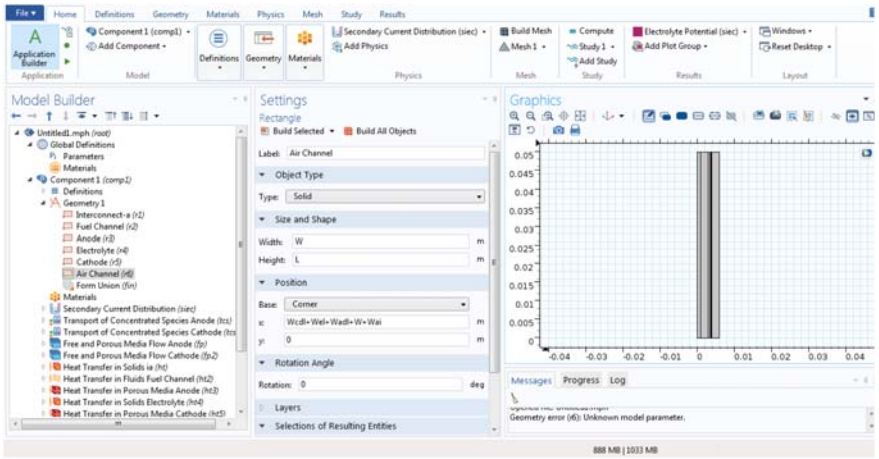

FIGURE A.16

Air channel geometry.

Similarly, as shown in Fig. A.19, select the fuel channel and anode domains. The variables *wH2* and *wH2O* are defined as the *mass fraction* of the species in *Anode Transport of Concentrated Species* physics.

As shown in Fig. A.20 select the air channel and cathode domains. The variables *wO2* and *wN2* are defined as the *mass fraction* of the species in *Cathode Transport* of *Concentrated Species* physics. Since H_2O and N_2 do not participate in the electrochemical reactions, their amount is calculated from their mass

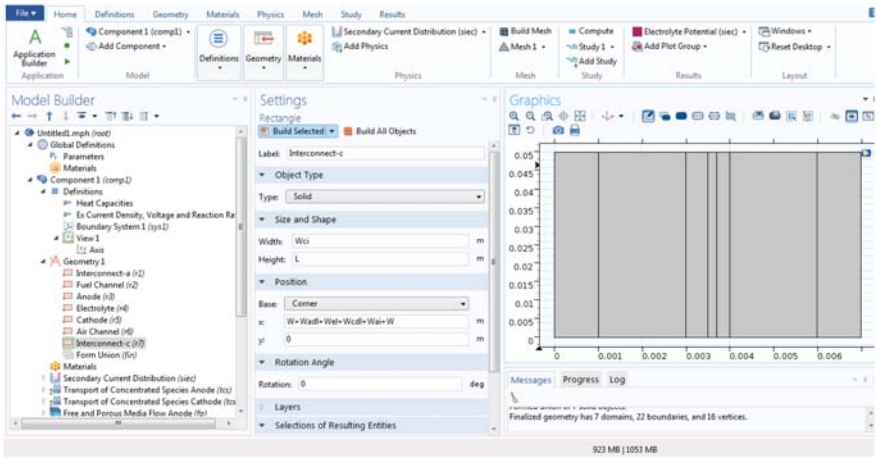

FIGURE A.17

Cathode interconnect geometry.

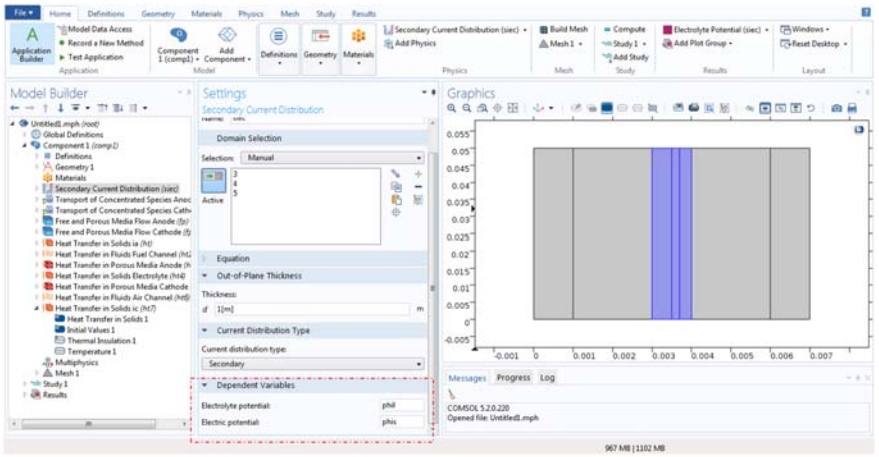

FIGURE A.18

Dependent variables (*Secondary Current Distribution*).

balance. In order to indicate this property, these variables are selected in the *From Mass Constraint* drop-down menu.

As shown in Figs. A.21 and A.22 select the fuel channel free and porous media flow, and air channel free and porous media flow, respectively. The *velocity field* of fuel and air in the anode and cathode porous electrodes and free channels are defined as *u* (*u,v,w*), *u2* (*u21x,u21y,u21z*). *p*, *p2* are defined as the pressure profiles of the anode and cathode porous electrodes, and free channels.

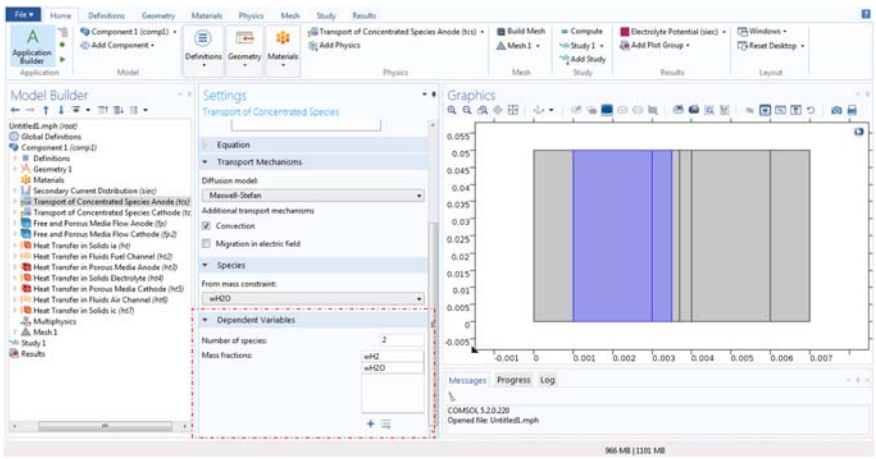

FIGURE A.19

Dependent variables (Fuel Channel Transport of Concentrated Species).

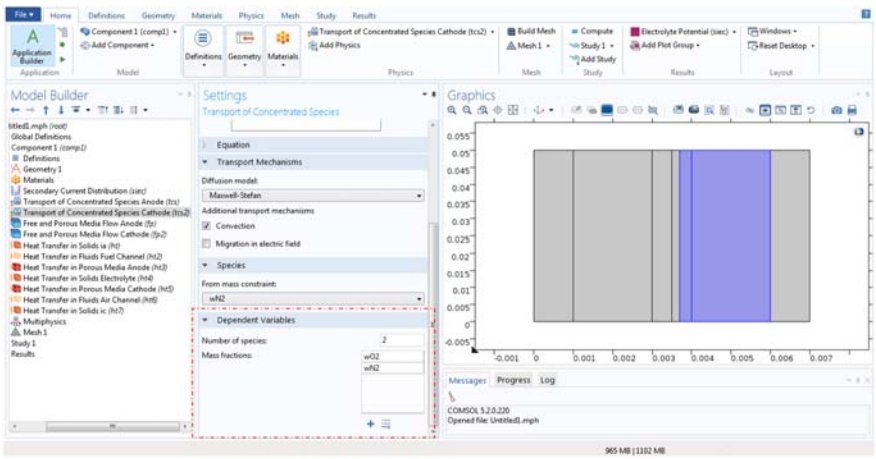

FIGURE A.20

Dependent variables (Air Channel Transport of Concentrated Species).

As shown in Figs. A.23–A.29 the temperature profiles of the seven rectangular domains of the planar SOFC system (i.e., anode interconnect, fuel channel, anode, electrolyte, cathode, air channel, cathode interconnect) are defined as *Tai, T1, T2, T3, T4, T5,* and *Tci*, respectively.

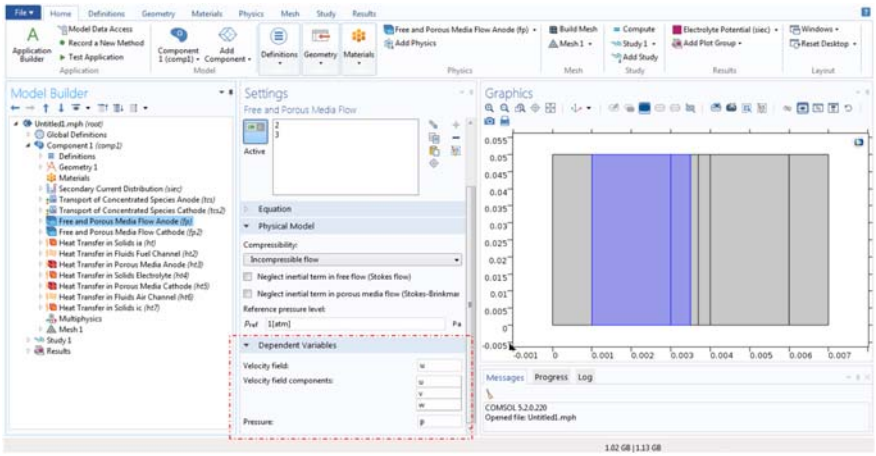

FIGURE A.21

Dependent variables (Fuel Channel Free and Porous Media Flow Physics).

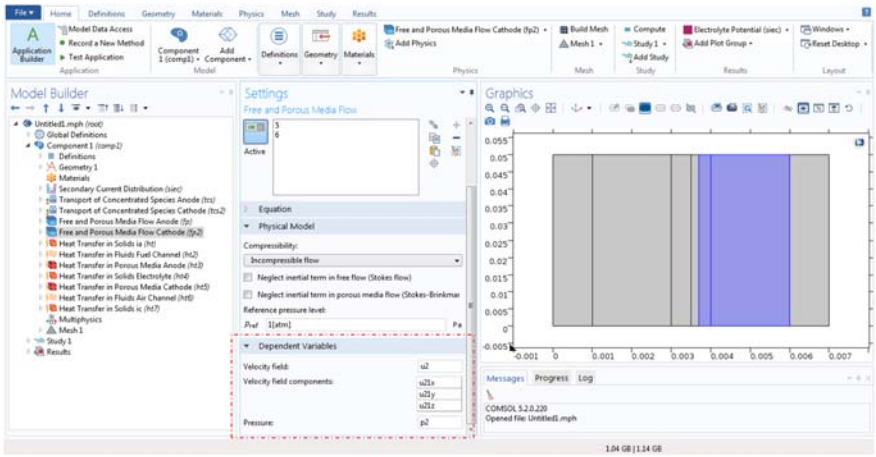

FIGURE A.22

Dependent variables (Air Channel Free and Porous Media Flow Physics).

A.6 Physics selection and boundary or interfacial conditions for the solid oxide fuel cell domains

The next step is to specify the physics of each geometric object. Table A.7 lists the physics for the seven domains of the planar SOFC as shown in Fig. A.1.

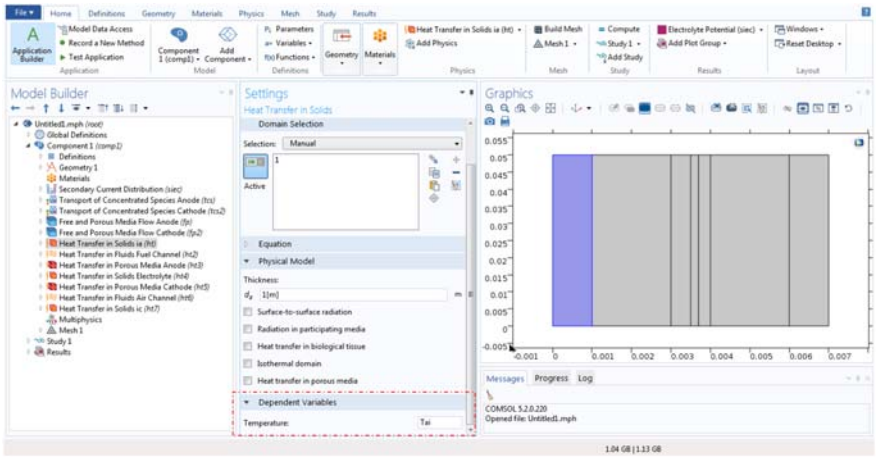

FIGURE A.23

Dependent variables (Anode Interconnect Heat-Transfer Physics).

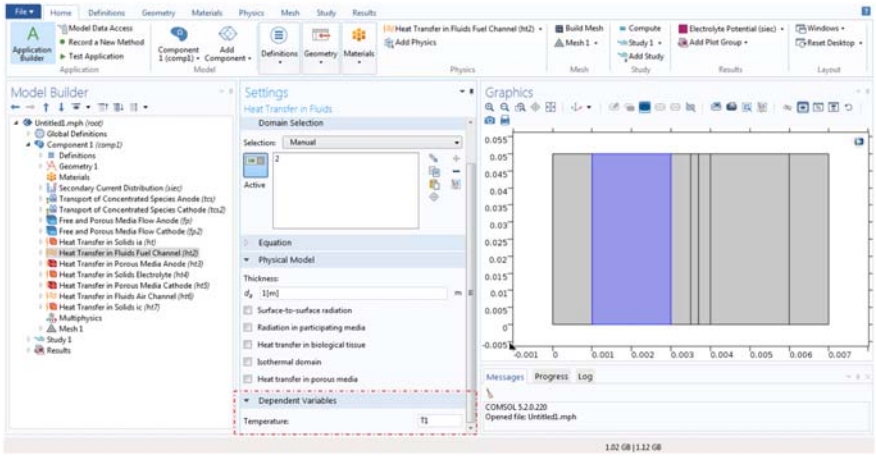

FIGURE A.24

Dependent variables (Fuel Channel Heat-Transfer Physics).

The boundary (*BC*) and interfacial (*IFC*) conditions are specified for all the external boundaries as well as for the internal interfaces of the SOFC computational domain. As can be seen in Fig. A.30 there is a total of 22 distinct surfaces, 16 of which are external boundaries and 6 of which are internal interfaces. The BCs and IFCs will be presented next for the mass, energy, and charge transport models, separately.

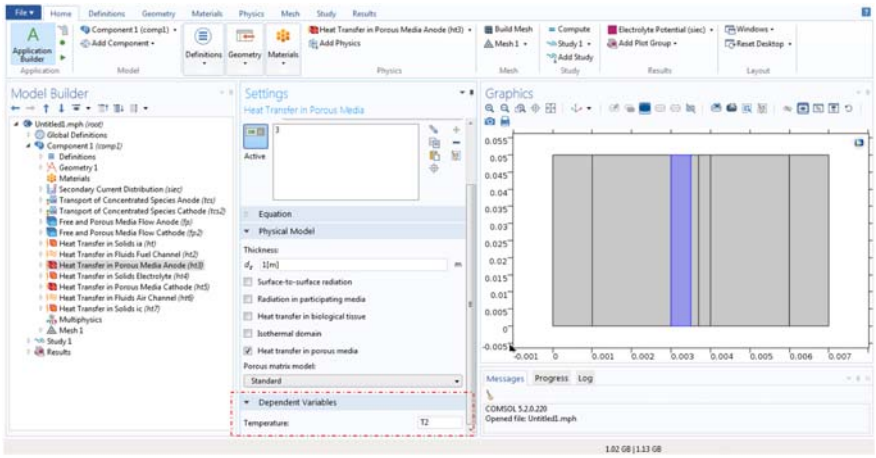

FIGURE A.25

Dependent variables (Anode Porous Electrode Heat-Transfer Physics).

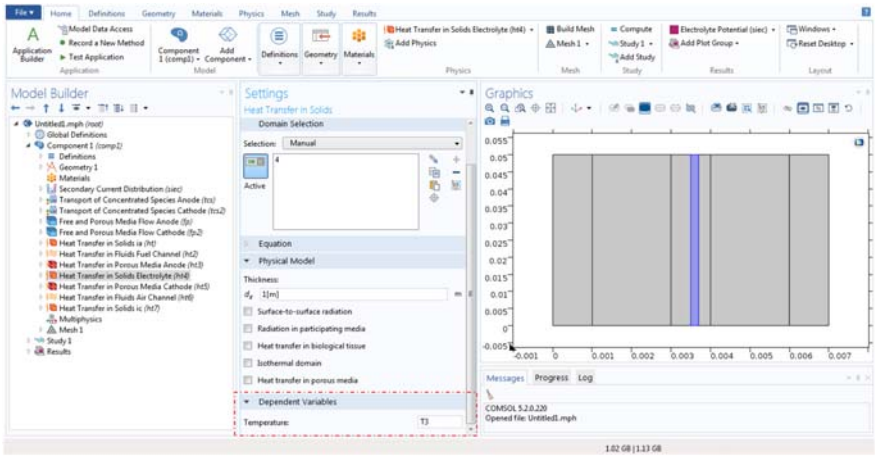

FIGURE A.26

Dependent variables (Electrolyte Heat-Transfer Physics).

A.6.1 Electrochemical cell domains (anode/cathode/electrolyte) physics and boundary conditions

An electrolytic cell has three component domains, namely an electrolyte and two electrodes (a cathode and an anode) that allow positively charged hydrogen ions (protons) to move between the two sides of the SOFC. At the anode, fuel is oxidized and then generates electrons. The electrons flow from the anode to the cathode through the electrolyte. At the cathode hydrogen ions, electrons, and oxygen react to

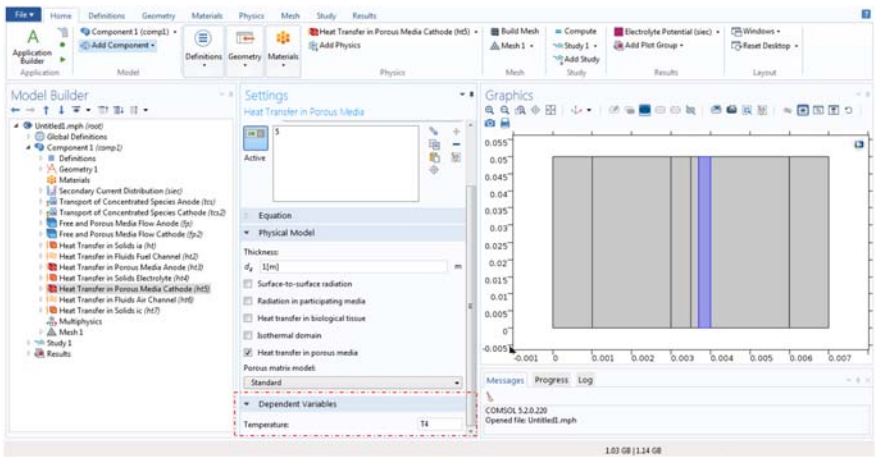

FIGURE A.27

Dependent variables (Cathode Heat-Transfer Physics).

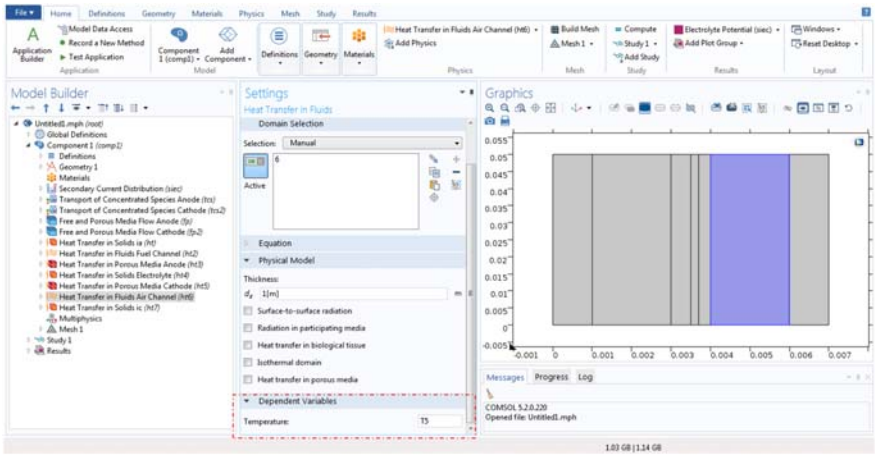

FIGURE A.28

Dependent variables (Air Channel Heat-Transfer Physics).

form water. The created voltage and current densities corresponding to the electrochemical reactions are computed by the *Current Density Distribution* physics. The electrochemical reactions that take place at the planar SOFC electrodes are:

$$\text{Anode side}: \quad H_2 + O^{2-} \rightarrow H_2O + 2e^-$$

$$\text{Cathode side}: \quad 1/2O_2 + 2e^- \rightarrow O^{2-}$$

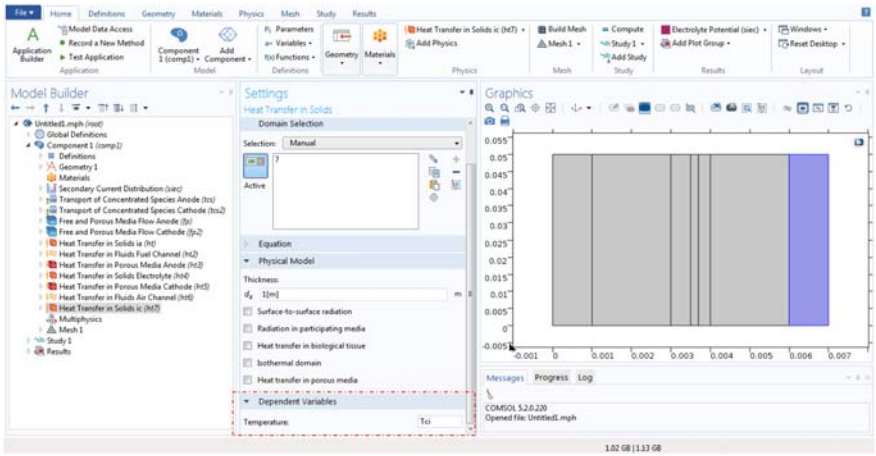

FIGURE A.29

Dependent variables (Cathode Interconnect Heat-Transfer Physics).

A.6.1.1 Current density distribution physics

The electric potential is defined as *phis* at the two electrode subdomains and the electrolyte potential *phil* at the electrolyte subdomain are calculated by solving the charge-conservation equation. The governing equations which describe the charge conservation are:

$$\frac{\partial \rho_l}{\partial t} = -\nabla.(\sigma_l \nabla \varnothing_l) + Q_l \tag{A.1}$$

$$\frac{\partial \rho_s}{\partial t} = -\nabla.(\sigma_s \nabla \varnothing_s) + Q_s \tag{A.2}$$

where ρ_l and ρ_s are the electric and ionic charge densities, respectively. σ_l refers to the effective electric conductivity of the electrodes and σ_s refers to the ionic conductivity of the electrolyte. $\varnothing_l$ and $\varnothing_s$ are the electric and ionic voltage, and Q_l and Q_s represent the electric and ionic charge sources, respectively.

As shown in Fig. A.31 by the highlighted areas, for the *Current Density Distribution* physics in the *Graphics* section, select the three domains of the anode, cathode, and electrolyte.

As shown in Fig. A.32 the variable *ec* stands for the *electrolyte conductivity* in the *Electrolyte* section.

In Fig. A.33 the anode porous electrode is selected and its main specifications such as *electrolyte conductivity* (*eea*) and *electrical conductivity* (*sea*) are defined. *No correction* is chosen for the *effective conductivity correction*.

As shown in Fig. A.34, by scrolling down in the *Settings* section, the *porous electrode reaction* specification for the anode is defined. The temperature and *anode equilibrium potential* are defined as *T* and *Eeq_a*. In the kinetic-expression

Table A.7 The physics associated with the seven domains of the planar solid oxide fuel cell.

Domains	Related physics	Variables	Boundary/interfacial conditions
Anode interconnects	Heat Transfer in Solids	Temperature profile (*Tai*)	$IFC4: -n(-k_{AIC}\nabla T_{AIC}) = h_{FC/AIC}(T_{FC} - T_{AIC})$
Fuel channel	Transport of Concentrated Species	Mass fraction of H_2 (wH_2) Mass fraction of H_2O (wH_2O)	$BC5: x_i^{FC} = x_i^{In} \cdot i = H_2.H_2O$ $BC6: J_i^{FC} = 0 \cdot i = H_2.H_2O$ $IFC7: x_i^{FC} = x_i^{AE} N_i^{FC} = N_i^{AE} \cdot i = H_2 \cdot H_2O$
	Free and Porous Media Flow	Velocity profile (u) Pressure profile (p)	$BC5: u_i^{FC} = u_i^{In} \cdot i = H_2 \cdot H_2O$ $BC6: p_i^{FC} = 0 \cdot i = H_2 \cdot H_2O$
	Heat Transfer in Fluids	Temperature profile ($T1$)	$BC5: T_{FC} = T_{FC}^{In}$ $BC6: -n(-k_{FC}\nabla T_{FC}) = 0$ $IFC4: -n(-k_{AIC}\nabla T_{AIC}) = h_{FC/AIC}(T_{FC} - T_{AIC})$ $IFC7: -n(-k_{AE}\nabla T_{AE}) = h_{FC/AE}(T_{FC} - T_{AE})$
Anode electrode	Secondary Current Distribution	Electrode potential ($phis$)	$IFC7: V_{el} = 0$
	Transport of Concentrated Species	Mass fraction of H_2 (wH_2) Mass fraction of H_2O (wH_2O)	$IFC10: N_{H_2}^{AE} = -\frac{I_C^{AE}}{2F}$ $IFC10: N_{H_2O}^{AE} = +\frac{I_C^{AE}}{2F}$
	Free and Porous Media Flow	Velocity profile (u) Pressure profile (p)	$IFC10: \rho\nabla \cdot u^{AE} = \frac{I_C^{AE} M_{H_2}}{2F} - \frac{I_C^{AE} M_{H_2O}}{2F}$
	Heat Transfer in Porous Media	Temperature profile ($T2$)	$IFC7: -n(-k_{AE}\nabla T_{AE}) = h_{FC/AE}(T_{FC} - T_{AE})$ $IFC10: -n(-k_{AE}\nabla T_{AE}) = h_{EL/AE}(T_{AE} - T_{EL})$

Electrolyte	Secondary Current Distribution	Electrolyte potential (*phil*)	*IFC*10: $-n(-\sigma\nabla V_{el}) = -I_C^{AE} = -I_0^{AE}\left[\exp\left(a^{AE}\frac{n_e F}{RT}\eta^{AE}\right) - \exp\left(-\left(1-a^{AE}\right)\frac{n_e F}{RT}\eta^{AE}\right)\right]$
			*IFC*10: $-n(-\sigma\nabla V_{io}) = -I_C^{AE} = -I_0^{AE}\left[\exp\left(a^{AE}\frac{n_e F}{RT}\eta^{AE}\right) - \exp\left(-\left(1-a^{AE}\right)\frac{n_e F}{RT}\eta^{AE}\right)\right]$
			*IFC*13: $-n(-\sigma\nabla V_{el}) = -I_C^{CE} = -I_0^{CE}\left[\exp\left(a^{CE}\frac{n_e F}{RT}\eta^{CE}\right) - \exp\left(-\left(1-a^{CE}\right)\frac{n_e F}{RT}\eta^{CE}\right)\right]$
			*IFC*13: $-n(-\sigma\nabla V_{io}) = -I_C^{CE} = -I_0^{CE}\left[\exp\left(a^{CE}\frac{n_e F}{RT}\eta^{CE}\right) - \exp\left(-\left(1-a^{CE}\right)\frac{n_e F}{RT}\eta^{CE}\right)\right]$
	Heat Transfer in Solids	Temperature profile (*T3*)	*IFC*10: $-n(-k_{AE}\nabla T_{AE}) - n(-k_{EL}\nabla T_{EL}) = \frac{I_C^{AE}}{2F}T\Delta S^{AE} + I_C^{AE}\eta_{act}^{AE}$
			*IFC*13: $-n(-k_{EL}\nabla T_{EL}) - n(-k_{CE}\nabla T_{CE}) = \frac{I_C^{CE}}{2F}T\Delta S^{CE} + I_C^{CE}\eta_{act}^{CE}$
Cathode electrode	Secondary Current Distribution	Electrode potential (*phis*)	*IFC*16: $V_{el} = V_C$
	Transport of Concentrated Species	Mass fraction of O_2 (*wO2*) Mass fraction of N_2 (*wN2*)	*IFC*13: $N_{O_2}^{CE} = -\frac{I_C^{CE}}{4F}$
	Free and Porous Media Flow	Velocity profile (*u2*) Pressure profile (*p2*)	*IFC*13: $\rho\nabla\cdot u^{CE} = -\frac{I_C^{CE}M_{O_2}}{4F}$
	Heat Transfer in Porous Media	Temperature profile (*T4*)	*IFC*13: $-n(-k_{CE}\nabla T_{CE}) = h_{EL}(T_{AC} - T_{EL})$
			*IFC*16: $-n(-k_{CE}\nabla T_{CE}) = h_{AC/CE}(T_{AC} - T_{CE})$
Air channel	Transport of Concentrated Species	Mass fraction of O_2 (*wO2*) Mass fraction of N_2 (*wN2*)	*BC*17: $x_j^{AC} = x_j^{In}\cdot j = O_2\cdot N_2$ *BC*18: $J_j^{AC} = 0\cdot j = O_2\cdot N_2$ *IFC*16: $x_j^{AC} = x_j^{CE}N_j^{AC} = N_j^{CE}\cdot j = O_2\cdot N_2$
	Free and Porous Media Flow	Velocity profile (*u2*) Pressure profile (*p2*)	*BC*17: $u_j^{AC} = u_j^{In}\cdot j = O_2\cdot N_2$ *BC*18: $p_j^{AC} = 0\cdot j = O_2\cdot N_2$
	Heat Transfer in Fluids	Temperature profile (*T5*)	*BC*17: $T_{AC} = T_{AC}^{In}$ *BC*18: $-n(-k_{AC}\nabla T_{AC}) = 0$ *IFC*16: $-n(-k_{CE}\nabla T_{CE}) = h_{AC/CE}(T_{AC} - T_{CE})$ *IFC*19: $-n(-k_{ClC}\nabla T_{ClC}) = h_{AC/ClC}(T_{AC} - T_{ClC})$
Cathode interconnect	Heat Transfer in Solids	Temperature profile (*Tcl*)	*IFC*19: $-n(-k_{ClC}\nabla T_{ClC}) = h_{AC/ClC}(T_{AC} - T_{ClC})$

BC, *Boundary condition;* IFC, *interfacial condition.*

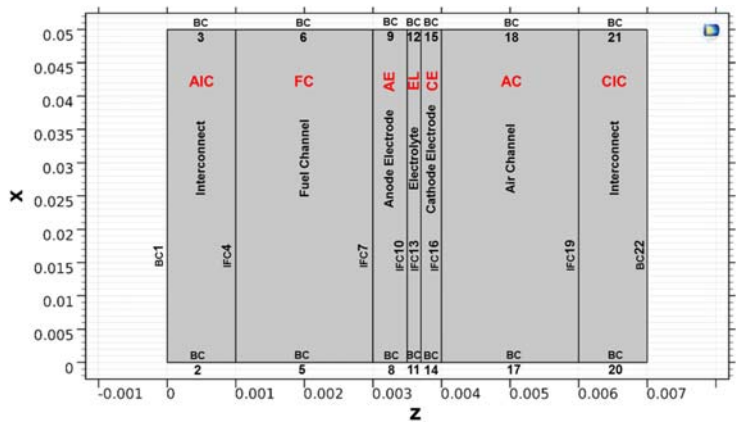

FIGURE A.30

Schematic of the subdomains, boundaries, and interfaces of a planar solid oxide fuel cell [1].

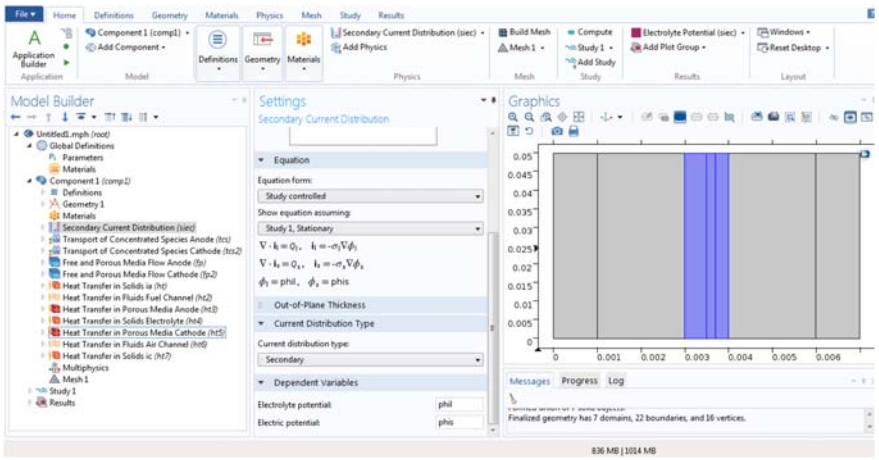

FIGURE A.31

Secondary Current Distribution physics.

type, *Butler−Volmer* is chosen. The *Butler−Volmer* parameters of *exchange current density* (*i0a*), *anode transfer coefficient*, *cathodic transfer coefficient*, and *active specific surface area* (*ssa*) are specified.

Similarly, as shown in Fig. A.35, in the *porous electrode* section the main specifications of the cathode, namely *electrolyte conductivity* (*eec*) and *electrical conductivity* (*sec*), are defined.

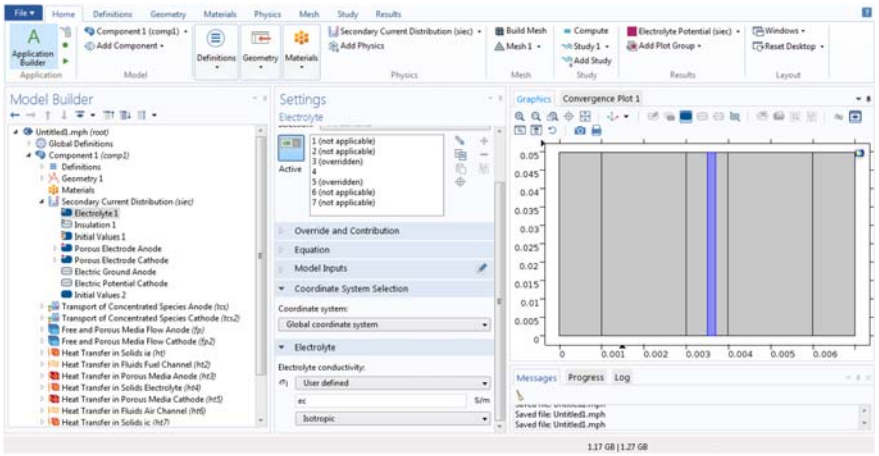

FIGURE A.32

Electrolyte specifications.

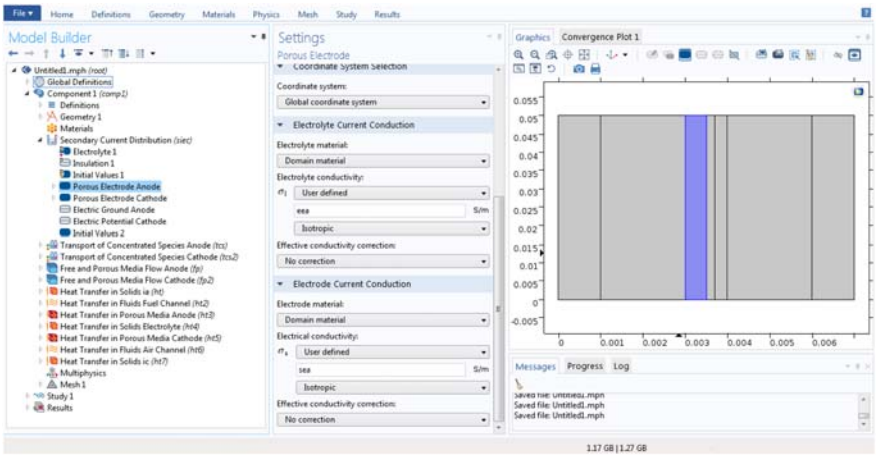

FIGURE A.33

Anode porous electrode specifications.

As shown in Fig. A.36, by scrolling down in the *Settings* section, in the *porous electrode reaction* specification the reaction kinetics of the cathode domain can be specified. The temperature and cathode *equilibrium potential* are defined as *T* and *Eeq_c*. In the drop-down menu of the *kinetic-expression type*, select the *Butler−Volmer* option. *Butler−Volmer* parameters, namely *exchange current density* (*i0c*), *anodic transfer coefficient, cathodic transfer coefficient*, and *active specific surface area* (*ssc*), are defined.

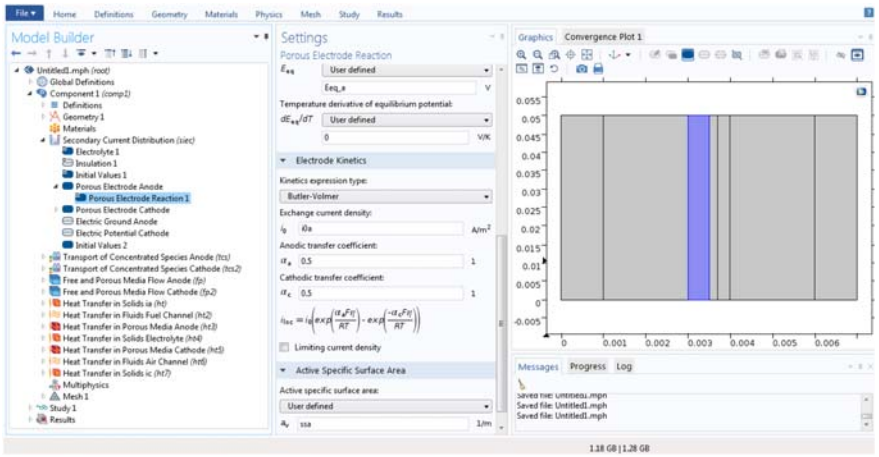

FIGURE A.34

Electrochemical reaction of anode porous electrode.

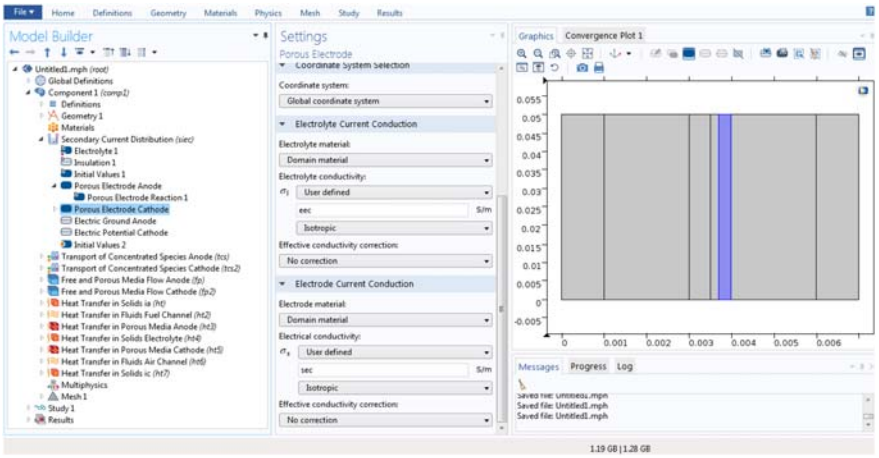

FIGURE A.35

Cathode porous electrode specifications.

As shown in Figs. A.37 and A.38, under the *Physics* tab, click *Electrode Boundaries* and choose *Electric Ground* and *Electric Potential* and select boundaries 7 and 16, respectively.

As shown in Fig. A.38, under the *Settings* window for *Electric Potential* locate the *Electric Potential* section and in the $\phi_{s,bnd}$ text field, type *Vcell*.

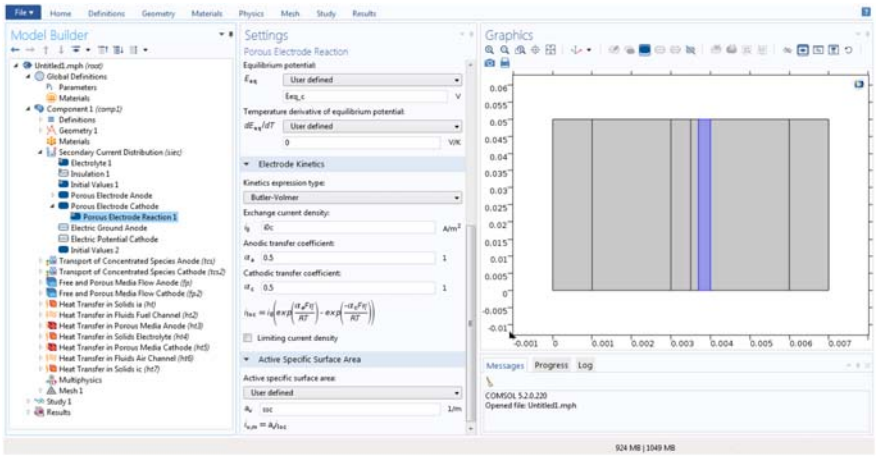

FIGURE A.36

Electrochemical reaction of cathode porous electrode.

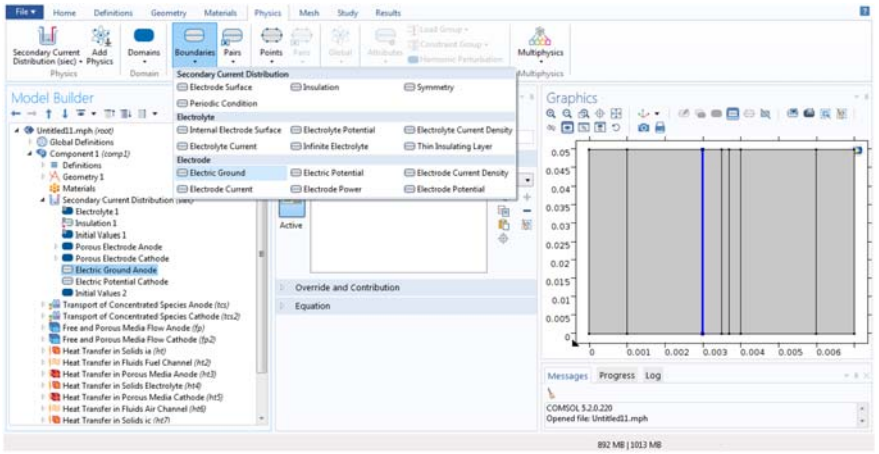

FIGURE A.37

Anode electric ground.

As shown in Fig. A.39, under the *Physics* tab click *Domains* and choose *Initial Values*. In the settings window for *Initial Values* select the cathode domain, then type *0* and *Vcell* in the *phil* and *phis* text fields, respectively.

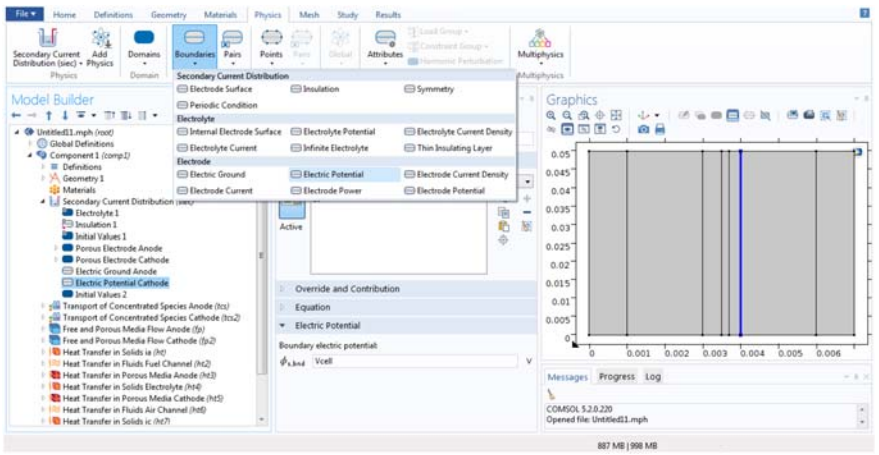

FIGURE A.38

Cathode electric potential.

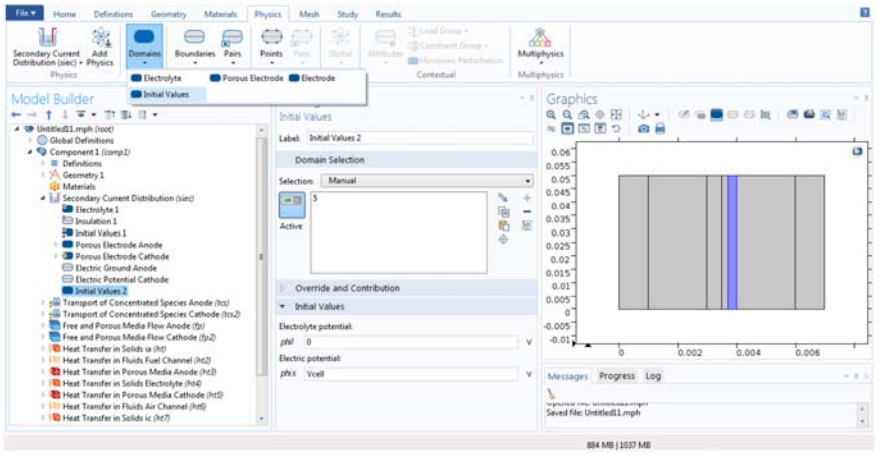

FIGURE A.39

Electrolyte potential initial values.

A.6.2 Mass transport phenomena

The involved physics and associated boundaries in the modeling of the mass transport phenomena are listed in Tables A.1 and A.7, respectively. The *Concentrated Species* physics was applied in all the involved elements including the anode, cathode, and fuel and air channels.

A.6.2.1 Transport of Concentrated Species in the anode electrode and fuel channel domains

As highlighted in Fig. A.40 the *Concentrated Species* physics is set up for the anode and fuel channels. The oxygen atoms from the cathode porous electrode penetrate the electrolyte and through their reaction with the hydrogen atoms produce water. The reaction between oxygen and hydrogen atoms occurs in the anode porous media. The water product is transported through the anode porous electrode and is released to the fuel channel.

As shown in Fig. A.40, in order to specify the transport of mass species in the porous domain, select domains 2 and 3 from the *Graphics* window, corresponding to the fuel channel and anode porous electrode, respectively. Then in the *Settings* window for the *transport of Concentrated Species* locate the *transport mechanisms* section. From the *Diffusion Model* drop-down menu, choose *Maxwell−Stefan*. In the *Species* section, from the drop-down menu named *From Mass Constraint*, choose wH_2O.

As shown in Fig. A.41 in the *Model Builder* window, expand the *Transport of Concentrated Species Anode* branch, then click *Transport Properties 1*. In the settings window for *transport properties* of the anode, locate the *density* and *diffusion* sections and in the text fields set up the *Mh2*, *Mh2o*, and *Dh2h2oeff*.

As shown in Fig. A.42, under the *Physics* tab, click *Domains* and choose *Transport Properties*. Under *Transport Properties 2* for the fuel channel, locate the *Density* and *Diffusion* sections and in the text fields set up the *Mh2*, *Mh2o*, and *Dh2h2o*. The *velocity field*, *temperature*, and *absolute pressure* are coupled with free and porous media flow and Heat Transfer in Fluids physics.

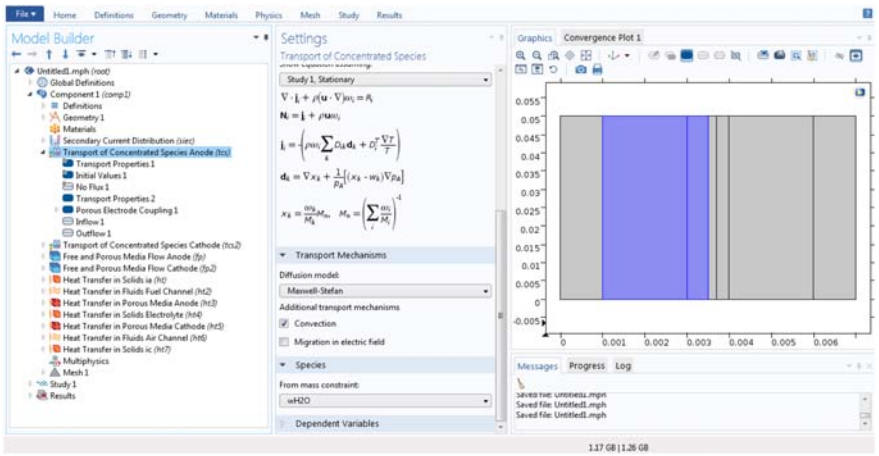

FIGURE A.40

Transport of Concentrated Species (anode side).

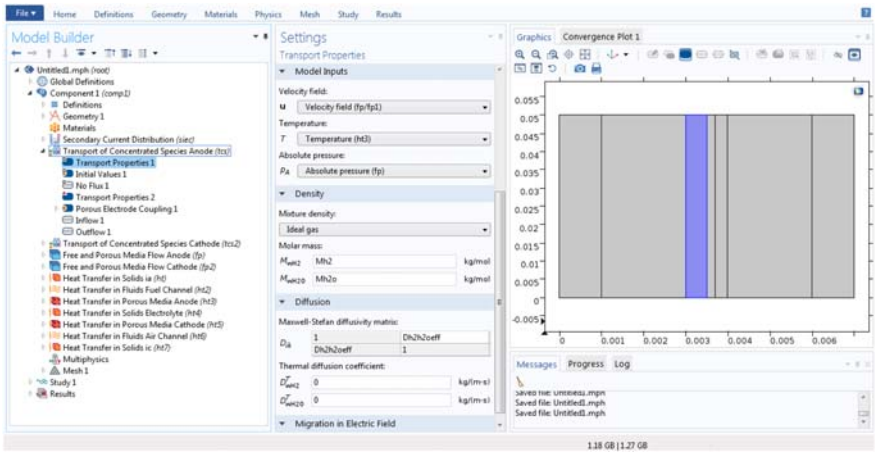

FIGURE A.41

Anode transport properties.

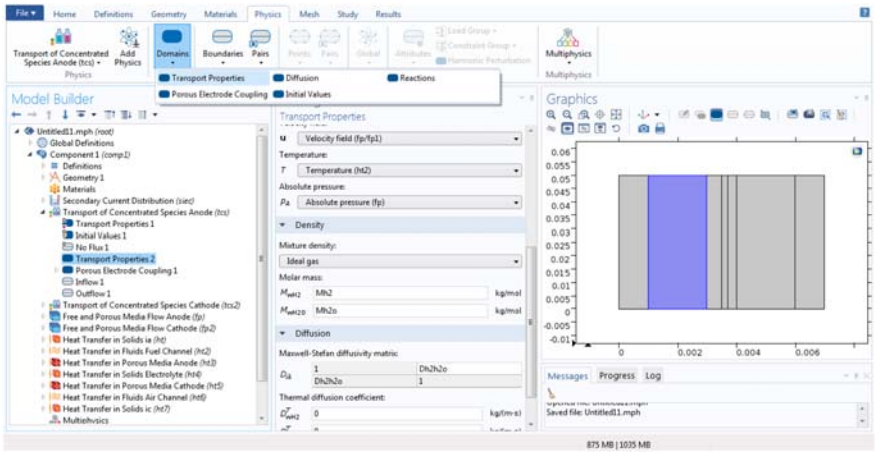

FIGURE A.42

Fuel channel transport properties.

Since in planar SOFCs the reaction between oxygen and hydrogen atoms occurs only in the anode porous electrode, the reaction coefficients are defined in this domain. As shown in Fig. A.43, under the *Physics* tab click *Domains* and choose *Porous Electrode Coupling*. Expand the *Porous Electrode Coupling 1* and click *Reaction Coefficients 1*. Then under the settings window for *Reaction Coefficients*, locate the *Model Inputs* section and under the *Coupled Reaction*

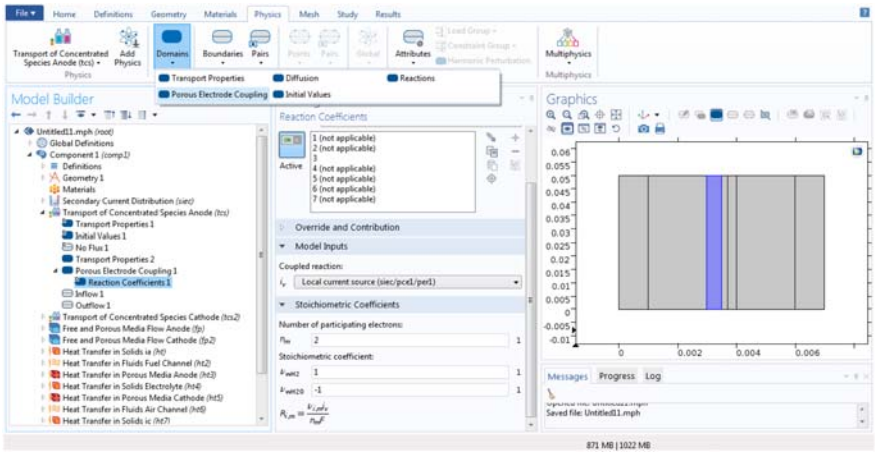

FIGURE A.43

Reaction coefficient coupling of anode porous electrode.

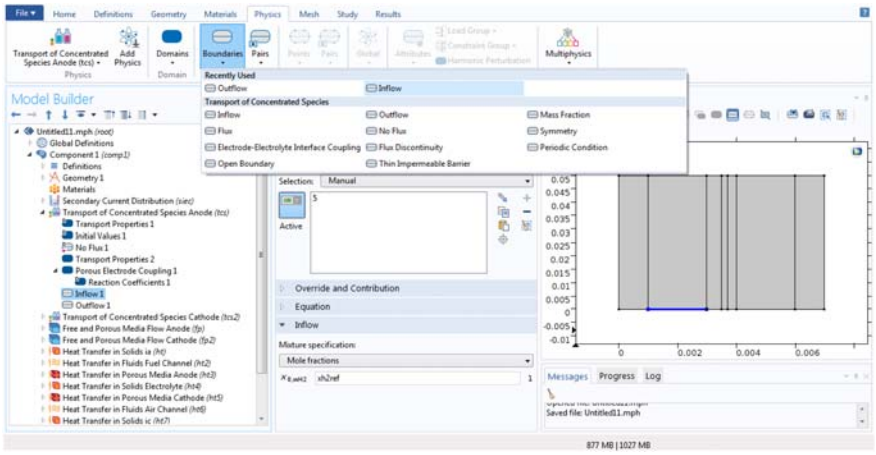

FIGURE A.44

Fuel inflow boundary condition.

drop-down menu, choose the *Local Current Source* (*siec/pce1/per1*) option. In the *Stoichiometric Coefficients* section, specify 2 as the *number of participating electrons*, and in the v_{wH2}, v_{wH2O} text fields, specify 1 and −1, respectively.

As shown in Figs. A.44 and A.45, under the *Physics* tab click *Boundaries* and choose the *Inflow* and *Outflow* commands, select the boundaries 5 and 6 (as shown in Fig. A.30). Under the *Inflow* section, locate the *Mixture Specification* and type *xh2ref* in the text field, as the mole fraction of H_2 in the inlet flow.

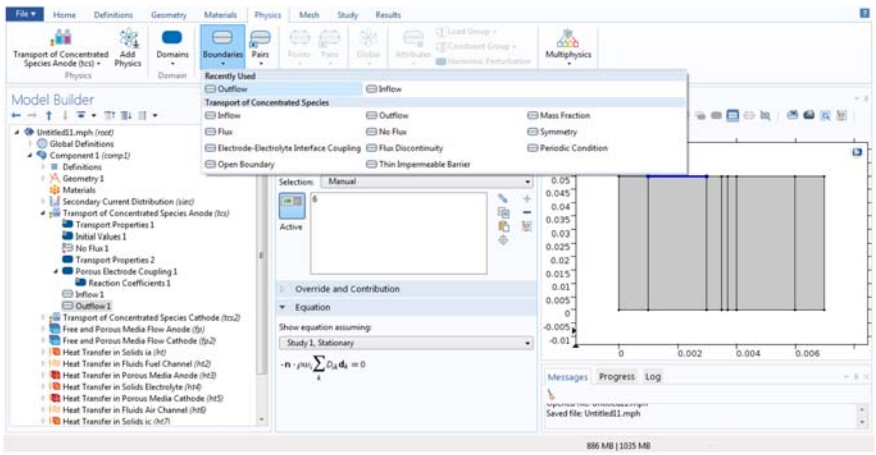

FIGURE A.45

Fuel outflow boundary condition.

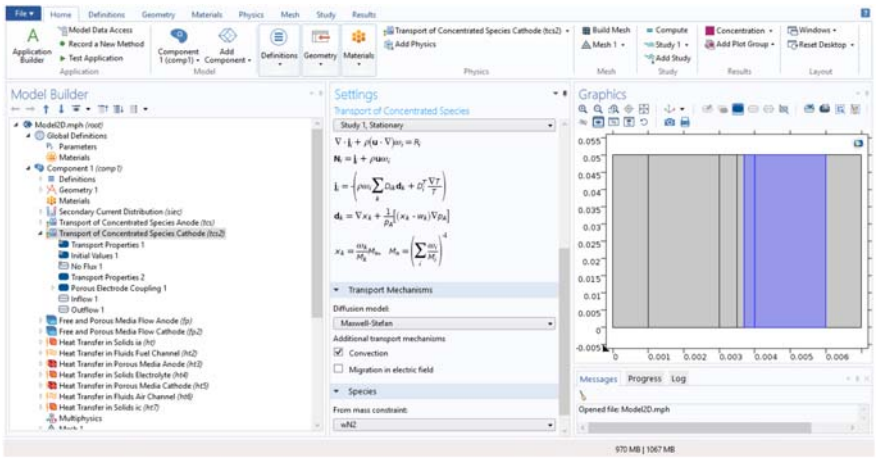

FIGURE A.46

Transport of Concentrated Species (Cathode side).

A.6.2.2 Transport of Concentrated Species in the cathode electrode and air channel domains

Similarly to the process applied for the anode domain, we need to set up the mass transport model for the cathode porous electrode domain. The porous electrode reaction consisting of the ionization of oxygen atoms gives rise to species mass transport in the cathode porous electrode domain. As shown in Fig. A.46, under

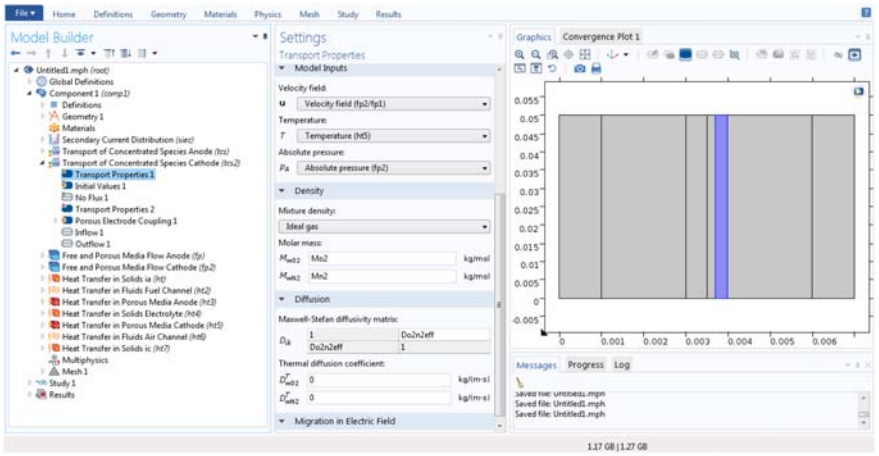

FIGURE A.47

Cathode transport properties.

the *Graphics* window select domains 5 and 6 for the air channel and cathode porous electrode, respectively. In the *Settings* window for *Transport of Concentrated Species* locate the *Transport Mechanisms* section. From the *Diffusion Model* drop-down menu, choose *Maxwell−Stefan*. Under the *Species* section, from the *From Mass Constraint* drop-down menu, choose *wN2*.

In the *Model Builder* window, expand the *Transport of Concentrated Species Cathode* and click *Transport Properties 1*. In the *Settings* window for *Transport Properties* of the cathode, locate the *Density* and *Diffusion* sections, and in the text fields specify *Mo2*, *Mn2*, and *Do2n2eff*, respectively, as shown in Fig. A.47.

As shown in Fig. A.48, under the *Physics* tab click *Domains* and choose *Transport Properties*. In *Transport Properties 2* for the *Air Channel* locate the *Density* and *Diffusion* sections and in the text fields specify *Mo2*, *Mn2*, and *Do2n2*, respectively. The *velocity field*, *temperature*, and *absolute pressure* are coupled with *Free and Porous Media Flow* and *Heat Transfer in Fluids* physics.

In the cathode porous electrode domain, we need to specify the ionization of oxygen reactions. As shown in Fig. A.49, under the *Physics* tab click *Domains* and choose *Porous Electrode Coupling*. Expand the *Porous Electrode Coupling 1* window and click *Reaction Coefficients 1*. Then under the *Settings* window for *Reaction Coefficients* locate the *Model Inputs* section and choose the *Local Current Source* (*siec/pce2/per1*). In the *Stoichiometric Coefficients* section specify 4 as a *Number of Participating Electrons* and in the v_{wO2}, v_{wN2} text fields specify −1 and 0, respectively.

As shown in Figs. A.50 and A.51, under the *Physics* tab click *Boundaries* and choose *Inflow* and *Outflow* commands, select boundaries 17 and 18 (as shown in Fig. A.30). Locate the *Mixture Specification* option and specify *xo2ref* in the text field as the mole fraction of O_2 in the inlet flow.

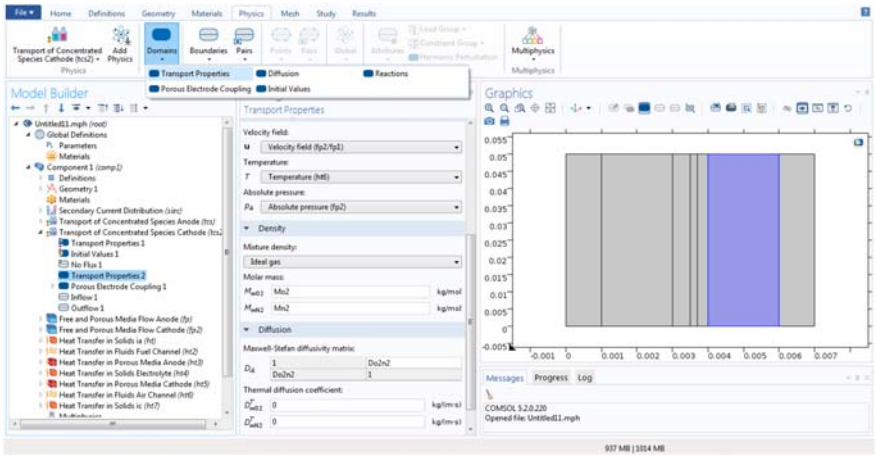

FIGURE A.48

Air channel transport properties.

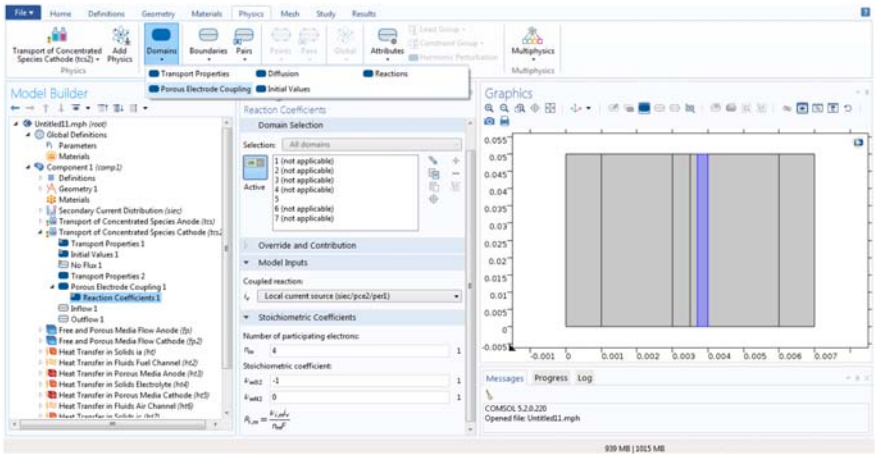

FIGURE A.49

Reaction coefficient coupling of cathode porous electrode.

A.6.3 Momentum transport phenomena

The momentum transfer should be specified for the anode and cathode porous electrodes, as well as the fuel and air channels. The required procedure is discussed in Section A.6.3.1.

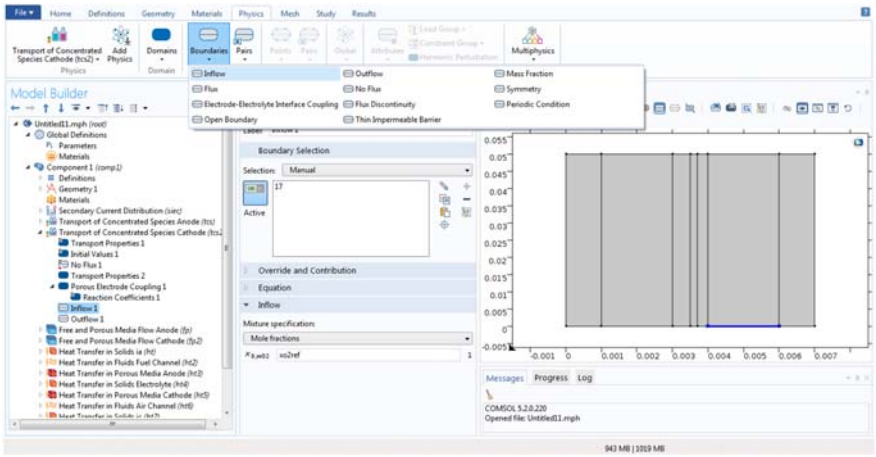

FIGURE A.50

Air-inflow boundary condition.

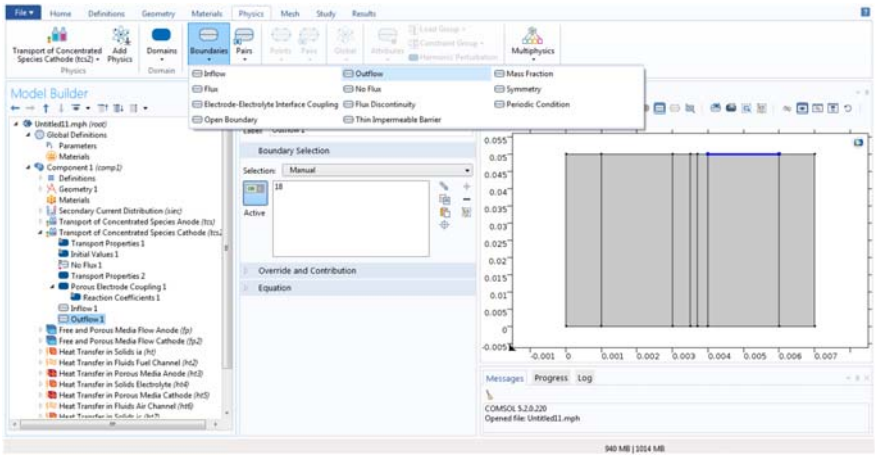

FIGURE A.51

Air-outflow boundary condition.

A.6.3.1 Free and Porous Media Flow in anode electrode and fuel channel domains

As shown in Fig. A.52 in order to set up the convective flow model on the anode domain, first select domains 2 and 3 for fuel channel and anode porous electrode in the *Graphics* window. Then, in the *Settings* window for *Free and Porous Media Flow*, locate the *Physical Model* section. In the *Compressibility* drop-down menu, choose *Incompressible Flow* ($Ma < 0.3$) and define the *Reference Pressure Level*.

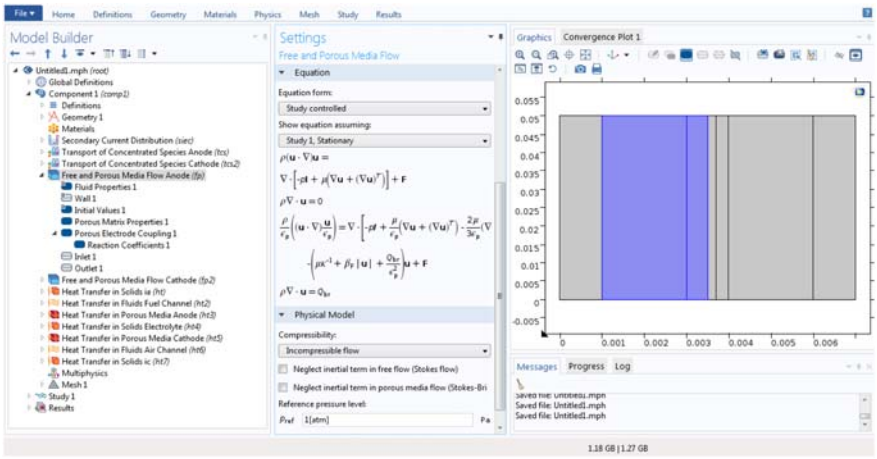

FIGURE A.52

Free and Porous Media Flow in the anode porous electrode and fuel channel domains.

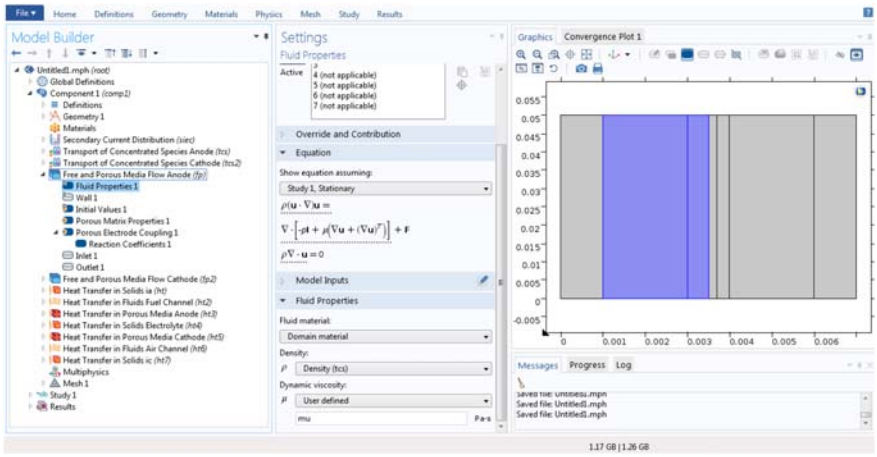

FIGURE A.53

Fuel channel and anode fluid properties.

As shown in Fig. A.53, under the *Model Builder* window expand *Free and Porous Media Flow Anode* (*fp*) and click *Fluid Properties 1*. In the *Settings* window for *Fluid Properties* of the anode, locate the *Fluid Properties* section and from the drop-down menu choose *Density* (*tcs*) for ρ, choose *User* defined for μ, and in the associated text field specify *mu*. The notation *Density* (*tcs*) implies that the density is actually calculated from the *Transport of Concentrated Species* (*tcs*) and is, in fact, coupled to that physics.

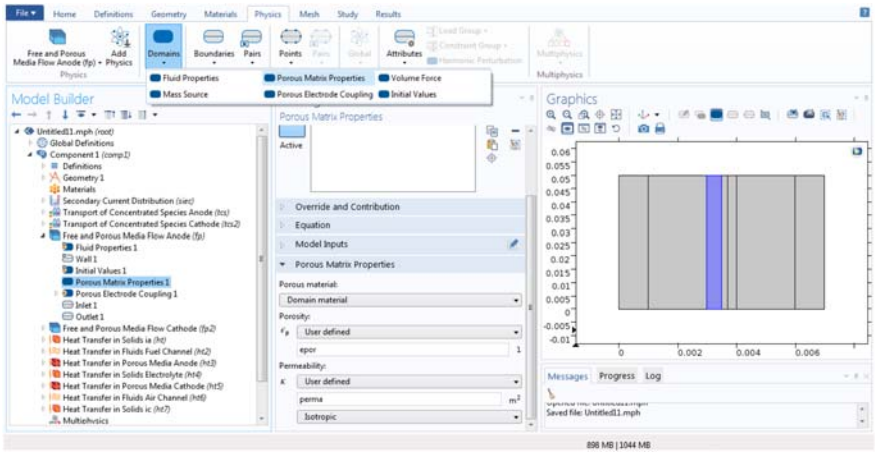

FIGURE A.54

Anode porous electrode properties.

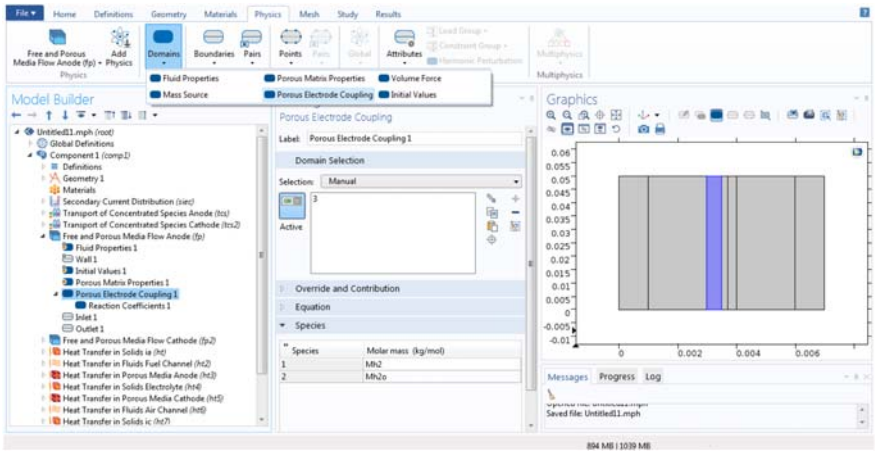

FIGURE A.55

Porous electrode coupling.

As shown in Fig. A.54, under the *Physics* tab click *Domains* and choose *Porous Matrix Properties*. In this section the *Porosity* and *Permeability* of the anode porous electrode are defined as *epor* and *perma* by the user.

As shown in Fig. A.55, under the *Physics* tab click *Domains* and choose *Porous Electrode Coupling*. Click on it and specify the *Molar Mass* of species *Mh2* and *Mh2o* in the *Species* section.

The effects of reactions on momentum transport also need to be specified. To this end, as shown in Fig. A.56, first expand the *Porous Electrode Coupling 1*, then click on *Reaction Coefficients 1*. In the *Settings* window for *Reaction*

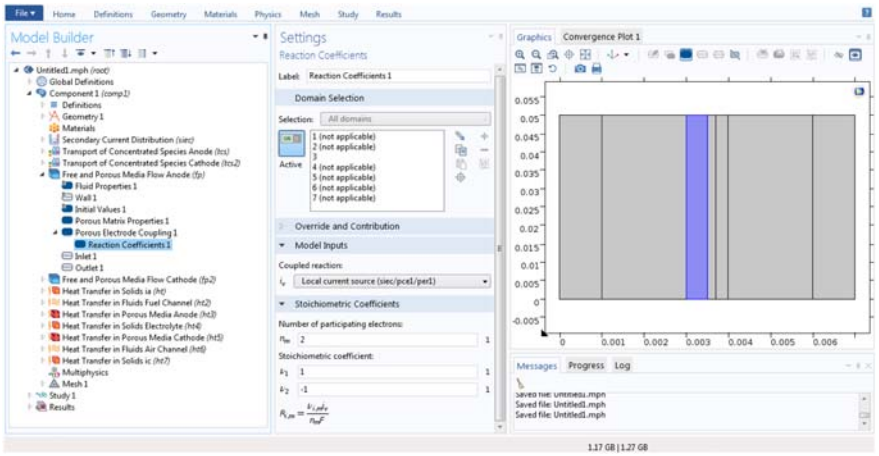

FIGURE A.56

Reaction coefficient of the anode porous electrode.

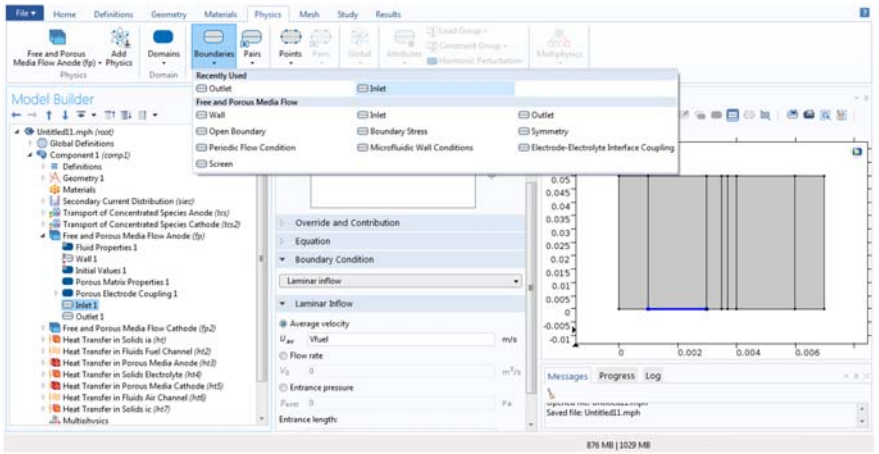

FIGURE A.57

Fuel-inlet boundary condition.

Coefficients locate the *Model Inputs* section and under the *Coupled Reaction* drop-down menu choose the *Local Current Source* (*siec/pce1/per1*). In the *Stoichiometric Coefficients* section specify 2 as the *Number of participating electrons* and in the v_{H2} and v_{H2O} text fields, specify 1 and −1, respectively.

As shown in Fig. A.57, under the *Physics* tab click *Boundaries* and choose *Inlet* and *Outlet*. Select boundaries 5 and 6 in the *Graphics* window. Locate the *Laminar Inflow* drop-down menu and choose *Average Velocity* and type *Vfuel* in the text field as a fluid-inlet velocity.

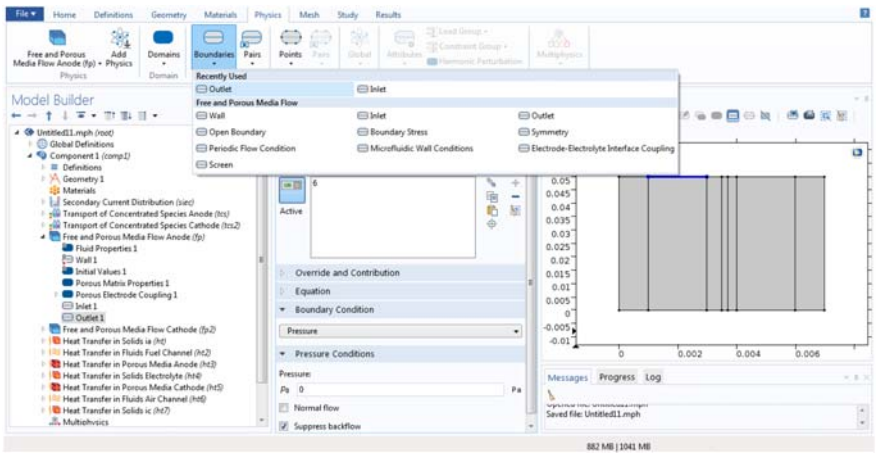

FIGURE A.58

Fuel-outlet boundary condition.

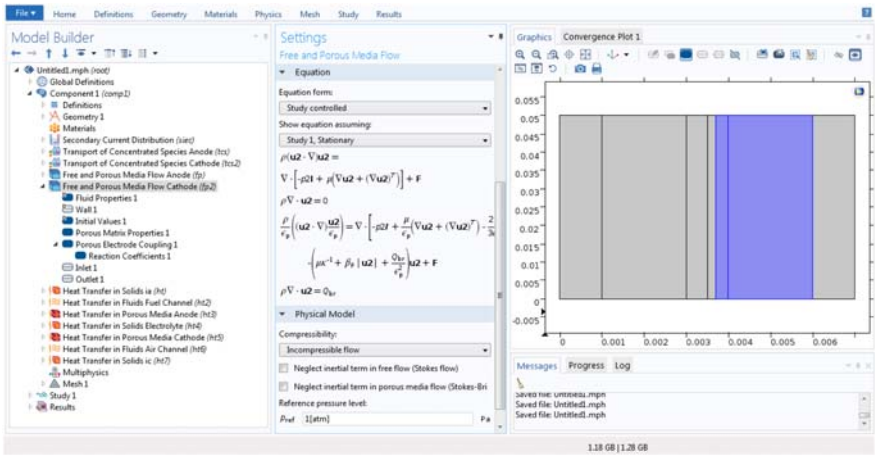

FIGURE A.59

Free and Porous Media Flow in the cathode porous electrode and air channel domains.

As shown in Fig. A.58, under the *Outlet* boundary condition, locate the *Pressure conditions*. Choose *Pressure* and specify 0 in the text field as a fluid-inlet velocity.

A.6.3.2 Free and Porous Media Flow in the cathode porous electrode and air channel domains

As shown in Fig. A.59 in order to set up the convective flow model on the cathode domain, first select domains 5 and 6 for air channel and cathode porous

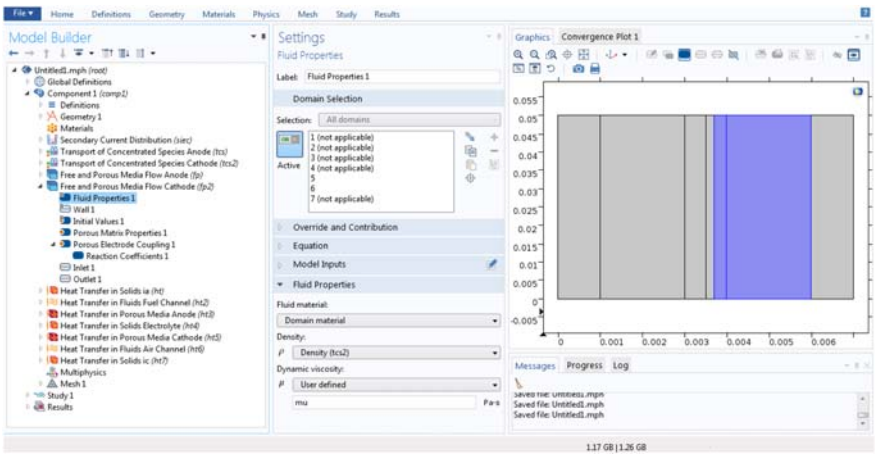

FIGURE A.60

Air channel and cathode fluid properties.

electrode in the *Graphics* window. Then in the *Settings* window for *Free and Porous Media Flow*, locate the *Physical Model* section. In the *Compressibility* drop-down menu choose *Incompressible flow* ($Ma < 0.3$) and define the *Reference Pressure Level*.

As shown in Fig. A.60, under the *Model Builder* window, expand the *Free and Porous Media Flow Cathode* (*fp2*) and click *Fluid Properties 1*. In the *Settings* window for *Fluid Properties* of the cathode locate the *Fluid Properties* section and from the drop-down menu choose *Density* (*tcs2*) for ρ and choose user defined for *Dynamic viscosity* (μ); in the associated text field specify *mu*. The notation *Density* (*tcs2*) implies that the density is actually calculated from the *Transport of Concentrated Species* (*tcs2*) and is, in fact, coupled to that physics.

As shown in Fig. A.61, under the *Physics* tab click *Domains* and choose *Porous Matrix Properties*. In the *Porous Matrix Properties* section, *Porosity* and *Permeability* of *Cathode Porous Electrode* are defined as *epor* and *permc* by the user.

As shown in Fig. A.62, under the *Physics* tab, click *Domains* and choose *Porous Electrode Coupling*. Click on it and specify the *Molar Mass* of species as *Mo2*, *Mh2o*, and *Mn2* in the *Species* section.

The effects of reactions is also need to be specified in the momentum transport. To this end, as shown in Fig. A.63, expand the *Porous Electrode Coupling 1* option and click *Reaction Coefficients 1*. In the *Settings* window for *Reaction Coefficients* locate the *Model Inputs* section and under the *Coupled Reaction* drop-down menu choose the *Local Current Source* (*siec/pce2/per1*). In the *Stoichiometric Coefficients* section specify 4 as the *Number of participating electrons* and in the v_{O2}, v_{H2O}, and v_{N2} text fields specify -1, 0, and 0, respectively.

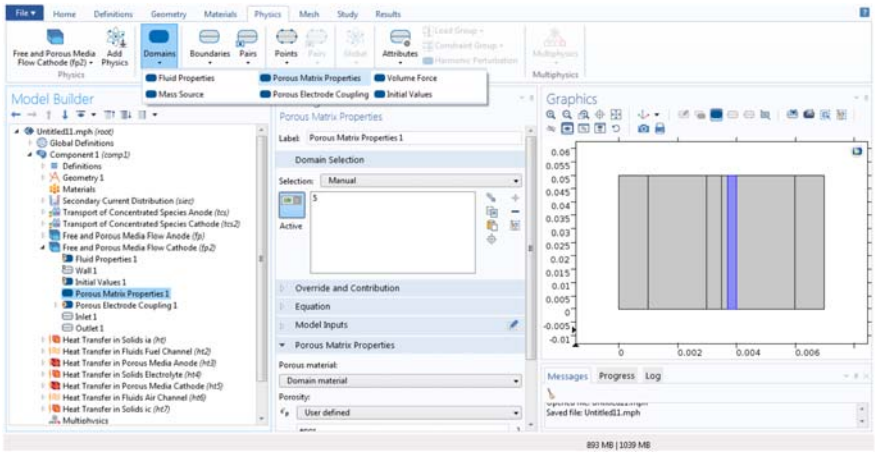

FIGURE A.61

Cathode porous electrode properties.

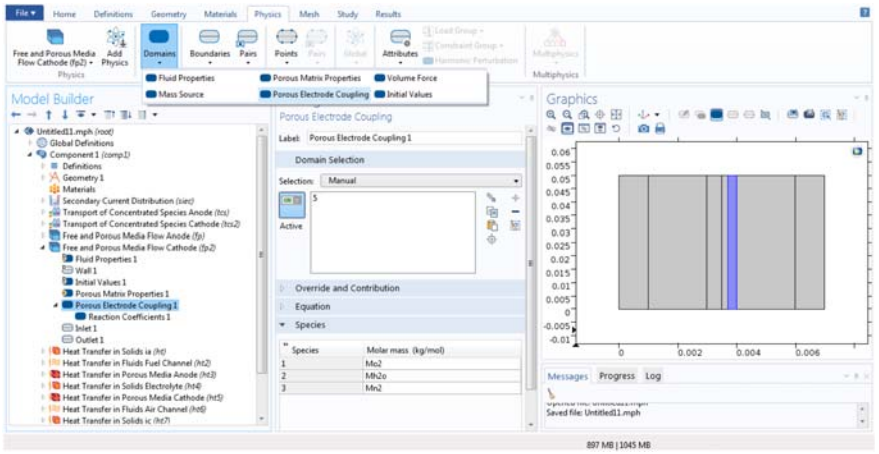

FIGURE A.62

Cathode porous electrode coupling.

As shown in Fig. A.64, under the *Physics* tab click *Boundaries* and choose *Inlet* and *Outlet* and select boundaries 17 and 18 in the *Graphics* window. Locate the *Laminar Inflow* drop-down menu, and choose *Average Velocity* and type *Vair* in the text field as a fluid-inlet velocity.

As shown in Fig. A.65, under the *Outlet* boundary condition locate the *Pressure conditions*, choose *Pressure* and specify 0 in the text field as the fluid-inlet velocity.

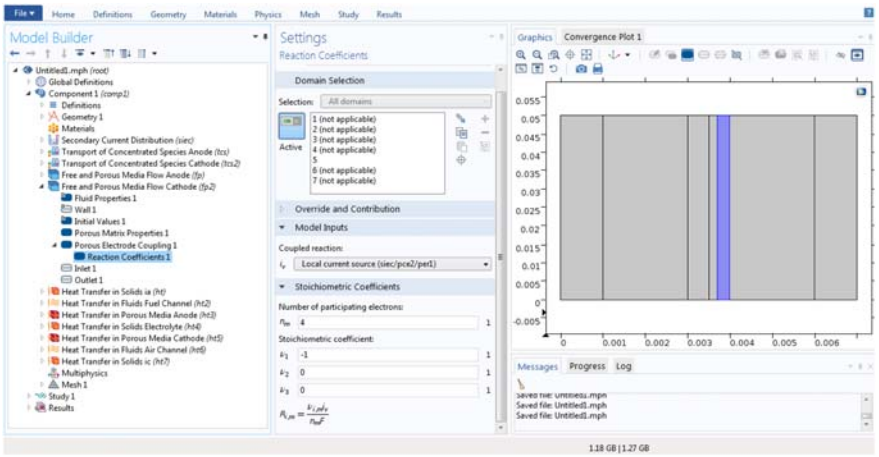

FIGURE A.63

Reaction coefficient of cathode porous electrode.

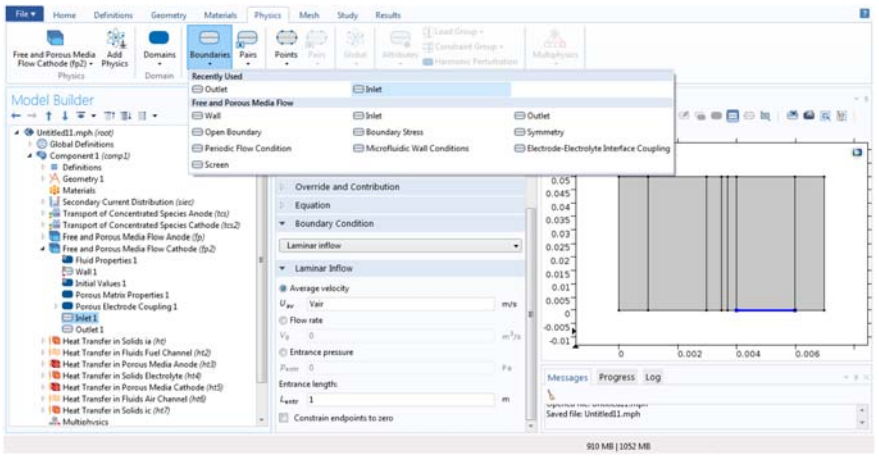

FIGURE A.64

Air channel inlet boundary condition.

A.6.4 Heat-transport phenomena

The heat-transfer phenomena involve the generation of heat at the solid electrolyte and its dissipation from the anode and cathode porous electrodes. The generated energy is transported to the air and fuel channels and eventually leaves the system through the fluid flows. The key heat-transfer mechanism in the electrolyte, anode interconnect, and cathode interconnect domains is conduction. The

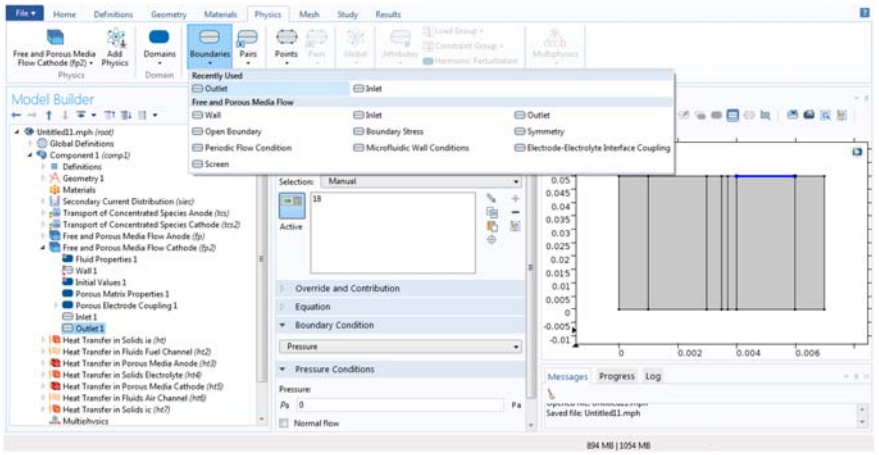

FIGURE A.65

Air channel outlet boundary condition.

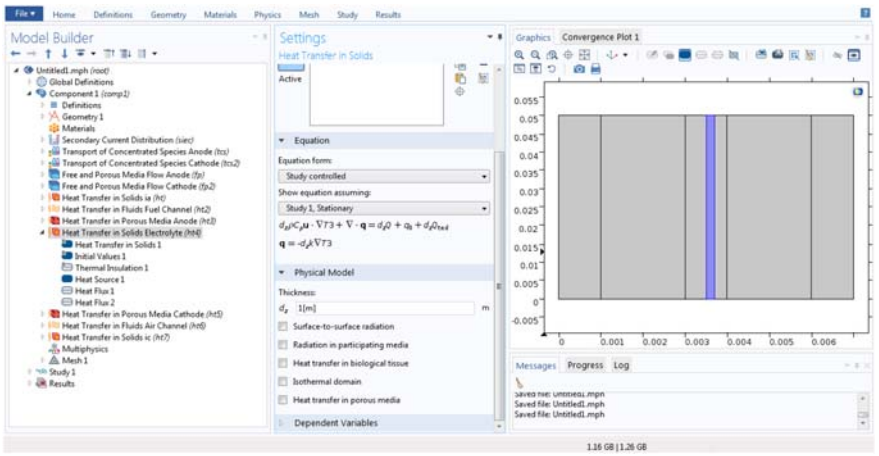

FIGURE A.66

The settings of the heat-transfer phenomena in the solid electrolyte.

key heat-transfer mechanisms in the cathode and anode porous electrodes are conduction and convention, respectively. The key heat-transfer mechanism in the air and fuel channels is convection. Specifying these physics are discussed in the following sections.

A.6.4.1 Heat transfer in the electrolyte domain

The thermal energy transport equation is solved for the solid electrolyte domain in this model as shown in Fig. A.66. The dominating phenomena in the solid

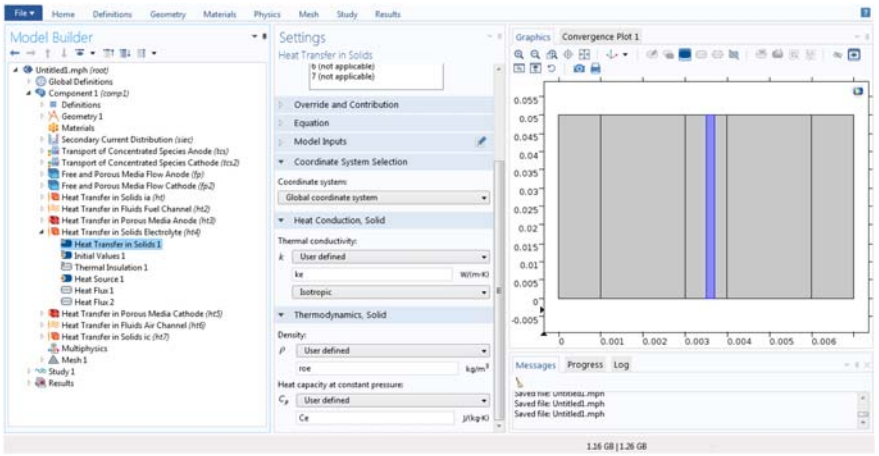

FIGURE A.67

Electrolyte heat-transfer properties.

electrolyte domain are conductive and convective heat flux, while thermal-energy transport by the radiation mechanism is negligible. The following equation describes the thermal-energy balance:

$$\frac{\partial \rho c_P T_{el}}{\partial t} = -\nabla \cdot (-k_{el} \nabla T_{el} + \rho c_P u T_{el}) + Q_h \tag{A.3}$$

where the *el* index refers to the solid electrolyte domain, Q_h represents the generated heat, and k_{el} is the effective thermal conductivity. Its parameters need to be specified, as discussed next.

As shown in Fig. A.67 in the *Heat Conduction* section, the value of the *thermal conductivity* of the solid electrolyte (*ke*) is specified. In addition, in the *Thermodynamic* section, parameters such as *Density* (*roe*) and *Heat Capacity* (*Ce*) are specified.

The term corresponding to the heat generated from the electrochemical reactions must also be defined. Under the *Physics* tab click *Domains* and choose *Heat Source*. As shown in Fig. A.68 in the *Heat Source* section, choose the first option, *General source*, and from the drop-down menu select the *Total Power Dissipation Density* (*siec*) option.

As shown in Fig. A.69 it is now necessary to specify the heat transfer-boundary conditions for the solid electrolyte domain. The boundaries are shared with the anode and cathode porous electrodes domains. Under the *Physics* tab click *Boundaries* and choose *Heat Flux* for the two boundaries.

Figs. A.69 and A.70 show the value of heat flux specified for the boundary conditions. Based on the stoichiometry of the electrochemical reaction, the *general inward heat flux* through the cathode and anode porous electrodes are defined by the O_2 and H_2 reaction rates, respectively.

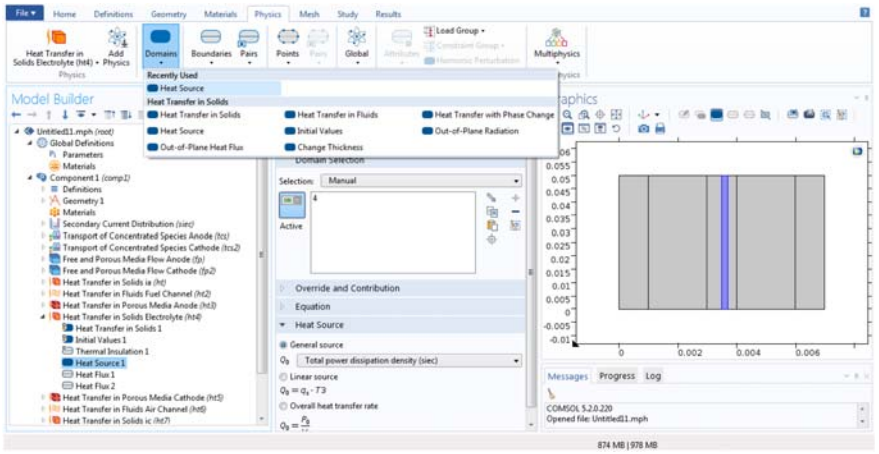

FIGURE A.68

The electrochemical reaction heat source.

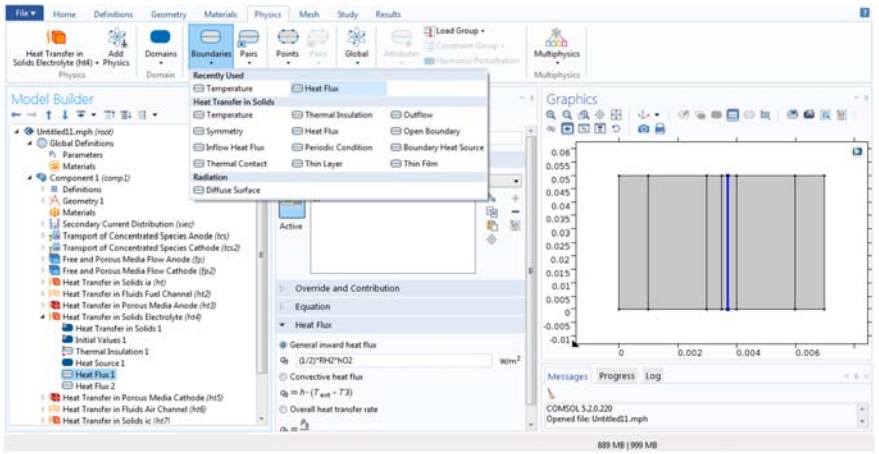

FIGURE A.69

Cathode porous electrode side heat flux boundary condition.

$$\text{Cathode inward heat flux}: \frac{1}{2} \times R_{H_2} \times h_{O_2} \tag{A.4}$$

$$\text{Anode inward heat flux}: R_{H_2} \times h_{H_2} - R_{H_2} \times h_{H_2O} \tag{A.5}$$

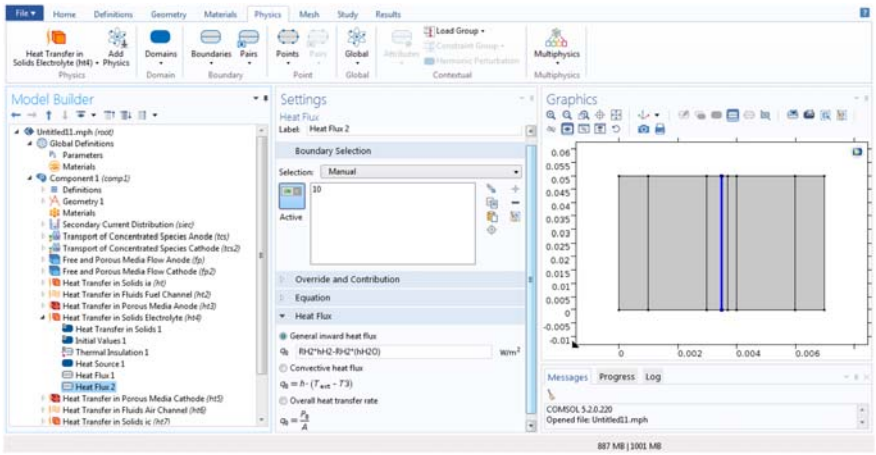

FIGURE A.70

Anode porous electrode side heat flux boundary condition.

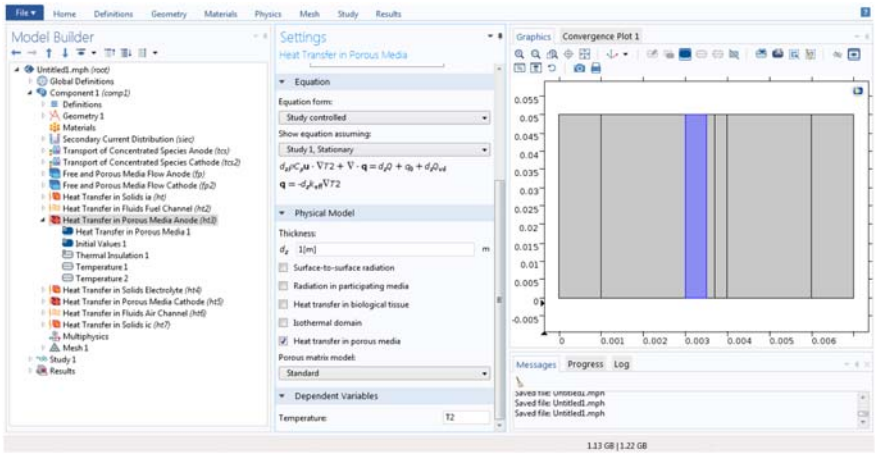

FIGURE A.71

Heat Transfer in Porous Media for the anode.

A.6.4.2 Heat transfer in the anode electrode porous media domain

The thermal energy transport equation is also solved for the anode porous electrode domain, as highlighted in Fig. A.71. The dominating phenomena in the anode porous electrode domain are conductive and convective heat flux, while

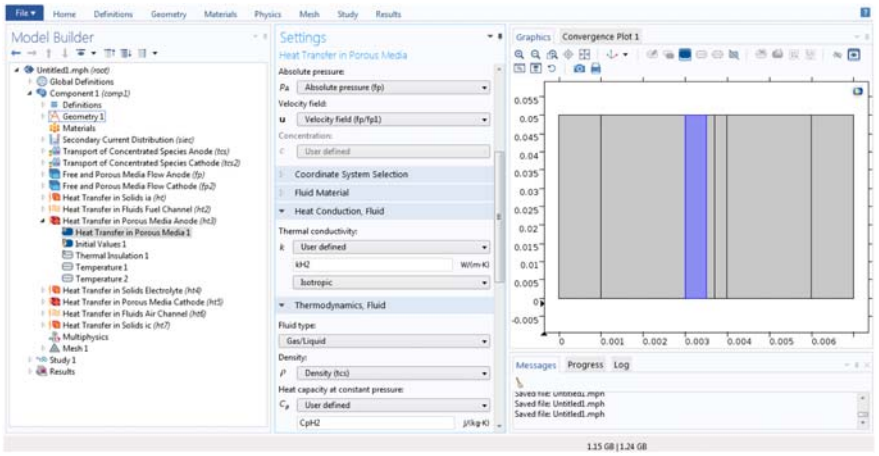

FIGURE A.72

Anode porous electrode heat-transfer properties.

thermal energy transport by the radiation mechanism is negligible. In addition, there is no heat generation in this domain. The following equation describes the energy balance:

$$\frac{\partial \rho c_P T_{an}}{\partial t} = -\nabla \cdot (-k_{an} \nabla T_{an} + \rho c_P u T_{an}) + Q_h \tag{A.6}$$

where the *an* index refers to the anode porous electrode domain. Q_h represents the generated heat and is equal to zero. k_{an} is the effective thermal conductivity, and its parameters need to be specified, as discussed next.

The *Heat Transfer in Porous Media* physics is required to determine the specification of porous media and fluid as the main data. The *Absolute Pressure* and *Velocity Field* are calculated through the *Free and Porous Media Flow* physics. The *Thermal conductivity* (*kH2*) and *Heat capacity* (*CpH2*) of fluid are defined by the user, and the *Density* of the fluid is calculated through the *Transport of Concentrated Species* physics as shown in Fig. A.72.

As shown in Fig. A.73 it is required to specify the parameters of the anode porous electrode material in the anode porous media *Heat Conduction* and *Thermodynamics* tabs. Enter the values of *ka*, *roa*, and *Ca* for *Thermal Conductivity*, *Density*, and *Specific-Heat Capacity*, in the corresponding fields, respectively.

Two boundary conditions are coupled with the temperature profile of the fuel channel and electrolyte. The left wall is the interface between the anode and fuel channel. On the *Physics* tab, click *Boundaries* and choose *Temperature*. Fig. A.74 shows the *Temperature* option, and the temperature of the interface, *T1*, is specified by the user.

The other boundary condition concerns with the other wall that is the interface between the anode and electrolyte. On the *Physics* tab, click *Boundaries* and choose *Temperature*. Fig. A.75 shows the *Temperature* option, and the temperature of the interface, *T3*, is specified by the user.

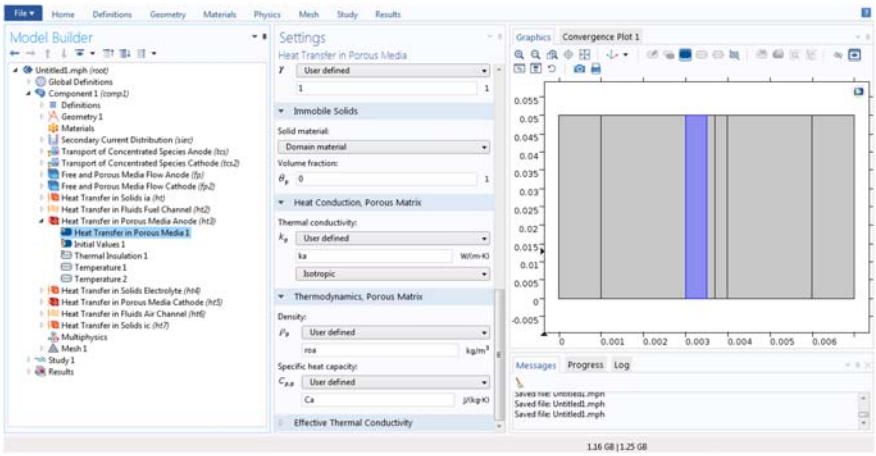

FIGURE A.73

Anode porous electrode heat-transfer properties.

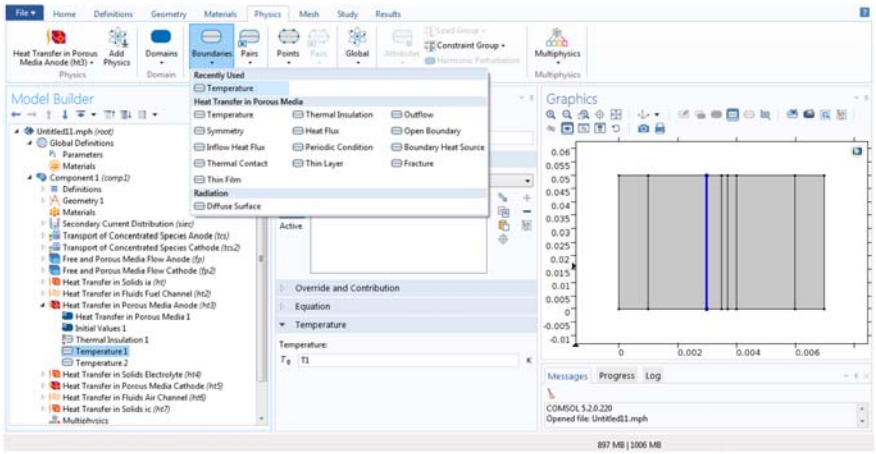

FIGURE A.74

Fuel channel side temperature boundary condition.

A.6.4.3 Heat transfer in the cathode electrode porous media domain

The thermal energy transport equation is also solved for the porous media in the Anode domain, as highlighted in Fig. A.76. The dominating phenomena in the *Solid Electrolyte* domain are conductive heat flux and convective heat flux, while

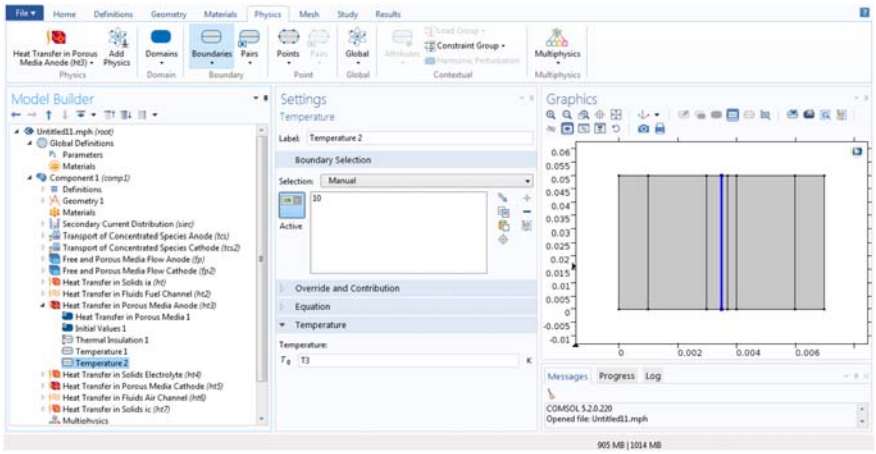

FIGURE A.75

Electrolyte side temperature boundary condition.

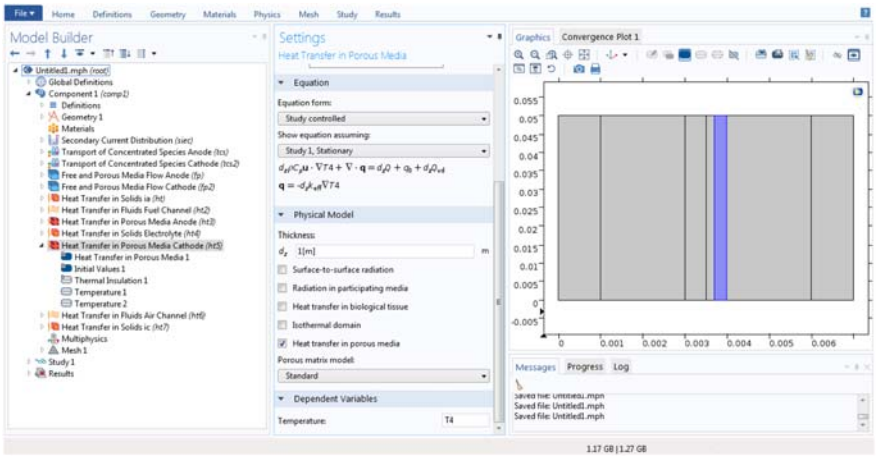

FIGURE A.76

Heat Transfer in Porous Media for cathode.

thermal energy transport by the radiation mechanism is negligible. In addition, there is no heat generation in this domain. The following equation describes the energy balance:

$$\frac{\partial \rho c_P T_{ca}}{\partial t} = -\nabla \cdot (-k_{ca} \nabla T_{ca} + \rho c_P u T_{ca}) + Q_h \tag{A.7}$$

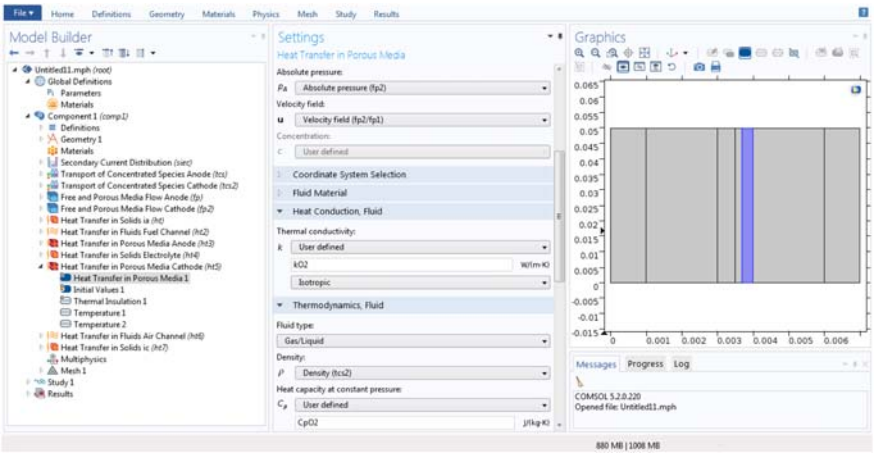

FIGURE A.77

Cathode porous electrode heat transfer properties.

where the *ca* index refers to the cathode porous electrode domain. Q_h represents the generated heat and is equal to zero. k_{ca} is the effective thermal conductivity, and its parameters need to be specified, as discussed next.

For solving effective thermal conductivity the *Heat Transfer in Porous Media* physics is required to determine the specification of porous media and fluid as the main data. The *Absolute Pressure* and *Velocity Field* are calculated through the *Free and Porous Media Flow* physics. The *Thermal Conductivity* (*kO2*) and *Heat Capacity* (*CpO2*) of the fluid are defined by the user, and the *Density* of the fluid is calculated through the *Transport of Concentrated Species* physics as shown in Fig. A.77.

As shown in Fig. A.78 it is required to specify the parameters of the cathode porous electrode material in the *Heat Conduction* and *Thermodynamics* tabs. Enter the values of *kc*, *roc*, and *Cc* for *Thermal Conductivity*, *Density*, and *Specific Heat Capacity* in the corresponding fields, respectively.

Two boundary conditions are coupled with the temperature profile of the air channel and electrolyte. The right wall is the interface between the cathode porous electrode and electrolyte. On the *Physics* tab, click *Boundaries* and choose *Temperature*. Fig. A.79 shows the *Temperature* option and the temperature of the interface *T3* is specified by the user.

The other boundary condition concerns with the other wall is the interface between the cathode porous electrode and air channel, Fig. A.80 shows the *Temperature* option, and the temperature of interface *T5* is specified by the user.

A.6.4.4 Heat transfer in the fuel channel domain

The thermal energy transport equation is also solved for the fuel channel domain, as highlighted in Fig. A.81. The dominating phenomena in the fuel channel

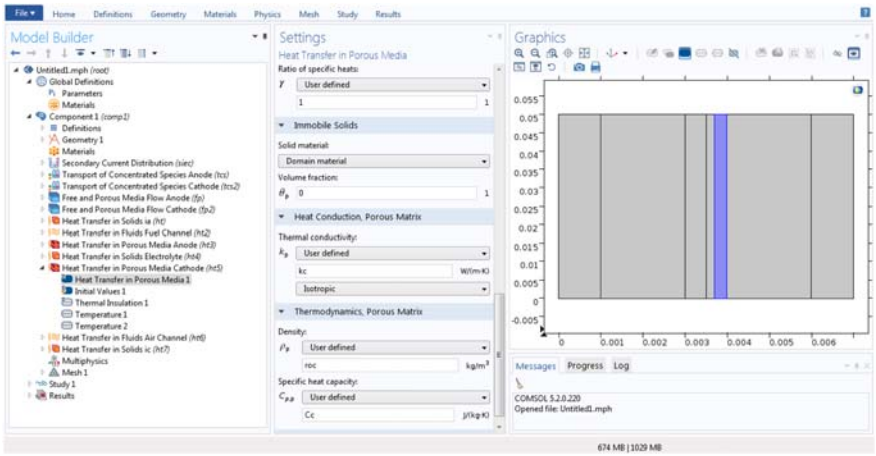

FIGURE A.78

Cathode porous electrode heat transfer properties.

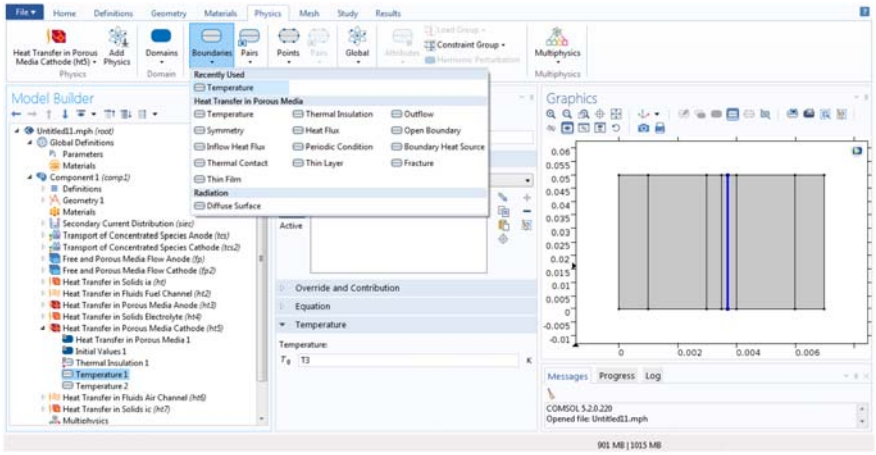

FIGURE A.79

Electrolyte side temperature boundary condition.

domain are conductive heat flux and convective heat flux, while the thermal energy transport by the radiation mechanism is negligible. In addition, there is no heat generation in this domain. The following equation describes the energy balance:

$$\frac{\partial \rho c_P T_{an.ch}}{\partial t} = -\nabla \cdot (-k_{an.ch} \nabla T_{an.ch} + \rho c_P u T_{an.ch}) + Q_h \tag{A.8}$$

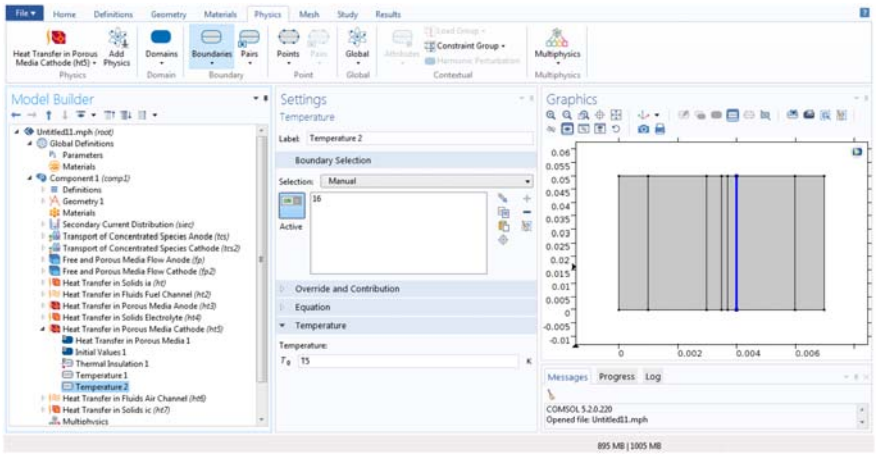

FIGURE A.80

Air channel side temperature boundary condition.

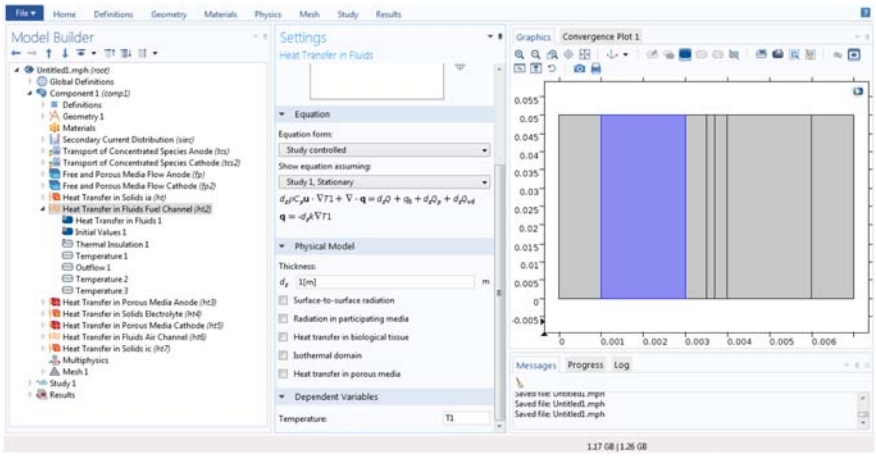

FIGURE A.81

Heat Transfer in Fluids for fuel channel.

where the *ca* index refers to the Fuel Channel domain. Q_h represents the generated heat and is equal to zero. $k_{an.ch}$ is the effective thermal conductivity, and its parameters need to be specified, as discussed next.

For solving the *Heat Transfer in Fluids*, physics is required to determine the specification of fluid as the main data. The *Absolute Pressure* and *Velocity Field* are calculated through the *Free and Porous Media Flow* physics. The *Thermal*

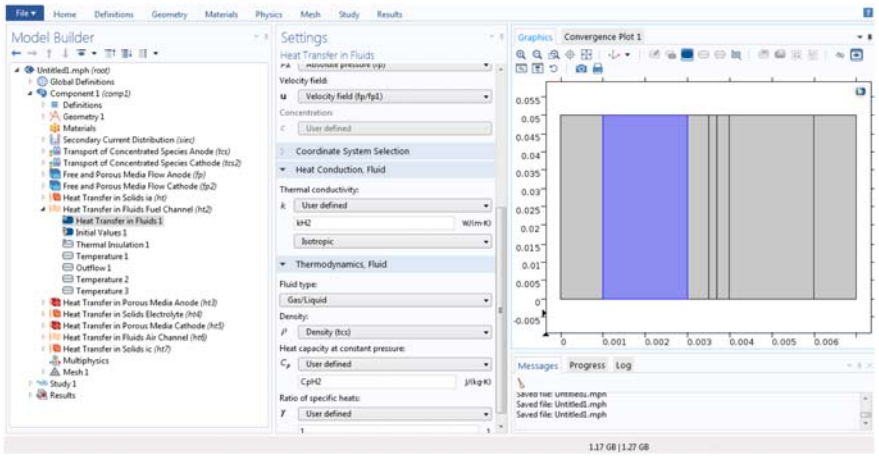

FIGURE A.82

Fuel channel heat-transfer properties.

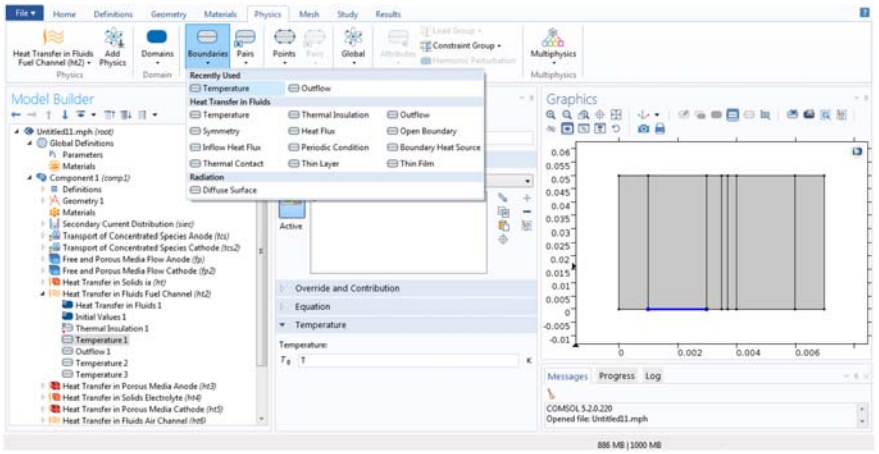

FIGURE A.83

Fuel-inlet temperature boundary condition.

Conductivity (*kH2*) and *Heat Capacity* (*CpH2*) of fluid are defined by the user and the *Density* of the fluid is calculated through the *Transport of Concentrated Species* Physics as shown in Fig. A.82.

As shown in Figs. A.83 and A.84, under the *Physics* tab click on *Boundaries* and choose *Temperature* and *Outflow*. Select boundaries 5 and 6, respectively. Locate the *Temperature* and type *T* in the text field as the inlet-flow temperature.

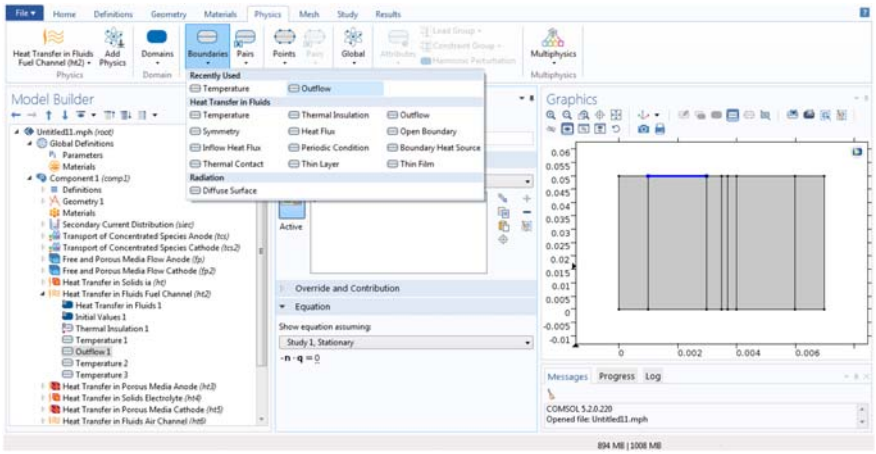

FIGURE A.84

Fuel-outlet boundary condition.

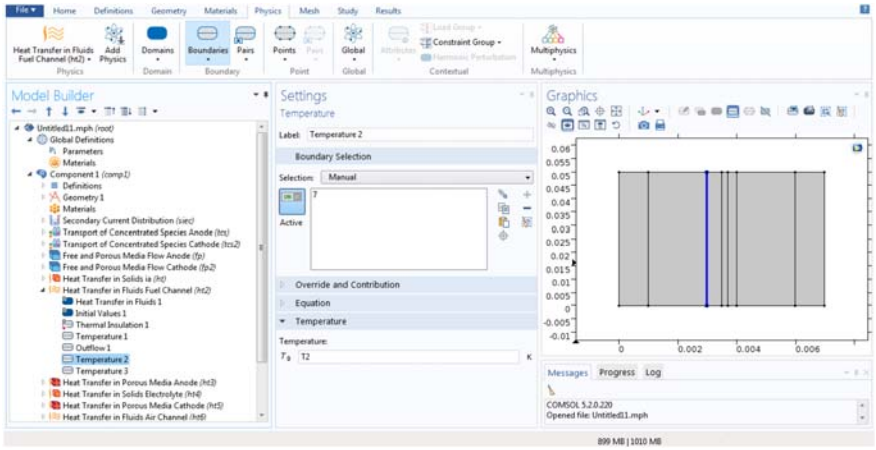

FIGURE A.85

Anode side temperature boundary condition.

The walls boundary condition are coupled with a temperature profile of the anode porous electrode and interconnect. The left wall is the interface between the fuel channel and anode porous electrode. On the *Physics* tab click *Boundaries* and choose *Temperature*. Fig. A.85 shows the *Temperature* option and the temperature profile of the interface *T2* is specified by the user.

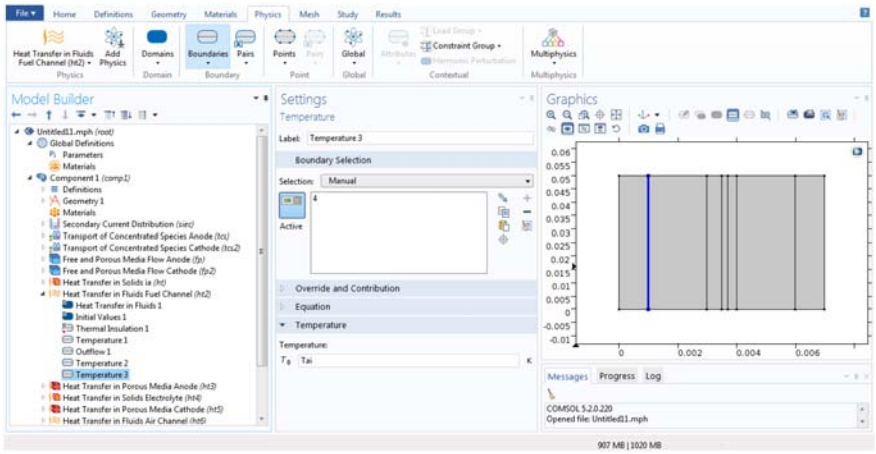

FIGURE A.86

Anode interconnect side temperature boundary condition.

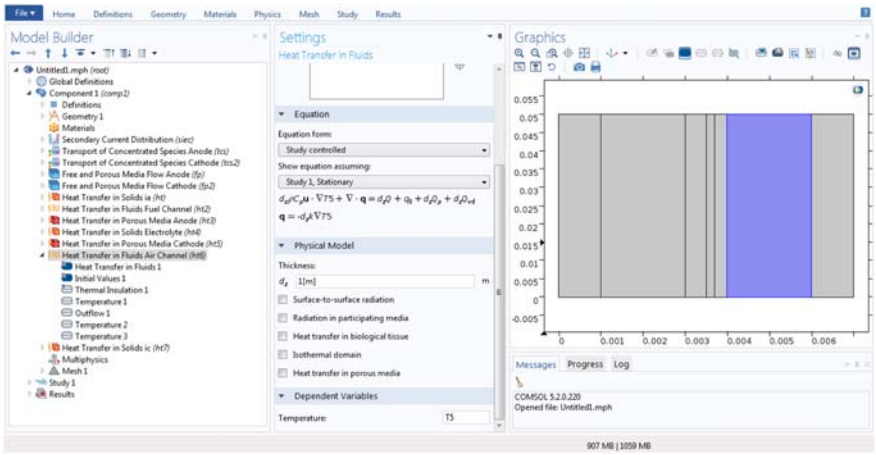

FIGURE A.87

Heat Transfer in Fluids for the air channel.

The other boundary condition concerns with the other wall that is the interface between the fuel channel and interconnect. On the *Physics* tab click *Boundaries* and choose *Temperature*. Fig. A.86 shows the *Temperature* option and the temperature of the interface *Tai* is specified by the user.

A.6.4.5 Heat transfer in the air channel domain

The thermal energy transport equation is also solved for the air channel domain as highlighted in Fig. A.87. The dominating phenomena in the air channel domain

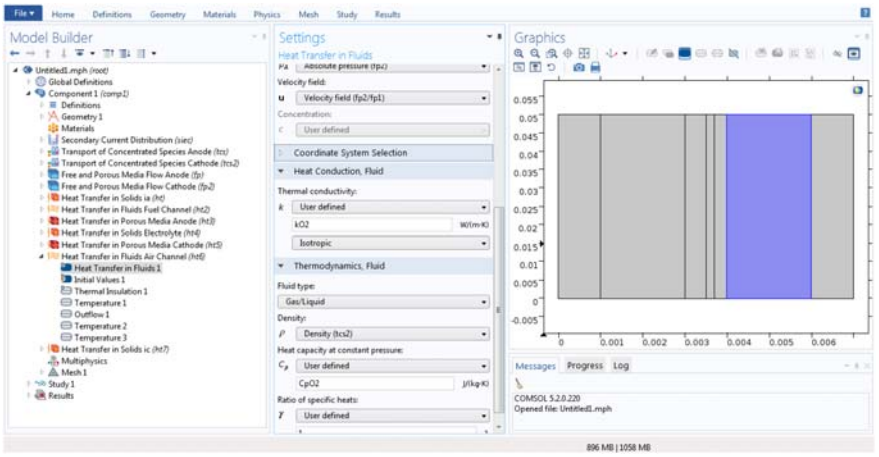

FIGURE A.88

Air channel heat-transfer properties.

are conductive heat flux and convective heat flux, while thermal energy transport by the radiation mechanism is negligible. In addition, there is no heat generation in this domain. The following equation describes the energy balance:

$$\frac{\partial \rho c_P T_{ca.ch}}{\partial t} = -\nabla \cdot (-k_{ca.ch} \nabla T_{ca.ch} + \rho c_P u T_{ca.ch}) + Q_h \tag{A.9}$$

where the *ca.ch* index refers to the air channel domain, Q_h represents the generated heat equal to zero, $k_{ca.ch}$ is the effective thermal conductivity, and its parameters need to be specified, as discussed next.

For solving the *Heat Transfer in Fluids* physics, it is required to determine the specification of fluid as the main data. The absolute pressure and velocity fields are calculated through the *Free and Porous Media Flow* physics. *Thermal Conductivity* (*kO2*) and *Heat Capacity* (*CpO2*) of fluid are defined by user and the *Density* of the fluid is calculated through the *Transport of Concentrated Species* physics as shown in Fig. A.88.

As shown in Figs. A.89 and A.90, under the *Physics* tab click *Boundaries* and choose *Temperature* and *Outflow*, and select boundaries 17 and 18, respectively. Locate the *Temperature* and type *T* in the text field as the inlet-flow temperature.

The walls boundary condition are coupled with the temperature profile of the cathode porous electrode and interconnect. The left wall is the interface between the air channel and cathode porous electrode. On the *Physics* tab click *Boundaries* and choose *Temperature*. Fig. A.91 shows the *Temperature* option and the temperature of the interface *T4* is specified by the user.

For another wall that is the interface between the air channel and interconnect, on the *Physics* tab click on *Boundaries* and choose *Temperature*. Fig. A.92 shows the *Temperature* option and the temperature of the interface *Tci* is specified by the user.

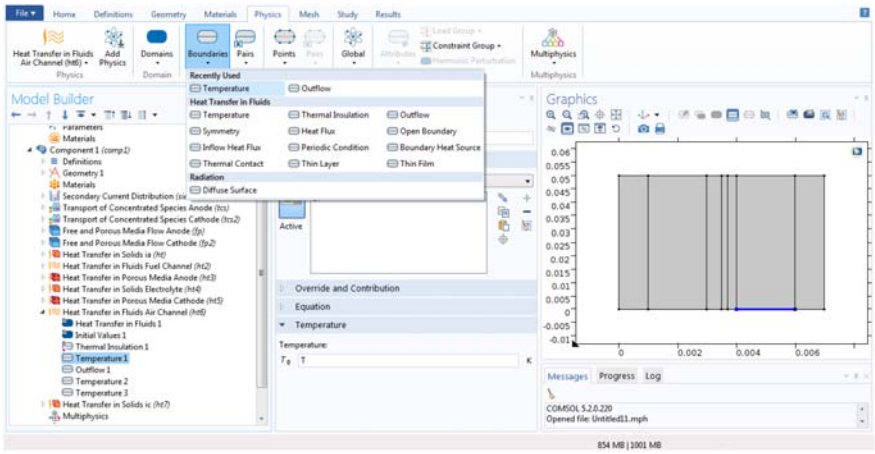

FIGURE A.89

Air-inlet temperature boundary condition.

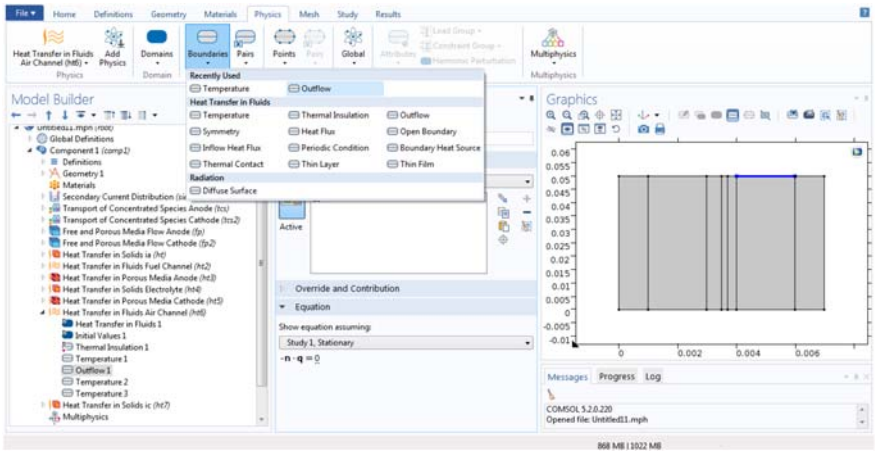

FIGURE A.90

Air-outlet boundary condition.

A.6.4.6 Heat transfer in the anode interconnect domain

The thermal energy transport equation is also solved for the anode interconnect domain, as highlighted in Fig. A.93. The dominating phenomenon in the anode interconnect domain is conductive heat flux, while thermal energy transport by the radiation mechanism is negligible. In addition, there is no heat generation in this domain. The following equation describes the energy balance:

$$\frac{\partial \rho c_P T_{an.int}}{\partial t} = -\nabla \cdot (-k_{an.int} \nabla T_{an.int}) + Q_h \tag{A.10}$$

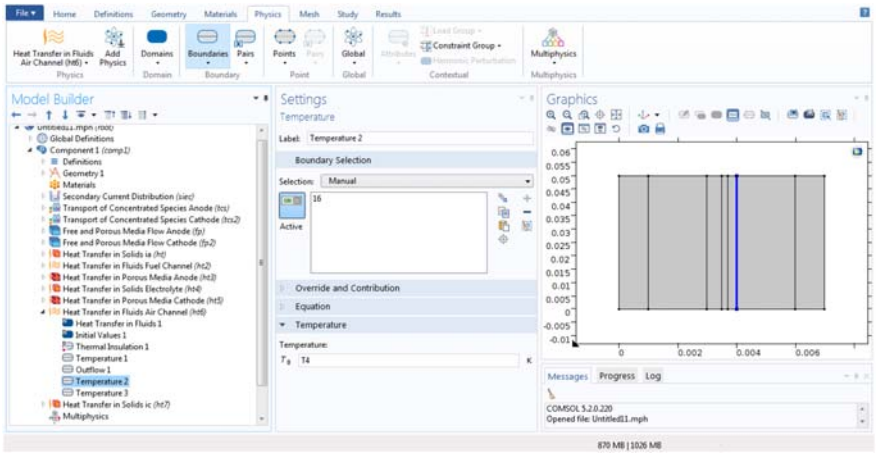

FIGURE A.91

Cathode porous electrode side temperature boundary condition.

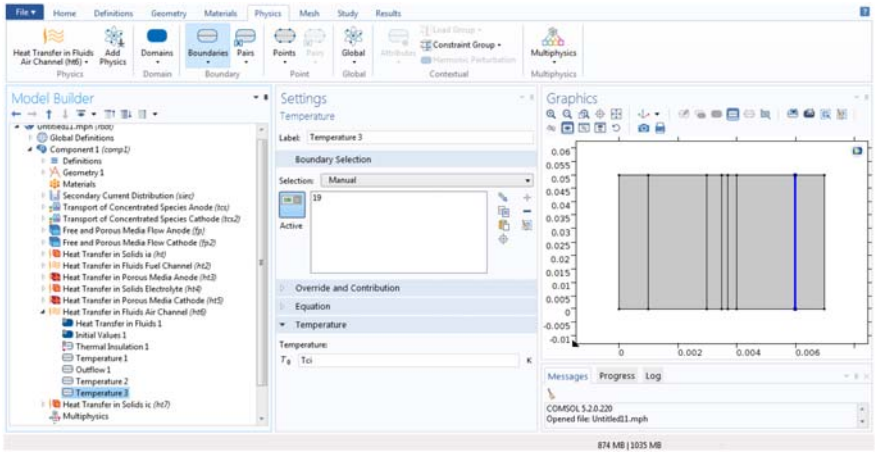

FIGURE A.92

Cathode interconnect side temperature boundary condition.

where the *an.int* index refers to the anode interconnect domain, Q_h represents the generated heat equal to zero, $k_{an.int}$ is the effective thermal conductivity and its parameters need to be specified, as discussed next.

For solving the *Heat Transfer in Solids* physics for the anode interconnect, it is required to determine the specification of the anode interconnect as the main data. *Thermal Conductivity* (*ki*), *Density* (*roi*), and *Heat Capacity* (*Ci*) of fluid are defined by the user as shown in Fig. A.94.

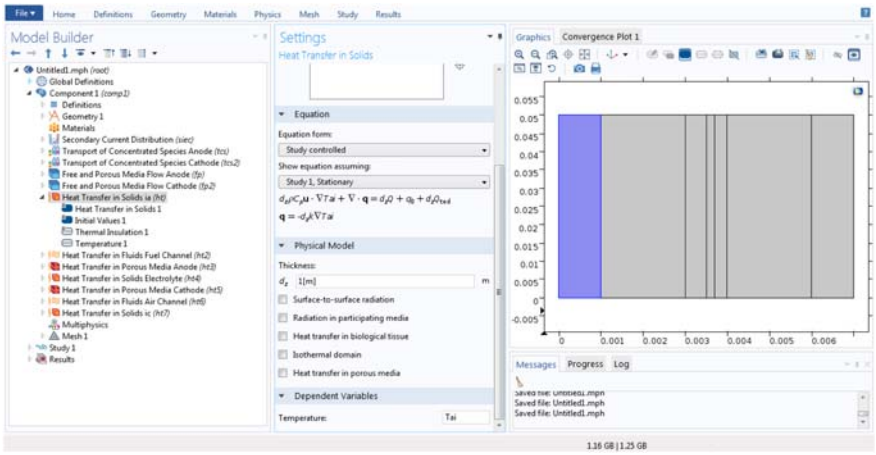

FIGURE A.93

Heat Transfer in Solids for the anode interconnect.

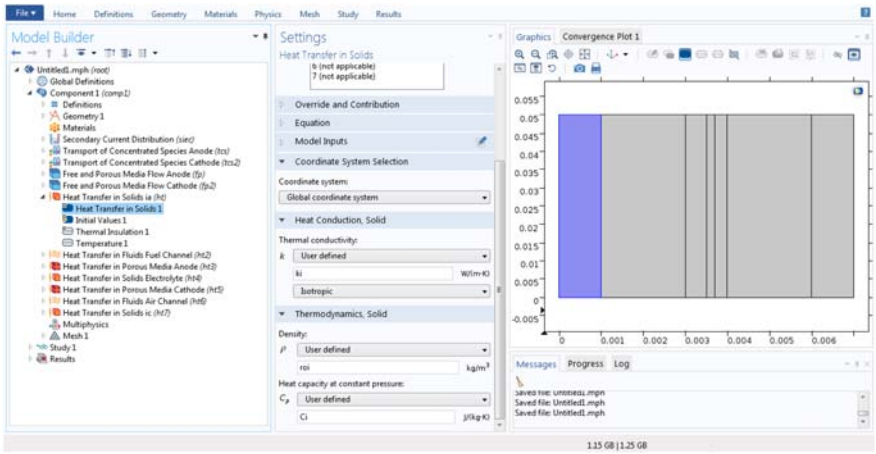

FIGURE A.94

Anode interconnect heat-transfer properties.

For the interface boundary between the interconnect and fuel channel, on the *Physics* tab click on *Boundaries* and choose *Temperature*. Fig. A.95 shows the *Temperature* option and the temperature of the interface *T1* is specified by the user.

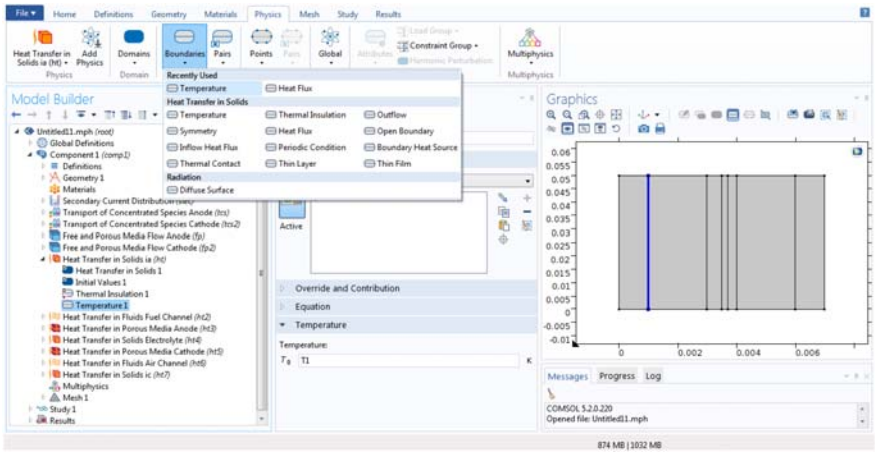

FIGURE A.95

Fuel channel side temperature boundary condition.

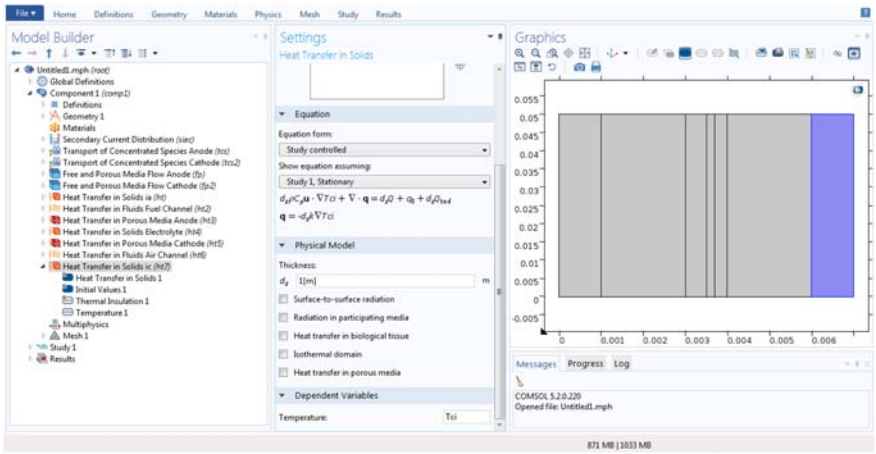

FIGURE A.96

Heat Transfer in Solids for the cathode interconnect.

A.6.4.7 Heat transfer in the cathode interconnect domain

The thermal energy transport equation is also solved for the cathode interconnect domain, as highlighted in Fig. A.96. The dominating phenomenon in the cathode interconnect domain is conductive heat flux, while thermal energy transport by

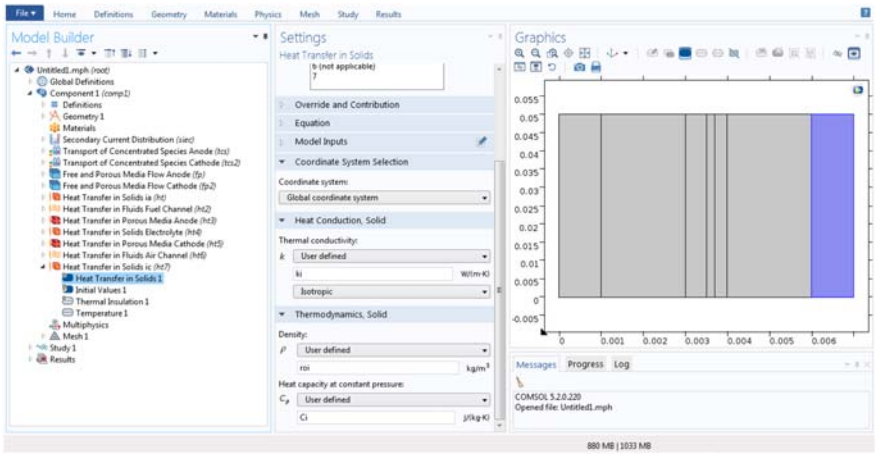

FIGURE A.97

Cathode interconnect heat-transfer properties.

the radiation mechanism is negligible. In addition, there is no heat generation in this domain. The following equation describes the energy balance:

$$\frac{\partial \rho c_P T_{ca.int}}{\partial t} = -\nabla \cdot (-k_{ca.int} \nabla T_{ca.int}) + Q_h \tag{A.11}$$

where the *ca.int* index refers to the cathode interconnect domain. Q_h represents the generated heat and is equal to zero. $k_{ca.int}$ is the effective thermal conductivity and its parameters need to be specified, as discussed next.

For solving the *Heat Transfer in Solids* physics for the cathode interconnect it is required to determine the specification of the cathode interconnect as the main data. *Thermal Conductivity* (*ki*), *Density* (*roi*), and *Heat Capacity* (*Ci*) of fluid are defined by the user as shown in Fig. A.97.

To determine the interface boundary between the *interconnect* and *air channel*, on the *Physics* tab click on *Boundaries* and choose *Temperature*. Fig. A.98 shows the *Temperature* option and the temperature of the interface *T5* is specified by the user.

A.7 Mesh generation

The physics settings for the model is now complete. In this study the seven graphical domains are discretized according to the mapped mesh strategy. As shown in Fig. A.99, in order to specify the meshing strategy the following steps are taken. First, in the *Model Builder* window under *Component 1* (*comp1* right-click on *Mesh 1* and choose the *Mapped* options. Then right-click *Mapped 1* and choose

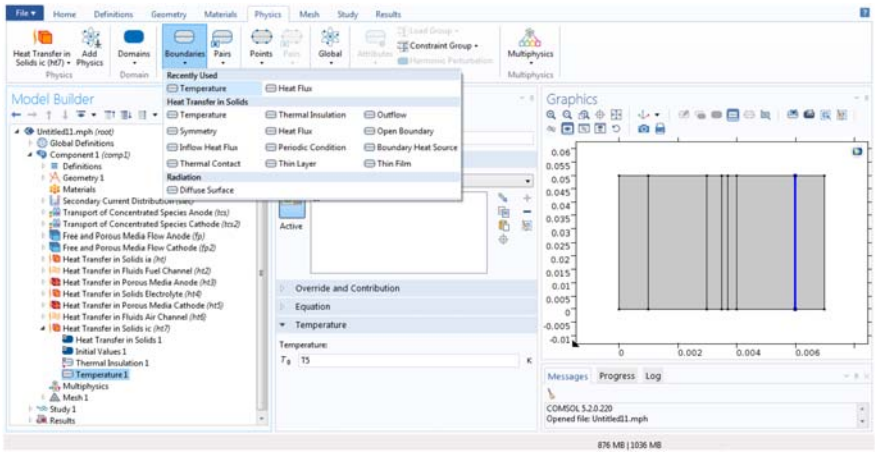

FIGURE A.98

Air channel side temperature boundary condition.

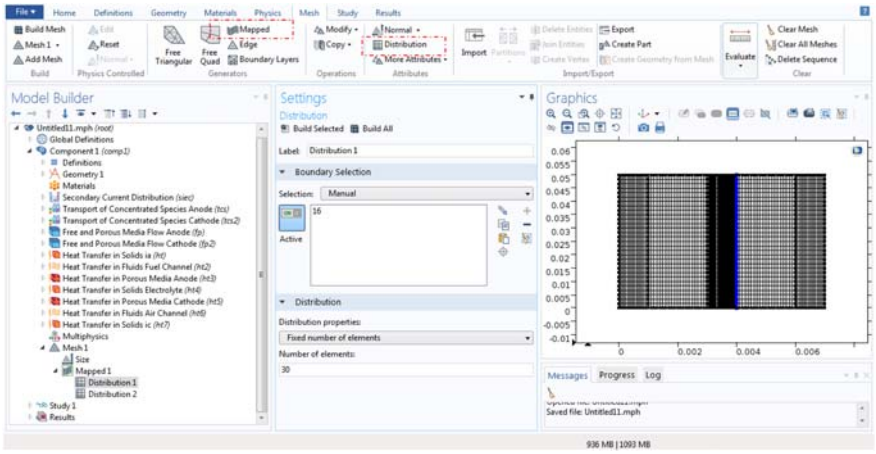

FIGURE A.99

Mapped distribution on the anode side.

the *Distribution 1* option. Select boundary 16 and in the *Settings* window for *Distribution*, locate the *Distribution* section. From the drop-down menu choose the *Fixed Number of Elements* distribution type.

Considering that a higher resolution for the mapped mesh results in higher accuracy, this however comes at the price of higher computational costs. Therefore a trade-off must be established. Type 30 in the *Number of the Elements* text field as shown in Fig. A.99.

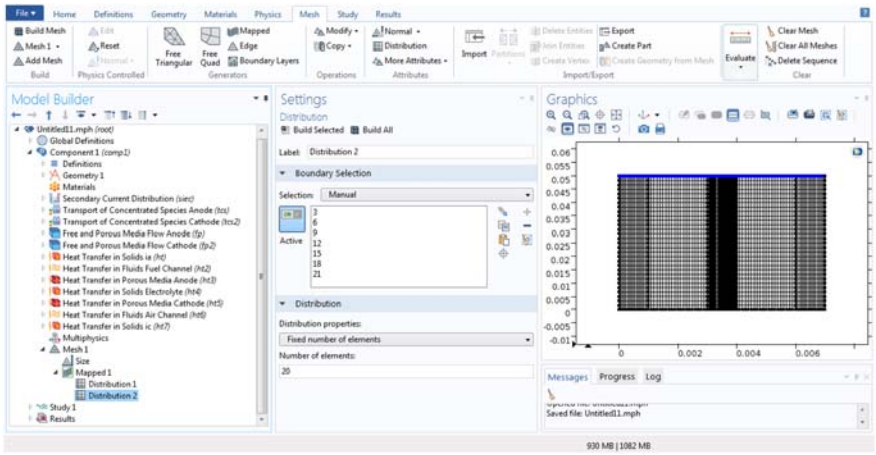

FIGURE A.100

Mapped distribution on top.

Similarly, right-click on *Mapped 1* and choose *Distribution 2*, select *Boundaries* 3, 6, 9, 12, 15, 18, and 21. In the *Settings* window for *Distribution*, locate the *Distribution* section. From the *Distribution Properties* drop-down menu choose *Fixed Number of Elements* distribution type. Type 20 in the *Number of the Elements* text field as shown in Fig. A.100.

A.8 Study

The problem is now ready to be solved. The solver setting is shown in Fig. A.101. The integrated nonlinear solver (*Fully Coupled*), which uses a constant *Damping factor* form of the *Constant Newton method*, was selected for the solution of the nonlinear system with its relative *tolerance factor* set to 10^{-3}, and the *maximum number of iterations* set to *25*.

For the inversion of the Jacobian matrix at each iteration, the *Linear Direct Solver* was used since for this particular system it showed better performance compared to the iterative linear solvers. In *Direct 1*, locate the *General* section and from the *Solver* drop-down menu choose *PARADISO* as shown in Fig. A.102.

A.9 Results

In Fig. A.103 the H_2 and O_2 mole fractions at the fuel channel and air channel are illustrated. Hydrogen and oxygen flow in the fuel and air channels,

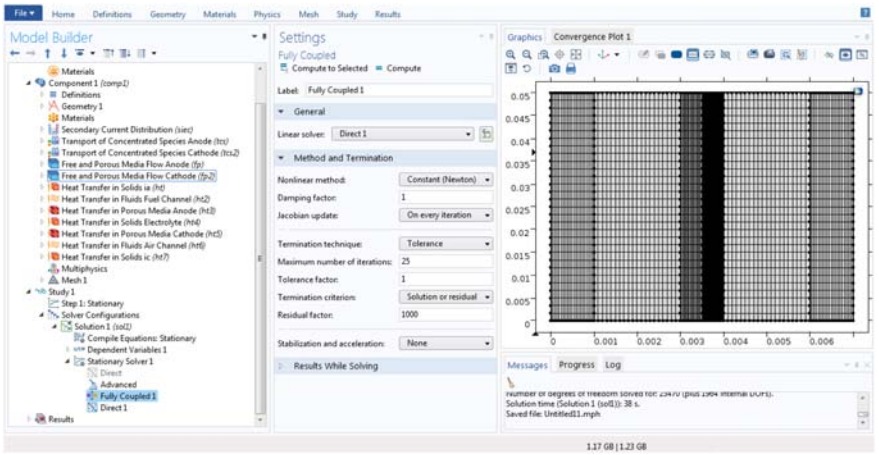

FIGURE A.101

Fully coupled method and termination setting.

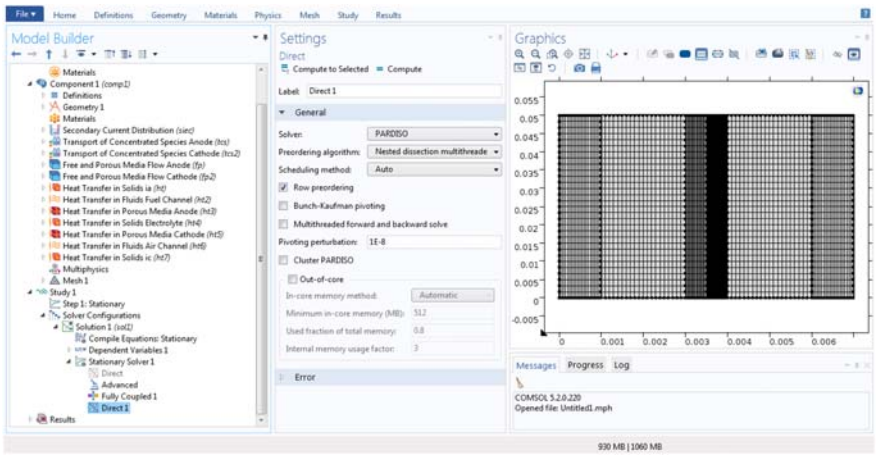

FIGURE A.102

Direct solver setting.

respectively. They diffuse through the anode and cathode porous electrodes where they are consumed at the electrode/electrolyte interfaces by the electrochemical oxidation and reduction reactions.

In order to produce the above figure, first, as shown in Fig. A.104, on the *Home* tab click *Add Plot Group* and choose *2D Plot Group*. In the *Settings* window for *2D Plot Group*, locate the *Data* section and choose *Study 1/Solution 1*. Change the label of the 2D plot to *Concentration* and then right-click on it and choose *Surface 1* and *2*.

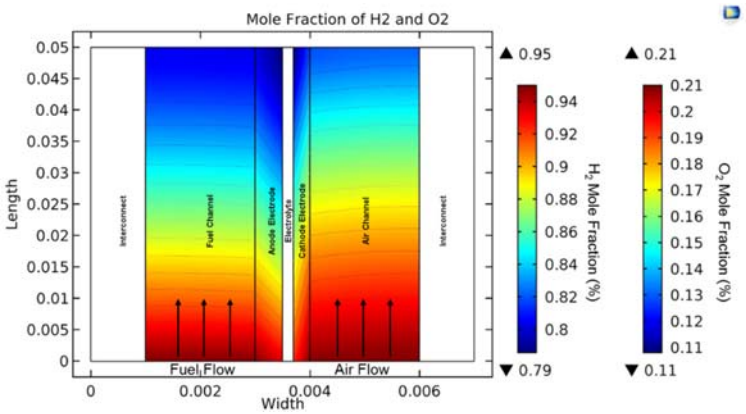

FIGURE A.103

H_2 and O_2 mole-fraction distributions in the fuel and air channels and anode and cathode porous electrodes.

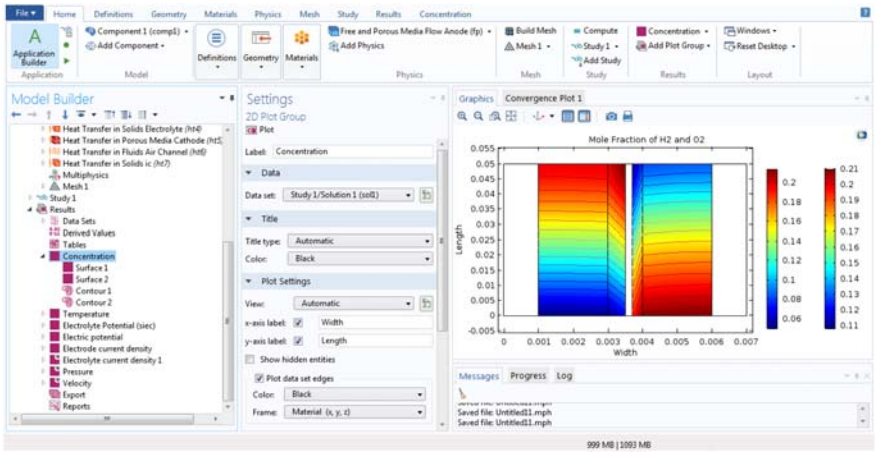

FIGURE A.104

Concentration 2D plot group.

Figs. A.105 and A.106 show the surface concentration of O_2 and H_2, respectively. In the *Settings* window for *Surface 1* click on *Replace Expression* in the upper-right corner of the *Expression* section. From the drop-down menu, choose *Component 1*, *Transport of Concentrated Species Cathode*, mole fraction, *tcs2.x_wO2*. Similarly as *Surface 1*, consider *tcs.x_wH2* for defining the expression of *Surface 2*.

Fig. A.107 shows the temperature distribution in the SOFC. Heat is absorbed from the anode electrochemical reaction and is released through the cathode

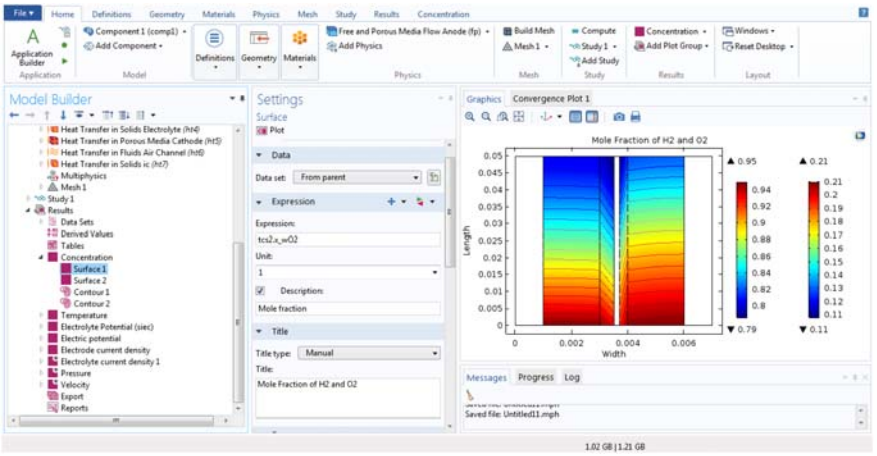

FIGURE A.105

Surface O_2 concentration.

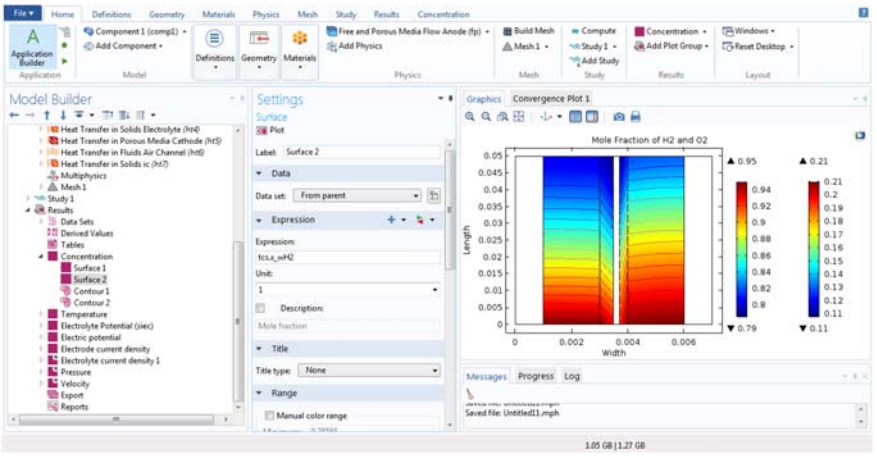

FIGURE A.106

Surface H_2 concentration.

channel. Overall, the heat released is transferred along the *z*-direction mainly by conduction to the gas streams where it is transferred along the *x*-direction via convection by the flow of the gas mixtures. The slightly higher temperature observed at the cathode side is related to the exothermic reaction of the oxygen reduction. Heat is also generated at the solid domains of the SOFC due to the ohmic resistance.

As shown in Fig. A.108, under the *Home* tab, click on *Add Plot Group* and choose *2D Plot Group*. In the *Settings* window for *2D Plot Group* locate the *Data*

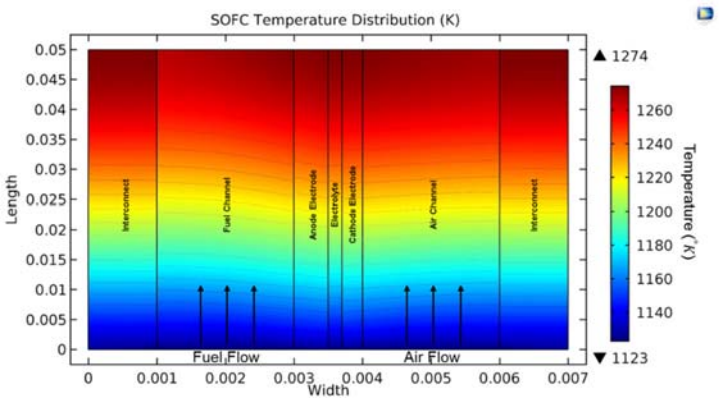

FIGURE A.107

Temperature distribution in an solid oxide fuel cell.

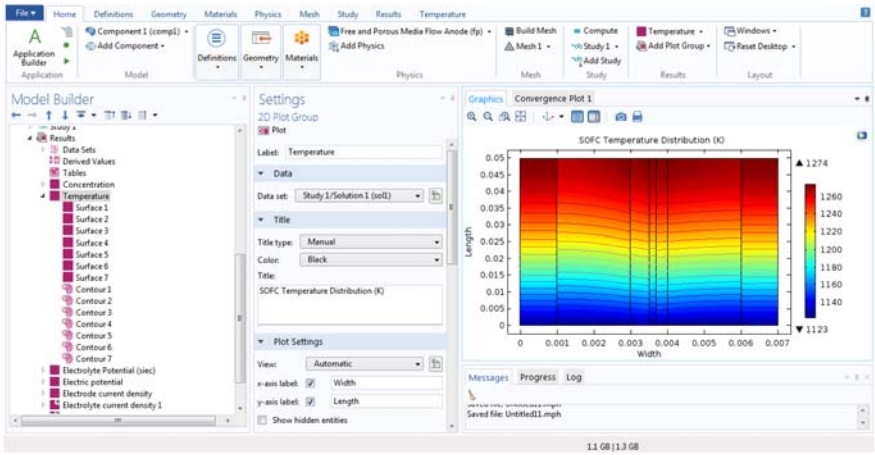

FIGURE A.108

Temperature 2D plot group.

section and choose *Study 1/Solution 1*. Change the label of the 2D plot to *Temperature* and then right-click on it and add surfaces 1−7 (i.e., anode interconnect, fuel channel, anode porous electrode, electrolyte, cathode porous electrode, air channel, cathode interconnect).

As shown in Fig. A.109 in the *Settings* window *Surface 1* is defined as an anode interconnect, click *Replace Expression* in the upper-right corner of the *Expression* section. From the drop-down menu, choose *Component 1*, *Heat Transfer in Solids* via *Temperature*, *Tai*. A similar procedure can be applied for defining the *Temperature Surfaces* of the other six elements of the planar SOFC.

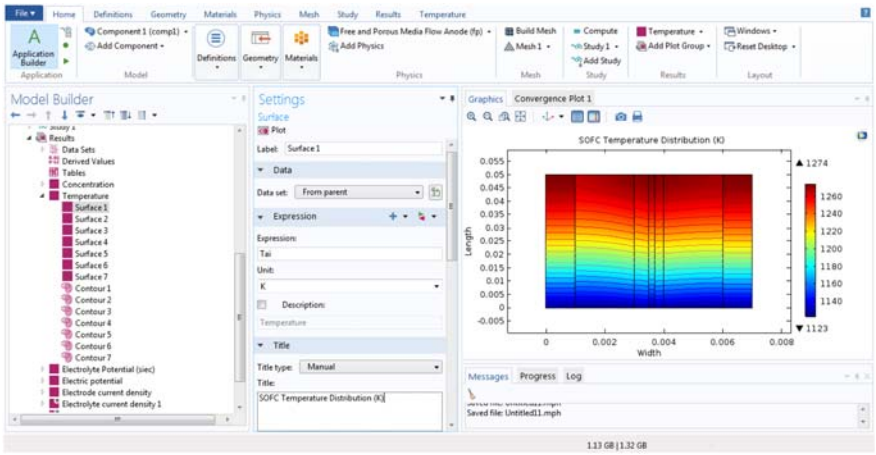

FIGURE A.109

Surface temperature distribution.

Conclusion

This Appendix presented a pictorial tutorial for modeling a planar SOFC using a computational fluid dynamics software tool, called COMSOL Multiphysics. The SOFC model was developed through the formulation of the mass transport, energy transport, and electrochemical phenomena that take place in the fuel and air channels, porous electrodes, electrolyte, and interconnects. The required procedure comprises six main stages incorporating Model initialization, Model Geometry creation, setting up the Subdomain Equations and Boundary conditions, specifying the transport phenomena for each domain, meshing the Geometry, conducting steady-state study, and analyzing the results. The developed model can provide a benchmark and starting point for future studies such as the design and scale-up of other SOFC-based industrial systems.

References

[1] K. Tseronis, I. Bonis, I.K. Kookos, C. Theodoropoulos, Parametric and transient analysis of non-isothermal, planar solid oxide fuel cells, Int. J. Hydrogen Energy 37 (1) (2012) 530–547.

[2] Introduction to COMSOL Multiphysics®, version 5.2, COMSOL, Inc. www.comsol.com/documentation.

[3] R.H. Perry, D.W. Green, J.O. Maloney, seventh ed., Chemical Engineers' Handbook, vol. 27, McGraw-Hill, 1997.

Glossary

Mahdi Sharifzadeh, Wenqian Chen, Giorgio Triulzi, Mirko Hu, Majid Saidi, Venkatesan Krishnan, Maryam Ghadrdan, Meysam Qadrdan, Yingru Zhao, Alireza Mohammadzadeh, Seyedeh Kiana Naghib Zadeh, Mohammad Hassan Saidi, Davood Rashtchian and Nilay Shah

Active constraint region Active constraints are related to variables that should be kept at their limiting value to achieve optimality. These can be related to manipulated variables (MVs) or controlled variables (CVs). The MVs correspond to the dynamic (physical) degrees of freedom (DoF) used by the control system, and a typical MV constraint is the maximum opening of a valve. Active constraints may change due to disturbances. Different disturbances may lead to a situation where a different set of variables become active. This will separate the disturbance space to different active constraint regions.

Active constraint A constraint becomes active when the value of the objective function cannot be improved by moving from borders of the feasible region back into an interior point in the region, the optimization algorithm makes this inequality constraint to an equality constraint. Intersection of objective function contours with the constraint line will define the optimal value.

Anaerobic digestion Anaerobic digestion is a series of biological processes in which microorganisms break down biodegradable material in the absence of oxygen. One of the end products is biogas, which is then combusted to generate electricity and heat, or can be processed into renewable natural gas or utilized as a feedstock to fuel cell systems.

Anode-supported solid oxide fuel cell (AS-SOFC) An anode-supported SOFC is one of the component-supported SOFCs in which the anode is the thickest portion of the cell and provides mechanical strength to it.

Anode An anode is an electrode through which conventional current flows into a polarized, electrical device.

Auxiliary power unit A device that provides the energy for functions other than the propulsion of a vehicle.

Battery A device that converts chemical energy into electrical energy and vice versa.

Bibliometrics Statistical analysis of written texts such as books, articles, and patents.

Biofuel cell A class of fuel cells comprising fuel cells with biological electrolytes and fuel cells using biofuels.

Biogas Biogas is a gas produced by the biological breakdown of organic matter in the absence of oxygen. Biogas originates from biogenic material and is a type of biofuel.

Bottoming cycle A cycle that is attached to a primary power producer, which makes use of the available heat and utilizes it effectively to generate further electrical power.

Bulk patent data A big quantity of data.

Carnot efficiency Theoretical maximum efficiency for a heat engine.

Cathode-supported SOFC A cathode-supported SOFC is one of the component-supported SOFCs in which the cathode layer is the thickest portion of the cell and provides the main mechanical strength to it.

Cathode A cathode is the electrode from which a conventional current leaves a polarized electrical device.

Cell stacking A device for saving power in a fuel cell system to obtain the suitable voltage output from the device.

Centrality Related to a network, centrality can be defined as the measure of the importance of a node in a network, for example, if there are many paths passing through the node.

Cermet A composite material made of ceramics and metals.

Classification overlap method A method to extract patent data related to a technological domain (subdomain) using classification systems.

Coefficient of performance The ratio between the output and input of a chiller or heat pump.

Coefficient of thermal expansion A material property which shows its response to temperature change. This coefficient describes by how much the size of a solid object changes with respect to a change in its temperature.

Coelectrolysis This term is utilized in fuel cell systems when water and carbon dioxide are used to produce syngas.

Cogeneration Cogeneration (also CHP) is the application of a heat engine or a power station to simultaneously generate electricity and useful heat.

Combined heating and power A generator that produces power and heat simultaneously.

Comma-separated values file A type of file containing data that can be easily transformed in a table.

Commercialization Introduction of technology to the market.

Component-supported SOFC The SOFC in which the component (anode, cathode, etc.) is the thickest portion of the cell and provides mechanical strength to it.

Condition number The condition number of a matrix is defined as the ratio between the maximum and minimum singular values. The condition number has been used as an input−output controllability measure. It is suggested that a high-condition number indicates sensitivity to uncertainty.

Continuity equation A mathematical representation that describes transport of some quantity. Here it refers to the mass continuity of fluid flow in the SOFC.

Control input The inputs that the controller can manipulate to control the process (MVs).

Control-loop pairing Pairing up measured variables and MVs in an multiple input multiple output system.

Control structure design Deals with the structural decisions of the control system, including what to control and how to pair the manipulated and controlled variables.

Control variable The variable in a control system that is kept constant or follows a profile.

Controllability The ability to achieve acceptable control performance. More precisely, to keep the outputs within specified bounds from their set points, despite unknown changes (e.g., disturbances and plant changes) using available inputs and measurements.

Cost reduction The decrease in the cost due to several reasons such as improvement of production processes or economies-of-scale effects.

Creep A slow change of the materials with the passage of time.

Current–voltage ($I-V$) curve One of the characteristic curves of an SOFC that shows the SOFC's behavior, that is, voltage changes with respect to current changes.

Cyclic processes A process is termed cyclic when it operates in multiple sequential stages, usually with a working fluid, and returns to its starting point in terms of pressure and temperature, only to repeat itself, for example, taking in the heat from a high-temperature reservoir, converting it to useful work, releasing waste heat and then returning to its original state due to external work. This sequence of steps repeats themselves, and hence, is a cyclic process.

Degradation Change in the composition or microstructure of different parts of a cell.

Delamination Detachment of the electrolyte and the electrode layer.

Diffusion The spread of a technology in the market.

Dip coating A method of layer fabrication where a base shape is soaked in a bath of slurry. Due to the viscosity of the slurry, with the exiting base shape from the bath a layer of slurry is attached to it and a new layer is fabricated.

District-heating system A pipeline network for distributing heat generated in a centralized heat producer for space heating and/or water heating.

Ebb generation The method of a tidal lagoon operation that generates electricity when the tide is going out of the lagoon.

Economies of scale Reduction of costs due to the better management of raw material and energy costs.

Electrode An electrical conductor used to make contact with a nonmetallic part of a circuit.

Electrolysis This term is utilized in fuel cell systems when the only reactant in the system is steam.

Electrolyte-supported SOFC Electrolyte A substance that can become electrically conducting when dissolved in a polar solvent.

Electrolyte The electrolyte is a dense layer of ceramic that conducts oxygen ions in the fuel cell system.

ENE-FARM A demonstration project for fuel cell-stationary applications in residential buildings in Japan.

ENE-FIELD A demonstration project for fuel cell-stationary applications in the residential building sector in European Union.

Energy equation The mathematical form of the conservation of an energy law that is used for the energy analysis of an SOFC system.

Energy storage In the context of electricity storage refers to capturing electricity produced by renewable and non-renewable resources and storing it for discharge when required.

Exergetic efficiency In energy device applications, the efficiency is normally defined as work done or heat input. However, when the Second Law clearly postulates that only the Gibbs free energy component is useful for work—that is, the rest of the enthalpy term ($T\Delta S$) is simply unusable for work—it makes much more sense to redefine efficiency. The exergetic efficiency is therefore the ratio of the work done to the exergy available (not the enthalpy).

Exergy Initially postulated as the extent of departure of a system in its existing state from a reference state, which is quite simply the Earth's atmosphere, that is, if a system has its temperature, pressure, or composition different from the environment then the system has exergy. A classic argument is made to distinguish exergy from energy, that is, the atmosphere around us has considerable energy but no exergy, which means that any system in equilibrium with the atmosphere (or the reference state) in terms of

temperature, pressure, and composition is incapable of doing work. Therefore exergy refers to a system having a certain potential for doing work, and once this work is completed the system will reach a final state of equilibrium with the surroundings.

External supporting SOFC When the auxiliary parts are used as the supporting section (porous substrate, or interconnector) the fuel cells are called external supporting SOFCs.

Feed-forward control In a feed-forward system the control variable adjustment is based on knowledge about the process in the form of a mathematical model of the process and knowledge about (or measurements of) the process disturbances.

Finite element analysis Finite element analysis is one of the numerical methods for solving engineering problems based on the finite element method. It is typically used to solve problems in structural analysis, heat transfer (thermal modeling), fluid flow, species transport, and electric currents and is, thus, one of the common numerical methods used for simulating SOFC physics.

Flare-gas recovery The process of recovering the waste gases that would normally be flared so that they can be used as fuel gas elsewhere in facilities like energy generating systems (e.g., SOFCs). This results in reduced emissions and cost savings.

Flexibility Modifying generation and/or consumption patterns in reaction to an external signal (such as a change in price) to provide a service within the energy system.

Flood generation Tidal lagoon turbines are used when the tide is coming in, and the sluices are opened when the tide is going out.

Fossil fuel Natural fuel derived from the remains of living organisms.

Fuel cell Fuel utilization (FU) In a chemical reactor the word "conversion" or "conversion per pass" is used; similarly in SOFCs, FU is very prevalent in terms of usage. FU may be per pass or overall, and this distinction is notable in cases of fuel exhaust recycling from SOFC stacks. FU is a critical parameter in optimizing electrical efficiencies in SOFCs and SOFC−hybrid cycle power plants.

Functional layer Layers which only provide their electrochemical function in an SOFC.

Green power technologies Technologies aimed to generate power with low or zero emission of carbon dioxide and harmful substances.

Growth rate Growth velocity that can be measured in several ways.

Heat engine A device that converts thermal energy into mechanical energy.

Heat recovery steam generation A process of extracting the maximum residual heat from the primary power cycle for heating or additional power production.

Heat transfer equation The mathematical representation (partial differential equation) that describes temperation evolution over time and its distribution in a solid or fluid medium.

Hybrid cycles When more than one type of heat engine is used, usually in series. For example, natural gas can be converted to electrical power using an SOFC and the exit temperature is high enough to generate additional power via a cyclic heat engine or a combination of more than one heat engine.

Hybrid SOFC energy systems Hybrid energy systems are capable of exploiting the advantages of two or more energy technologies, simultaneously. The SOFC as a high-temperature technology can be combined with bottoming cycles such as gas turbines and steam turbines in cascade to meet higher efficiency suggesting great potential as a green, decentralized, CHP system.

Hydrogen economy The vision of using hydrogen as a fuel.

Improvement rate See performance growth.

Inferential control In inferential control the controlled variables that are difficult to measure are estimated by combining some of the measured variables and then used in feedback control.

Interconnect A component between the anode of one cell to the cathode of the adjacent cell in a multiple-cell SOFC.

Interconnector or metallic-supported SOFC One of the external supporting SOFCs in which the metallic interconnector is the thickest portion of the cell and provides mechanical strength.

International Patent Classification Hierarchical patent classification system created by the World Intellectual Property Organization.

Irreversibility All processes in nature are irreversible, that is, they are not incremental. Therefore they cannot be reversed, for example, dropping a ball cannot be reversed. In a chemical or mechanical engineering parlance, if one operates a system at infinitesima' rates, only then, is a reversible process ensured. In SOFCs the accepted goal is to operate the cell at low-current densities and high voltages, which are not far away from the open circuit voltage, and therefore minimize the irreversibility to the extent that is feasible.

Learning-by-doing One of the factors that push technological growth, mainly based on production.

Learning-by-searching One of the factors that push technological growth, mainly based on research funding.

Levelized cost of energy A cost indicator by levelizing the capital cost plus whole lifetime operation cost to each unit of energy produced.

Life-cycle assessment (LCA) Also known as life-cycle analysis, LCA is an environmental management tool that enables quantification of environmental burdens accompanied with the life cycle of both renewable and fossil fuel-based systems.

Logistic curve S-shaped curve usually used in biological systems.

Manipulated variable The variable in a control system that is changed to keep the control variable at set point.

Market saturation The phenomenon where a technology is no longer desired by the market.

Mass-produced Produced in series and high quantities, usually possible because of the simplicity of the product.

Maturity stage An intermediate stage in the technological life cycle; during this stage the diffusion is highest.

Membrane electrode assembly (MEA) MEA in solid oxide fuel cells, a series of a porous anode, dense electrolyte, and porous cathode connected to each other is called membrane electrode assembly. Similarly, in ReSOC structures, it include a solid electrolyte, oxygen electrode, and fuel electrode. In other words, MEA is the chemical part of SOFCs and ReSOCs.

Mircotubular SOFC A tubular SOFC with a diameter of less than, or about, 3 mm.

(m)GT (Micro) gas turbine.

Model predictive control An advanced method to control a process while satisfying a set of constraints. The aim is to optimize the process at the current time step by considering the previous measurements and the predicted states and control inputs.

Molten carbon fuel cell A fuel cell with molten-carbonates electrolyte.

Momentum equations A statement of Newton's Second Law which correlates the sum of forces acting on an infinitesimal fluid element to the element's acceleration. Sets of equation which are a mathematical representation of Newton's Second Law which describes fluid flow.

Moore's law Improvement of the performance of technology in time.

Multivariable control Process controllers that control multiple process variables simultaneously. Multivariable control can be useful when multiple, single-control loops are highly interactive.

Municipal solid waste (MSW) Broadly speaking, MSW is nonhazardous refuse generated by households, institutions, industries, agriculture, and sewage that varies due to the community jurisdiction and nutrition/diet. It is made up of waste, compostable, and recyclable materials with the municipality overseeing its disposal. Typically this refuse is collected, separated, and sent to either a landfill or a municipal recycling center for processing.

Nernst potential In thermodynamics, the Gibbs free energy (ΔG) represents the maximum energy that can be converted to work. The equivalent in terms of voltage, is the Nernst potential, that is, $\Delta G/nF$, where n is the number of electrons consumed per mole of limiting reactant in an electrochemical reaction and F, the Faraday's constant ($F = 96{,}487$ Coulomb/mol of electrons). The Nernst potential is equal to, and used interchangeably, with open circuit voltage (OCV) (except in case of mixed ion−electron conductor electrolyte SOFCs when OCV is lower than the Nernst potential).

Net present value An indicator of how much value an investment holds through the means of a discount rate.

Overpotential Is the extent to which the operating voltage is lower than the OCV due to ohmic and nonohmic irreversibilities occurring during cell operation, that is, current flow. An analogous term that defines overpotential is polarization. The more the cell is "polarized," the more is its overpotential. The differential of overpotential with respect to current density is termed area-specific resistance.

Oxygen reduction reaction The conversion of oxygen into oxide.

Patents view An online patent database containing patents from all over the world registered in the United States.

Performance growth The increase of qualities and capabilities of a technology.

Performance measure The measure of the capabilities of a technology; each technology has different fields of application.

Photovoltaic panels A generator that can generate power from solar energy.

Plastic deformation When stress is applied to a material which is higher than its tensile stress, irreversible deformation occurs in the material. This type of irreversible deformation is called plastic deformation. The reversible deformation is called elastic deformation.

Polymer electrolyte membrane A semipermeable membrane designed to conduct protons and used as an electronic insulator and reactant barrier.

Porous substrate-supported SOFC In some SOFCs an additional porous layer is used for structurally supporting the SOFC cell.

Positive electrode−electrolyte−negative electrode (PEN) The basic structure of SOFCs is the positive electrode−electrolyte−negative electrode (PEN) which is a three-layer assembly.

Power-to-gas A technology that converts electricity to a gas fuel.

Predictor Property of a phenomenon that helps to infer something about the phenomenon's future.

Primary variable The variable of primary importance that is linked to the overall control objective of the process (in other words CVs in the supervisory control layer)

Process innovation Discovery of new knowledge and techniques related to the production of a technology.

Process-intensive Dependent very much on the production process.

Product innovation Discovery of new knowledge and techniques related to the architecture and composition of a technology.

Propulsion The forward moving of an object.

Rationalization Elaboration of results by comparing them with theoretical information.

Redox (reduction−oxidation) The reduction of Ni in an Ni-based anode due to fuel shortage.

Reforming A chemical process in which hydrogen-containing fuels react with steam, oxygen, or both to produce a hydrogen-rich gas stream (syngas).

Regenerative fuel cell Fuel cells with round-trip energy conversion capabilities.

Regulatory control layer The regulatory layer is designed to facilitate stable operation and to regulate and keep the operation in the linear-operating range. Its performance can be quantified using the state-drift criterion.

Renewable energy Generally defined as energy that is collected from resources that are naturally replenished on the human timescale, such as sunlight, wind, rain, tides, waves, and geothermal heat.

Residual stress When stress is applied to a solid, after removing it, an amount of stress remains in the solid, called residual stress.

Reversible solid oxide cell (ReSOC) Systems can be used in two alternative operating modes, i.e. generating electricity from fuel, as well as producing hydrogen by consuming electricity.

Round-trip efficiency Energy storage typically consumes electricity and saves it in some manner, then hands it back to the grid. The ratio of energy put in (MWh) to energy retrieved from storage (MWh) is the round-trip efficiency, expressed in percent (%).

Scientometrics A measure of science and scientific research.

Screen printing A fabrication process. In this method ink or paste is transferred by a squeegee on a stencil and a layer of ink or paste is fabricated on the beneath layer.

Search path node pair A method to estimate the centrality of a node in a network.

Secondary variable An independent variable which includes information of primary variables.

Self-optimizing control A strategy for selecting controlled variables. An economic objective function is adopted as a selection criterion. The aim is to systematically select the controlled variables so that by controlling them at constant set points the impact of uncertainty and varying disturbances on the economic optimality is minimized. If a selection leads to an acceptable economic loss compared to perfectly optimal operation, then the chosen control structure is referred to as "self-optimizing."

Self-supporting SOFC When the main parts are used as supporting section (i.e., cathode, anode, or electrolyte) the cell is called self-supporting.

Sintering Compressing or heating a solid material for forming it. The heating is not for the purpose of melting the solid and only increases its temperature in the solid phase.

Slurry spin coating A method of layer fabrication where the slurry is put on the rotating disk and with the spin of the disk, slurry is distributed and make a thin layer based on the speed of the rotation. Centrifugal force is the concept of this method of fabrication.

SOFC stack A combination of single SOFCs.

Soft sensor Soft sensor or virtual sensor is a common name for software where several measurements are processed together to estimate the value of an unmeasured variable.

Solid loading The concentration of the solid particles in a slurry.

Solid oxide electrolyzer cell A solid oxide fuel cell that runs in regenerative mode to achieve the electrolysis of water (and/or carbon dioxide) by using a solid oxide, or ceramic, electrolyte to produce hydrogen gas (and/or CO) and oxygen.

Solid oxide fuel cell (SOFC) A fuel cell with solid oxide or ceramic electrolyte. An electrochemical conversion device that produces electricity directly from oxidizing a fuel.

Species transport equation A mathematical equation that shows the concentration of species change over time and in a domain due to convection and diffusion based on conservation of chemical species.

Spray method of fabrication A coating fabrication methods where a molten substance or suspension is sprayed onto the surface and a layer is fabricated. Based on the method of molting and spraying this method has two main branches, electrical and chemical spraying.

S-shaped curve The curve representing the technological life cycle, see logistic curve.

State estimation When the states are not available, they need to be estimated from the measurements.

State variable A state variable is used to describe the mathematical "state" of a dynamical system. The states of a system together with the input variables define the system and determine its future behavior in the absence of any external forces affecting the system.

Static estimation When the final steady-state values of variables are estimated.

Steady-state multiplicity Multiple steady states.

Supercapacitor A device that stores electric charge.

Supported layer Layers which are thicker than the usual size and used for structural support.

Tape casting A method of fabrication where a mold is filled with molten metal or other considering solid material and then solidified for making the solid the shape of the mold. Tape casting is casting using a sheet of ceramics.

Technological changes Evolution of a technology that transformed from its initial stage to its current form.

Technological development See technological changes.

Technological domain The area comprising the knowledge, processes, and tools related a technology.

Technological forecasting Attempts of predicting the evolution of a technology in a quantitative or qualitative way.

Technological life cycle Fixed stages which a technology that passes through from its early stage to its substitution.

Thermal expansion coefficient The fractional increase in size with increase in temperature at constant pressure.

Thermal management A technique used with the purpose of safe operation and maintenance of an SOFC system as well as efficient use of the available thermal energy.

Thermal modeling Refers to all the methods used (simulations, analyses, assumptions, etc.) that are capable of calculating temperature profiles through solving the heat transfer equation. The main goals of thermal modeling are to find thermal behavior of the SOFC, predict thermal stresses, predict transient behavior of the system, reduce thermal losses, and increase thermal efficiency.

Thermal transient Refers to the transient heat transfer phenomenon.

Throughput manipulator A degree of freedom that affects the network flow and is not directly or indirectly determined by the control of the individual units, including their inventory control.

Tidal lagoon A generator that uses the movement of the oceans to create power.

Triad The three half-hour settlement periods with highest system demand between November and February in the United Kingdom separated by at least ten clear days.

Trigeneration The process by which some of the heat produced by a CHP plant is used to generate chilled water for air conditioning or refrigeration.

Triple-phase boundary The place where three phases of the electrolyte, electrode, and fuel meet each other.

United States Patent Classification (UPC) A classification system created by USPTO, but replaced by UPC in 2015.

United States Patent and Trademark Office (USPTO) Federal agency that grants patents filed in the United States and registers trademarks.

Vehicle An entity designed for the transportation of people and/or materials.

Waste management The collection, transportation, and disposal of garbage, sewage, MSW, and other waste products. Waste management encompasses management of all processes and resources for proper handling of waste materials, employing several waste control and disposal methods such as source reduction, recycling, reuse, incineration, landfilling, or power-plant systems for minimizing the environmental impact of commercial and industrial waste streams in order to comply with health codes and environmental regulations.

Waste-to-energy systems Thermal treatment plants associated with energy and further fuel production.

Wind turbine A generator that can generate power from wind.

Wright's law Improvement of the performance of technology for doubling of the production capacity.

This page intentionally left blank

Index

Note: Page numbers followed by "*f*" and "*t*" refer to figures and tables, respectively.

D

E

I

J

K

L

M

N

O

P

R

S

T

U

V

W

Y

Z

Design and Operation of Solid Oxide Fuel Cells

The Systems Engineering Vision for Industrial Application

A multidisciplinary, comprehensive, and critical review of the latest research and technological advances in the field of SOFC, with a focus on theory, applications, and computational tools in a variety of power plants.

Edited by
Dr. Mahdi Sharifzadeh

Design and Operation of Solid Oxide Fuel Cells: The Systems Engineering Vision for Industrial Application presents a comprehensive, authoritative, critical, and accessible review of the latest research in the field of solid oxide fuel cells (SOFCs). On discussing the theoretical aspects of the field, the book explores a diverse range of power applications, such as hybrid power plants, polygeneration, distributed electricity generation, energy storage, and waste management, to name just a few, with a focus on modeling and computational skills.

Dr. Sharifzadeh presents the associated risks and limitations throughout the discussion, providing a very complete and thorough analysis of SOFCs, their control and operation in power plants. Written by an international team of experts from multiple disciplines, including Chemical Engineering, Electrical Engineering, and Mechanical Engineering, chapters provide a diverse and futuristic vision for the design and operation of solid oxide fuel cell technologies. The first of its kind, this book will be of particular interest to energy engineers, industry experts, and academic researchers in the energy, power, and transportation industries, as well as to those working and researching in the chemical, environmental, and material sectors.

- Closes the gap between various power engineering disciples by considering a diverse variety of applications and sectors
- Presents and reviews a variety of modeling techniques and considers regulations throughout
- Includes Computational Fluid Dynamics (CFD) modeling examples, and process simulation and optimization programming guidance

About the Editor

Dr. Sharifzadeh is an expert in the optimal design and operation of energy-efficient industrial processes, with a special focus on low carbon power generation, which is evidenced by solid academic background in Energy Systems Engineering, and 28 highly cited publications including a publication with detailed analysis of SOFC hybrid power plants. His research interests include the intersection of process design and control, with a focus on energy and environmental applications. He is furthermore very interested in the development of advanced optimization algorithms to address large-scale problems.

ELSEVIER

ACADEMIC PRESS
An imprint of Elsevier
elsevier.com/books-and-journals

ISBN 978-0-12-815253-9